TECHNISCHE UNIVERSITÄT
CHEMNITZ

Fakultät für Mathematik
Professur Angewandte Funktionalanalysis

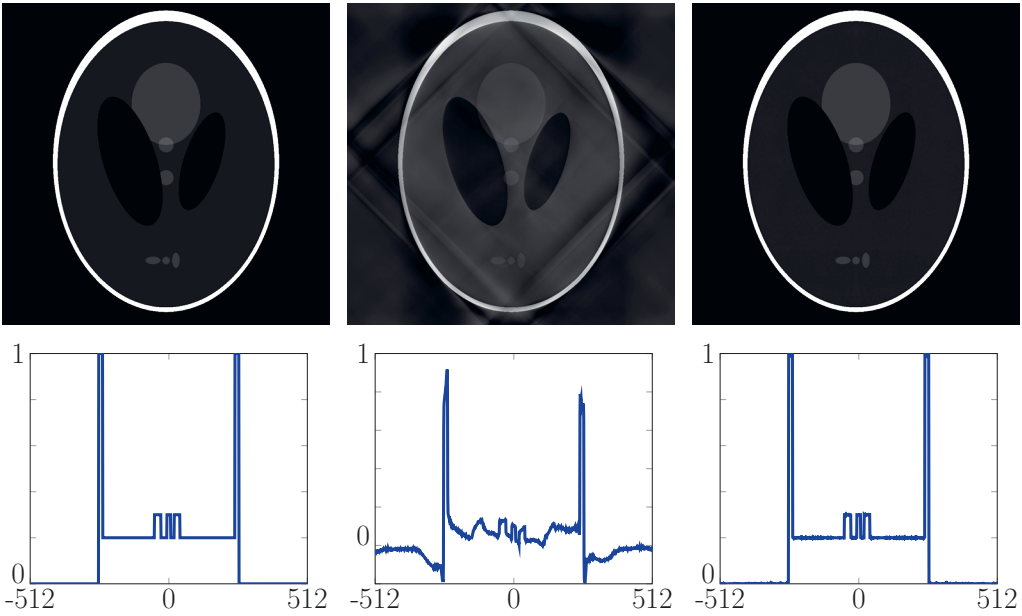

Melanie Kircheis

Fast Fourier Methods for Trigonometric Polynomials and Bandlimited Functions

Melanie Kircheis

Fast Fourier Methods for Trigonometric Polynomials and Bandlimited Functions

Berichte aus der Mathematik

Melanie Kircheis

Fast Fourier Methods for Trigonometric Polynomials and Bandlimited Functions

D 93 (Diss. TU Chemnitz)

Shaker Verlag
Düren 2024

Bibliographic information published by the Deutsche Nationalbibliothek
The Deutsche Nationalbibliothek lists this publication in the Deutsche Nationalbibliografie; detailed bibliographic data are available in the Internet at http://dnb.d-nb.de.

Zugl.: Chemnitz, Techn. Univ., Diss., 2024

Satz/Layout, Titelgrafik: Melanie Kircheis

Printed in Germany.

Print-ISBN 978-3-8440-9731-3
PDF-ISBN 978-3-8440-9831-0
ISSN 0945-0882
eISSN 2944-1463
https://doi.org/10.2370/9783844098310

Shaker Verlag GmbH • Am Langen Graben 15a • 52353 Düren
Phone: 0049/2421/99011-0 • Telefax: 0049/2421/99011-9
Internet: www.shaker.de • e-mail: info@shaker.de

Fast Fourier Methods for Trigonometric Polynomials and Bandlimited Functions

von der Fakultät für Mathematik
der Technischen Universität Chemnitz
genehmigte

Dissertation

zur Erlangung des akademischen Grades

doctor rerum naturalium
(Dr. rer. nat.)

vorgelegt

von Melanie Kircheis, M. Sc.

Tag der Einreichung: 28. Juni 2024

Betreuer: Prof. Dr. Daniel Potts, Technische Universität Chemnitz

Gutachter: Prof. Dr. Daniel Potts, Technische Universität Chemnitz
Prof. Dr. Brigitte Forster-Heinlein, Universität Passau
Prof. PhD Heather Denise Wilber, University of Washington

Tag der öffentlichen Prüfung: 18. Oktober 2024

Contents

1 Introduction **9**

2 Nonequispaced fast Fourier transforms **23**
2.1 Preliminaries and Definitions 23
2.2 The NFFT 25
2.3 The adjoint NFFT 30
2.4 The NNFFT 31

3 Direct inversion methods for the NFFT **37**
3.1 Problem formulation 37
3.2 Density compensation factors 42
3.2.1 Exact quadrature weights for trigonometric polynomials 45
3.2.2 Practical computation schemes 50
3.2.3 Bounds on the approximation error 53
3.2.4 Linking to approaches in literature 57
3.3 Optimization of the sparse matrix $\boldsymbol{B}$ 69
3.3.1 Frobenius norm minimization 70
3.3.2 Practical computation schemes 73
3.3.3 Bounds on the approximation error 78
3.3.4 Linking to approaches in literature 81
3.4 Numerical examples & summary 87

4 Regularized Shannon sampling formulas **105**
4.1 Bandlimited functions and the sampling theorem 105
4.2 Poor convergence of Shannon sampling sums 112
4.3 Univariate regularized Shannon sampling formulas 122
4.3.1 Regularization with a window function in frequency domain 124
4.3.2 Regularization with a window function in spatial domain 141
4.3.3 Comparison of the two regularization methods . . . 183
4.4 Multivariate regularized Shannon sampling formulas 183
4.5 Numerical examples & summary 200

5 Fast sinc methods **217**
5.1 Discrete sinc transform 217
5.1.1 Approximation of the sinc function by exponential sums 219
5.1.2 The fast sinc transform 227
5.2 Application to regularized Shannon sampling formulas . . . 233
5.2.1 Fast approximation using frequency window functions 233
5.2.2 Fast approximation using spatial window functions 236
5.3 Approximation of bandlimited functions based on Fourier data 239
5.3.1 Derivation of the fast algorithm 240
5.3.2 Comparison to the classical NFFT 244
5.4 Numerical examples & summary 248

6 Reconstruction of the Fourier transform of bandlimited functions from nonequispaced spatial data **261**
6.1 Density compensation factors 261
6.1.1 Reconsideration as trigonometric polynomials . . . 262
6.1.2 Linking to approaches in literature 265
6.1.3 Exactness condition in the sense of tempered distributions 269
6.2 Optimization of the sparse matrix $\boldsymbol{B}$ 272
6.3 Numerical examples & summary 272

Bibliography **277**

Alphabetical Index **293**

List of Symbols **297**

1 Introduction

The well-known fast Fourier transform (FFT) is one of the most important and widely used algorithms in a variety of fields including engineering, natural sciences, scientific computing, and signal processing. The reason for this is that the FFT enables the fast evaluation of trigonometric sums at equispaced nodes, reducing the number of arithmetic operations from $\mathcal{O}(N^2)$ for the naive computation to only $\mathcal{O}(N \log N)$, where N denotes the number of given nodes. This efficient computation is based on a divide-and-conquer strategy exploiting the underlying trigonometric structure, which was first described by C.F. Gauss around 1800, cf. [HJB85, Pre16], and was brought to a wider attention by Cooley and Tukey in 1965, see [CT65].

In the case of nonequispaced nodes, however, the evaluation of a trigonometric polynomial is not possible via the classical FFT, which led to the development of the nonequispaced fast Fourier transform (NFFT), also referred to as the nonuniform fast Fourier transform (NUFFT), see for instance [DR93, Bey95, Ste98a, War98, DS99, PST01, GL04, KKP09, BMK19, PT21a]. This efficient algorithm realizes the approximation of a trigonometric polynomial by a linear combination of translates of a 1-periodic window function, resulting in a three-step approximation procedure that consists of a convolution step, an ordinary FFT, and a deconvolution step, thus possessing the same arithmetic complexity as the FFT.

Nevertheless, numerous applications such as magnetic resonance imaging (MRI), cf. [NW01, GLI06, DAP22, EKP22], synthetic aperture radar (SAR), cf. [GJG23], solution of partial differential equations (PDEs), cf. [Fas07], etc., are interested in an inverse transform. In other words, there is a demand for fast algorithms for the approximation of Fourier data from given nonequispaced function evaluations of trigonometric polynomials, or even of bandlimited functions. For this reason, the present thesis is divided into two parts. The first part focuses on efficient inversion methods for the nonequispaced fast Fourier transform (NFFT), while the second part addresses the generalizations of these methods to the setting of bandlimited functions.

More precisely, the first objective of this work is the study of efficient methods for the discrete inversion problem, i. e., computing the Fourier

coefficients $\hat{f}_{\boldsymbol{k}} \in \mathbb{C}$, $\boldsymbol{k} \in \mathcal{I}_{\boldsymbol{M}}$, of a trigonometric polynomial

$$f(\boldsymbol{x}) = \sum_{\boldsymbol{k} \in \mathcal{I}_{\boldsymbol{M}}} \hat{f}_{\boldsymbol{k}} \, \mathrm{e}^{2\pi \mathrm{i} \boldsymbol{k} \boldsymbol{x}} \tag{1.1}$$

from given evaluations $f(\boldsymbol{x}_j)$, $j = 1, \dots, N$, at given nonequispaced points $\boldsymbol{x}_j \in \left[-\frac{1}{2}, \frac{1}{2}\right)^d$, where $N \in \mathbb{N}$ and $\mathcal{I}_{\boldsymbol{M}} \coloneqq \mathbb{Z}^d \cap \left[-\frac{M}{2}, \frac{M}{2}\right)^d$ with $|\mathcal{I}_{\boldsymbol{M}}| = M^d$. Since in general the number N of the nodes $\boldsymbol{x}_j$ does not coincide with the number $|\mathcal{I}_{\boldsymbol{M}}|$ of the Fourier coefficients $\hat{f}_{\boldsymbol{k}}$, the nonequispaced Fourier matrix

$$\boldsymbol{A} = \left(\mathrm{e}^{2\pi \mathrm{i} \boldsymbol{k} \boldsymbol{x}_j}\right)_{j=1,\, \boldsymbol{k} \in \mathcal{I}_{\boldsymbol{M}}}^{N} \in \mathbb{C}^{N \times |\mathcal{I}_{\boldsymbol{M}}|},$$

is rectangular and hence a regular inverse does not exist. Therefore, we can only expect approximate inverse nonequispaced fast Fourier transforms. Here we describe two methods for finding a left-inverse matrix, which can be seen as generalizations of the equispaced setting, where the inverse of the FFT is simply given by its scaled adjoint. Thus, the main contribution of the first part of this thesis is the presentation of fast methods that can be realized with the complexity of an adjoint NFFT, due to a precomputation that depends only on the nodes $\boldsymbol{x}_j$, $j = 1, \dots, N$. In particular, based on an extensive study of the so-called density compensation methods, which compute a diagonal matrix of weights, we introduce a condition for exactness and consequently a scheme for the computation of weights that are exact under proper assumptions on the nodes. Moreover, we successfully generalize this concept of density compensation to the modification of a sparse matrix in the factorization of the adjoint NFFT, thereby allowing more freedom in the optimization and thus relaxing the assumptions to be made.

The second objective of this work is the generalization of the obtained efficient methods to the continuous inversion problem. In this case, instead of trigonometric polynomials (1.1), we deal with bandlimited functions, which are functions whose Fourier transform

$$\hat{f}(\boldsymbol{v}) \coloneqq \int_{\mathbb{R}^d} f(\boldsymbol{x}) \, \mathrm{e}^{-2\pi \mathrm{i} \boldsymbol{v} \boldsymbol{x}} \, \mathrm{d}\boldsymbol{x}, \quad \boldsymbol{v} \in \mathbb{R}^d, \tag{1.2}$$

is supported on $\left[-\frac{M}{2}, \frac{M}{2}\right]^d$. Accordingly, our goal is to compute point evaluations $\hat{f}(\boldsymbol{k}) \in \mathbb{C}$, $\boldsymbol{k} \in \mathcal{I}_{\boldsymbol{M}}$, of the Fourier transform $\hat{f}$ from given samples $f(\boldsymbol{x}_j)$, $j = 1, \dots, N$, at nonequispaced nodes $\boldsymbol{x}_j \in \left[-\frac{1}{2}, \frac{1}{2}\right)^d$.

The main contributions of this part can be summarized as follows. In order to address this more challenging problem, we firstly examine bandlimited functions in greater detail. Here, more efficient and accurate numerical realizations of the famous Whittaker–Kotelnikov–Shannon sampling theorem, see [Whi15, Kot01, Sha49], are obtained by the systematic transfer of the NFFT window functions in combination with a new approach for estimating the approximation error. In particular, we present the first comprehensive overview of the regularized Shannon sampling formulas and, for the first time, extend these results to the multivariate setting with $d > 1$. Based on this, we introduce a new NFFT-like approach for the continuous problem of computing the samples $f(\boldsymbol{x}_j)$, $j = 1, \dots, N$, from given point evaluations $\hat{f}(\boldsymbol{k}) \in \mathbb{C}$, $\boldsymbol{k} \in \mathcal{I}_{\boldsymbol{M}}$, of the Fourier transform $\hat{f}$ of a bandlimited function f. Since this approach is specifically designed for the case of bandlimited functions, it can be demonstrated that it yields a significant improvement in comparison to the classical NFFT. Finally, considering the continuous inversion problem, we give a detailed study of the relation between the cases of trigonometric polynomials and bandlimited functions. Thereby, we are able to show that the previously introduced efficient inversion methods from the discrete setting can be generalized to the continuous setting and that the error in the resulting reconstruction is dominated by the fact that the bandlimited function f is typically not known on whole $\mathbb{R}^d$, but only on a bounded domain.

Outline of this thesis

In addition to this introductory part, the present thesis comprises five chapters. In the following, we provide a brief overview of the individual topics. For a more detailed introduction, please refer to the opening of each chapter.

Chapter 2: Nonequispaced fast Fourier transforms

The second chapter is dedicated to the introduction of the fundamental algorithms utilized for the efficient evaluation of trigonometric sums at nonequispaced nodes. Initially, we recall some basic definitions and present the concept of the well-known fast Fourier transform (FFT) in Section 2.1. Subsequently, in Section 2.2 we describe the previously mentioned fast Fourier transform for nonequispaced data in the spatial domain (NFFT),

which is summarized in Algorithm 2.2. Its adjoint version for nonequispaced data in the frequency domain, the adjoint NFFT, is then given in Algorithm 2.5 in Section 2.3. Afterwards, this approach is further generalized in Section 2.4, where the fast Fourier transform for nonequispaced data in the spatial domain and in the frequency domain (NNFFT) is detailed and finally stated in Algorithm 2.6.

Chapter 3: Direct inversion methods for the NFFT

Since numerous applications are interested in an inversion of the nonequispaced fast Fourier transform, see above, the third chapter is attributed to this task. That is to say, instead of the evaluation of a trigonometric polynomial (1.1) at given points $\boldsymbol{x}_j$, $j = 1, \dots, N$, now the aim is computing the Fourier coefficients $\hat{f}_{\boldsymbol{k}}$, $\boldsymbol{k} \in \mathcal{I}_{\boldsymbol{M}}$, from given nonequispaced data $f(\boldsymbol{x}_j)$, $j = 1, \dots, N$.

Through a detailed study of the literature, we recognize that the existing methods can be divided into two distinct categories: iterative and direct procedures. While iteration schemes require multiple iteration steps, the so-called direct methods consist of only one precomputational step and one reconstruction step. Since in the context of the nonequispaced fast Fourier transform (NFFT) being a direct method means that the reconstruction can be realized with the same number of arithmetic operations as a single application of an adjoint NFFT, the reconstruction step is very efficient. Thus, although the necessary precomputations might be rather costly, they need to be done only once for a given set of points $\boldsymbol{x}_j$, $j = 1, \dots, N$, and therefore direct methods are especially beneficial in the case of multiple measurements at the same points. For this reason, this work focuses on approaches of this kind.

In Section 3.1 we introduce the general idea of our procedures. By having a closer look at the special case of equispaced points and the fact that the adjoint NFFT does not yield an inversion of the NFFT per se, see (3.2), it becomes evident that in the nonequispaced case some kind of re-weighting according to the points is compulsory. In particular, we aim to find a left-inverse matrix $\boldsymbol{X} \in \mathbb{C}^{|\mathcal{I}_{\boldsymbol{M}}| \times N}$ with $\boldsymbol{X}\boldsymbol{A} \approx \boldsymbol{I}_{|\mathcal{I}_{\boldsymbol{M}}|}$ that exhibits a similar structure $\boldsymbol{D}^* \boldsymbol{F}^* \boldsymbol{B}^*$ as the adjoint NFFT. Therefore, we present two different approaches for the realization of this precomputational step.

Firstly, in Section 3.2 we consider the very well-known approach of so-called sampling density compensation. In these methods, the

aforementioned precomputations consist of computing a diagonal matrix $\boldsymbol{W} \coloneqq \operatorname{diag}(w_j)_{j=1}^N$ of suitable weights $w_j \in \mathbb{C}$. The subsequent reconstruction step then involves only one adjoint NFFT applied to the scaled coefficient vector $\boldsymbol{W}\boldsymbol{f}$, as illustrated in Algorithm 3.2. Through our investigation, we demonstrate that optimal density compensation weights need to fulfill the condition

$$\sum_{j=1}^{N} w_j \, \mathrm{e}^{2\pi \mathrm{i} \boldsymbol{k} \boldsymbol{x}_j} = \delta_{\boldsymbol{0},\boldsymbol{k}}, \quad \boldsymbol{k} \in \mathcal{I}_{\boldsymbol{2M}},$$

to ensure an exact reconstruction, as evidenced by Theorem 3.6. Based on this fact, we show that the exactness condition can also be used to compute the optimal weights numerically, leading to Algorithm 3.10.

Secondly, in Section 3.3 we generalize the idea of sampling density compensation to find an optimal sparse matrix instead of a diagonal matrix of weights. More precisely, here the idea is using the matrix representation $\boldsymbol{A} \approx \boldsymbol{B}\boldsymbol{F}\boldsymbol{D}$ of the NFFT to modify one of the matrix factors. Then the precomputational step consists of computing the optimal sparse matrix $\boldsymbol{B}_{\mathrm{opt}}$ based on the minimization problem

$$\underset{\tilde{\boldsymbol{B}} \in \mathbb{R}^{N \times |\mathcal{I}_{\boldsymbol{M}\boldsymbol{\sigma}}|} \colon \tilde{\boldsymbol{B}} \ (2m+1)^d\text{-sparse}}{\operatorname{Minimize}} \left\| \boldsymbol{D}^* \boldsymbol{F}^* \tilde{\boldsymbol{B}}^* \boldsymbol{A} - \boldsymbol{I}_{|\mathcal{I}_{\boldsymbol{M}}|} \right\|_{\mathrm{F}}^2,$$

where $\| \cdot \|_{\mathrm{F}}$ denotes the Frobenius norm. As outlined in Algorithm 3.21, this enables that the actual reconstruction step includes only one modified adjoint NFFT applied to the coefficient vector $\boldsymbol{f}$. In addition to these theoretical results, we also discuss methods for the numerical computation, summarized in Algorithm 3.25.

Finally, several numerical examples are presented in Section 3.4, with special emphasis on comparing the new approaches both among themselves and with selected methods from the literature. Especially, in compliance with the obtained exactness condition, the superiority of the newly proposed density compensation factors computed by Algorithm 3.10 is demonstrated in Figure 3.6. In addition, the enhanced results that can be achieved under less rigorous assumptions using the novel matrix optimization approach, in contrast to the density compensation approach, are clearly evident in Figure 3.11.

Chapter 4: Regularized Shannon sampling formulas

Having considered the evaluation problem and the reconstruction problem for trigonometric polynomials (1.1), our aim is now to study the analogous problems for the so-called bandlimited functions. While trigonometric polynomials (1.1) are periodic functions on the torus $\mathbb{T}^d$ with only a finite number of nonzero Fourier coefficients, we now move on to functions on $\mathbb{R}^d$ that exhibit a similar property with respect to the continuous Fourier transform. More precisely, a function $f\colon \mathbb{R}^d \to \mathbb{C}$ is called bandlimited with bandwidth $M \in \mathbb{N}$, if the support of its (continuous) Fourier transform (1.2) is contained in $\left[-\frac{M}{2}, \frac{M}{2}\right]^d$. For such a function, the fundamental Whittaker–Kotelnikov–Shannon sampling theorem, see [Whi15, Kot01, Sha49], ensures that for all $L \geq M$ it can be recovered from its samples $f\big(\frac{\boldsymbol{\ell}}{L}\big)$, $\boldsymbol{\ell} \in \mathbb{Z}^d$, by

$$f(\boldsymbol{x}) = \sum_{\boldsymbol{\ell} \in \mathbb{Z}^d} f\big(\tfrac{\boldsymbol{\ell}}{L}\big) \operatorname{sinc}\big(L\pi\big(\boldsymbol{x} - \tfrac{\boldsymbol{\ell}}{L}\big)\big), \quad \boldsymbol{x} \in \mathbb{R}^d, \tag{1.3}$$

with the sinc function (3.31). In other words, this sampling theorem plays an essential role in signal processing, as it describes the close relation between a bandlimited function and its equidistant samples.

Unfortunately, the practical use of this sampling theorem is limited, since it requires infinitely many samples, which is impossible in practice. The partial sums, however, exhibit a rather poor convergence, due to the slow decay of the sinc function, see [Jag66]. Moreover, in the presence of noise or quantization in the samples $f\big(\frac{\boldsymbol{\ell}}{L}\big)$, $\boldsymbol{\ell} \in \mathbb{Z}^d$, the convergence of Shannon sampling series may even break down completely, see [Fei92a, DD03].

Therefore, suitable methods for the numerical realization of the sampling theorem are discussed in this fourth chapter. In particular, in Section 4.1 we specify some important preliminaries as well as the famous sampling theorem of Whittaker–Kotelnikov–Shannon, while Section 4.2 gives evidence for the poor convergence rate and the lack of numerical robustness of classical Shannon sampling sums. To overcome these shortcomings, the proposed numerical realizations of the sampling theorem are based on additional regularization techniques, where a so-called window function is employed. Since such a window function can be chosen either in frequency domain or in spatial domain, we survey both approaches for the univariate setting in Section 4.3. In doing so, we put a special emphasis on the comparison of the two approaches in terms of error decay rates.

Firstly, in Section 4.3.1 we study the regularization with a window

function in the frequency domain. In literature this is often realized by substituting the sinc function in (1.3) by a function ψ that is compactly supported in the frequency domain, cf. e. g. [Dau92, Nat86a, Rap96, Par97, ST05]. More specifically, ones chooses a window function of the form

$$\hat{\psi}(v) \coloneqq \begin{cases} 1 & : |v| \leq \frac{M}{2}, \\ \xi(|v|) & : \frac{M}{2} < |v| < \frac{L}{2}, \\ 0 & : |v| \geq \frac{L}{2}. \end{cases}$$

However, due to this structure, the uncertainty principle implies that the corresponding sampling series still requires infinitely many samples. Therefore, we approximate a function f by the T-th partial sum

$$(P_{\psi,T} f)(x) \coloneqq \sum_{\ell=-T}^{T} f\big(\tfrac{\ell}{L}\big)\, \frac{1}{L}\, \psi\big(x - \tfrac{\ell}{L}\big), \quad x \in \mathbb{R}.$$

In this work, we present the first general result on the uniform approximation error

$$\max_{x \in [-1,\,1]} \big| f(x) - (P_{\psi,T} f)(x) \big|.$$

in Theorem 4.10. Moreover, by specifying this result for several window functions we obtain more explicit versions of previously existing bounds. Nevertheless, our investigations show that for the regularization in the frequency domain only algebraic error decay rates are achievable.

Secondly, in Section 4.3.2 we study the regularization with a window function in the spatial domain. Here for some $m \in \mathbb{N} \setminus \{1\}$ a suitable window function $\varphi_m \colon \mathbb{R} \to [0,\, 1]$ with compact support $\big[-\frac{m}{L},\, \frac{m}{L}\big]$ and $\varphi_m(0) = 1$ is chosen, such that a function f can be approximated by the regularized Shannon sampling formula

$$(R_{\varphi,m} f)(x) \coloneqq \sum_{\ell \in \mathbb{Z}} f\big(\tfrac{\ell}{L}\big)\, \operatorname{sinc}\big(L\pi \left(x - \tfrac{\ell}{L}\right)\big)\, \varphi_m\big(x - \tfrac{\ell}{L}\big), \quad x \in \mathbb{R}.$$

Due to the assumptions made on the window function φ_m we show that this regularized Shannon sampling formula exhibits the interpolation property (4.75) for $x \in \frac{1}{L}\,\mathbb{Z}$ and requires only $2m+1$ samples $f\big(\frac{\ell}{L}\big)$ for fixed $x \in \mathbb{R} \setminus \frac{1}{L}\,\mathbb{Z}$. Note that in literature this approach was only considered for the truncated Gaussian window function (4.60), cf.

e. g. [Qia03, SS07, MXZ09, LZ17, CZ19]. In contrast, we present the first general result on the uniform approximation error

$$\|f - R_{\varphi,m} f\|_{C_0(\mathbb{R})} \coloneqq \max_{x \in \mathbb{R}} \big| f(x) - (R_{\varphi,m} f)(x) \big|$$

in Theorem 4.25. Furthermore, by specifying this result for window functions which are known to be excellent in the context of the NFFT, we show that exponential error decay rates are obtained.

All in all, we present the first systematic approach, comparing the different regularization techniques and window functions both theoretically and numerically, see also Table 4.1 in Section 4.3.3. As it turns out that the best results are obtained by oversampling and the newly suggested regularization in the spatial domain, these regularized Shannon sampling formulas are generalized to the multivariate setting for the first time in Section 4.4.

In the final Section 4.5 several numerical examples illustrate the theoretical results. These include a comparison of several window functions in frequency domain in Figure 4.16 and a comparison of several window functions in spatial domain in Figure 4.25. In addition, a concluding comparison of the two approaches in Figure 4.26 clearly emphasizes the superiority of the newly proposed NFFT window functions.

Chapter 5: Fast sinc methods

As already seen, the sinc function plays an important role in the context of the sampling theorem and the regularized Shannon sampling formulas, but is also needed in many other applications, see [LB92, Ste93]. Therefore, this interluding fifth chapter emphasizes the value of the sinc function by focusing on efficient and accurate algorithms in which the sinc function is a crucial ingredient.

Firstly, in Section 5.1 we consider the so-called discrete sinc transform (see [GLI06, LB11])

$$h(\boldsymbol{b}_\ell) = \sum_{k \in \mathcal{I}_K} c_k \operatorname{sinc}\big(M\pi\,(\boldsymbol{b}_\ell - \boldsymbol{a}_k)\big), \quad \ell \in \mathcal{I}_L, \tag{1.4}$$

with complex coefficients $c_k \in \mathbb{C}$ and given points $\boldsymbol{a}_k, \boldsymbol{b}_\ell \in \left[-\frac{1}{2}, \frac{1}{2}\right]^d$, $k \in \mathcal{I}_K$ and $\ell \in \mathcal{I}_L$ for $K, L \in 2\mathbb{N}$, which can be nonequispaced. In order to

derive a fast algorithm for the computation of these values, we approximate the sinc function $\operatorname{sinc}(M\pi\boldsymbol{x})$ for all $\boldsymbol{x} \in [-1,1]^d$ by an exponential sum

$$\sum_{j=0}^{n} w_j \, \mathrm{e}^{-2\pi \mathrm{i} M \boldsymbol{z}_j \boldsymbol{x}}$$

with explicitly known coefficients $w_j > 0$, $j = 0, \ldots, n$, for given points $\boldsymbol{z}_j \in \left[-\frac{1}{2}, \frac{1}{2}\right]^d$. Namely, by applying a Clenshaw–Curtis quadrature rule to an integral representation of the sinc function, we derive a new error estimate in Theorem 5.4. Thereby, the evaluation of the discrete sinc transform (1.4) can be realized efficiently by means of two fast Fourier transforms for nonequispaced data in the spatial domain and in the frequency domain (NNFFTs). In addition, the explicit error estimate indicates that for a given target accuracy, the parameters M and n can be fixed, thereby enabling the realization of the so-called fast sinc transform in Algorithm 5.10 with only $\mathcal{O}(K+L)$ arithmetic operations.

Subsequently, in Section 5.2 similar techniques are employed to extend this fast sinc transform to the evaluation of the regularized Shannon sampling formulas from Section 4.3. More precisely, in case these numerical realizations of the sampling theorem still require a huge amount of samples and therefore the direct evaluation is too costly, we describe analogous efficient approximation procedures. In particular, in Section 5.2.1 we concentrate on the regularization in the frequency domain from Section 4.3.1. The resulting approximation procedure is summarized in Algorithm 5.14, whose accuracy is based on the new error estimate of Theorem 5.13. Additionally, in Section 5.2.2 we address the regularization in the spatial domain from Section 4.3.2, with the resulting procedure outlined in Algorithm 5.15.

Afterwards, we are equipped with all the necessary tools to change the focus and revisit the aforementioned evaluation problem for bandlimited functions in Section 5.3. More precisely, for given values $\hat{f}(\boldsymbol{k})$, $\boldsymbol{k} \in \mathcal{I}_{\boldsymbol{M}}$, of the Fourier transform of a bandlimited function f, we are looking for function evaluations $f(\boldsymbol{x}_j)$ at given nonequispaced points $\boldsymbol{x}_j$, $j = 1, \ldots N$. Note that if a trigonometric polynomial $f \in L_2(\mathbb{T}^d)$ is given, it is already known by Chapter 2 that this evaluation of (1.1) can be realized by means of the nonequispaced fast Fourier transform (NFFT). Hence, for the first time we introduce an NFFT-like procedure for bandlimited functions in Algorithm 5.16, which is based on the regularized Shannon sampling formulas of Chapter 4 and therefore the sinc function plays an

important role in this approximation. In particular, we discuss the relation of this new method to the classical NFFT, where the evident superiority of this novel approach is illustrated in Figure 5.1.

Finally, Section 5.4 contains several numerical examples that demonstrate the accuracy and efficiency of the new approaches. Specifically, the accuracy of the fast sinc transform is confirmed in Figure 5.5, while Figures 5.6 and 5.7 illustrate the quality of the analogous methods for the fast evaluation of the regularized Shannon sampling formulas. Furthermore, a comparison of the approximation errors of the newly proposed NFFT-like method and the classical NFFT is displayed in Figure 5.8, once more showing the considerable improvement that can be obtained through this novel approach.

Chapter 6: Reconstruction of the Fourier transform of bandlimited functions from nonequispaced spatial data

In the last chapter we address the reconstruction problem for bandlimited functions. As previously discussed in Chapter 3, there are several approaches that are based on the setting of trigonometric polynomials. However, numerous applications, e. g. magnetic resonance imaging (MRI), cf. [GLI06, EKP22], are concerned with the analogous continuous inversion problem, where the aim is the reconstruction of point evaluations $\hat{f}(\boldsymbol{k}) \in \mathbb{C}$, $\boldsymbol{k} \in \mathcal{I}_{\boldsymbol{M}}$, of the Fourier transform $\hat{f}$ from given measurements $f(\boldsymbol{x}_j)$, $j = 1, \dots, N$, of the form

$$f(\boldsymbol{x}) = \int_{\left[-\frac{M}{2}, \frac{M}{2}\right)^d} \hat{f}(\boldsymbol{v}) \, \mathrm{e}^{2\pi \mathrm{i} \boldsymbol{v} \boldsymbol{x}} \, \mathrm{d}\boldsymbol{v}, \quad \boldsymbol{x} \in \mathbb{R}^d.$$

To address this problem, note that the given problem can also be seen as a generalization of the discrete problem in Chapter 3, such that we immediately obtain direct inversion methods by reviewing several approaches and extending these techniques to the setting of bandlimited functions.

In particular, in Section 6.1 we investigate the aforementioned density compensation technique. Using the fact that the 1-periodization $\tilde{f}(\boldsymbol{x}) = \sum_{\boldsymbol{r} \in \mathbb{Z}^d} f(\boldsymbol{x} + \boldsymbol{r})$ of a bandlimited function can be represented in the form

$$\tilde{f}(\boldsymbol{x}) \coloneqq \sum_{\boldsymbol{k} \in \mathbb{Z}^d} c_{\boldsymbol{k}}(\tilde{f}) \, \mathrm{e}^{2\pi \mathrm{i} \boldsymbol{k} \boldsymbol{x}} = \sum_{\boldsymbol{k} \in \mathcal{I}_{\boldsymbol{M}}} \hat{f}(\boldsymbol{k}) \, \mathrm{e}^{2\pi \mathrm{i} \boldsymbol{k} \boldsymbol{x}},$$

it becomes evident that this is a trigonometric polynomial (1.1). Thus, if we had access to the periodization $\tilde{f}$, the density compensation approach from Algorithm 3.2 using the weights computed by Algorithm 3.10 would guarantee an exact reconstruction. However, in practical applications the periodization $\tilde{f}$ cannot be sampled, since f is typically only known on a bounded domain. Nevertheless, this shows that the density compensation approach is also suitable for bandlimited functions.

Similarly, we also comment on the analogous use of the matrix optimization approach from Algorithm 3.21 using the optimized sparse matrix computed by Algorithm 3.25 in Section 6.2.

Finally, in Section 6.3 we show some numerical examples, where Figure 6.2 clearly demonstrates that the error in the approximation solely occurs because the bandlimited function f is not known on whole $\mathbb{R}^d$.

Publications by the author

Parts of this thesis have already been published in peer-reviewed journals and proceedings. In particular, most of Chapter 3 on direct inversion methods for the nonequispaced fast Fourier transform (NFFT) can be found similarly in [KP23a]. Moreover, the approach for exact density compensation factors in Section 3.2.1 and the practical computations schemes in Section 3.2.2 are also part of [KP23b], while Section 3.2.4 is based on an analogous survey of density compensation methods in [EKP22] which was done for the sinc matrix. In addition, the matrix optimization approach in Section 3.3.1 was briefly introduced in [KP21], and the frame theoretical approach mentioned in Section 3.3.4 was studied more thoroughly in [KP19]. Besides, the results of Sections 4.2 and 4.3 on the poor convergence properties of Shannon sampling sums and the univariate regularized Shannon sampling formulas are already known by [KPT24], except for some generalizations and editorial changes. More precisely, the regularized Shannon sampling formulas with localized sampling in Section 4.3.2 and the corresponding numerical examples in Section 4.5 have already been subject of study in [KPT22]. A one-dimensional version of the fast sinc transform in Section 5.1 and the corresponding numerical examples in Section 5.4 have previously been established in [KPT23]. Furthermore, Sections 6.1.1 and 6.1.2 on the generalization of density compensation methods to bandlimited functions and the corresponding numerical examples in Section 6.3 are adapted from [KP23b], while the comments in the context of tempered

distributions in Section 6.1.3 are already included in [KP23a]. Elements such as lemmas, theorems, or examples that are taken almost verbatim are identified as such in the appropriate sections.

Beyond that, all code files for the experiments presented in this thesis are publicly available on [Kir].

Acknowledgements

On the way to this dissertation I have benefited from the support of many people, and I would like to take this opportunity to thank them all.

First and foremost, I would like to express my deepest gratitude to my supervisor Prof. Dr. Daniel Potts, who has made this whole work possible from the very start. Without him, I am sure, I would not have even started a project like this. And even though it was hard sometimes, especially in the beginning of the project when everything seemed to be a dead end, he never lost the faith in our project and in me, even when I did. His kind guidance, outstanding support and constant encouragement have kept me motivated over the past few years and ultimately made this thesis happen.

I also gratefully acknowledge Prof. Dr. Brigitte Forster-Heinlein and Prof. PhD Heather Denise Wilber for their willingness to serve as reviewers for this thesis. Special thanks to them for reading my doctoral thesis so thoroughly, for writing such detailed and positive reviews, and for dedicating their time to attend my defense.

Moreover, I would also like to express my thanks to my co-authors. I am especially obliged to Prof. Dr. Manfred Tasche for his longstanding and fruitful cooperation on the regularized Shannon sampling formulas, which became an essential part of this thesis. Additionally, I also appreciate Holger Eggers, who drew my attention to the density compensation methods frequently used in MRI.

Furthermore, I would like to thank all the members of our working group for the excellent working environment. I am especially grateful to Dr. Franziska Nestler, who has been my elder sister and good example for so many years now. Whatever small or big task I was struggling with, she always had a sympathetic ear for me, and also proofread most parts of this thesis. I also want to give credit to my colleague Fabian Taubert, who consistently took the teaching load off my shoulders when there was another deadline to be met. In addition, I would like to thank Dr. Roman

Unger for his technical support, which has been most helpful at several stages from the preparation of this thesis to its defense.

Finally, it would be remiss of me not to express my sincerest gratitude to my entire family and friends for their unconditional support throughout these years. I am particularly grateful to my parents, my grandmother, and my aunt for their unwavering belief in me and their constant reassurance. Additional thanks to my mom, who is always the first to stand by my side and to cheer me up. Moreover, I would like to thank my best friend Lena Marie Uhlmann, who has always been a great comfort to me and who has also been a proofreader of this thesis. Last but definitely not least, I am deeply thankful to Florian Pasch, who always kept my head up and who always made me smile, especially when I was more in the mood for tears.

At the end, I would like to acknowledge the financial support provided in part by the European Union and the Free State of Saxony (ESF), as well as the BMBF grant 01|S20053A (project SAℓE).

2 Nonequispaced fast Fourier transforms

This introductory chapter covers some important concepts in the field of Fourier analysis and their numerical realizations. Among them, the well-known fast Fourier transform (FFT) is one of the most important algorithms for a wide range of applications in engineering, natural sciences, scientific computing, and signal processing. Nevertheless, the limitation to equispaced data represents a significant disadvantage, which led to the development of the nonequispaced fast Fourier transform (NFFT).

In the following, we firstly introduce some fundamental notation and the basic concept of the FFT in Section 2.1. Secondly, we describe the fast evaluation of trigonometric sums at nonequispaced nodes. More specifically, in Sections 2.2 and 2.3, a unified approach to the fast Fourier transform for nonequispaced data in either the spatial domain (NFFT) or the frequency domain (adjoint NFFT) is presented. Subsequently, this approach is further generalized in Section 2.4, investigating the fast Fourier transform for nonequispaced data in the spatial domain and in the frequency domain (NNFFT).

2.1 Preliminaries and Definitions

Let

$$\mathbb{T}^d := \mathbb{R}^d \setminus \mathbb{Z}^d \cong \left[-\tfrac{1}{2}, \tfrac{1}{2}\right)^d = \left\{\boldsymbol{x} \in \mathbb{R}^d \colon\ -\tfrac{1}{2} \leq x_t < \tfrac{1}{2},\ t = 1, \ldots, d\right\}$$

denote the *d-dimensional torus* with $d \in \mathbb{N}$. For $\boldsymbol{M} := (M_1, \ldots, M_d)^\top$ with $M_t \in 2\mathbb{N}$ for all $t = 1, \ldots, d$, we define the multi-index set

$$\mathcal{I}_{\boldsymbol{M}} := \mathbb{Z}^d \cap \prod_{t=1}^{d} \left[-\tfrac{M_t}{2}, \tfrac{M_t}{2}\right) = \left\{\boldsymbol{k} \in \mathbb{Z}^d \colon\ -\tfrac{M_t}{2} \leq k_t < \tfrac{M_t}{2},\ t = 1, \ldots, d\right\} \tag{2.1}$$

with cardinality $|\mathcal{I}_{\boldsymbol{M}}| = \prod_{t=1}^{d} M_t$. The inner product of two vectors $\boldsymbol{x}, \boldsymbol{y} \in \mathbb{R}^d$ shall be defined as usual as $\boldsymbol{x}\boldsymbol{y} := x_1 y_1 + \cdots + x_d y_d$. Additionally, we define the componentwise product of two vectors as $\boldsymbol{x} \odot \boldsymbol{y} := (x_1 y_1, \ldots, x_d y_d)^\top$, the all ones vector $\mathbf{1}_d := (1, \ldots, 1)^\top \in \mathbb{Z}^d$ and

the reciprocal of a vector $\boldsymbol{M} \in \mathbb{Z}^d$ with nonzero components shall be given by $\boldsymbol{M}^{-1} \coloneqq \left(M_1^{-1}, \dots, M_d^{-1}\right)^\top$.

We consider the Hilbert space $L_2(\mathbb{T}^d)$ of all 1-periodic, complex-valued functions, which possesses the orthonormal basis $\{\mathrm{e}^{2\pi\mathrm{i}\boldsymbol{k}\boldsymbol{x}} : \boldsymbol{k} \in \mathbb{Z}^d\}$. Therefore, every function $f \in L_2(\mathbb{T}^d)$ is uniquely representable in the form

$$f(\boldsymbol{x}) = \sum_{\boldsymbol{k}\in\mathbb{Z}^d} c_{\boldsymbol{k}}(f)\, \mathrm{e}^{2\pi\mathrm{i}\boldsymbol{k}\boldsymbol{x}} \tag{2.2}$$

with the coefficients

$$c_{\boldsymbol{k}}(f) \coloneqq \int_{\mathbb{T}^d} f(\boldsymbol{x})\, \mathrm{e}^{-2\pi\mathrm{i}\boldsymbol{k}\boldsymbol{x}}\, \mathrm{d}\boldsymbol{x}, \quad \boldsymbol{k} \in \mathbb{Z}^d, \tag{2.3}$$

where the sum in (2.2) converges to f in the $L_2(\mathbb{T}^d)$-norm, cf. [PPST23, Theorem 4.5]. A series of the form (2.2) is called *Fourier series* with the *Fourier coefficients* (2.3). Numerically, the Fourier coefficients (2.3) are approximated on the uniform grid $\{\boldsymbol{M}^{-1} \odot \boldsymbol{\ell}, \boldsymbol{\ell} \in \mathcal{I}_{\boldsymbol{M}}\}$ by the trapezoidal rule for numerical integration as

$$c_{\boldsymbol{k}}(f) \approx \frac{1}{|\mathcal{I}_{\boldsymbol{M}}|} \sum_{\boldsymbol{\ell}\in\mathcal{I}_{\boldsymbol{M}}} f(\boldsymbol{M}^{-1} \odot \boldsymbol{\ell})\, \mathrm{e}^{-2\pi\mathrm{i}\boldsymbol{k}(\boldsymbol{M}^{-1}\odot\boldsymbol{\ell})}, \quad \boldsymbol{k} \in \mathbb{Z}^d, \tag{2.4}$$

which is an acceptable approximation for $\boldsymbol{k} \in \mathcal{I}_{\boldsymbol{M}}$, see e. g. [PPST23, p. 248]. The fast evaluation of (2.4) can then be realized by means of the famous *fast Fourier transform (FFT)* with an arithmetic complexity of $\mathcal{O}(|\mathcal{I}_{\boldsymbol{M}}| \log(|\mathcal{I}_{\boldsymbol{M}}|))$. Here, the efficiency is obtained by a divide-and-conquer strategy proposed by Cooley and Tukey [CT65] in 1965. Moreover, it is know that this transformation is invertible and that the inverse problem of computing

$$f(\boldsymbol{M}^{-1} \odot \boldsymbol{\ell}) = \sum_{\boldsymbol{k}\in\mathcal{I}_{\boldsymbol{M}}} \hat{f}_{\boldsymbol{k}}\, \mathrm{e}^{2\pi\mathrm{i}\boldsymbol{k}(\boldsymbol{M}^{-1}\odot\boldsymbol{\ell})}, \quad \boldsymbol{\ell} \in \mathcal{I}_{\boldsymbol{M}},$$

with $\hat{f}_{\boldsymbol{k}} \approx c_{\boldsymbol{k}}(f)$, $\boldsymbol{k} \in \mathcal{I}_{\boldsymbol{M}}$, can be realized by means of an *inverse fast Fourier transform (iFFT)*, which is basically the same algorithm except for some reordering and scaling, cf. [PPST23, Lemma 3.17].

Since the restriction to equispaced data is a significant disadvantage in a variety of applications, now suppose we are given nonequispaced

nodes $\boldsymbol{x}_j \in \mathbb{T}^d,\ j = 1, \ldots, N$, instead. For given $\hat{f}_{\boldsymbol{k}} \in \mathbb{C}$, $\boldsymbol{k} \in \mathcal{I}_{\boldsymbol{M}}$, we consider the computation of the sums

$$f_j \coloneqq f(\boldsymbol{x}_j) = \sum_{\boldsymbol{k} \in \mathcal{I}_{\boldsymbol{M}}} \hat{f}_{\boldsymbol{k}}\, \mathrm{e}^{2\pi \mathrm{i} \boldsymbol{k} \boldsymbol{x}_j}, \quad j = 1, \ldots, N, \tag{2.5}$$

as well as the adjoint problem of computing the sums

$$h_{\boldsymbol{k}} = \sum_{j=1}^{N} f_j\, \mathrm{e}^{-2\pi \mathrm{i} \boldsymbol{k} \boldsymbol{x}_j}, \quad \boldsymbol{k} \in \mathcal{I}_{\boldsymbol{M}}, \tag{2.6}$$

for given values $f_j \in \mathbb{C}$, $j = 1, \ldots, N$. By defining the *nonequispaced Fourier matrix*

$$\boldsymbol{A} = \boldsymbol{A}_{|\mathcal{I}_{\boldsymbol{M}}|} \coloneqq \left(\mathrm{e}^{2\pi \mathrm{i} \boldsymbol{k} \boldsymbol{x}_j}\right)_{j=1,\, \boldsymbol{k} \in \mathcal{I}_{\boldsymbol{M}}}^{N} \in \mathbb{C}^{N \times |\mathcal{I}_{\boldsymbol{M}}|}, \tag{2.7}$$

as well as the vectors $\boldsymbol{f} \coloneqq (f_j)_{j=1}^{N}$, $\hat{\boldsymbol{f}} \coloneqq (\hat{f}_{\boldsymbol{k}})_{\boldsymbol{k} \in \mathcal{I}_{\boldsymbol{M}}}$ and $\boldsymbol{h} \coloneqq (h_{\boldsymbol{k}})_{\boldsymbol{k} \in \mathcal{I}_{\boldsymbol{M}}}$, the computation of sums of the form (2.5) and (2.6) can be written as $\boldsymbol{f} = \boldsymbol{A}\hat{\boldsymbol{f}}$ and $\boldsymbol{h} = \boldsymbol{A}^* \boldsymbol{f}$, where $\boldsymbol{A}^* \coloneqq \overline{\boldsymbol{A}}^T$ denotes the adjoint matrix of $\boldsymbol{A}$ in (2.7).

Note that the naive computation of (2.5) and (2.6) is of complexity $\mathcal{O}(N \cdot |\mathcal{I}_{\boldsymbol{M}}|)$. Since this is not feasible for practical applications, a fast approximate algorithm, the so-called *nonequispaced fast Fourier transform (NFFT)*, is briefly described below. We will demonstrate that the NFFT asymptotically requires the same computational cost as the FFT, as we only intend to compute the result up to a finite precision. For more information see e. g. [DR93, Bey95, Ste98a, GL04, KKP09] or [PPST23, pp. 413–417].

Remark 2.1. The algorithms presented in this chapter (Algorithms 2.2, 2.5 and 2.6) are part of the NFFT software package [KKP]. For algorithmic details we refer to [KKP09]. Note that an alternative implementation is available at [BMK]. ◇

2.2 The NFFT

Firstly, we restrict our attention to problem (2.5), which is equivalent to the evaluation of a *trigonometric polynomial*

$$f(\boldsymbol{x}) = \sum_{\boldsymbol{k} \in \mathcal{I}_{\boldsymbol{M}}} \hat{f}_{\boldsymbol{k}}\, \mathrm{e}^{2\pi \mathrm{i} \boldsymbol{k} \boldsymbol{x}} \tag{2.8}$$

with given $\hat{f}_{\boldsymbol{k}} \in \mathbb{C}$, $\boldsymbol{k} \in \mathcal{I}_{\boldsymbol{M}}$, at given nonequispaced nodes $\boldsymbol{x}_j \in \mathbb{T}^d$, $j = 1, \dots, N$. Let $\varphi \in L_2(\mathbb{R}^d) \cap L_1(\mathbb{R}^d)$ be a so-called *window function* $\varphi\colon \mathbb{R}^d \to [0,1]^d$, which is well localized in space and frequency domain. For typical choices of window functions please refer to Remark 2.3. Now we define the 1-periodic function $\tilde{\varphi}(\boldsymbol{x}) \coloneqq \sum_{\boldsymbol{r} \in \mathbb{Z}^d} \varphi(\boldsymbol{x} + \boldsymbol{r})$ with absolute convergent Fourier series. As a consequence, the Fourier coefficients of the periodization $\tilde{\varphi}$ have the form

$$c_{\boldsymbol{k}}(\tilde{\varphi}) = \int_{\mathbb{T}^d} \tilde{\varphi}(\boldsymbol{x})\, \mathrm{e}^{-2\pi \mathrm{i} \boldsymbol{k}\boldsymbol{x}}\, \mathrm{d}\boldsymbol{x} = \int_{\mathbb{R}^d} \varphi(\boldsymbol{x})\, \mathrm{e}^{-2\pi \mathrm{i} \boldsymbol{k}\boldsymbol{x}}\, \mathrm{d}\boldsymbol{x} =: \hat{\varphi}(\boldsymbol{k}), \quad \boldsymbol{k} \in \mathbb{Z}^d.$$

For a given d-dimensional *oversampling factor* $\boldsymbol{\sigma} \coloneqq (\sigma_1, \dots, \sigma_d)^\top \geq \mathbf{1}_d$, we define $(M_\sigma)_t \coloneqq 2\lceil \lceil \sigma_t M_t \rceil / 2 \rceil \in 2\mathbb{N}$, $t = 1, \dots, d$, as well as the respective vector $\boldsymbol{M}_{\boldsymbol{\sigma}} \coloneqq ((M_\sigma)_1, \dots, (M_\sigma)_d)^\top$. Then we approximate f by a linear combination of translates of the periodized window function, i. e.,

$$f(\boldsymbol{x}) \approx s(\boldsymbol{x}) \coloneqq \sum_{\boldsymbol{\ell} \in \mathcal{I}_{\boldsymbol{M}_{\boldsymbol{\sigma}}}} g_{\boldsymbol{\ell}}\, \tilde{\varphi}\big(\boldsymbol{x} - \boldsymbol{M}_{\boldsymbol{\sigma}}^{-1} \odot \boldsymbol{\ell}\big), \tag{2.9}$$

where the coefficients $g_{\boldsymbol{\ell}} \in \mathbb{C}$, $\boldsymbol{\ell} \in \mathcal{I}_{\boldsymbol{M}_{\boldsymbol{\sigma}}}$, are to be determined such that (2.9) yields a good approximation. By means of the *convolution theorem* (see [PPST23, Lemma 4.1]), the approximant $s \in L_2(\mathbb{T}^d)$ in (2.9) can be represented as

$$\begin{aligned} s(\boldsymbol{x}) &= \sum_{\boldsymbol{k} \in \mathbb{Z}^d} c_{\boldsymbol{k}}(s)\, \mathrm{e}^{2\pi \mathrm{i} \boldsymbol{k}\boldsymbol{x}} \\ &= \sum_{\boldsymbol{k} \in \mathcal{I}_{\boldsymbol{M}}} \hat{g}_{\boldsymbol{k}}\, c_{\boldsymbol{k}}(\tilde{\varphi})\, \mathrm{e}^{2\pi \mathrm{i} \boldsymbol{k}\boldsymbol{x}} \\ &\quad + \sum_{\boldsymbol{r} \in \mathbb{Z}^d \setminus \{\mathbf{0}\}} \sum_{\boldsymbol{k} \in \mathcal{I}_{\boldsymbol{M}}} \hat{g}_{\boldsymbol{k}}\, c_{\boldsymbol{k} + \boldsymbol{M}_{\boldsymbol{\sigma}} \odot \boldsymbol{r}}(\tilde{\varphi})\, \mathrm{e}^{2\pi \mathrm{i} (\boldsymbol{k} + \boldsymbol{M}_{\boldsymbol{\sigma}} \odot \boldsymbol{r}) \boldsymbol{x}}, \end{aligned} \tag{2.10}$$

where the *discrete Fourier transform* of the coefficients $g_{\boldsymbol{\ell}}$ is defined as

$$\hat{g}_{\boldsymbol{k}} \coloneqq \sum_{\boldsymbol{\ell} \in \mathcal{I}_{\boldsymbol{M}_{\boldsymbol{\sigma}}}} g_{\boldsymbol{\ell}}\, \mathrm{e}^{-2\pi \mathrm{i} \boldsymbol{k} (\boldsymbol{M}_{\boldsymbol{\sigma}}^{-1} \odot \boldsymbol{\ell})}, \quad \boldsymbol{k} \in \mathcal{I}_{\boldsymbol{M}}. \tag{2.11}$$

Comparing (2.5) and (2.10) then yields

$$\hat{g}_{\boldsymbol{k}} = \begin{cases} \dfrac{\hat{f}_{\boldsymbol{k}}}{\hat{\varphi}(\boldsymbol{k})} & : \boldsymbol{k} \in \mathcal{I}_{\boldsymbol{M}}, \\ 0 & : \boldsymbol{k} \in \mathcal{I}_{\boldsymbol{M}_{\boldsymbol{\sigma}}} \setminus \mathcal{I}_{\boldsymbol{M}}. \end{cases}$$

Consequently, the coefficients $g_{\boldsymbol{\ell}}$ in (2.9) can be obtained by inverting (2.11), i. e., by the application of an iFFT.

Furthermore, we assume that φ is *well localized*, such that it is small outside the square $\prod_{t=1}^{d}\left[-{}^{m}/_{(M_\sigma)_t}, {}^{m}/_{(M_\sigma)_t}\right]$, $m \ll (M_\sigma)_t$, for all $t = 1, \dots, d$. In this case, the window function φ can be approximated by the compactly supported function

$$\varphi_m(\boldsymbol{x}) \coloneqq \begin{cases} \varphi(\boldsymbol{x}) & : \boldsymbol{x} \in \prod_{t=1}^{d}\left[-\frac{m}{(M_\sigma)_t}, \frac{m}{(M_\sigma)_t}\right], \\ 0 & : \text{otherwise.} \end{cases}$$

Then we approximate $s(\boldsymbol{x}_j)$ in (2.9) by the short sums

$$\begin{aligned} f(\boldsymbol{x}_j) \approx s(\boldsymbol{x}_j) \approx \tilde{f}_j &\coloneqq \sum_{\boldsymbol{\ell} \in \mathcal{I}_{\boldsymbol{M}_{\boldsymbol{\sigma}}}} g_{\boldsymbol{\ell}}\, \tilde{\varphi}_m\big(\boldsymbol{x}_j - \boldsymbol{M}_{\boldsymbol{\sigma}}^{-1} \odot \boldsymbol{\ell}\big) \\ &= \sum_{\boldsymbol{\ell} \in \mathcal{I}_{\boldsymbol{M}_{\boldsymbol{\sigma}},m}(\boldsymbol{x}_j)} g_{\boldsymbol{\ell}}\, \tilde{\varphi}_m\big(\boldsymbol{x}_j - \boldsymbol{M}_{\boldsymbol{\sigma}}^{-1} \odot \boldsymbol{\ell}\big), \end{aligned}$$

where the index set of the nonzero entries

$$\begin{aligned} \mathcal{I}_{\boldsymbol{M}_{\boldsymbol{\sigma}},m}(\boldsymbol{x}_j) \coloneqq \big\{ \boldsymbol{\ell} \in \mathcal{I}_{\boldsymbol{M}_{\boldsymbol{\sigma}}} : \exists \boldsymbol{z} \in \mathbb{Z}^d \text{ with } \\ -m \cdot \mathbf{1}_d \le \boldsymbol{M}_{\boldsymbol{\sigma}} \odot (\boldsymbol{x}_j + \boldsymbol{z}) - \boldsymbol{\ell} \le m \cdot \mathbf{1}_d \big\} \end{aligned} \tag{2.12}$$

contains at most $(2m+1)^d$ entries for each fixed $\boldsymbol{x}_j$. Thus, the obtained algorithm can be summarized as follows.

Algorithm 2.2 (NFFT)**.**

For $d, N \in \mathbb{N}$ and $\boldsymbol{M} = (M_1, \dots, M_d)^\top \in (2\mathbb{N})^d$ let $\boldsymbol{x}_j \in \mathbb{T}^d$, $j = 1, \dots, N$, be given nodes as well as $\hat{f}_{\boldsymbol{k}} \in \mathbb{C}$, $\boldsymbol{k} \in \mathcal{I}_{\boldsymbol{M}}$, given Fourier coefficients. Furthermore, we are given the d-dimensional oversampling factor $\boldsymbol{\sigma} \ge \mathbf{1}_d$, the vector $\boldsymbol{M}_{\boldsymbol{\sigma}} \coloneqq ((M_\sigma)_1, \dots, (M_\sigma)_d)^\top$ with $2\mathbb{N} \ni (M_\sigma)_t \coloneqq 2\lceil \lceil \sigma_t M_t \rceil / 2 \rceil$, as well as the window function φ, the truncated function φ_m with $m \ll (M_\sigma)_t$, $t = 1, \dots, d$, and their 1-periodic versions $\tilde{\varphi}$ and $\tilde{\varphi}_m$.

0. Precomputation:
   a) Compute the nonzero Fourier coefficients $\hat{\varphi}(\boldsymbol{k})$ for $\boldsymbol{k} \in \mathcal{I}_{\boldsymbol{M}}$, cf. (2.1).
   b) Compute the values $\tilde{\varphi}_m\big(\boldsymbol{x}_j - \boldsymbol{M}_{\boldsymbol{\sigma}}^{-1} \odot \boldsymbol{\ell}\big)$ for $j = 1, \dots, N$, and $\boldsymbol{\ell} \in \mathcal{I}_{\boldsymbol{M}_{\boldsymbol{\sigma}},m}(\boldsymbol{x}_j)$, cf. (2.12).

1. Set $\mathcal{O}(|\mathcal{I}_{\boldsymbol{M}}|)$

$$\hat{g}_{\boldsymbol{k}} \coloneqq \begin{cases} \frac{\hat{f}_{\boldsymbol{k}}}{\hat{\varphi}(\boldsymbol{k})} & : \boldsymbol{k} \in \mathcal{I}_{\boldsymbol{M}}, \\ 0 & : \boldsymbol{k} \in \mathcal{I}_{\boldsymbol{M}_{\boldsymbol{\sigma}}} \setminus \mathcal{I}_{\boldsymbol{M}}. \end{cases}$$

2. Compute $\mathcal{O}(|\mathcal{I}_{\boldsymbol{M}}| \log(|\mathcal{I}_{\boldsymbol{M}}|))$

$$g_{\boldsymbol{\ell}} \coloneqq \frac{1}{|\mathcal{I}_{\boldsymbol{M}_{\boldsymbol{\sigma}}}|} \sum_{\boldsymbol{k} \in \mathcal{I}_{\boldsymbol{M}}} \hat{g}_{\boldsymbol{k}}\, \mathrm{e}^{2\pi \mathrm{i} \boldsymbol{k} (\boldsymbol{M}_{\boldsymbol{\sigma}}^{-1} \odot \boldsymbol{\ell})}, \quad \boldsymbol{\ell} \in \mathcal{I}_{\boldsymbol{M}_{\boldsymbol{\sigma}}},$$

by means of a d-variate iFFT.

3. Compute the short sums $\mathcal{O}(N)$

$$\tilde{f}_j \coloneqq \sum_{\boldsymbol{\ell} \in \mathcal{I}_{\boldsymbol{M}_{\boldsymbol{\sigma}}, m}(\boldsymbol{x}_j)} g_{\boldsymbol{\ell}}\, \tilde{\varphi}_m\big(\boldsymbol{x}_j - \boldsymbol{M}_{\boldsymbol{\sigma}}^{-1} \odot \boldsymbol{\ell}\big), \quad j = 1, \ldots, N.$$

Output: $\tilde{f}_j \approx f_j$, $j = 1, \ldots, N$, cf. (2.5).

Complexity: $\mathcal{O}(|\mathcal{I}_{\boldsymbol{M}}| \log(|\mathcal{I}_{\boldsymbol{M}}|) + N)$

Remark 2.3. As window function one usually uses d-variate functions $\varphi\colon \mathbb{R}^d \to \mathbb{R}$, that arise as the *tensor product*

$$\varphi(\boldsymbol{x}) = \prod_{t=1}^{d} \varphi(x_t), \quad \boldsymbol{x} = (x_1, \ldots, x_d) \in \mathbb{R}^d, \tag{2.13}$$

of a univariate window function, which is also denoted by $\varphi\colon \mathbb{R} \to \mathbb{R}$ for the sake of simplicity. For the Fourier transform of these d-variate window functions we obtain

$$\hat{\varphi}(\boldsymbol{k}) = \prod_{t=1}^{d} \hat{\varphi}(k_t), \quad \boldsymbol{k} = (k_1, \ldots, k_d) \in \mathbb{Z}^d.$$

Therefore, it suffices to specify the univariate window function φ and compute its univariate Fourier transform $\hat{\varphi}$.

For instance, in [DR93, DS99] the *Gaussian window function* was used, cf. (4.60), while [Bey95, Ste98a] studied the *B–spline window function*, cf. (4.61). More recent results like [PT21a] suggest for example the *sinh-type*

window function, cf. (4.62), or the *continuous Kaiser–Bessel window function*, cf. (4.63). In addition, also related window functions, where an analytic expression of the Fourier transform is unknown, were discussed in [BMK, BMK19, Bar21]. Examples of this form include the *continuous exp-type window function*

$$\varphi_{\exp}(x) \coloneqq \begin{cases} \frac{1}{\mathrm{e}^{\beta}-1}\left(\mathrm{e}^{\beta\sqrt{1-(M_\sigma x/m)^2}}-1\right) & : x \in \left[-\frac{m}{M_\sigma}, \frac{m}{M_\sigma}\right], \\ 0 & : x \in \mathbb{R} \setminus \left[-\frac{m}{M_\sigma}, \frac{m}{M_\sigma}\right], \end{cases}$$

see [PT21a, Section 6], with a discontinuous version suggested in [BMK19, Bar21], as well as the *continuous cosh-type window function*

$$\varphi_{\cosh}(x) \coloneqq \begin{cases} \frac{\cosh\left(\beta\sqrt{1-\left(\frac{M_\sigma x}{m}\right)^2}\right)-1}{\cosh\beta-1} & : x \in \left[-\frac{m}{M_\sigma}, \frac{m}{M_\sigma}\right], \\ 0 & : x \in \mathbb{R} \setminus \left[-\frac{m}{M_\sigma}, \frac{m}{M_\sigma}\right], \end{cases}$$

see [PT21a, Section 7], with a discontinuous version proposed in [BMK19, Remark 13]. We remark that the FINUFFT software [BMK] is based on the exp-type window function $\varphi_{\exp}$.

For more information on suitable window functions and corresponding error estimates see e. g. [Fou03, GL04, KKP09, BMK19, PT21b, PPST23] and references therein. ◇

Next we give the matrix-vector representation of the NFFT. To this end, we define the diagonal matrix

$$\boldsymbol{D} \coloneqq \operatorname{diag}\left(\frac{1}{|\mathcal{I}_{\boldsymbol{M}_\sigma}| \cdot \hat{\varphi}(\boldsymbol{k})}\right)_{\boldsymbol{k}\in\mathcal{I}_{\boldsymbol{M}}} \in \mathbb{C}^{|\mathcal{I}_{\boldsymbol{M}}|\times|\mathcal{I}_{\boldsymbol{M}}|}, \tag{2.14}$$

the truncated *Fourier matrix*

$$\boldsymbol{F} \coloneqq \left(\mathrm{e}^{2\pi\mathrm{i}\boldsymbol{k}(\boldsymbol{M}_\sigma^{-1}\odot\boldsymbol{\ell})}\right)_{\boldsymbol{\ell}\in\mathcal{I}_{\boldsymbol{M}_\sigma},\,\boldsymbol{k}\in\mathcal{I}_{\boldsymbol{M}}} \in \mathbb{C}^{|\mathcal{I}_{\boldsymbol{M}_\sigma}|\times|\mathcal{I}_{\boldsymbol{M}}|}, \tag{2.15}$$

and the sparse matrix

$$\boldsymbol{B} \coloneqq \left(\tilde{\varphi}_m\big(\boldsymbol{x}_j - \boldsymbol{M}_\sigma^{-1}\odot\boldsymbol{\ell}\big)\right)_{j=1,\,\boldsymbol{\ell}\in\mathcal{I}_{\boldsymbol{M}_\sigma}}^{N} \in \mathbb{R}^{N\times|\mathcal{I}_{\boldsymbol{M}_\sigma}|}, \tag{2.16}$$

where by definition (2.12) each row of $\boldsymbol{B}$ contains at most $(2m+1)^d$ nonzeros. In doing so, the NFFT in Algorithm 2.2 can be formulated in

matrix-vector notation such that we receive the approximation $\boldsymbol{A} \approx \boldsymbol{BFD}$ of (2.7), cf. [PPST23, p. 419]. This is to say, using the definition of the matrices, the NFFT performs the approximation

$$\mathrm{e}^{2\pi\mathrm{i}\boldsymbol{k}\boldsymbol{x}_j} \approx \frac{1}{|\mathcal{I}_{\boldsymbol{M}_\sigma}| \cdot \hat{\varphi}(\boldsymbol{k})} \sum_{\boldsymbol{\ell} \in \mathcal{I}_{\boldsymbol{M}_\sigma, m}(\boldsymbol{x}_j)} \mathrm{e}^{2\pi\mathrm{i}\boldsymbol{k}(\boldsymbol{M}_\sigma^{-1} \odot \boldsymbol{\ell})} \, \tilde{\varphi}_m\big(\boldsymbol{x}_j - \boldsymbol{M}_\sigma^{-1} \odot \boldsymbol{\ell}\big) \,. \tag{2.17}$$

Remark 2.4. It should be noted that, for reasons of consistency, the factor $|\mathcal{I}_{\boldsymbol{M}_\sigma}|^{-1}$ is here not located in the matrix $\boldsymbol{F}$ as usual but in the matrix $\boldsymbol{D}$. ◇

2.3 The adjoint NFFT

Now we proceed with the adjoint problem (2.6). As shown above, this can be written as $\boldsymbol{h} = \boldsymbol{A}^* \boldsymbol{f}$ with the adjoint matrix $\boldsymbol{A}^*$ of (2.7). Thus, using the matrices (2.14), (2.15) and (2.16) we receive the approximation $\boldsymbol{A}^* \approx \boldsymbol{D}^* \boldsymbol{F}^* \boldsymbol{B}^*$, such that the algorithm for the adjoint problem can be denoted as follows.

Algorithm 2.5 (adjoint NFFT)**.**

For $d, N \in \mathbb{N}$ let $\boldsymbol{x}_j \in \mathbb{T}^d$, $j = 1, \ldots, N$, be given nodes as well as $f_j \in \mathbb{C}$ given coefficients. Furthermore, we are given the d-dimensional oversampling factor $\boldsymbol{\sigma} \geq \mathbf{1}_d$, the vector $\boldsymbol{M}_{\boldsymbol{\sigma}} \coloneqq ((M_\sigma)_1, \ldots, (M_\sigma)_d)^\top$ with $2\mathbb{N} \ni (M_\sigma)_t \coloneqq 2\lceil \lceil \sigma_t M_t \rceil / 2 \rceil$ and $\boldsymbol{M} = (N_1, \ldots, M_d)^\top \in (2\mathbb{N})^d$, as well as the window function φ, the truncated function φ_m with $m \ll (M_\sigma)_t$, $t = 1, \ldots, d$, and their 1-periodic versions $\tilde{\varphi}$ and $\tilde{\varphi}_m$.

0. Precomputation:
   a) Compute the nonzero Fourier coefficients $\hat{\varphi}(\boldsymbol{k})$ for $\boldsymbol{k} \in \mathcal{I}_{\boldsymbol{M}}$, cf. (2.1).
   b) Compute the values $\tilde{\varphi}_m\big(\boldsymbol{x}_j - \boldsymbol{M}_{\boldsymbol{\sigma}}^{-1} \odot \boldsymbol{\ell}\big)$ for $j = 1, \ldots, N$, and $\boldsymbol{\ell} \in \mathcal{I}_{\boldsymbol{M}_\sigma, m}(\boldsymbol{x}_j)$, cf. (2.12).
1. Compute the sparse sums $\mathcal{O}(N)$

$$g_{\boldsymbol{\ell}} \coloneqq \sum_{j=1}^{N} f_j \, \tilde{\varphi}_m\big(\boldsymbol{x}_j - \boldsymbol{M}_{\boldsymbol{\sigma}}^{-1} \odot \boldsymbol{\ell}\big) \,, \quad \boldsymbol{\ell} \in \mathcal{I}_{\boldsymbol{M}_\sigma} . \tag{2.18}$$

2. Compute $\mathcal{O}(|\mathcal{I}_{\boldsymbol{M}}| \log(|\mathcal{I}_{\boldsymbol{M}}|))$

$$\hat{g}_{\boldsymbol{k}} := \frac{1}{|\mathcal{I}_{\boldsymbol{M}_\sigma}|} \sum_{\boldsymbol{\ell} \in \mathcal{I}_{\boldsymbol{M}_\sigma}} g_{\boldsymbol{\ell}} \, \mathrm{e}^{-2\pi \mathrm{i} \boldsymbol{k} (\boldsymbol{M}_\sigma^{-1} \odot \boldsymbol{\ell})}, \quad \boldsymbol{k} \in \mathcal{I}_{\boldsymbol{M}},$$

by means of a d-variate FFT.

3. Set $\mathcal{O}(|\mathcal{I}_{\boldsymbol{M}}|)$

$$\tilde{h}_{\boldsymbol{k}} := \frac{\hat{g}_{\boldsymbol{k}}}{\hat{\varphi}(\boldsymbol{k})}, \quad \boldsymbol{k} \in \mathcal{I}_{\boldsymbol{M}}.$$

Output: $\tilde{h}_{\boldsymbol{k}} \approx h_{\boldsymbol{k}}$, $\boldsymbol{k} \in \mathcal{I}_{\boldsymbol{M}}$, cf. (2.6)

Complexity: $\mathcal{O}(|\mathcal{I}_{\boldsymbol{M}}| \log(|\mathcal{I}_{\boldsymbol{M}}|) + N)$

2.4 The NNFFT

The previously presented algorithms of Sections 2.2 and 2.3 are methods for nonequispaced nodes in the spatial domain or the frequency domain, and equispaced nodes in the respective other domain. Next, we generalize these methods to nonequispaced nodes in both the spatial domain and the frequency domain, cf. [PPST23, Section 7.3]. For this purpose, let the so-called the *nonharmonic bandwidth* $M \in \mathbb{N}$ with $M \gg 1$ and the numbers $N_1, N_2 \in 2\mathbb{N}$ be given. Then we consider the exponential sums

$$f(\boldsymbol{x}) = \sum_{k \in \mathcal{I}_{N_1}} f_k \, \mathrm{e}^{-2\pi \mathrm{i} M \boldsymbol{v}_k \boldsymbol{x}}, \quad \boldsymbol{x} \in \left[-\tfrac{1}{2}, \tfrac{1}{2}\right]^d, \tag{2.19}$$

where $\boldsymbol{v}_k \in \left[-\frac{1}{2}, \frac{1}{2}\right]^d$, $k \in \mathcal{I}_{N_1}$, are nonequispaced nodes in the frequency domain and $f_k \in \mathbb{C}$ are given coefficients. Note that in comparison to the trigonometric polynomial (2.8), the exponential sum (2.19) is not periodic, since for arbitrary points $\boldsymbol{v}_k$ we have $M\boldsymbol{v}_k \notin \mathbb{Z}^d$. For arbitrary nodes $\boldsymbol{x}_j \in \left[-\frac{1}{2}, \frac{1}{2}\right]^d$, $j \in \mathcal{I}_{N_2}$, in the spatial domain, we consider the fast computation of the N_2 values

$$f(\boldsymbol{x}_j) = \sum_{k \in \mathcal{I}_{N_1}} f_k \, \mathrm{e}^{-2\pi \mathrm{i} M \boldsymbol{v}_k \boldsymbol{x}_j}, \quad j \in \mathcal{I}_{N_2}. \tag{2.20}$$

A fast algorithm for the evaluation of the sums (2.20) is called *fast Fourier transform for nonequispaced data in spatial and frequency domain* (NNFFT), which was introduced in [Elb98, ES98], see also [PST01]. Note that this algorithm is also called nonuniform FFT of type 3, see [LG05]. As known (see [ES98, PST01]), the NNFFT is a combination of Algorithms 2.2 and 2.5, which shall be explained in the following.

For a given window function $\varphi_1 : \mathbb{R}^d \to [0,1]^d$ we introduce the auxiliary function

$$h(\boldsymbol{t}) := \sum_{k \in \mathcal{I}_{N_1}} f_k \, \varphi_1(\boldsymbol{t} - \boldsymbol{v}_k), \quad \boldsymbol{t} \in \mathbb{R}^d,$$

which has the continuous Fourier transform (cf. (4.1))

$$\begin{aligned} \hat{h}(M\boldsymbol{x}) &= \int_{\mathbb{R}^d} h(\boldsymbol{t}) \, \mathrm{e}^{-2\pi \mathrm{i} M \boldsymbol{x} \boldsymbol{t}} \, \mathrm{d}\boldsymbol{t} \\ &= \sum_{k \in \mathcal{I}_{N_1}} f_k \int_{\mathbb{R}^d} \varphi_1(\boldsymbol{t} - \boldsymbol{v}_k) \, \mathrm{e}^{-2\pi \mathrm{i} M \boldsymbol{x} \boldsymbol{t}} \, \mathrm{d}\boldsymbol{t} \qquad (2.21) \\ &= \sum_{k \in \mathcal{I}_{N_1}} f_k \, \mathrm{e}^{-2\pi \mathrm{i} M \boldsymbol{v}_k \boldsymbol{x}} \, \hat{\varphi}_1(M\boldsymbol{x}) = f(\boldsymbol{x}) \, \hat{\varphi}_1(M\boldsymbol{x}), \quad \boldsymbol{x} \in \mathbb{R}^d. \end{aligned}$$

Hence, for arbitrary nodes $\boldsymbol{x}_j \in \left[-\frac{1}{2}, \frac{1}{2}\right]^d$, $j \in \mathcal{I}_{N_2}$, we have

$$f(\boldsymbol{x}_j) = \frac{\hat{h}(M\boldsymbol{x}_j)}{\hat{\varphi}_1(M\boldsymbol{x}_j)}, \quad j \in \mathcal{I}_{N_2}.$$

Since the Fourier coefficients $\hat{\varphi}_1(M\boldsymbol{x}_j)$, $j \in \mathcal{I}_{N_2}$, can be precomputed for a given window function φ_1, it only remains to approximate the values $\hat{h}(M\boldsymbol{x}_j)$, $j \in \mathcal{I}_{N_2}$, in (2.21).

To this end, for a given oversampling factor $\sigma_1 > 1$ we set $M_{\sigma_1} := \sigma_1 M$ such that $M_{\sigma_1} \in 2\mathbb{N}$, and choose a truncation parameter $m_1 \in \mathbb{N} \setminus \{1\}$ with $2m_1 \ll M_{\sigma_1}$. As the window function φ_1 is assumed to be well-localized in spatial domain, it can be approximated by the compactly supported function

$$\varphi_{m_1}(\boldsymbol{x}) := \begin{cases} \varphi_1(\boldsymbol{x}) & : \boldsymbol{x} \in \left[-\frac{m_1}{M_{\sigma_1}}, \frac{m_1}{M_{\sigma_1}}\right]^d, \\ 0 & : \text{otherwise.} \end{cases}$$

In addition, we introduce the constant $a \coloneqq 1 + \frac{2m_1}{M_{\sigma_1}} > 1$ and, without loss of generality, we assume that $\boldsymbol{v}_k \in \left[-\frac{1}{2a}, \frac{1}{2a}\right]^d$, $k \in \mathcal{I}_{N_1}$. If $\boldsymbol{v}_k \in \left[-\frac{1}{2}, \frac{1}{2}\right]^d$, then we replace the nonharmonic bandwidth M by $M^* \coloneqq M + \lceil \frac{2m_1}{\sigma_1} \rceil$ and set $\boldsymbol{v}_k^* \coloneqq \frac{M}{M^*}\, \boldsymbol{v}_k \in \left[-\frac{1}{2a}, \frac{1}{2a}\right]^d$ such that $M\, \boldsymbol{v}_k = M^* \boldsymbol{v}_k^*$, $k \in \mathcal{I}_{N_1}$.

Thereby, since $\operatorname{supp}(\varphi_{m_1}) = \left[-\frac{m_1}{M_{\sigma_1}}, \frac{m_1}{M_{\sigma_1}}\right]$ we have for arbitrary points $\boldsymbol{v}_k \in \left[-\frac{1}{2a}, \frac{1}{2a}\right]^d$ that

$$\varphi_{m_1}(\boldsymbol{t} - \boldsymbol{v}_k) = 0 \quad \text{for all} \quad |\boldsymbol{t}| > \tfrac{1}{2a} + \tfrac{m_1}{M_{\sigma_1}} = \tfrac{a}{2} - \left(\tfrac{1}{2} - \tfrac{1}{2a}\right).$$

This implies

$$\operatorname{supp}(\varphi_{m_1}(\cdot - \boldsymbol{v}_k)) \subset \left[-\tfrac{a}{2}, \tfrac{a}{2}\right]^d, \quad k \in \mathcal{I}_{N_1},$$

since $\frac{1}{2} - \frac{1}{2a} > 0$. Thus, by (2.21) we obtain

$$\hat{h}(M\boldsymbol{x}) \approx s_1(M\boldsymbol{x}) \coloneqq \sum_{k \in \mathcal{I}_{N_1}} f_k \int\limits_{\left[-\frac{a}{2}, \frac{a}{2}\right]^d} \varphi_{m_1}(\boldsymbol{t} - \boldsymbol{v}_k)\, \mathrm{e}^{-2\pi \mathrm{i} M \boldsymbol{x} \boldsymbol{t}}\, \mathrm{d}\boldsymbol{t}, \quad \boldsymbol{x} \in \mathbb{R}^d.$$

Discretization of this integral using the rectangular rule then yields the approximation

$$\begin{aligned} \hat{h}(M\boldsymbol{x}) &\approx s_1(M\boldsymbol{x}) \\ &\approx s_2(M\boldsymbol{x}) \coloneqq \sum_{k \in \mathcal{I}_{N_1}} f_k\, M_{\sigma_1}^{-d} \sum_{\boldsymbol{\ell} \in \mathcal{I}_{\boldsymbol{a}\boldsymbol{M}_{\boldsymbol{\sigma_1}}}} \varphi_{m_1}\left(\tfrac{\boldsymbol{\ell}}{M_{\sigma_1}} - \boldsymbol{v}_k\right) \mathrm{e}^{-2\pi \mathrm{i} \boldsymbol{x} \boldsymbol{\ell} / \sigma_1} \end{aligned}$$

for all $\boldsymbol{x} \in \mathbb{R}^d$, where $\boldsymbol{a}\boldsymbol{M}_{\boldsymbol{\sigma_1}} \coloneqq a M_{\sigma_1} \cdot \mathbf{1}_d$. Changing the order of summation we finally obtain

$$s_2(M\boldsymbol{x}) = \sum_{\boldsymbol{\ell} \in \mathcal{I}_{\boldsymbol{a}\boldsymbol{M}_{\boldsymbol{\sigma_1}}}} \left(M_{\sigma_1}^{-d} \sum_{k \in \mathcal{I}_{N_1}} f_k\, \varphi_{m_1}\left(\tfrac{\boldsymbol{\ell}}{M_{\sigma_1}} - \boldsymbol{v}_k\right) \right) \mathrm{e}^{-2\pi \mathrm{i} \boldsymbol{x} \boldsymbol{\ell} / \sigma_1}, \quad \boldsymbol{x} \in \mathbb{R}^d.$$

Note that the inner sums

$$g_{\boldsymbol{\ell}} \coloneqq M_{\sigma_1}^{-d} \sum_{k \in \mathcal{I}_{N_1}} f_k\, \varphi_{m_1}\left(\tfrac{\boldsymbol{\ell}}{M_{\sigma_1}} - \boldsymbol{v}_k\right), \quad \boldsymbol{\ell} \in \mathcal{I}_{\boldsymbol{a}\boldsymbol{M}_{\boldsymbol{\sigma_1}}},$$

are sparse since by $\operatorname{supp}(\varphi_{m_1}) = \big[-\frac{m_1}{M_{\sigma_1}}, \frac{m_1}{M_{\sigma_1}}\big]$ we have for each fixed $\boldsymbol{v}_k$ that $\varphi_{m_1}\big(\frac{\boldsymbol{\ell}}{M_{\sigma_1}} - \boldsymbol{v}_k\big) \neq 0$ only for $\boldsymbol{\ell} \in \mathcal{I}'_{\boldsymbol{M_{\sigma_1}},m_1}(\boldsymbol{v}_k)$, where

$$\mathcal{I}'_{\boldsymbol{M_{\sigma_1}},m_1}(\boldsymbol{v}_k) \coloneqq \Big\{\boldsymbol{\ell} \in \mathcal{I}_{\boldsymbol{aM_{\sigma_1}}} : \big|\tfrac{\boldsymbol{\ell}}{M_{\sigma_1}} - \boldsymbol{v}_k\big| < \tfrac{m_1}{M_{\sigma_1}}\Big\}. \tag{2.22}$$

The remaining outer sum

$$s_2(M\boldsymbol{x}) = \sum_{\boldsymbol{\ell} \in \mathcal{I}_{\boldsymbol{aM_{\sigma_1}}}} g_{\boldsymbol{\ell}}\, \mathrm{e}^{-2\pi \mathrm{i} \boldsymbol{x}\boldsymbol{\ell}/\sigma_1}, \quad j \in \mathcal{I}_{N_2}.$$

can then be evaluated by means of an NFFT, see Algorithm 2.2. This NFFT uses a second window function φ_2 and $M_{\sigma_2} \coloneqq \sigma_2\, aM_{\sigma_1} \in 2\mathbb{N}$ with parameters $\sigma_2 > 1$ and $m_2 \in \mathbb{N} \setminus \{1\}$ with $2m_2 \leq \big(1 - \frac{1}{\sigma_1}\big) M_{\sigma_2}$. Denoting the result of this NFFT as $s(M\boldsymbol{x}_j)$, then $s(M\boldsymbol{x}_j)/\hat{\varphi}_1(M\boldsymbol{x}_j)$ is an approximate value of $f(\boldsymbol{x}_j)$, $j \in \mathcal{I}_{N_2}$. Hence, the obtained algorithm can be summarized as follows.

Algorithm 2.6 (NNFFT)**.**

For $d, M \in \mathbb{N}$ with $M \gg 1$ and $N_1,\, N_2 \in 2\mathbb{N}$ let $\boldsymbol{v}_k \in \big[-\frac{1}{2a}, \frac{1}{2a}\big]^d$, $k \in \mathcal{I}_{N_1}$, and $\boldsymbol{x}_j \in \big[-\frac{1}{2}, \frac{1}{2}\big]^d$, $j \in \mathcal{I}_{N_2}$, be given nodes as well as $f_k \in \mathbb{C}$ given coefficients. Furthermore, we are given the oversampling factors $\sigma_1, \sigma_2 > 1$, $M_{\sigma_1} = \sigma_1\, M \in 2\mathbb{N}$ and $M_{\sigma_2} = \sigma_2\, aM_{\sigma_1} \in 2\mathbb{N}$ with $a = 1 + \frac{2m_1}{M_{\sigma_1}}$, as well as the window functions φ_1 and φ_2, their truncated versions $\varphi_{m_1}, \varphi_{m_2}$ with $m_1, m_2 \in \mathbb{N} \setminus \{1\}$, $2m_1 \ll M_{\sigma_1}$ and $2m_2 \leq \big(1 - \frac{1}{\sigma_1}\big) M_{\sigma_2}$, and the 1-periodized function $\tilde{\varphi}_{m_2}$.

0. Precomputation:
   a) Compute the nonzero Fourier coefficients $\hat{\varphi}_1(M\boldsymbol{x}_j)$ for $j \in \mathcal{I}_{N_2}$, cf. (2.1).
   b) Compute $\varphi_{m_1}\big(\frac{\boldsymbol{\ell}}{M_{\sigma_1}} - \boldsymbol{v}_k\big)$ for $k \in \mathcal{I}_{N_1}$ and $\boldsymbol{\ell} \in \mathcal{I}'_{\boldsymbol{M_{\sigma_1}},m_1}(\boldsymbol{v}_k)$, cf. (2.22).
   c) Compute the nonzero Fourier coefficients $\hat{\varphi}_2\big(\boldsymbol{\ell}\big)$ for $\boldsymbol{\ell} \in \mathcal{I}_{\boldsymbol{aM_{\sigma_1}}}$, cf. (2.1).
   d) Compute $\tilde{\varphi}_{m_2}\big(\frac{\boldsymbol{x}_j}{\sigma_1} - \frac{\boldsymbol{n}}{M_{\sigma_2}}\big)$ for $j \in \mathcal{I}_{N_2}$ and $\boldsymbol{n} \in \mathcal{I}_{\boldsymbol{M_{\sigma_2}},m_2}(\boldsymbol{x}_j)$, cf. (2.12).

1. Compute the sparse sums $\mathcal{O}(N_1)$

$$g_{\boldsymbol{\ell}} \coloneqq M_{\sigma_1}^{-d} \sum_{k \in \mathcal{I}_{N_1}} f_k \, \varphi_{m_1}\big(\tfrac{\boldsymbol{\ell}}{M_{\sigma_1}} - \boldsymbol{v}_k\big), \quad \boldsymbol{\ell} \in \mathcal{I}_{\boldsymbol{a}\boldsymbol{M}_{\boldsymbol{\sigma_1}}}.$$

2. Set $\mathcal{O}(|\mathcal{I}_{\boldsymbol{M}}|)$

$$\hat{g}_{\boldsymbol{\ell}} \coloneqq \frac{g_{\boldsymbol{\ell}}}{\hat{\varphi}_2(\boldsymbol{\ell})}, \quad \boldsymbol{\ell} \in \mathcal{I}_{\boldsymbol{a}\boldsymbol{M}_{\boldsymbol{\sigma_1}}}.$$

3. Compute $\mathcal{O}(|\mathcal{I}_{\boldsymbol{M}}| \log(|\mathcal{I}_{\boldsymbol{M}}|))$

$$h_{\boldsymbol{n}} \coloneqq M_{\sigma_2}^{-d} \sum_{\boldsymbol{\ell} \in \mathcal{I}_{\boldsymbol{a}\boldsymbol{M}_{\boldsymbol{\sigma_1}}}} \hat{g}_{\boldsymbol{\ell}} \, \mathrm{e}^{-2\pi \mathrm{i} \boldsymbol{\ell}\boldsymbol{n}/M_{\sigma_2}}, \quad \boldsymbol{n} \in \mathcal{I}_{\boldsymbol{M}_{\boldsymbol{\sigma_2}}},$$

   by means of a d-variate FFT.

4. Compute the short sums $\mathcal{O}(N_2)$

$$s(M\boldsymbol{x}_j) \coloneqq \sum_{\boldsymbol{n} \in \mathcal{I}_{\boldsymbol{M}_{\boldsymbol{\sigma_2}}, m_2}(\boldsymbol{x}_j)} h_{\boldsymbol{n}} \, \tilde{\varphi}_{m_2}\Big(\frac{\boldsymbol{x}_j}{\sigma_1} - \frac{\boldsymbol{n}}{M_{\sigma_2}}\Big), \quad j \in \mathcal{I}_{N_2}.$$

5. Set $\mathcal{O}(N_2)$

$$S(\boldsymbol{x}_j) \coloneqq \frac{s(M\boldsymbol{x}_j)}{\hat{\varphi}_1(M\boldsymbol{x}_j)}, \quad j \in \mathcal{I}_{N_2}.$$

Output: $S(\boldsymbol{x}_j) \approx f(\boldsymbol{x}_j)$, cf. (2.20).

Complexity: $\mathcal{O}(|\mathcal{I}_{\boldsymbol{M}}| \log(|\mathcal{I}_{\boldsymbol{M}}|) + N_1 + N_2)$

Remark 2.7. For estimates on the approximation error of Algorithm 2.6 we refer to [ES98, KPT23]. ◇

Note that an important application of the NNFFT is the fast sinc transform introduced in [KPT23], cf. Section 5.1.

3 Direct inversion methods for the NFFT

Having introduced the fast Fourier transform for nonequispaced data in the previous chapter, we remark that numerous applications such as magnetic resonance imaging (MRI), cf. [NW01, GLI06, DAP22, EKP22], synthetic aperture radar (SAR), cf. [GJG23], solution of partial differential equations (PDEs), cf. [Fas07], etc., are interested in the inverse problem, i. e., instead of the evaluation of the sums (2.5) the aim is computing the Fourier coefficients $\hat{f}_{\boldsymbol{k}}$, $\boldsymbol{k} \in \mathcal{I}_{\boldsymbol{M}}$, from given nonequispaced data $f(\boldsymbol{x}_j)$, $j = 1, \dots, N$. Therefore, the present chapter is attributed to this task.

Initially, in Section 3.1 we have a closer look at the inversion problem itself and explain the main challenges of using nonequispaced data, which can be seen by comparison to the case of equispaced data. Afterwards, we provide an overview of existing methods, including a discussion of the advantages of iterative and direct procedures, and introduce the idea of two different direct approaches in a general framework. In Section 3.2 we firstly examine the approach of so-called sampling density compensation, where the general idea is to compute a diagonal matrix of weights to re-weight the adjoint NFFT appropriately. Secondly, we study a matrix optimization approach in Section 3.3, which can be viewed as a generalization, since here the aim is to compute an optimal sparse matrix based on a certain minimization problem. Finally, in Section 3.4 several numerical examples are presented, justifying the accuracy of the new approaches and comparing them with each other as well as with those mentioned from the literature, followed by a short summary.

3.1 Problem formulation

To clarify the major dissimilarity between equispaced and nonequispaced data, we start considering the equispaced case. In particular, when evaluating at the grid points $x_{\boldsymbol{j}} = \frac{1}{n}\boldsymbol{j} \in \mathbb{T}^d$, $\boldsymbol{j} \in \mathcal{I}_{\boldsymbol{n}}$, with $\boldsymbol{n} \coloneqq n \cdot \mathbf{1}_d$ and $|\mathcal{I}_{\boldsymbol{n}}| = N$, the nonequispaced Fourier matrix $\boldsymbol{A} \in \mathbb{C}^{N \times |\mathcal{I}_{\boldsymbol{M}}|}$ in (2.7) turns into the equispaced Fourier matrix $\boldsymbol{F} \in \mathbb{C}^{|\mathcal{I}_{\boldsymbol{M}_\sigma}| \times |\mathcal{I}_{\boldsymbol{M}}|}$ from (2.15) with $|\mathcal{I}_{\boldsymbol{M}_\sigma}| = N$.

Thereby, it results from the geometric sum formula that

$$\boldsymbol{F}^*\boldsymbol{F} = \left(\sum_{\boldsymbol{j}\in\mathcal{I}_{\boldsymbol{n}}} \mathrm{e}^{2\pi\mathrm{i}(\boldsymbol{k}-\boldsymbol{\ell})\boldsymbol{j}/n} \right)_{\boldsymbol{k},\boldsymbol{\ell}\in\mathcal{I}_{\boldsymbol{M}}} = N\boldsymbol{I}_{|\mathcal{I}_{\boldsymbol{M}}|}, \quad \text{if } |\mathcal{I}_{\boldsymbol{M}}| \leq N, \tag{3.1}$$

as well as

$$\boldsymbol{F}\boldsymbol{F}^* = \left(\sum_{\boldsymbol{k}\in\mathcal{I}_{\boldsymbol{M}}} \mathrm{e}^{2\pi\mathrm{i}\boldsymbol{k}(\boldsymbol{j}-\boldsymbol{h})/n} \right)_{\boldsymbol{j},\boldsymbol{h}\in\mathcal{I}_{\boldsymbol{n}}} = |\mathcal{I}_{\boldsymbol{M}}| \cdot \boldsymbol{I}_N, \quad \text{if } |\mathcal{I}_{\boldsymbol{M}}| \geq N$$

and $|\mathcal{I}_{\boldsymbol{M}}|$ is divisible by N. Thus, in the equispaced setting a one-sided inverse is given by the (scaled) adjoint matrix. However, when considering arbitrary points $\boldsymbol{x}_j \in \mathbb{T}^d$, $j = 1, \ldots, N$, this property is lost, i. e., for the nonequispaced Fourier matrix $\boldsymbol{A} \in \mathbb{C}^{N\times|\mathcal{I}_{\boldsymbol{M}}|}$ in (2.7) we have

$$\boldsymbol{A}^*\boldsymbol{A} \neq N\boldsymbol{I}_{|\mathcal{I}_{\boldsymbol{M}}|} \quad \text{and} \quad \boldsymbol{A}\boldsymbol{A}^* \neq |\mathcal{I}_{\boldsymbol{M}}| \cdot \boldsymbol{I}_N. \tag{3.2}$$

Because of this, more effort is needed to obtain a solution to the inverse problem in the nonequispaced setting. In general, we face the following two problems.

(1) Solve the linear system

$$\boldsymbol{A}\hat{\boldsymbol{f}} = \boldsymbol{f}, \tag{3.3}$$

i. e., reconstruct the Fourier coefficients $\hat{\boldsymbol{f}} = (\hat{f}_{\boldsymbol{k}})_{\boldsymbol{k}\in\mathcal{I}_{\boldsymbol{M}}}$ from given function values $\boldsymbol{f} = (f(\boldsymbol{x}_j))_{j=1}^N$. This problem is referred to as *inverse NDFT (iNDFT)* and an efficient solver shall be called *inverse NFFT (iNFFT)*.

(2) Solve the linear system

$$\boldsymbol{A}^*\boldsymbol{f} = \boldsymbol{h}, \tag{3.4}$$

i. e., reconstruct the spatial coefficients $\boldsymbol{f} = (f_j)_{j=1}^N$ from given data $\boldsymbol{h} = (h_{\boldsymbol{k}})_{\boldsymbol{k}\in\mathcal{I}_{\boldsymbol{M}}}$. This problem is referred to as *inverse adjoint NDFT (iNDFT*)* and an efficient solver shall be called *inverse adjoint NFFT (iNFFT*)*.

Remark 3.1. We remark that according to the solvability criterion, the linear system of equations (3.3) has at least one solution if and only if the matrix $\boldsymbol{A}$ and the augmented coefficient matrix $(\boldsymbol{A}|\boldsymbol{f})$ have the same rank, which is always satisfied since (2.5) is equivalent to the evaluation of a trigonometric polynomial (2.8) at given nonequispaced nodes $\boldsymbol{x}_j \in \mathbb{T}^d$, $j = 1, \dots, N$. In other words, the rank of the nonequispaced Fourier matrix $\boldsymbol{A} \in \mathbb{C}^{N \times |\mathcal{I}_{\boldsymbol{M}}|}$ in (2.7) depends solely on the given points $\boldsymbol{x}_j$.

Additionally, note that in both problems (3.3) and (3.4), the number N of nodes $\boldsymbol{x}_j$ is generally independent of the number $|\mathcal{I}_{\boldsymbol{M}}|$ of Fourier coefficients $\hat{f}_{\boldsymbol{k}}$. Hence, the nonequispaced Fourier matrix $\boldsymbol{A} \in \mathbb{C}^{N \times |\mathcal{I}_{\boldsymbol{M}}|}$ in (2.7) is rectangular in most cases, and therefore a regular inverse matrix does not exist. In general, this forces us to consider the least squares problem of minimizing the residual norm $\|\boldsymbol{A}\hat{\boldsymbol{f}} - \boldsymbol{f}\|_2$ instead. The corresponding least squares solution is known to be unique in case the nonequispaced Fourier matrix $\boldsymbol{A}$ has full rank. Indeed, eigenvalue estimates in [FGS95, BG04, BP07, KP08, KN21] confirm that this condition is satisfied for sufficiently nice points $\boldsymbol{x}_j$, i. e., points that are not too far from being equispaced. Certain measures for this "nonuniformity" will be discussed later in this chapter. ◇

In the literature a variety of approaches for an inverse NFFT (iNFFT) can be found. This is why we give a short overview. First of all, we consider *iterative inversion procedures* for the problem (3.3). These methods require multiple iteration steps by definition, and therefore multiple matrix vector multiplications with the system matrix $\boldsymbol{A}$, or rather multiple applications of the NFFT (see Algorithm 2.2), are needed to compute a solution. For the one-dimensional setting $d = 1$ with $|\mathcal{I}_{\boldsymbol{M}}| = N$ an algorithm was published in [RAT18], which is specifically designed for jittered equispaced points and is based on the *conjugate gradient (CG) algorithm* in connection with low rank approximation, while an approach for the overdetermined case $|\mathcal{I}_{\boldsymbol{M}}| \leq N$ can be found in [FGS95] that uses the Toeplitz structure of the matrix product $\boldsymbol{A}^*\boldsymbol{W}\boldsymbol{A}$ with a diagonal matrix $\boldsymbol{W} \coloneqq \operatorname{diag}(w_j)_{j=1}^N$ of Voronoi weights in connection with the CG algorithm. For higher dimensional problems with $d \geq 1$ several approaches exist which compute a least squares approximation to the linear system $\boldsymbol{A}\hat{\boldsymbol{f}} = \boldsymbol{f}$. On the one hand, in the overdetermined case $|\mathcal{I}_{\boldsymbol{M}}| \leq N$ the given data can typically only be approximated up to a residual $\boldsymbol{r} \coloneqq \boldsymbol{A}\hat{\boldsymbol{f}} - \boldsymbol{f}$. Therefore, the weighted least

squares problem

$$\underset{\hat{\boldsymbol{f}}\in\mathbb{C}^{|\mathcal{I}_{\boldsymbol{M}}|}}{\text{Minimize}} \sum_{j=1}^{N} w_j \left| \sum_{\boldsymbol{k}\in\mathcal{I}_{\boldsymbol{M}}} \hat{f}_{\boldsymbol{k}}\, \mathrm{e}^{2\pi\mathrm{i}\boldsymbol{k}\boldsymbol{x}_j} - f(\boldsymbol{x}_j) \right|^2$$

is considered, which is equivalent to solving the weighted normal equations of first kind $\boldsymbol{A}^*\boldsymbol{W}\boldsymbol{A}\hat{\boldsymbol{f}} = \boldsymbol{A}^*\boldsymbol{W}\boldsymbol{f}$ with the diagonal matrix $\boldsymbol{W} \coloneqq \operatorname{diag}(w_j)_{j=1}^N$ of weights in time domain. In [SFN01, FS03, KKP07] these normal equations are solved iteratively by means of the CG algorithm using the NFFT to realize fast matrix-vector multiplications involving $\boldsymbol{A}$, whereas in [PW01] a fast convolution is used for this purpose. On the other hand, in the consistent underdetermined case $|\mathcal{I}_{\boldsymbol{M}}| > N$ the data can be interpolated exactly and therefore one can choose a specific solution, e. g. the one that solves the constrained minimization problem

$$\underset{\hat{\boldsymbol{f}}\in\mathbb{C}^{|\mathcal{I}_{\boldsymbol{M}}|}}{\text{Minimize}} \sum_{\boldsymbol{k}\in\mathcal{I}_{\boldsymbol{M}}} \frac{|\hat{f}_{\boldsymbol{k}}|^2}{\hat{w}_{\boldsymbol{k}}} \quad \text{subject to} \quad \boldsymbol{A}\hat{\boldsymbol{f}} = \boldsymbol{f}.$$

It was shown in [KP07] that this interpolation problem is equivalent to the weighted normal equations of second kind $\boldsymbol{A}\hat{\boldsymbol{W}}\boldsymbol{A}^*\boldsymbol{y} = \boldsymbol{f}$, $\hat{\boldsymbol{f}} = \hat{\boldsymbol{W}}\boldsymbol{A}^*\boldsymbol{y}$ with the diagonal matrix $\hat{\boldsymbol{W}} \coloneqq \operatorname{diag}(\hat{w}_{\boldsymbol{k}})_{\boldsymbol{k}\in\mathcal{I}_{\boldsymbol{M}}}$ of weights in frequency domain, such that the CG method was used in connection with the NFFT to iteratively compute a solution to this problem, see also [PPST23, Section 7.6.2].

Moreover, there are several regularization techniques for the multidimensional setting $d \geq 1$. For example, [SRG10, WAG15, AGP16] all solve the ℓ_1-regularized problem

$$\underset{\hat{\boldsymbol{f}}\in\mathbb{C}^{|\mathcal{I}_{\boldsymbol{M}}|}}{\text{Minimize}} \ \tfrac{1}{2}\|\boldsymbol{A}\hat{\boldsymbol{f}} - \boldsymbol{f}\|_2^2 + \lambda\|\mathcal{L}^m\hat{\boldsymbol{f}}\|_1$$

with regularization parameter $\lambda > 0$ and the m-th order polynomial annihilation operator $\mathcal{L}^m \in \mathbb{R}^{N\times|\mathcal{I}_{\boldsymbol{M}}|}$ as sparsifying transform, see [AGY05]. Based on this, weighted ℓ_p-schemes

$$\underset{\hat{\boldsymbol{f}}\in\mathbb{C}^{|\mathcal{I}_{\boldsymbol{M}}|}}{\text{Minimize}} \ \tfrac{1}{2}\|\boldsymbol{A}\hat{\boldsymbol{f}} - \boldsymbol{f}\|_2^2 + \tfrac{1}{p}\|\boldsymbol{W}\mathcal{L}^m\hat{\boldsymbol{f}}\|_p^p$$

were introduced in [CWB08, CY08, DDFG10, LMFL12], which are designed to reduce the penalty at locations where $\mathcal{L}^m\hat{\boldsymbol{f}}$ is nonzero. For instance, [CAG19, SG19] each state a two step method, that firstly uses edge detection

to create a mask, i. e., a weighting matrix which indicates where nonzero entries are expected in the *total variation (TV)* domain, and then targets weighted ℓ_2-norm TV regularization appropriately to smooth regions of the function in a second minimization step.

In contrast to these iterated procedures, we rather concentrate on so-called *direct methods* to reduce the computational effort. In the setting of problem (3.3) we hereby mean methods, where for a fixed set of points $\boldsymbol{x}_j$, $j = 1, \dots, N$, the reconstruction of $\hat{\boldsymbol{f}} \in \mathbb{C}^{|\mathcal{I}_{\boldsymbol{M}}|}$ from given $\boldsymbol{f} \in \mathbb{C}^N$ can be realized with the same number of arithmetic operations as a single application of an adjoint NFFT (see Algorithm 2.5). To achieve this, a certain precomputational step is compulsory, since the adjoint NFFT does not yield an inversion of the NFFT per se, see (3.2). Although this precomputations might be rather costly, they need to be done only once for a given set of points $\boldsymbol{x}_j$, $j = 1, \dots, N$, while the actual reconstruction step is very efficient. This is why direct methods are especially beneficial in case we are given fixed nodes for several problems with different measurement vectors $\boldsymbol{f} = (f(\boldsymbol{x}_j))_{j=1}^N$.

Already in [DR95] a direct method for the setting $d = 1$ and $|\mathcal{I}_{\boldsymbol{M}}| = N$ was explained, which uses Lagrange interpolation in combination with fast multipole methods (FMM). Based on this, further methods were deduced for the same setting, which also use Lagrange interpolation, but additionally incorporate an imaginary shift in [Sel18], or utilize the NFFT in [KP19] for the fast evaluation of occurring sums, see also [PPST23, Section 7.6.1]. In the overdetermined setting $|\mathcal{I}_{\boldsymbol{M}}| \leq N$ another approach for computing an inverse NFFT can be obtained by using the fact that $\boldsymbol{A}^*\boldsymbol{A}$ is of Toeplitz structure. Therefore, the Gohberg-Semencul formula, see [HR84], can be used to solve the normal equations $\boldsymbol{A}^*\boldsymbol{A}\hat{\boldsymbol{f}} = \boldsymbol{A}^*\boldsymbol{f}$ exactly by analogy with [ASS16]. Here the computation of the components of the Gohberg–Semencul formula can be viewed as a precomputational step. In addition, also a frame-theoretical approach is known from [GS14], which provides a link between the adjoint NFFT and frame approximation, and could therefore be seen as a way to invert the NFFT. Recently, a new fast algorithm was presented in [WEB24] that exploits the structure of so-called Cauchy-like matrices or rather a low-rank approximation of such, and is especially useful for very irregular grids (e. g. pairwise colliding points). For the multidimensional setting $d > 1$ several methods have been developed in [ACD$^+$06, ACD$^+$08] that are tailored to the special structure of the linogram or pseudo-polar grid, respectively, see Figure 3.4c, such

that the inversion involves only one-dimensional FFTs and interpolations. However, these techniques are exclusively applicable for the special case of the linogram grid, whereas we are interested in more generally applicable methods.

More specifically, we seek to find a suitable matrix $\boldsymbol{X} \in \mathbb{C}^{|\mathcal{I}_M| \times N}$ with $\boldsymbol{X}\boldsymbol{A} \approx \boldsymbol{I}_{|\mathcal{I}_M|}$, since then we can simply compute an approximation of the Fourier coefficients by means of $\boldsymbol{X}\boldsymbol{f} = \boldsymbol{X}\boldsymbol{A}\hat{\boldsymbol{f}} \approx \hat{\boldsymbol{f}}$. The previously mentioned precomputational step then consists of computing an appropriate matrix $\boldsymbol{X}$. To find this left-inverse $\boldsymbol{X}$, we utilize the fact that in the equispaced case (3.1) holds. In addition, we also incorporate the approximate factorization $\boldsymbol{A}^* \approx \boldsymbol{D}^*\boldsymbol{F}^*\boldsymbol{B}^*$ of the adjoint NFFT, cf. Section 2.3, with the matrices $\boldsymbol{D} \in \mathbb{C}^{|\mathcal{I}_M| \times |\mathcal{I}_M|}$, $\boldsymbol{F} \in \mathbb{C}^{|\mathcal{I}_{M_\sigma}| \times |\mathcal{I}_M|}$ and $\boldsymbol{B} \in \mathbb{R}^{N \times |\mathcal{I}_{M_\sigma}|}$ defined in (2.14), (2.15) and (2.16). That is to say, in accordance with the equispaced setting we choose $\boldsymbol{X} = \boldsymbol{D}^*\boldsymbol{F}^*\boldsymbol{B}^* \cdot N^{-1}$.

Based on this observation, this chapter is organized as follows. At first, in Section 3.2 we study so-called density compensation techniques, which make use of the simplest generalization $\boldsymbol{X} = \boldsymbol{D}^*\boldsymbol{F}^*\boldsymbol{B}^*\boldsymbol{W}$ with some additional weighting $\boldsymbol{W} = \operatorname{diag}(w_j)_{j=1}^N \in \mathbb{C}^{N \times N}$ due to the nonequispaced sampling. Afterwards, in Section 3.3 this approach is further generalized to $\boldsymbol{X} = \boldsymbol{D}^*\boldsymbol{F}^*\boldsymbol{B}_{\text{opt}}^*$, where $\boldsymbol{B}_{\text{opt}} \in \mathbb{R}^{N \times |\mathcal{I}_{M_\sigma}|}$ is a modified matrix resulting from a certain matrix optimization problem. In the end, both approaches are compared in the numerical examples of Section 3.4.

3.2 Density compensation factors

In this section we focus on a direct inversion method for solving problem (3.3) that utilizes so-called *sampling density compensation*, as done in [KP23a]. To this end, we consider the Fourier coefficients in (2.3) and introduce a new quadrature formula for this integral representation. In contrast to the already known equispaced approximation (2.4) we now assume given arbitrary, nonequispaced points $\boldsymbol{x}_j \in \mathbb{T}^d$, $j = 1, \dots, N$. Thereby, the Fourier coefficients (2.3) are approximated by a general quadrature rule using quadrature weights $w_j \in \mathbb{C}$, $j = 1, \dots, N$, which are needed for sampling density compensation due to the nonequispaced sampling. Thus, for

a trigonometric polynomial (2.8) we have

$$\hat{f}_{\boldsymbol{k}} = c_{\boldsymbol{k}}(f) \approx h^{\mathrm{w}}_{\boldsymbol{k}} \coloneqq \sum_{j=1}^{N} w_j \, f(\boldsymbol{x}_j) \, \mathrm{e}^{-2\pi \mathrm{i} \boldsymbol{k} \boldsymbol{x}_j}, \quad \boldsymbol{k} \in \mathcal{I}_{\boldsymbol{M}}. \tag{3.5}$$

Using the nonequispaced Fourier matrix $\boldsymbol{A} \in \mathbb{C}^{N \times |\mathcal{I}_{\boldsymbol{M}}|}$ in (2.7), the diagonal matrix of weights $\boldsymbol{W} \coloneqq \operatorname{diag}(w_j)_{j=1}^{N} \in \mathbb{C}^{N \times N}$ as well as the vector $\boldsymbol{h}^{\mathrm{w}} \coloneqq (h^{\mathrm{w}}_{\boldsymbol{k}})_{\boldsymbol{k} \in \mathcal{I}_{\boldsymbol{M}}}$, the nonequispaced quadrature rule (3.5) can be written as $\hat{\boldsymbol{f}} \approx \boldsymbol{h}^{\mathrm{w}} \coloneqq \boldsymbol{A}^* \boldsymbol{W} \boldsymbol{f}$. For achieving a fast computation method we make use of the approximation of the adjoint NFFT, cf. Section 2.3, i. e., the final approximation is given by

$$\hat{\boldsymbol{f}} \approx \tilde{\boldsymbol{h}}^{\mathrm{w}} \coloneqq \boldsymbol{D}^* \boldsymbol{F}^* \boldsymbol{B}^* \boldsymbol{W} \boldsymbol{f}, \tag{3.6}$$

with the matrices $\boldsymbol{D} \in \mathbb{C}^{|\mathcal{I}_{\boldsymbol{M}}| \times |\mathcal{I}_{\boldsymbol{M}}|}$, $\boldsymbol{F} \in \mathbb{C}^{|\mathcal{I}_{\boldsymbol{M}_{\boldsymbol{\sigma}}}| \times |\mathcal{I}_{\boldsymbol{M}}|}$ and $\boldsymbol{B} \in \mathbb{R}^{N \times |\mathcal{I}_{\boldsymbol{M}_{\boldsymbol{\sigma}}}|}$ defined in (2.14), (2.15) and (2.16). In other words, for density compensation methods the already mentioned precomputations consist of computing the quadrature weights $w_j \in \mathbb{C}$, $j = 1, \ldots, N$, while the actual reconstruction step includes only one adjoint NFFT (see Algorithm 2.5) applied to the scaled measurement vector $\boldsymbol{W} \boldsymbol{f}$. Hence, density compensation methods can be summarized as follows.

Algorithm 3.2 (iNFFT – density compensation approach)**.**

For $d, N \in \mathbb{N}$ let $\boldsymbol{x}_j \in \mathbb{T}^d$, $j = 1, \ldots, N$, be given nodes as well as $\boldsymbol{f} \in \mathbb{C}^N$ given coefficients. In addition, we are given $\boldsymbol{M} = (M_1, \ldots, M_d)^{\top} \in (2\mathbb{N})^d$.

0. Precompute a suitable weight matrix $\boldsymbol{W} = \operatorname{diag}(w_j)_{j=1}^{N}$.
1. Compute $\tilde{\boldsymbol{h}}^{\mathrm{w}} \coloneqq \boldsymbol{D}^* \boldsymbol{F}^* \boldsymbol{B}^* \boldsymbol{W} \boldsymbol{f}$, cf. (3.6), by means of an adjoint NFFT.

Output: $\tilde{\boldsymbol{h}}^{\mathrm{w}} \approx \hat{\boldsymbol{f}} \in \mathbb{C}^{|\mathcal{I}_{\boldsymbol{M}}|}$, cf. (3.3).

Complexity: $\mathcal{O}(|\mathcal{I}_{\boldsymbol{M}}| \log(|\mathcal{I}_{\boldsymbol{M}}|) + N)$

The aim of all density compensation techniques is then to choose appropriate weights $w_j \in \mathbb{C}$, $j = 1, \ldots, N$, such that the underlying quadrature (3.5) is preferably exact. In the following we have a look at the specific choice of the so-called *density compensation factors* w_j.

An intuitive approach for density compensation is based on geometry, where each sample is considered as representative of a certain surrounding area, as in numerical integration. The weights for each sample can be obtained for instance by constructing a Voronoi diagram and calculating the area of each cell, see e. g. [RPS+99]. This approach of *Voronoi weights* is well-known and widely used in practice. However, it does not necessarily yield a good approximation (3.6), cf. Figure 3.6, which is why we examine some more sophisticated approaches in the remainder of this section.

For this purpose, this section is organized as follows. Firstly, in Section 3.2.1 we introduce density compensation factors $w_j,\ j = 1, \dots, N$, that lead to an exact reconstruction formula (3.5) for all trigonometric polynomials (2.8) of degree $\boldsymbol{M}$. In addition to the theoretical results, we also discuss methods for the numerical computation in Section 3.2.2. Subsequently, in Section 3.2.3 we present an error bound on density compensation factors computed based on the previous optimality condition. Finally, in Section 3.2.4 we reconsider certain approaches from literature and illustrate how they relate to each other and to the method from Section 3.2.1.

Remark 3.3. Before doing so, we have a closer look at some possible interpretation perspectives on the reconstruction (3.6).

(i) If we define $\boldsymbol{g} \coloneqq \boldsymbol{W}\boldsymbol{f}$, i. e., each entry of $\boldsymbol{f}$ is scaled with respect to the nodes $\boldsymbol{x}_j$, $j = 1, \dots, N$, the approximation (3.6) can be written as $\hat{\boldsymbol{f}} \approx \boldsymbol{D}^* \boldsymbol{F}^* \boldsymbol{B}^* \boldsymbol{g}$. As mentioned before, this coincides with an ordinary adjoint NFFT applied to a modified coefficient vector $\boldsymbol{g}$.

(ii) By defining the matrix $\tilde{\boldsymbol{B}} \coloneqq \boldsymbol{W}^* \boldsymbol{B}$, i. e., scaling the rows of $\boldsymbol{B}$ with respect to the nodes $\boldsymbol{x}_j$, $j = 1, \dots, N$, the approximation (3.6) can be written as $\hat{\boldsymbol{f}} \approx \boldsymbol{D}^* \boldsymbol{F}^* \tilde{\boldsymbol{B}}^* \boldsymbol{f}$. In this sense, density compensation can also be seen as a modification of the adjoint NFFT and its application to the original coefficient vector.

Note that (i) is the common viewpoint. However, we keep (ii) in mind, since this allows treating density compensation methods as an optimization of the sparse matrix $\boldsymbol{B} \in \mathbb{R}^{N \times |\mathcal{I}_{\boldsymbol{M}_\sigma}|}$ in (2.16), as it shall be done in Section 3.3. In addition, we remark that density compensation methods only use N degrees of freedom. ◇

3.2.1 Exact quadrature weights for trigonometric polynomials

Similar to [GKP09], we aim for density compensation factors w_j, $j = 1, \dots, N$, that lead to an exact reconstruction formula (3.5) for all trigonometric polynomials (2.8) of degree $\boldsymbol{M}$. To this end, we firstly examine certain properties that arise from (3.5) being exact, as considered in [KP23a, Theorem 3.2].

Theorem 3.4. *Let a polynomial degree $\boldsymbol{M} \in (2\mathbb{N})^d$, nonequispaced nodes $\boldsymbol{x}_j \in \mathbb{T}^d$, $j = 1, \dots, N$, and quadrature weights $w_j \in \mathbb{C}$ be given. Then an exact reconstruction formula* (3.5) *for trigonometric polynomials* (2.8) *with maximum degree $\boldsymbol{M}$ satisfying*

$$\hat{f}_{\boldsymbol{k}} = c_{\boldsymbol{k}}(f) = h^{\mathrm{w}}_{\boldsymbol{k}}, \quad \boldsymbol{k} \in \mathcal{I}_{\boldsymbol{M}}, \tag{3.7}$$

implies the following equivalent statements.

(i) The quadrature rule

$$\int_{\mathbb{T}^d} f(\boldsymbol{x}) \,\mathrm{d}\boldsymbol{x} = \sum_{j=1}^{N} w_j f(\boldsymbol{x}_j) \tag{3.8}$$

is exact for all trigonometric polynomials (2.8) *with maximum degree $\boldsymbol{M}$.*

(ii) The linear system of equations

$$\left[\boldsymbol{A}^\top \boldsymbol{w}\right]_{\boldsymbol{k}} = \sum_{j=1}^{N} w_j \,\mathrm{e}^{2\pi \mathrm{i} \boldsymbol{k}\boldsymbol{x}_j} = \delta_{\boldsymbol{0},\boldsymbol{k}} = \left\{ \begin{array}{ll} 1 & : \boldsymbol{k} = \boldsymbol{0} \\ 0 & : \textit{otherwise} \end{array} \right\}, \quad \boldsymbol{k} \in \mathcal{I}_{\boldsymbol{M}}, \tag{3.9}$$

is fulfilled with the nonequispaced Fourier matrix $\boldsymbol{A} \in \mathbb{C}^{N \times |\mathcal{I}_{\boldsymbol{M}}|}$ in (2.7)*, $\boldsymbol{w} := (w_j)_{j=1}^{N}$ and the* Kronecker symbol $\delta_{\boldsymbol{0},\boldsymbol{k}}$.

Proof.

(3.7) $\Rightarrow$ (i): By inserting the definition (2.8) of a trigonometric polynomial of degree $\boldsymbol{M}$ into the integral considered in (3.8) we have

$$\int_{\mathbb{T}^d} f(\boldsymbol{x}) \,\mathrm{d}\boldsymbol{x} = \sum_{\boldsymbol{k} \in \mathcal{I}_{\boldsymbol{M}}} \hat{f}_{\boldsymbol{k}} \cdot \int_{\mathbb{T}^d} \mathrm{e}^{2\pi \mathrm{i} \boldsymbol{k}\boldsymbol{x}} \,\mathrm{d}\boldsymbol{x} = \sum_{\boldsymbol{k} \in \mathcal{I}_{\boldsymbol{M}}} \hat{f}_{\boldsymbol{k}} \cdot \delta_{\boldsymbol{0},\boldsymbol{k}} = \hat{f}_{\boldsymbol{0}}. \tag{3.10}$$

Now using the property (3.7) as well as the definition (3.5) of $h_{\boldsymbol{k}}^{\mathrm{w}}$ we proceed with

$$\hat{f}_{\boldsymbol{0}} = h_{\boldsymbol{0}}^{\mathrm{w}} = \sum_{j=1}^{N} w_j f(\boldsymbol{x}_j)\,\mathrm{e}^{0} = \sum_{j=1}^{N} w_j f(\boldsymbol{x}_j),$$

such that a combination with (3.10) yields the assertion (3.8).

(i) $\Rightarrow$ (ii): Inserting the definition (2.8) of a trigonometric polynomial of degree $\boldsymbol{M}$ into the right-hand side of (3.8) implies

$$\sum_{j=1}^{N} w_j f(\boldsymbol{x}_j) = \sum_{j=1}^{N} w_j \sum_{\boldsymbol{k}\in\mathcal{I}_{\boldsymbol{M}}} \hat{f}_{\boldsymbol{k}}\,\mathrm{e}^{2\pi\mathrm{i}\boldsymbol{k}\boldsymbol{x}_j} = \sum_{\boldsymbol{k}\in\mathcal{I}_{\boldsymbol{M}}} \hat{f}_{\boldsymbol{k}} \sum_{j=1}^{N} w_j\,\mathrm{e}^{2\pi\mathrm{i}\boldsymbol{k}\boldsymbol{x}_j}. \quad (3.11)$$

This together with the property (i) and (3.10) leads to

$$\hat{f}_{\boldsymbol{0}} = \sum_{\boldsymbol{k}\in\mathcal{I}_{\boldsymbol{M}}} \hat{f}_{\boldsymbol{k}} \sum_{j=1}^{N} w_j\,\mathrm{e}^{2\pi\mathrm{i}\boldsymbol{k}\boldsymbol{x}_j}$$

and thus to assertion (3.9).

(ii) $\Rightarrow$ (i): Combining (3.10), (3.9) and (3.11) yields the assertion via

$$\int_{\mathbb{T}^d} f(\boldsymbol{x})\,\mathrm{d}\boldsymbol{x} = \sum_{\boldsymbol{k}\in\mathcal{I}_{\boldsymbol{M}}} \hat{f}_{\boldsymbol{k}} \cdot \delta_{\boldsymbol{0},\boldsymbol{k}} = \sum_{\boldsymbol{k}\in\mathcal{I}_{\boldsymbol{M}}} \hat{f}_{\boldsymbol{k}} \sum_{j=1}^{N} w_j\,\mathrm{e}^{2\pi\mathrm{i}\boldsymbol{k}\boldsymbol{x}_j} = \sum_{j=1}^{N} w_j f(\boldsymbol{x}_j).$$

■

Remark 3.5. Comparable results can also be found in the literature. A fundamental theorem in numerical integration, see [Tch57], states that for any integral $\int_{\mathbb{T}^d} f(\boldsymbol{x})\,\mathrm{d}\boldsymbol{x}$ there exists an exact quadrature rule (3.8), i. e., optimal points $\boldsymbol{x}_j \in \mathbb{T}^d$ and weights $w_j \in \mathbb{C}$, $j = 1, \ldots, N$, such that (3.8) is fulfilled. In [Grö20, Lemma 2.6] it was shown that for given points $\boldsymbol{x}_j \in \mathbb{T}^d$, $j = 1, \ldots, N$, certain quadrature weights w_j can be stated by means of frame theoretical considerations which lead to an exact quadrature rule (3.8) by definition. Moreover, it was shown in [Grö20, Lemma 3.6] that these weights are the ones with minimal (weighted) ℓ_2-norm, which are already known under the name "least squares quadrature", see [Huy09]. According to [Huy09, Section 2.1] these quadrature weights w_j, $j = 1, \ldots, N$, can be

found by solving a linear system of equations $\boldsymbol{\Phi}\boldsymbol{w} = \boldsymbol{v}$, where for a set of basis functions $\{\phi_{\boldsymbol{k}}\}_{\boldsymbol{k}\in\mathcal{I}_{\boldsymbol{M}}}$ one defines $\Phi_{\boldsymbol{k},j} \coloneqq \phi_{\boldsymbol{k}}(\boldsymbol{x}_j)$ and $v_{\boldsymbol{k}} \coloneqq \int_{\mathbb{T}^d} \phi_{\boldsymbol{k}}(\boldsymbol{x})\,\mathrm{d}\boldsymbol{x}$. In our setting we have $\phi_{\boldsymbol{k}}(\boldsymbol{x}) = \mathrm{e}^{2\pi\mathrm{i}\boldsymbol{k}\boldsymbol{x}}$, and therefore

$$\boldsymbol{\Phi} = \left(\mathrm{e}^{2\pi\mathrm{i}\boldsymbol{k}\boldsymbol{x}_j}\right)_{\boldsymbol{k},j} = \boldsymbol{A}^\top \quad \text{and} \quad v_{\boldsymbol{k}} = \int_{\mathbb{T}^d} 1\cdot \mathrm{e}^{2\pi\mathrm{i}\boldsymbol{k}\boldsymbol{x}}\,\mathrm{d}\boldsymbol{x} = \delta_{\boldsymbol{0},\boldsymbol{k}},$$

i. e., the same linear system of equations as in (3.9). However, we remark that both [Grö20] and [Huy09] state the results only in the case $d = 1$. ⋄

Note that the two statements (i) and (ii) of Theorem 3.4 are not equivalent to the exact reconstruction property (3.7), since by (3.5) and (2.8) we have

$$\begin{aligned} h_{\boldsymbol{k}}^{\mathrm{w}} &= \sum_{j=1}^{N} w_j \left(\sum_{\boldsymbol{\ell}\in\mathcal{I}_{\boldsymbol{M}}} \hat{f}_{\boldsymbol{\ell}}\, \mathrm{e}^{2\pi\mathrm{i}\boldsymbol{\ell}\boldsymbol{x}_j} \right) \mathrm{e}^{-2\pi\mathrm{i}\boldsymbol{k}\boldsymbol{x}_j} = \sum_{\boldsymbol{\ell}\in\mathcal{I}_{\boldsymbol{M}}} \hat{f}_{\boldsymbol{\ell}} \sum_{j=1}^{N} w_j\, \mathrm{e}^{2\pi\mathrm{i}(\boldsymbol{\ell}-\boldsymbol{k})\boldsymbol{x}_j} \\ &= \sum_{\substack{\boldsymbol{\ell}\in\mathcal{I}_{\boldsymbol{M}} \\ (\boldsymbol{\ell}-\boldsymbol{k})\in\mathcal{I}_{\boldsymbol{M}}}} \hat{f}_{\boldsymbol{\ell}} \sum_{j=1}^{N} w_j\, \mathrm{e}^{2\pi\mathrm{i}(\boldsymbol{\ell}-\boldsymbol{k})\boldsymbol{x}_j} \\ &\qquad + \sum_{\substack{\boldsymbol{\ell}\in\mathcal{I}_{\boldsymbol{M}} \\ (\boldsymbol{\ell}-\boldsymbol{k})\notin\mathcal{I}_{\boldsymbol{M}}}} \hat{f}_{\boldsymbol{\ell}} \sum_{j=1}^{N} w_j\, \mathrm{e}^{2\pi\mathrm{i}(\boldsymbol{\ell}-\boldsymbol{k})\boldsymbol{x}_j}, \quad \boldsymbol{k}\in\mathcal{I}_{\boldsymbol{M}}. \end{aligned}$$

Due to the fact that (3.9) only holds for $\boldsymbol{k},\boldsymbol{\ell}\in\mathcal{I}_{\boldsymbol{M}}$ with $(\boldsymbol{\ell}-\boldsymbol{k})\in\mathcal{I}_{\boldsymbol{M}}$, this implies

$$h_{\boldsymbol{k}}^{\mathrm{w}} = \hat{f}_{\boldsymbol{k}} + \sum_{\substack{\boldsymbol{\ell}\in\mathcal{I}_{\boldsymbol{M}} \\ (\boldsymbol{\ell}-\boldsymbol{k})\notin\mathcal{I}_{\boldsymbol{M}}}} \hat{f}_{\boldsymbol{\ell}} \sum_{j=1}^{N} w_j\, \mathrm{e}^{2\pi\mathrm{i}(\boldsymbol{\ell}-\boldsymbol{k})\boldsymbol{x}_j}, \quad \boldsymbol{k}\in\mathcal{I}_{\boldsymbol{M}},$$

where for all $\boldsymbol{k}\in\mathcal{I}_{\boldsymbol{M}}\setminus\{\boldsymbol{0}\}$ there exists an $\boldsymbol{\ell}\in\mathcal{I}_{\boldsymbol{M}}$ with $(\boldsymbol{\ell}-\boldsymbol{k})\in\mathcal{I}_{\boldsymbol{2M}}\setminus\mathcal{I}_{\boldsymbol{M}}$. In other words, the two statements (i) and (ii) of Theorem 3.4 only ensure that $h_{\boldsymbol{0}}^{\mathrm{w}} = \hat{f}_{\boldsymbol{0}}$.

However, based on similar considerations as in Theorem 3.4 the following result can be shown, cf. [KP23a, Corollary 3.4] and [KP23b, Theorem II.1].

Theorem 3.6. *Let $|\mathcal{I}_{\boldsymbol{2M}}| \le N$ and $\boldsymbol{x}_j\in\mathbb{T}^d$, $j = 1,\dots,N$, be given. Then the density compensation factors $w_j\in\mathbb{C}$ satisfying*

$$\sum_{j=1}^{N} w_j\, \mathrm{e}^{2\pi\mathrm{i}\boldsymbol{k}\boldsymbol{x}_j} = \delta_{\boldsymbol{0},\boldsymbol{k}}, \quad \boldsymbol{k}\in\mathcal{I}_{\boldsymbol{2M}}, \tag{3.12}$$

are optimal, since for all trigonometric polynomials of degree $\boldsymbol{M}$*, see* (2.8)*, an exact reconstruction of the Fourier coefficients* $\hat{f}_{\boldsymbol{k}}$ *is given by*

$$\hat{f}_{\boldsymbol{k}} = h^{\mathrm{w}}_{\boldsymbol{k}} = \sum_{j=1}^{N} w_j \, f(\boldsymbol{x}_j) \, \mathrm{e}^{-2\pi \mathrm{i} \boldsymbol{k} \boldsymbol{x}_j}, \quad \boldsymbol{k} \in \mathcal{I}_{\boldsymbol{M}}.$$

Proof. It is known that $\{\mathrm{e}^{2\pi \mathrm{i} \boldsymbol{\ell} \boldsymbol{x}} : \boldsymbol{\ell} \in \mathbb{Z}^d\}$ forms an orthonormal basis of the Hilbert space $L_2(\mathbb{T}^d)$ of all 1-periodic, complex-valued functions, see [PPST23, p. 177]. To achieve an exact reconstruction for all trigonometric polynomials (2.8) with maximum degree $\boldsymbol{M}$ it suffices to consider the set of basis functions with $\boldsymbol{\ell} \in \mathcal{I}_{\boldsymbol{M}}$. For each of these basis functions with fixed $\boldsymbol{\ell} \in \mathcal{I}_{\boldsymbol{M}}$ we have

$$h^{\mathrm{w}}_{\boldsymbol{k}} = \sum_{j=1}^{N} w_j \, \mathrm{e}^{2\pi \mathrm{i} (\boldsymbol{\ell} - \boldsymbol{k}) \boldsymbol{x}_j}, \quad \boldsymbol{k} \in \mathcal{I}_{\boldsymbol{M}},$$

and

$$\hat{f}_{\boldsymbol{k}} = c_{\boldsymbol{k}}(f) = \int_{\mathbb{T}^d} \mathrm{e}^{2\pi \mathrm{i} (\boldsymbol{\ell} - \boldsymbol{k}) \boldsymbol{x}} \, \mathrm{d}\boldsymbol{x} = \delta_{\boldsymbol{k}, \boldsymbol{\ell}}, \quad \boldsymbol{k} \in \mathcal{I}_{\boldsymbol{M}},$$

with the Kronecker symbol $\delta_{\boldsymbol{k}, \boldsymbol{\ell}} = \delta_{(\boldsymbol{\ell} - \boldsymbol{k}), \boldsymbol{0}}$. Thus, in order to obtain $\hat{f}_{\boldsymbol{k}} = h^{\mathrm{w}}_{\boldsymbol{k}}$ for each of these basis functions we need to assure that the weights satisfy

$$\sum_{j=1}^{N} w_j \, \mathrm{e}^{2\pi \mathrm{i} (\boldsymbol{\ell} - \boldsymbol{k}) \boldsymbol{x}_j} = \delta_{\boldsymbol{k}, \boldsymbol{\ell}}, \quad \boldsymbol{\ell}, \boldsymbol{k} \in \mathcal{I}_{\boldsymbol{M}}. \tag{3.13}$$

Since for $\boldsymbol{k}, \boldsymbol{\ell} \in \mathcal{I}_{\boldsymbol{M}}$ we have $(\boldsymbol{\ell} - \boldsymbol{k}) \in \mathcal{I}_{\boldsymbol{2M}}$, the property (3.13) is fulfilled by the more general condition (3.12). That is to say, the condition (3.12) ensures the exact reconstruction for all trigonometric polynomials (2.8) with maximum degree $\boldsymbol{M}$. However, it was already shown in [Huy09, Section 3.1] that the condition (3.12) can only be fulfilled exactly, if (3.12) is an underdetermined system with $|\mathcal{I}_{\boldsymbol{2M}}| \leq N$. ∎

In other words, by defining the nonequispaced Fourier matrix $\boldsymbol{A}_{|\mathcal{I}_{\boldsymbol{2M}}|} \in \mathbb{C}^{N \times |\mathcal{I}_{\boldsymbol{2M}}|}$ as in (2.7) as well as $\boldsymbol{w} \coloneqq (w_j)_{j=1}^{N}$, an exact solution to the linear system of equations

$$\boldsymbol{A}^{\top}_{|\mathcal{I}_{\boldsymbol{2M}}|} \, \boldsymbol{w} = \boldsymbol{e}_{\boldsymbol{0}} \coloneqq (\delta_{\boldsymbol{0}, \boldsymbol{k}})_{\boldsymbol{k} \in \mathcal{I}_{\boldsymbol{2M}}} \tag{3.14}$$

yields an exact reconstruction for all trigonometric polynomials (2.8) of degree $\boldsymbol{M}$.

Remark 3.7. We remark, that since $\delta_{(\boldsymbol{\ell}-\boldsymbol{k}),\mathbf{0}} = \delta_{\boldsymbol{k},\boldsymbol{\ell}}$, the condition (3.12) implies

$$\delta_{\boldsymbol{k},\boldsymbol{\ell}} = \sum_{j=1}^{N} w_j \, \mathrm{e}^{2\pi\mathrm{i}(\boldsymbol{\ell}-\boldsymbol{k})\boldsymbol{x}_j} = \sum_{j=1}^{N} \mathrm{e}^{-2\pi\mathrm{i}\boldsymbol{k}\boldsymbol{x}_j} \left(w_j \, \mathrm{e}^{2\pi\mathrm{i}\boldsymbol{\ell}\boldsymbol{x}_j} \right), \quad \boldsymbol{k}, \boldsymbol{\ell} \in \mathcal{I}_{\boldsymbol{M}}.$$

By using the nonequispaced Fourier matrix $\boldsymbol{A} \in \mathbb{C}^{N \times |\mathcal{I}_{\boldsymbol{M}}|}$ in (2.7), the diagonal matrix of weights $\boldsymbol{W} = \operatorname{diag}(w_j)_{j=1}^{N} \in \mathbb{C}^{N \times N}$ and the identity matrix $\boldsymbol{I}_{|\mathcal{I}_{\boldsymbol{M}}|}$ of size $|\mathcal{I}_{\boldsymbol{M}}|$ this can be written in matrix-vector notation as $\boldsymbol{A}^* \boldsymbol{W} \boldsymbol{A} = \boldsymbol{I}_{|\mathcal{I}_{\boldsymbol{M}}|}$. Note that this matrix equation immediately shows that we have an exact reconstruction of the form (3.7), since by (3.3) the properties $\boldsymbol{A}^* \boldsymbol{W} \boldsymbol{A} = \boldsymbol{I}_{|\mathcal{I}_{\boldsymbol{M}}|}$ and $\hat{\boldsymbol{f}} = \boldsymbol{A}^* \boldsymbol{W} \boldsymbol{f}$ are equivalent. ◇

Remark 3.8. Let $f \in L_2(\mathbb{T}^d)$ be an arbitrary 1-periodic function. Then by definitions (3.5) and (2.2) the optimality condition (3.12) yields

$$\begin{aligned} h_{\boldsymbol{k}}^{\mathrm{w}} &= \sum_{\boldsymbol{\ell} \in \mathbb{Z}^d} c_{\boldsymbol{\ell}}(f) \sum_{j=1}^{N} w_j \, \mathrm{e}^{2\pi\mathrm{i}(\boldsymbol{\ell}-\boldsymbol{k})\boldsymbol{x}_j} \\ &= \sum_{\substack{\boldsymbol{\ell} \in \mathbb{Z}^d \\ (\boldsymbol{\ell}-\boldsymbol{k}) \in \mathcal{I}_{\boldsymbol{2M}}}} c_{\boldsymbol{\ell}}(f) \sum_{j=1}^{N} w_j \, \mathrm{e}^{2\pi\mathrm{i}(\boldsymbol{\ell}-\boldsymbol{k})\boldsymbol{x}_j} + \sum_{\substack{\boldsymbol{\ell} \in \mathbb{Z}^d \\ (\boldsymbol{\ell}-\boldsymbol{k}) \notin \mathcal{I}_{\boldsymbol{2M}}}} c_{\boldsymbol{\ell}}(f) \sum_{j=1}^{N} w_j \, \mathrm{e}^{2\pi\mathrm{i}(\boldsymbol{\ell}-\boldsymbol{k})\boldsymbol{x}_j} \\ &= c_{\boldsymbol{k}}(f) + \sum_{\substack{\boldsymbol{\ell} \in \mathbb{Z}^d \\ (\boldsymbol{\ell}-\boldsymbol{k}) \notin \mathcal{I}_{\boldsymbol{2M}}}} c_{\boldsymbol{\ell}}(f) \sum_{j=1}^{N} w_j \, \mathrm{e}^{2\pi\mathrm{i}(\boldsymbol{\ell}-\boldsymbol{k})\boldsymbol{x}_j}, \quad \boldsymbol{k} \in \mathcal{I}_{\boldsymbol{M}}. \end{aligned}$$

That is to say, for a function $f \in L_2(\mathbb{T}^d)$ we only have a good approximation in case the coefficients $c_{\boldsymbol{\ell}}(f)$ are small for $\boldsymbol{\ell} \notin \mathcal{I}_{\boldsymbol{M}}$, whereas this reconstruction can only be exact for f being a trigonometric polynomial (2.8). ◇

Remark 3.9. In [Huy09, Section 2.3] it was stated that stability of a quadrature rule (3.8) is directly imposed by its weights. Namely, if all quadrature weights $w_j \in \mathbb{C}$, $j = 1, \ldots, N$, are positive, the corresponding quadrature rule is stable. A commonly used measure of stability is $\kappa(\boldsymbol{w}) \coloneqq \sum_{j=1}^{N} |w_j|$. Note that if the quadrature rule (3.8) is exact for all trigonometric polynomials (2.8) with maximum degree $\boldsymbol{M}$, this especially holds for a trigonometric polynomial of degree $\mathbf{0}$, i. e., a constant function $f(\boldsymbol{x}) = \hat{f}_{\mathbf{0}}$. In this case,

the quadrature rule (3.8) can be written as

$$\hat{f}_{\mathbf{0}} = \int_{\mathbb{T}^d} f(\boldsymbol{x}) \,\mathrm{d}\boldsymbol{x} = \sum_{j=1}^{N} w_j f(\boldsymbol{x}_j) = \hat{f}_{\mathbf{0}} \sum_{j=1}^{N} w_j.$$

Thus, if $w_j > 0$, $j = 1, \ldots, N$, this implies

$$\kappa(\boldsymbol{w}) = \sum_{j=1}^{N} w_j = 1.$$

Additionally note that by Theorem 3.4 the properties (3.8) and (3.9) are equivalent, and that for $\boldsymbol{k} = \mathbf{0}$ the linear system (3.9) reads as

$$\left[\boldsymbol{A}^{\top}\boldsymbol{w}\right]_{\mathbf{0}} = \sum_{j=1}^{N} w_j = 1.$$

In other words, the linear system of equations (3.9), and thus also (3.12), already includes the condition $\sum_{j=1}^{N} w_j = 1$, which guarantees stable quadrature in case of positive weights $w_j > 0$, $j = 1, \ldots, N$. ◇

3.2.2 Practical computation schemes

Since by Theorem 3.6 an exact solution $\boldsymbol{w} = (w_j)_{j=1}^{N}$ of the linear system (3.12) leads to an exact reconstruction formula (3.5) for all trigonometric polynomials (2.8) with maximum degree $\boldsymbol{M}$, we now aim to use this condition (3.12) to find the optimal density compensation factors $w_j \in \mathbb{C}$, $j = 1, \ldots, N$, numerically.

We remark that in contrast to (3.3) using the matrix $\boldsymbol{A} \in \mathbb{C}^{N \times |\mathcal{I}_{\boldsymbol{M}}|}$, in (3.14) we now deal with the enlarged matrix $\boldsymbol{A}_{|\mathcal{I}_{\mathbf{2}\boldsymbol{M}}|} \in \mathbb{C}^{N \times |\mathcal{I}_{\mathbf{2}\boldsymbol{M}}|}$, such that single matrix operations are more costly. Nevertheless, Theorem 3.6 yields a direct inversion method for (3.3), where the system (3.14) needs to be solved only once for a fixed set of nodes $\boldsymbol{x}_j \in \mathbb{T}^d$, $j = 1, \ldots, N$. Its solution $\boldsymbol{w}$ can then be used to efficiently approximate $\hat{\boldsymbol{f}} \in \mathbb{C}^{|\mathcal{I}_{\boldsymbol{M}}|}$ for multiple measurement vectors $\boldsymbol{f} \in \mathbb{C}^N$, whereas iterative methods for (3.3) need to solve $\boldsymbol{A}\hat{\boldsymbol{f}} = \boldsymbol{f}$ each time.

Practical computation in the underdetermined setting $|\mathcal{I}_{2M}| \leq N$

As already mentioned in [Huy09, Section 3.1] an exact solution to (3.12) can only be found if $|\mathcal{I}_{2M}| \leq N$, i. e., in case (3.14) is an underdetermined system of equations. By [Huy09, Lemma 3.1] this system has at least one solution, which is why we may choose the one with minimal ℓ_2-norm.

If $\operatorname{rank}(\boldsymbol{A}_{|\mathcal{I}_{2M}|}) = |\mathcal{I}_{2M}|$, then the system (3.14) is consistent and the unique solution is given by the *normal equations of second kind*

$$\boldsymbol{A}_{|\mathcal{I}_{2M}|}^{\top} \overline{\boldsymbol{A}_{|\mathcal{I}_{2M}|}}\, \boldsymbol{v} = \boldsymbol{e_0}, \quad \overline{\boldsymbol{A}_{|\mathcal{I}_{2M}|}}\, \boldsymbol{v} = \boldsymbol{w}. \tag{3.15}$$

More precisely, if the condition number of $\boldsymbol{A}_{|\mathcal{I}_{2M}|} \in \mathbb{C}^{N \times |\mathcal{I}_{2M}|}$ is sufficiently small, we may compute the vector $\boldsymbol{v} \in \mathbb{C}^{|\mathcal{I}_{2M}|}$ in (3.15) using an iterative procedure like the CG algorithm, such that only matrix multiplications with $\boldsymbol{A}_{|\mathcal{I}_{2M}|}^{\top}$ and $\overline{\boldsymbol{A}_{|\mathcal{I}_{2M}|}}$ are needed. Since fast multiplication with $\boldsymbol{A}_{|\mathcal{I}_{2M}|}^{\top}$ and $\overline{\boldsymbol{A}_{|\mathcal{I}_{2M}|}}$ can easily be realized by means of an adjoint NFFT (see Algorithm 2.5) and an NFFT (see Algorithm 2.2), respectively, computing the solution $\boldsymbol{w} = (w_j)_{j=1}^N$ to (3.15) is of complexity $\mathcal{O}(|\mathcal{I}_{2M}| \log(|\mathcal{I}_{2M}|) + N)$, where

$$|\mathcal{I}_{2M}| = \prod_{t=1}^{d} (2M_t) = 2^d \cdot \prod_{t=1}^{d} M_t = 2^d\, |\mathcal{I}_{M}|.$$

Hence, this procedure can be used to efficiently compute the exact quadrature weights $w_j \in \mathbb{C}$, $j = 1, \ldots, N$, via (3.15), as long as the full rank condition $\operatorname{rank}(\boldsymbol{A}_{|\mathcal{I}_{2M}|}) = |\mathcal{I}_{2M}|$ is satisfied.

In case of a low rank matrix $\boldsymbol{A}_{|\mathcal{I}_{2M}|} \in \mathbb{C}^{N \times |\mathcal{I}_{2M}|}$ with $|\mathcal{I}_{2M}| \leq N$, we cannot expect a unique solution but we may still use (3.15) to obtain a least squares approximation to (3.12), if the condition number of $\boldsymbol{A}_{|\mathcal{I}_{2M}|}$ is sufficiently small.

Practical computation in the overdetermined setting $|\mathcal{I}_{2M}| > N$

However, when $|\mathcal{I}_{2M}| > N$ there is no theoretical guarantee and therefore we cannot expect to find an exact solution $\boldsymbol{w} = (w_j)_{j=1}^N$ to (3.12), since we have to deal with an overdetermined system possessing more conditions than variables. Nevertheless, we still aim to find optimal density compensation factors $w_j \in \mathbb{C}$, $j = 1, \ldots, N$, numerically by considering a least squares approximation to (3.12) that minimizes $\left\| \boldsymbol{A}_{|\mathcal{I}_{2M}|}^{\top} \boldsymbol{w} - \boldsymbol{e_0} \right\|_2$.

In [Bjö96, Theorem 1.1.2] it was shown that every least squares solution satisfies the *normal equations of first kind*

$$\overline{\boldsymbol{A}_{|\mathcal{I}_{\boldsymbol{2M}}|}}\,\boldsymbol{A}_{|\mathcal{I}_{\boldsymbol{2M}}|}^{\top}\,\boldsymbol{w} = \overline{\boldsymbol{A}_{|\mathcal{I}_{\boldsymbol{2M}}|}}\,\boldsymbol{e_0}. \tag{3.16}$$

By means of the definitions of the matrix $\boldsymbol{A}_{|\mathcal{I}_{\boldsymbol{2M}}|} \in \mathbb{C}^{N\times|\mathcal{I}_{\boldsymbol{2M}}|}$, cf. (2.7), and the vector $\boldsymbol{e_0} = (\delta_{\boldsymbol{0},\boldsymbol{k}})_{\boldsymbol{k}\in\mathcal{I}_{\boldsymbol{2M}}}$ we simplify the right-hand side of (3.16) via

$$\overline{\boldsymbol{A}_{|\mathcal{I}_{\boldsymbol{2M}}|}}\,\boldsymbol{e_0} = \left(\sum_{\boldsymbol{k}\in\mathcal{I}_{\boldsymbol{2M}}} \delta_{\boldsymbol{0},\boldsymbol{k}}\,\mathrm{e}^{-2\pi\mathrm{i}\boldsymbol{k}\boldsymbol{x}_j}\right)_{j=1}^{N} = \boldsymbol{1}_N.$$

Since fast multiplication with $\boldsymbol{A}_{|\mathcal{I}_{\boldsymbol{2M}}|}^{\top}$ and $\overline{\boldsymbol{A}_{|\mathcal{I}_{\boldsymbol{2M}}|}}$ can easily be realized by means of an adjoint NFFT (see Algorithm 2.5) and an NFFT (see Algorithm 2.2), respectively, the solution $\boldsymbol{w} = (w_j)_{j=1}^{N}$ to (3.16) can be computed iteratively by means of the CG algorithm in $\mathcal{O}(|\mathcal{I}_{\boldsymbol{2M}}|\log(|\mathcal{I}_{\boldsymbol{2M}}|) + N)$ arithmetic operations. Note that the solution to (3.16) is only unique if the full rank condition $\operatorname{rank}(\boldsymbol{A}_{|\mathcal{I}_{\boldsymbol{2M}}|}) = N$ is satisfied, cf. [Bjö96, p. 7]. We remark that the computed weight matrix $\boldsymbol{W} = \operatorname{diag}(\boldsymbol{w})$ can also be used in an iterative procedure as in [PPST23, Alg. 7.35] to further improve the approximation of $\hat{\boldsymbol{f}} \in \mathbb{C}^{|\mathcal{I}_{\boldsymbol{M}}|}$.

The previous considerations lead to the following algorithm to compute a suitable weight matrix $\boldsymbol{W} = \operatorname{diag}(w_j)_{j=1}^{N}$ based on the condition (3.14). For further details see [KP23a].

Algorithm 3.10 (Computation of the optimal density compensation factors)**.** For $d, N \in \mathbb{N}$ let the nonequispaced nodes $\boldsymbol{x}_j \in \mathbb{T}^d$, $j = 1,\dots,N$, as well as the vector $\boldsymbol{M} = (M_1,\dots,M_d)^{\top} \in (2\mathbb{N})^d$, be given.

1. If $|\mathcal{I}_{\boldsymbol{2M}}| \le N$:

   Compute the solution $\boldsymbol{v} \in \mathbb{C}^{|\mathcal{I}_{\boldsymbol{2M}}|}$ to (3.15) iteratively using the NFFT. $\mathcal{O}(|\mathcal{I}_{\boldsymbol{2M}}|\log(|\mathcal{I}_{\boldsymbol{2M}}|) + N)$

   Compute the weights $\boldsymbol{w} = \overline{\boldsymbol{A}_{|\mathcal{I}_{\boldsymbol{2M}}|}}\,\boldsymbol{v}$, see (3.15), using an NFFT. $\mathcal{O}(|\mathcal{I}_{\boldsymbol{2M}}|\log(|\mathcal{I}_{\boldsymbol{2M}}|) + N)$

   elseif $|\mathcal{I}_{\boldsymbol{2M}}| > N$:

   Compute the solution $\boldsymbol{w} = (w_j)_{j=1}^{N}$ to (3.16) iteratively using the NFFT. $\mathcal{O}(|\mathcal{I}_{\boldsymbol{2M}}|\log(|\mathcal{I}_{\boldsymbol{2M}}|) + N)$

2. Compose $\boldsymbol{W} = \operatorname{diag}(\boldsymbol{w}) \in \mathbb{C}^{N \times N}$. $\mathcal{O}(N)$

Output: weight matrix $\boldsymbol{W}$

Complexity: $\mathcal{O}(|\mathcal{I}_{\boldsymbol{2M}}| \log(|\mathcal{I}_{\boldsymbol{2M}}|) + N)$

3.2.3 Bounds on the approximation error

Analogous to [KP23a, Theorem 3.14] we now summarize the previous findings by presenting an error bound on density compensation factors based on the optimality condition (3.12).

Theorem 3.11. *Let $p, q \in \{1, 2, \infty\}$ with $\frac{1}{p} + \frac{1}{q} = 1$. For given $d, N \in \mathbb{N}$, vector $\boldsymbol{M} \in (2\mathbb{N})^d$ and nonequispaced nodes $\boldsymbol{x}_j \in \left[-\frac{1}{2}, \frac{1}{2}\right)^d$, $j = 1, \dots, N$, let $\boldsymbol{A} \in \mathbb{C}^{N \times |\mathcal{I}_{\boldsymbol{M}}|}$ be the nonequispaced Fourier matrix in (2.7). Furthermore, we assume that we can compute density compensation factors $\boldsymbol{W} = \operatorname{diag}\left(w_j\right)_{j=1}^{N} \in \mathbb{C}^{N \times N}$ by means of Algorithm 3.10, such that*

$$\sum_{j=1}^{N} w_j \, \mathrm{e}^{2\pi \mathrm{i} \boldsymbol{k} \boldsymbol{x}_j} = \delta_{\boldsymbol{0},\boldsymbol{k}} + \varepsilon_{\boldsymbol{k}}, \quad \boldsymbol{k} \in \mathcal{I}_{\boldsymbol{2M}}, \tag{3.17}$$

with small $\varepsilon_{\boldsymbol{k}} \in \mathbb{R}$ for all $\boldsymbol{k} \in \mathcal{I}_{\boldsymbol{2M}}$. Then there exists an $\varepsilon \geq 0$ such that the corresponding density compensation procedure satisfies the following error bounds.

(i) For any trigonometric polynomial $f \in L_2(\mathbb{T}^d)$ of degree $\boldsymbol{M}$ as in (2.8) we have

$$\left\| \hat{\boldsymbol{f}} - \boldsymbol{A}^* \boldsymbol{W} \boldsymbol{f} \right\|_p \leq |\mathcal{I}_{\boldsymbol{M}}| \, \varepsilon \cdot \left\| \hat{\boldsymbol{f}} \right\|_p, \tag{3.18}$$

where $\hat{\boldsymbol{f}} \coloneqq (\hat{f}_{\boldsymbol{k}})_{\boldsymbol{k} \in \mathcal{I}_{\boldsymbol{M}}}$ are the coefficients in (2.8).

(ii) For any 1-periodic function $f \in L_2(\mathbb{T}^d) \cap C(\mathbb{T}^d)$ as in (2.2) we have

$$\begin{aligned} \left\| \hat{\boldsymbol{f}} - \boldsymbol{A}^* \boldsymbol{W} \boldsymbol{f} \right\|_p \leq{}& |\mathcal{I}_{\boldsymbol{M}}| \, \varepsilon \cdot \left\| \hat{\boldsymbol{f}} \right\|_p \\ &+ \left(N \, |\mathcal{I}_{\boldsymbol{M}}|\right)^{1/p} \|\boldsymbol{w}\|_q \cdot \|f - p_{\boldsymbol{M}}\|_{C(\mathbb{T}^d)}, \end{aligned} \tag{3.19}$$

where $\hat{\boldsymbol{f}} \coloneqq (c_{\boldsymbol{k}}(f))_{\boldsymbol{k} \in \mathcal{I}_{\boldsymbol{M}}}$ are the first $|\mathcal{I}_{\boldsymbol{M}}|$ coefficients in (2.2) and $p_{\boldsymbol{M}}$ is the best approximating trigonometric polynomial of degree $\boldsymbol{M}$ of f.

Proof. We start with some general considerations that are independent of the function f. By (3.17) we can find $\varepsilon \coloneqq \max_{\boldsymbol{k}\in\mathcal{I}_{\boldsymbol{M}}} |\varepsilon_{\boldsymbol{k}}| \geq 0$, such that $|\varepsilon_{\boldsymbol{k}}| \leq \varepsilon$, $\boldsymbol{k} \in \mathcal{I}_{\boldsymbol{2M}}$, and thereby

$$\left| \sum_{j=1}^{N} w_j \, \mathrm{e}^{2\pi \mathrm{i} \boldsymbol{k} \boldsymbol{x}_j} - \delta_{\boldsymbol{0},\boldsymbol{k}} \right| \leq \varepsilon, \quad \boldsymbol{k} \in \mathcal{I}_{\boldsymbol{2M}}.$$

Then for all $\boldsymbol{k}, \boldsymbol{\ell} \in \mathcal{I}_{\boldsymbol{M}}$ with $(\boldsymbol{\ell} - \boldsymbol{k}) \in \mathcal{I}_{\boldsymbol{2M}}$ this yields

$$\left| [\boldsymbol{E}_{\mathrm{r}}]_{\boldsymbol{k},\boldsymbol{\ell}} \right| = \left| \sum_{j=1}^{N} w_j \, \mathrm{e}^{2\pi \mathrm{i} (\boldsymbol{\ell}-\boldsymbol{k}) \boldsymbol{x}_j} - \delta_{\boldsymbol{k},\boldsymbol{\ell}} \right| \leq \varepsilon,$$

where $\boldsymbol{E}_{\mathrm{r}} \coloneqq \boldsymbol{A}^* \boldsymbol{W} \boldsymbol{A} - \boldsymbol{I}_{|\mathcal{I}_{\boldsymbol{M}}|}$. Hence, we have

$$\left\| \boldsymbol{A}^* \boldsymbol{W} \boldsymbol{A} - \boldsymbol{I}_{|\mathcal{I}_{\boldsymbol{M}}|} \right\|_1 = \max_{\boldsymbol{\ell}\in\mathcal{I}_{\boldsymbol{M}}} \sum_{\boldsymbol{k}\in\mathcal{I}_{\boldsymbol{M}}} \left| [\boldsymbol{E}_{\mathrm{r}}]_{\boldsymbol{k},\boldsymbol{\ell}} \right| \leq \max_{\boldsymbol{\ell}\in\mathcal{I}_{\boldsymbol{M}}} \sum_{\boldsymbol{k}\in\mathcal{I}_{\boldsymbol{M}}} \varepsilon = |\mathcal{I}_{\boldsymbol{M}}| \, \varepsilon, \tag{3.20}$$

$$\left\| \boldsymbol{A}^* \boldsymbol{W} \boldsymbol{A} - \boldsymbol{I}_{|\mathcal{I}_{\boldsymbol{M}}|} \right\|_\infty = \max_{\boldsymbol{k}\in\mathcal{I}_{\boldsymbol{M}}} \sum_{\boldsymbol{\ell}\in\mathcal{I}_{\boldsymbol{M}}} \left| [\boldsymbol{E}_{\mathrm{r}}]_{\boldsymbol{k},\boldsymbol{\ell}} \right| \leq \max_{\boldsymbol{k}\in\mathcal{I}_{\boldsymbol{M}}} \sum_{\boldsymbol{\ell}\in\mathcal{I}_{\boldsymbol{M}}} \varepsilon = |\mathcal{I}_{\boldsymbol{M}}| \, \varepsilon, \tag{3.21}$$

and

$$\begin{aligned} \left\| \boldsymbol{A}^* \boldsymbol{W} \boldsymbol{A} - \boldsymbol{I}_{|\mathcal{I}_{\boldsymbol{M}}|} \right\|_{\mathrm{F}} &= \sqrt{\sum_{\boldsymbol{k}\in\mathcal{I}_{\boldsymbol{M}}} \sum_{\boldsymbol{\ell}\in\mathcal{I}_{\boldsymbol{M}}} \left| [\boldsymbol{E}_{\mathrm{r}}]_{\boldsymbol{k},\boldsymbol{\ell}} \right|^2} \\ &\leq \sqrt{\sum_{\boldsymbol{k}\in\mathcal{I}_{\boldsymbol{M}}} \sum_{\boldsymbol{\ell}\in\mathcal{I}_{\boldsymbol{M}}} \varepsilon^2} = |\mathcal{I}_{\boldsymbol{M}}| \, \varepsilon, \end{aligned} \tag{3.22}$$

where $\| \cdot \|_{\mathrm{F}}$ denotes the *Frobenius norm* of a matrix. This can be used to estimate the approximation error of (3.5), since

$$\begin{aligned} \left\| \hat{\boldsymbol{f}} - \boldsymbol{A}^* \boldsymbol{W} \boldsymbol{f} \right\|_p &\leq \left\| \hat{\boldsymbol{f}} - \boldsymbol{A}^* \boldsymbol{W} \boldsymbol{A} \hat{\boldsymbol{f}} \right\|_p + \left\| \boldsymbol{A}^* \boldsymbol{W} \boldsymbol{A} \hat{\boldsymbol{f}} - \boldsymbol{A}^* \boldsymbol{W} \boldsymbol{f} \right\|_p \\ &= \left\| \left(\boldsymbol{A}^* \boldsymbol{W} \boldsymbol{A} - \boldsymbol{I}_{|\mathcal{I}_{\boldsymbol{M}}|} \right) \hat{\boldsymbol{f}} \right\|_p + \left\| \boldsymbol{A}^* \boldsymbol{W} \left(\boldsymbol{A} \hat{\boldsymbol{f}} - \boldsymbol{f} \right) \right\|_p \\ &\leq \left\| \boldsymbol{A}^* \boldsymbol{W} \boldsymbol{A} - \boldsymbol{I}_{|\mathcal{I}_{\boldsymbol{M}}|} \right\|_p \cdot \left\| \hat{\boldsymbol{f}} \right\|_p + \left\| \boldsymbol{A}^* \boldsymbol{W} \right\|_p \cdot \left\| \boldsymbol{A} \hat{\boldsymbol{f}} - \boldsymbol{f} \right\|_p. \end{aligned} \tag{3.23}$$

Using $\boldsymbol{A} \in \mathbb{C}^{N \times |\mathcal{I}_{\boldsymbol{M}}|}$ from (2.7) as well as $\boldsymbol{W} = \operatorname{diag}(w_j)_{j=1}^N = \operatorname{diag}(\boldsymbol{w})$ we have

$$\begin{aligned}\left\|\boldsymbol{A}^* \boldsymbol{W}\right\|_1 &= \max_{j=1,\dots,N} \sum_{\boldsymbol{k} \in \mathcal{I}_{\boldsymbol{M}}} |w_j| \cdot \left|\mathrm{e}^{-2\pi \mathrm{i} \boldsymbol{k} \boldsymbol{x}_j}\right| \\ &\leq \max_{j=1,\dots,N} |w_j| \cdot \sum_{\boldsymbol{k} \in \mathcal{I}_{\boldsymbol{M}}} 1 = |\mathcal{I}_{\boldsymbol{M}}| \cdot \|\boldsymbol{w}\|_\infty,\end{aligned}$$

$$\left\|\boldsymbol{A}^* \boldsymbol{W}\right\|_\infty = \max_{\boldsymbol{k} \in \mathcal{I}_{\boldsymbol{M}}} \sum_{j=1}^N |w_j| \cdot \left|\mathrm{e}^{-2\pi \mathrm{i} \boldsymbol{k} \boldsymbol{x}_j}\right| \leq \sum_{j=1}^N |w_j| \cdot \max_{\boldsymbol{k} \in \mathcal{I}_{\boldsymbol{M}}} 1 = \|\boldsymbol{w}\|_1,$$

and

$$\begin{aligned}\left\|\boldsymbol{A}^* \boldsymbol{W}\right\|_{\mathrm{F}} &= \sqrt{\sum_{\boldsymbol{k} \in \mathcal{I}_{\boldsymbol{M}}} \sum_{j=1}^N |w_j|^2 \cdot \left|\mathrm{e}^{-2\pi \mathrm{i} \boldsymbol{k} \boldsymbol{x}_j}\right|^2} \\ &\leq \sqrt{\sum_{j=1}^N |w_j|^2 \cdot |\mathcal{I}_{\boldsymbol{M}}|} = \sqrt{|\mathcal{I}_{\boldsymbol{M}}|} \cdot \|\boldsymbol{w}\|_2.\end{aligned}$$

Hence, from (3.20) – (3.23) and $\|\cdot\|_2 \leq \|\cdot\|_{\mathrm{F}}$ it follows that

$$\left\|\hat{\boldsymbol{f}} - \boldsymbol{A}^* \boldsymbol{W} \boldsymbol{f}\right\|_p \leq |\mathcal{I}_{\boldsymbol{M}}|\, \varepsilon \cdot \left\|\hat{\boldsymbol{f}}\right\|_p + \left\|\boldsymbol{A} \hat{\boldsymbol{f}} - \boldsymbol{f}\right\|_p \cdot |\mathcal{I}_{\boldsymbol{M}}|^{1/p}\, \|\boldsymbol{w}\|_q \qquad (3.24)$$

for $p \in \{1, 2, \infty\}$ with $\frac{1}{p} + \frac{1}{q} = 1$. Now it merely remains to estimate $\left\|\boldsymbol{A} \hat{\boldsymbol{f}} - \boldsymbol{f}\right\|_p$ for the specific choice of f.

(i): Since a trigonometric polynomial (2.8) of degree $\boldsymbol{M}$ satifies $\boldsymbol{A} \hat{\boldsymbol{f}} = \boldsymbol{f}$, the second term in (3.24) vanishes and we obtain the assertion (3.18).

(ii): When considering an arbitrary 1-periodic function given by (2.2) we have

$$\begin{aligned}\left|\left[\boldsymbol{A} \hat{\boldsymbol{f}} - \boldsymbol{f}\right]_j\right| &= \left|f(\boldsymbol{x}_j) - \sum_{\boldsymbol{k} \in \mathcal{I}_{\boldsymbol{M}}} c_{\boldsymbol{k}}(f)\, \mathrm{e}^{2\pi \mathrm{i} \boldsymbol{k} \boldsymbol{x}_j}\right| \\ &\leq \max_{\boldsymbol{x} \in \mathbb{T}^d} \left| \sum_{\boldsymbol{k} \in \mathbb{Z}^d \setminus \mathcal{I}_{\boldsymbol{M}}} c_{\boldsymbol{k}}(f)\, \mathrm{e}^{2\pi \mathrm{i} \boldsymbol{k} \boldsymbol{x}} \right| \\ &= \|f - p_{\boldsymbol{M}}\|_{C(\mathbb{T}^d)}, \quad j = 1, \dots, N,\end{aligned}$$

with the best approximating trigonometric polynomial $p_{\boldsymbol{M}}$ of de-

gree $\boldsymbol{M}$ of f. This yields $\left\|\boldsymbol{A}\hat{\boldsymbol{f}} - \boldsymbol{f}\right\|_p \leq N^{1/p} \left\|f - p_{\boldsymbol{M}}\right\|_{C(\mathbb{T}^d)}$ and by (3.24) the assertion (3.19). ∎

Remark 3.12. For the solution of (3.12) we consider the least squares solution with $\|\boldsymbol{w}\|_2 \to \min$, which is the straightforward approach. Note that since the error bound in Theorem 3.11 is based on the condition (3.17), it might be possible to obtain even better results by considering the constraints $\|\boldsymbol{w}\|_1 \to \min$ or $|\varepsilon_{\boldsymbol{k}}| < \varepsilon$, $\boldsymbol{k} \in \mathcal{I}_{\boldsymbol{2M}}$. However, these modifications are not addressed in this investigation and might be subject to further research. ◇

As known by Remark 3.7, an exact reconstruction (3.7) of trigonometric polynomials (2.8) is equivalent to the matrix product $\boldsymbol{A}^*\boldsymbol{W}\boldsymbol{A}$ being equal to identity $\boldsymbol{I}_{|\mathcal{I}_{\boldsymbol{M}}|}$. Note that there is a similar relation between the error of the reconstruction (3.5) and the error matrix $\boldsymbol{E}_{\mathrm{r}} = \boldsymbol{A}^*\boldsymbol{W}\boldsymbol{A} - \boldsymbol{I}_{|\mathcal{I}_{\boldsymbol{M}}|}$. More specifically, as an immediate implication of Theorem 3.11, the following estimate on the condition of the matrix $\boldsymbol{A}^*\boldsymbol{W}\boldsymbol{A}$ can be given, cf. [KP23a, Theorem 3.15].

Corollary 3.13. *Let $\boldsymbol{A} \in \mathbb{C}^{N\times|\mathcal{I}_{\boldsymbol{M}}|}$ in (2.7), $\boldsymbol{W} = \operatorname{diag}(w_j)_{j=1}^N$ and $\varepsilon \geq 0$ be given as in Theorem 3.11. If additionally $\varepsilon\,|\mathcal{I}_{\boldsymbol{M}}| < 1$ is fulfilled, this implies*

$$1 \leq \kappa_2(\boldsymbol{A}^*\boldsymbol{W}\boldsymbol{A}) \leq \frac{1+\varepsilon\,|\mathcal{I}_{\boldsymbol{M}}|}{1-\varepsilon\,|\mathcal{I}_{\boldsymbol{M}}|}$$

with the condition number $\kappa_2(\boldsymbol{X}) \coloneqq \|\boldsymbol{X}\|_2\|\boldsymbol{X}^{-1}\|_2$.

Proof. In order to estimate the condition number $\kappa_2(\boldsymbol{A}^*\boldsymbol{W}\boldsymbol{A})$ we need to determine the norms $\left\|\boldsymbol{A}^*\boldsymbol{W}\boldsymbol{A}\right\|_2$ and $\left\|(\boldsymbol{A}^*\boldsymbol{W}\boldsymbol{A})^{-1}\right\|_2$. To this end, we use the fact that by (3.17) it is known that $\boldsymbol{A}^*\boldsymbol{W}\boldsymbol{A} = \boldsymbol{I}_{|\mathcal{I}_{\boldsymbol{M}}|} + \boldsymbol{\mathcal{E}}$, where $\boldsymbol{\mathcal{E}} \coloneqq (\varepsilon_{\boldsymbol{\ell}-\boldsymbol{k}})_{\boldsymbol{\ell},\boldsymbol{k}\in\mathcal{I}_{\boldsymbol{M}}}$, and therefore we have

$$\left\|\boldsymbol{A}^*\boldsymbol{W}\boldsymbol{A}\right\|_2 = \left\|\boldsymbol{I}_{|\mathcal{I}_{\boldsymbol{M}}|} + \boldsymbol{\mathcal{E}}\right\|_2 \leq \left\|\boldsymbol{I}_{|\mathcal{I}_{\boldsymbol{M}}|}\right\|_2 + \|\boldsymbol{\mathcal{E}}\|_2. \tag{3.25}$$

Moreover, it is known by the theory of Neumann series, cf. [Ste98b, Theorem 4.20], that if $\left\|\boldsymbol{I}_{|\mathcal{I}_{\boldsymbol{M}}|} - \boldsymbol{T}\right\|_2 < 1$ holds for a matrix $\boldsymbol{T} \in \mathbb{C}^{|\mathcal{I}_{\boldsymbol{M}}|\times|\mathcal{I}_{\boldsymbol{M}}|}$, then $\boldsymbol{T}$ is invertible and its inverse is given by

$$\boldsymbol{T}^{-1} = \sum_{n=0}^{\infty} \left(\boldsymbol{I}_{|\mathcal{I}_{\boldsymbol{M}}|} - \boldsymbol{T}\right)^n.$$

Using this property for $\boldsymbol{T} = \boldsymbol{A}^*\boldsymbol{W}\boldsymbol{A}$ we have

$$\left\|(\boldsymbol{A}^*\boldsymbol{W}\boldsymbol{A})^{-1}\right\|_2 = \left\|\sum_{n=0}^{\infty}\left(\boldsymbol{I}_{|\mathcal{I}_{\boldsymbol{M}}|} - \boldsymbol{A}^*\boldsymbol{W}\boldsymbol{A}\right)^n\right\|_2 = \left\|\sum_{n=0}^{\infty}\boldsymbol{\mathcal{E}}^n\right\|_2 \leq \sum_{n=0}^{\infty}\|\boldsymbol{\mathcal{E}}^n\|_2\,, \tag{3.26}$$

in case that $\left\|\boldsymbol{I}_{|\mathcal{I}_{\boldsymbol{M}}|} - \boldsymbol{A}^*\boldsymbol{W}\boldsymbol{A}\right\|_2 = \|\boldsymbol{\mathcal{E}}\|_2 < 1$. Hence, by (3.25) and (3.26) we find

$$\kappa_2(\boldsymbol{A}^*\boldsymbol{W}\boldsymbol{A}) \leq (1 + \|\boldsymbol{\mathcal{E}}\|_2) \cdot \left(\sum_{n=0}^{\infty}\|\boldsymbol{\mathcal{E}}^n\|_2\right). \tag{3.27}$$

Additionally, we know that $|\varepsilon_{\boldsymbol{k}}| \leq \varepsilon$, $\boldsymbol{k} \in \mathcal{I}_{\boldsymbol{2M}}$, with some $\varepsilon \geq 0$, and therefore

$$\|\boldsymbol{\mathcal{E}}\|_2 \leq \|\boldsymbol{\mathcal{E}}\|_{\mathrm{F}} = \sqrt{\sum_{\boldsymbol{k}\in\mathcal{I}_{\boldsymbol{M}}}\sum_{\boldsymbol{\ell}\in\mathcal{I}_{\boldsymbol{M}}}|\varepsilon_{\boldsymbol{\ell}-\boldsymbol{k}}|^2} \leq \sqrt{\sum_{\boldsymbol{k}\in\mathcal{I}_{\boldsymbol{M}}}\sum_{\boldsymbol{\ell}\in\mathcal{I}_{\boldsymbol{M}}}\varepsilon^2} = \varepsilon\,|\mathcal{I}_{\boldsymbol{M}}|. \tag{3.28}$$

In other words, the correctness of (3.26) is ensured if $\varepsilon\,|\mathcal{I}_{\boldsymbol{M}}| < 1$. Since the spectral norm is a sub-multiplicative norm, the estimate (3.28) also implies $\|\boldsymbol{\mathcal{E}}^n\|_2 \leq \|\boldsymbol{\mathcal{E}}\|_2^n \leq (\varepsilon\,|\mathcal{I}_{\boldsymbol{M}}|)^n$. Consequently, we have by the geometric sum formula that

$$\sum_{n=0}^{\infty}\|\boldsymbol{\mathcal{E}}^n\|_2 \leq \sum_{n=0}^{\infty}(\varepsilon\,|\mathcal{I}_{\boldsymbol{M}}|)^n = \frac{1}{1-\varepsilon\,|\mathcal{I}_{\boldsymbol{M}}|}. \tag{3.29}$$

Thus, combining (3.27), (3.28) and (3.29) yields the assertion. ■

3.2.4 Linking to approaches in literature

In the literature a variety of density compensation approaches can be found. Although many of them use a variant of (3.5) incorporating the *sinc matrix*

$$\boldsymbol{C} \coloneqq \left(|\mathcal{I}_{\boldsymbol{M}}|\,\mathrm{sinc}\left(M\pi\left(\boldsymbol{x}_j - \boldsymbol{M}^{-1}\odot\boldsymbol{\ell}\right)\right)\right)_{j=1,\,\boldsymbol{\ell}\in\mathcal{I}_{\boldsymbol{M}}}^{N} \in \mathbb{R}^{N\times|\mathcal{I}_{\boldsymbol{M}}|} \tag{3.30}$$

with the *d-variate sinc function*

$$\mathrm{sinc}(\boldsymbol{x}) \coloneqq \prod_{t=1}^{d}\mathrm{sinc}(x_t), \quad \mathrm{sinc}(x) \coloneqq \begin{cases} \frac{\sin x}{x} & : x \in \mathbb{R}\setminus\{0\}, \\ 1 & : x = 0, \end{cases} \tag{3.31}$$

instead of the nonequispaced Fourier matrix $\boldsymbol{A} \in \mathbb{C}^{N \times |\mathcal{I}_M|}$ in (2.7), some of these approaches shall be reconsidered here using a unified optimization approach, cf. [EKP22]. Similar to [KP23a, Section 3.4] we focus in particular on the connection of the approaches among each other as well as to the method introduced in Section 3.2.1.

Density compensation using the pseudoinverse

Due to the fact that the inversion problem (3.3) is in general not exactly solvable, we study the corresponding *least squares* problem, i. e., we look for the approximant that minimizes the residual norm $\left\|\boldsymbol{f} - \boldsymbol{A}\hat{\boldsymbol{f}}\right\|_2$. It is known (e. g. [Bjö96, p. 15]) that this problem always has the unique solution

$$\hat{\boldsymbol{f}} \approx \tilde{\boldsymbol{h}}^{\mathrm{pinv}} \coloneqq \boldsymbol{A}^{\dagger}\boldsymbol{f} \tag{3.32}$$

with the *Moore-Penrose pseudoinverse* $\boldsymbol{A}^{\dagger} \in \mathbb{C}^{|\mathcal{I}_M| \times N}$. Since the pseudoinverse generally is a dense matrix, the evaluation of (3.32) is not computationally efficient. However, comparing (3.32) to the density compensation approach (3.5), the weights $w_j \in \mathbb{C}$, $j = 1, \dots, N$, should be chosen such that the matrix product $\boldsymbol{A}^*\boldsymbol{W}$ approximates the pseudoinverse $\boldsymbol{A}^{\dagger}$ as best as possible. In other words, we consider the approximation error

$$\left\|\boldsymbol{h}^{\mathrm{w}} - \tilde{\boldsymbol{h}}^{\mathrm{pinv}}\right\|_2^2 = \left\|\boldsymbol{A}^*\boldsymbol{W}\boldsymbol{f} - \boldsymbol{A}^{\dagger}\boldsymbol{f}\right\|_2^2 \leq \left\|\boldsymbol{A}^*\boldsymbol{W} - \boldsymbol{A}^{\dagger}\right\|_{\mathrm{F}}^2 \cdot \left\|\boldsymbol{f}\right\|_2^2,$$

and study the optimization problem

$$\underset{\boldsymbol{W} = \mathrm{diag}(w_j)_{j=1}^N}{\text{Minimize}} \left\|\boldsymbol{A}^*\boldsymbol{W} - \boldsymbol{A}^{\dagger}\right\|_{\mathrm{F}}^2. \tag{3.33}$$

Based on the definition of the Frobenius norm of a matrix and the Euclidean norm of a vector, we obtain for $\boldsymbol{z}_j \in \mathbb{C}^n$ being the columns of a matrix $\boldsymbol{Z} \in \mathbb{C}^{k \times n}$ that

$$\|\boldsymbol{Z}\|_F^2 = \sum_{i=1}^{k}\sum_{j=1}^{n} |z_{ij}|^2 = \sum_{j=1}^{n} \|\boldsymbol{z}_j\|_2^2. \tag{3.34}$$

Hence, we rewrite the norm of the error matrix $\boldsymbol{E} \coloneqq \boldsymbol{A}^*\boldsymbol{W} - \boldsymbol{A}^{\dagger} \in \mathbb{C}^{|\mathcal{I}_M| \times N}$ in (3.33) as

$$\|\boldsymbol{E}\|_{\mathrm{F}}^2 = \left\|\boldsymbol{A}^*\boldsymbol{W} - \boldsymbol{A}^{\dagger}\right\|_{\mathrm{F}}^2 = \sum_{j=1}^{N} \left\|\boldsymbol{A}^*\boldsymbol{w}_j - (\boldsymbol{A}^{\dagger})_j\right\|_2^2, \tag{3.35}$$

where the vectors $\boldsymbol{w}_j \in \mathbb{C}^N$ and $(\boldsymbol{A}^\dagger)_j \in \mathbb{C}^{|\mathcal{I}_M|}$ are the columns of the matrices $\boldsymbol{W} = \operatorname{diag}(w_j)_{j=1}^N \in \mathbb{C}^{N\times N}$ and $\boldsymbol{A}^\dagger \in \mathbb{C}^{|\mathcal{I}_M|\times N}$, respectively. Since we aim for a diagonal matrix $\boldsymbol{W}$, only the diagonal entries $w_j = [\boldsymbol{W}]_{j,j}$ shall be nonzero and therefore it suffices to consider only these entries. In doing so, we may rewrite (3.35) requiring only the j-th column $\boldsymbol{a}_j \in \mathbb{C}^{|\mathcal{I}_M|}$ of $\boldsymbol{A}^* \in \mathbb{C}^{|\mathcal{I}_M|\times N}$ as

$$\|\boldsymbol{E}\|_{\mathrm{F}}^2 = \sum_{j=1}^{N} \left\|\boldsymbol{a}_j w_j - (\boldsymbol{A}^\dagger)_j\right\|_2^2.$$

In other words, we found that the optimization problem (3.33) is equivalent to

$$\underset{w_j\in\mathbb{C}}{\text{Minimize}} \quad \left\|\boldsymbol{a}_j w_j - (\boldsymbol{A}^\dagger)_j\right\|_2^2, \quad j = 1,\dots,N.$$

The solution of these least-squares problems can be computed using the pseudoinverse as $w_j = \boldsymbol{a}_j^\dagger (\boldsymbol{A}^\dagger)_j \in \mathbb{C}$, and since the column vectors $\boldsymbol{a}_j \in \mathbb{C}^{|\mathcal{I}_M|}$ have full column rank, this can be written as

$$w_j = \left(\boldsymbol{a}_j^*\boldsymbol{a}_j\right)^{-1} \boldsymbol{a}_j^*(\boldsymbol{A}^\dagger)_j = \frac{[\boldsymbol{A}\boldsymbol{A}^\dagger]_{j,j}}{[\boldsymbol{A}\boldsymbol{A}^*]_{j,j}}, \quad j = 1,\dots N. \tag{3.36}$$

By (2.7) it is easy to see that for the denominators we have

$$[\boldsymbol{A}\boldsymbol{A}^*]_{j,j} = \sum_{\boldsymbol{k}\in\mathcal{I}_M} \mathrm{e}^{2\pi\mathrm{i}\boldsymbol{k}(\boldsymbol{x}_j - \boldsymbol{x}_j)} = |\mathcal{I}_{\boldsymbol{M}}|.$$

For the numerators we utilize the *singular value decomposition (SVD)* of the matrix $\boldsymbol{A} \in \mathbb{C}^{N\times|\mathcal{I}_M|}$ in (2.7), which is given by $\boldsymbol{A} = \boldsymbol{\Theta}\boldsymbol{\Sigma}\boldsymbol{\Omega}^*$ with unitary matrices $\boldsymbol{\Theta} \in \mathbb{C}^{N\times N}$, $\boldsymbol{\Omega} \in \mathbb{C}^{|\mathcal{I}_M|\times|\mathcal{I}_M|}$ and the rectangular diagonal matrix $\boldsymbol{\Sigma} \in \mathbb{R}^{N\times|\mathcal{I}_M|}$. Then the pseudoinverse $\boldsymbol{A}^\dagger$ possesses the factorization $\boldsymbol{A}^\dagger = \boldsymbol{\Omega}\boldsymbol{\Sigma}^\dagger\boldsymbol{\Theta}^*$, see e. g. [Bjö96, p. 15], such that for $r \coloneqq \operatorname{rank}(\boldsymbol{A})$ we may notate

$$\boldsymbol{A}\boldsymbol{A}^\dagger = (\boldsymbol{\Theta}\boldsymbol{\Sigma}\boldsymbol{\Omega}^*)(\boldsymbol{\Omega}\boldsymbol{\Sigma}^\dagger\boldsymbol{\Theta}^*) = \boldsymbol{\Theta}\boldsymbol{\Sigma}\boldsymbol{\Sigma}^\dagger\boldsymbol{\Theta}^* = \boldsymbol{\Theta}\begin{pmatrix} \boldsymbol{I}_r & \boldsymbol{0}_{r\times(N-r)} \\ \boldsymbol{0}_{(N-r)\times r} & \boldsymbol{0}_{N-r} \end{pmatrix}\boldsymbol{\Theta}^*. \tag{3.37}$$

An analogous approach for full column rank was studied in [SN00] considering the sinc matrix (3.30) instead of the nonequispaced Fourier

matrix $\boldsymbol{A}$ in (3.5). There it was claimed (without proof) that weights obtained by a scheme analogous to (3.36) are always positive. In order to show this, let $\boldsymbol{Z} \in \mathbb{C}^{k \times n}$ as well as $\boldsymbol{z}_j \in \mathbb{C}^k$ be the j-th column of $\boldsymbol{Z}$. Then we have

$$[\boldsymbol{Z}\boldsymbol{I}_n\, \boldsymbol{Z}^*]_{j,j} = \boldsymbol{z}_j \boldsymbol{z}_j^* = |z_{j,1}|^2 + \cdots + |z_{j,n}|^2 \geq 0.$$

Hence, choosing $n = r$ and $\boldsymbol{Z} = [\boldsymbol{\Theta}_t]_{t=1}^n$ for the numerator in (3.36), where $\boldsymbol{\Theta}_t \in \mathbb{C}^N$ is the t-th column of $\boldsymbol{\Theta} \in \mathbb{C}^{N \times N}$, yields the non-negativity of the weights computed by (3.36).

Nevertheless, it can be seen that the calculations in (3.36) are very costly due to the SVD, which is necessary to compute the numerators by (3.37). Since we end up lacking a fast computation technique for $\boldsymbol{A}\boldsymbol{A}^\dagger \in \mathbb{C}^{N \times N}$, we remain with the high complexity of $\mathcal{O}(N^2\,|\mathcal{I}_{\boldsymbol{M}}| + |\mathcal{I}_{\boldsymbol{M}}|^3)$. Moreover, to compute an SVD the matrix $\boldsymbol{A} \in \mathbb{C}^{N \times |\mathcal{I}_{\boldsymbol{M}}|}$ in (2.7) has to be assembled completely, which results in huge memory requirements for larger problems. Therefore, this density compensation technique is in general not feasible in practice, which is why we study some more sophisticated approaches in the remainder of this section.

Density compensation using weighted normal equations of first kind

Having a closer look at least squares problems, it is known, see e. g. [Bjö96, Theorem 1.1.2], that every least squares solution satisfies the weighted normal equations of first kind

$$\boldsymbol{A}^*\boldsymbol{W}\boldsymbol{A}\hat{\boldsymbol{f}} = \boldsymbol{A}^*\boldsymbol{W}\boldsymbol{f}. \tag{3.38}$$

We remark that a unique solution to (3.38) exists if and only if $\operatorname{rank}(\boldsymbol{A}) = |\mathcal{I}_{\boldsymbol{M}}|$, cf. [Bjö96, p. 7], i. e., if $\boldsymbol{A} \in \mathbb{C}^{N \times |\mathcal{I}_{\boldsymbol{M}}|}$ in (2.7) has full column rank. Note that by Remark 3.7 an exact reconstruction $\hat{\boldsymbol{f}} = \boldsymbol{A}^*\boldsymbol{W}\boldsymbol{f}$ is equivalent to $\boldsymbol{A}^*\boldsymbol{W}\boldsymbol{A} = \boldsymbol{I}_{|\mathcal{I}_{\boldsymbol{M}}|}$. We also recognize by (3.38) that one may try to find suitable weights by considering the optimization problem

$$\underset{\boldsymbol{W}=\operatorname{diag}(w_j)_{j=1}^N}{\text{Minimize}} \quad \left\|\boldsymbol{A}^*\boldsymbol{W}\boldsymbol{A} - \boldsymbol{I}_{|\mathcal{I}_{\boldsymbol{M}}|}\right\|_{\mathrm{F}}^2. \tag{3.39}$$

In other words, we look for the multilevel block Toeplitz matrix

$$\boldsymbol{A}^*\boldsymbol{W}\boldsymbol{A} = \left(\sum_{j=1}^N w_j\, \mathrm{e}^{-2\pi \mathrm{i}(\boldsymbol{k}-\boldsymbol{\ell})\boldsymbol{x}_j}\right)_{\boldsymbol{k},\boldsymbol{\ell} \in \mathcal{I}_{\boldsymbol{M}}}, \tag{3.40}$$

that approximates the identity best, and therefore yields the smallest reconstruction error in (3.5). Since $\operatorname{rank}(\boldsymbol{A}^*\boldsymbol{W}\boldsymbol{A}) = \operatorname{rank}(\boldsymbol{A}) \leq \min\{N, |\mathcal{I}_{\boldsymbol{M}}|\}$, we observe that we only receive a full-rank approximation if the condition $N \geq |\mathcal{I}_{\boldsymbol{M}}|$ is satisfied, i. e., if we are in the overdetermined setting of (3.3). Otherwise, when considering the underdetermined setting $N < |\mathcal{I}_{\boldsymbol{M}}|$ we can only expect rank-deficient approximations.

An analogous approach has already been studied in [Ros98, SN00], where the sinc matrix $\boldsymbol{C} \in \mathbb{R}^{N \times |\mathcal{I}_{\boldsymbol{M}}|}$ in (3.30) was used instead of the nonequispaced Fourier matrix $\boldsymbol{A} \in \mathbb{C}^{N \times |\mathcal{I}_{\boldsymbol{M}}|}$ in (2.7). By similar considerations as in [SN00] the optimization problem (3.39) could also be derived from (3.33) by introducing an additional right-hand scaling in the domain of measured data and minimizing the Frobenius norm of the weighted error matrix $\boldsymbol{E}_{\mathrm{r}} \coloneqq (\boldsymbol{E} \cdot \boldsymbol{A}) \in \mathbb{C}^{|\mathcal{I}_{\boldsymbol{M}}| \times |\mathcal{I}_{\boldsymbol{M}}|}$, where $\boldsymbol{E} = (\boldsymbol{A}^*\boldsymbol{W} - \boldsymbol{A}^\dagger) \in \mathbb{C}^{|\mathcal{I}_{\boldsymbol{M}}| \times N}$ is the error matrix in (3.33).

By inserting the equation (2.5) into the approximation (3.5), i. e., considering $\hat{\boldsymbol{f}} \approx \boldsymbol{h}^{\mathrm{w}} = \boldsymbol{A}^*\boldsymbol{W}\boldsymbol{f} = \boldsymbol{A}^*\boldsymbol{W}\boldsymbol{A}\hat{\boldsymbol{f}}$, we recognize that we can control the approximation error by

$$\left\|\boldsymbol{h}^{\mathrm{w}} - \hat{\boldsymbol{f}}\right\|_2^2 = \left\|\boldsymbol{A}^*\boldsymbol{W}\boldsymbol{A}\hat{\boldsymbol{f}} - \hat{\boldsymbol{f}}\right\|_2^2 \leq \left\|\boldsymbol{A}^*\boldsymbol{W}\boldsymbol{A} - \boldsymbol{I}_{|\mathcal{I}_{\boldsymbol{M}}|}\right\|_{\mathrm{F}}^2 \cdot \left\|\hat{\boldsymbol{f}}\right\|_2^2. \tag{3.41}$$

Thus, the minimization of the Frobenius norm as in (3.39) results in a decrease of the approximation error as well.

Obviously, the easiest choice for $\boldsymbol{W} \in \mathbb{C}^{N \times N}$ satisfying $\boldsymbol{A}^*\boldsymbol{W}\boldsymbol{A} \approx \boldsymbol{I}_{|\mathcal{I}_{\boldsymbol{M}}|}$ would be the dense pseudoinverse $\boldsymbol{W} = (\boldsymbol{A}^*)^\dagger\boldsymbol{A}^\dagger$. However, since the aim is achieving a diagonal matrix of weights, we have to search for the best diagonal approximation of this dense matrix. To this end, we rewrite the norm in (3.39) using (3.40), the Kronecker symbol $\delta_{\boldsymbol{k},\boldsymbol{\ell}}$ and the property (3.34) as

$$\begin{aligned}
&\left\|\boldsymbol{A}^*\boldsymbol{W}\boldsymbol{A} - \boldsymbol{I}_{|\mathcal{I}_{\boldsymbol{M}}|}\right\|_{\mathrm{F}}^2 \\
&\quad= \left\| \left(\sum_{j=1}^{N} w_j \, \mathrm{e}^{-2\pi\mathrm{i}(\boldsymbol{k}-\boldsymbol{\ell})\boldsymbol{x}_j} \right)_{\boldsymbol{k},\boldsymbol{\ell} \in \mathcal{I}_{\boldsymbol{M}}} - \left(\delta_{\boldsymbol{k},\boldsymbol{\ell}}\right)_{\boldsymbol{k},\boldsymbol{\ell} \in \mathcal{I}_{\boldsymbol{M}}} \right\|_{\mathrm{F}}^2 \\
&\quad= \sum_{\boldsymbol{\ell} \in \mathcal{I}_{\boldsymbol{M}}} \left\| \left(\mathrm{e}^{-2\pi\mathrm{i}(\boldsymbol{k}-\boldsymbol{\ell})\boldsymbol{x}_j} \right)_{\boldsymbol{k} \in \mathcal{I}_{\boldsymbol{M}},\, j=1}^{N} \cdot \left(w_j\right)_{j=1}^{N} - \left(\delta_{\boldsymbol{k},\boldsymbol{\ell}}\right)_{\boldsymbol{k} \in \mathcal{I}_{\boldsymbol{M}}} \right\|_2^2 \\
&\quad= \sum_{\boldsymbol{\ell} \in \mathcal{I}_{\boldsymbol{M}}} \left\|\boldsymbol{X}_{\boldsymbol{\ell}}\,\boldsymbol{w} - \boldsymbol{e}_{\boldsymbol{\ell}}\right\|_2^2,
\end{aligned} \tag{3.42}$$

where

$$\boldsymbol{X}_{\boldsymbol{\ell}} \coloneqq \left(\mathrm{e}^{-2\pi\mathrm{i}(\boldsymbol{k}-\boldsymbol{\ell})\boldsymbol{x}_j}\right)_{\boldsymbol{k}\in\mathcal{I}_{\boldsymbol{M}},\, j=1}^{N}, \quad \boldsymbol{w} \coloneqq (w_j)_{j=1}^{N}, \quad \boldsymbol{e}_{\boldsymbol{\ell}} \coloneqq (\delta_{\boldsymbol{k},\boldsymbol{\ell}})_{\boldsymbol{k}\in\mathcal{I}_{\boldsymbol{M}}}.$$

However, this formulation (3.42) is not separable for single $w_j \in \mathbb{C}$, $j = 1, \ldots, N$, and inconsistent solutions $\boldsymbol{w} \in \mathbb{C}^N$ may occur when separating for different $\boldsymbol{\ell} \in \mathcal{I}_{\boldsymbol{M}}$. To circumvent this issue, we reshape (3.42) by stacking into the highly overdetermined system

$$\sum_{\boldsymbol{\ell}\in\mathcal{I}_{\boldsymbol{M}}} \left\|\boldsymbol{X}_{\boldsymbol{\ell}}\,\boldsymbol{w} - \boldsymbol{e}_{\boldsymbol{\ell}}\right\|_2^2 = \left\|(\boldsymbol{X}_{\boldsymbol{\ell}})_{\boldsymbol{\ell}\in\mathcal{I}_{\boldsymbol{M}}} \cdot \boldsymbol{w} - (\boldsymbol{e}_{\boldsymbol{\ell}})_{\boldsymbol{\ell}\in\mathcal{I}_{\boldsymbol{M}}}\right\|_2^2,$$

where we used the property

$$\|\boldsymbol{y}_1\|_2^2 + \cdots + \|\boldsymbol{y}_n\|_2^2 = \left\|(\boldsymbol{y}_1 \ \cdots \ \boldsymbol{y}_n)^{\top}\right\|_2^2.$$

Thus, similar to [Ros98], the density compensation factors $\boldsymbol{w} \in \mathbb{C}^N$ can be found by solving the normal equations $\boldsymbol{S}\boldsymbol{w} = \boldsymbol{b}$, where by definition (2.7) we have

$$\boldsymbol{A}\boldsymbol{A}^* = \left(\sum_{\boldsymbol{k}\in\mathcal{I}_{\boldsymbol{M}}} \mathrm{e}^{2\pi\mathrm{i}\boldsymbol{k}(\boldsymbol{x}_j-\boldsymbol{x}_h)}\right)_{j,h=1}^{N}, \tag{3.43}$$

and therefore

$$\begin{aligned}
\boldsymbol{S} &\coloneqq ((\boldsymbol{X}_{\boldsymbol{\ell}})_{\boldsymbol{\ell}\in\mathcal{I}_{\boldsymbol{M}}})^* \cdot (\boldsymbol{X}_{\boldsymbol{\ell}})_{\boldsymbol{\ell}\in\mathcal{I}_{\boldsymbol{M}}} = \sum_{\boldsymbol{\ell}\in\mathcal{I}_{\boldsymbol{M}}} \boldsymbol{X}_{\boldsymbol{\ell}}^*\boldsymbol{X}_{\boldsymbol{\ell}} \\
&= \sum_{\boldsymbol{\ell}\in\mathcal{I}_{\boldsymbol{M}}} \left(\mathrm{e}^{2\pi\mathrm{i}(\boldsymbol{k}-\boldsymbol{\ell})\boldsymbol{x}_j}\right)_{j=1,\,\boldsymbol{k}\in\mathcal{I}_{\boldsymbol{M}}}^{N} \cdot \left(\mathrm{e}^{-2\pi\mathrm{i}(\boldsymbol{k}-\boldsymbol{\ell})\boldsymbol{x}_h}\right)_{\boldsymbol{k}\in\mathcal{I}_{\boldsymbol{M}},\, h=1}^{N} \\
&= \left(\left(\sum_{\boldsymbol{k}\in\mathcal{I}_{\boldsymbol{M}}} \mathrm{e}^{2\pi\mathrm{i}\boldsymbol{k}(\boldsymbol{x}_j-\boldsymbol{x}_h)}\right)\left(\sum_{\boldsymbol{\ell}\in\mathcal{I}_{\boldsymbol{M}}} \mathrm{e}^{-2\pi\mathrm{i}\boldsymbol{\ell}(\boldsymbol{x}_j-\boldsymbol{x}_h)}\right)\right)_{j,h=1}^{N} \\
&= \left(\left|[\boldsymbol{A}\boldsymbol{A}^*]_{j,h}\right|^2\right)_{j,h=1}^{N} \in \mathbb{R}^{N\times N}
\end{aligned} \tag{3.44}$$

as well as

$$\begin{aligned}
\boldsymbol{b} &\coloneqq ((\boldsymbol{X}_{\boldsymbol{\ell}})_{\boldsymbol{\ell}\in\mathcal{I}_{\boldsymbol{M}}})^* \cdot (\boldsymbol{e}_{\boldsymbol{\ell}})_{\boldsymbol{\ell}\in\mathcal{I}_{\boldsymbol{M}}} \\
&= \sum_{\boldsymbol{\ell}\in\mathcal{I}_{\boldsymbol{M}}} \boldsymbol{X}_{\boldsymbol{\ell}}^*\boldsymbol{e}_{\boldsymbol{\ell}} = \left(\sum_{\boldsymbol{\ell}\in\mathcal{I}_{\boldsymbol{M}}} \mathrm{e}^{0}\right)_{j=1}^{N} = |\mathcal{I}_{\boldsymbol{M}}| \cdot \boldsymbol{1}_N.
\end{aligned}$$

Nevertheless, these normal equations $\boldsymbol{S}\boldsymbol{w} = \boldsymbol{b}$ are still not separable for single $w_j \in \mathbb{C}$. Therefore, the solution $\boldsymbol{w} \in \mathbb{C}^N$ shall be computed iteratively by means of the CG algorithm, which is of high complexity $\mathcal{O}(N^3)$. Analogous to Section 3.2.4, there is also the problem of memory requirement for assembling huge matrices. This is why the authors in [SN00] restricted themselves to a maximal image size of 64×64 pixels, which corresponds to setting $\boldsymbol{M} = (64, 64)^\top$.

Remark 3.14. The CG algorithm requires a symmetric, positive semidefinite system matrix. Obviously, the symmetry property is fulfilled for $\boldsymbol{S} \in \mathbb{R}^{N \times N}$ in (3.44). In order to show that $\boldsymbol{S}$ is also positive semidefinite, we use the Schur product theorem, see [HJ13, Theorem. 7.5.3]. This theorem states that for two positive semidefinite matrices $\boldsymbol{P}, \boldsymbol{R} \in \mathbb{C}^{k \times n}$ the elementwise product, also called *Hadamard product*,

$$[\boldsymbol{P} \circ \boldsymbol{R}]_{j,h} \coloneqq p_{j,h} \cdot r_{j,h}$$

is positive semidefinite as well. Therefore, let $\boldsymbol{P} \coloneqq \boldsymbol{A}\boldsymbol{A}^* \in \mathbb{C}^{N \times N}$ and $\boldsymbol{R} \coloneqq \overline{\boldsymbol{A}\boldsymbol{A}^*} \in \mathbb{C}^{N \times N}$. Since a matrix is positive semidefinite if and only if it can be decomposed as a product of a matrix and its adjoint, cf. [HJ13, Theorem 7.2.7], both matrices are positive semidefinite. Moreover, we have

$$[\boldsymbol{S}]_{j,h} = [\boldsymbol{P} \circ \boldsymbol{R}]_{j,h} = [\boldsymbol{A}\boldsymbol{A}^*]_{j,h} \cdot \overline{[\boldsymbol{A}\boldsymbol{A}^*]}_{j,h} = \left|[\boldsymbol{A}\boldsymbol{A}^*]_{j,h}\right|^2,$$

such that $\boldsymbol{S} \in \mathbb{R}^{N \times N}$ is positive semidefinite as well. ◇

We notice that for the normal equations $\boldsymbol{S}\boldsymbol{w} = \boldsymbol{b}$ we have $\boldsymbol{S} \in \mathbb{R}^{N \times N}$ as well as $\boldsymbol{b} \in \mathbb{R}^N$, and therefore $\boldsymbol{w} \in \mathbb{R}^N$, whereas non-negativity cannot be guaranteed.

Remark 3.15. Since the high complexity in the computation of the weights $\boldsymbol{w} \in \mathbb{C}^N$ by $\boldsymbol{S}\boldsymbol{w} = \boldsymbol{b}$ arises from solving with the system matrix $\boldsymbol{S}$, we investigate if the multiplication with the matrix $\boldsymbol{S} \in \mathbb{R}^{N \times N}$ in (3.44) could be improved by means of the NFFT from Section 2.2. To this end, note that by (3.44) we have

$$[\boldsymbol{S}]_{j,h} = \sum_{\boldsymbol{k} \in \mathcal{I}_{\boldsymbol{M}}} \sum_{\boldsymbol{\ell} \in \mathcal{I}_{\boldsymbol{M}}} \mathrm{e}^{2\pi \mathrm{i}(\boldsymbol{k}(\boldsymbol{x}_j - \boldsymbol{x}_h) + \boldsymbol{\ell}(\boldsymbol{x}_h - \boldsymbol{x}_j))} = \sum_{\boldsymbol{s} \in \mathcal{I}_{\boldsymbol{M}}^{2d}} \mathrm{e}^{2\pi \mathrm{i} \boldsymbol{s}(\boldsymbol{y}_j - \boldsymbol{y}_h)},$$

where we introduced the double-length vectors

$$\boldsymbol{s} \coloneqq \begin{pmatrix} \boldsymbol{k} \\ \boldsymbol{\ell} \end{pmatrix} \in \mathbb{R}^{2d}, \quad \boldsymbol{y}_j \coloneqq \begin{pmatrix} \boldsymbol{x}_j \\ -\boldsymbol{x}_j \end{pmatrix} \in \mathbb{R}^{2d} \quad \text{and} \quad \boldsymbol{y}_h \coloneqq \begin{pmatrix} \boldsymbol{x}_h \\ -\boldsymbol{x}_h \end{pmatrix} \in \mathbb{R}^{2d}.$$

Hence, the multiplication of $\boldsymbol{S} \in \mathbb{R}^{N \times N}$ with a vector $\boldsymbol{v} \in \mathbb{C}^N$ can be written as

$$[\boldsymbol{S}\boldsymbol{v}]_j = \sum_{h=1}^{N} v_h \sum_{\boldsymbol{t} \in \mathcal{I}_{\boldsymbol{M}}^{2d}} \mathrm{e}^{2\pi \mathrm{i} \boldsymbol{s}(\boldsymbol{y}_j - \boldsymbol{y}_h)} = \sum_{\boldsymbol{t} \in \mathcal{I}_{\boldsymbol{M}}^{2d}} \mathrm{e}^{2\pi \mathrm{i} \boldsymbol{s} \boldsymbol{y}_j} \left(\sum_{h=1}^{N} v_h \, \mathrm{e}^{-2\pi \mathrm{i} \boldsymbol{s} \boldsymbol{y}_h} \right), \tag{3.45}$$

with the $2d$-dimensional multi-index set

$$\begin{aligned} \mathcal{I}_{\boldsymbol{M}}^{2d} &\coloneqq \mathbb{Z}^{2d} \cap \prod_{t=1}^{2d} \left[-\tfrac{M_t}{2}, \tfrac{M_t}{2} \right) \\ &= \left\{ \boldsymbol{k} \in \mathbb{Z}^{2d} \colon \, -\tfrac{M_t}{2} \leq k_t < \tfrac{M_t}{2}, \, t = 1, \ldots, 2d \right\}, \end{aligned}$$

cf. (2.1). In other words, the inner sum in (3.45) corresponds to a $2d$-dimensional adjoint NFFT and the outer sum to a $2d$-dimensional NFFT. Therefore, the multiplication of the matrix $\boldsymbol{S} \in \mathbb{R}^{N \times N}$ by a vector $\boldsymbol{v} \in \mathbb{C}^N$ is of arithmetic complexity

$$\mathcal{O}(|\mathcal{I}_{\boldsymbol{M}}^{2d}| \log(|\mathcal{I}_{\boldsymbol{M}}^{2d}|) + N) = \mathcal{O}(|\mathcal{I}_{\boldsymbol{M}}|^2 \log(|\mathcal{I}_{\boldsymbol{M}}|) + N).$$

For computing a solution to the system $\boldsymbol{S}\boldsymbol{w} = \boldsymbol{b}$ this technique would need to be incorporated into an iterative procedure such as the CG algorithm, i. e., multiple iteration steps and therefore multiple applications of the $2d$-dimensional NFFT are needed. Note, however, that the NFFT is only feasible for small dimensions $d \in \{1, 2, 3\}$, such that this approach is already not applicable for $d = 2$ since the 4-dimensional NFFT quickly becomes unaffordable, while for $d = 1$ it only pays off for very large problem sizes, where the naive computation fails due to memory limitations. Thus, this technique can be helpful as it may enable the computation of the weights when this is not possible otherwise, even though this technique is still costly. ◇

Density compensation using weighted normal equations of second kind

Another approach for density compensation factors is based on the weighted normal equations of second kind

$$\boldsymbol{A}\boldsymbol{A}^*\boldsymbol{W}\boldsymbol{y} = \boldsymbol{f}, \quad \boldsymbol{A}^*\boldsymbol{W}\boldsymbol{y} = \hat{\boldsymbol{f}}. \tag{3.46}$$

We remark that there exists a unique solution to (3.46) if and only if $\operatorname{rank}(\boldsymbol{A}) = N$, i. e., if $\boldsymbol{A} \in \mathbb{C}^{N \times |\mathcal{I}_{\boldsymbol{M}}|}$ in (2.7) has full row rank, cf. [Bjö96, p. 7].

In order to achieve an approximation $\hat{\boldsymbol{f}} \approx \boldsymbol{A}^*\boldsymbol{W}\boldsymbol{f}$ of the Fourier coefficients as in (3.5), we recognize by (3.46) that we need to fulfill $\boldsymbol{A}\boldsymbol{A}^*\boldsymbol{W} \approx \boldsymbol{I}_N$, since then $\boldsymbol{y} \approx \boldsymbol{f}$. To achieve this, we consider the optimization problem

$$\underset{\boldsymbol{W}=\operatorname{diag}(w_j)_{j=1}^N}{\text{Minimize}} \quad \|\boldsymbol{A}\boldsymbol{A}^*\boldsymbol{W} - \boldsymbol{I}_N\|_{\mathrm{F}}^2. \tag{3.47}$$

Since $\operatorname{rank}(\boldsymbol{A}\boldsymbol{A}^*\boldsymbol{W}) = \operatorname{rank}(\boldsymbol{A}) \leq \min\{N, |\mathcal{I}_{\boldsymbol{M}}|\}$, we observe that we only receive a full-rank approximation, if the condition $N \leq |\mathcal{I}_{\boldsymbol{M}}|$ is satisfied, i. e., if we are in the underdetermined setting of (3.3). Otherwise, when considering the overdetermined setting $N > |\mathcal{I}_{\boldsymbol{M}}|$ we can only expect rank-deficient approximations. As in Section 3.2.4, we remark that the optimization problem (3.47) could also be derived from (3.33) by introducing an additional left-hand scaling in the Fourier domain and minimizing the Frobenius norm of the weighted error matrix $\boldsymbol{E}_{\mathrm{l}} \coloneqq (\boldsymbol{A} \cdot \boldsymbol{E}) \in \mathbb{C}^{N \times N}$.

Remark 3.16. An analogous approach was already studied in [PM99], considering the sinc matrix $\boldsymbol{C} \in \mathbb{R}^{N \times |\mathcal{I}_{\boldsymbol{M}}|}$ in (3.30) instead of the nonequispaced Fourier matrix $\boldsymbol{A} \in \mathbb{C}^{N \times |\mathcal{I}_{\boldsymbol{M}}|}$ in (2.7). Another version of a sinc matrix was studied in [CM98, GLI06], cf. Section 6.1.2, where it was claimed that this approach coincides with the one in [PM99]. However, we will show in Remark 6.3 that this claim only holds asymptotically for $|\mathcal{I}_{\boldsymbol{M}}| \to \infty$ in the setting of the sinc matrix (3.30).

In contrast, when using the nonequispaced Fourier matrix $\boldsymbol{A} \in \mathbb{C}^{N \times |\mathcal{I}_{\boldsymbol{M}}|}$ in (2.7) this equality can directly be seen. In this case, the analog to [GLI06] utilizes an approximation of the form $\boldsymbol{f} \approx \boldsymbol{H}\boldsymbol{W}\boldsymbol{f}$, where the matrix $\boldsymbol{H} \in \mathbb{C}^{N \times N}$ is defined as the system matrix of (3.3) evaluated at pointwise differences of the nonequispaced nodes, i. e.,

$$\boldsymbol{H} \coloneqq \left(\sum_{\boldsymbol{k} \in \mathcal{I}_{\boldsymbol{M}}} \mathrm{e}^{2\pi \mathrm{i} \boldsymbol{k}(\boldsymbol{x}_j - \boldsymbol{x}_h)} \right)_{j,h=1}^{N}.$$

Since $\boldsymbol{H} = \boldsymbol{A}\boldsymbol{A}^*$ by (3.43), we recognize that considering the minimization of the approximation error

$$\|\boldsymbol{H}^*\boldsymbol{W}\boldsymbol{f} - \boldsymbol{f}\|_2^2 = \|\boldsymbol{A}\boldsymbol{A}^*\boldsymbol{W}\boldsymbol{f} - \boldsymbol{f}\|_2^2 \leq \|\boldsymbol{A}\boldsymbol{A}^*\boldsymbol{W} - \boldsymbol{I}_N\|_{\mathrm{F}}^2 \cdot \|\boldsymbol{f}\|_2^2,$$

leads to the optimization problem (3.47) as well. ◇

Remark 3.17. Note that by left-hand multiplication with $\boldsymbol{A} \in \mathbb{C}^{N \times |\mathcal{I}_M|}$ in (2.7) and insertion of (3.3), an exact reconstruction of the form (3.7) immediately implies

$$\boldsymbol{f} = \boldsymbol{A}\hat{\boldsymbol{f}} = \boldsymbol{A}\boldsymbol{A}^*\boldsymbol{W}\boldsymbol{f},$$

and thereby the property $\boldsymbol{A}\boldsymbol{A}^*\boldsymbol{W} = \boldsymbol{I}_N$. However, in constrast to Remark 3.7 these two properties are not equivalent, since $\boldsymbol{A}\boldsymbol{A}^*\boldsymbol{W} = \boldsymbol{I}_N$ does not imply an exact reconstruction of the form $\hat{\boldsymbol{f}} = \boldsymbol{A}^*\boldsymbol{W}\boldsymbol{f}$. ◇

Obviously, the easiest choice for $\boldsymbol{W} \in \mathbb{C}^{N \times N}$ satisfying $\boldsymbol{A}\boldsymbol{A}^*\boldsymbol{W} \approx \boldsymbol{I}_N$ would be the dense pseudoinverse $\boldsymbol{W} = (\boldsymbol{A}\boldsymbol{A}^*)^\dagger$. However, since we aim for a diagonal matrix of weights, we have to search for the best diagonal approximation of this dense matrix. In other words, since only the diagonal entries $w_j = [\boldsymbol{W}]_{j,j}$ of $\boldsymbol{W}$ are nonzero, we may rewrite (3.47) only considering the j-th column of $\boldsymbol{A}\boldsymbol{A}^* \in \mathbb{C}^{N \times N}$. For this purpose we denote the j-th column of $\boldsymbol{A}^* \in \mathbb{C}^{|\mathcal{I}_M| \times N}$ once more as $\boldsymbol{a}_j \in \mathbb{C}^{|\mathcal{I}_M|}$ as well as the columns of $\boldsymbol{W}$ and $\boldsymbol{I}_N$ as $\boldsymbol{w}_j \in \mathbb{C}^N$ and $\boldsymbol{e}_j \in \mathbb{R}^N$, respectively. Then we have by (3.34) that

$$\|\boldsymbol{A}\boldsymbol{A}^*\boldsymbol{W} - \boldsymbol{I}_N\|_{\mathrm{F}}^2 = \sum_{j=1}^{N} \|\boldsymbol{A}\boldsymbol{A}^*\boldsymbol{w}_j - \boldsymbol{e}_j\|_2^2 = \sum_{j=1}^{N} \|\boldsymbol{A}\boldsymbol{a}_j w_j - \boldsymbol{e}_j\|_2^2,$$

such that the solution to the minimization problem can be computed using the pseudoinverse as $w_j = (\boldsymbol{A}\boldsymbol{a}_j)^\dagger \boldsymbol{e}_j \in \mathbb{C}$, $j = 1, \ldots, N$. Since

$$\begin{aligned}\boldsymbol{A}\boldsymbol{a}_j &= \left(\mathrm{e}^{2\pi \mathrm{i} \boldsymbol{k}\boldsymbol{x}_h}\right)_{h=1,\, \boldsymbol{k} \in \mathcal{I}_M}^{N} \cdot \left(\mathrm{e}^{-2\pi \mathrm{i} \boldsymbol{k}\boldsymbol{x}_j}\right)_{\boldsymbol{k} \in \mathcal{I}_M} \\ &= \left(\sum_{\boldsymbol{k} \in \mathcal{I}_M} \mathrm{e}^{-2\pi \mathrm{i} \boldsymbol{k}(\boldsymbol{x}_j - \boldsymbol{x}_h)} \right)_{h=1}^{N} \in \mathbb{C}^N\end{aligned}$$

as a vector has full column rank, these weights can be written as $w_j = \left((\boldsymbol{A}\boldsymbol{a}_j)^* \boldsymbol{A}\boldsymbol{a}_j\right)^{-1} (\boldsymbol{A}\boldsymbol{a}_j)^* \boldsymbol{e}_j$. Similar to (3.44) this can be simplified

via

$$\begin{aligned}(\boldsymbol{A}\boldsymbol{a}_j)^*\boldsymbol{A}\boldsymbol{a}_j &= \left(\left(\sum_{\boldsymbol{k}\in\mathcal{I}_{\boldsymbol{M}}} \mathrm{e}^{2\pi\mathrm{i}\boldsymbol{k}(\boldsymbol{x}_j-\boldsymbol{x}_h)}\right)_{h=1}^{N}\right)^{\top}\left(\sum_{\boldsymbol{\ell}\in\mathcal{I}_{\boldsymbol{M}}} \mathrm{e}^{-2\pi\mathrm{i}\boldsymbol{\ell}(\boldsymbol{x}_j-\boldsymbol{x}_h)}\right)_{h=1}^{N} \\ &= \sum_{h=1}^{N}\left(\sum_{\boldsymbol{k}\in\mathcal{I}_{\boldsymbol{M}}} \mathrm{e}^{2\pi\mathrm{i}\boldsymbol{k}(\boldsymbol{x}_j-\boldsymbol{x}_h)}\right)\left(\sum_{\boldsymbol{\ell}\in\mathcal{I}_{\boldsymbol{M}}} \mathrm{e}^{-2\pi\mathrm{i}\boldsymbol{\ell}(\boldsymbol{x}_j-\boldsymbol{x}_h)}\right) \\ &= \sum_{h=1}^{N}\left|\left[\boldsymbol{A}\boldsymbol{A}^*\right]_{j,h}\right|^2\end{aligned}$$

and

$$(\boldsymbol{A}\boldsymbol{a}_j)^*\boldsymbol{e}_j = \sum_{h=1}^{N}\delta_{j,h}\sum_{\boldsymbol{k}\in\mathcal{I}_{\boldsymbol{M}}} \mathrm{e}^{-2\pi\mathrm{i}\boldsymbol{k}(\boldsymbol{x}_j-\boldsymbol{x}_h)} = \sum_{\boldsymbol{k}\in\mathcal{I}_{\boldsymbol{M}}} \mathrm{e}^{0} = |\mathcal{I}_{\boldsymbol{M}}|,$$

such that we obtain

$$w_j = \frac{|\mathcal{I}_{\boldsymbol{M}}|}{\sum_{h=1}^{N}\left|\left[\boldsymbol{A}\boldsymbol{A}^*\right]_{j,h}\right|^2}, \quad j = 1,\dots,N. \tag{3.48}$$

Note that in (3.48) we only deal with the nonnegative numbers $|\mathcal{I}_{\boldsymbol{M}}|$ and $\left|\left[\boldsymbol{A}\boldsymbol{A}^*\right]_{j,h}\right|^2$, $j,h = 1,\dots,N$, such that w_j in (3.48) are nonnegative for all $j = 1,\dots,N$.

Due to the representation (3.43), the computation of $\left[\boldsymbol{A}\boldsymbol{A}^*\right]_{j,h}$, $h = 1,\dots,N$, for fixed j is of arithmetic complexity $\mathcal{O}(N\cdot|\mathcal{I}_{\boldsymbol{M}}|)$, such that the overall complexity for the naive computation of the weights (3.48) is given by $\mathcal{O}(N^2\cdot|\mathcal{I}_{\boldsymbol{M}}|)$.

Remark 3.18. Similar to Remark 3.15 one might also try to incorporate the NFFT from Section 2.2 for the computation of (3.48). On the one hand, one could apply an NFFT for the computation of $\left[\boldsymbol{A}\boldsymbol{A}^*\right]_{j,h}$, $h = 1,\dots,N$, for fixed j, such that this step takes $\mathcal{O}(|\mathcal{I}_{\boldsymbol{M}}|\log(|\mathcal{I}_{\boldsymbol{M}}|)+N)$ arithmetic operations and the overall complexity is given by $\mathcal{O}(N\cdot|\mathcal{I}_{\boldsymbol{M}}|\log(|\mathcal{I}_{\boldsymbol{M}}|)+N^2)$. On the other hand, one could use the procedure in (3.45) with $\boldsymbol{v} = \boldsymbol{1}_N$ yielding the complexity $\mathcal{O}(|\mathcal{I}_{\boldsymbol{M}}^{2d}|\log(|\mathcal{I}_{\boldsymbol{M}}^{2d}|)+N) = \mathcal{O}(|\mathcal{I}_{\boldsymbol{M}}|^2\log(|\mathcal{I}_{\boldsymbol{M}}|)+N)$. However, a similar comment as in Remark 3.15 applies to this second method, as it is not applicable for $d = 2$ and for $d = 1$ it is only beneficial for very large problem sizes with $N \geq 40000$. ◇

As mentioned in [PM99] one could also consider a simplified version of the optimization problem (3.47) by reducing the number of conditions, e. g. by summing the columns on both sides of $\boldsymbol{A}\boldsymbol{A}^*\boldsymbol{W} = \boldsymbol{I}_N$ as

$$\sum_{j=1}^{N} w_j \sum_{\boldsymbol{k}\in\mathcal{I}_{\boldsymbol{M}}} \mathrm{e}^{2\pi\mathrm{i}\boldsymbol{k}(\boldsymbol{x}_h-\boldsymbol{x}_j)} = \sum_{j=1}^{N} \delta_{j,h} = 1, \quad h = 1,\dots,N.$$

By means of (3.43) this can be written as

$$\boldsymbol{A}\boldsymbol{A}^*\boldsymbol{w} = \boldsymbol{1}_N. \tag{3.49}$$

Note that due to the summation over the columns every solution $\boldsymbol{W} = \operatorname{diag}(\boldsymbol{w}) = \operatorname{diag}(w_j)_{j=1}^N$ of the original problem $\boldsymbol{A}\boldsymbol{A}^*\boldsymbol{W} = \boldsymbol{I}_N$ also solves the relaxed problem (3.49), while the reversal only holds true, if the matrix $\boldsymbol{A}\boldsymbol{A}^* \in \mathbb{C}^{N\times N}$ is diagonal.

Since a fast multiplication with $\boldsymbol{A}\boldsymbol{A}^*$ can easily be realized by applying an adjoint NFFT (see Algorithm 2.5) and an NFFT (see Algorithm 2.2) afterwards, a solution to problem (3.49) can be computed by means of an iterative procedure such as the CG algorithm in $\mathcal{O}(|\mathcal{I}_{\boldsymbol{M}}|\log(|\mathcal{I}_{\boldsymbol{M}}|) + N)$ arithmetic operations.

Remark 3.19. Finally, we investigate the connection of this approach to the method introduced in Section 3.2.1. To this end, assume that the linear system (3.9) is fulfilled with exactness for given $\boldsymbol{w} \in \mathbb{C}^N$, i. e., by $\boldsymbol{A}^* = \overline{\boldsymbol{A}^\top}$ we have $(\delta_{\boldsymbol{0},\boldsymbol{k}})_{\boldsymbol{k}\in\mathcal{I}_{\boldsymbol{M}}} = \overline{\boldsymbol{A}^\top\boldsymbol{w}} = \boldsymbol{A}^*\overline{\boldsymbol{w}}$. Then left-hand multiplication with $\boldsymbol{A} \in \mathbb{C}^{N\times|\mathcal{I}_{\boldsymbol{M}}|}$ in (2.7) yields

$$\boldsymbol{A}\boldsymbol{A}^*\overline{\boldsymbol{w}} = \boldsymbol{A}\cdot(\delta_{\boldsymbol{0},\boldsymbol{k}})_{\boldsymbol{k}\in\mathcal{I}_{\boldsymbol{M}}} = \left(\sum_{\boldsymbol{k}\in\mathcal{I}_{\boldsymbol{M}}} \delta_{\boldsymbol{0},\boldsymbol{k}}\cdot\mathrm{e}^{2\pi\mathrm{i}\boldsymbol{k}\boldsymbol{x}_j}\right)_{j=1}^{N} = \boldsymbol{1}_N.$$

In other words, an exact solution $\boldsymbol{w}$ to the linear system (3.9) implies that the conjugate complex weights $\overline{\boldsymbol{w}}$ exactly solve the system (3.49). However, the reversal does not hold true and therefore (3.49) is not equivalent to (3.9). Moreover, we have seen in Theorem 3.6 that an augmented variant of (3.9), namely (3.12), is necessary to obtain an exact reconstruction $\hat{f}_{\boldsymbol{k}} = h^{\mathrm{w}}_{\boldsymbol{k}}$ in (3.5) for trigonometric polynomials (2.8) of maximum degree $\boldsymbol{M}$, which is why this relaxation approach is not expected to work properly. ◇

Summary

Overall, in this section a broad variety of density compensation approaches has been presented. For a comparison of the mentioned methods, we refer to the numerical examples in Section 3.4. More specifically, in Example 3.32 we investigate the accuracy of the density compensation method from Algorithm 3.2 with the weights computed by Algorithm 3.10 and check the theoretical error bound of Theorem 3.11. In addition, a comparison with the approaches of Section 3.2.4 is shown in Example 3.33, i. e., the weights computed by means of Algorithm 3.10 are compared to the approaches from Section 3.2.4 for using Algorithm 3.2.

In summary, we will see the optimality of the weights computed by means of Algorithm 3.10 for the setting $|\mathcal{I}_{\boldsymbol{2M}}| \leq N$, cf. Figure 3.6. However, in the setting $|\mathcal{I}_{\boldsymbol{2M}}| > N$ we will see that Algorithm 3.10 is not capable of producing a good reconstruction. In this setting the weights computed using (3.44) and (3.48), respectively, appear to be more promising, cf. Figures 3.8d and 3.8e. Nevertheless, we have to keep in mind that comparatively small choices of M are necessary for these methods to be computationally affordable, see Remarks 3.15 and 3.18.

3.3 Optimization of the sparse matrix B

As observed in Remark 3.3, the density compensation techniques studied so far can be viewed as an optimization of the sparse matrix $\boldsymbol{B} \in \mathbb{R}^{N \times |\mathcal{I}_{\boldsymbol{M}_\sigma}|}$ in (2.16) from the NFFT decomposition, see Section 2.2. However, since density compensation presumably suffers from the fact that only N degrees of freedom are used, this restriction shall now be relaxed, i. e., instead of searching for optimal scaling factors for the rows of $\boldsymbol{B}$, we now study the optimization of each nonzero entry of the sparse matrix $\boldsymbol{B}$, as introduced in [KP21, KP23a]. More precisely, we aim to modify the matrix $\boldsymbol{B}$ such that its sparse structure with at most $(2m+1)^d$ entries per row and consequently the arithmetic complexity of its application to a vector is preserved. Note that a matrix satisfying this property we call $(2m+1)^d$-*sparse*.

To this end, this section is organized as follows. Firstly, in Section 3.3.1 we introduce the Frobenius norm minimization problem and the resulting modified matrix $\boldsymbol{B}_{\text{opt}}$. In addition to the theoretical results, we also discuss methods for the numerical computation in Section 3.3.2. Subsequently, in Section 3.3.3 we present an error bound on the approximation error

based on the previously considered optimization approach. Finally, in Section 3.3.4 we reconsider certain approaches from literature and illustrate their connection to the method in Section 3.3.1.

3.3.1 Frobenius norm minimization

Let $\tilde{\boldsymbol{B}} \in \mathbb{R}^{N \times |\mathcal{I}_{M_\sigma}|}$ be a $(2m+1)^d$-sparse matrix. By defining the approximation $\tilde{\boldsymbol{h}} \coloneqq \boldsymbol{D}^* \boldsymbol{F}^* \tilde{\boldsymbol{B}}^* \boldsymbol{f}$ and inserting (3.3), we recognize that the minimization of the approximation error

$$\begin{aligned} \left\|\tilde{\boldsymbol{h}} - \hat{\boldsymbol{f}}\right\|_2 &= \left\|\boldsymbol{D}^* \boldsymbol{F}^* \tilde{\boldsymbol{B}}^* \boldsymbol{f} - \hat{\boldsymbol{f}}\right\|_2 = \left\|\boldsymbol{D}^* \boldsymbol{F}^* \tilde{\boldsymbol{B}}^* \boldsymbol{A} \hat{\boldsymbol{f}} - \hat{\boldsymbol{f}}\right\|_2 \\ &= \left\|\left(\boldsymbol{D}^* \boldsymbol{F}^* \tilde{\boldsymbol{B}}^* \boldsymbol{A} - \boldsymbol{I}_{|\mathcal{I}_M|}\right) \hat{\boldsymbol{f}}\right\|_2 \\ &\leq \left\|\boldsymbol{D}^* \boldsymbol{F}^* \tilde{\boldsymbol{B}}^* \boldsymbol{A} - \boldsymbol{I}_{|\mathcal{I}_M|}\right\|_{\mathrm{F}} \left\|\hat{\boldsymbol{f}}\right\|_2 \end{aligned} \tag{3.50}$$

implies the optimization problem

$$\underset{\tilde{\boldsymbol{B}} \in \mathbb{R}^{N \times |\mathcal{I}_{M_\sigma}|} :\, \tilde{\boldsymbol{B}}\ (2m+1)^d\text{-sparse}}{\text{Minimize}} \left\|\boldsymbol{D}^* \boldsymbol{F}^* \tilde{\boldsymbol{B}}^* \boldsymbol{A} - \boldsymbol{I}_{|\mathcal{I}_M|}\right\|_{\mathrm{F}}^2. \tag{3.51}$$

Note that a similar approach for the one-dimensional setting was firstly explored in [KP19], while a similar idea for the forward problem, i. e., the evaluation of (2.5), was already studied in [NS03].

Remark 3.20. We remark that in (3.50) we estimated the Euclidean vector norm $\|\cdot\|_2$ not by its induced matrix norm $\|\boldsymbol{Z}\|_2 = \sigma_{\max}(\boldsymbol{Z})$, where $\sigma_{\max}(\boldsymbol{Z})$ denotes the largest singular value of a matrix $\boldsymbol{Z} \in \mathbb{C}^{k \times n}$, but by means of the consistent Frobenius norm $\|\cdot\|_{\mathrm{F}}$. This is mainly due to the expensive computation of this so-called *spectral norm* $\|\cdot\|_2$ and the fact that we especially target our minimization to the sparse structure of the matrix $\boldsymbol{B}$, which is hard to implement for the spectral norm as well.

However, note that for the Frobenius norm (3.34) we are given the equivalent characterization by the *Schatten 2-norm* as

$$\|\boldsymbol{Z}\|_{\mathrm{F}} = \left(\sum_{j=1}^{\min\{k,n\}} \sigma_j(\boldsymbol{Z})^2 \right)^{\frac{1}{2}},$$

cf. e. g. [Bjö96, pp. 25]. Therefore, the Frobenius norm may be larger than necessary, which tends to make the bound (3.50) not as sharp as it

might be. Nevertheless, as we still have $\frac{1}{\sqrt{n}}\|\boldsymbol{Z}\|_{\mathrm{F}} \leq \|\boldsymbol{Z}\|_2 \leq \|\boldsymbol{Z}\|_{\mathrm{F}}$ for any matrix $\boldsymbol{Z} \in \mathbb{C}^{k\times n}$, the minimization of the Frobenius norm in (3.51) also implies a decrease in the spectral norm of the same matrix. ◇

To derive an explicit representation of the optimal $(2m+1)^d$-sparse matrix $\boldsymbol{B}$, some rearrangement of the optimization problem (3.51) has to be done, cf. [KP21, KP23a]. By the definition of the Frobenius norm we have $\|\boldsymbol{Z}\|_{\mathrm{F}} = \|\boldsymbol{Z}^*\|_{\mathrm{F}}$, such that (3.51) is equivalent to its adjoint

$$\underset{\tilde{\boldsymbol{B}}\in\mathbb{R}^{N\times|\mathcal{I}_{\boldsymbol{M}_{\boldsymbol{\sigma}}}|}\colon \tilde{\boldsymbol{B}}\ (2m+1)^d\text{-sparse}}{\text{Minimize}} \big\|\boldsymbol{A}^*\tilde{\boldsymbol{B}}\boldsymbol{F}\boldsymbol{D} - \boldsymbol{I}_{|\mathcal{I}_M|}\big\|_{\mathrm{F}}^2. \tag{3.52}$$

Since it is known by (2.15) that $\boldsymbol{F}^*\boldsymbol{F} = |\mathcal{I}_{\boldsymbol{M}_{\boldsymbol{\sigma}}}|\,\boldsymbol{I}_{|\mathcal{I}_M|}$ and $\boldsymbol{D} \in \mathbb{R}^{|\mathcal{I}_M|\times|\mathcal{I}_M|}$ is diagonal by (2.14), we have $\frac{1}{|\mathcal{I}_{\boldsymbol{M}_{\boldsymbol{\sigma}}}|}\boldsymbol{D}^{-1}\boldsymbol{F}^*\boldsymbol{F}\boldsymbol{D} = \boldsymbol{I}_{|\mathcal{I}_M|}$. Thus, due to the fact that the Frobenius norm is a submultiplicative norm, this implies

$$\begin{aligned}\big\|\boldsymbol{A}^*\tilde{\boldsymbol{B}}\boldsymbol{F}\boldsymbol{D} - \boldsymbol{I}_{|\mathcal{I}_M|}\big\|_{\mathrm{F}} &= \big\|\big(\boldsymbol{A}^*\tilde{\boldsymbol{B}} - \tfrac{1}{|\mathcal{I}_{\boldsymbol{M}_{\boldsymbol{\sigma}}}|}\boldsymbol{D}^{-1}\boldsymbol{F}^*\big)\boldsymbol{F}\boldsymbol{D}\big\|_{\mathrm{F}} \\ &\leq \big\|\boldsymbol{A}^*\tilde{\boldsymbol{B}} - \tfrac{1}{|\mathcal{I}_{\boldsymbol{M}_{\boldsymbol{\sigma}}}|}\boldsymbol{D}^{-1}\boldsymbol{F}^*\big\|_{\mathrm{F}}\,\big\|\boldsymbol{F}\boldsymbol{D}\big\|_{\mathrm{F}}. \end{aligned}\tag{3.53}$$

Therefore, we proceed with the modified optimization problem

$$\underset{\tilde{\boldsymbol{B}}\in\mathbb{R}^{N\times|\mathcal{I}_{\boldsymbol{M}_{\boldsymbol{\sigma}}}|}\colon \tilde{\boldsymbol{B}}\ (2m+1)^d\text{-sparse}}{\text{Minimize}} \big\|\boldsymbol{A}^*\tilde{\boldsymbol{B}} - \tfrac{1}{|\mathcal{I}_{\boldsymbol{M}_{\boldsymbol{\sigma}}}|}\boldsymbol{D}^{-1}\boldsymbol{F}^*\big\|_{\mathrm{F}}^2. \tag{3.54}$$

Since we aim to preserve the property that $\boldsymbol{B} \in \mathbb{R}^{N\times|\mathcal{I}_{\boldsymbol{M}_{\boldsymbol{\sigma}}}|}$ in (2.16) is a $(2m+1)^d$-sparse matrix, we rewrite the norm in (3.54) by the property (3.34) in terms of the columns of $\tilde{\boldsymbol{B}}$, additionally considering only the nonzero entries of each column. To this end, analogous to (2.12), we define the index set

$$\begin{aligned}\mathcal{I}_{\boldsymbol{M}_{\boldsymbol{\sigma}},m}(\boldsymbol{\ell}) \coloneqq \big\{j\in\{1,\dots,N\}\colon \exists \boldsymbol{z}\in\mathbb{Z}^d \text{ with} \\ -m\cdot\mathbf{1}_d \leq \boldsymbol{M}_{\boldsymbol{\sigma}}\odot(\boldsymbol{x}_j+\boldsymbol{z}) - \boldsymbol{\ell} \leq m\cdot\mathbf{1}_d\big\}\end{aligned}\tag{3.55}$$

of the nonzero entries of the $\boldsymbol{\ell}$-th column of $\boldsymbol{B} \in \mathbb{R}^{N\times|\mathcal{I}_{\boldsymbol{M}_{\boldsymbol{\sigma}}}|}$. Thus, by (3.34) we have

$$\big\|\boldsymbol{A}^*\tilde{\boldsymbol{B}} - \tfrac{1}{|\mathcal{I}_{\boldsymbol{M}_{\boldsymbol{\sigma}}}|}\boldsymbol{D}^{-1}\boldsymbol{F}^*\big\|_{\mathrm{F}}^2 = \sum_{\boldsymbol{\ell}\in\mathcal{I}_{\boldsymbol{M}_{\boldsymbol{\sigma}}}} \big\|\boldsymbol{H}_{\boldsymbol{\ell}}\tilde{\boldsymbol{b}}_{\boldsymbol{\ell}} - \tfrac{1}{|\mathcal{I}_{\boldsymbol{M}_{\boldsymbol{\sigma}}}|}\boldsymbol{D}^{-1}\boldsymbol{f}_{\boldsymbol{\ell}}\big\|_2^2, \tag{3.56}$$

where $\tilde{\boldsymbol{b}}_{\boldsymbol{\ell}} \in \mathbb{R}^{|\mathcal{I}_{\boldsymbol{M}_\sigma,m}(\boldsymbol{\ell})|}$ denote the vectors of the nonzeros of each column of $\tilde{\boldsymbol{B}} \in \mathbb{R}^{N\times|\mathcal{I}_{\boldsymbol{M}_\sigma}|}$, the matrices

$$\boldsymbol{H}_{\boldsymbol{\ell}} := \left(\mathrm{e}^{-2\pi\mathrm{i}\boldsymbol{k}\boldsymbol{x}_j}\right)_{\boldsymbol{k}\in\mathcal{I}_{\boldsymbol{M}},\, j\in\mathcal{I}_{\boldsymbol{M}_\sigma,m}(\boldsymbol{\ell})} \in \mathbb{C}^{|\mathcal{I}_{\boldsymbol{M}}|\times|\mathcal{I}_{\boldsymbol{M}_\sigma,m}(\boldsymbol{\ell})|} \tag{3.57}$$

are the corresponding submatrices of $\boldsymbol{A}^* \in \mathbb{C}^{|\mathcal{I}_{\boldsymbol{M}}|\times N}$, cf. (2.7), and the vectors $\boldsymbol{f}_{\boldsymbol{\ell}} \in \mathbb{C}^{|\mathcal{I}_{\boldsymbol{M}}|}$ are the columns of $\boldsymbol{F}^* \in \mathbb{C}^{|\mathcal{I}_{\boldsymbol{M}}|\times|\mathcal{I}_{\boldsymbol{M}_\sigma}|}$, cf. (2.15). Hence, we may rewrite (3.54) as

$$\underset{\tilde{\boldsymbol{b}}_{\boldsymbol{\ell}}\in\mathbb{R}^{|\mathcal{I}_{\boldsymbol{M}_\sigma,m}(\boldsymbol{\ell})|}}{\text{Minimize}} \left\|\boldsymbol{H}_{\boldsymbol{\ell}}\tilde{\boldsymbol{b}}_{\boldsymbol{\ell}} - \tfrac{1}{|\mathcal{I}_{\boldsymbol{M}_\sigma}|}\boldsymbol{D}^{-1}\boldsymbol{f}_{\boldsymbol{\ell}}\right\|_2^2, \quad \boldsymbol{\ell}\in\mathcal{I}_{\boldsymbol{M}_\sigma}. \tag{3.58}$$

Thus, if the matrix (3.57) has full column rank, the solution of the least squares problem (3.58) can be computed by means of the pseudoinverse $\boldsymbol{H}_{\boldsymbol{\ell}}^\dagger$ as

$$\boldsymbol{b}_{\boldsymbol{\ell}}^{\mathrm{opt}} := \tfrac{1}{|\mathcal{I}_{\boldsymbol{M}_\sigma}|}\left(\boldsymbol{H}_{\boldsymbol{\ell}}^*\boldsymbol{H}_{\boldsymbol{\ell}}\right)^{-1}\boldsymbol{H}_{\boldsymbol{\ell}}^*\boldsymbol{D}^{-1}\boldsymbol{f}_{\boldsymbol{\ell}}, \quad \boldsymbol{\ell}\in\mathcal{I}_{\boldsymbol{M}_\sigma}. \tag{3.59}$$

Having these vectors $\boldsymbol{b}_{\boldsymbol{\ell}}^{\mathrm{opt}}$ we compose the optimized matrix $\boldsymbol{B}_{\mathrm{opt}}$, observing that $\boldsymbol{b}_{\boldsymbol{\ell}}^{\mathrm{opt}}$ only consist of the nonzero entries of $\boldsymbol{B}_{\mathrm{opt}}$. Then the approximation of the Fourier coefficients is given by

$$\hat{\boldsymbol{f}} \approx \boldsymbol{h}_{\mathrm{opt}} := \boldsymbol{D}^*\boldsymbol{F}^*\boldsymbol{B}_{\mathrm{opt}}^*\boldsymbol{f}, \tag{3.60}$$

i. e., our approach for an inverse NFFT by modifying the adjoint NFFT can be summarized as follows.

Algorithm 3.21 (iNFFT – optimization approach)**.**

For $d, N \in \mathbb{N}$ let $\boldsymbol{x}_j \in \mathbb{T}^d$, $j = 1,\dots,N$, be given nodes as well as $\boldsymbol{f} \in \mathbb{C}^N$. Furthermore, let the d-dimensional oversampling factor $\boldsymbol{\sigma} \geq \boldsymbol{1}_d$, the vector $\boldsymbol{M}_{\boldsymbol{\sigma}} := ((M_\sigma)_1,\dots,(M_\sigma)_d)^\top$ with $2\mathbb{N} \ni (M_\sigma)_t := 2\lceil\lceil\sigma_t M_t\rceil/2\rceil$ and $\boldsymbol{M} = (M_1,\dots,M_d)^\top \in (2\mathbb{N})^d$, as well as a truncation parameter $m \ll (M_\sigma)_t$, $t = 1,\dots,d$, be given.

0. Precompute the optimal $(2m+1)^d$-sparse matrix $\boldsymbol{B}_{\mathrm{opt}} \in \mathbb{R}^{N\times|\mathcal{I}_{\boldsymbol{M}_\sigma}|}$, cf. (3.59).
1. Compute $\boldsymbol{h}_{\mathrm{opt}} := \boldsymbol{D}^*\boldsymbol{F}^*\boldsymbol{B}_{\mathrm{opt}}^*\boldsymbol{f}$, cf. (3.60), by means of a modified adjoint NFFT.

Output: $\boldsymbol{h}_{\mathrm{opt}} \approx \hat{\boldsymbol{f}} \in \mathbb{C}^{|\mathcal{I}_{\boldsymbol{M}}|}$, cf. (3.3).

Complexity: $\mathcal{O}(|\mathcal{I}_{\boldsymbol{M}}|\log(|\mathcal{I}_{\boldsymbol{M}}|) + N)$

Remark 3.22. Note that since

$$\operatorname{rank}(\boldsymbol{D}^*\boldsymbol{F}^*\boldsymbol{B}_{\text{opt}}^*\boldsymbol{A}) \leq \operatorname{rank}(\boldsymbol{A}) \leq \min\{N, |\mathcal{I}_{\boldsymbol{M}}|\},$$

we can only obtain a full-rank approximation $\boldsymbol{D}^*\boldsymbol{F}^*\boldsymbol{B}_{\text{opt}}^*\boldsymbol{A} \approx \boldsymbol{I}_{|\mathcal{I}_{\boldsymbol{M}}|}$ of the identity in (3.51), if the constraint $|\mathcal{I}_{\boldsymbol{M}}| \leq N$ is fulfilled, i. e., if we are in the overdetermined setting of (3.3). This is why, our procedure in Algorithm 3.21 works best in the overdetermined setting $|\mathcal{I}_{\boldsymbol{M}}| \leq N$, while in the underdetermined setting $|\mathcal{I}_{\boldsymbol{M}}| > N$ it produces rather poor results, see Example 3.34.

We further remark that if (3.3) is underdetermined, we have found that the straightforward analogue to (3.51), i. e., searching for an approximation of the form $\boldsymbol{B}_{\text{opt}}\boldsymbol{F}\boldsymbol{D}\boldsymbol{A}^* \approx \boldsymbol{I}_N$, does not succeed either. Rather, additional assumptions on the data and more sophisticated regularization techniques are supposedly needed, but were not considered in this work. ◇

Remark 3.23. Up to now, we focused only on the problem (3.3). Nevertheless, considering the inverse adjoint NFFT in (3.4), we recognize that this problem can also be solved by means of the optimization procedure above. As in Remark 3.22 assume $|\mathcal{I}_{\boldsymbol{M}}| \leq N$, which is the underdetermined setting of the adjoint problem (3.4). Therefore, the minimum norm solution of (3.4) is given by the normal equations of second kind

$$\boldsymbol{A}^*\boldsymbol{A}\boldsymbol{y} = \boldsymbol{h}, \quad \boldsymbol{f} = \boldsymbol{A}\boldsymbol{y}.$$

Incorporating the matrix decomposition of the NFFT, cf. Section 2.2, we recognize that a modification $\boldsymbol{B}_{\text{opt}} \in \mathbb{R}^{N \times |\mathcal{I}_{\boldsymbol{M}_\sigma}|}$ of the matrix $\boldsymbol{B} \in \mathbb{R}^{N \times |\mathcal{I}_{\boldsymbol{M}_\sigma}|}$ such that $\boldsymbol{A}^*\boldsymbol{B}_{\text{opt}}\boldsymbol{F}\boldsymbol{D} \approx \boldsymbol{I}_{|\mathcal{I}_{\boldsymbol{M}}|}$ implies $\boldsymbol{y} \approx \boldsymbol{h}$ and hence $\boldsymbol{f} \approx \boldsymbol{B}_{\text{opt}}\boldsymbol{F}\boldsymbol{D}\boldsymbol{h}$. Thus, the optimization problem (3.52) is also the one to consider for (3.4). In other words, our approach provides both, an inverse NFFT as well as an inverse adjoint NFFT. ◇

3.3.2 Practical computation schemes

To receive an efficient algorithm for the computation of the least squares solution (3.59), we now have a closer look at its computation scheme. For this purpose, let

$$D_n(x) := \sum_{k=-n}^{n} \mathrm{e}^{2\pi \mathrm{i} k x} = \frac{\sin((2n+1)\pi x)}{\sin(\pi x)}$$

denote the one-dimensional *Dirichlet kernel*, cf. [PPST23, Example 1.14]. Then the matrix $\boldsymbol{H}_{\boldsymbol{\ell}}^* \boldsymbol{H}_{\boldsymbol{\ell}}$ in (3.59) can be stated explicitly by (3.57) as

$$\begin{aligned} \boldsymbol{H}_{\boldsymbol{\ell}}^* \boldsymbol{H}_{\boldsymbol{\ell}} &= \left(\sum_{\boldsymbol{k} \in \mathcal{I}_{\boldsymbol{M}}} \mathrm{e}^{2\pi \mathrm{i} \boldsymbol{k} (\boldsymbol{x}_h - \boldsymbol{x}_j)} \right)_{h,j \in \mathcal{I}_{\boldsymbol{M}_{\boldsymbol{\sigma}},m}(\boldsymbol{\ell})} \\ &= \left(\prod_{t=1}^{d} \left(\sum_{k_t = -\frac{M_t}{2}}^{\frac{M_t}{2}-1} \mathrm{e}^{2\pi \mathrm{i} k_t (x_{h_t} - x_{j_t})} \right) \right)_{h,j \in \mathcal{I}_{\boldsymbol{M}_{\boldsymbol{\sigma}},m}(\boldsymbol{\ell})} \\ &= \left(\prod_{t=1}^{d} \left(D_{\frac{M_t}{2}-1}(x_{ht} - x_{j_t}) + \mathrm{e}^{-M_t \pi \mathrm{i} (x_{h_t} - x_{j_t})} \right) \right)_{h,j \in \mathcal{I}_{\boldsymbol{M}_{\boldsymbol{\sigma}},m}(\boldsymbol{\ell})} . \end{aligned} \tag{3.61}$$

In other words, in contrast to the naive computation with a complexity of $\mathcal{O}(|\mathcal{I}_{\boldsymbol{M}}| \cdot |\mathcal{I}_{\boldsymbol{M}_{\boldsymbol{\sigma}},m}(\boldsymbol{\ell})|^2)$, for fixed $\boldsymbol{\ell} \in \mathcal{I}_{\boldsymbol{M}_{\boldsymbol{\sigma}}}$ the matrix $\boldsymbol{H}_{\boldsymbol{\ell}}^* \boldsymbol{H}_{\boldsymbol{\ell}}$ can be determined in $\mathcal{O}(|\mathcal{I}_{\boldsymbol{M}_{\boldsymbol{\sigma}},m}(\boldsymbol{\ell})|^2)$ operations. Considering the right hand sides $\boldsymbol{v}_{\boldsymbol{\ell}} \coloneqq \frac{1}{|\mathcal{I}_{\boldsymbol{M}_{\boldsymbol{\sigma}}}|} \boldsymbol{H}_{\boldsymbol{\ell}}^* \boldsymbol{D}^{-1} \boldsymbol{f}_{\boldsymbol{\ell}}$ of (3.59), we have by definitions (3.57), (2.14) and (2.15) that

$$\boldsymbol{v}_{\boldsymbol{\ell}} = \left(\sum_{\boldsymbol{k} \in \mathcal{I}_{\boldsymbol{M}}} \hat{\varphi}(\boldsymbol{k}) \, \mathrm{e}^{2\pi \mathrm{i} \boldsymbol{k} \left(\boldsymbol{x}_j - \boldsymbol{M}_{\boldsymbol{\sigma}}^{-1} \odot \boldsymbol{\ell} \right)} \right)_{j \in \mathcal{I}_{\boldsymbol{M}_{\boldsymbol{\sigma}},m}(\boldsymbol{\ell})}, \quad \boldsymbol{\ell} \in \mathcal{I}_{\boldsymbol{M}_{\boldsymbol{\sigma}}}. \tag{3.62}$$

Thus, since $\frac{1}{|\mathcal{I}_{\boldsymbol{M}_{\boldsymbol{\sigma}}}|} \boldsymbol{D}^{-1} = \operatorname{diag}(\hat{\varphi}(\boldsymbol{k}))_{\boldsymbol{k} \in \mathcal{I}_{\boldsymbol{M}}}$, the computation of $\boldsymbol{v}_{\boldsymbol{\ell}}$ in (3.62) involves neither multiplication with nor division by the (possibly) huge number $|\mathcal{I}_{\boldsymbol{M}_{\boldsymbol{\sigma}}}|$ and is therefore numerically stable. Nevertheless, for a general window function $\varphi : \mathbb{R}^d \to [0,1]^d$ and fixed $\boldsymbol{\ell} \in \mathcal{I}_{\boldsymbol{M}_{\boldsymbol{\sigma}}}$ the computation of $\boldsymbol{v}_{\boldsymbol{\ell}}$ in (3.62) is still of high complexity $\mathcal{O}(|\mathcal{I}_{\boldsymbol{M}}| \cdot |\mathcal{I}_{\boldsymbol{M}_{\boldsymbol{\sigma}},m}(\boldsymbol{\ell})|)$.

Remark 3.24. Note that in the previous explanations we basically assumed a given matrix $\boldsymbol{B} \in \mathbb{R}^{N \times |\mathcal{I}_{\boldsymbol{M}_{\boldsymbol{\sigma}}}|}$ in (2.16) and subsequent optimization of its entries, i. e., a fixed window function $\varphi : \mathbb{R}^d \to [0,1]^d$ and a fixed truncation parameter $m \in \mathbb{N}$. In fact, we are free to choose a suitable window function φ, as it also appears in the matrix $\boldsymbol{D} = \frac{1}{|\mathcal{I}_{\boldsymbol{M}_{\boldsymbol{\sigma}}}|} \operatorname{diag}(\hat{\varphi}(\boldsymbol{k})^{-1})_{\boldsymbol{k} \in \mathcal{I}_{\boldsymbol{M}}}$, see (2.14). The corresponding truncation parameter m can also be chosen freely. More specifically, this parameter acts as a scaling parameter to adjust the number $(2m+1)^d$ of entries to be chosen in each row of $\boldsymbol{B}$, but with a trade-off in the complexity of the resulting algorithms. ◇

Therefore, we aim to find a good window function $\varphi : \mathbb{R}^d \to [0,1]^d$ that further reduces the complexity of the computation of (3.62), and hence the entire algorithm. It is easy to see that the complexity of computing (3.62) is greatly decreased if $\hat{\varphi}(\boldsymbol{k})$ is independent of $\boldsymbol{k} \in \mathcal{I}_{\boldsymbol{M}}$, e. g., by setting $\hat{\varphi}(\boldsymbol{k}) = 1$, $\boldsymbol{k} \in \mathcal{I}_{\boldsymbol{M}}$, we obtain for each $\boldsymbol{\ell} \in \mathcal{I}_{\boldsymbol{M}_{\boldsymbol{\sigma}}}$ that

$$\begin{aligned} \boldsymbol{v}_{\boldsymbol{\ell}} &= \left(\sum_{\boldsymbol{k} \in \mathcal{I}_{\boldsymbol{M}}} \mathrm{e}^{2\pi \mathrm{i} \boldsymbol{k} \left(\boldsymbol{x}_j - \boldsymbol{M}_{\boldsymbol{\sigma}}^{-1} \odot \boldsymbol{\ell} \right)} \right)_{j \in \mathcal{I}_{\boldsymbol{M}_{\boldsymbol{\sigma}}, m}(\boldsymbol{\ell})} \\ &= \left(\prod_{t=1}^{d} \left(D_{\frac{M}{2}-1} \left(x_{j\,t} - \tfrac{l_t}{\sigma_t M_t} \right) + \mathrm{e}^{-M\pi \mathrm{i} \left(x_{j\,t} - \frac{l_t}{\sigma_t M_t} \right)} \right) \right)_{j \in \mathcal{I}_{\boldsymbol{M}_{\boldsymbol{\sigma}}, m}(\boldsymbol{\ell})} \end{aligned} \tag{3.63}$$

In other words, for fixed $\boldsymbol{\ell} \in \mathcal{I}_{\boldsymbol{M}_{\boldsymbol{\sigma}}}$ each entry of $\boldsymbol{v}_{\boldsymbol{\ell}}$ can be stated explicitly and thus the computation of $\boldsymbol{v}_{\boldsymbol{\ell}}$ in (3.63) simplifies to a complexity of $\mathcal{O}(|\mathcal{I}_{\boldsymbol{M}_{\boldsymbol{\sigma}}, m}(\boldsymbol{\ell})|)$. Note that for this specific choice of the $\hat{\varphi}(\boldsymbol{k})$, $\boldsymbol{k} \in \mathcal{I}_{\boldsymbol{M}}$, the matrix $\boldsymbol{D} \in \mathbb{C}^{|\mathcal{I}_{\boldsymbol{M}}|}$ in (2.14) reduces to $\boldsymbol{D} = \frac{1}{|\mathcal{I}_{\boldsymbol{M}_{\boldsymbol{\sigma}}}|} \boldsymbol{I}_{|\mathcal{I}_{\boldsymbol{M}}|}$. The corresponding window function is given by the (asymmetric) *Dirichlet window function*

$$\varphi_{\mathrm{D}} \coloneqq \sum_{\boldsymbol{k} \in \mathcal{I}_{\boldsymbol{M}}} \mathrm{e}^{2\pi \mathrm{i} \boldsymbol{k} \boldsymbol{x}} = \prod_{t=1}^{d} \left(D_{\frac{M_t}{2}-1}(x_t) + \mathrm{e}^{-M_t \pi \mathrm{i} x_t} \right). \tag{3.64}$$

We additionally remark that the theoretical results in Theorem 3.28 also support the assumption that φ_{D} in (3.64) is the best window function to use. Therefore, Algorithm 3.25 is given only for this window function. Nevertheless, this algorithm could still be used for some general window function $\varphi : \mathbb{R}^d \to [0,1]^d$, as in Example 3.34, only changing the complexity of the computation of $\boldsymbol{v}_{\boldsymbol{\ell}}$ in (3.62), and thus resulting in an overall complexity of $\mathcal{O}(|\mathcal{I}_{\boldsymbol{M}}|^2 \cdot |\mathcal{I}_{\boldsymbol{M}_{\boldsymbol{\sigma}}, m}(\boldsymbol{\ell})| + |\mathcal{I}_{\boldsymbol{M}}| \cdot |\mathcal{I}_{\boldsymbol{M}_{\boldsymbol{\sigma}}, m}(\boldsymbol{\ell})|^3)$, instead.

In summary, this leads to the following algorithm.

Algorithm 3.25 (Optimization of the sparse matrix $\boldsymbol{B}$)**.**

For $d, N \in \mathbb{N}$ let $\boldsymbol{x}_j \in \mathbb{T}^d$, $j = 1, \ldots, N$, be given nodes. Furthermore, we are given the d-dimensional oversampling factor $\boldsymbol{\sigma} \geq \boldsymbol{1}_d$, the vector $\boldsymbol{M}_{\boldsymbol{\sigma}} \coloneqq ((M_\sigma)_1, \ldots, (M_\sigma)_d)^\top$ with $2\mathbb{N} \ni (M_\sigma)_t \coloneqq 2\lceil \lceil \sigma_t M_t \rceil / 2 \rceil$ and $\boldsymbol{M} = (M_1, \ldots, M_d)^\top \in (2\mathbb{N})^d$, as well as a truncation parameter $m \ll (M_\sigma)_t$, $t = 1, \ldots, d$.

1. For $\boldsymbol{\ell} \in \mathcal{I}_{\boldsymbol{M}_\sigma}$:

Determine the index set $\mathcal{I}_{\boldsymbol{M}_\sigma,m}(\boldsymbol{\ell})$, cf. (3.55).	$\mathcal{O}(\lvert\mathcal{I}_{\boldsymbol{M}_\sigma,m}(\boldsymbol{\ell})\rvert)$
Compute the right side $\boldsymbol{v}_{\boldsymbol{\ell}}$ via (3.63).	$\mathcal{O}(\lvert\mathcal{I}_{\boldsymbol{M}_\sigma,m}(\boldsymbol{\ell})\rvert)$
Determine $\boldsymbol{H}_{\boldsymbol{\ell}}^* \boldsymbol{H}_{\boldsymbol{\ell}}$ via (3.61).	$\mathcal{O}(\lvert\mathcal{I}_{\boldsymbol{M}_\sigma,m}(\boldsymbol{\ell})\rvert^2)$
Solve $(\boldsymbol{H}_{\boldsymbol{\ell}}^* \boldsymbol{H}_{\boldsymbol{\ell}})\, \boldsymbol{b}_{\boldsymbol{\ell}}^{\mathrm{opt}} = \boldsymbol{v}_{\boldsymbol{\ell}}$ for $\boldsymbol{b}_{\boldsymbol{\ell}}^{\mathrm{opt}}$, cf. (3.59).	$\mathcal{O}(\lvert\mathcal{I}_{\boldsymbol{M}_\sigma,m}(\boldsymbol{\ell})\rvert^3)$

2. Compose $\boldsymbol{B}_{\mathrm{opt}} \in \mathbb{R}^{N \times \lvert\mathcal{I}_{\boldsymbol{M}_\sigma}\rvert}$ columnwise of the $\boldsymbol{b}_{\boldsymbol{\ell}}^{\mathrm{opt}} \in \mathbb{R}^{\lvert\mathcal{I}_{\boldsymbol{M}_\sigma,m}(\boldsymbol{\ell})\rvert}$ observing sparsity and periodicity. $\mathcal{O}(\lvert\mathcal{I}_{\boldsymbol{M}}\rvert)$

Output: optimized matrix $\boldsymbol{B}_{\mathrm{opt}}$

Complexity: $\mathcal{O}(\lvert\mathcal{I}_{\boldsymbol{M}}\rvert \cdot \max_{\boldsymbol{\ell} \in \mathcal{I}_{\boldsymbol{M}_\sigma}} \lvert\mathcal{I}_{\boldsymbol{M}_\sigma,m}(\boldsymbol{\ell})\rvert^3)$

Remark 3.26. Note that it is not possible to give a general statement about the dimensions of the matrix $\boldsymbol{H}_{\boldsymbol{\ell}} \in \mathbb{C}^{\lvert\mathcal{I}_{\boldsymbol{M}}\rvert \times \lvert\mathcal{I}_{\boldsymbol{M}_\sigma,m}(\boldsymbol{\ell})\rvert}$ in (3.57), since the size of the index set $\mathcal{I}_{\boldsymbol{M}_\sigma,m}(\boldsymbol{\ell})$ in (3.55) strongly depends on the distribution of the nonequispaced nodes $\boldsymbol{x}_j \in \mathbb{T}^d$, $j = 1, \ldots, N$. To visualize this circumstance, we depicted some exemplary patterns of the nonzero entries of the original matrix $\boldsymbol{B} \in \mathbb{R}^{N \times \lvert\mathcal{I}_{\boldsymbol{M}_\sigma}\rvert}$ in (2.16) in Figure 3.1. It can easily be seen that for all choices of the nodes, each row contains the same number of nonzero entries, i. e., all index sets (2.12) are of the same size of maximum $(2m+1)^d$. However, when considering the columns instead, we recognize an evident discrepancy in the number of nonzero entries. We notice that, due to the fact that each row of $\boldsymbol{B} \in \mathbb{R}^{N \times \lvert\mathcal{I}_{\boldsymbol{M}_\sigma}\rvert}$ contains at most $(2m+1)^d$ entries, each column contains $\frac{N}{\lvert\mathcal{I}_{\boldsymbol{M}_\sigma}\rvert}(2m+1)^d$ entries on average, while a more precise statement about the maximum size of the index sets (3.55) cannot be made. Roughly speaking, the more irregular the distribution of the nodes $\boldsymbol{x}_j \in \mathbb{T}^d$ is, the larger the index sets (3.55) can be. In general, however, the number $\lvert\mathcal{I}_{\boldsymbol{M}_\sigma,m}(\boldsymbol{\ell})\rvert$ is a small constant compared to $\lvert\mathcal{I}_{\boldsymbol{M}}\rvert$, such that Algorithm 3.25 ends up with a total computational cost of approximately $\mathcal{O}(\lvert\mathcal{I}_{\boldsymbol{M}}\rvert)$.

Note that if $\lvert\mathcal{I}_{\boldsymbol{M}_\sigma,m}(\boldsymbol{\ell})\rvert$ is large for all $\boldsymbol{\ell}$, i. e., $\lvert\mathcal{I}_{\boldsymbol{M}_\sigma,m}(\boldsymbol{\ell})\rvert \sim N$, $\boldsymbol{\ell} \in \mathcal{I}_{\boldsymbol{M}_\sigma}$, then the complexity of Algorithm 3.21 amounts to $\mathcal{O}(\lvert\mathcal{I}_{\boldsymbol{M}}\rvert N^3)$, which is way too costly for applications. However, in this case we can make use of the NFFT to accelerate the procedure. For fixed $\boldsymbol{\ell} \in \mathcal{I}_{\boldsymbol{M}_\sigma}$, the NFFT can be used to compute the vectors $\boldsymbol{v}_{\boldsymbol{\ell}}$ in (3.62) and can be incorporated into an iterative solver such as the CG algorithm to solve $(\boldsymbol{H}_{\boldsymbol{\ell}}^* \boldsymbol{H}_{\boldsymbol{\ell}})\, \boldsymbol{b}_{\boldsymbol{\ell}}^{\mathrm{opt}} = \boldsymbol{v}_{\boldsymbol{\ell}}$. Since both steps require $\mathcal{O}(\lvert\mathcal{I}_{\boldsymbol{M}}\rvert \log(\lvert\mathcal{I}_{\boldsymbol{M}}\rvert) + N)$ arithmetic operations, the total complexity is then $\mathcal{O}(\lvert\mathcal{I}_{\boldsymbol{M}}\rvert^2 \log(\lvert\mathcal{I}_{\boldsymbol{M}}\rvert) + N\lvert\mathcal{I}_{\boldsymbol{M}}\rvert)$. ◇

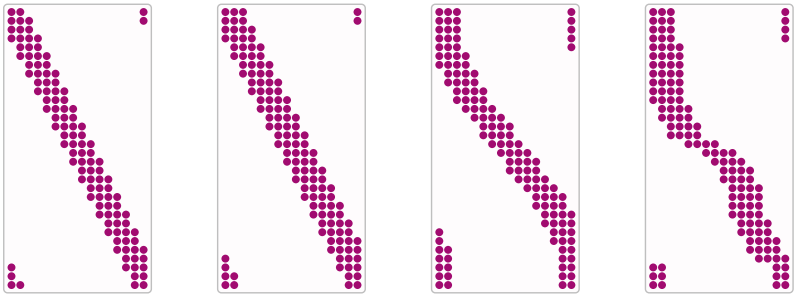

(a) Equispaced points (b) Jittered points (c) Chebyshev points (d) Random points

Figure 3.1: Nonzero entries of the matrix $\boldsymbol{B} \in \mathbb{R}^{N \times |\mathcal{I}_{\boldsymbol{M}_\sigma}|}$ for several choices of the nodes $\boldsymbol{x}_j \in \mathbb{T}^d$, $j = 1, \dots, N$, with $d = 1$, $M_\sigma = M = 16$, $N = 2M$ and $m = 2$.

Remark 3.27. As a measure for the "nonuniformity" of the given nodes $\boldsymbol{x}_j \in \mathbb{T}^d$, $j = 1, \dots, N$, one could utilize the *mesh norm* and the *separation distance*

$$\delta := 2 \max_{\boldsymbol{z} \in \mathbb{T}^d} \min_{j=1,\dots,N} \operatorname{dist}(\boldsymbol{x}_j, \boldsymbol{z}), \qquad q := \min_{\substack{j,h=1,\dots,N \\ j \neq h}} \operatorname{dist}(\boldsymbol{x}_j, \boldsymbol{x}_h),$$

where for two points on the torus $\mathbb{T}^d$ the notion of distance is defined by

$$\operatorname{dist}(\boldsymbol{x}, \boldsymbol{y}) := \min_{\boldsymbol{k} \in \mathbb{Z}^d} \|(\boldsymbol{y} + \boldsymbol{k}) - \boldsymbol{x}\|_\infty.$$

While the separation distance q is the minimal distance between neighboring nodes, the mesh norm δ can be interpreted as the corresponding maximum distance. A visualization of the mesh norm for equispaced nodes can be found in Figure 3.2. It is known from [KP07] that $q \leq N^{-1/d} \leq \delta$, with equality for equispaced nodes. Therefore, sampling points $\boldsymbol{x}_j \in \mathbb{T}^d$, $j = 1, \dots, N$, are said to be highly *nonuniform*, if the separation distance q is very small compared to the mesh norm δ. ◇

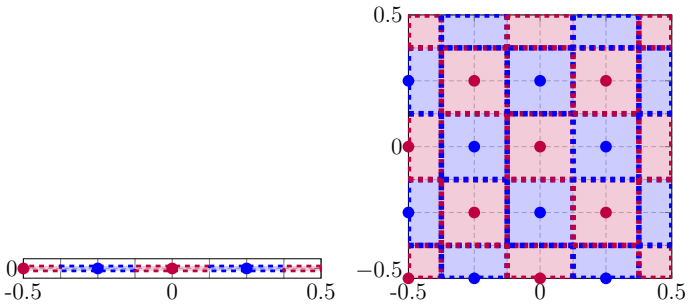

(a) $d = 1$ (b) $d = 2$

Figure 3.2: Visualization of the mesh norm for equispaced grids in one and two dimensions.

3.3.3 Bounds on the approximation error

Analogous to [KP23a, Theorem 4.5] we now summarize the previous findings by presenting an error bound on the optimization procedure in Algorithm 3.21, which also provides a criterion for the choice of the window function $\varphi : \mathbb{R}^d \to [0,1]^d$ used for the diagonal matrix $\boldsymbol{D} \in \mathbb{C}^{|\mathcal{I}_M| \times |\mathcal{I}_M|}$ in (2.14).

Theorem 3.28. *Let $\boldsymbol{B}_{\text{opt}} \in \mathbb{R}^{N \times |\mathcal{I}_{M_\sigma}|}$ be the optimized matrix composed by the vectors in* (3.59) *and let $\boldsymbol{h}_{\text{opt}} = \boldsymbol{D}^* \boldsymbol{F}^* \boldsymbol{B}_{\text{opt}}^* \boldsymbol{f} \in \mathbb{C}^{|\mathcal{I}_M|}$ be the corresponding approximation of $\hat{\boldsymbol{f}}$ computed by means of Algorithm 3.21. Furthermore, assume that each column $\boldsymbol{b}_{\boldsymbol{\ell}}^{\text{opt}} \in \mathbb{R}^{|\mathcal{I}_{M_\sigma, m}|}$ of $\boldsymbol{B}_{\text{opt}} \in \mathbb{R}^{N \times |\mathcal{I}_{M_\sigma}|}$ as solution to* (3.58) *possesses a small residual*

$$\left\| \boldsymbol{H}_{\boldsymbol{\ell}} \boldsymbol{b}_{\boldsymbol{\ell}}^{\text{opt}} - \tfrac{1}{|\mathcal{I}_{M_\sigma}|} \boldsymbol{D}^{-1} \boldsymbol{f}_{\boldsymbol{\ell}} \right\|_2^2 = \varepsilon_{\boldsymbol{\ell}} > 0, \quad \boldsymbol{\ell} \in \mathcal{I}_{M_\sigma}. \tag{3.65}$$

Then there exists an $\varepsilon > 0$ such that

$$\left\| \boldsymbol{h}_{\text{opt}} - \hat{\boldsymbol{f}} \right\|_2^2 \leq \varepsilon \sum_{\boldsymbol{k} \in \mathcal{I}_M} \frac{1}{\hat{\varphi}(\boldsymbol{k})^2} \cdot \left\| \hat{\boldsymbol{f}} \right\|_2^2.$$

Moreover, the (asymmetric) Dirichlet window function φ_{D} in (3.64) *is the optimal window function for the inverse NFFT in Algorithm 3.21.*

Proof. As in (3.50) the approximation error can be estimated by

$$\begin{aligned}\left\|\boldsymbol{h}_{\mathrm{opt}}-\hat{\boldsymbol{f}}\right\|_2^2 &= \left\|\left(\boldsymbol{D}^*\boldsymbol{F}^*\boldsymbol{B}_{\mathrm{opt}}^*\boldsymbol{A}-\boldsymbol{I}_{|\mathcal{I}_M|}\right)\hat{\boldsymbol{f}}\right\|_2^2 \\ &\leq \left\|\boldsymbol{D}^*\boldsymbol{F}^*\boldsymbol{B}_{\mathrm{opt}}^*\boldsymbol{A}-\boldsymbol{I}_{|\mathcal{I}_M|}\right\|_{\mathrm{F}}^2 \left\|\hat{\boldsymbol{f}}\right\|_2^2. \end{aligned} \tag{3.66}$$

Using the same arguments as for (3.52) and (3.53) we proceed with

$$\begin{aligned}\left\|\boldsymbol{D}^*\boldsymbol{F}^*\boldsymbol{B}_{\mathrm{opt}}^*\boldsymbol{A}-\boldsymbol{I}_{|\mathcal{I}_M|}\right\|_{\mathrm{F}}^2 &= \left\|\boldsymbol{A}^*\boldsymbol{B}_{\mathrm{opt}}\boldsymbol{F}\boldsymbol{D}-\boldsymbol{I}_{|\mathcal{I}_M|}\right\|_{\mathrm{F}}^2 \\ &\leq \left\|\boldsymbol{A}^*\boldsymbol{B}_{\mathrm{opt}}-\tfrac{1}{|\mathcal{I}_{M_\sigma}|}\boldsymbol{D}^{-1}\boldsymbol{F}^*\right\|_{\mathrm{F}}^2 \left\|\boldsymbol{F}\boldsymbol{D}\right\|_{\mathrm{F}}^2. \end{aligned} \tag{3.67}$$

To estimate the first Frobenius norm in (3.67), we rewrite it by analogy with (3.56) columnwise as

$$\left\|\boldsymbol{A}^*\boldsymbol{B}_{\mathrm{opt}}-\tfrac{1}{|\mathcal{I}_{M_\sigma}|}\boldsymbol{D}^{-1}\boldsymbol{F}^*\right\|_{\mathrm{F}}^2 = \sum_{\boldsymbol{\ell}\in\mathcal{I}_{M_\sigma}} \left\|\boldsymbol{H}_{\boldsymbol{\ell}}\boldsymbol{b}_{\boldsymbol{\ell}}^{\mathrm{opt}}-\tfrac{1}{|\mathcal{I}_{M_\sigma}|}\boldsymbol{D}^{-1}\boldsymbol{f}_{\boldsymbol{\ell}}\right\|_2^2,$$

where $\boldsymbol{b}_{\boldsymbol{\ell}}^{\mathrm{opt}} \in \mathbb{R}^{|\mathcal{I}_{M_\sigma,m}(\boldsymbol{\ell})|}$ denote the nonzero entries of the columns of $\boldsymbol{B}_{\mathrm{opt}} \in \mathbb{R}^{N\times|\mathcal{I}_{M_\sigma}|}$, $\boldsymbol{H}_{\boldsymbol{\ell}} \in \mathbb{C}^{|\mathcal{I}_M|\times|\mathcal{I}_{M_\sigma,m}(\boldsymbol{\ell})|}$ in (3.57) are the corresponding submatrices of $\boldsymbol{A}^* \in \mathbb{C}^{|\mathcal{I}_M|\times N}$, cf. (2.7), and $\boldsymbol{f}_{\boldsymbol{\ell}} \in \mathbb{C}^{|\mathcal{I}_M|}$ are the columns of $\boldsymbol{F}^* \in \mathbb{C}^{|\mathcal{I}_M|\times|\mathcal{I}_{M_\sigma}|}$, cf. (2.15). Since $\boldsymbol{b}_{\boldsymbol{\ell}}^{\mathrm{opt}} \in \mathbb{R}^{|\mathcal{I}_{M_\sigma,m}|}$ as solutions to the least squares problems (3.58) satisfy (3.65), we can find $\varepsilon := \max_{\boldsymbol{\ell}\in\mathcal{I}_{M_\sigma}} \varepsilon_{\boldsymbol{\ell}} \geq 0$, such that $\varepsilon_{\boldsymbol{\ell}} \leq \varepsilon$, $\boldsymbol{\ell} \in \mathcal{I}_{\boldsymbol{M}_\sigma}$, and thereby

$$\sum_{\boldsymbol{\ell}\in\mathcal{I}_{M_\sigma}} \left\|\boldsymbol{H}_{\boldsymbol{\ell}}\boldsymbol{b}_{\boldsymbol{\ell}}^{\mathrm{opt}}-\tfrac{1}{|\mathcal{I}_{M_\sigma}|}\boldsymbol{D}^{-1}\boldsymbol{f}_{\boldsymbol{\ell}}\right\|_2^2 \leq \sum_{\boldsymbol{\ell}\in\mathcal{I}_{M_\sigma}} \varepsilon_{\boldsymbol{\ell}} \leq \varepsilon\,|\mathcal{I}_{M_\sigma}|.$$

Thus, we may write (3.67) as

$$\left\|\boldsymbol{D}^*\boldsymbol{F}^*\boldsymbol{B}_{\mathrm{opt}}^*\boldsymbol{A}-\boldsymbol{I}_{|\mathcal{I}_M|}\right\|_{\mathrm{F}}^2 \leq \varepsilon\,|\mathcal{I}_{M_\sigma}| \cdot \left\|\boldsymbol{F}\boldsymbol{D}\right\|_{\mathrm{F}}^2. \tag{3.68}$$

Hence, it remains to estimate the Frobenius norm $\left\|\boldsymbol{F}\boldsymbol{D}\right\|_{\mathrm{F}}^2$. By the definitions of the Frobenius norm and the trace $\mathrm{tr}(\boldsymbol{Z}) = \sum_{j=1}^n z_{j,j}$ of a matrix $\boldsymbol{Z} = (z_{j,k})_{j,k=1}^n \in \mathbb{C}^{n\times n}$, we have $\|\boldsymbol{Z}\|_{\mathrm{F}}^2 = \mathrm{tr}(\boldsymbol{Z}^*\boldsymbol{Z})$. Since in addition $\boldsymbol{F}^*\boldsymbol{F} = |\mathcal{I}_{\boldsymbol{M}_\sigma}|\,\boldsymbol{I}_{|\mathcal{I}_M|}$ by (2.15), this yields

$$\left\|\boldsymbol{F}\boldsymbol{D}\right\|_{\mathrm{F}}^2 = \mathrm{tr}(\boldsymbol{D}^*\boldsymbol{F}^*\boldsymbol{F}\boldsymbol{D}) = |\mathcal{I}_{\boldsymbol{M}_\sigma}| \cdot \mathrm{tr}(\boldsymbol{D}^*\boldsymbol{D}) = |\mathcal{I}_{\boldsymbol{M}_\sigma}| \cdot \left\|\boldsymbol{D}\right\|_{\mathrm{F}}^2. \tag{3.69}$$

Using the definition (2.14) of the diagonal matrix $\boldsymbol{D} \in \mathbb{R}^{|\mathcal{I}_{\boldsymbol{M}}| \times |\mathcal{I}_{\boldsymbol{M}}|}$, we obtain

$$\left\|\boldsymbol{D}\right\|_{\mathrm{F}}^2 = \frac{1}{|\mathcal{I}_{\boldsymbol{M}_\sigma}|^2} \sum_{\boldsymbol{k} \in \mathcal{I}_{\boldsymbol{M}}} \frac{1}{\hat{\varphi}(\boldsymbol{k})^2}.$$

Then combining this with (3.68) and (3.69) implies

$$\left\|\boldsymbol{D}^* \boldsymbol{F}^* \boldsymbol{B}_{\mathrm{opt}}^* \boldsymbol{A} - \boldsymbol{I}_{|\mathcal{I}_{\boldsymbol{M}}|}\right\|_{\mathrm{F}}^2 \leq \varepsilon \sum_{\boldsymbol{k} \in \mathcal{I}_{\boldsymbol{M}}} \frac{1}{\hat{\varphi}(\boldsymbol{k})^2}, \tag{3.70}$$

such that (3.66) yields the assertion.

Since $0 \leq \hat{\varphi}(\boldsymbol{k}) \leq 1$, $\boldsymbol{k} \in \mathcal{I}_{\boldsymbol{M}}$, holds for suitable window functions of the NFFT, cf. [PT21b], we have

$$1 \leq \frac{1}{\hat{\varphi}(\boldsymbol{k})} \leq \frac{1}{\hat{\varphi}(\boldsymbol{k})^2}$$

and therefore

$$\sum_{\boldsymbol{k} \in \mathcal{I}_{\boldsymbol{M}}} \frac{1}{\hat{\varphi}(\boldsymbol{k})^2} \geq \sum_{\boldsymbol{k} \in \mathcal{I}_{\boldsymbol{M}}} 1 = |\mathcal{I}_{\boldsymbol{M}}|.$$

Hence, the smallest constant is obtained in (3.70) when $\hat{\varphi}(\boldsymbol{k}) = 1$, $\boldsymbol{k} \in \mathcal{I}_{\boldsymbol{M}}$, i. e., the (asymmetric) Dirichlet window function (3.64) is the optimal window function for the inverse NFFT in Algorithm 3.21. ■

Note that for the reconstruction of trigonometric polynomials (2.8) the error bound of Theorem 3.28 with the optimal window function (3.64) gives the same guarantee as (3.18) in Theorem 3.11 with the optimal density compensation factors of Algorithm 3.10.

Remark 3.29. We remark that due to the fact that we consider the optimization problem (3.54) while actually aiming for $\boldsymbol{D}^* \boldsymbol{F}^* \tilde{\boldsymbol{B}}^* \boldsymbol{A} \approx \boldsymbol{I}_{|\mathcal{I}_{\boldsymbol{M}}|}$, cf. (3.50), one might ask whether this approximation may be improved by a subsequent optimization of the diagonal matrix $\boldsymbol{D}$, i. e., considering the optimization problem

$$\underset{\tilde{\boldsymbol{D}} \in \mathbb{C}^{|\mathcal{I}_{\boldsymbol{M}}| \times |\mathcal{I}_{\boldsymbol{M}}|} :\ \tilde{\boldsymbol{D}} \text{ diagonal}}{\text{Minimize}} \left\|\boldsymbol{A}^* \boldsymbol{B}_{\mathrm{opt}} \boldsymbol{F} \tilde{\boldsymbol{D}} - \boldsymbol{I}_{|\mathcal{I}_{\boldsymbol{M}}|}\right\|_{\mathrm{F}}^2.$$

By the property (3.34) and the fact that $\tilde{\boldsymbol{D}}$ is a diagonal matrix, this Frobenius norm can be rewritten as

$$\begin{aligned}\left\|\boldsymbol{A}^*\boldsymbol{B}_{\mathrm{opt}}\boldsymbol{F}\tilde{\boldsymbol{D}}-\boldsymbol{I}_{|\mathcal{I}_{\boldsymbol{M}}|}\right\|_{\mathrm{F}}^2 &= \sum_{\boldsymbol{k}\in\mathcal{I}_{\boldsymbol{M}}}\left\|\boldsymbol{A}^*\boldsymbol{B}_{\mathrm{opt}}\boldsymbol{F}\,\tilde{\boldsymbol{d}}_{\boldsymbol{k}}-\boldsymbol{e}_{\boldsymbol{k}}\right\|_2^2\\ &= \sum_{\boldsymbol{k}\in\mathcal{I}_{\boldsymbol{M}}}\left\|\boldsymbol{A}^*\boldsymbol{B}_{\mathrm{opt}}\boldsymbol{F}_{\boldsymbol{k}}\,\tilde{d}_{\boldsymbol{k},\boldsymbol{k}}-\boldsymbol{e}_{\boldsymbol{k}}\right\|_2^2,\end{aligned}$$

where $\boldsymbol{F}_{\boldsymbol{k}}$, $\tilde{\boldsymbol{d}}_{\boldsymbol{k}}$ and $\boldsymbol{e}_{\boldsymbol{k}}$ denote the $\boldsymbol{k}$-th columns of the matrices $\boldsymbol{F}\in\mathbb{C}^{|\mathcal{I}_{\boldsymbol{M}_{\boldsymbol{\sigma}}}|\times|\mathcal{I}_{\boldsymbol{M}}|}$ in (2.15), $\tilde{\boldsymbol{D}}\in\mathbb{C}^{|\mathcal{I}_{\boldsymbol{M}}|\times|\mathcal{I}_{\boldsymbol{M}}|}$ and $\boldsymbol{I}_{|\mathcal{I}_{\boldsymbol{M}}|}\in\mathbb{C}^{|\mathcal{I}_{\boldsymbol{M}}|\times|\mathcal{I}_{\boldsymbol{M}}|}$, and $\tilde{d}_{\boldsymbol{k},\boldsymbol{k}}\in\mathbb{C}$ is the diagonal entry of $\tilde{\boldsymbol{D}}\in\mathbb{C}^{|\mathcal{I}_{\boldsymbol{M}}|\times|\mathcal{I}_{\boldsymbol{M}}|}$. Thus, since the vector $\boldsymbol{\beta}_{\boldsymbol{k}}=(\beta_{\boldsymbol{k},\boldsymbol{\ell}})_{\boldsymbol{\ell}\in\mathcal{I}_{\boldsymbol{M}}}\coloneqq\boldsymbol{A}^*\boldsymbol{B}_{\mathrm{opt}}\boldsymbol{F}_{\boldsymbol{k}}\in\mathbb{C}^{|\mathcal{I}_{\boldsymbol{M}}|}$ has full column rank for all $\boldsymbol{k}\in\mathcal{I}_{\boldsymbol{M}}$, the solution $\boldsymbol{D}_{\mathrm{opt}}=\operatorname{diag}\left(d_{\boldsymbol{k},\boldsymbol{k}}^{\mathrm{opt}}\right)_{\boldsymbol{k}\in\mathcal{I}_{\boldsymbol{M}}}$ of the above least squares problem can be computed by means of the pseudoinverse as

$$d_{\boldsymbol{k},\boldsymbol{k}}^{\mathrm{opt}}\coloneqq(\boldsymbol{\beta}_{\boldsymbol{k}}^*\boldsymbol{\beta}_{\boldsymbol{k}})^{-1}\boldsymbol{\beta}_{\boldsymbol{k}}^*\boldsymbol{e}_{\boldsymbol{k}}=\frac{\overline{\beta_{\boldsymbol{k},\boldsymbol{k}}}}{\sum_{\boldsymbol{\ell}\in\mathcal{I}_{\boldsymbol{M}}}|\beta_{\boldsymbol{k},\boldsymbol{\ell}}|^2}\in\mathbb{C},\quad\boldsymbol{k}\in\mathcal{I}_{\boldsymbol{M}}.\tag{3.71}$$

However, the theoretical results in Theorem 3.28 suggest that the (asymmetric) Dirichlet window function φ_{D} in (3.64) with $\boldsymbol{D}=\frac{1}{|\mathcal{I}_{\boldsymbol{M}_{\boldsymbol{\sigma}}}|}\boldsymbol{I}_{|\mathcal{I}_{\boldsymbol{M}}|}$ is already optimal, i. e., that the norm (3.70) cannot be made smaller. Note that the numerical results in Example 3.34 confirm this to be true, also showing that by the optimization of the matrix $\boldsymbol{D}$ there is barely any difference in the norm for other window functions φ as well. In other words, this shows that the optimization procedure in Algorithm 3.25 is indeed optimal with respect to the minimization problem (3.51). ◇

3.3.4 Linking to approaches in literature

There are also some approaches in the literature that attempt to expand the notion of density compensation. This is why, we examine these approaches more closely, presenting them using a unified optimization approach. Similar to Section 3.2.4, we particularly focus on the connection of these approaches to the method introduced in Section 3.3.1.

Sparse approximation of the pseudoinverse

First of all, let us recall the basic idea mentioned in Section 3.1 that we seek to find a matrix $\boldsymbol{X}\in\mathbb{C}^{|\mathcal{I}_{\boldsymbol{M}}|\times N}$ that fulfills $\boldsymbol{X}\boldsymbol{A}\approx\boldsymbol{I}_{|\mathcal{I}_{\boldsymbol{M}}|}$

and therefore $\boldsymbol{X}\boldsymbol{f} = \boldsymbol{X}\boldsymbol{A}\hat{\boldsymbol{f}} \approx \hat{\boldsymbol{f}}$. By incorporating the approximate factorization $\boldsymbol{A} \approx \boldsymbol{B}\boldsymbol{F}\boldsymbol{D}$ of the NFFT, cf. Section 2.2, with the matrices $\boldsymbol{D} \in \mathbb{C}^{|\mathcal{I}_M|\times|\mathcal{I}_M|}$, $\boldsymbol{F} \in \mathbb{C}^{|\mathcal{I}_{M_\sigma}|\times|\mathcal{I}_M|}$ and $\boldsymbol{B} \in \mathbb{R}^{N\times|\mathcal{I}_{M_\sigma}|}$ defined in (2.14), (2.15) and (2.16), this can be reformulated that we are looking for a matrix $\boldsymbol{X}$ with $\boldsymbol{X}\boldsymbol{B}\boldsymbol{F}\boldsymbol{D} \approx \boldsymbol{I}_{|\mathcal{I}_M|}$. Additionally, using the fact that $\boldsymbol{F}^*\boldsymbol{F} = |\mathcal{I}_{M_\sigma}|\,\boldsymbol{I}_{|\mathcal{I}_M|}$ by (2.15) and $\boldsymbol{D}$ in (2.14) is a diagonal matrix, we know that

$$\tfrac{1}{|\mathcal{I}_{M_\sigma}|}\,\boldsymbol{D}^{-1}\boldsymbol{F}^*\boldsymbol{B}^\dagger\boldsymbol{B}\boldsymbol{F}\boldsymbol{D} \approx \boldsymbol{I}_{|\mathcal{I}_M|}, \tag{3.72}$$

if the pseudoinverse $\boldsymbol{B}^\dagger \in \mathbb{R}^{|\mathcal{I}_{M_\sigma}|\times N}$ of (2.16) exists. In other words, the simplest method to obtain a suitable left-inverse matrix $\boldsymbol{X}$ is by using the pseudoinverse $\boldsymbol{B}^\dagger$. However, in general the pseudoinverse $\boldsymbol{B}^\dagger$ of the sparse matrix $\boldsymbol{B}$ will be a full matrix, so the reconstruction using $\boldsymbol{X} = \frac{1}{|\mathcal{I}_{M_\sigma}|}\,\boldsymbol{D}^{-1}\boldsymbol{F}^*\boldsymbol{B}^\dagger$ will not be efficient. Therefore, we look for a sparse approximation $\boldsymbol{S}$ of $\boldsymbol{B}^\dagger$ with $\boldsymbol{S} \approx \frac{1}{|\mathcal{I}_{M_\sigma}|}\,\boldsymbol{B}^\dagger$, or more precisely we consider the matrix optimization problem

$$\underset{\boldsymbol{S}\in\mathbb{R}^{|\mathcal{I}_{M_\sigma}|\times N}\colon\,\boldsymbol{S}\,(2m+1)^d\text{-sparse}}{\text{Minimize}} \quad \big\|\boldsymbol{S}\boldsymbol{B} - \tfrac{1}{|\mathcal{I}_{M_\sigma}|}\,\boldsymbol{I}_{|\mathcal{I}_{M_\sigma}|}\big\|_{\mathrm{F}}^2. \tag{3.73}$$

We remark that a similar approach, the so-called *block uniform resampling algorithm* was introduced in [Ros98] using the sinc matrix $\boldsymbol{C} \in \mathbb{R}^{N\times|\mathcal{I}_M|}$ in (3.30) instead of the sparse matrix $\boldsymbol{B} \in \mathbb{C}^{N\times|\mathcal{I}_{M_\sigma}|}$ in (2.16).

To find a solution to the optimization problem (3.73) we rewrite the respective norm by the property (3.34) as

$$\begin{aligned}\big\|\boldsymbol{S}\boldsymbol{B} - \tfrac{1}{|\mathcal{I}_{M_\sigma}|}\,\boldsymbol{I}_{|\mathcal{I}_{M_\sigma}|}\big\|_{\mathrm{F}}^2 &= \big\|\boldsymbol{B}^*\boldsymbol{S}^* - \tfrac{1}{|\mathcal{I}_{M_\sigma}|}\,\boldsymbol{I}_{|\mathcal{I}_{M_\sigma}|}\big\|_{\mathrm{F}}^2\\ &= \sum_{\boldsymbol{\ell}\in\mathcal{I}_{M_\sigma}} \big\|\boldsymbol{B}_{\boldsymbol{\ell}}^*\tilde{\boldsymbol{s}}_{\boldsymbol{\ell}} - \tfrac{1}{|\mathcal{I}_{M_\sigma}|}\,\boldsymbol{e}_{\boldsymbol{\ell}}\big\|_2^2,\end{aligned}$$

where $\boldsymbol{e}_{\boldsymbol{\ell}} \in \mathbb{R}^{|\mathcal{I}_{M_\sigma}|}$ again denote the columns of the identity matrix $\boldsymbol{I}_{|\mathcal{I}_{M_\sigma}|}$, $\tilde{\boldsymbol{s}}_{\boldsymbol{\ell}} \in \mathbb{R}^{|\mathcal{I}_{M_\sigma,m}(\boldsymbol{\ell})|}$ denote the vectors of the nonzeros of the columns of $\boldsymbol{S}^* \in \mathbb{R}^{N\times|\mathcal{I}_{M_\sigma}|}$, and $\boldsymbol{B}_{\boldsymbol{\ell}}^* \in \mathbb{R}^{|\mathcal{I}_{M_\sigma}|\times|\mathcal{I}_{M_\sigma,m}(\boldsymbol{\ell})|}$ are the corresponding submatrices of $\boldsymbol{B}^* \in \mathbb{R}^{|\mathcal{I}_{M_\sigma}|\times N}$, cf. (2.16). Hence, the solution to (3.73) can be computed using the pseudoinverse as

$$\tilde{\boldsymbol{s}}_{\boldsymbol{\ell}}^{\,\mathrm{opt}} \coloneqq (\boldsymbol{B}_{\boldsymbol{\ell}}^*)^\dagger \cdot \tfrac{1}{|\mathcal{I}_{M_\sigma}|}\,\boldsymbol{e}_{\boldsymbol{\ell}}.$$

That is to say, the nonzero entries of the columns of the optimized matrix $\boldsymbol{S}^*_{\text{opt}}$ are set as the elements of the columns of the pseudoinverse matrix $(\boldsymbol{B}^*_{\boldsymbol{\ell}})^\dagger$.

Note that so far we have used the same techniques as in Section 3.3.1 applied to a different matrix optimization problem in order to exploit the structure of the desired matrix. In [Ros98], however, the authors take one step further and introduce a second simplification by considering only a submatrix $\tilde{\boldsymbol{B}}^*_{\boldsymbol{\ell}} \in \mathbb{R}^{n\times|\mathcal{I}_{\boldsymbol{M}_{\boldsymbol{\sigma}},m}(\boldsymbol{\ell})|}$ of $\boldsymbol{B}^*_{\boldsymbol{\ell}} \in \mathbb{R}^{|\mathcal{I}_{\boldsymbol{M}_{\boldsymbol{\sigma}}}|\times|\mathcal{I}_{\boldsymbol{M}_{\boldsymbol{\sigma}},m}(\boldsymbol{\ell})|}$ and therefore also a subvector $\tilde{\boldsymbol{e}}_{\boldsymbol{\ell}} \in \mathbb{R}^n$ of $\boldsymbol{e}_{\boldsymbol{\ell}} \in \mathbb{R}^{|\mathcal{I}_{\boldsymbol{M}_{\boldsymbol{\sigma}}}|}$. In particular, the size $n = (2r+1)^d \leq |\mathcal{I}_{\boldsymbol{M}_{\boldsymbol{\sigma}}}|$ results from considering only the indices $\boldsymbol{k} \in \mathcal{I}_{\boldsymbol{M}_{\boldsymbol{\sigma}}}$ in (2.16) with $\|\boldsymbol{\ell}-\boldsymbol{k}\|_\infty \leq r \in \mathbb{N}$. In other words, for $n < |\mathcal{I}_{\boldsymbol{M}_{\boldsymbol{\sigma}}}|$ this means a loss of information by omitting data, and therefore considering a different problem instead of simply rewriting by using the structure. However, we have seen in our numerical experiments, see Example 3.35, that except for very tiny choices of r, the results using this additional simplification seem to be as good as the untruncated version above.

Frame theoretical approach

A completely different path is taken in [GS14, KP19], where for $d = 1$ the frame approximation is connected to the adjoint NFFT, which can thus be seen as a method for inverting the NFFT. In order to explain this method, we firstly summarize the main ideas of frames and frame approximation, basically adapted from [GS14] and [Chr16].

Let $\mathcal{H}$ be a separable Hilbert space with inner product $\langle\cdot,\cdot\rangle$. Then a sequence $\{\vartheta_j\}_{j=1}^\infty \subset \mathcal{H}$ is called *frame* if there exist constants $A, B > 0$ such that

$$A\|f\|^2 \leq \sum_{j=1}^{\infty} |\langle f, \vartheta_j\rangle|^2 \leq B\|f\|^2, \quad f \in \mathcal{H}.$$

The operator $S\colon \mathcal{H} \to \mathcal{H}$, $Sf = \sum_{j=1}^\infty \langle f, \vartheta_j\rangle\vartheta_j$, is named the *frame operator*. Then one of the most important results in frame theory, the so-called *frame decomposition*, states that every element of $\mathcal{H}$ can be represented as a linear combination of the elements of the frame, i. e.,

$$f = \sum_{j=1}^{\infty} \langle f, S^{-1}\vartheta_j\rangle\vartheta_j = \sum_{j=1}^{\infty} \langle f, \vartheta_j\rangle S^{-1}\vartheta_j, \quad f \in \mathcal{H}, \tag{3.74}$$

which is a property similar to an orthonormal basis. However, to apply (3.74), it is necessary to explicitly state the inverse operator S^{-1}, which is usually difficult or even impossible, and thus it is necessary to approximate S^{-1}. It was shown in [GS13, GS14] that if $\{\psi_\ell\}_{\ell=-\infty}^{\infty}$ is a so-called admissible frame with respect to the frame $\{\vartheta_j\}_{j=1}^{\infty}$, see [GS14, Definition 1], the dual frame $\{S^{-1}\vartheta_j\}_{j=1}^{\infty}$ can be approximated by

$$S^{-1}\vartheta_j \approx \tilde{\vartheta}_j := \sum_{\ell\in\mathcal{I}_{\boldsymbol{M}_\sigma}} p_{\ell,j}\,\psi_\ell, \quad j=1,\dots,N, \tag{3.75}$$

where $\boldsymbol{\Theta}^\dagger =: (p_{\ell,j})_{\ell\in\mathcal{I}_{\boldsymbol{M}_\sigma},\,j=1}^{N}$ is the Moore-Penrose pseudoinverse of the matrix

$$\boldsymbol{\Theta} := (\langle\vartheta_j,\psi_\ell\rangle)_{j=1,\,\ell\in\mathcal{I}_{\boldsymbol{M}_\sigma}}^{N}. \tag{3.76}$$

Thus, truncating the series (3.74) and inserting (3.75) yields the approximation

$$f \approx \sum_{j=1}^{N}\sum_{\ell\in\mathcal{I}_{\boldsymbol{M}_\sigma}} \langle f,\vartheta_j\rangle\, p_{\ell,j}\,\psi_\ell. \tag{3.77}$$

Now, in order to link the frame approximation (3.77) and the adjoint NFFT from Section 2.3, we consider a discrete version of the frames proposed in [GS14], i. e.,

$$\{\vartheta_j(k) := \mathrm{e}^{-2\pi\mathrm{i}kx_j},\, j\in\mathbb{N}\}, \quad \left\{\psi_\ell(k) := \frac{\mathrm{e}^{-2\pi\mathrm{i}k\ell/M_\sigma}}{M_\sigma\,\hat{\varphi}(k)},\, \ell\in\mathbb{Z}\right\}, \quad k\in\mathbb{Z}. \tag{3.78}$$

Note that in comparison to [GS14] we changed time and frequency domain to match our notations in Section 2.2. Thereby, we receive the scalar product

$$\langle\vartheta_j,\psi_\ell\rangle_{\ell_2} = \sum_{k=-\infty}^{\infty}\vartheta_j(k)\,\overline{\psi_\ell(k)} = \sum_{k=-\infty}^{\infty}\frac{1}{M_\sigma\,\hat{\varphi}(k)}\,\mathrm{e}^{-2\pi\mathrm{i}k\left(x_j-\frac{\ell}{M_\sigma}\right)},$$

such that truncating the infinite sum to $k\in\mathcal{I}_{\boldsymbol{M}}$ yields an approximation of the matrix $\boldsymbol{\Theta}$ in (3.76) by

$$\boldsymbol{\Theta}_{\ell_2} = (\boldsymbol{F}\boldsymbol{D}\boldsymbol{A}^*)^\top = \overline{\boldsymbol{A}\boldsymbol{D}^*\boldsymbol{F}^*} \tag{3.79}$$

with $\boldsymbol{A}\in\mathbb{C}^{N\times|\mathcal{I}_{\boldsymbol{M}}|}$ in (2.7), $\boldsymbol{D}\in\mathbb{C}^{|\mathcal{I}_{\boldsymbol{M}}|\times|\mathcal{I}_{\boldsymbol{M}}|}$ in (2.14), and $\boldsymbol{F}\in\mathbb{C}^{|\mathcal{I}_{\boldsymbol{M}_\sigma}|\times|\mathcal{I}_{\boldsymbol{M}}|}$ in (2.15).

Remark 3.30. It was already mentioned in [GS14, DGS16] that for points $x_j \in \mathbb{T}$ other than the jittered equispaced nodes, cf. (3.85), the admissibility condition for (3.78) may not hold or even the conditions for constituting a frame may fail. In addition, it was observed that for a general window function φ the corresponding conditions can only be satisfied for finite frames, i. e., finite versions of (3.78). In what follows, we assume that all conditions for the frame reconstruction are met. For a detailed study of when this is fulfilled, we refer to [GS13, GS14, DGS16]. ◇

Finally, to apply this method to the problem (3.3) we now consider the frame approximation (3.77) for a function $\hat{f}$ in the frequency domain, i. e.,

$$\begin{aligned}\hat{f}(k) \approx \tilde{\tilde{h}}(k) &= \sum_{j=1}^{N} \sum_{\ell \in \mathcal{I}_{\boldsymbol{M}_\sigma}} \langle \hat{f}, \vartheta_j \rangle \, p_{\ell,j} \, \psi_\ell(k) \\ &= \sum_{\ell \in \mathcal{I}_{\boldsymbol{M}_\sigma}} d_\ell \, \psi_\ell(k), \quad k \in \mathcal{I}_{\boldsymbol{M}}, \end{aligned} \tag{3.80}$$

where by the definition of $p_{\ell,j}$, cf. (3.75), the coefficients can be abbreviated as $\boldsymbol{d} \coloneqq (d_\ell)_{\ell \in \mathcal{I}_{\boldsymbol{M}_\sigma}} = \boldsymbol{\Theta}^\dagger \boldsymbol{f}$ with $\boldsymbol{f} \coloneqq \big(\langle \hat{f}, \vartheta_j \rangle\big)_{j=1}^{N} = (f_j)_{j=1}^{N}$, cf. [GS14]. In other words, the equispaced samples of the function $\hat{f}$, which are now treated as Fourier coefficients of the respective function f, shall be reconstructed from given data $\langle \hat{f}, \vartheta_j \rangle =: f_j$, $j = 1, \dots, N$. Note that this can be seen as a generalization of the problem (3.3) and will be studied more closely in Chapter 6.

Now given this very accurate but hard to compute approximation (3.80), the aim of [GS14, KP19] is to modify the adjoint NFFT in Algorithm 2.5 appropriately, such that we can use this simple method to invert the NFFT, i. e., we are looking for an approximation of the form $\tilde{\boldsymbol{h}} \approx \tilde{\tilde{\boldsymbol{h}}} \approx \hat{\boldsymbol{f}}$, where $\tilde{\boldsymbol{h}} \coloneqq (\tilde{h}_k)_{k \in \mathcal{I}_{\boldsymbol{M}}}$, $\tilde{\tilde{\boldsymbol{h}}} \coloneqq (\tilde{\tilde{h}}_k)_{k \in \mathcal{I}_{\boldsymbol{M}}}$ and $\hat{\boldsymbol{f}} \coloneqq (\hat{f}(k))_{k \in \mathcal{I}_{\boldsymbol{M}}}$.

In [GS14, Section 2.3] firstly the approximation (3.6) using density compensation is considered, which can be written as

$$\begin{aligned}\tilde{h}_k^{\mathrm{w}} &= \sum_{\ell \in \mathcal{I}_{\boldsymbol{M}_\sigma}} \sum_{j=1}^{N} w_j f_j \, \tilde{\varphi}_m\Big(x_j - \tfrac{l}{M_\sigma}\Big) \, \psi_\ell(k) \\ &= \sum_{\ell \in \mathcal{I}_{\boldsymbol{M}_\sigma}} c_\ell \, \psi_\ell(k), \quad k \in \mathcal{I}_{\boldsymbol{M}}, \end{aligned} \tag{3.81}$$

with coefficients vector $\boldsymbol{c} \coloneqq (c_\ell)_{\ell \in \mathcal{I}_{\boldsymbol{M}_\sigma}} = \boldsymbol{B}^* \boldsymbol{W} \boldsymbol{f}$. By additionally defining the matrix $\boldsymbol{\Psi} \coloneqq (\psi_\ell(k))_{k \in \mathcal{I}_{\boldsymbol{M}}, \ell \in \mathcal{I}_{\boldsymbol{M}_\sigma}} = \boldsymbol{D}^* \boldsymbol{F}^*$, the approximations (3.80) and (3.81) can be denoted as $\tilde{\tilde{\boldsymbol{h}}} = \boldsymbol{\Psi} \boldsymbol{d}$ and $\tilde{\boldsymbol{h}}^{\mathrm{w}} = \boldsymbol{\Psi} \boldsymbol{c}$. Hence, the aim is to improve the approximation (3.81) by modifying the diagonal matrix $\boldsymbol{W}$, such that the difference to approximation (3.80) is minimal. It was shown in [GS14, Theorem 2.4] that this norm $\left\| \tilde{\boldsymbol{h}} - \tilde{\tilde{\boldsymbol{h}}} \right\|_2$ is bounded from above by the Frobenius norm $\| \boldsymbol{\Theta}^* \boldsymbol{\Theta} \boldsymbol{B}^* \boldsymbol{W} - \boldsymbol{\Theta}^* \|_{\mathrm{F}}^2$. We remark that by (3.79) and additionally using the fact that the Frobenius norm is a submultiplicative norm, we have

$$\begin{aligned} \| \boldsymbol{\Theta}^* \boldsymbol{\Theta} \boldsymbol{B}^* \boldsymbol{W} - \boldsymbol{\Theta}^* \|_{\mathrm{F}} &= \left\| \boldsymbol{F} \boldsymbol{D} \boldsymbol{A}^* \boldsymbol{A} \boldsymbol{D}^* \boldsymbol{F}^* \boldsymbol{B}^* \boldsymbol{W} - \boldsymbol{F} \boldsymbol{D} \boldsymbol{A}^* \right\|_{\mathrm{F}} \\ &\leq \left\| \boldsymbol{F} \boldsymbol{D} \boldsymbol{A}^* \right\|_{\mathrm{F}} \left\| \boldsymbol{A} \boldsymbol{D}^* \boldsymbol{F}^* \boldsymbol{B}^* \boldsymbol{W} - \boldsymbol{I}_N \right\|_{\mathrm{F}}, \end{aligned}$$

such that this approach yields the optimization problem

$$\underset{\boldsymbol{W} = \operatorname{diag}(w_j)_{j=1}^N}{\text{Minimize}} \ \| \boldsymbol{A} \boldsymbol{D}^* \boldsymbol{F}^* \boldsymbol{B}^* \boldsymbol{W} - \boldsymbol{I}_N \|_{\mathrm{F}}^2,$$

cf. (3.47). Based on this, a generalization using a $(2s-1)$-sparse matrix $\boldsymbol{\Lambda} \in \mathbb{R}^{N \times N}$ instead of the diagonal matrix $\boldsymbol{W}$ was considered in [GS14, Remark 3], which implies the optimization problem

$$\underset{\boldsymbol{\Lambda} \in \mathbb{R}^{N \times N} \colon \boldsymbol{\Lambda}\ (2s-1)\text{-sparse}}{\text{Minimize}} \ \| \boldsymbol{A} \boldsymbol{D}^* \boldsymbol{F}^* \boldsymbol{B}^* \boldsymbol{\Lambda} - \boldsymbol{I}_N \|_{\mathrm{F}}^2. \tag{3.82}$$

In other words, instead of scaling the entries of $\boldsymbol{B}^*$ as in density compensation methods, this approach employs a linear combination of the entries of $\boldsymbol{B}^*$.

Nevertheless, compared to the approach in Section 3.3.1, where we are free to optimize each entry of $\boldsymbol{B}$ by itself, this approach is still less flexible. Thus, by analogy with [KP19], we also rewrite the approximation $\tilde{h}_k$ of the adjoint NFFT in Algorithm (2.5) as

$$\tilde{h}_k = \sum_{\ell \in \mathcal{I}_{\boldsymbol{M}_\sigma}} g_\ell \, \psi_\ell(k), \quad k \in \mathcal{I}_{\boldsymbol{M}},$$

with coefficients vector $\boldsymbol{g} \coloneqq (g_\ell)_{\ell \in \mathcal{I}_{\boldsymbol{M}_\sigma}} = \boldsymbol{B}^* \boldsymbol{f}$, see (2.18), Then it was shown in [KP19, Theorem 4.3], that the difference $\left\| \tilde{\boldsymbol{h}} - \tilde{\tilde{\boldsymbol{h}}} \right\|_2$ is upper

bounded by the Frobenius norm $\|\boldsymbol{B}^*\boldsymbol{\Theta} - \boldsymbol{I}_{|\mathcal{I}_{\boldsymbol{M}_\sigma}|}\|_{\mathrm{F}}$. Note that by (3.79) we have $\boldsymbol{B}^*\boldsymbol{\Theta} = (\boldsymbol{F}\boldsymbol{D}\boldsymbol{A}^*\boldsymbol{B})^\top$ and hence this yields the optimization problem

$$\underset{\boldsymbol{B}\in\mathbb{R}^{N\times|\mathcal{I}_{\boldsymbol{M}_\sigma}|}:\ \boldsymbol{B}\ (2m+1)\text{-sparse}}{\text{Minimize}} \quad \|\boldsymbol{F}\boldsymbol{D}\boldsymbol{A}^*\boldsymbol{B} - \boldsymbol{I}_{M_\sigma}\|_{\mathrm{F}}^2. \tag{3.83}$$

We remark that this is closely connected to the optimization problem (3.54). Similar to (3.53) we can use that $\boldsymbol{F}^*\boldsymbol{F} = |\mathcal{I}_{\boldsymbol{M}_\sigma}|\,\boldsymbol{I}_{|\mathcal{I}_{\boldsymbol{M}}|}$ by (2.15) and $\boldsymbol{D} \in \mathbb{R}^{|\mathcal{I}_{\boldsymbol{M}}|\times|\mathcal{I}_{\boldsymbol{M}}|}$ in (2.14) is diagonal, such that we have $\frac{1}{|\mathcal{I}_{\boldsymbol{M}_\sigma}|}\boldsymbol{D}^{-1}\boldsymbol{F}^*\boldsymbol{F}\boldsymbol{D} = \boldsymbol{I}_{|\mathcal{I}_{\boldsymbol{M}}|}$. Additionally using the fact that the Frobenius norm is a submultiplicative norm, this implies

$$\begin{aligned}\big\|\boldsymbol{A}^*\tilde{\boldsymbol{B}} - \tfrac{1}{|\mathcal{I}_{\boldsymbol{M}_\sigma}|}\boldsymbol{D}^{-1}\boldsymbol{F}^*\big\|_{\mathrm{F}} &= \big\|\tfrac{1}{|\mathcal{I}_{\boldsymbol{M}_\sigma}|}\boldsymbol{D}^{-1}\boldsymbol{F}^*\boldsymbol{F}\boldsymbol{D}\boldsymbol{A}^*\tilde{\boldsymbol{B}} - \tfrac{1}{|\mathcal{I}_{\boldsymbol{M}_\sigma}|}\boldsymbol{D}^{-1}\boldsymbol{F}^*\big\|_{\mathrm{F}} \\ &\le \big\|\tfrac{1}{|\mathcal{I}_{\boldsymbol{M}_\sigma}|}\boldsymbol{D}^{-1}\boldsymbol{F}^*\big\|_{\mathrm{F}}\,\big\|\boldsymbol{F}\boldsymbol{D}\boldsymbol{A}^*\tilde{\boldsymbol{B}} - \boldsymbol{I}_{|\mathcal{I}_{\boldsymbol{M}_\sigma}|}\big\|_{\mathrm{F}},\end{aligned}$$

such that the approach of [KP19] also implies a decrease in (3.54). However, as the method in [KP19] is designed for $d = 1$ and we have encountered that it can not be generalized to $d = 2$, we rather prefer the optimization problem (3.54). For a closer study of the frame theoretic approach we refer to [KP19].

Summary

In summary, in this section we presented approaches that broaden the notion of the previously considered density compensation procedures. Namely, instead of searching optimal scaling factors for the rows of $\boldsymbol{B}$, now the optimization of each nonzero entry of the sparse matrix $\boldsymbol{B} \in \mathbb{R}^{N\times|\mathcal{I}_{\boldsymbol{M}_\sigma}|}$ in (2.16) was studied.

For numerical results, we refer to the examples in Section 3.4. More specifically, in Example 3.34 we examine the norm minimization properties of the optimized matrix computed by Algorithm 3.25. Additionally, a comparison with the optimization approaches of Section 3.3.4 is shown in Example 3.35, while a comparison to the density compensation methods from Section 3.2 is given in Example 3.36.

3.4 Numerical examples & summary

Concluding this chapter, we have a look at some numerical examples, cf. [KP23a]. Besides comparing the density compensation approach from

Section 3.2 to the optimization approach from Section 3.3 (see Example 3.36), we also demonstrate the accuracy of both approaches (see Examples 3.32–3.33 as well as Examples 3.34–3.35).

Remark 3.31. Before getting started, firstly we introduce some exemplary grids. For the sake of simplicity, we restrict ourselves here to the two-dimensional setting $d = 2$.

(i) On the one hand, we study sampling schemes that possess a random part. The simplest choice for this is the *random grid*

$$\boldsymbol{x}_{s,t} := \frac{1}{2}\,(\eta_1, \eta_2)^\top, \quad s = 1, \dots, N_1,\ t = 1, \dots, N_2, \tag{3.84}$$

where $\eta_1, \eta_2 \sim U(-1, 1)$, and $U(-1, 1)$ denotes the uniform distribution on the interval $(-1, 1)$, see Figure 3.3a. Additionally, we also consider a sampling scheme, that is somehow closer to the Cartesian grid. More precisely, we start with a Cartesian grid and add a two-dimensional perturbation, i. e.,

$$\boldsymbol{x}_{s,t} := \left(-\frac{1}{2} + \frac{2t-1}{N_1}, -\frac{1}{2} + \frac{2s-1}{N_2}\right)^\top + \left(\frac{1}{N_1}\,\eta_1,\ \frac{1}{N_2}\,\eta_2\right)^\top, \tag{3.85}$$

with $s = 1, \dots, N_1$, $t = 1, \dots, N_2$, and $\eta_1, \eta_2 \sim U(-1, 1)$. A visualization of this *jittered grid* can be found in Figure 3.3b.

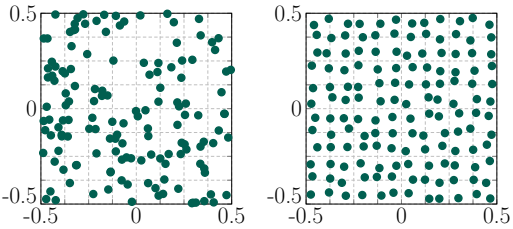

(a) Random grid (3.84) (b) Jittered grid (3.85)

Figure 3.3: Exemplary grids of random kind of size $N_1 = N_2 = 12$.

(ii) On the other hand, we examine grids of polar kind, as mentioned in [FKP07]. For $R, T \in 2\mathbb{N}$ the points of the so-called *polar*

grid are given by a signed radius $r_s \coloneqq \frac{s}{R} \in \left[-\frac{1}{2}, \frac{1}{2}\right)$ and an angle $\theta_t \coloneqq \frac{\pi t}{T} \in \left[-\frac{\pi}{2}, \frac{\pi}{2}\right)$ as

$$\boldsymbol{x}_{s,t} \coloneqq r_s \left(\cos\theta_t, \sin\theta_t\right)^\top, \quad (s,t)^\top \in \mathcal{I}_R \times \mathcal{I}_T. \tag{3.86}$$

Since it is known that the inversion problem is ill-conditioned for this grid, we additionally consider a modification. For the *modified polar grid*

$$\boldsymbol{x}_{s,t} \coloneqq r_s \left(\cos\theta_t, \sin\theta_t\right)^\top, \quad (s,t)^\top \in \mathcal{I}_{\sqrt{2}R} \times \mathcal{I}_T, \tag{3.87}$$

we added more concentric circles and excluded the points outside the unit square, see Figure 3.4b. Another sampling scheme which is known for more stable results than the polar grid is the *linogram* or *pseudo-polar grid*, where the points lie on concentric squares instead of concentric circles, see Figure 3.4c, as defined by the two sets of points

$$\boldsymbol{x}_{s,t}^{BH} \coloneqq \left(\frac{s}{R}, \frac{4st}{RT}\right)^\top, \quad \boldsymbol{x}_{s,t}^{BV} \coloneqq \left(-\frac{4st}{RT}, \frac{s}{R}\right)^\top, \quad (s,t)^\top \in \mathcal{I}_R \times \mathcal{I}_{\frac{T}{2}}. \tag{3.88}$$

(iii) A further modification of these polar grids was introduced in [H+19], where the angles θ_t are not chosen equidistantly, but are obtained by golden angle increments. For the *golden angle polar grid* we only exchange the equispaced angles of the polar grid by

$$\theta_t = \operatorname{mod}\Big(\frac{\pi}{2} + t\,\frac{2\pi}{1+\sqrt{5}}, \pi\Big) - \frac{\pi}{2}, \quad t = 0, \dots, T-1, \tag{3.89}$$

see Figure 3.4d. The *golden angle linogram grid* is given by

$$\boldsymbol{x}_{s,t} \coloneqq \left\{ \begin{array}{ll} \left(\frac{2s+1}{2R}, \frac{2s+1}{2R}\tan\left(\theta_t - \frac{\pi}{4}\right)\right)^\top & : \theta_t \in \left[0, \frac{\pi}{2}\right) \\ \left(-\frac{2s+1}{2R}\cot\left(\theta_t - \frac{\pi}{4}\right), \frac{2s+1}{2R}\right)^\top & : \theta_t \in \left[-\frac{\pi}{2}, 0\right) \end{array} \right\}, \quad s \in \mathcal{I}_R, \tag{3.90}$$

with θ_t in (3.89), as illustrated in Figure 3.4e.

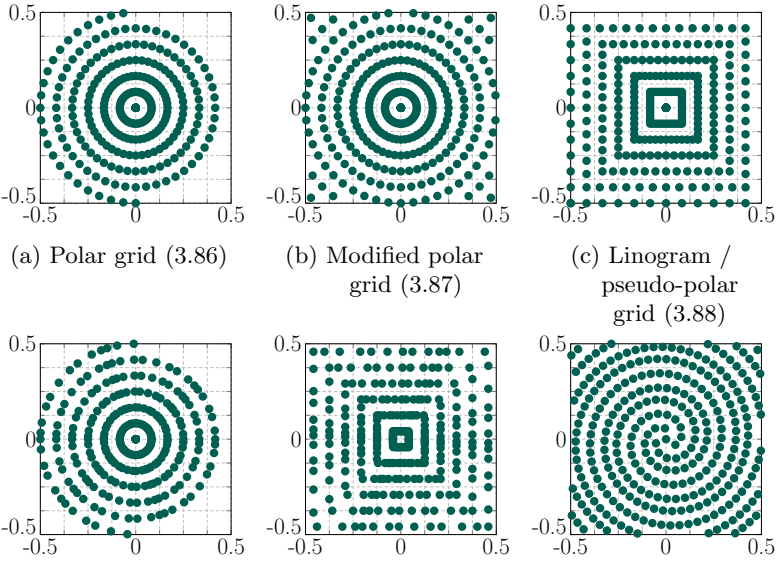

(a) Polar grid (3.86) (b) Modified polar grid (3.87) (c) Linogram / pseudo-polar grid (3.88)

(d) Golden angle polar grid, cf. (3.89) (e) Golden angle linogram grid (3.90) (f) Spiral grid (3.91)

Figure 3.4: Exemplary grids of polar kind of size $R = 12$ and $T = 2R$.

(iv) In addition, we also consider the *spiral grid*, which consists of the 3 sets of points

$$\boldsymbol{x}_{s,t} \coloneqq r_s \cdot \boldsymbol{R}_{\frac{2\pi}{3}}^{t-1} \left(\cos(\alpha_s), \sin(\alpha_s)\right)^\top, \quad t \in \{1,2,3\}, \tag{3.91}$$

where radius and angle are given by

$$r_s = \frac{\sqrt{15(s-1)}}{4\sqrt{RT}}, \quad \alpha_s = \pi\sqrt{\frac{15(s-1)}{8RT}}\left(\sqrt{\frac{RT}{5}} - 1\right),$$

for $s = 1, \ldots, \lfloor \frac{8}{15} RT \rfloor$, respectively, and the matrix

$$\boldsymbol{R}_{\frac{2\pi}{3}} \coloneqq \begin{pmatrix} \cos\left(\frac{2\pi}{3}\right) & -\sin\left(\frac{2\pi}{3}\right) \\ \sin\left(\frac{2\pi}{3}\right) & \cos\left(\frac{2\pi}{3}\right) \end{pmatrix}$$

realizes a rotation by 120 degrees. Again, we have excluded the points outside the unit square, see Figure 3.4f.

Note that in all the definitions above it was necessary to denote the sampling points by $\boldsymbol{x}_{s,t}$ with different index sets for s and t in order to obtain a rigorous representation. However, using some suitable reordering and N being the total number of points, we may again use the notation $\boldsymbol{x}_j$, $j = 1, \dots, N$, as in the remainder of this work. ◇

Now we examine the quality of the different approaches from Sections 3.2 and 3.3 for the grids mentioned in Remark 3.31.

Density compensation

Firstly, we investigate the accuracy of the density compensation method from Algorithm 3.2 with the weights computed by Algorithm 3.10. More specifically, in Example 3.32 we check the theoretical error bound of Theorem 3.11, and in Example 3.33 we show a comparison with the approaches of Section 3.2.4.

Example 3.32. As in [KP23a, Example 5.2], we first examine the quality of our density compensation factors in Algorithm 3.10 for a trigonometric polynomial f in (2.8) with given Fourier coefficients $\hat{f}_{\boldsymbol{k}} \in [1, 10]$, $\boldsymbol{k} \in \mathcal{I}_{\boldsymbol{M}}$. For the corresponding function evaluations of (2.8) at given points $\boldsymbol{x}_j \in \left[-\frac{1}{2}, \frac{1}{2}\right)^d$, $j = 1, \dots, N$, we test how well these Fourier coefficients can be approximated. More precisely, we consider the estimate $\tilde{\boldsymbol{h}}^{\mathrm{w}} = \boldsymbol{D}^* \boldsymbol{F}^* \boldsymbol{B}^* \boldsymbol{W} \boldsymbol{f}$, cf. (3.6), with the matrix $\boldsymbol{W} = \operatorname{diag}(w_j)_{j=1}^N$ of density compensation factors computed by means of Algorithm 3.10, i. e., by (3.15), in case $|\mathcal{I}_{\boldsymbol{2M}}| \leq N$, or by (3.16), if $|\mathcal{I}_{\boldsymbol{2M}}| > N$. Subsequently, we compute the relative errors

$$e_p \coloneqq \frac{\|\tilde{\boldsymbol{h}}^{\mathrm{w}} - \hat{\boldsymbol{f}}\|_p}{\|\hat{\boldsymbol{f}}\|_p}, \quad p \in \{2, \infty\}, \tag{3.92}$$

and we demonstrate that

$$e_p \leq |\mathcal{I}_{\boldsymbol{M}}|\, \varepsilon, \quad p \in \{2, \infty\},$$

holds with the residual $\varepsilon = \left\| \boldsymbol{A}_{|\mathcal{I}_{\boldsymbol{2M}}|}^{\top} \boldsymbol{w} - \boldsymbol{e}_{\boldsymbol{0}} \right\|_\infty \geq 0$, cf. (3.17), as stated by the theoretical error bound (3.18).

This test is performed for several dimensions $d \in \{1, 2, 3\}$. In our experiment we use random points (3.84) with $N_t = 2^{9-d}$, $t = 1, \dots, d$, and for several problem sizes $\boldsymbol{M} = M \cdot \boldsymbol{1}_d$, $M = 2^c$ with $c = 1, \dots, 11 - d$, we

choose random Fourier coefficients $\hat{f}_{\boldsymbol{k}} \in [1, 10]$, $\boldsymbol{k} \in \mathcal{I}_{\boldsymbol{M}}$. Afterwards, we compute the evaluations of the trigonometric polynomial (2.8) by means of an NFFT and use the resulting vector $\boldsymbol{f}$ as input for the reconstruction. Due to the randomness we repeat this process 10 times and then calculate the maximum error. The corresponding results are displayed in Figure 3.5. We recognize that for $|\mathcal{I}_{\boldsymbol{2M}}| < N$, i. e., as long as $M < \frac{N_1}{2} = 2^{8-d}$ is satisfied, the weights computed by means of (3.15) indeed yield an exact reconstruction of the given Fourier coefficients. However, it can be seen that for $|\mathcal{I}_{\boldsymbol{2M}}| > N$ the least squares approximation via (3.16) no longer produces good results. In both cases the theoretical error estimate (3.18) provides a suitable upper bound on the relative errors (3.92). This shows that the approximation error is indeed mainly influenced by the residual of the linear system (3.12). ◇

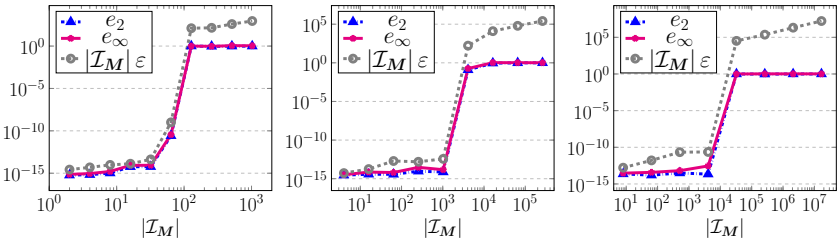

(a) $d = 1$ (b) $d = 2$ (c) $d = 3$

Figure 3.5: Relative errors (3.92) of the reconstruction of the Fourier coefficients of a trigonometric polynomial (2.8) with given $\hat{f}_{\boldsymbol{k}} \in [1, 10]$, $\boldsymbol{k} \in \mathcal{I}_{\boldsymbol{M}}$, computed using the density compensation factors from Algorithm 3.10, for random grids with $N_t = 2^{9-d}$, $t = 1, \ldots, d$, and $\boldsymbol{M} = M \cdot \mathbf{1}_d$, $M = 2^c$ with $c = 1, \ldots, 11 - d$.

Example 3.33. Next, we survey the different density compensation methods from Section 3.2, i. e., we compare the weights computed by means of Algorithm 3.10 with the approaches from Section 3.2.4 when using Algorithm 3.2.

(a) Firstly, we consider the setting $|\mathcal{I}_{\boldsymbol{2M}}| \leq N$ and show the optimality of the weights computed by means of Algorithm 3.10, i. e., using (3.15). For this purpose, we compare the reconstruction of given Fourier coefficients $\hat{f}_{\boldsymbol{k}}$, $\boldsymbol{k} \in \mathcal{I}_{\boldsymbol{M}}$, of a trigonometric polynomial (2.8) computed by means of Algo-

rithm 3.2 using Voronoi weights as well as the density compensation factors from (3.15), (3.36), (3.44), and (3.48) for several $M = 2^c$, $c = 1, \dots, 10$. To make this affordable for all the approaches, we restrict ourselves to the one-dimensional setting $d = 1$.

In this experiment, the Fourier coefficients shall be chosen deterministically as integer evaluations of the *triangular pulse function*

$$g(v) \coloneqq \left(1 - \left|\tfrac{v}{b}\right|\right) \cdot \chi_{[-b,b]}(v), \quad b \coloneqq \left\lceil \tfrac{3M}{8} \right\rceil. \tag{3.93}$$

Then for given jittered points (3.85) with $N = 2M$ we compute the evaluations of the trigonometric polynomial (2.8) by means of an NFFT and use the resulting vector as input for Algorithm 3.2. For the corresponding reconstruction $\tilde{\boldsymbol{h}}^{\mathrm{w}}$ we compute the relative errors (3.92). Due to the randomness in the nodes we repeat this process 10 times and then calculate the maximum error. The corresponding results are depicted in Figure 3.6. It is easy to see that the density compensation factors computed using Algorithm 3.10, or more precisely by (3.15), indeed produce the best results and therefore are the optimal ones. Note additionally that (3.36) and (3.48) are not even as good as the Voronoi weights. Merely the density compensation factors computed using (3.44) provide reasonable results, although not as good as (3.15).

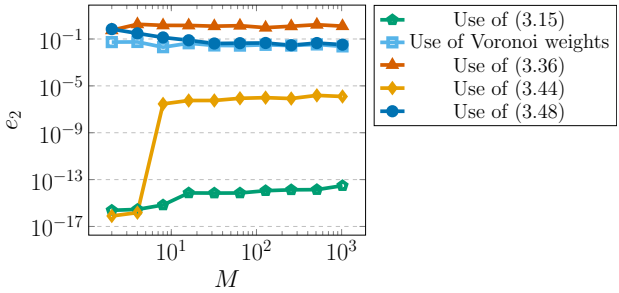

Figure 3.6: Relative errors (3.92) of the reconstruction of the Fourier coefficients of a trigonometric polynomial (2.8) with given $\hat{f}_{\boldsymbol{k}}$, $\boldsymbol{k} \in \mathcal{I}_{\boldsymbol{M}}$, computed by means of Algorithm 3.2 using Voronoi weights as well as the density compensation factors from (3.15), (3.36), (3.44), (3.48), for one-dimensional jittered grids (3.85) with $N = 2M$ and $M = 2^c$, $c = 1, \dots, 10$.

In addition, for the setting $M = 8$ and $N = 16$, Figure 3.7 shows the distribution of some exemplarily chosen jittered nodes $x_j \in \mathbb{T}$, $j = 1, \ldots, N$, cf. (3.85), and the corresponding density compensation factors $w_j \in \mathbb{R}$. We recognize that the weights computed using (3.44) indeed look most similar to those computed by means of (3.15) and (3.16), which are identical, and that (3.48) basically resembles the Voronoi weights. Moreover, note that except for (3.36), all density compensation factors are nonnegative.

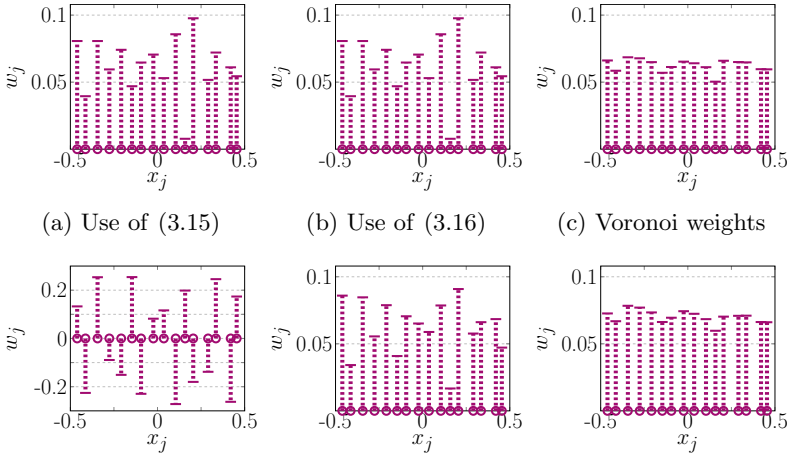

(a) Use of (3.15) (b) Use of (3.16) (c) Voronoi weights

(d) Use of (3.36) (e) Use of (3.44) (f) Use of (3.48)

Figure 3.7: Exemplary density compensation factors w_j for given jittered nodes x_j, $j = 1, \ldots, N$, cf. (3.85), computed using (3.15), (3.16), (3.36), (3.44) and (3.48), as well as Voronoi weights with $d = 1$, $M = 8$ and $N = 2M$.

(b) Secondly, we consider $|\mathcal{I}_{\boldsymbol{2M}}| > N$ for the two-dimensional setting $d = 2$. For this purpose, analogous to [KP23b, Example IV.1], we have a look at the reconstruction of the Shepp-Logan phantom, see Figure 3.8a. Here the phantom data shall be treated as Fourier coefficients $\hat{\boldsymbol{f}} := (\hat{f}_{\boldsymbol{k}})_{\boldsymbol{k} \in \mathcal{I}_{\boldsymbol{M}}}$ of a trigonometric polynomial (2.8). For given points $\boldsymbol{x}_j \in \mathbb{T}^2$, $j = 1, \ldots, N$, we then compute the evaluations of the trigonometric polynomial (2.8) by means of an NFFT and use the resulting vector as input for the reconstruction. More precisely, for the spiral grid (3.91), cf. Figure 3.4f, of size $R = M$, $T = 2R$, we study (3.16), (3.44) and (3.48).

The corresponding reconstruction of the phantom of size $M = 64$ is presented in Figure 3.8 (top) including a detailed view of the 52nd row (bottom). Since the exactness condition $|\mathcal{I}_{\mathbf{2M}}| \leq N$ (see Theorem 3.4) is violated, the weights computed by (3.15) do not yield an exact reconstruction, cf. Figure 3.8b. Moreover, note that the results using the least squares approximation by (3.16) are just as bad, cf. Figure 3.8c. In fact, in this setting the weights computed using (3.44) and (3.48), respectively, appear to be more promising, see Figures 3.8d and 3.8e, since there are no artifacts and the differences to the original phantom are no longer visible. However, we remark that the comparatively small choice of $M = 64$ is necessary for (3.44) and (3.48) to be computationally affordable, cf. also Remarks 3.15 and 3.18. ◇

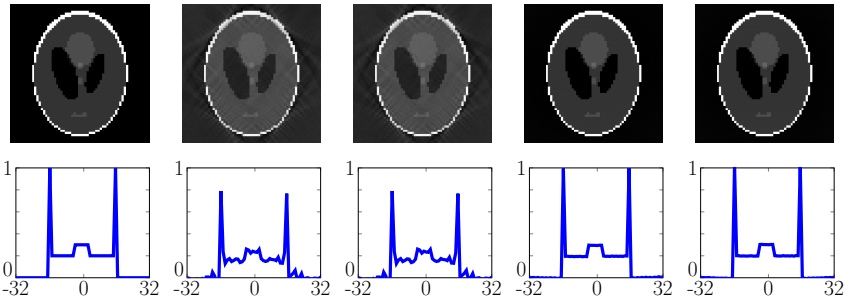

(a) Original phantom

(b) Use of (3.15) with e_2=2.11e−01

(c) Use of (3.16) with e_2=2.11e−01

(d) Use of (3.44) with e_2=2.83e−02

(e) Use of (3.48) with e_2=3.61e−02

Figure 3.8: Reconstruction of the Shepp-Logan phantom of size $M = 64$ (top) via Algorithm 3.2 using density compensation factors computed by (3.15), (3.16), (3.44) and (3.48) for the spiral grid (3.91) of size $R = M$, $T = 2R$; as well as a detailed view of the 52nd row (bottom).

Matrix optimization

Secondly, we investigate the accuracy of the matrix optimization method from Algorithm 3.21 with the optimized sparse matrix computed by Algorithm 3.25. More precisely, in Example 3.34 we investigate whether the

norm minimization aimed at in Section 3.3 is successful and in Example 3.35 we show the superiority of this procedure compared to the approaches from Section 3.3.4.

Example 3.34. (a) In order to study the quality of our optimization method from Section 3.3, we compare the original and optimized Frobenius norms

$$n_{\mathrm{F}}(\varphi, m, \sigma) := \left\| \boldsymbol{A}^* \boldsymbol{B} \boldsymbol{F} \boldsymbol{D} - \boldsymbol{I}_{|\mathcal{I}_{\boldsymbol{M}}|} \right\|_{\mathrm{F}}, \tag{3.94}$$

$$n_{\mathrm{F}}^{\mathrm{opt}}(\varphi, m, \sigma) := \left\| \boldsymbol{A}^* \boldsymbol{B}_{\mathrm{opt}} \boldsymbol{F} \boldsymbol{D} - \boldsymbol{I}_{|\mathcal{I}_{\boldsymbol{M}}|} \right\|_{\mathrm{F}}, \tag{3.95}$$

as well as the respective spectral norms

$$n_2(\varphi, m, \sigma) := \left\| \boldsymbol{A}^* \boldsymbol{B} \boldsymbol{F} \boldsymbol{D} - \boldsymbol{I}_{|\mathcal{I}_{\boldsymbol{M}}|} \right\|_2, \tag{3.96}$$

$$n_2^{\mathrm{opt}}(\varphi, m, \sigma) := \left\| \boldsymbol{A}^* \boldsymbol{B}_{\mathrm{opt}} \boldsymbol{F} \boldsymbol{D} - \boldsymbol{I}_{|\mathcal{I}_{\boldsymbol{M}}|} \right\|_2, \tag{3.97}$$

similar to [KP23a, Example 5.3], where $\boldsymbol{B}$ denotes the original matrix (2.16) from the NFFT and $\boldsymbol{B}_{\mathrm{opt}}$ denotes the optimized matrix generated by Algorithm 3.25. Since we are free to choose a suitable window function used in the computation of this optimized matrix $\boldsymbol{B}_{\mathrm{opt}}$, we now compare the common B–spline window function φ_{B}, cf. (4.61) with the Dirichlet window function φ_{D} in (3.64), which is optimal by Theorem 3.28. For the original matrix $\boldsymbol{B}$ we utilize only the B–spline window function φ_{B}, since the Dirichlet window function φ_{D} is not an appropriate window for the NFFT.

Due to memory limitations in the computation of the norms (3.94)–(3.97), we have to be content with very small problems, which nevertheless show the functionality of Algorithm 3.25. For this reason we consider $d = 2$ and choose $\boldsymbol{M} = (12, 12)^\top$ as well as $N_1 = N_2 = R = 2^\mu$, $\mu \in \{2, \dots, 7\}$, and $T = 2R$ for the grids mentioned in Remark 3.31. In other words, we test Algorithm 3.25 in the underdetermined setting $|\mathcal{I}_{\boldsymbol{M}}| > N$ as well as in the overdetermined setting $|\mathcal{I}_{\boldsymbol{M}}| \leq N$.

Having a look at the results for the grids of Remark 3.31, it becomes apparent that they separate into two groups. Figure 3.9a displays the results for the polar grid (3.86), which are the same as for the golden angle polar grid, cf. (3.89). In these cases, the optimization yields only a slight improvement. However, for all other grids mentioned, the minimization procedure in Algorithm 3.25 is very effective. The results for these grids are depicted in Figure 3.9b, exemplified for the modified polar grid (3.87).

One reason for the different behavior of polar and modified polar grid could be the ill-posedness of the inversion problem for the polar grid, which

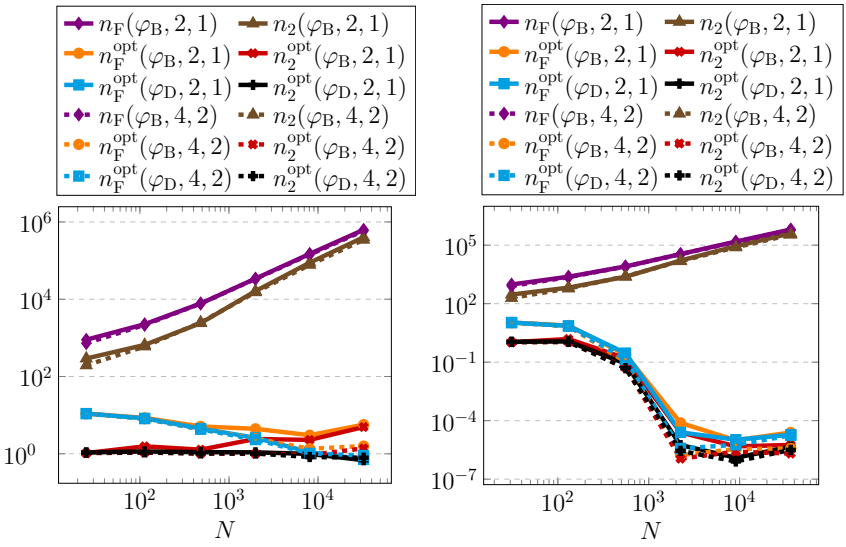

(a) Polar grid (3.86)

(b) Modified polar grid (3.87)

Figure 3.9: Frobenius norms (3.94) and (3.95) as well as spectral norms (3.96) and (3.97) of the original matrix $\boldsymbol{B}$ and the optimized matrix $\boldsymbol{B}_{\mathrm{opt}}$ generated by Algorithm 3.25 using the B–spline window function φ_{B} as well as the Dirichlet window function φ_{D} from (3.64) with $R = 2^{\mu}$, $\mu \in \{2, \dots, 7\}$, and $T = 2R$ as well as $\boldsymbol{M} = (12, 12)^{\top}$, $m \in \{2, 4\}$, and $\sigma \in \{1, 2\}$.

results in huge condition numbers of $\boldsymbol{H}_{\boldsymbol{\ell}}^{*}\boldsymbol{H}_{\boldsymbol{\ell}}$, while the problem is well-posed for the modified polar grid. Another reason might be found in the optimization procedure itself. Having a closer look at the polar grid, see Figure 3.4a, we recognize that there are no grid points in the corners of the unit square. Therefore, some of the index sets $\mathcal{I}_{\boldsymbol{M}_{\boldsymbol{\sigma}},m}(\boldsymbol{\ell})$ in (3.55) are empty and no optimization can be done for the corresponding matrix columns. This could also lead to worse minimization properties of the polar grid.

Furthermore, it can be seen that our optimization procedure in Algorithm 3.25 is most effective in the overdetermined setting $|\mathcal{I}_{\boldsymbol{M}}| \leq N$, and

for the use of the Dirichlet window function (3.64). The choice of the truncation parameter m and the oversampling factor σ, however, only seems to have a minor impact. Additionally, note that although our optimization procedure in Algorithm 3.25 focuses on the Frobenius norm, the spectral norm behaves similarly, as stated in Remark 3.20.

(b) Finally, considering the approach of subsequent optimization of the diagonal matrix $\boldsymbol{D}$ from Remark 3.29, we recorded the norms

$$\left\| \boldsymbol{A}^* \boldsymbol{B}_{\mathrm{opt}} \boldsymbol{F} \boldsymbol{D}_{\mathrm{opt}} - \boldsymbol{I}_{|\mathcal{I}_{\boldsymbol{M}}|} \right\|_{\mathrm{F}} \tag{3.98}$$

and $\|\boldsymbol{D} - \boldsymbol{D}_{\mathrm{opt}}\|_\infty$ as well. The respective results for the modified polar grid (3.87) with $m = 2$ and $\sigma = 1$ are printed in Table 3.1. It can be seen that for both window functions this approach provides hardly any improvement, and thus our optimization procedure in Algorithm 3.25 is indeed optimal with respect to problem (3.51). ◇

	$n_{\mathrm{F}}^{\mathrm{opt}}(\varphi, m, \sigma)$ in (3.95)		$\tilde{n}_{\mathrm{F}}^{\mathrm{opt}}(\varphi, m, \sigma)$ in (3.98)		$\|\boldsymbol{D} - \boldsymbol{D}_{\mathrm{opt}}\|_\infty$	
N	φ_{B}	φ_{D}	φ_{B}	φ_{D}	φ_{B}	φ_{D}
31	1.07e+01	1.07e+01	1.07e+01	1.07e+01	1.24e+01	1.54e−03
131	7.57e+00	7.25e+00	7.43e+00	7.20e+00	2.83e+01	1.40e−03
555	2.47e−01	2.92e−01	2.47e−01	2.88e−01	8.50e−02	1.13e−04
2239	5.11e−06	1.96e−06	5.11e−06	1.96e−06	3.00e−07	1.93e−10
9083	8.62e−06	2.90e−06	8.62e−06	2.89e−06	2.24e−07	3.45e−10
36535	1.58e−05	9.15e−06	1.58e−05	9.12e−06	6.83e−07	1.22e−09

Table 3.1: Matrix norms using the original matrix $\boldsymbol{D}$ in (2.14) and the optimized matrix $\boldsymbol{D}_{\mathrm{opt}}$ generated by (3.71) for the B–spline window function φ_{B} as well as the Dirichlet window function φ_{D} from (3.64) using the modified polar grid (3.87) with $R = 2^\mu$, $\mu \in \{2, \dots, 7\}$, and $T = 2R$ as well as $\boldsymbol{M} = (12, 12)^\top$, $m = 2$ and $\sigma = 1$.

Example 3.35. Next, we survey the different matrix optimization methods from Section 3.3, i. e., we compare our method from Algorithm 3.21 to the approaches mentioned in Section 3.3.4. Note that since all of these approaches are designed for the overdetermined setting $|\mathcal{I}_{\boldsymbol{M}}| < N$ and some only for $d = 1$, we restrict ourselves to this setting and study the pointwise reconstruction and error for a specific set of parameters with $M = 64$,

$\sigma = 1.0$ and $m = 2$. Similar to Example 3.33, the Fourier coefficients $\hat{\boldsymbol{f}}$ shall be chosen deterministically as integer evaluations of the triangular pulse function (3.93). Then for given jittered points (3.85) with $N = 2M$ we compute the evaluations of the trigonometric polynomial (2.8) by means of an NFFT and use the resulting vector $\boldsymbol{f}$ as input for the different reconstruction methods. For the corresponding reconstruction $\tilde{\boldsymbol{h}}$ we compute the pointwise errors $|\hat{\boldsymbol{f}} - \tilde{\boldsymbol{h}}|$.

In particular, we examine the reconstruction $\frac{1}{|\mathcal{I}_{M_\sigma}|}\boldsymbol{D}^{-1}\boldsymbol{F}^*\boldsymbol{B}^\dagger\boldsymbol{f}$ using the pseudoinverse, cf. (3.72), the reconstruction $\boldsymbol{D}^{-1}\boldsymbol{F}^*\boldsymbol{S}_{\text{opt}}\boldsymbol{f}$, cf. [Ros98], where $\boldsymbol{S}_{\text{opt}}$ is the solution to (3.73), and $\boldsymbol{D}^*\boldsymbol{F}^*\boldsymbol{B}^*\boldsymbol{\Lambda}\boldsymbol{f}$, where $\boldsymbol{\Lambda}$ is the solution to (3.82) with $s = \lceil \log(N) \rceil = 5$ as proposed in [GS14]. For comparison to [Ros98], we also considered the matrix $\boldsymbol{B}^\dagger_{\text{sub}}$, which is formed by simply stamping out the desired sparsity pattern from $\boldsymbol{B}^\dagger$. Note that in all of these approaches we choose the B–spline window function φ_{B}. Moreover, we also study the reconstruction by Algorithm 3.21, where we use $\tilde{\boldsymbol{B}}_{\text{opt}}$ as solution to (3.83), cf. [KP19], and $\boldsymbol{B}_{\text{opt}}$ computed by means of Algorithm 3.25. In these two cases we make use of the Dirichlet window function φ_{D} in (3.64), such that $\boldsymbol{D} = \frac{1}{|\mathcal{I}_{M_\sigma}|}\boldsymbol{I}_{|\mathcal{I}_M|}$.

The corresponding results are depicted in Figure 3.10. It can clearly be seen that cutting the desired sparsity pattern out of $\boldsymbol{B}^\dagger$ is somewhat different and much worse than the optimization procedure in (3.73). However, also the sparse approximation $\boldsymbol{S}$ from (3.73) is not as good as the dense pseudoinverse $\boldsymbol{B}^\dagger$. Interestingly, for using a submatrix with $n = 2r + 1 < |\mathcal{I}_{M_\sigma}|$ as proposed in [Ros98] we found that for all $r \geq 3$ we receive the same maximum reconstruction error, only for $r \leq 2$ the error got worse. Considering the frame theoretical approach in (3.82), we recognize that this yields results similar to the sparse approximation of the pseudoinverse, cf. (3.73). Only our optimization procedure from Algorithm 3.25 and the related method from [KP19], cf. (3.83), produce much better reconstructions, which is presumably due to the highest degree of freedom in the optimization process. ◇

Comparison of the two approaches

Finally, we compare the density compensation approach from Section 3.2 with the matrix optimization approach from Section 3.3, as done in [KP23a, Example 5.4].

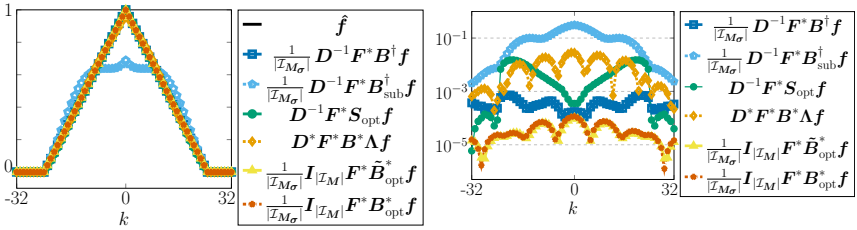

(a) Reconstruction

(b) Pointwise reconstruction error

Figure 3.10: Reconstructions of the triangular pulse (3.93) and pointwise errors for the different matrix optimization methods from Section 3.3 with $d = 1$, $M = 64$, $\sigma = 1.0$, $m = 2$ and $N = 2M$ jittered points (3.85).

Example 3.36. To compare the density compensation approach of Algorithm 3.2 using the weights computed by Algorithm 3.10, with the optimization approach of Algorithm 3.21 using the modified matrix $\boldsymbol{B}_{\text{opt}}$ computed by Algorithm 3.25, we restrict ourselves to the two-dimensional setting $d = 2$ to simplify the visualization of the results. In addition, we again consider the Shepp-Logan phantom as Fourier coefficients of a trigonometric polynomial (2.8) of degree $\boldsymbol{M}$.

(a) In a first experiment, we test the inversion methods of Sections 3.2 and 3.3 as in [ACD+08] for increasing input sizes. For this we choose $\boldsymbol{M} = (M, M)^\top$, $M = 2^c$ with $c = 3, \dots, 10$, and linogram grids (3.88) of size $R = 2M$, $T = 2R$, i. e., we consider the setting $|\mathcal{I}_{\boldsymbol{2M}}| < N$. To use Algorithm 3.21, we additionally choose the oversampling factor $\sigma = 1.0$ and the truncation parameter $m = 4$. For each input size we measure the computation time of the precomputational steps, i. e., the computation of the weight matrix $\boldsymbol{W} = \operatorname{diag}(w_j)_{j=1}^N$ or the computation of the optimized sparse matrix $\boldsymbol{B}_{\text{opt}} \in \mathbb{R}^{N \times |\mathcal{I}_{\boldsymbol{M_\sigma}}|}$, see Algorithms 3.10 and 3.25, as well as the time needed for the reconstruction, i. e., the corresponding adjoint NFFT, see Algorithms 3.2 and 3.21. Moreover, for the reconstruction $\tilde{\boldsymbol{h}} \in \{\tilde{\boldsymbol{h}}^{\text{w}}, \boldsymbol{h}_{\text{opt}}\}$, cf. (3.6) and (3.60), we consider the relative errors

$$e_2 := \frac{\|\tilde{\boldsymbol{h}} - \hat{\boldsymbol{f}}\|_2}{\|\hat{\boldsymbol{f}}\|_2}. \tag{3.99}$$

The corresponding results can be found in Table 3.2. We remark that since we ensured $|\mathcal{I}_{\boldsymbol{2M}}| < N$, the density compensation method in Algorithm 3.2 with weights computed by (3.15) indeed produces nearly exact results. Although, our optimization procedure from Algorithm 3.21 achieves small errors as well, this reconstruction is not as good as the one by means of our density compensation method.

Note that in comparison to [ACD+08] our method in Algorithm 3.2 using density compensation produces errors of the same order, but is much more effective for solving multiple problems with the same points $\boldsymbol{x}_j \in \mathbb{T}^d$, $j = 1, \dots, N$, for different input values $\boldsymbol{f} \in \mathbb{C}^N$. Since our precomputations have to be done only once in this setting, we strongly benefit from the fact that we only need to perform an adjoint NFFT as reconstruction, which is very fast, whereas in [ACD+08] they would need to execute their whole routine each time again.

	Relative error e_2		Precomputation time		Reconstruction time	
M	Alg. 3.2	Alg. 3.21	Alg. 3.10	Alg. 3.25	Alg. 3.2	Alg. 3.21
8	1.33e−15	6.86e−14	9.83e−02	1.92e+00	6.25e−04	2.24e−03
16	7.23e−15	1.57e−07	1.62e−01	8.33e+00	2.51e−03	3.48e−03
32	2.34e−14	4.58e−07	3.30e−01	4.32e+01	3.19e−03	7.48e−03
64	2.59e−14	4.75e−07	3.43e+00	2.41e+02	5.04e−03	4.93e−03
128	7.90e−14	6.00e−07	9.47e+00	1.21e+03	2.99e−02	5.51e−02
256	2.64e−13	4.09e−06	3.84e+01	5.84e+03	6.64e−02	6.78e−01
512	1.09e−12	2.02e−06	1.40e+02	2.92e+04	2.17e−01	3.27e+00
1024	4.26e−12	1.35e−05	7.22e+02	1.43e+05	7.49e−01	1.61e+01

Table 3.2: Relative errors (3.99) of the reconstruction of the Shepp-Logan phantom of size M as well as the runtime in seconds for the density compensation method from Algorithm 3.2 compared to Algorithm 3.21 with $\sigma = 1.0$ and $m = 4$, using linogram grids (3.88) of size $R = 2M,\ T = 2R$.

(b) In a second experiment we aim to decrease the amount of overdetermination, i. e., we keep the size $|\mathcal{I}_{\boldsymbol{M}}|$ of the phantom, but reduce the number N of the nonequispaced points $\boldsymbol{x}_j \in \mathbb{T}^d$, $j = 1, \dots, N$. To this end, we now consider linogram grids (3.88) of the smaller size $R = M$, $T = 2R$, i. e., we now have $|\mathcal{I}_{\boldsymbol{2M}}| > N$. The reconstruction of the phantom of size 1024×1024 is presented in Figure 3.11 (top) including a detailed view of the 832nd row of this reconstruction (bottom) for both the density

compensation method of Algorithm 3.2 using weights computed by means of Algorithm 3.10 as well as the optimization method of Algorithm 3.21 using the modified matrix computed by means of Algorithm 3.25. The corresponding relative errors (3.99) are included in Figure 3.11 as well.

Note that although we have previously seen that in the setting $|\mathcal{I}_{\boldsymbol{2M}}| > N$ the weights computed using (3.44) and (3.48) might be more promising than the weights computed by means of Algorithm 3.10, these weights cannot be computed for the considered phantom size of Figure 3.11, cf. Remarks 3.15 and 3.18.

Due to the fact that the exactness condition $|\mathcal{I}_{\boldsymbol{2M}}| < N$ (cf. Section 3.2.2) is violated, it can be seen in Figure 3.11b that the density compensation method using the weights computed by means of (3.16) does not yield an exact reconstruction in this setting. On the contrary, we recognize that our optimization method, see Figure 3.11c, achieves a huge improvement in comparison to the density compensation technique in Figure 3.11b, since is does not show any artifacts. Presumably, this is due to the higher amount of degrees of freedom in the optimization of the matrix $\boldsymbol{B}$ from Section 3.3 than in the density compensation techniques from Section 3.2, cf. Remark 3.3. We remark that although the errors are not as small as in Table 3.2, by comparing Figures 3.11a and 3.11c it becomes apparent that the differences are not even visible anymore.

Finally, note that for this result the number N of points is about 4 times lower than for the results shown in Table 3.2. That is to say, we needed only twice as many function values as Fourier coefficients, whereas e. g. in [ACD+08] they needed a factor of more than 4. ◇

Remark 3.37. Note that the code files for all the experiments in this section are available at [Kir] under `https://github.com/melaniekircheis/dissertation/tree/main/3-Direct_inversion_methods_for_the_NFFT`. ◇

Summary

In this chapter, we have investigated direct inversion methods for solving problem (3.3) and gave a comprehensive overview of the existing approaches. In particular, we have presented a recently developed sampling density compensation technique as well as matrix optimization procedure, which can be seen as a generalized approach. In addition, both methods were considered and compared to several approaches known from the literature.

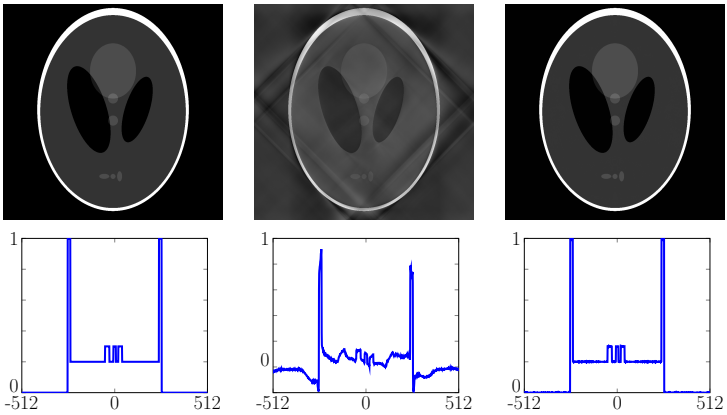

(a) Original phantom

(b) Algorithm 3.2 with e_2=5.0585e-01

(c) Algorithm 3.21 with e_2=2.2737e-03

Figure 3.11: Reconstruction of the Shepp-Logan phantom of size 1024×1024 (top) via the density compensation method from Algorithm 3.2 using weights computed by Algorithm 3.10 compared to the optimization method from Algorithm 3.21 using the modified matrix computed by Algorithm 3.25 for the linogram grid (3.88) of size $R = M = 1024$, $T = 2R$; as well as a detailed view of the 832nd row each (bottom).

All in all, we have seen that our new methods introduced in Sections 3.2 and 3.3 both are optimal in their appropriate setting, outperforming comparable approaches. More specifically, in case of the highly overdetermined setting $|\mathcal{I}_{\mathbf{2}\boldsymbol{M}}| < N$ of problem (3.3) it was demonstrated that the density compensation approach from Algorithm 3.2 using the weights computed by means of Algorithm 3.10 does indeed yield exact results. Considering the overdetermined setting of problem (3.3) with $|\mathcal{I}_{\boldsymbol{M}}| < N < |\mathcal{I}_{\mathbf{2}\boldsymbol{M}}|$, instead, the matrix optimization approach from Algorithm 3.21 using the optimized sparse matrix computed by means of Algorithm 3.25 has proven to be the best.

4 Regularized Shannon sampling formulas

So far, we have focused exclusively on trigonometric polynomials (2.8), which are periodic functions on the torus $\mathbb{T}^d$ possessing only a finite number of nonzero Fourier coefficients. Moving forward, we will broaden our attention to functions on $\mathbb{R}^d$ that exhibit a similar property with respect to the continuous Fourier transform, known as bandlimited functions.

For this purpose, we start Section 4.1 with some important preliminaries, including the definition and properties of bandlimited functions, as well as the famous sampling theorem of Whittaker–Kotelnikov–Shannon. Secondly, in Section 4.2 we proceed with practical aspects regarding this theorem, presenting evidence for the poor convergence rate and the lack of numerical robustness of classical Shannon sampling sums. Therefore, the proposed numerical realizations of the Whittaker–Kotelnikov–Shannon sampling theorem are based on an additional regularization. These regularized Shannon sampling formulas are presented in Section 4.3 for the univariate setting and generalized to the multivariate setting in Section 4.4. In conclusion, the final Section 4.5 includes several numerical examples, such as visualizations of theoretical results and comparisons of the different approaches, as well as a short summary.

4.1 Bandlimited functions and the sampling theorem

A function $f\colon \mathbb{R}^d \to \mathbb{C}$ is said to be *bandlimited* with *bandwidth* $M \in \mathbb{N}$, if the support of its *(continuous) Fourier transform*

$$\hat{f}(\boldsymbol{v}) \coloneqq \int_{\mathbb{R}^d} f(\boldsymbol{x})\, \mathrm{e}^{-2\pi \mathrm{i} \boldsymbol{v}\boldsymbol{x}}\, \mathrm{d}\boldsymbol{x}, \quad \boldsymbol{v} \in \mathbb{R}^d, \tag{4.1}$$

is contained in $\left[-\frac{M}{2}, \frac{M}{2}\right]^d$. Since $|f(\boldsymbol{x})\, \mathrm{e}^{-2\pi \mathrm{i} \boldsymbol{v}\boldsymbol{x}}| = |f(\boldsymbol{x})|$, the Fourier transform (4.1) is well-defined on the Banach space $L_1(\mathbb{R}^d)$ of measurable func-

tions $f\colon \mathbb{R}^d \to \mathbb{C}$ with finite norm

$$\|f\|_{L_1(\mathbb{R}^d)} \coloneqq \int_{\mathbb{R}^d} |f(\boldsymbol{x})| \,\mathrm{d}\boldsymbol{x} < \infty,$$

where almost equal functions are identified. Additionally, it is known (see e. g. [PPST23, Theorem 4.21] or [Par97, Proposition 7.1.2]) that the Fourier transform (4.1) on $L_1(\mathbb{R}^d)$ is a continuous mapping into the Banach space $C_0(\mathbb{R}^d)$ of continuous functions $f\colon \mathbb{R}^d \to \mathbb{C}$ vanishing as $\|\boldsymbol{x}\|_2 \to \infty$, with the norm

$$\|f\|_{C_0(\mathbb{R}^d)} \coloneqq \max_{\boldsymbol{x}\in\mathbb{R}^d} |f(\boldsymbol{x})|. \tag{4.2}$$

Since function evaluations of f will be relevant for our purposes, we require at least $f \in L_1(\mathbb{R}^d) \cap C_0(\mathbb{R}^d)$. Additionally, considering the Hilbert space $L_2(\mathbb{R}^d)$ with inner product and norm

$$\langle f, g\rangle_{L_2(\mathbb{R}^d)} \coloneqq \int_{\mathbb{R}^d} f(\boldsymbol{x})\,\overline{g(\boldsymbol{x})}\,\mathrm{d}\boldsymbol{x}, \quad \|f\|_{L_2(\mathbb{R}^d)} \coloneqq \left(\int_{\mathbb{R}^d} |f(\boldsymbol{x})|^2 \,\mathrm{d}\boldsymbol{x}\right)^{1/2},$$

we obviously have $L_1(\mathbb{R}^d) \cap C_0(\mathbb{R}^d) \subseteq L_2(\mathbb{R}^d)$, since

$$\begin{aligned}\|f\|_{L_2(\mathbb{R}^d)}^2 = \int_{\mathbb{R}^d} |f(\boldsymbol{x})|^2 \,\mathrm{d}\boldsymbol{x} &\le \max_{\boldsymbol{x}\in\mathbb{R}^d} |f(\boldsymbol{x})| \cdot \int_{\mathbb{R}^d} |f(\boldsymbol{x})| \,\mathrm{d}\boldsymbol{x} \\ &= \|f\|_{C_0(\mathbb{R}^d)}^2 \cdot \|f\|_{L_1(\mathbb{R}^d)}^2.\end{aligned}$$

Furthermore, the Fourier transform can be uniquely extended to $L_2(\mathbb{R}^d)$, see e. g. [PPST23, Theorem 4.25]. Therefore, let the space of all bandlimited functions with bandwidth $M \in \mathbb{N}$ be denoted by

$$\mathcal{B}_{M/2}(\mathbb{R}^d) \coloneqq \left\{ f \in L_2(\mathbb{R}^d) \colon \operatorname{supp}(\hat{f}) \subseteq \left[-\tfrac{M}{2}, \tfrac{M}{2}\right]^d \right\}, \tag{4.3}$$

which is also known as the *Paley–Wiener space*.

By definition, the Paley–Wiener space $\mathcal{B}_{M/2}(\mathbb{R}^d)$ consists of equivalence classes of almost equal functions. However, it can be shown that there is always a smooth representation. To this end, let $C^r(\mathbb{R}^d)$ denote the class of r-times continuously differentiable functions, where for all multi-indices $\boldsymbol{\alpha} \coloneqq (\alpha_t)_{t=1}^d \in \mathbb{N}_0^d$ with $|\boldsymbol{\alpha}| \coloneqq \alpha_1 + \cdots + \alpha_d \le r$ the partial derivatives

$$(D^{\boldsymbol{\alpha}} f)(\boldsymbol{x}) \coloneqq \frac{\partial^{\boldsymbol{\alpha}} f}{\partial x_1^{\alpha_1} \partial x_2^{\alpha_2} \dots \partial x_d^{\alpha_d}}$$

exist and are continuous. Then the following embedding can be shown.

Lemma 4.1. *For the Paley–Wiener space* (4.3) *we have*

$$\mathcal{B}_{M/2}(\mathbb{R}^d) \subseteq L_2(\mathbb{R}^d) \cap C_0(\mathbb{R}^d) \cap C^\infty(\mathbb{R}^d).$$

Proof. Let $f \in \mathcal{B}_{M/2}(\mathbb{R}^d)$. By the theorem of Plancherel (see e. g. [PPST23, Theorem 4.25]) the Fourier transform is a linear, continuous and invertible mapping from $L_2(\mathbb{R}^d)$ onto itself with $\|f\|_{L_2(\mathbb{R}^d)} = \|\hat{f}\|_{L_2(\mathbb{R}^d)}$, i. e., we have $\hat{f} \in L_2(\mathbb{R}^d)$. Now using the Cauchy–Schwarz inequality we obtain

$$\begin{aligned}
\|\hat{f}\|_{L_1(\mathbb{R}^d)} &= \int_{\mathbb{R}^d} |\hat{f}(\boldsymbol{v})| \,\mathrm{d}\boldsymbol{v} = \int_{\left[-\frac{M}{2},\frac{M}{2}\right]^d} 1 \cdot |\hat{f}(\boldsymbol{v})| \,\mathrm{d}\boldsymbol{v} \\
&\leq \left(\int_{\left[-\frac{M}{2},\frac{M}{2}\right]^d} 1^2 \,\mathrm{d}\boldsymbol{v} \right)^{1/2} \left(\int_{\left[-\frac{M}{2},\frac{M}{2}\right]^d} |\hat{f}(\boldsymbol{v})|^2 \,\mathrm{d}\boldsymbol{v} \right)^{1/2} \\
&= \sqrt{|\mathcal{I}_{\boldsymbol{M}}|} \cdot \|\hat{f}\|_{L_2(\mathbb{R}^d)} < \infty.
\end{aligned}$$

In other words, we have $f \in L_2(\mathbb{R}^d)$ and $\hat{f} \in L_1(\mathbb{R}^d)$. Thus, by the Fourier inversion theorem, see e. g. [PPST23, Theorem 2.23], the *inverse Fourier transform* of f can be written as

$$f(\boldsymbol{x}) = \int_{\mathbb{R}^d} \hat{f}(\boldsymbol{v}) \, \mathrm{e}^{2\pi \mathrm{i} \boldsymbol{v}\boldsymbol{x}} \,\mathrm{d}\boldsymbol{v} = \int_{\left[-\frac{M}{2},\frac{M}{2}\right]^d} \hat{f}(\boldsymbol{v}) \, \mathrm{e}^{2\pi \mathrm{i} \boldsymbol{v}\boldsymbol{x}} \,\mathrm{d}\boldsymbol{v}, \quad \boldsymbol{x} \in \mathbb{R}^d. \tag{4.4}$$

Since it is additionally known that the inverse Fourier transform (4.4) is a continuous mapping from $L_1(\mathbb{R}^d)$ into $C_0(\mathbb{R}^d)$ (see e. g. [Par97, Proposition 7.1.2]), we have $\mathcal{B}_{M/2}(\mathbb{R}^d) \subseteq L_2(\mathbb{R}^d) \cap C_0(\mathbb{R}^d)$. Moreover, the inverse Fourier transform (4.4) also implies

$$\begin{aligned}
(D^{\boldsymbol{\alpha}} f)(\boldsymbol{x}) &= \int_{\left[-\frac{M}{2},\frac{M}{2}\right]^d} \hat{f}(\boldsymbol{v}) \, \left(D^{\boldsymbol{\alpha}} \mathrm{e}^{2\pi \mathrm{i} \boldsymbol{v}\boldsymbol{x}} \right)(\boldsymbol{x}) \,\mathrm{d}\boldsymbol{v} \\
&= \int_{\left[-\frac{M}{2},\frac{M}{2}\right]^d} \hat{f}(\boldsymbol{v}) \, (2\pi \mathrm{i} \boldsymbol{v})^{\boldsymbol{\alpha}} \, \mathrm{e}^{2\pi \mathrm{i} \boldsymbol{v}\boldsymbol{x}} \,\mathrm{d}\boldsymbol{v}.
\end{aligned}$$

Using the Cauchy–Schwarz inequality again, one can show that $(2\pi \mathrm{i} \cdot)^{\boldsymbol{\alpha}} \hat{f} \in L_1(\mathbb{R}^d)$ such that $D^{\boldsymbol{\alpha}} f \in C_0(\mathbb{R}^d)$ for all $\boldsymbol{\alpha} \in \mathbb{N}_0^d$, and therefore $f \in \mathbb{C}^\infty(\mathbb{R}^d)$ as well. ∎

To examine further properties of the bandlimited functions $f \in \mathcal{B}_{M/2}(\mathbb{R}^d)$, let us consider the set $\big\{\sqrt{|\mathcal{I}_{\boldsymbol{M}}|}\,\mathrm{sinc}(M\pi(\cdot - \frac{\boldsymbol{\ell}}{M})) : \boldsymbol{\ell} \in \mathbb{Z}^d\big\}$. It is easy to see that this set constitutes an orthonormal system in $L_2(\mathbb{R}^d)$, since by the shifting property of the Fourier transform and the definition of the sinc function (3.31) the Fourier transform of $\mathrm{sinc}(M\pi(\cdot - \frac{\boldsymbol{\ell}}{M}))$ is equal to

$$\frac{1}{|\mathcal{I}_{\boldsymbol{M}}|}\,\mathrm{e}^{-2\pi\mathrm{i}\boldsymbol{\ell}\boldsymbol{v}/M}\,\chi_{[-\frac{M}{2},\,\frac{M}{2}]^d}(\boldsymbol{v}), \quad \boldsymbol{v} \in \mathbb{R}^d,$$

and by Parseval's identity we have for all $\boldsymbol{k}$, $\boldsymbol{\ell} \in \mathbb{Z}^d$ that

$$\begin{aligned}\big\langle \sqrt{|\mathcal{I}_{\boldsymbol{M}}|}\,\mathrm{sinc}(M\pi(\cdot - \tfrac{\boldsymbol{k}}{M})), \sqrt{|\mathcal{I}_{\boldsymbol{M}}|}\,\mathrm{sinc}(M\pi(\cdot - \tfrac{\boldsymbol{\ell}}{M}))\big\rangle_{L_2(\mathbb{R}^d)} \\ = \frac{1}{|\mathcal{I}_{\boldsymbol{M}}|} \int\limits_{[-\frac{M}{2},\frac{M}{2}]^d} \mathrm{e}^{2\pi\mathrm{i}(\boldsymbol{\ell}-\boldsymbol{k})\boldsymbol{v}/M}\,\mathrm{d}\boldsymbol{v} = \delta_{\boldsymbol{k},\boldsymbol{\ell}}\end{aligned} \tag{4.5}$$

with the *Kronecker symbol*

$$\delta_{\boldsymbol{k},\boldsymbol{\ell}} \coloneqq \prod_{t=1}^{d} \delta_{k_t,\ell_t} = \begin{cases} 1 & : \boldsymbol{k} = \boldsymbol{\ell}, \\ 0 & : \boldsymbol{k} \neq \boldsymbol{\ell}. \end{cases}$$

Moreover, it is known that the system $\big\{\sqrt{|\mathcal{I}_{\boldsymbol{M}}|}\,\mathrm{sinc}(M\pi(\cdot - \frac{\boldsymbol{\ell}}{M})) : \boldsymbol{\ell} \in \mathbb{Z}^d\big\}$ even forms an orthonormal basis of $\mathcal{B}_{M/2}(\mathbb{R}^d)$, see e. g. [LB92, Theorem 2.7]. That is to say, all $f \in \mathcal{B}_{M/2}(\mathbb{R}^d)$ possess the unique representation

$$f(\boldsymbol{x}) = \sum_{\boldsymbol{\ell}\in\mathbb{Z}^d} \nu_{\boldsymbol{\ell}}\,\mathrm{sinc}(M\pi(\boldsymbol{x} - \tfrac{\boldsymbol{\ell}}{M})), \quad \boldsymbol{x} \in \mathbb{R}^d,$$

where the coefficients are given by

$$\begin{aligned}\nu_{\boldsymbol{\ell}} &= |\mathcal{I}_{\boldsymbol{M}}| \cdot \big\langle f,\, \mathrm{sinc}(M\pi(\cdot - \tfrac{\boldsymbol{\ell}}{M}))\big\rangle_{L_2(\mathbb{R}^d)} \\ &= |\mathcal{I}_{\boldsymbol{M}}| \int\limits_{\mathbb{R}^d} f(\boldsymbol{x})\,\mathrm{sinc}(M\pi(\boldsymbol{x} - \tfrac{\boldsymbol{\ell}}{M}))\,\mathrm{d}\boldsymbol{x}, \quad \boldsymbol{\ell} \in \mathbb{Z}^d.\end{aligned} \tag{4.6}$$

In addition, since

$$\begin{aligned}\int_{-M/2}^{M/2} \mathrm{e}^{2\pi\mathrm{i}v(x-\ell/M)}\,\mathrm{d}v &= \frac{\mathrm{e}^{M\pi\mathrm{i}(x-\frac{\ell}{M})} - \mathrm{e}^{-M\pi\mathrm{i}(x-\frac{\ell}{M})}}{2\mathrm{i}\cdot\pi(x-\frac{\ell}{M})} \\ &= M\,\mathrm{sinc}(M\pi(x-\tfrac{\ell}{M})),\end{aligned}$$

we can rewrite the coefficients (4.6) by means of (4.1) and (4.4) as

$$\begin{aligned}\nu_{\boldsymbol{\ell}} &= \int_{\mathbb{R}^d} f(\boldsymbol{x}) \int_{\left[-\frac{M}{2},\frac{M}{2}\right]^d} \mathrm{e}^{2\pi\mathrm{i}\boldsymbol{v}(\boldsymbol{x}-\boldsymbol{\ell}/M)}\,\mathrm{d}\boldsymbol{v}\,\mathrm{d}\boldsymbol{x} \\ &= \int_{\left[-\frac{M}{2},\frac{M}{2}\right]^d} \left(\int_{\mathbb{R}^d} f(\boldsymbol{x})\,\mathrm{e}^{2\pi\mathrm{i}\boldsymbol{v}\boldsymbol{x}}\,\mathrm{d}\boldsymbol{x} \right) \mathrm{e}^{-2\pi\mathrm{i}\boldsymbol{v}\boldsymbol{\ell}/M}\,\mathrm{d}\boldsymbol{v} \\ &= \int_{\left[-\frac{M}{2},\frac{M}{2}\right]^d} \hat{f}(\boldsymbol{v})\,\mathrm{e}^{2\pi\mathrm{i}\boldsymbol{v}\boldsymbol{\ell}/M}\,\mathrm{d}\boldsymbol{v} = f\left(\tfrac{\boldsymbol{\ell}}{M}\right), \quad \boldsymbol{\ell} \in \mathbb{Z}^d.\end{aligned}$$

A more general version of this result is known as the classical *Whittaker–Kotelnikov–Shannon sampling theorem*, see Theorem 4.2, which plays a fundamental role in signal processing, since it describes the close relation between a bandlimited function and its equidistant samples. It was discovered independently by the mathematician E. T. Whittaker [Whi15] as well as the electrical engineers V. A. Kotelnikov [Kot01] and C. E. Shannon [Sha49]. However, since Shannon was the first to recognize the relevance of the sampling theorem in digital signal processing, it is frequently attributed to him exclusively.

Theorem 4.2 (**Sampling theorem of Whittaker–Kotelnikov–Shannon**). *Let $f \in \mathcal{B}_{M/2}(\mathbb{R}^d)$ be bandlimited with bandwidth $M \in \mathbb{N}$. Further let $L \geq M$, $L \in \mathbb{N}$. Then f is completely determined by its values $f\left(\frac{\boldsymbol{\ell}}{L}\right)$, $\boldsymbol{\ell} \in \mathbb{Z}^d$, and f can be represented in the form*

$$f(\boldsymbol{x}) = \sum_{\boldsymbol{\ell}\in\mathbb{Z}^d} f\left(\tfrac{\boldsymbol{\ell}}{L}\right) \operatorname{sinc}\left(L\pi\left(\boldsymbol{x} - \tfrac{\boldsymbol{\ell}}{L}\right)\right), \quad \boldsymbol{x} \in \mathbb{R}^d, \tag{4.7}$$

where the series converges absolutely and uniformly on $\mathbb{R}^d$.

Proof. (cf. e. g. [PPST23, Theorem 2.31])

(i) For $L \geq M$ we have $\mathcal{B}_{M/2}(\mathbb{R}^d) \subseteq \mathcal{B}_{L/2}(\mathbb{R}^d)$ by definition (4.3), because of the simple embedding $\left[-\frac{M}{2}, \frac{M}{2}\right]^d \subseteq \left[-\frac{L}{2}, \frac{L}{2}\right]^d$. Hence, each $f \in \mathcal{B}_{M/2}(\mathbb{R}^d)$ can be regarded as a function $f \in \mathcal{B}_{L/2}(\mathbb{R}^d)$ and therefore (4.7) holds as shown above.

(ii) Considering the absolute convergence, the Cauchy–Schwarz inequality implies

$$\sum_{\boldsymbol{\ell}\in\mathbb{Z}^d} \big|f\big(\tfrac{\boldsymbol{\ell}}{L}\big)\big| \cdot \big|\mathrm{sinc}\big(L\pi\big(\boldsymbol{x}-\tfrac{\boldsymbol{\ell}}{L}\big)\big)\big| \leq \left(\sum_{\boldsymbol{\ell}\in\mathbb{Z}^d} \big|f\big(\tfrac{\boldsymbol{\ell}}{L}\big)\big|^2\right)^{1/2} \left(\sum_{\boldsymbol{\ell}\in\mathbb{Z}^d} \big[\mathrm{sinc}(L\pi\boldsymbol{x}-\pi\boldsymbol{\ell})\big]^2\right)^{1/2}. \tag{4.8}$$

For the first term it is known by the representation (4.7) and the orthonormality property (4.5) that for any $f \in \mathcal{B}_{M/2}(\mathbb{R}^d) \subseteq \mathcal{B}_{L/2}(\mathbb{R}^d)$ with $L \geq M$ we have

$$\|f\|^2_{L_2(\mathbb{R}^d)} = \langle f, f\rangle_{L_2(\mathbb{R}^d)} = \frac{1}{L^d} \sum_{\boldsymbol{\ell}\in\mathbb{Z}^d} \big|f\big(\tfrac{\boldsymbol{\ell}}{L}\big)\big|^2, \tag{4.9}$$

cf. [Nik75]. For the second term we consider the 1-periodic function $h(\boldsymbol{t}) \coloneqq \mathrm{e}^{2\pi\mathrm{i}L\boldsymbol{t}\boldsymbol{x}}$, $\boldsymbol{t} \in \big[-\frac{1}{2},\frac{1}{2}\big)^d$, for fixed $\boldsymbol{x} \in \mathbb{R}^d$, whose Fourier series is given by

$$h(\boldsymbol{t}) = \sum_{\boldsymbol{k}\in\mathbb{Z}^d} c_{\boldsymbol{k}}(h)\,\mathrm{e}^{2\pi\mathrm{i}\boldsymbol{k}\boldsymbol{t}}, \quad \boldsymbol{t} \in \big[-\tfrac{1}{2},\tfrac{1}{2}\big)^d,$$

with the Fourier coefficients

$$c_{\boldsymbol{k}}(h) = \int_{\left[-\frac{1}{2},\frac{1}{2}\right]^d} \mathrm{e}^{2\pi\mathrm{i}\boldsymbol{t}(L\boldsymbol{x}-\boldsymbol{k})}\,\mathrm{d}\boldsymbol{t} = \mathrm{sinc}(L\pi\boldsymbol{x}-\pi\boldsymbol{k}), \quad \boldsymbol{k}\in\mathbb{Z}^d.$$

Then, using the Parseval's identity we obtain for each fixed $\boldsymbol{x} \in \mathbb{R}^d$ that

$$\sum_{\boldsymbol{k}\in\mathbb{Z}^d} \big[\mathrm{sinc}(L\pi\boldsymbol{x}-\pi\boldsymbol{k})\big]^2 = \|h\|_{L_2\left(\left[-\frac{1}{2},\frac{1}{2}\right]^d\right)} = 1. \tag{4.10}$$

Thus, by (4.8), (4.9), and (4.10), for each $\boldsymbol{x} \in \mathbb{R}^d$ the series in (4.7) is absolutely convergent with

$$\sum_{\boldsymbol{\ell}\in\mathbb{Z}^d} \big|f\big(\tfrac{\boldsymbol{\ell}}{L}\big)\big| \cdot \big|\mathrm{sinc}\big(L\pi\big(\boldsymbol{x}-\tfrac{\boldsymbol{\ell}}{L}\big)\big)\big| \leq L^{d/2}\,\|f\|_{L_2(\mathbb{R}^d)}.$$

(iii) Regarding the uniform convergence, we need to show that

$$\lim_{T\to\infty} \|f - S_T f\|_{C_0(\mathbb{R}^d)} = 0, \tag{4.11}$$

where $S_T f$ denotes the *T-th Shannon sampling sum*

$$(S_T f)(\boldsymbol{x}) \coloneqq \sum_{\|\boldsymbol{\ell}\|_\infty \le T} f\big(\tfrac{\boldsymbol{\ell}}{L}\big)\,\operatorname{sinc}(L\pi\boldsymbol{x} - \pi\boldsymbol{\ell}), \quad \boldsymbol{x} \in \mathbb{R}^d. \tag{4.12}$$

By the representations (4.7) and (4.12) we have

$$f(\boldsymbol{x}) - (S_T f)(\boldsymbol{x}) = \sum_{\|\boldsymbol{\ell}\|_\infty > T} f\big(\tfrac{\boldsymbol{\ell}}{L}\big)\,\operatorname{sinc}(L\pi\boldsymbol{x} - \pi\boldsymbol{\ell}), \quad \boldsymbol{x} \in \mathbb{R}^d.$$

Then the Cauchy–Schwarz inequality yields

$$\begin{aligned}&\big|f(\boldsymbol{x}) - (S_T f)(\boldsymbol{x})\big| \\ &\qquad \le \Bigg(\sum_{\|\boldsymbol{\ell}\|_\infty > T} \big|f\big(\tfrac{\boldsymbol{\ell}}{L}\big)\big|^2\Bigg)^{1/2} \Bigg(\sum_{\|\boldsymbol{\ell}\|_\infty > T} \big[\operatorname{sinc}(L\pi\boldsymbol{x} - \pi\boldsymbol{\ell})\big]^2\Bigg)^{1/2}.\end{aligned} \tag{4.13}$$

Since both series converge by (4.9) and (4.10), the partial sums satisfy

$$\lim_{T\to\infty} \sum_{\|\boldsymbol{\ell}\|_\infty > T} \big|f\big(\tfrac{\boldsymbol{\ell}}{L}\big)\big|^2 = 0 \quad \text{and} \quad \lim_{T\to\infty} \sum_{\|\boldsymbol{\ell}\|_\infty > T} \big[\operatorname{sinc}(L\pi\boldsymbol{x} - \pi\boldsymbol{\ell})\big]^2 = 0. \tag{4.14}$$

Hence, the uniform convergence property (4.11) is implied by (4.13) and (4.14). ∎

Unfortunately, the numerical use of this classical Whittaker–Kotelnikov–Shannon sampling theorem (see Theorem 4.2) is limited, since it requires infinitely many samples, which is impossible in practice. Based on this observation, numerous approaches for numerical realizations have been developed. To provide an overview on this subject, this chapter is organized as follows. Firstly, in Section 4.2 we show the poor convergence and non-robustness of the classical Shannon sampling sums (4.12) and improve results on the upper and lower bounds of the norm of the Shannon sampling operator. Consequently, we study several regularization techniques that can mitigate these drawbacks. Specifically, in Section 4.3 we firstly limit our focus to the simpler univariate setting. Afterwards, the most efficient method is generalized to the multivariate setting in Section 4.4. Finally, we compare the approaches from Sections 4.3.1 and 4.3.2, and illustrate our theoretical findings by the numerical examples in Section 4.5.

4.2 Poor convergence of Shannon sampling sums

Due to the fact that the sinc function has rather poor decay, the *Shannon sampling series*

$$\sum_{\boldsymbol{\ell}\in\mathbb{Z}^d} f\big(\tfrac{\boldsymbol{\ell}}{L}\big)\,\mathrm{sinc}(L\pi\boldsymbol{x}-\pi\boldsymbol{\ell}),\quad \boldsymbol{x}\in\mathbb{R}^d, \tag{4.15}$$

converges very slowly. In order to demonstrate this fact, we truncate the series (4.15) with $T\in\mathbb{N}$ and analyze the T-th Shannon sampling sum (4.12) in greater detail. More precisely, since these sums can be constructed for every $f\in C_0(\mathbb{R}^d)$, we firstly examine the norm $\|S_T\|$ of the corresponding operator.

Lemma 4.3. *The linear operator $S_T : C_0(\mathbb{R}^d)\to C_0(\mathbb{R}^d)$ in (4.12) has the norm*

$$\|S_T\| = \max_{\boldsymbol{x}\in\mathbb{R}^d} \sum_{\|\boldsymbol{\ell}\|_\infty\le T} |\mathrm{sinc}(L\pi\boldsymbol{x}-\pi\boldsymbol{\ell})|. \tag{4.16}$$

Proof. For each $f\in C_0(\mathbb{R}^d)$ and $\boldsymbol{x}\in\mathbb{R}^d$ the definition (4.12) of the T-th Shannon sampling operator and the definition of the norm (4.2) imply

$$\begin{aligned}\big|(S_Tf)(\boldsymbol{x})\big| &\le \sum_{\|\boldsymbol{\ell}\|_\infty\le T} \big|f\big(\tfrac{\boldsymbol{\ell}}{L}\big)\big|\,\big|\mathrm{sinc}(L\pi\boldsymbol{x}-\boldsymbol{\ell}\pi)\big| \\ &\le \sum_{\|\boldsymbol{\ell}\|_\infty\le T} \big|\mathrm{sinc}(L\pi\boldsymbol{x}-\boldsymbol{\ell}\pi)\big|\,\|f\|_{C_0(\mathbb{R}^d)},\end{aligned}$$

such that

$$\|S_Tf\|_{C_0(\mathbb{R}^d)} \le \max_{\boldsymbol{x}\in\mathbb{R}^d} \sum_{\|\boldsymbol{\ell}\|_\infty\le T} \big|\mathrm{sinc}(L\pi\boldsymbol{x}-\boldsymbol{\ell}\pi)\big|\,\|f\|_{C_0(\mathbb{R}^d)}.$$

Thus, assuming that the even nonnegative function

$$s_T(\boldsymbol{x}) \coloneqq \sum_{\|\boldsymbol{\ell}\|_\infty\le T} \big|\mathrm{sinc}(L\pi\boldsymbol{x}-\boldsymbol{\ell}\pi)\big|,\quad \boldsymbol{x}\in\mathbb{R}^d, \tag{4.17}$$

which is contained in $C_0(\mathbb{R}^d)$, has its maximum at a point we denote as $\boldsymbol{x}^* \coloneqq (x_1^*, \dots, x_d^*)^\top \in \mathbb{R}^d$, this yields

$$\|S_T\| = \sup\left\{\|S_T f\|_{C_0(\mathbb{R}^d)} \colon \|f\|_{C_0(\mathbb{R}^d)} = 1\right\} \leq s_T(\boldsymbol{x}^*).$$

The other way around, we consider the linear spline $g \in C_0(\mathbb{R})$ with

$$g\left(\tfrac{\ell}{L}\right) = \begin{cases} \operatorname{sign}\bigl(\operatorname{sinc}(L\pi x_t^* - \ell\pi)\bigr) & : \ell = -T, \dots, T, \\ 0 & : \ell \in \mathbb{Z} \setminus \{-T, \dots, T\}. \end{cases}$$

Then its tensorized version $g(\boldsymbol{\ell}) \coloneqq \prod_{t=1}^d g(\ell_t)$ satisfies $\|g\|_{C_0(\mathbb{R}^d)} = 1$ and by the product structure of the sinc function (3.31) we have

$$\begin{aligned}(S_T g)(\boldsymbol{x}) &= \sum_{\|\boldsymbol{\ell}\|_\infty \leq T} \left(\prod_{t=1}^d \operatorname{sign}\bigl(\operatorname{sinc}(L\pi x_t^* - \ell_t\pi)\bigr)\right) \operatorname{sinc}(L\pi\boldsymbol{x} - \boldsymbol{\ell}\pi) \\ &\leq s_T(\boldsymbol{x}^*).\end{aligned}$$

Thus, evaluation at the point $\boldsymbol{x} = \boldsymbol{x}^*$, i. e.,

$$(S_T g)(\boldsymbol{x}^*) = \sum_{\|\boldsymbol{\ell}\|_\infty \leq T} \bigl|\operatorname{sinc}(L\pi\boldsymbol{x}^* - \boldsymbol{\ell}\pi)\bigr| = \max_{\boldsymbol{x}\in\mathbb{R}^d} s_T(\boldsymbol{x}) = s_T(\boldsymbol{x}^*),$$

implies

$$\|S_T\| \geq \|S_T g\|_{C_0(\mathbb{R}^d)} = \max_{\boldsymbol{x}\in\mathbb{R}^d} \bigl|(S_T g)(\boldsymbol{x})\bigr| = s_T(\boldsymbol{x}^*).$$

and hence (4.16). ∎

Note that Lemma 4.3 generalizes the result from [KPT24, Lemma 2.1] to $d > 1$. Now we show that the norm $\|S_T\|$ is unbounded with respect to $T \in \mathbb{N}$.

Lemma 4.4. *The norm of the operator $S_T \colon C_0(\mathbb{R}^d) \to C_0(\mathbb{R}^d)$ can be estimated by*

$$\begin{aligned}\left(\frac{2}{\pi}(\ln T + c) - \frac{1}{\pi T(2T+1)}\right)^d &< \|S_T\| \\ &< \left(\frac{2}{\pi}(\ln T + c) + \frac{T+2}{\pi T(T+1)}\right)^d,\end{aligned} \tag{4.18}$$

where $c \coloneqq 2\ln 2 + \gamma$ *with the* Euler constant

$$\gamma = \lim_{T\to\infty}\left(\sum_{k=1}^{T}\frac{1}{k} - \ln T\right) = 0.57721566\ldots.$$

Proof. For ease of notation we start with the case $d = 1$, as done in [KPT24, Theorem 2.2]. As suggested in [Ste93, Problem 3.1.5] we represent (4.17) in the form

$$s_T(x) = \sum_{\ell=1}^{T+1} a_\ell(x), \quad x \in \mathbb{R},$$

with

$$a_\ell(x) \coloneqq \begin{cases} \left|\operatorname{sinc}(L\pi x - \ell\pi)\right| + \left|\operatorname{sinc}(L\pi x + (\ell-1)\pi)\right| & : \ell = 1, \ldots, T, \\ \left|\operatorname{sinc}(L\pi x + T\pi)\right| & : \ell = T+1. \end{cases}$$

Since the function s_T in (4.17) is even, we estimate its maximum only for $x \geq 0$. For $\ell = 1, \ldots, T$, we have $a_\ell(0) = a_\ell\big(\frac{1}{L}\big) = 0$ and by the trigonometric identities we obtain for $x \in \big(0,\, \frac{1}{L}\big)$ that

$$a_\ell(x) = \frac{\sin(L\pi x)}{\pi}\left(\frac{1}{\ell - 1 + Lx} + \frac{1}{\ell - Lx}\right) = \frac{(2\ell-1)\,\sin(L\pi x)}{\pi\left[(\ell-1)\ell + Lx\,(1-Lx)\right]}.$$

By defining the functions $b_\ell\colon (0,\,1) \to \mathbb{R}$, $\ell = 1, \ldots, T$, via

$$b_\ell(x) \coloneqq \frac{\pi}{(2\ell-1)}\,a_\ell\big(\tfrac{x}{L}\big) = \frac{\sin(\pi x)}{(\ell-1)\ell + x(1-x)}, \quad x \in (0,\,1),$$

we have the symmetry property $b_\ell(x) = b_\ell(1-x)$, i. e., each b_ℓ is symmetric with respect to $\frac{1}{2}$. Furthermore, by $b_\ell'(x) \geq 0$ for $x \in \big(0,\, \frac{1}{2}\big]$, the function b_ℓ is non-decreasing on $\big(0,\, \frac{1}{2}\big]$ and therefore has its maximum at $x = \frac{1}{2}$. Thus, the function $a_\ell\colon \big[0,\, \frac{1}{L}\big] \to \mathbb{R}$ has its maximum at $x = \frac{1}{2L}$, i. e.,

$$\max_{x\in[0,\,1/L]} a_\ell(x) = a_\ell\big(\tfrac{1}{2L}\big) = \frac{4}{(2\ell-1)\pi}, \quad \ell = 1, \ldots, T.$$

Additionally, the function $a_{T+1}(x)$ can be written as

$$a_{T+1}(x) = \frac{\sin(L\pi x)}{\pi\,(T + Lx)}, \quad x \in \left[0,\, \tfrac{1}{L}\right],$$

such that

$$0 < \max_{x\in[0,\,1/L]} a_{T+1}(x) < \frac{1}{\pi T}.$$

Note that in the case $T \gg 1$ the function $a_{T+1}\colon \left[0,\,\frac{1}{L}\right] \to \mathbb{R}$ has its maximum close to $x = \frac{1}{2L}$. Hence, in summary this yields

$$\frac{4}{\pi}\sum_{\ell=1}^{T}\frac{1}{2\ell-1} < \max_{x\in[0,\,1/L]} s_T(x) < \frac{4}{\pi}\sum_{\ell=1}^{T}\frac{1}{2\ell-1} + \frac{1}{\pi T}.$$

For $x \in \left[\frac{k}{L},\,\frac{k+1}{L}\right]$ with arbitrary $k \in \mathbb{N}$, the sum $s_T(x)$ in (4.17) is less than it is for $x \in \left[0,\,\frac{1}{L}\right]$, since for each $x \in \left(0,\,\frac{1}{L}\right)$ we have $\sin(L\pi x - n\pi) = (-1)^n \sin(L\pi x)$, $n \in \mathbb{Z}$, and

$$\sum_{\ell=-T}^{T}\frac{\sin(L\pi x)}{|L\pi x - (\ell-k)\pi|} < \sum_{\ell=-T}^{T}\frac{\sin(L\pi x)}{|L\pi x - \ell\pi|}, \quad k \in \mathbb{N},$$

such that $s_T\left(\frac{k}{L} + x\right) < s_T(x)$. Thus, for the even function $s_T(x)$ in (4.17) we obtain

$$\frac{4}{\pi}\sum_{\ell=1}^{T}\frac{1}{2\ell-1} < \max_{x\in\mathbb{R}} s_T(x) < \frac{4}{\pi}\sum_{\ell=1}^{T}\frac{1}{2\ell-1} + \frac{1}{\pi T},$$

which, by Lemma 4.3, can also be written as

$$\frac{4}{\pi}\sum_{\ell=1}^{T}\frac{1}{2\ell-1} < \|S_T\| < \frac{4}{\pi}\sum_{\ell=1}^{T}\frac{1}{2\ell-1} + \frac{1}{\pi T}. \tag{4.19}$$

Note that for $T \gg 1$ the value

$$s_T\left(\tfrac{1}{2L}\right) = \frac{4}{\pi}\sum_{\ell=1}^{T}\frac{1}{2\ell-1} + \frac{2}{\pi\,(2T+1)} \tag{4.20}$$

is a good approximation of the norm $\|S_T\|$.

Now we estimate $\|S_T\|$ by $\ln T$. For this purpose we denote the *T-th harmonic number* by

$$H_T := \sum_{k=1}^{T}\frac{1}{k}, \quad T \in \mathbb{N},$$

such that

$$\sum_{\ell=1}^{T} \frac{1}{2\ell-1} = \sum_{\ell=1}^{T} \left(\frac{1}{2\ell-1} + \frac{1}{2\ell} \right) - \sum_{\ell=1}^{T} \frac{1}{2\ell} = H_{2T} - \frac{1}{2} H_T. \tag{4.21}$$

Using *Euler's constant* $\gamma := \lim_{T\to\infty} \big(H_T - \ln T\big)$, the estimates

$$\frac{1}{2T+2} < H_T - \ln T - \gamma < \frac{1}{2T}$$

are known, cf. [You91], such that

$$\begin{aligned} \frac{1}{2}\left(\ln T + 2\ln 2 + \gamma\right) - \frac{1}{4T\,(2T+1)} &< H_{2T} - \frac{1}{2} H_T \\ &< \frac{1}{2}\left(\ln T + \ln 2 + \gamma\right) + \frac{1}{4T\,(T+1)}. \end{aligned} \tag{4.22}$$

Therefore, applying (4.19), (4.21), and (4.22) yields the assertion (4.18) for $d = 1$.

For $d > 1$ we then use the fact that by the product structure of the d-variate sinc function (3.31) we have

$$\begin{aligned} s_T(\boldsymbol{x}) &= \sum_{\|\boldsymbol{\ell}\|_\infty \le T} |\operatorname{sinc}(L\pi\boldsymbol{x} - \pi\boldsymbol{\ell})| \\ &= \prod_{t=1}^{d} \left(\sum_{\ell=-T}^{T} |\operatorname{sinc}(L\pi x_t - \pi\ell)| \right) = \prod_{t=1}^{d} s_T(x_t), \end{aligned} \tag{4.23}$$

and thus

$$\|S_T\| = \max_{\boldsymbol{x}\in\mathbb{R}^d} s_T(\boldsymbol{x}) = \max_{\boldsymbol{x}\in\mathbb{R}^d} \left(\prod_{t=1}^{d} s_T(x_t) \right) = \left(\max_{x\in\mathbb{R}} s_T(x) \right)^d \tag{4.24}$$

in connection with the previous result for $d = 1$ implies the assertion (4.18). ∎

Note that Lemma 4.4 improves a former result of [Ste93, p. 142, Problem 3.1.5], which only contains a coarse proof sketch for the upper bound, while (4.18) gives a very precise nesting, see also Figure 4.14.

In addition, it should be pointed out that Lemma 4.4 shows that although the Shannon sampling sums (4.12) can be formed for each $f \in C_0(\mathbb{R}^d)$, this is not a meaningful operator in this general setting. Since by Lemma 4.4 the norm of the linear operator $S_T \colon C_0(\mathbb{R}^d) \to C_0(\mathbb{R}^d)$ is unbounded with respect to T, the theorem of Banach–Steinhaus implies that an arbitrary function $f \in C_0(\mathbb{R}^d)$ cannot be represented in the form (4.15). For bandlimited functions $f \in \mathcal{B}_{M/2}(\mathbb{R}^d) \subseteq C_0(\mathbb{R}^d)$, however, the series (4.15) converges absolutely and uniformly on whole $\mathbb{R}^d$, as known from the Whittaker–Kotelnikov–Shannon sampling theorem, see Theorem 4.2. Therefore, the Shannon sampling operator S_T should be considered for bandlimited functions $f \in \mathcal{B}_{M/2}(\mathbb{R}^d)$ only.

Nevertheless, also for bandlimited functions the convergence of the Shannon sampling series (4.15) is very slow due to the poor decay of the sinc function, as can be seen from the sharp upper and lower bounds of the norm of the Shannon sampling operator, see Lemma 4.4. More precisely, considering the one-dimensional setting we only have a convergence rate of $1/\sqrt{T}$, as mentioned in [Jag66, Zay93, ST06]. For the multivariate setting we will provide a rigorous analysis of the approximation error in Lemma 4.6. Before doing so, we need the following intermediate lemma, which is frequently referred to as the *integral test for convergence of series*, also known as the *Maclaurin–Cauchy test*, see e. g. [WW20, p. 71].

Lemma 4.5. *Let $g \colon \mathbb{R} \to \mathbb{R}$ be a function, which is continuous and monotonously decreasing on the interval $[A, \infty)$ with $A \in \mathbb{N}_0$. Then the series $\sum_{k=A}^{\infty} g(k)$ converges if and only if the improper integral $\int_A^{\infty} g(x) \, \mathrm{d}x$ is finite. More precisely, we have*

$$\int_A^{\infty} g(x) \, \mathrm{d}x \leq \sum_{k=A}^{\infty} g(k) \leq g(A) + \int_A^{\infty} g(x) \, \mathrm{d}x. \tag{4.25}$$

Proof. Since the function g is monotonously decreasing on the interval $[A, \infty)$ by assumption, we have $g(k) \leq g(x)$ for all $k \geq x \geq A$. Hence, this yields

$$g(k) = \int_{k-1}^{k} g(k) \, \mathrm{d}x \leq \int_{k-1}^{k} g(x) \, \mathrm{d}x, \quad k \geq A + 1,$$

since g is continuous and therefore integrable on the interval $[A, \infty)$. By

summation over all $k \in \{A, A+1, \dots, B\}$, $B \in \mathbb{N}$, we obtain

$$\sum_{k=A}^{B} g(k) = g(A) + \sum_{k=A+1}^{B} g(k)$$
$$\leq g(A) + \sum_{k=A+1}^{B} \int_{k-1}^{k} g(x)\,\mathrm{d}x = g(A) + \int_{A}^{B} g(x)\,\mathrm{d}x, \qquad (4.26)$$

such that the limit process $B \to \infty$ implies the right-hand side of (4.25). Analogously, one can also show the left inequality in (4.25). This completes the proof. ∎

Now we are fully equipped to provide a rigorous analysis of the approximation error, which can be seen as a generalization of [Jag66, Theorem 1] to $d > 1$.

Lemma 4.6. *Let $f \in \mathcal{B}_{M/2}(\mathbb{R})$ be a bandlimited function with bandwidth $M \in \mathbb{N}$. Then, for $T, L \in \mathbb{N}$ with $T > L \geq M$ we obtain the error estimate*

$$\max_{\boldsymbol{x} \in [-1,\,1]^d} \big|f(\boldsymbol{x}) - (S_T f)(\boldsymbol{x})\big| \leq \left(\frac{2L}{\pi^2}\right)^{d/2} (T-L)^{-d/2}\, \|f\|_{L_2(\mathbb{R}^d)}.$$

Proof. By (4.13) and (4.9) we immediately have

$$\big|f(\boldsymbol{x}) - (S_T f)(\boldsymbol{x})\big| \leq L^{d/2}\, \|f\|_{L_2(\mathbb{R}^d)} \left(\sum_{\|\boldsymbol{\ell}\|_\infty > T} \big[\operatorname{sinc}(L\pi\boldsymbol{x} - \pi\boldsymbol{\ell})\big]^2 \right)^{1/2}.$$

For estimating the sinc series we recognize that equivalently to (4.23) we can write

$$\sum_{\|\boldsymbol{\ell}\|_\infty > T} \big[\operatorname{sinc}(L\pi\boldsymbol{x} - \pi\boldsymbol{\ell})\big]^2 = \prod_{t=1}^{d} \left(\sum_{|\ell| > T} \big[\operatorname{sinc}(L\pi x_t - \pi\ell)\big]^2 \right)$$
$$\leq \frac{1}{\pi^{2d}} \cdot \prod_{t=1}^{d} \left(\sum_{\ell=T+1}^{\infty} \frac{1}{(Lx_t - \ell)^2} + \sum_{\ell=T+1}^{\infty} \frac{1}{(Lx_t + \ell)^2} \right).$$

Then the integral test for convergence of series, see Lemma 4.5, yields

$$\sum_{\ell=T+1}^{\infty} \frac{1}{(Lx_t - \ell)^2} < \int_{T}^{\infty} \frac{1}{(Lx_t - v)^2}\,\mathrm{d}v = \frac{1}{T - Lx_t}, \quad T > Lx_t,$$

$$\sum_{\ell=T+1}^{\infty} \frac{1}{(Lx_t+\ell)^2} < \int_T^{\infty} \frac{1}{(Lx_t+v)^2}\,\mathrm{d}v = \frac{1}{T+Lx_t}, \quad T > -Lx_t,$$

cf. [Jag66, Theorem 1], such that for $T > L$ we obtain

$$\max_{\boldsymbol{x}\in[-1,\,1]^d} \Bigg(\sum_{\|\boldsymbol{\ell}\|_\infty > T} \big[\operatorname{sinc}(L\pi\boldsymbol{x}-\pi\boldsymbol{\ell})\big]^2 \Bigg)^{1/2} \le \frac{1}{\pi^d} \cdot \left(\prod_{t=1}^{d} \frac{2}{T-L} \right)^{1/2}$$

and thereby the assertion. ∎

Note that several works, such as [Jag66, YT66, Pip75, BES82, CM82, Mar92, Zay93], have studied a pointwise error decay when additional conditions are imposed on $f \in \mathcal{B}_{M/2}(\mathbb{R}^d)$. General results on whole $\mathbb{R}^d$, however, are not feasible for arbitrary $f \in \mathcal{B}_{M/2}(\mathbb{R}^d)$. Rather, the uniform approximation error $\|f - S_T f\|_{C_0(\mathbb{R}^d)}$ can only be studied under the additional assumption that $f \in \mathcal{B}_{M/2}(\mathbb{R}^d)$ satisfies certain decay conditions, see [Li98, JG03].

In addition to this rather poor convergence, it is known, see [Fei92a, Fei92b, DD03], that in the presence of noise in the samples $f\big(\frac{\boldsymbol{\ell}}{L}\big)$, $\boldsymbol{\ell} \in \mathbb{Z}^d$, of a bandlimited function $f \in \mathcal{B}_{M/2}(\mathbb{R}^d)$, the convergence of Shannon sampling series (4.15) may even break down completely. To show this, let $f \in \mathcal{B}_{M/2}(\mathbb{R}^d)$ be a given bandlimited function with bandwidth $M \in \mathbb{N}$ and let $T \in \mathbb{N}$ be sufficiently large. For given samples $f\big(\frac{\boldsymbol{\ell}}{L}\big)$ with $\boldsymbol{\ell} \in \mathbb{Z}^d$ and $L \ge M$, $L \in \mathbb{N}$, we consider finitely many erroneous samples

$$\tilde{f}_{\boldsymbol{\ell}} := \begin{cases} f\big(\frac{\boldsymbol{\ell}}{L}\big) + \varepsilon_{\boldsymbol{\ell}} & : \|\boldsymbol{\ell}\|_\infty \le T, \\ f\big(\frac{\boldsymbol{\ell}}{L}\big) & : \|\boldsymbol{\ell}\|_\infty > T, \end{cases}$$

with error terms $\varepsilon_{\boldsymbol{\ell}}$ which are uniformly bounded by $|\varepsilon_{\boldsymbol{\ell}}| \le \varepsilon$ for $\|\boldsymbol{\ell}\|_\infty \le T$. Then the approximation

$$\begin{aligned} \tilde{f}(\boldsymbol{x}) &:= \sum_{\boldsymbol{\ell}\in\mathbb{Z}^d} \tilde{f}_{\boldsymbol{\ell}} \operatorname{sinc}(L\pi\boldsymbol{x}-\pi\boldsymbol{\ell}) \\ &= f(\boldsymbol{x}) + \sum_{\|\boldsymbol{\ell}\|_\infty \le T} \varepsilon_{\boldsymbol{\ell}} \operatorname{sinc}(L\pi\boldsymbol{x}-\pi\boldsymbol{\ell}), \quad \boldsymbol{x} \in \mathbb{R}^d. \end{aligned}$$

satisfies the following error bounds, see [KPT24, Theorem 2.3].

Theorem 4.7. *Let $f \in \mathcal{B}_{M/2}(\mathbb{R}^d)$ be an arbitrary bandlimited function with bandwidth $M \in \mathbb{N}$. Further let $T, L \in \mathbb{N}$ with $L \geq M$, and $\varepsilon > 0$ be given. Then we have*

$$\big\|\tilde{f} - f\big\|_{C_0(\mathbb{R}^d)} < \varepsilon \left(\frac{2}{\pi} \ln T + \frac{5}{4} + \frac{1}{2T}\right)^d. \tag{4.27}$$

Moreover, for the special error terms

$$\varepsilon_{\boldsymbol{\ell}} = \varepsilon \operatorname{sign}\big(\operatorname{sinc}(\tfrac{\pi}{2}\mathbf{1}_d - \pi\boldsymbol{\ell})\big) = \varepsilon\,(-1)^{\ell_1+\ldots+\ell_d+d} \prod_{t=1}^{d} \operatorname{sign}(2\ell_t - 1) \tag{4.28}$$

for $\boldsymbol{\ell} = (\ell_1, \ldots, \ell_d) \in \mathbb{Z}^d$ with $\|\boldsymbol{\ell}\|_\infty \leq T$ we have

$$\big\|\tilde{f} - f\big\|_{C_0(\mathbb{R}^d)} \geq \varepsilon \left(\frac{2}{\pi} \ln T + \frac{4}{\pi} \ln 2 + \frac{2\gamma}{\pi}\right)^d > \varepsilon \left(\frac{2}{\pi} \ln T + \frac{5}{4}\right)^d, \tag{4.29}$$

such that the Shannon sampling series (4.15) *is not numerically robust.*

Proof. By (4.24), (4.19) and (4.22) we are given the upper error bound

$$\begin{aligned}\big\|\tilde{f} - f\big\|_{C_0(\mathbb{R}^d)} &\leq \varepsilon \max_{\boldsymbol{x}\in\mathbb{R}^d} s_T(\boldsymbol{x}) < \varepsilon \left(\frac{4}{\pi} \sum_{\ell=1}^{T} \frac{1}{2\ell - 1} + \frac{1}{\pi T}\right)^d \\ &< \frac{2\varepsilon}{\pi} \left(\ln T + 2\ln 2 + \gamma + \frac{T+2}{2T(T+1)}\right)^d.\end{aligned}$$

Since

$$\frac{4}{\pi} \ln 2 + \frac{2\gamma}{\pi} = 1.2500093\ldots \tag{4.30}$$

and the sequence $\mu_T \coloneqq \frac{T+2}{T+1} = 1 + \frac{1}{T+1}$ is monotonously decreasing with $\max_{T\in\mathbb{N}} \mu_T = \mu_1 = \frac{3}{2}$, we have

$$\frac{4}{\pi} \ln 2 + \frac{2\gamma}{\pi} + \frac{1}{\pi T} \cdot \mu_T \leq \frac{5}{4} + \frac{1}{2T},$$

which yields (4.27).

Next, we proceed with the lower bound. By the special choice of the finitely many error terms $\varepsilon_{\boldsymbol{\ell}}$ in (4.28) we obtain

$$\tilde{f}(\boldsymbol{x}) - f(\boldsymbol{x}) = \varepsilon \sum_{\|\boldsymbol{\ell}\|_\infty \le T} \operatorname{sign}\big(\operatorname{sinc}(\tfrac{\pi}{2}\mathbf{1}_d - \pi\boldsymbol{\ell})\big) \operatorname{sinc}(L\pi\boldsymbol{x} - \pi\boldsymbol{\ell}), \quad \boldsymbol{x} \in \mathbb{R}^d. \tag{4.31}$$

Thus, by (4.23) as well as (4.20) – (4.22) we conclude that

$$\begin{aligned} \big\|\tilde{f} - f\big\|_{C_0(\mathbb{R})^d} &\ge \big|\tilde{f}(\tfrac{1}{2L}\mathbf{1}_d) - f(\tfrac{1}{2L}\mathbf{1}_d)\big| = \varepsilon \sum_{\|\boldsymbol{\ell}\|_\infty \le T} \big|\operatorname{sinc}(\tfrac{\pi}{2}\mathbf{1}_d - \pi\boldsymbol{\ell})\big| \\ &= \varepsilon \, \big(s_T\big(\tfrac{1}{2L}\big)\big)^d > \varepsilon \left(\frac{2}{\pi} \ln T + \frac{4}{\pi} \ln 2 + \frac{2\gamma}{\pi}\right)^d, \end{aligned}$$

such that (4.30) completes the proof. ∎

Note that (4.27) specifies a corresponding remark of [DD03, p. 681] as it makes the constant explicit. In addition, we remark that the norm $\big\|\tilde{f} - f\big\|_{C_0(\mathbb{R}^d)}$ does not depend on the special choice of the function $f \in \mathcal{B}_{M/2}(\mathbb{R}^d)$ or the so–called *oversampling parameter* $\lambda \coloneqq \frac{L-M}{M} \ge 0$ for $L \ge M$, see Figure 4.14. Furthermore, Figure 4.14 also illustrates that for $T \to \infty$ the error behavior shown in Theorem 4.7 is not satisfactory. Thus, in the presence of noise in the samples $f\big(\frac{\boldsymbol{\ell}}{L}\big)$, $\boldsymbol{\ell} \in \mathbb{Z}^d$, the convergence of the Shannon sampling series (4.15) may even break down completely.

Remark 4.8. In the above worst case analysis we have seen that the approximation of $f \in \mathcal{B}_{M/2}(\mathbb{R}^d)$ by the T-th partial sum (4.12) of its Shannon sampling series with $L \ge M$ is not numerically robust in the deterministic sense. On the other hand, a simple average case study, see [KPT24, Remark 2.5], shows that this approximation is numerically robust in the stochastic sense. Therefore, we compute (4.12) as an inner product of the real $(2T+1)^d$-dimensional vectors

$$\Big(f\big(\tfrac{\boldsymbol{\ell}}{L}\big)\Big)_{\|\boldsymbol{\ell}\|_\infty \le T} \quad \text{and} \quad \big(\operatorname{sinc}(L\pi\boldsymbol{x} - \boldsymbol{\ell}\pi)\big)_{\|\boldsymbol{\ell}\|_\infty \le T}.$$

Now assume that instead of the exact samples $f\big(\frac{\boldsymbol{\ell}}{L}\big)$, $\|\boldsymbol{\ell}\|_\infty \le T$, only perturbed samples $\tilde{f}\big(\frac{\boldsymbol{\ell}}{L}\big) \coloneqq f\big(\frac{\boldsymbol{\ell}}{L}\big) + X_{\boldsymbol{\ell}}$, $\|\boldsymbol{\ell}\|_\infty \le T$, are given. In this case, the error terms are modeled as real random variables $X_{\boldsymbol{\ell}}$, $\boldsymbol{\ell} \in \mathbb{Z}^d$, that

are uncorrelated, each having vanishing expectation $\mathbb{E}(X_{\boldsymbol{\ell}}) = 0$ and constant variance $\mathbb{V}(X_{\boldsymbol{\ell}}) = \mathbb{E}(|X_{\boldsymbol{\ell}}|^2) = \rho^2$ with $\rho > 0$. Then we consider the stochastic approximation error

$$\begin{aligned}\Delta_T &\coloneqq \sum_{\|\boldsymbol{\ell}\|_\infty \le T} \tilde{f}\left(\tfrac{\boldsymbol{\ell}}{L}\right) \operatorname{sinc}(L\pi\boldsymbol{x} - \boldsymbol{\ell}\pi) - \sum_{\|\boldsymbol{\ell}\|_\infty \le T} f\left(\tfrac{\boldsymbol{\ell}}{L}\right) \operatorname{sinc}(L\pi\boldsymbol{x} - \boldsymbol{\ell}\pi) \\ &= \sum_{\|\boldsymbol{\ell}\|_\infty \le T} X_{\boldsymbol{\ell}} \operatorname{sinc}(L\pi t\boldsymbol{x} - \boldsymbol{\ell}\pi)\,.\end{aligned}$$

Obviously, this error term Δ_T has the expectation

$$\mathbb{E}(\Delta_T) = \sum_{\|\boldsymbol{\ell}\|_\infty \le T} \operatorname{sinc}(L\pi\boldsymbol{x} - \boldsymbol{\ell}\pi)\, \mathbb{E}(X_{\boldsymbol{\ell}}) = 0$$

and the variance

$$\begin{aligned}\mathbb{V}(\Delta_T) &= \sum_{\|\boldsymbol{\ell}\|_\infty \le T} \left|\operatorname{sinc}(L\pi\boldsymbol{x} - \boldsymbol{\ell}\pi)\right|^2 \mathbb{V}(X_{\boldsymbol{\ell}}) \\ &= \rho^2 \sum_{\|\boldsymbol{\ell}\|_\infty \le T} \left|\operatorname{sinc}(L\pi\boldsymbol{x} - \boldsymbol{\ell}\pi)\right|^2 .\end{aligned}$$

Thus, by (4.10) we obtain $\mathbb{V}(\Delta_T) \le \rho^2$. ◇

4.3 Univariate regularized Shannon sampling formulas

As seen in Section 4.2, the practical use of the classical Shannon sampling series (4.15) is limited, since it requires infinitely many samples, has rather poor convergence, and is not numerically robust in the deterministic sense. Therefore, we will now discuss some numerical realizations of the Whittaker–Kotelnikov–Shannon sampling theorem, where for the sake of simplicity, we initially focus on the univariate setting $d = 1$.

To address the demonstrated shortcomings, a so-called *oversampling* is frequently used, i. e., a function $f \in \mathcal{B}_{M/2}(\mathbb{R})$ of bandwidth $M \in \mathbb{N}$ is sampled on a finer grid $\frac{1}{L}\mathbb{Z}$ with $L > M$, where the oversampling is quantified by the oversampling parameter $\lambda \coloneqq \frac{L-M}{M} \ge 0$. In addition, we study several regularization techniques, i. e., generalizations of the classical Shannon

sampling series (4.15) which are of the form

$$\sum_{\ell\in\mathbb{Z}} f\big(\tfrac{\ell}{L}\big)\,\psi\big(x-\tfrac{\ell}{L}\big) \tag{4.32}$$

with some suitable function $\psi\colon \mathbb{R}\to[-1,1]$. More precisely, similar to [SS00], we examine regularization functions ψ that are either bandlimited or timelimited, meaning that they are compactly supported in the frequency domain or in the spatial domain, respectively.

On the one hand, we investigate the regularization in frequency domain, as done for instance in [Dau92, Nat86a, Rap96, Par97, ST05]. This approach is based on choosing a so–called window function $\hat{\psi}$ that is compactly supported in the frequency domain. Afterwards, in order to compute the approximation (4.32), the corresponding function ψ in spatial domain has be to determined by means of inverse Fourier transform (4.4). However, by the uncertainty principle (see [PPST23, Lemma 2.39]) it is known that $\operatorname{supp}(\psi)=\mathbb{R}$, such that (4.32) still requires infinitely many samples. Thus, for numerical realizations an additional truncation of the series is required, such that we approximate a function $f\in\mathcal{B}_{M/2}(\mathbb{R})$ by the T-th partial sum of (4.32).

On the other hand, we consider the regularization in spatial domain, which was introduced for example in [Qia03, SS07, MXZ09, LZ17, CZ19, KPT22]. Here for some $m\in\mathbb{N}\setminus\{1\}$ a suitable window function $\varphi_m\colon\mathbb{R}\to[0,1]$ with compact support $\big[-\frac{m}{L},\frac{m}{L}\big]$ and $\varphi_m(0)=1$ is chosen in spatial domain. Then the regularization function ψ in (4.32) is given by $\psi(x)=\operatorname{sinc}(L\pi x)\,\varphi_m(x)$. Since this implies $\psi\big(x-\frac{\ell}{L}\big)\big|_{x=\frac{k}{L}}=\delta_{k,\ell}$ for all $k,\ell\in\mathbb{Z}$, this method is an interpolating approximation. Moreover, by the use of the compactly supported window function φ_m the computation of (4.32) for $x\in\mathbb{R}\setminus\frac{1}{L}\,\mathbb{Z}$ only requires $2m+1$ samples $f\big(\frac{\ell}{L}\big)$, where $\ell\in\mathbb{Z}$ fulfills the condition $|\ell-Lx|\le m$.

In the following, we study both approaches, propose new error estimates for several choices of the window functions $\hat{\psi}$ and φ_m, and compare the theoretical and numerical approximation properties in terms of error decay rates.

To this end, this section is organized as follows. Firstly, in Section 4.3.1 we start with the regularization using a window function in frequency domain. After recapitulating a known general result in Theorem 4.9, we consider several window functions of different regularity and present the

corresponding algebraic error decay rates based on a general result in Theorem 4.10. Subsequently, in Section 4.3.2 we proceed with the regularization using a window function in spatial domain. Here we also review a known general result in Theorem 4.25 and demonstrate the exponential decay of the considered window functions afterwards.

4.3.1 Regularization with a window function in frequency domain

To overcome the drawbacks of poor convergence and numerical instability of the Shannon sampling series (4.15), one can apply regularization with a convenient window function either in the frequency domain or in the spatial domain.

Similar to [KPT24], we firstly consider the *regularization with a frequency window function* of the form

$$\hat{\psi}(v) \coloneqq \begin{cases} 1 & : |v| \le \frac{M}{2}, \\ \xi(|v|) & : \frac{M}{2} < |v| < \frac{L}{2}, \\ 0 & : |v| \ge \frac{L}{2}, \end{cases} \tag{4.33}$$

cf. [Dau92, Par97, ST05], where $\xi\colon \left[\frac{M}{2}, \frac{L}{2}\right] \to [0, 1]$ is frequently chosen as some monotonously decreasing, continuous function with $\xi\left(\frac{M}{2}\right) = 1$ and $\xi\left(\frac{L}{2}\right) = 0$. Applying the inverse Fourier transform (4.4), we determine the corresponding function in spatial domain by

$$\psi(x) = \int_{\mathbb{R}} \hat{\psi}(v)\, \mathrm{e}^{2\pi \mathrm{i} v x}\, \mathrm{d}v = 2 \int_0^{L/2} \hat{\psi}(v)\, \cos(2\pi v x)\, \mathrm{d}v. \tag{4.34}$$

Analogous to [Dau92, p. 19] and [Par97, Theorem 7.2.5], we obtain the following representation result, see also [KPT24, Theorem 3.3].

Theorem 4.9. *Let $f \in \mathcal{B}_{M/2}(\mathbb{R})$ be a bandlimited function with bandwidth $M \in \mathbb{N}$ and let $L \coloneqq M\,(1+\lambda) \in \mathbb{N}$ with $\lambda > 0$. Further assume that the samples $f\left(\frac{\ell}{L}\right)$, $\ell \in \mathbb{Z}$, fulfill the condition*

$$\sum_{\ell \in \mathbb{Z}} \left| f\left(\tfrac{\ell}{L}\right) \right| < \infty. \tag{4.35}$$

Using oversampling and regularization with a frequency window function $\hat{\psi}$

of the form (4.33)*, the function* f *can be represented as*

$$f(x) = \sum_{\ell\in\mathbb{Z}} f\big(\tfrac{\ell}{L}\big)\, \frac{1}{L}\, \psi\big(x - \tfrac{\ell}{L}\big), \quad x \in \mathbb{R}, \tag{4.36}$$

where the series (4.36) *converges absolutely and uniformly on* $\mathbb{R}$*.*

Proof. Since by assumption $f \in \mathcal{B}_{M/2}(\mathbb{R})$ is bandlimited with bandwidth M, we have $\operatorname{supp}(\hat{f}) \subseteq \big[-\frac{M}{2}, \frac{M}{2}\big] \subset \big[-\frac{L}{2}, \frac{L}{2}\big]$ and therefore the function $\hat{f}$ restricted on $\big[-\frac{L}{2}, \frac{L}{2}\big]$ can be represented by its L-periodic Fourier series

$$\hat{f}(v) = \sum_{\ell\in\mathbb{Z}} c_\ell(\hat{f})\, \mathrm{e}^{2\pi \mathrm{i}\ell v/L}, \quad v \in \big[-\tfrac{L}{2}, \tfrac{L}{2}\big],$$

with the Fourier coefficients

$$c_\ell(\hat{f}) = \frac{1}{L} \int_{-L/2}^{L/2} \hat{f}(v)\, \mathrm{e}^{-2\pi \mathrm{i}\ell v/L}\, \mathrm{d}v.$$

Using the definition of the inverse Fourier transform (4.4), we recognize that $c_\ell(\hat{f}) = \frac{1}{L}\, f\big(-\frac{\ell}{L}\big)$. Hence, we may denote $\hat{f}$ as

$$\hat{f}(v) = \frac{1}{L} \sum_{\ell\in\mathbb{Z}} f\big(\tfrac{\ell}{L}\big)\, \mathrm{e}^{-2\pi \mathrm{i}\ell v/L}, \quad v \in \big[-\tfrac{L}{2}, \tfrac{L}{2}\big]. \tag{4.37}$$

By the Weierstrass M-test and assumption (4.35), the Fourier series (4.37) converges absolutely and uniformly on $\big[-\frac{L}{2}, \frac{L}{2}\big]$. Additionally, by assumption we have $\operatorname{supp}(\hat{f}) \subseteq \big[-\frac{M}{2}, \frac{M}{2}\big]$ as well as $\hat{\psi}(v) = 1$ for $v \in \big[-\frac{M}{2}, \frac{M}{2}\big]$ by (4.33), such that $\hat{f}(v) = \hat{f}(v)\, \hat{\psi}(v)$ for all $v \in \mathbb{R}$. Therefore, by inserting (4.37) into the inverse Fourier transform (4.4), we obtain

$$\begin{aligned} f(x) &= \int_{\mathbb{R}} \hat{f}(v)\, \mathrm{e}^{2\pi \mathrm{i}xv}\, \mathrm{d}v = \int_{-L/2}^{L/2} \hat{f}(v)\, \mathrm{e}^{2\pi \mathrm{i}xv}\, \mathrm{d}v \\ &= \int_{-L/2}^{L/2} \hat{f}(v)\, \hat{\psi}(v)\, \mathrm{e}^{2\pi \mathrm{i}xv}\, \mathrm{d}v = \sum_{\ell\in\mathbb{Z}} \frac{1}{L}\, f\big(\tfrac{\ell}{L}\big) \int_{-L/2}^{L/2} \hat{\psi}(v)\, \mathrm{e}^{2\pi \mathrm{i}(x-\ell/L)v}\, \mathrm{d}v \\ &= \sum_{\ell\in\mathbb{Z}} f\big(\tfrac{\ell}{L}\big)\, \frac{1}{L}\, \psi\big(x - \tfrac{\ell}{L}\big), \quad x \in \mathbb{R}, \end{aligned}$$

where summation and integration may be interchanged by the theorem of Fubini–Tonelli, if

$$\frac{1}{L} \sum_{\ell \in \mathbb{Z}} \left| f\left(\tfrac{\ell}{L}\right) \right| \cdot \int_{-L/2}^{L/2} |\hat{\psi}(v)| \, \mathrm{d}v < \infty \,,$$

which is fulfilled, since we have (4.35) and $|\hat{\psi}(v)| \leq 1$ by definition (4.33). Additionally, note that from (4.33) and (4.34) it follows that

$$|\psi(x)| \leq 2 \int_0^{L/2} \left| \cos(2\pi v x) \right| \mathrm{d}v < L \,, \quad x \in \mathbb{R} \,.$$

Hence, we have $\frac{1}{L} \left| \psi\big(x - \frac{\ell}{L}\big) \right| < 1$ for all $x \in \mathbb{R}$ and $\ell \in \mathbb{Z}$, and consequently the series (4.36) converges absolutely and uniformly on $\mathbb{R}$ by (4.35) and the Weierstrass M-test. ∎

Note that (4.36) is not an interpolating representation, since in general we have

$$\frac{1}{L} \, \psi\big(x - \tfrac{\ell}{L}\big) \Big|_{x = \frac{k}{L}} \neq \delta_{k,\ell}, \quad k, \ell \in \mathbb{Z}.$$

Moreover, since the frequency window function $\hat{\psi}$ in (4.33) is compactly supported, the *uncertainty principle* (see e. g. [PPST23, Lemma 2.39]) yields $\operatorname{supp}(\psi) = \mathbb{R}$, such that (4.36) does not imply localized sampling for any choice of $\hat{\psi}$. In other words, the representation (4.36) still requires infinitely many samples $f\big(\frac{\ell}{L}\big)$, $\ell \in \mathbb{Z}$.

For practical realizations we therefore need to consider a truncated version of (4.36). Hence, for $T \in \mathbb{N}$ we introduce the T-th partial sum

$$(P_{\psi,T} f)(x) \coloneqq \sum_{\ell=-T}^{T} f\big(\tfrac{\ell}{L}\big) \, \frac{1}{L} \, \psi\big(x - \tfrac{\ell}{L}\big), \quad x \in \mathbb{R}, \tag{4.38}$$

and show the following new convergence result.

Theorem 4.10. *Let $f \in \mathcal{B}_{M/2}(\mathbb{R})$ be a bandlimited function with bandwidth $M \in \mathbb{N}$ and let $L = M\,(1+\lambda) \in \mathbb{N}$ with $\lambda > 0$. Further assume that the samples $f\big(\frac{\ell}{L}\big)$, $\ell \in \mathbb{Z}$, fulfill the condition* (4.35)*. Using oversampling and regularization with a frequency window function of the form* (4.33)*, the*

T-th partial sums $P_{\psi,T}f$ uniformly converge to f on $[-1,\,1]$ as $T \to \infty$. If additionally the decay condition

$$\big|\psi(x)\big| \le c\,|x|^{-r}, \quad x \in \mathbb{R} \setminus \{0\}, \tag{4.39}$$

holds, for $T > L$ we obtain the error estimate

$$\max_{x\in[-1,\,1]} \big|f(x) - (P_{\psi,T}f)(x)\big| \le cL^{r-1}\sqrt{\tfrac{2L}{2r-1}}\,(T-L)^{(-2r+1)/2}\,\|f\|_{L_2(\mathbb{R})}. \tag{4.40}$$

Proof. By (4.36) and (4.38) we have

$$f(x) - (P_{\psi,T}f)(x) = \sum_{|\ell|>T} f\big(\tfrac{\ell}{L}\big)\,\frac{1}{L}\,\psi\big(x - \tfrac{\ell}{L}\big),$$

such that the Cauchy–Schwarz inequality implies

$$\big|f(x) - (P_{\psi,T}f)(x)\big| \le \bigg(\sum_{|\ell|>T} \big|f\big(\tfrac{\ell}{L}\big)\big|^2\bigg)^{1/2} \bigg(\sum_{|\ell|>T} \big|\tfrac{1}{L}\,\psi\big(x - \tfrac{\ell}{L}\big)\big|^2\bigg)^{1/2}. \tag{4.41}$$

Since $f \in \mathcal{B}_{M/2}(\mathbb{R})$ is bandlimited with bandwidth $M \in \mathbb{N}$ and $L > M$, we obtain by (4.9) that

$$\bigg(\sum_{|\ell|>T} \big|f\big(\tfrac{\ell}{L}\big)\big|^2\bigg)^{1/2} \le \sqrt{L}\,\|f\|_{L_2(\mathbb{R})}. \tag{4.42}$$

Since by assumption the decay condition (4.39) is satisfied, we have

$$\big|\psi\big(x - \tfrac{\ell}{L}\big)\big|^2 \le c^2 L^{2r}\,(Lx - \ell)^{-2r}.$$

Thus, for $T > L$ and $x \in [-1,\,1]$ we obtain

$$\begin{aligned}
\bigg(\sum_{|\ell|>T} \big|\tfrac{1}{L}\,\psi\big(x - \tfrac{\ell}{L}\big)\big|^2\bigg)^{1/2} &\le cL^{r-1}\bigg(\sum_{|\ell|>T} (Lx-\ell)^{-2r}\bigg)^{1/2} \\
&= cL^{r-1}\bigg(\sum_{\ell=T+1}^{\infty} (Lx+\ell)^{-2r} + \sum_{\ell=T+1}^{\infty} (Lx-\ell)^{-2r}\bigg)^{1/2} \\
&\le cL^{r-1}\bigg(2\sum_{\ell=T+1}^{\infty} (\ell-L)^{-2r}\bigg)^{1/2}.
\end{aligned}$$

Using the integral test for convergence of series, see Lemma 4.5, we conclude

$$\sum_{\ell=T+1}^{\infty} (\ell - L)^{-2r} \leq \int_{T}^{\infty} (y - L)^{-2r} \,\mathrm{d}y = \tfrac{1}{2r-1} \, (T - L)^{-2r+1},$$

which yields

$$\Big(\sum_{|\ell|>T} \big|\psi\big(x - \tfrac{\ell}{L}\big)\big|^2 \Big)^{1/2} \leq cL^{r-1} \sqrt{\tfrac{2}{2r-1}} \, (T - L)^{(-2r+1)/2}. \tag{4.43}$$

Hence, the estimates (4.41), (4.42), and (4.43) imply the assertion (4.40). ∎

Note that for the frequency window functions $\hat{\psi}$ in (4.33) only error estimates on certain compact intervals (such as for example $[-1, 1]$) can be given, while results on whole $\mathbb{R}$ are not feasible. We remark that in the univariate setting $d = 1$ the error estimate in Lemma 4.6 coincides with the one of Theorem 4.10 using $r = 1$ and $c = \frac{1}{\pi}$. Therefore, the result in Theorem 4.10 can be viewed as a generalization to window functions ψ in (4.34) with faster decay than the sinc function (3.31).

Remark 4.11. In [SS00, Lemma 2] it was shown that by considering the *Bernstein spaces* of bandlimited functions

$$\mathcal{B}^p_{M/2}(\mathbb{R}) \coloneqq \Big\{ f \in \mathscr{S}'(\mathbb{R}) \cap L^p(\mathbb{R}) \colon \operatorname{supp}(\hat{f}) \subseteq \big[-\tfrac{M}{2}, \, \tfrac{M}{2}\big] \Big\} \subseteq C^\infty(\mathbb{R}),$$

where $\mathscr{S}'(\mathbb{R})$ denotes the set of tempered distributions, cf. Section 6.1.3, the Marcinkiewicz–Zygmund–like inequality

$$\frac{1}{L} \Big(\sum_{\ell \in \mathbb{Z}} \big|f\big(\tfrac{\ell}{L}\big)\big|^p \Big)^{1/p} \leq \Big(1 + \frac{1}{2 + 2\lambda} \Big) \, \|f\|_{L^p(\mathbb{R})}$$

holds for all $f \in \mathcal{B}^p_{M/2}(\mathbb{R})$ with $1 \leq p < \infty$. Thus, by using Hölder's inequality

$$\big|f(x) - (P_{\psi,T} f)(x)\big| \leq \Big(\sum_{|\ell|>T} \big|f\big(\tfrac{\ell}{L}\big)\big|^p \Big)^{1/p} \Big(\sum_{|\ell|>T} \big|\tfrac{1}{L} \, \psi\big(x - \tfrac{\ell}{L}\big)\big|^q \Big)^{1/q}$$

with $\frac{1}{p} + \frac{1}{q} = 1$ instead of (4.41), the L^p-version

$$\max_{x \in [-1,\,1]} \left| f(x) - (P_{\psi,T} f)(x) \right| \leq \frac{cL^r\,(3+2\lambda)}{2+2\lambda} \left(\frac{2}{qr-1} \right)^{1/q} (T-L)^{-r+1/q}\, \|f\|_{L^p(\mathbb{R})}$$

of Theorem 4.10 can be shown analogously for all $f \in \mathcal{B}^p_{M/2}(\mathbb{R})$ with $1 \leq p < \infty$. ◇

Additionally, note that in Theorem 4.10 we require the inverse Fourier transform ψ in (4.34) of the frequency window function $\hat{\psi}$ in (4.33) to satisfy the decay condition (4.39), since this is the property used in the proof of the error bound (4.40). However, there is a correlation between the smoothness of $\hat{\psi}$ in (4.33) and the decay rate of ψ in (4.34) given by the following lemma.

Lemma 4.12. *For $r \geq 0$ let $\hat{\psi} \in C^r(\mathbb{R})$ with smoother $\xi \in C^{r+2}\left(\left[-\frac{M}{2}, \frac{L}{2}\right]\right)$ in* (4.33)*. Then the corresponding function ψ in spatial domain fulfills the decay condition* (4.39)*.*

Proof. Considering (4.33) we recognize that $\hat{\psi} \in C^r(\mathbb{R})$ holds if and only if

$$\begin{aligned} \xi\left(\tfrac{M}{2}\right) = 1, \quad \xi^{(p)}\left(\tfrac{M}{2}\right) = 0, \qquad & p = 1, \ldots, r, \\ \xi^{(p)}\left(\tfrac{L}{2}\right) = 0, \qquad & p = 0, \ldots, r. \end{aligned}$$

By means of this fact and the $(r+2)$-times differentiability of ξ, the function ψ in (4.34) can be computed using $(r+2)$-fold application of partial integration as

$$\begin{aligned} \psi(x) &= 2 \int_0^{M/2} \cos(2\pi v x)\,\mathrm{d}v + 2 \int_{M/2}^{L/2} \xi(v)\,\cos(2\pi v x)\,\mathrm{d}v \\ &= -\frac{2}{2\pi x} \int_{M/2}^{L/2} \xi'(v)\,\sin(2\pi v x)\,\mathrm{d}v = \ldots \\ &= \begin{cases} (-1)^{\frac{r+1}{2}}\, \dfrac{2}{(2\pi x)^{r+1}} \displaystyle\int_{M/2}^{L/2} \xi^{(r+1)}(v)\,\cos(2\pi v x)\,\mathrm{d}v & : r\,\text{odd}, \\ (-1)^{\frac{r+2}{2}}\, \dfrac{2}{(2\pi x)^{r+1}} \displaystyle\int_{M/2}^{L/2} \xi^{(r+1)}(v)\,\sin(2\pi v x)\,\mathrm{d}v & : r\,\text{even}, \end{cases} \end{aligned}$$

$$= \begin{cases} \dfrac{2\cdot(-1)^{\frac{r+1}{2}}}{(2\pi x)^{r+2}} \left(\Big[\xi^{(r+1)}(v)\, \sin(2\pi v x) \Big]_{M/2}^{L/2} \right. \\ \qquad\qquad \left. - \displaystyle\int_{M/2}^{L/2} \xi^{(r+2)}(v)\, \sin(2\pi v x)\, \mathrm{d}v \right) & : r \text{ odd}, \\ \dfrac{2\cdot(-1)^{\frac{r}{2}}}{(2\pi x)^{r+2}} \left(\Big[\xi^{(r+1)}(v)\, \cos(2\pi v x) \Big]_{M/2}^{L/2} \right. \\ \qquad\qquad \left. - \displaystyle\int_{M/2}^{L/2} \xi^{(r+2)}(v)\, \cos(2\pi v x)\, \mathrm{d}v \right) & : r \text{ even}. \end{cases}$$

Therefore, employing the triangle inequality twice we obtain

$$|\psi(x)| \le |x|^{-(r+2)} \cdot \frac{2}{(2\pi)^{r+2}} \left(\max_{v\in\left[\frac{M}{2},\frac{L}{2}\right]} \xi^{(r+1)}(v) \cdot 2 \right. \\ \left. + \max_{v\in\left[\frac{M}{2},\frac{L}{2}\right]} \xi^{(r+2)}(v) \cdot \int_{M/2}^{L/2} \mathrm{d}v \right)$$

and thus an estimate of the form (4.39). ∎

Remark 4.13. Let us consider the issue of numerical robustness, i. e., suppose that the samples $f\big(\frac{\ell}{L}\big)$, $\ell \in \mathbb{Z}$, of a bandlimited function $f \in \mathcal{B}_{M/2}(\mathbb{R})$ are not known exactly, but rather erroneous samples $\tilde{f}_\ell := f\big(\frac{\ell}{L}\big) + \varepsilon_\ell$ with $|\varepsilon_\ell| \le \varepsilon$, $\ell \in \mathbb{Z}$, and $\varepsilon > 0$ are given. Then for $T \in \mathbb{N}$ we denote the T-th partial sum with erroneous samples $\tilde{f}_\ell$ by

$$(P_{\psi,T}\tilde{f})(x) := \frac{1}{L} \sum_{\ell=-T}^{T} \tilde{f}_\ell\, \psi\big(x - \tfrac{\ell}{L}\big), \quad x \in \mathbb{R}.$$

Using this definition as well as (4.38) we have

$$\begin{aligned} (P_{\psi,T}\tilde{f})(x) - (P_{\psi,T}f)(x) &= \frac{1}{L} \sum_{\ell=-T}^{T} \Big(\tilde{f}_\ell - f\big(\tfrac{\ell}{L}\big) \Big)\, \psi\big(x - \tfrac{\ell}{L}\big) \\ &= \frac{1}{L} \sum_{\ell=-T}^{T} \varepsilon_\ell\, \psi\big(x - \tfrac{\ell}{L}\big), \quad x \in \mathbb{R}. \end{aligned}$$

Since we already know that $\frac{1}{L}\left|\psi\big(x-\frac{\ell}{L}\big)\right| < 1$ for all $x \in \mathbb{R}$ and $\ell \in \mathbb{Z}$, the uniform perturbation error can be estimated by

$$\begin{aligned}\big\|P_{\psi,T}\tilde{f} - P_{\psi,T}f\big\|_{C_0(\mathbb{R})} &\leq \max_{x\in\mathbb{R}} \sum_{\ell=-T}^{T} |\varepsilon_\ell| \cdot \tfrac{1}{L}\left|\psi\big(x-\tfrac{\ell}{L}\big)\right| \\ &\leq \varepsilon \sum_{\ell=-T}^{T} 1 = \varepsilon\,(2T+1).\end{aligned}$$

Thus, for fixed $T \in \mathbb{N}$ the T-th partial sum (4.38) is numerically robust. However, since a lower bound similar to Theorem 4.7 is not yet known, the numerical robustness of the regularization (4.36) in the Fourier domain remains unclear. ◇

Linear frequency window function

Now given the general results, let us consider some possible choices of window functions. A simple example of a window function (4.33) in frequency domain is the *linear frequency window function*

$$\hat{\psi}_{\mathrm{lin}}(v) \coloneqq \begin{cases} 1 & : |v| \leq \frac{M}{2}, \\ 1 - \frac{2|v|-M}{L-M} & : \frac{M}{2} < |v| < \frac{L}{2}, \\ 0 & : |v| \geq \frac{L}{2}, \end{cases} \tag{4.44}$$

cf. [Dau92, pp. 18–19], [Par97, pp. 210–212] or [SS00, Example 2]. Note that in the trigonometric setting a function of the form (4.44) is also often referred to as *trapezoidal* or *de La Vallée-Poussin type* window function, respectively. Obviously, the window function $\hat{\psi}_{\mathrm{lin}}(v)$ is a continuous linear spline supported on $\left[-\frac{L}{2}, \frac{L}{2}\right]$, see Figure 4.1a. By (4.34) we obtain the corresponding function in spatial domain as

$$\begin{aligned}\psi_{\mathrm{lin}}(x) &= 2\int_0^{M/2} \cos(2\pi v x)\,\mathrm{d}v + 2\int_{M/2}^{L/2} \left(1 - \frac{2v-M}{L-M}\right) \cos(2\pi v x)\,\mathrm{d}v \\ &= \frac{1}{(L-M)\,(\pi x)^2}\,\big(\cos(M\pi x) - \cos(L\pi x)\big) \\ &= \frac{L+M}{2}\,\mathrm{sinc}\big(\tfrac{L+M}{2}\,\pi x\big)\,\mathrm{sinc}\big(\tfrac{L-M}{2}\,\pi x\big), \quad x \in \mathbb{R}\setminus\{0\},\end{aligned} \tag{4.45}$$

and $\psi_{\mathrm{lin}}(0) = \frac{L+M}{2}$. This function $\frac{1}{L}\,\psi_{\mathrm{lin}}$ is even, supported on whole $\mathbb{R}$, and has its maximum at $x = 0$ such that

$$\left\| \frac{1}{L}\,\psi_{\mathrm{lin}} \right\|_{C_0(\mathbb{R})} = \frac{1}{L}\,\psi_{\mathrm{lin}}(0) = \frac{L+M}{2L} < 1.$$

In addition, the function $\frac{1}{L}\,\psi_{\mathrm{lin}}(x)$ has a faster decay than $\operatorname{sinc}(L\pi x)$ for $|x| \to \infty$, cf. Figure 4.1b, while for $L \to +M$ we have

$$\lim_{L \to +M} \frac{1}{L}\,\psi_{\mathrm{lin}}(x) = \operatorname{sinc}(M\pi x).$$

Moreover, for the linear frequency window function (4.44) we have the following convergence result, cf. [KPT24, Theorem 3.4].

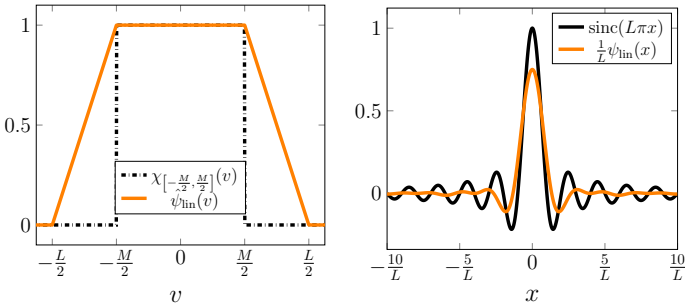

(a) $\hat{\psi}_{\mathrm{lin}}$ in (4.44) (b) $\frac{1}{L}\,\psi_{\mathrm{lin}}$ in (4.45)

Figure 4.1: The linear frequency window function (4.44) and its scaled inverse Fourier transform (4.45).

Theorem 4.14. *Let $f \in \mathcal{B}_{M/2}(\mathbb{R})$ be a bandlimited function with bandwidth $M \in \mathbb{N}$ and let $L = M\,(1+\lambda) \in \mathbb{N}$ with $\lambda > 0$. Further assume that the samples $f\big(\frac{\ell}{L}\big)$, $\ell \in \mathbb{Z}$, fulfill the condition (4.35). Using oversampling and regularization with the linear frequency window function (4.44), the T-th partial sums $P_{\mathrm{lin},T} f$ converge uniformly to f on $[-1,\,1]$ as $T \to \infty$. For $T > L$ we obtain the error estimate*

$$\max_{x \in [-1,\,1]} \big| f(x) - (P_{\mathrm{lin},T} f)(x) \big| \le \sqrt{\frac{2L}{3}}\,\frac{2\,(1+\lambda)}{\pi^2 \lambda}\,(T-L)^{-3/2}\,\|f\|_{L_2(\mathbb{R})}. \tag{4.46}$$

Proof. By Theorem 4.10 we only have to check the decay rate of the function ψ_{lin} corresponding to the linear frequency window function (4.44). It can easily be seen that ψ_{lin} in (4.45) satisfies the decay condition

$$\big|\psi_{\mathrm{lin}}(x)\big| \leq \frac{2}{M\lambda\,\pi^2}\,|x|^{-2}, \quad x \in \mathbb{R} \setminus \{0\},$$

and thus (4.40) implies the estimate (4.46). ∎

Higher order frequency window functions by means of interpolation

In order to obtain convergence rates better than the one in Theorem 4.14, one may consider frequency window functions (4.33) of higher smoothness, cf. Corollary 4.12. Therefore, our next step is to construct a continuously differentiable frequency window function by polynomial interpolation as done in [KPT24]. Since the frequency window function (4.33) is even, it suffices to consider $\xi\colon \left[\frac{M}{2}, \frac{L}{2}\right] \to [0, 1]$ only at the interval boundaries $\frac{M}{2}$ and $\frac{L}{2}$. Clearly, the linear frequency window function $\hat{\psi}_{\mathrm{lin}}$ in (4.44) fulfills

$$\lim_{v \to \frac{M}{2}} \xi(v) = 1, \quad \lim_{v \to \frac{L}{2}} \xi(v) = 0.$$

Thus, to obtain a smoother frequency window function, we need to additionally satisfy the first order conditions

$$\lim_{v \to \frac{M}{2}} \xi'(v) = 0, \quad \lim_{v \to \frac{L}{2}} \xi'(v) = 0.$$

Then the corresponding interpolation polynomial yields the *cubic frequency window function*

$$\hat{\psi}_{\mathrm{cub}}(v) \coloneqq \begin{cases} 1 & : |v| \leq \frac{M}{2}, \\ \frac{16}{(L-M)^3}\left(|v| - \frac{L}{2}\right)^2\left(|v| - \frac{3M-L}{4}\right) & : \frac{M}{2} < |v| < \frac{L}{2}, \\ 0 & : |v| \geq \frac{L}{2}, \end{cases} \tag{4.47}$$

see Figure 4.2a. By (4.34) the inverse Fourier transform of (4.47) is given by

$$\psi_{\mathrm{cub}}(x) = \frac{L+M}{2}\,\mathrm{sinc}\big(\tfrac{L+M}{2}\,\pi x\big) \cdot \frac{12\left(\mathrm{sinc}\big(\frac{L-M}{2}\,\pi x\big) - \cos\left(\frac{L-M}{2}\,\pi x\right)\right)}{\pi^2 x^2 (L-M)^2} \tag{4.48}$$

for $x \in \mathbb{R} \setminus \{0\}$ and $\psi_{\mathrm{cub}}(0) = \frac{L+M}{2}$, cf. Figure 4.2b. Hence, analogous to Theorem 4.10, the following error estimate can be derived, cf. also [KPT24, Theorem 3.7].

Theorem 4.15. *Let $f \in \mathcal{B}_{M/2}(\mathbb{R})$ be a bandlimited function with bandwidth $M \in \mathbb{N}$ and let $L = M(1+\lambda) \in \mathbb{N}$ with $\lambda > 0$. Further assume that the samples $f\left(\frac{\ell}{L}\right)$, $\ell \in \mathbb{Z}$, fulfill the condition (4.35). Using oversampling and regularization with the cubic frequency window function (4.47), the T-th partial sums $P_{\mathrm{cub},T} f$ converge uniformly to f on $[-1, 1]$ as $T \to \infty$. For $T > L$ the following estimate holds*

$$\max_{x \in [-1,\,1]} \left| f(x) - (P_{\mathrm{cub},T} f)(x) \right| \leq \sqrt{\frac{2L}{5}}\, \frac{14\,(1+\lambda)^2}{\pi^3 \lambda^2}\, (T-L)^{-5/2}\, \|f\|_{L_2(\mathbb{R})}. \tag{4.49}$$

Proof. By Theorem 4.10 we only have to check the decay of the function ψ_{cub} corresponding to the cubic frequency window function (4.47). It can easily be seen by graphical representation that ψ_{cub} in (4.48) satisfies the decay condition

$$\left|\psi_{\mathrm{cub}}(x)\right| \leq \frac{14}{\pi^3 (L-M)^2}\, |x|^{-3}, \quad x \in \mathbb{R} \setminus \{0\},$$

and thus (4.40) implies the estimate (4.49). ∎

Remark 4.16. Another continuously differentiable frequency window function is given in [Rap96] as the *raised cosine frequency window function*

$$\hat{\psi}_{\cos}(v) := \begin{cases} 1 & : |v| \leq \frac{M}{2}, \\ \frac{1}{2} + \frac{1}{2}\, \cos\left(\frac{2|v|-M}{L-M}\pi\right) & : \frac{M}{2} < |v| < \frac{L}{2}, \\ 0 & : |v| \geq \frac{L}{2}, \end{cases} \tag{4.50}$$

see Figure 4.2a. By (4.34) the corresponding function in spatial domain can be determined as

$$\psi_{\cos}(x) = \frac{L+M}{2}\, \operatorname{sinc}\left(\tfrac{L+M}{2}\,\pi x\right) \cdot \frac{\cos\left(\frac{L-M}{2}\,\pi x\right)}{1 - x^2 (L-M)^2}, \quad x \in \mathbb{R} \setminus \left\{\pm \tfrac{1}{L-M}\right\}, \tag{4.51}$$

and $\psi_{\cos}\left(\pm\frac{1}{L-M}\right) = \frac{L-M}{4}\cos\left(\frac{M\pi}{L-M}\right)$, cf. also [SS00, Example 6] and [QO05, Corollary 2.1], see Figure 4.2b. Note that graphical representation shows that this function $\psi_{\cos}$ satisfies the decay condition

$$\left|\psi_{\cos}(x)\right| \le \frac{2}{\pi(L-M)^2}\,|x|^{-3}, \quad x \in \mathbb{R}\setminus\{0\},$$

and thus (4.40) implies an error decay of the same rate as in (4.49), but with a slightly larger constant. By Corollary 4.12 this can also be seen in (4.50) and (4.47), since $\hat{\psi}_{\cos} \in C^1(\mathbb{R})$ and $\hat{\psi}_{\mathrm{cub}} \in C^1(\mathbb{R})$ possess the same regularity, and therefore both frequency window functions meet the same error bound (4.49), cf. Figure 4.16. ◇

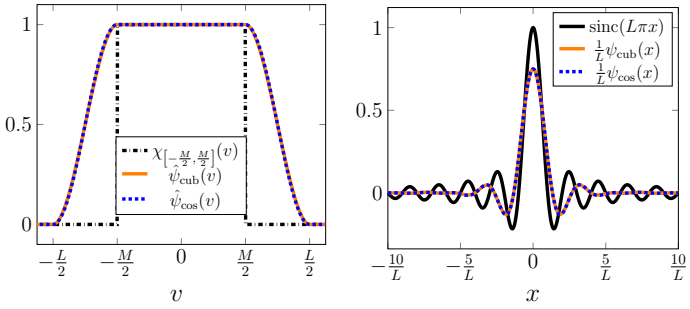

(a) $\hat{\psi}_{\mathrm{cub}}$ and $\hat{\psi}_{\cos}$ (b) $\frac{1}{L}\,\psi_{\mathrm{cub}}$ and $\frac{1}{L}\,\psi_{\cos}$

Figure 4.2: The frequency window functions (4.47) and (4.50), and their scaled inverse Fourier transforms (4.48) and (4.51).

Higher order frequency window functions by means of convolution

Note that by (4.45) and the convolution property

$$(f * g)\hat{} = \hat{f}\,\hat{g} \in C_0(\mathbb{R}), \quad f,\, g \in L_1(\mathbb{R}), \tag{4.52}$$

of the Fourier transform, where for $f,\, g \in L_1(\mathbb{R})$ the *convolution* is defined by

$$(f * g)(x) := \int_{\mathbb{R}} f(x-t)\,g(t)\,\mathrm{d}t, \quad x \in \mathbb{R},$$

the linear frequency window function (4.44) can be written as

$$\hat{\psi}_{\mathrm{lin}}(v) = \frac{2}{L-M}\left(\chi_{\left[-\frac{L+M}{4},\,\frac{L+M}{4}\right]} * \chi_{\left[-\frac{L-M}{4},\,\frac{L-M}{4}\right]}\right)(v).$$

Therefore, instead of determining smoother frequency window functions of the form (4.33) by means of interpolation, they can also be constructed by means of convolution, cf. [Nat86b] and [KPT24, Lemma 3.9].

Lemma 4.17. *Let $L > M$ be given. Further assume that $\rho\colon \mathbb{R} \to [0,\,\infty)$ is an even integrable function with $\operatorname{supp}(\rho) = \left[-\frac{L-M}{4},\,\frac{L-M}{4}\right]$ and $\int_{\mathbb{R}} \rho(v)\,\mathrm{d}v = 1$. Then the convolution*

$$\hat{\psi}_{\mathrm{conv}}(v) = \left(\chi_{\left[-\frac{L+M}{4},\,\frac{L+M}{4}\right]} * \rho\right)(v), \quad v \in \mathbb{R}, \tag{4.53}$$

is a frequency window function of the form (4.33)*.*

Proof. By assumption we have $\rho \in L_1(\mathbb{R})$. Since $\chi_{\left[-\frac{L+M}{4},\,\frac{L+M}{4}\right]} \in L_1(\mathbb{R})$ as well, their convolution $\hat{\psi}_{\mathrm{conv}} \in L_1(\mathbb{R})$ can be written as

$$\hat{\psi}_{\mathrm{conv}}(v) = \int_{-(L+M)/4}^{(L+M)/4} \rho(v-w)\,\mathrm{d}w = \int_{v-(L+M)/4}^{v+(L+M)/4} \rho(w)\,\mathrm{d}w. \tag{4.54}$$

Since the convolution of two even functions is again an even function, it is sufficient to consider (4.54) only for $v \geq 0$.

For $v \in \left[0,\,\frac{M}{2}\right]$ we have $v - \frac{L+M}{4} \leq -\frac{L-M}{4} < \frac{L-M}{4} \leq v + \frac{L+M}{4}$ and thus the assumption $\operatorname{supp}(\rho) = \left[-\frac{L-M}{4},\,\frac{L-M}{4}\right]$ yields

$$\hat{\psi}_{\mathrm{conv}}(v) = \int_{-(L-M)/4}^{(L-M)/4} \rho(w)\,\mathrm{d}w = 1, \quad v \in \left[0,\,\tfrac{M}{2}\right].$$

For $v \in \left[\frac{M}{2},\,\frac{L}{2}\right]$ we can write

$$\hat{\psi}_{\mathrm{conv}}(v) = \int_{v-(L+M)/4}^{(L-M)/4} \rho(w)\,\mathrm{d}w \geq 0, \quad v \in \left[\tfrac{M}{2},\,\tfrac{L}{2}\right],$$

where $\hat{\psi}_{\mathrm{conv}}\left(\frac{M}{2}\right) = 1$, $\hat{\psi}_{\mathrm{conv}}\left(\frac{L}{2}\right) = 0$, and $\hat{\psi}_{\mathrm{conv}}\colon \left[\frac{M}{2},\,\frac{L}{2}\right] \to [0,\,1]$ is monotonously non-increasing, since $\rho(w) \geq 0$ for all $w \in \mathbb{R}$ by assumption. Finally, for $v \in \left[\frac{L}{2},\,\infty\right)$ we have $v - \frac{L+M}{4} \geq \frac{L-M}{4}$, which implies by assumption $\operatorname{supp}(\rho) = \left[-\frac{L-M}{4},\,\frac{L-M}{4}\right]$ that

$$\hat{\psi}_{\mathrm{conv}}(v) = \int_{v-(L+M)/4}^{v+(L+M)/4} \rho(w)\,\mathrm{d}w = 0, \quad v \geq \tfrac{L}{2}.$$

Thus, the window function $\hat{\psi}_{\mathrm{conv}}$ defined by (4.53) is of the form (4.33). ■

Given such a frequency window function $\hat{\psi}_{\mathrm{conv}}$ in (4.53), its inverse Fourier transform (4.34) is known by the convolution property (4.52) as

$$\psi_{\mathrm{conv}}(x) = \frac{L+M}{2} \operatorname{sinc}\bigl(\tfrac{L+M}{2}\,\pi x\bigr)\,\check{\rho}(x). \tag{4.55}$$

Thus, to obtain a suitable window function (4.53), we need to assure that the inverse Fourier transform

$$\check{\rho}(x) = \int_{\mathbb{R}} \rho(v)\,\mathrm{e}^{2\pi \mathrm{i} x v}\,\mathrm{d}v = \int_{-(L-M)/4}^{(L-M)/4} \rho(v)\,\mathrm{e}^{2\pi \mathrm{i} x v}\,\mathrm{d}v$$

of ρ is explicitly known.

Remark 4.18. We remark that the frequency window functions $\hat{\psi}_{\mathrm{cub}}$ in (4.47) and $\hat{\psi}_{\mathrm{cos}}$ in (4.50) lack a convolutional representation (4.53). Although the corresponding functions (4.48) and (4.51) in spatial domain are of the form (4.55), for both frequency windows the Fourier transform of the respective function $\check{\rho}$ is not explicitly known (only in the sense of tempered distributions, cf. Section 6.1.3). ◇

As before, proper error estimates for the *convolutional frequency window function* $\hat{\psi}_{\mathrm{conv}}$ in (4.53) can be achieved by means of Theorem 4.10. However, note that Lemma 4.12 is not applicable in this setting, since the smoothness properties of the function ξ in (4.33) are unknown. Nevertheless, it can be shown that the smoothness of the window function (4.53) in spatial domain as well as the decay of the respective function (4.55) is determined by the smoothness of the chosen function ρ in (4.53), as the following lemma shows.

Lemma 4.19. *For $r > 0$ let the function ρ in* (4.53) *satisfy $\rho \in C^{r-1}(\mathbb{R})$ as well as $\rho \in C^{r+1}(\mathbb{R} \setminus \{-\frac{L-M}{4}, \frac{L-M}{4}\})$. Then $\hat{\psi}_{\mathrm{conv}} \in C^r(\mathbb{R})$ and the corresponding function ψ_{conv} in* (4.55) *in spatial domain fulfills the decay condition* (4.39).

Proof. Obviously, the function ρ is integrable, since $\rho \in C(\mathbb{R})$ by assumption. Let P be an antiderivative of ρ, then the representation (4.54) yields

$$\hat{\psi}'_{\mathrm{conv}}(v) = \left(\int_{v-(L+M)/4}^{v+(L+M)/4} \rho(w)\,\mathrm{d}w\right)' = \Bigl(P\bigl(v+\tfrac{L+M}{4}\bigr) - P\bigl(v-\tfrac{L+M}{4}\bigr)\Bigr)'$$

$$= \rho\big(v + \tfrac{L+M}{4}\big) - \rho\big(v - \tfrac{L+M}{4}\big) \in C^{r-1}(\mathbb{R}),$$

such that $\hat{\psi}_{\mathrm{conv}} \in C^r(\mathbb{R})$.

In addition, analogous to the proof of Corollary 4.12, it can be shown that by $\rho \in C^{r-1}(\mathbb{R})$ we have $\rho^{(r-1)}\big(\pm \tfrac{L-M}{4}\big) = 0$, and therefore

$$|\check{\rho}(x)| \le c_\rho\, |x|^{-(r+1)}, \quad x \in \mathbb{R} \setminus \{0\}.$$

Since it is additionally known that

$$\check{\chi}_{[-\frac{L+M}{4},\,\frac{L+M}{4}]} = \hat{\chi}_{[-\frac{L+M}{4},\,\frac{L+M}{4}]} = \frac{L+M}{2}\,\mathrm{sinc}\big(\tfrac{L+M}{2}\,\pi x\big),$$

we obtain

$$\begin{aligned} |\psi_{\mathrm{conv}}(x)| &= \Big|\big(\chi_{[-\frac{L+M}{4},\,\frac{L+M}{4}]} * \rho\big)\check{}\,(x)\Big| \\ &= \Big|\check{\chi}_{[-\frac{L+M}{4},\,\frac{L+M}{4}]}(x) \cdot \check{\rho}(x)\Big| \le \frac{1}{\pi|x|} \cdot c_\rho\, |x|^{-(r+1)} \end{aligned}$$

and thus the assertion. ∎

For the special choice of $\rho_n(v) = \frac{2n}{L-M}\, B_n\big(\frac{2n}{L-M} v\big)$ with $n \in \mathbb{N}$, where B_n is the centered cardinal B–spline of order n, cf. [SS00, Example 3], we have

$$\check{\rho}_n(x) = \Big(\mathrm{sinc}\big(\tfrac{L-M}{2n}\,\pi x\big)\Big)^n. \tag{4.56}$$

The corresponding convolutional frequency window functions (4.53) shall be denoted as $\hat{\psi}_{\mathrm{conv},n}$ and their inverse Fourier transforms (4.55) as $\psi_{\mathrm{conv},n}$, see Figure 4.3 for a visualization for $n \in \{1, \dots, 6\}$. Note that using $n = 1$ again yields (4.45), whereas for $n = 2$ we obtain

$$\psi_{\mathrm{conv},2}(x) = \frac{L+M}{2}\,\mathrm{sinc}\big(\tfrac{L+M}{2}\,\pi x\big)\,\Big(\mathrm{sinc}\big(\tfrac{L-M}{4}\,\pi x\big)\Big)^2. \tag{4.57}$$

It is easy to see that this function (4.57) satisfies the decay condition

$$\big|\psi_{\mathrm{conv},2}(x)\big| \le \frac{16}{\pi^3 (L-M)^2}\, |x|^{-3}, \quad x \in \mathbb{R} \setminus \{0\},$$

and thus (4.40) implies an error decay of the same rate as in (4.49), but with a slightly larger constant. This can also be seen by Corollary 4.12, since $\hat{\psi}_{\mathrm{conv},2} \in C^1(\mathbb{R})$ in (4.57) possesses the same regularity as $\hat{\psi}_{\mathrm{cub}} \in C^1(\mathbb{R})$ in (4.47) and $\hat{\psi}_{\mathrm{cos}} \in C^1(\mathbb{R})$ in (4.50), and therefore they all meet the same error bound (4.49), cf. Figure 4.16.

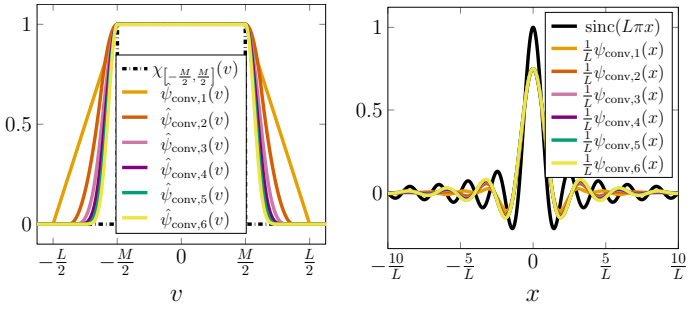

(a) $\hat{\psi}_{\mathrm{conv},n}$ in (4.53) (b) $\frac{1}{L}\,\psi_{\mathrm{conv},n}$ in (4.55)

Figure 4.3: The convolutional frequency window functions $\hat{\psi}_{\mathrm{conv},n}$ in (4.53) with $\rho_n(v) = \frac{2n}{L-M}\,B_n\big(\frac{2n}{L-M}v\big)$ for $n \in \{1,\dots,6\}$, and their scaled inverse Fourier transforms (4.55).

Remark 4.20. Note that the convolutional frequency window functions $\hat{\psi}_{\mathrm{conv},n}$ as well as their inverse Fourier transforms $\psi_{\mathrm{conv},n}$ are properly defined for all $n \in \mathbb{N}$. Therefore, one could attempt to find an infinitely differentiable frequency window function $\hat{\psi}_{\mathrm{conv},n}$ with accompanying rapidly decaying function in time domain $\psi_{\mathrm{conv},n}$ by sending $n \to \infty$. To compute the corresponding limit of (4.56) we set $a \coloneqq \frac{L-M}{2}\,\pi$ and define the sequence $\beta(n) \coloneqq \mathrm{sinc}\big(\frac{ax}{n}\big) - 1$, i. e., we consider

$$\lim_{n\to\infty} \Big(\mathrm{sinc}\big(\tfrac{ax}{n}\big)\Big)^n = \lim_{n\to\infty} \Big[\Big(1+\beta(n)\Big)^{\frac{1}{\beta(n)}}\Big]^{n\cdot\beta(n)}.$$

Obviously, the term in brackets tends to e, such that we only need to compute the limit of the exponent. By substituting $y = \frac{1}{n}$ we see that this exponent can be written as

$$n\cdot\beta(n) = \mathrm{sinc}\big(\tfrac{ax}{n}\big) - 1 = \frac{\frac{\sin(axy)}{axy} - 1}{y} = \frac{\sin(axy) - axy}{axy^2}.$$

As $n \to \infty$ we have $y \to 0$, such that both numerator and denominator of this term tend to zero. Thus, applying the rule of l'Hospital twice, the limit of the exponent can be computed by

$$\lim_{y\to 0} \frac{\sin(axy) - axy}{axy^2} = \lim_{y\to 0} \frac{ax\,\cos(axy) - ax}{2axy} = \lim_{y\to 0} \frac{-a^2x^2\,\sin(axy)}{2ax} = 0.$$

For (4.56) we thereby obtain

$$\lim_{n\to\infty} \check{\rho}_n(x) = \lim_{n\to\infty} \left[\Big(1+\beta(n)\Big)^{\frac{1}{\beta(n)}} \right]^{n\cdot\beta(n)} = \mathrm{e}^0 = 1, \quad x \in \mathbb{R},$$

yielding

$$\psi_{\mathrm{conv},\infty}(x) \coloneqq \lim_{n\to\infty} \psi_{\mathrm{conv},n}(x) = \frac{L+M}{2} \operatorname{sinc}\big(\tfrac{L+M}{2}\,\pi x\big), \tag{4.58}$$

which obviously has slower decay than $\psi_{\mathrm{conv},n}$ for all $n \in \mathbb{N}$. This is to say, although $\psi_{\mathrm{conv},n}$ is defined for all $n \in \mathbb{N}$ and the limit for $n \to \infty$ exists, this approach does not provide a rapidly decaying function and therefore fast convergence of (4.38). ◇

Remark 4.21. Also in the literature several attempts were made to achieve an infinitely differentiable frequency window function $\hat{\psi}_{\mathrm{conv}}$ in (4.53) with accompanying rapidly decaying function (4.55). For instance, in [Nat86b] the infinitely differentiable function

$$\rho_\infty(v) = \begin{cases} c\,\exp\big(\big[\big(\frac{4v}{L-M}\big)^2 - 1\big]^{-1}\big) & : |v| < \frac{L-M}{4}, \\ 0 & : \text{otherwise}, \end{cases}$$

with the scaling factor

$$c = \frac{1}{2}\left(\int_0^{(L-M)/4} \exp\big(\big[\big(\tfrac{4v}{L-M}\big)^2 - 1\big]^{-1}\big)\,\mathrm{d}v \right)^{-1}$$

is considered. The corresponding frequency window function (4.53) is denoted by $\hat{\psi}_\infty$. However, since for this function ρ_∞ the inverse Fourier transform $\check{\rho}_\infty$ cannot explicitly be stated, the function (4.55) in spatial domain can only be approximated, which was done by a piecewise rational approximation $\check{\rho}_{\mathrm{rat}}$ in [Nat86b]. We remark that because of this additional approximation a numerical decay of the expected rate is doubtful, since the issue of robustness of the corresponding regularized Shannon series remained unclear. This effect can also be seen in Figure 4.16, where the corresponding frequency window function (4.53), denoted by $\hat{\psi}_{\mathrm{rat}}$, shows similar behavior as the classical Shannon sampling sums (4.12).

A similar comment applies to [ST05], where an infinitely differentiable window function $\hat{\psi}$ is aimed for as well. Since no such $\hat{\psi}$ with explicit

inverse Fourier transform (4.34) is known, in [ST05] the function ψ in spatial domain is estimated with some Gabor approximation. Although an efficient computation scheme via fast Fourier transform (FFT) was introduced in [ST06], the numerical nonrobustness of this approximation seems to be neglected in this work as well. ◇

Summary

Finally, it should be noted that it has already been established in [Dau92, p. 19] that a faster decay than for $\hat{\psi}_{\mathrm{lin}}$ in (4.44) can be obtained by choosing $\hat{\psi}$ in (4.33) smoother, but at the price of a very large constant. This can also be seen in Figure 4.16, where the results for the window functions $\hat{\psi}_{\mathrm{cub}}$ in (4.47), $\hat{\psi}_{\cos}$ in (4.50), $\hat{\psi}_{\mathrm{conv},n}$ with $n \in \{2, 3, 4\}$, cf. (4.57), and $\hat{\psi}_{\mathrm{rat}}$ from Remark 4.21 are plotted as well. For this reason many authors such as [Dau92, Par97] restricted themselves to the linear frequency window function $\hat{\psi}_{\mathrm{lin}}$ in (4.44).

In contrast, we have reviewed several existing approaches and proposed general convergence results based on a rigorous analysis of the respective properties. Additionally, we have put special emphasis on the relations among the considered approaches. For a comparison of the theoretical error decay rates of the frequency window functions we refer to Table 4.1 in Section 4.3.3, while a visualization of the error decay rates can be found in Examples 4.67 and 4.68. However, so far, only approaches with algebraic error decay rates are known, and all attempts to design infinitely differentiable window functions have seemingly been unsuccessful. Note that the numerical results in Figure 4.16 also encourage the suggestion that in practice only algebraic decay rates are achievable for the regularization with a frequency window function.

4.3.2 Regularization with a window function in spatial domain

In order to obtain preferably better decay rates, we now consider a second regularization technique, namely regularization with a convenient window function in the spatial domain as done in [KPT22, KPT24].

For this purpose, we introduce the set Φ of all window functions $\varphi\colon \mathbb{R} \to [0, 1]$ with the following properties:

- The window function φ belongs to $L_1(\mathbb{R}) \cap C_0(\mathbb{R})$ and is even.
- The function φ restricted to $[0, \infty)$ is monotonously non-increasing with $\varphi(0) = 1$.

Note that it is especially beneficial for obtaining explicit error estimates (cf. Theorems 4.24, 4.25 and 4.29), if the Fourier transform

$$\hat{\varphi}(v) = \int_{\mathbb{R}} \varphi(x)\, \mathrm{e}^{-2\pi \mathrm{i} v x}\, \mathrm{d}x = 2 \int_0^\infty \varphi(x)\, \cos(2\pi v x)\, \mathrm{d}x\,, \quad v \in \mathbb{R}\,, \tag{4.59}$$

of $\varphi \in \Phi$ is explicitly known.

Remark 4.22. As examples of such window functions we consider the *Gaussian window function*

$$\varphi_{\mathrm{Gauss}}(x) := \mathrm{e}^{-x^2/(2\alpha^2)}, \quad x \in \mathbb{R}, \tag{4.60}$$

with some $\alpha > 0$, the *modified* B*–spline window function*

$$\varphi_{\mathrm{B}}(x) := \frac{1}{B_{2s}(0)}\, B_{2s}\Big(\frac{Lxs}{m}\Big), \quad x \in \mathbb{R}, \tag{4.61}$$

where B_{2s} is the *centered cardinal* B*–spline* of even order $2s \in \mathbb{N}$ and $m \in \mathbb{N}$ with $2m \ll L$, the sinh*-type window function*

$$\varphi_{\sinh}(x) := \begin{cases} \frac{1}{\sinh \beta}\, \sinh\Big(\beta \sqrt{1 - \big(\frac{Lx}{m}\big)^2}\Big) & : x \in \big[-\frac{m}{L},\, \frac{m}{L}\big]\,, \\ 0 & : x \in \mathbb{R} \setminus \big[-\frac{m}{L},\, \frac{m}{L}\big]\,, \end{cases} \tag{4.62}$$

with certain $\beta > 0$, and the *continuous Kaiser–Bessel window function*

$$\varphi_{\mathrm{cKB}}(x) := \begin{cases} \frac{1}{I_0(\beta) - 1} \left(I_0\Big(\beta \sqrt{1 - \big(\frac{Lx}{m}\big)^2}\Big) - 1 \right) & : x \in \big[-\frac{m}{L},\, \frac{m}{L}\big]\,, \\ 0 & : x \in \mathbb{R} \setminus \big[-\frac{m}{L},\, \frac{m}{L}\big]\,, \end{cases} \tag{4.63}$$

with certain $\beta > 0$, where I_0 denotes the *modified Bessel function of first kind*. All these window functions are well-studied, see e. g. [PT21b] and references therein, in the context of the nonequispaced fast Fourier transform (NFFT), cf. Section 2. ◇

Then, for a fixed window function $\varphi \in \Phi$ we study the *regularized Shannon sampling formula*

$$(R_\varphi f)(x) \coloneqq \sum_{\ell \in \mathbb{Z}} f\big(\tfrac{\ell}{L}\big)\, \operatorname{sinc}\big(L\pi\big(x - \tfrac{\ell}{L}\big)\big)\, \varphi\big(x - \tfrac{\ell}{L}\big), \quad x \in \mathbb{R}. \tag{4.64}$$

Since by assumption $\varphi(0) = 1$ and $\operatorname{sinc}(\pi(k-\ell)) = \delta_{k,\ell}$ for all k, $\ell \in \mathbb{Z}$ with the Kronecker symbol $\delta_{k,\ell}$, we obtain

$$\operatorname{sinc}\big(L\pi\big(x - \tfrac{\ell}{L}\big)\big)\, \varphi\big(x - \tfrac{\ell}{L}\big)\,\big|_{x=\frac{k}{L}} = \delta_{k,\ell}.$$

Therefore, this procedure $R_\varphi f$ is an *interpolating approximation* of f on $\frac{1}{L}\,\mathbb{Z}$, i. e., we have

$$f\big(\tfrac{k}{L}\big) = (R_\varphi f)\big(\tfrac{k}{L}\big), \quad k \in \mathbb{Z}. \tag{4.65}$$

Before proceeding with error estimates of the regularized Shannon sampling formula (4.64), we need the following lemma on the *convolution property* of the Fourier transform in $L_2(\mathbb{R})$. Note that for f, $g \in L_2(\mathbb{R})$ the convolution property of the Fourier transform is not true in the form (4.52), since by Young's inequality $f * g \in C_0(\mathbb{R})$ and by Hölder's inequality $\hat{f}\,\hat{g} \in L_1(\mathbb{R})$, but the Fourier transform does not map $C_0(\mathbb{R})$ onto $L_1(\mathbb{R})$. Instead, it was shown in [KPT22, Lemma 2.1 and Lemma 2.2] that the convolution property of the Fourier transform in $L_2(\mathbb{R})$ has the following form.

Lemma 4.23. *For all f, $g \in L_2(\mathbb{R})$ we have*

$$\begin{aligned} f * g &= (\hat{f}\,\hat{g})\check{} \in C_0(\mathbb{R}), \\ \hat{f} * \hat{g} &= (f\,g)\check{} \in C_0(\mathbb{R}). \end{aligned} \tag{4.66}$$

Proof. See [KPT22, Lemma 2.1 and Lemma 2.2]. ∎

Now we estimate the *uniform regularization error*

$$\|f - R_\varphi f\|_{C_0(\mathbb{R})} \coloneqq \max_{x \in \mathbb{R}} \big|f(x) - (R_\varphi f)(x)\big|$$

of the regularized Shannon sampling formula (4.64), cf. [KPT22, Theorem 3.2].

Theorem 4.24. *Let $f \in \mathcal{B}_{M/2}(\mathbb{R})$ with $M, L \in \mathbb{N}$ and $L > M$ be given. Further let $\varphi \in \Phi$ be a given window function. Then the regularized Shannon sampling formula* (4.64) *satisfies*

$$\|f - R_\varphi f\|_{C_0(\mathbb{R})} \le \sqrt{M} \max_{v \in \left[-\frac{M}{2}, \frac{M}{2}\right]} \left| 1 - \int_{v-L/2}^{v+L/2} \hat{\varphi}(u)\,\mathrm{d}u \right| \|f\|_{L_2(\mathbb{R})}$$

$$=: E_{\mathrm{r}}(\varphi, M, L)\,\|f\|_{L_2(\mathbb{R})}. \tag{4.67}$$

Proof. For the regularized Shannon sampling formula (4.64) we define the *regularization error*

$$e_{\mathrm{r}}(x) := f(x) - (R_\varphi f)(x) = f(x) - \sum_{\ell \in \mathbb{Z}} f\left(\tfrac{\ell}{L}\right) \psi\left(x - \tfrac{\ell}{L}\right), \quad x \in \mathbb{R}, \tag{4.68}$$

with the *regularized sinc function*

$$\psi(x) := \operatorname{sinc}(L\pi x)\,\varphi(x). \tag{4.69}$$

By Lemma 4.23, the Fourier transform of ψ reads as

$$\hat{\psi}(v) = \frac{1}{L} \int_{\mathbb{R}} \chi_{\left[-\frac{L}{2}, \frac{L}{2}\right]}(v-u)\,\hat{\varphi}(u)\,\mathrm{d}u = \frac{1}{L} \int_{v-L/2}^{v+L/2} \hat{\varphi}(u)\,\mathrm{d}u. \tag{4.70}$$

Hence, using the shifting property of the Fourier transform, the Fourier transform of $\psi\left(\,\cdot\, - \frac{\ell}{L}\right)$ is given by

$$\frac{1}{L}\,\mathrm{e}^{-2\pi \mathrm{i} v \ell/L} \int_{v-L/2}^{v+L/2} \hat{\varphi}(u)\,\mathrm{d}u.$$

Therefore, the Fourier transform of the regularization error (4.68) has the form

$$\hat{e}_{\mathrm{r}}(v) = \hat{f}(v) - \left(\sum_{\ell \in \mathbb{Z}} f\left(\tfrac{\ell}{L}\right) \frac{1}{L}\,\mathrm{e}^{-2\pi \mathrm{i} v \ell/L} \right) \int_{v-L/2}^{v+L/2} \hat{\varphi}(u)\,\mathrm{d}u, \quad v \in \mathbb{R}. \tag{4.71}$$

Since $f \in \mathcal{B}_{M/2}(\mathbb{R})$, it is known that $\hat{f}$ can be represented by (4.37) as

$$\hat{f}(v) = \hat{f}(v)\,\chi_{\left[-\frac{M}{2}, \frac{M}{2}\right]}(v)$$

$$= \left(\sum_{k \in \mathbb{Z}} \frac{1}{L} f\left(\tfrac{k}{L}\right) \mathrm{e}^{-2\pi \mathrm{i} k v/L} \right) \chi_{\left[-\frac{M}{2}, \frac{M}{2}\right]}(v), \quad v \in \mathbb{R}.$$

Inserting this into (4.71) we see that $\hat{e}_{\mathrm{r}}(v) = \hat{f}(v)\,\eta(v)$ with the auxiliary function

$$\eta(v) \coloneqq \chi_{\left[-\frac{M}{2},\,\frac{M}{2}\right]}(v) - \int_{v-L/2}^{v+L/2} \hat{\varphi}(u)\,\mathrm{d}u, \quad v \in \mathbb{R}, \tag{4.72}$$

and thereby $|\hat{e}_{\mathrm{r}}(v)| \le |\hat{f}(v)|\,|\eta(v)|$. Thus, by inverse Fourier transform (4.4) we get

$$\begin{aligned} |e_{\mathrm{r}}(x)| &= \left| \int_{\mathbb{R}} \hat{e}_{\mathrm{r}}(v)\,\mathrm{e}^{2\pi \mathrm{i} x v}\,\mathrm{d}v \right| \le \int_{\mathbb{R}} |\hat{e}_{\mathrm{r}}(v)|\,\mathrm{d}v \le \int_{-M/2}^{M/2} |\hat{f}(v)|\,|\eta(v)|\,\mathrm{d}v \\ &\le \max_{v \in \left[-\frac{M}{2},\,\frac{M}{2}\right]} |\eta(v)| \int_{-M/2}^{M/2} |\hat{f}(v)|\,\mathrm{d}v, \quad x \in \mathbb{R}. \end{aligned}$$

Using the Cauchy–Schwarz inequality and Parseval's identity, we see that

$$\begin{aligned} \int_{-M/2}^{M/2} |\hat{f}(v)|\,\mathrm{d}v &\le \left(\int_{-M/2}^{M/2} 1^2\,\mathrm{d}v \right)^{1/2} \left(\int_{-M/2}^{M/2} |\hat{f}(v)|^2\,\mathrm{d}v \right)^{1/2} \\ &= \sqrt{M}\,\|\hat{f}\|_{L_2(\mathbb{R})} = \sqrt{M}\,\|f\|_{L_2(\mathbb{R})}. \end{aligned}$$

In summary, this yields

$$\|e_{\mathrm{r}}\|_{C_0(\mathbb{R})} \le E_{\mathrm{r}}(\varphi, M, L)\,\|f\|_{L_2(\mathbb{R})}$$

with the *regularization error constant* (4.67). ■

Nevertheless, we recognize that the evaluation of the regularized Shannon sampling formula (4.64) still requires an infinite number of samples $f\left(\frac{\ell}{L}\right)$, $\ell \in \mathbb{Z}$. Therefore, in practice we have to deal with a truncated version of (4.64) as well.

Similar to (4.12) and (4.38), one could consider a uniform truncation by introducing a truncation parameter $T \in \mathbb{N}$ and studying the partial sums

$$(R_{\varphi,T} f)(x) \coloneqq \sum_{\ell=-T}^{T} f\left(\tfrac{\ell}{L}\right) \operatorname{sinc}\left(L\pi\left(x - \tfrac{\ell}{L}\right)\right) \varphi\left(x - \tfrac{\ell}{L}\right), \quad x \in \mathbb{R}.$$

However, as before, in this case bounds on the uniform approximation error $\|f - R_{\varphi,T} f\|_{C_0(\mathbb{R})}$ are unattainable and only weaker results of the form

$$\max_{x \in [-1,\,1]} \left| f(x) - (R_{\varphi,T} f)(x) \right|$$

can be obtained, cf. Sections 4.2 and 4.3.1. Therefore, to achieve uniform error bounds and faster decay rates, a different approach is taken here.

In view of the slow convergence of the sinc function it has been proposed to modify the Shannon sampling series (4.15) by multiplying the sinc function with a more convenient window function, cf. e. g. [Qia03, LZ17]. For this purpose, for a given window function $\varphi \in \Phi$ and $m \in \mathbb{N}$ with $2m \ll L$ we now define the *truncated window function*

$$\varphi_m(x) \coloneqq \varphi(x)\, \chi_{\left[-\frac{m}{L},\, \frac{m}{L}\right]}(x), \quad x \in \mathbb{R}, \tag{4.73}$$

and study the *regularized Shannon sampling formula with localized sampling*

$$(R_{\varphi,m} f)(x) \coloneqq \sum_{\ell \in \mathbb{Z}} f\big(\tfrac{\ell}{L}\big)\, \operatorname{sinc}\big(L\pi \left(x - \tfrac{\ell}{L}\right)\big)\, \varphi_m\big(x - \tfrac{\ell}{L}\big), \quad x \in \mathbb{R}. \tag{4.74}$$

Note that the truncation of the window function $\varphi \in \Phi$ preserves the interpolation property (4.65), i. e., we still have

$$f\big(\tfrac{k}{L}\big) = (R_{\varphi,m} f)\big(\tfrac{k}{L}\big), \quad k \in \mathbb{Z}. \tag{4.75}$$

Furthermore, the use of the compactly supported window function φ_m in (4.73) leads to *localized sampling* of the bandlimited function $f \in \mathcal{B}_{M/2}(\mathbb{R})$. Namely, due to the definition of the characteristic function $\chi_{\left[-\frac{m}{L},\, \frac{m}{L}\right]}$, the computation of $(R_{\varphi,m} f)(x)$ requires only $2m+1$ samples $f\big(\frac{\ell}{L}\big)$ for fixed $x \in \mathbb{R} \setminus \frac{1}{L}\,\mathbb{Z}$, where $\ell \in \mathbb{Z}$ fulfills the condition $|\ell - Lx| \le m$. Therefore, we approximate f by $R_{\varphi,m} f$ separately on each open interval $\big(\frac{k}{L},\, \frac{k+1}{L}\big)$, $k \in \mathbb{Z}$. Especially for $x \in \big(0,\, \frac{1}{L}\big)$, the regularized Shannon sampling formula with localized sampling (4.74) reads as

$$\begin{aligned}(R_{\varphi,m} f)(x) &= \sum_{\ell \in \mathcal{J}_m} f\big(\tfrac{\ell}{L}\big)\, \operatorname{sinc}\big(L\pi \left(x - \tfrac{\ell}{L}\right)\big)\, \varphi_m\big(x - \tfrac{\ell}{L}\big) \\ &= \sum_{\ell \in \mathcal{J}_m} f\big(\tfrac{\ell}{L}\big)\, \psi\big(x - \tfrac{\ell}{L}\big)\end{aligned}$$

with the regularized sinc function (4.69) and the index set

$$\mathcal{J}_m \coloneqq \{-m+1,\, -m+2,\, \ldots,\, m\}. \tag{4.76}$$

For the reconstruction of f on any open interval $\left(\frac{k}{L},\, \frac{k+1}{L}\right)$ with $k \in \mathbb{Z}$, we use the representation

$$(R_{\varphi,m} f)\left(x + \tfrac{k}{L}\right) = \sum_{\ell \in \mathcal{J}_m} f\left(\tfrac{\ell+k}{L}\right) \psi\left(x - \tfrac{\ell}{L}\right), \quad x \in \left(0,\, \tfrac{1}{L}\right). \tag{4.77}$$

This concept of regularized Shannon sampling formulas with localized sampling has already been studied by numerous authors. A survey of different approaches for window functions can be found in [Qia04], while the prominent Gaussian window function (4.60) was examined for example in [Qia03, QC06a, QC06b, SS07, TSM08, LZ17, CZ19]. In the following, we will focus on the window functions $\varphi \in \Phi$ mentioned in Remark 4.22, similar to the approach in [KPT22, KPT24].

Analogous to [KPT22, Theorem 3.2], the *uniform approximation error*

$$\|f - R_{\varphi,m} f\|_{C_0(\mathbb{R})} \coloneqq \max_{x \in \mathbb{R}} \left| f(x) - (R_{\varphi,m} f)(x) \right| \tag{4.78}$$

of the regularized Shannon sampling formula with localized sampling (4.74) can be estimated for given $f \in \mathcal{B}_{M/2}(\mathbb{R})$ and $\varphi \in \Phi$ as follows.

Theorem 4.25. *Let $f \in \mathcal{B}_{M/2}(\mathbb{R})$ with $M \in \mathbb{N}$, $L = M(1+\lambda) \in \mathbb{N}$ with $\lambda \geq 0$ and $m \in \mathbb{N} \setminus \{1\}$. Further let $\varphi \in \Phi$ with the truncated window function* (4.73) *be given. Then the regularized Shannon sampling formula with localized sampling* (4.74) *satisfies*

$$\|f - R_{\varphi,m} f\|_{C_0(\mathbb{R})} \leq \left(E_{\mathrm{r}}(\varphi, M, L) + E_{\mathrm{t}}(\varphi, m, L) \right) \|f\|_{L_2(\mathbb{R})}, \tag{4.79}$$

with the regularization error constant (4.67) *and the* truncation error constant

$$E_{\mathrm{t}}(\varphi, m, L) \coloneqq \frac{\sqrt{2L}}{\pi} \left(\frac{1}{m^2}\, \varphi^2\left(\tfrac{m}{L}\right) + \frac{1}{L} \int_{m/L}^{\infty} \frac{\varphi^2(t)}{t^2}\, \mathrm{d}t \right)^{1/2}. \tag{4.80}$$

Proof. Initially, we consider only the interval $\left[0,\, \frac{1}{L}\right]$. Here we split the approximation error

$$f(x) - (R_{\varphi,m} f)(x) = e_{\mathrm{r}}(x) + e_{\mathrm{t},0}(x), \quad x \in \left[0,\, \tfrac{1}{L}\right],$$

into the regularization error (4.68) and the *truncation error*

$$e_{\mathrm{t},0}(x) \coloneqq (R_{\varphi} f)(x) - (R_{\varphi,m} f)(x), \quad x \in \left[0,\, \tfrac{1}{L}\right].$$

Since the regularization error (4.68) has already been estimated in (4.67), only the truncation error has to be considered. For $x \in \big(0,\, \frac{1}{L}\big)$ we have by (4.64) and (4.74) that

$$\begin{aligned} e_{\mathrm{t},0}(x) &= \sum_{\ell\in\mathbb{Z}} f\big(\tfrac{\ell}{L}\big)\, \mathrm{sinc}\big(L\pi\,\big(x-\tfrac{\ell}{L}\big)\big)\, \varphi\big(x-\tfrac{\ell}{L}\big)\, \big[1-\chi_{[-\frac{m}{L},\,\frac{m}{L}]}\big(x-\tfrac{\ell}{L}\big)\big] \\ &= \sum_{\ell\in\mathbb{Z}\setminus\mathcal{J}_m} f\big(\tfrac{\ell}{L}\big)\, \mathrm{sinc}\big(L\pi\,\big(x-\tfrac{\ell}{L}\big)\big)\, \varphi\big(x-\tfrac{\ell}{L}\big). \end{aligned}$$

Now we introduce the auxiliary function

$$h_m(x) \coloneqq \sum_{\ell\in\mathbb{Z}\setminus\mathcal{J}_m} \frac{1}{\pi^2\,|Lx-\ell|^2}\, \varphi^2\big(x-\tfrac{\ell}{L}\big) \geq 0, \quad x \in \big[0,\, \tfrac{1}{L}\big]. \tag{4.81}$$

Then the Cauchy–Schwarz inequality and (4.9) imply

$$\begin{aligned} |e_{\mathrm{t},0}(x)| &\leq \sum_{\ell\in\mathbb{Z}\setminus\mathcal{J}_m} \big|f\big(\tfrac{\ell}{L}\big)\big|\, \big|\mathrm{sinc}\big(L\pi\,\big(x-\tfrac{\ell}{L}\big)\big)\, \varphi\big(x-\tfrac{\ell}{L}\big)\big| \\ &\leq \sqrt{\sum_{\ell\in\mathbb{Z}\setminus\mathcal{J}_m} \big|f\big(\tfrac{\ell}{L}\big)\big|^2} \cdot \sqrt{\sum_{\ell\in\mathbb{Z}\setminus\mathcal{J}_m} \big[\mathrm{sinc}\big(L\pi\,\big(x-\tfrac{\ell}{L}\big)\big)\, \varphi\big(x-\tfrac{\ell}{L}\big)\big]^2} \\ &\leq \sqrt{L}\, \|f\|_{L_2(\mathbb{R})}\, \sqrt{h_m(x)}. \end{aligned}$$

Since $\varphi|_{[0,\,\infty)}$ is monotonously non-increasing by assumption $\varphi \in \Phi$, we can estimate the series $h_m(x)$ for $x \in \big(0,\, \frac{1}{L}\big)$ by

$$\begin{aligned} h_m(x) &= \frac{1}{\pi^2} \left(\sum_{\ell=-\infty}^{-m} + \sum_{\ell=m+1}^{\infty} \right) \frac{\varphi^2\big(x-\frac{\ell}{L}\big)}{|Lx-\ell|^2} \\ &= \frac{1}{\pi^2} \left(\sum_{\ell=m}^{\infty} \frac{\varphi^2\big(x+\frac{\ell}{L}\big)}{|Lx+\ell|^2} + \sum_{\ell=m+1}^{\infty} \frac{\varphi^2\big(x-\frac{\ell}{L}\big)}{|Lx-\ell|^2} \right) \\ &\leq \frac{1}{\pi^2} \left(\sum_{\ell=m}^{\infty} \frac{\varphi^2\big(\frac{\ell}{L}\big)}{\ell^2} + \sum_{\ell=m+1}^{\infty} \frac{\varphi^2\big(\frac{\ell-1}{L}\big)}{(\ell-1)^2} \right) = \frac{2}{\pi^2} \sum_{\ell=m}^{\infty} \frac{\varphi^2\big(\frac{\ell}{L}\big)}{\ell^2}. \end{aligned} \tag{4.82}$$

Using the integral test for convergence of series (see Lemma 4.5), we obtain that

$$\sum_{\ell=m}^{\infty} \frac{\varphi^2\big(\frac{\ell}{L}\big)}{\ell^2} = \frac{\varphi^2\big(\frac{m}{L}\big)}{m^2} + \sum_{\ell=m+1}^{\infty} \frac{\varphi^2\big(\frac{\ell}{L}\big)}{\ell^2} < \frac{\varphi^2\big(\frac{m}{L}\big)}{m^2} + \frac{1}{L}\int_{m/L}^{\infty} \frac{\varphi^2(t)}{t^2}\,\mathrm{d}t. \tag{4.83}$$

By the interpolation property (4.75) of $R_{\varphi,m}f$ we have $e_{\mathrm{t},0}(0) = e_{\mathrm{t},0}\big(\frac{1}{L}\big) = 0$, such that we obtain by (4.80) that

$$\max_{x\in[0,1/L]} |e_{\mathrm{t},0}(x)| \le E_{\mathrm{t}}(\varphi, m, L)\,\|f\|_{L_2(\mathbb{R})}.$$

By the same technique, this error estimate can be shown for each interval $\big[\frac{k}{L}, \frac{k+1}{L}\big]$ with $k \in \mathbb{Z}$. On any open interval $\big(\frac{k}{L}, \frac{k+1}{L}\big)$ with $k \in \mathbb{Z}$, we split the error by (4.77) as

$$f\big(x + \tfrac{k}{L}\big) - (R_{\varphi,m}f)\big(x + \tfrac{k}{L}\big) = e_{\mathrm{r}}\big(x + \tfrac{k}{L}\big) + e_{\mathrm{t},k}(x), \quad x \in \big(0, \tfrac{1}{L}\big),$$

with the regularization error (4.68) and the truncation errors

$$e_{\mathrm{t},k}(x) \coloneqq \sum_{\ell\in\mathbb{Z}\setminus\mathcal{J}_m} f\big(\tfrac{\ell+k}{L}\big)\,\psi\big(x - \tfrac{\ell}{L}\big).$$

As shown above, we have

$$|e_{\mathrm{t},k}(x)| \le E_{\mathrm{t}}(\varphi, m, L)\,\|f\|_{L_2(\mathbb{R})}, \quad x \in \big(0, \tfrac{1}{L}\big),$$

and $e_{\mathrm{t},0}\big(\frac{k}{L}\big) = e_{\mathrm{t},0}\big(\frac{k+1}{L}\big) = 0$ for each $k \in \mathbb{Z}$ by the interpolation property of $R_{\varphi,m}f$. Hence, it follows that

$$\begin{aligned}\max_{x\in[k/L,\,(k+1)/L]} |f(x) - (R_{\varphi,m}f)(x)| &\le \|e_{\mathrm{r}}\|_{C_0(\mathbb{R})} + \max_{x\in[0,\,1/L]} |e_{\mathrm{t},k}(x)| \\ &\le \big(E_{\mathrm{r}}(\varphi, M, L) + E_{\mathrm{t}}(\varphi, m, L)\big)\,\|f\|_{L_2(\mathbb{R})}.\end{aligned}$$

This completes the proof. ∎

Note that it is especially beneficial for the estimation of the error constant (4.67), if the Fourier transform (4.59) of $\varphi \in \Phi$ is explicitly known.

Corollary 4.26. *The error estimate of Theorem 4.25 can be simplified, if the window function $\varphi \in \Phi$ vanishes on $\mathbb{R} \setminus \left[-\frac{m}{L}, \frac{m}{L}\right]$. Then the truncation errors $e_{\mathrm{t},k}(x)$ are equal to zero for all $x \in \left(0, \frac{1}{L}\right)$ and $k \in \mathbb{Z}$, such that $E_{\mathrm{t}}(\varphi, m, L) = 0$. For such window functions $\varphi \in \Phi$ we obtain the simple error estimate*

$$\|f - R_{\varphi,m} f\|_{C_0(\mathbb{R})} \leq E_{\mathrm{r}}(\varphi, M, L)\, \|f\|_{L_2(\mathbb{R})}.$$

Remark 4.27. Note that Corollary 4.26 applies to the modified B–spline window function (4.61), the sinh-type window function (4.62), and the continuous Kaiser–Bessel window function (4.63). The only window function of Remark 4.22, where Corollary 4.26 does not hold, is the Gaussian window function (4.60), since φ_{Gauss} does not vanish. ◇

Remark 4.28. Additionally, note that although the *constant window function*

$$\varphi_{\mathrm{const}}(x) \coloneqq 1, \quad x \in \mathbb{R}, \tag{4.84}$$

does not meet the criteria of the set Φ, since it is neither in $L_1(\mathbb{R}) \cap C_0(\mathbb{R})$ nor does it have an explicit Fourier transform, one can still use Theorem 4.25 to obtain a suitable error estimate for this window function. Since no regularization is done for the constant window function (4.84), we obviously have $E_{\mathrm{r}}(\varphi, M, L) = 0$. Then Theorem 4.25 provides an estimate of the truncation error as

$$\|f - R_{\mathrm{const},m} f\|_{C_0(\mathbb{R})} \leq E_{\mathrm{t}}(\varphi, m, L)\, \|f\|_{L_2(\mathbb{R})} = \frac{\sqrt{2L}}{\pi} \sqrt{\frac{1}{m} + \frac{1}{m^2}}\, \|f\|_{L_2(\mathbb{R})},$$

which can be seen as a consequence of a result in [MXZ09]. In other words, only using localized sampling without further regularization is not sufficient to obtain fast convergence results for the Shannon sampling series (4.15). ◇

Now let us move on to the numerical robustness. As seen in Theorem 4.7, if the samples $f\left(\frac{\ell}{L}\right)$, $\ell \in \mathbb{Z}$, of a bandlimited function $f \in \mathcal{B}_{M/2}(\mathbb{R})$ are not known exactly, i. e., only erroneous samples $\tilde{f}_\ell \coloneqq f\left(\frac{\ell}{L}\right) + \varepsilon_\ell$ with $|\varepsilon_\ell| \leq \varepsilon$, $\ell \in \mathbb{Z}$, and $\varepsilon > 0$ are available, the corresponding Shannon sampling series (4.15) may differ appreciably from f. Here we denote the regularized Shannon sampling formula with erroneous samples $\tilde{f}_\ell$ by

$$(R_{\varphi,m} \tilde{f})(x) = \sum_{\ell \in \mathbb{Z}} \tilde{f}_\ell\, \mathrm{sinc}\big(L\pi \left(x - \tfrac{\ell}{L}\right)\big)\, \varphi_m\big(x - \tfrac{\ell}{L}\big), \quad x \in \mathbb{R}. \tag{4.85}$$

Then, in contrast to the Shannon sampling series (4.15), the regularized Shannon sampling formula with localized sampling (4.74) is numerically robust, i. e., the *uniform perturbation error*

$$\|R_{\varphi,m}\tilde{f} - R_{\varphi,m}f\|_{C_0(\mathbb{R})} \tag{4.86}$$

is small, as the following theorem shows, cf. [KPT22, Theorem 3.4].

Theorem 4.29. *Let $f \in \mathcal{B}_{M/2}(\mathbb{R})$ with $M \in \mathbb{N}$, $L = M(1+\lambda) \in \mathbb{N}$ with $\lambda \geq 0$ and $m \in \mathbb{N} \setminus \{1\}$ be given. Further let $\varphi \in \Phi$ with the truncated window function* (4.73) *as well as $\tilde{f}_\ell = f\big(\frac{\ell}{L}\big) + \varepsilon_\ell$, where $|\varepsilon_\ell| \leq \varepsilon$ for all $\ell \in \mathbb{Z}$, with $\varepsilon > 0$. Then the regularized Shannon sampling sum with localized sampling* (4.74) *satisfies*

$$\|R_{\varphi,m}\tilde{f} - R_{\varphi,m}f\|_{C_0(\mathbb{R})} \leq \varepsilon\,\big(2 + L\,\hat{\varphi}(0)\big), \tag{4.87}$$

$$\|f - R_{\varphi,m}\tilde{f}\|_{C_0(\mathbb{R})} \leq \|f - R_{\varphi,m}f\|_{C_0(\mathbb{R})} + \varepsilon\,\big(2 + L\,\hat{\varphi}(0)\big). \tag{4.88}$$

Proof. Initially, we only consider the interval $\big[0,\,\frac{1}{L}\big]$. By (4.74) and (4.85) we have

$$\begin{aligned}
\tilde{e}_0(x) &\coloneqq (R_{\varphi,m}\tilde{f})(x) - (R_{\varphi,m}f)(x) \\
&= \sum_{\ell\in\mathbb{Z}} \Big(\tilde{f}_\ell - f\big(\tfrac{\ell}{L}\big)\Big)\,\operatorname{sinc}\big(L\pi\,\big(x - \tfrac{\ell}{L}\big)\big)\,\varphi_m\big(x - \tfrac{\ell}{L}\big) \\
&= \sum_{\ell\in\mathcal{J}_m} \varepsilon_\ell\,\operatorname{sinc}\big(L\pi\,\big(x - \tfrac{\ell}{L}\big)\big)\,\varphi_m\big(x - \tfrac{\ell}{L}\big), \quad x \in \big(0,\,\tfrac{1}{L}\big).
\end{aligned}$$

Using the non-negativity of φ and $|\varepsilon_\ell| \leq \varepsilon$, we receive

$$|\tilde{e}_0(x)| \leq \sum_{\ell\in\mathcal{J}_m} |\varepsilon_\ell|\,\big|\operatorname{sinc}\big(L\pi\,\big(x - \tfrac{\ell}{L}\big)\big)\big|\,\varphi\big(x - \tfrac{\ell}{L}\big) \leq \varepsilon \sum_{\ell\in\mathcal{J}_m} \varphi\big(x - \tfrac{\ell}{L}\big).$$

Since $\varphi|_{[0,\,\infty)}$ is monotonously non-increasing by assumption $\varphi \in \Phi$, we can estimate the sum for $x \in \big(0,\,\frac{1}{L}\big)$ by

$$\begin{aligned}
\sum_{\ell\in\mathcal{J}_m} \varphi\big(x - \tfrac{\ell}{L}\big) &= \left(\sum_{\ell=-m+1}^{0} + \sum_{\ell=1}^{m}\right) \varphi\big(x - \tfrac{\ell}{L}\big) \\
&= \sum_{\ell=0}^{m-1} \varphi\big(x + \tfrac{\ell}{L}\big) + \sum_{\ell=1}^{m} \varphi\big(x - \tfrac{\ell}{L}\big)
\end{aligned}$$

$$\leq \sum_{\ell=0}^{m-1} \varphi\big(\tfrac{\ell}{L}\big) + \sum_{\ell=1}^{m} \varphi\big(\tfrac{1}{L} - \tfrac{\ell}{L}\big) = 2 \sum_{\ell=0}^{m-1} \varphi\big(\tfrac{\ell}{L}\big).$$

Using the integral test for convergence of series (4.26), we obtain that

$$\sum_{\ell=0}^{m-1} \varphi\big(\tfrac{\ell}{L}\big) < \varphi(0) + \int_0^{m-1} \varphi\big(\tfrac{t}{L}\big)\,\mathrm{d}t = \varphi(0) + L \int_0^{(m-1)/L} \varphi(t)\,\mathrm{d}t.$$

By the definition of the Fourier transform (4.1) we have for $\varphi \in \Phi$ that

$$\begin{aligned}\hat{\varphi}(0) = \int_{\mathbb{R}} \varphi(t)\,\mathrm{d}t &\geq \int_{-m/L}^{m/L} \varphi(t)\,\mathrm{d}t = 2 \int_0^{m/L} \varphi(t)\,\mathrm{d}t \\ &\geq 2 \int_0^{(m-1)/L} \varphi(t)\,\mathrm{d}t,\end{aligned}$$

and therefore

$$\begin{aligned}|\tilde{e}_0(x)| &\leq 2\,\varepsilon \sum_{\ell=0}^{m-1} \varphi\big(\tfrac{\ell}{L}\big) \leq 2\,\varepsilon\big(\varphi(0) + \tfrac{L}{2}\,\hat{\varphi}(0)\big) \\ &= \varepsilon\big(2\,\varphi(0) + L\,\hat{\varphi}(0)\big), \quad x \in \big(0,\, \tfrac{1}{L}\big).\end{aligned}$$

Additionally, by the interpolation property (4.75) we have $|\tilde{e}_0(0)| = |\varepsilon_0| \leq \varepsilon$ as well as $\big|\tilde{e}_0\big(\frac{1}{L}\big)\big| = |\varepsilon_1| \leq \varepsilon$. Since by $\varphi \in \Phi$ we have $\varphi(0) = 1$, we therefore obtain

$$\max_{x \in [0,1/L]} |\tilde{e}_0(x)| \leq \varepsilon\big(2 + L\,\hat{\varphi}(0)\big).$$

By the same technique, this error estimate can be shown for each interval $\big[\frac{k}{L}, \frac{k+1}{L}\big]$ with $k \in \mathbb{Z}$. On any open interval $\big(\frac{k}{L}, \frac{k+1}{L}\big)$ with $k \in \mathbb{Z}$, we use (4.77) to denote the error in the form

$$\begin{aligned}\tilde{e}_k(x) &\coloneqq (R_{\varphi,m}\tilde{f})\big(x + \tfrac{k}{L}\big) - (R_{\varphi,m} f)\big(x + \tfrac{k}{L}\big) \\ &= \sum_{\ell \in \mathcal{J}_m} \varepsilon_{\ell+k}\,\psi\big(x - \tfrac{\ell}{L}\big), \quad x \in \big(0,\, \tfrac{1}{L}\big).\end{aligned}$$

As shown above, we have

$$|\tilde{e}_k(x)| \leq \varepsilon\big(2\,\varphi(0) + L\,\hat{\varphi}(0)\big), \quad x \in \big(0,\, \tfrac{1}{L}\big),$$

and

$$\big|\tilde{e}_0\big(\tfrac{k}{L}\big)\big| = |\varepsilon_k| \leq \varepsilon, \quad \big|\tilde{e}_0\big(\tfrac{k+1}{L}\big)\big| = |\varepsilon_{k+1}| \leq \varepsilon$$

for each $k \in \mathbb{Z}$ by the interpolation property (4.75). Hence, we obtain

$$\max_{x \in [k/L,\,(k+1)/L]} |(R_{\varphi,m}\tilde{f})(x) - (R_{\varphi,m}f)(x)| \leq \varepsilon\big(2 + L\,\hat{\varphi}(0)\big).$$

Finally, the triangle inequality implies (4.88), which completes the proof. ■

In the remainder of this section we specify the results of Theorems 4.25 and 4.29 for the window functions in Remark 4.22. For this purpose, it merely remains to estimate the regularization error constant (4.67), the truncation error constant (4.80) as well as $\hat{\varphi}(0)$ for the different window functions $\varphi \in \Phi$, which shall be done in the subsequent subsections.

Remark 4.30. We remark that these results for the regularized Shannon sampling formulas with compactly supported window functions have recently been extended to a more general version of the Fourier transform (4.1). More precisely, in [FTV23] the authors focus on regularized Shannon sampling formulas related to the *special affine Fourier transform (SAFT)*

$$\mathscr{F}_A f(v) \coloneqq \int_{\mathbb{R}} f(x)\,\phi_A(x,v)\,\mathrm{d}x, \quad v \in \mathbb{R},$$

where

$$\phi_A(x,v) \coloneqq \frac{1}{\sqrt{2\pi|b|}} \exp\left(\frac{\mathrm{i}}{2b}\left(ax^2 + 2px - 2vx + dv^2 + 2(bq - dp)v\right)\right)$$

denotes a kernel depending on a vector $A = (a,b,c,d,p,q)^\top \in \mathbb{R}^6$ which satisfies the conditions $ad - cb = 1$ and $b \neq 0$. Note that for $A = (0,1,-1,0,0,0)^\top$ this transform reduces to the classical Fourier transform (4.1) and in this case the results of [FTV23] coincide with the ones in this section. ◇

Gaussian window function

Firstly, we consider the Gaussian window function (4.60) with some $\alpha > 0$ and the corresponding *Gaussian regularized sinc function*, cf. (4.69), given by

$$\psi_{\mathrm{Gauss}}(x) \coloneqq \mathrm{sinc}(L\pi x)\,\mathrm{e}^{-x^2/(2\alpha^2)}, \quad x \in \mathbb{R}. \tag{4.89}$$

Lemma 4.31. *Let $L \in \mathbb{N}$ and $\alpha > 0$ be given. Then the Fourier transform of the Gaussian regularized sinc function* (4.89) *reads as*

$$\begin{aligned}\hat{\psi}_{\mathrm{Gauss}}(v) &= \frac{1}{L\sqrt{\pi}} \int_{\sqrt{2}\pi\alpha(v-L/2)}^{\sqrt{2}\pi\alpha(v+L/2)} \mathrm{e}^{-x^2}\,\mathrm{d}x \qquad (4.90)\\ &= \frac{1}{2L}\Big[\operatorname{erf}\big(\sqrt{2}\pi\alpha\,(v+\tfrac{L}{2})\big) - \operatorname{erf}\big(\sqrt{2}\pi\alpha\,(v-\tfrac{L}{2})\big)\Big],\end{aligned}$$

with the error function *defined by*

$$\operatorname{erf}(x) \coloneqq \frac{2}{\sqrt{\pi}} \int_0^x \mathrm{e}^{-x^2}\,\mathrm{d}x < 1, \quad x \in \mathbb{R}.$$

The function $\hat{\psi}_{\mathrm{Gauss}}$ in (4.90) *is even, positive, belongs to $C^\infty(\mathbb{R})$, and is monotonously decreasing on $[0, \infty)$ with*

$$\max_{v\in\mathbb{R}} \hat{\psi}_{\mathrm{Gauss}}(v) = \hat{\psi}_{\mathrm{Gauss}}(0) = \frac{1}{L}\operatorname{erf}\big(\sqrt{2}\pi\alpha\,\tfrac{L}{2}\big) < \frac{1}{L}.$$

Proof. To compute the Fourier transform of (4.89) we apply the convolution property (4.66) using $f(x) = \operatorname{sinc}(L\pi x)$ and $g(x) = \mathrm{e}^{-x^2/(2\alpha^2)}$. These functions possess the Fourier transforms

$$\begin{aligned}\hat{f}(v) &= \tfrac{1}{L}\,\chi_{[-\frac{L}{2},\,\frac{L}{2}]}(v), \quad v \in \mathbb{R},\\ \hat{g}(v) &= \sqrt{2\pi}\,\alpha\,\mathrm{e}^{-2\pi^2\alpha^2 v^2}, \quad v \in \mathbb{R}, \qquad (4.91)\end{aligned}$$

see e. g. [PPST23]. Thus, we obtain

$$\begin{aligned}\hat{\psi}_{\mathrm{Gauss}}(v) &= \widehat{(f\,g)}(v) = (\hat{f} * \hat{g})(v) = \int_{\mathbb{R}} \hat{f}(v-u)\,\hat{g}(u)\,\mathrm{d}u\\ &= \frac{1}{L}\int_{v-L/2}^{v+L/2} \hat{g}(u)\,\mathrm{d}u = \frac{\sqrt{2\pi}\,\alpha}{L}\int_{v-L/2}^{v+L/2} \mathrm{e}^{-2\pi^2\alpha^2u^2}\,\mathrm{d}u\end{aligned}$$

and by substituting $x = \sqrt{2}\pi\alpha u$ we have the assertion (4.90). It is easy to see by (4.90) that $\hat{\psi}_{\mathrm{Gauss}}$ is even, positive on $\mathbb{R}$, and belongs to $C^\infty(\mathbb{R})$. Moreover, since (4.90) is an integral of fixed length over a positive, monotonously decreasing function, and $v \to \infty$ shifts the integral bounds towards infinity, which makes the integral smaller, the function (4.90) is monotonously decreasing on $[0, \infty)$ and attains its maximum at $v = 0$. ∎

A visualization of the Gaussian regularized sinc function (4.89) and its Fourier transform (4.90) can be found in Figure 4.4. Note that in comparison to Section 4.3.1 the function $\hat{\psi}_{\mathrm{Gauss}}$ is not of the form (4.34). In addition, the Gaussian regularized sinc function ψ_{Gauss} is not bandlimited on any interval. However, the following lemma shows that this function (4.89) is *essentially bandlimited* on the interval $\left[-\frac{L}{2}(1+\varepsilon), \frac{L}{2}(1+\varepsilon)\right]$ with certain $\varepsilon > 0$, such that $\hat{\psi}_{\mathrm{Gauss}}$ is negligible for $|v| > \frac{L}{2}(1+\varepsilon)$.

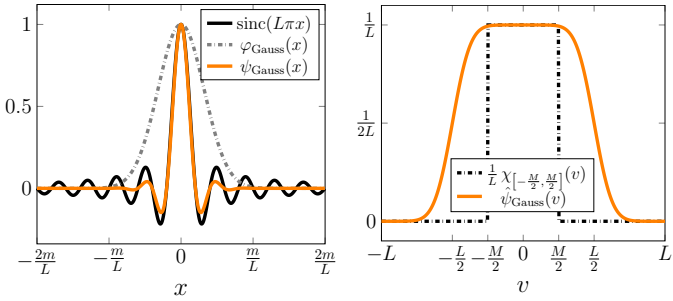

(a) ψ_{Gauss} in (4.89) (b) $\hat{\psi}_{\mathrm{Gauss}}$ in (4.90)

Figure 4.4: The Gaussian regularized sinc function ψ_{Gauss} as well as its Fourier transform $\hat{\psi}_{\mathrm{Gauss}}$ with $m = 5$ and $\alpha = \frac{1}{L}\sqrt{\frac{10}{\pi}}$.

Lemma 4.32. *The Gaussian regularized sinc function ψ_{Gauss} in (4.89) is essentially bandlimited on the interval $\left[-\frac{L}{2}(1+\varepsilon), \frac{L}{2}(1+\varepsilon)\right]$ with certain $\varepsilon \in (0, 1)$, i. e., for all $v \in \mathbb{R} \setminus \left[-\frac{L}{2}(1+\varepsilon), \frac{L}{2}(1+\varepsilon)\right]$ we have*

$$0 < \hat{\psi}_{\mathrm{Gauss}}(v) \leq \frac{1}{\sqrt{2\pi}\, L^2 \pi \alpha \varepsilon} \mathrm{e}^{-\pi^2 \alpha^2 L^2 \varepsilon^2/2}.$$

Proof. Since (4.90) is an integral over a positive function, we can estimate the Fourier transform of ψ_{Gauss} for $v \in \mathbb{R} \setminus \left[-\frac{L}{2}(1+\varepsilon), \frac{L}{2}(1+\varepsilon)\right]$ as

$$\begin{aligned} 0 < \hat{\psi}_{\mathrm{Gauss}}(v) &= \frac{1}{L\sqrt{\pi}} \int_{\sqrt{2}\pi\alpha(v-L/2)}^{\sqrt{2}\pi\alpha(v+L/2)} \mathrm{e}^{-x^2}\, \mathrm{d}x \\ &\leq \frac{1}{L\sqrt{\pi}} \int_{\sqrt{2}\pi\alpha(|v|-L/2)}^{\infty} \mathrm{e}^{-x^2}\, \mathrm{d}x. \end{aligned}$$

By [AS72, p. 298, Formula 7.1.13] we have the inequality

$$\frac{1}{t+\sqrt{t^2+2}}\,\mathrm{e}^{-t^2} \le \int_t^\infty \mathrm{e}^{-x^2}\,\mathrm{d}x \le \frac{1}{t+\sqrt{t^2+4/\pi}}\,\mathrm{e}^{-t^2}, \quad t \ge 0,$$

which can be simplified to

$$\frac{1}{(t+2)^2}\,\mathrm{e}^{-t^2} \le \int_t^\infty \mathrm{e}^{-x^2}\,\mathrm{d}x \le \frac{1}{2t}\,\mathrm{e}^{-t^2}, \quad t > 0. \tag{4.92}$$

Thereby, for $v \in \mathbb{R} \setminus \left[-\frac{L}{2}\,(1+\varepsilon),\ \frac{L}{2}\,(1+\varepsilon)\right]$ it follows by $|v| - \frac{L}{2} > \frac{L}{2}\,\varepsilon$ that

$$\begin{aligned} 0 < \hat{\psi}_{\mathrm{Gauss}}(v) &\le \frac{1}{2\sqrt{2\pi}\,L\pi\alpha\,(|v|-L/2)}\,\mathrm{e}^{-2\pi^2\alpha^2\,(|v|-L/2)^2} \\ &\le \frac{1}{\sqrt{2\pi}\,L^2\pi\alpha\varepsilon}\,\mathrm{e}^{-\pi^2\alpha^2L^2\varepsilon^2/2}. \end{aligned}$$

Thus, for fixed $\alpha > 0$ and convenient $\varepsilon > 0$, the Fourier transform $\hat{\psi}_{\mathrm{Gauss}}$ is negligible for $|v| > \frac{L}{2}\,(1+\varepsilon)$. ∎

Now we show that for the regularization with the Gaussian window function (4.60) the uniform approximation error (4.78) decays exponentially with respect to m, cf. [KPT22, Theorem 4.1].

Theorem 4.33. *Let $f \in \mathcal{B}_{M/2}(\mathbb{R})$ with $M \in \mathbb{N}$, $L = M(1+\lambda) \in \mathbb{N}$ with $\lambda > 0$, and $m \in \mathbb{N} \setminus \{1\}$ be given. Then the regularized Shannon sampling formula with localized sampling* (4.74) *using the Gaussian window function* (4.60) *and $\alpha = \frac{1}{M}\sqrt{\frac{m}{\pi(1+\lambda)\lambda}}$ satisfies the error estimate*

$$\|f - R_{\mathrm{Gauss},m} f\|_{C_0(\mathbb{R})} \le \frac{\sqrt{2Lm} + \sqrt{2L\lambda(1+m)}}{\pi m\sqrt{\lambda}}\,\mathrm{e}^{-m\pi\lambda/(2+2\lambda)}\,\|f\|_{L_2(\mathbb{R})}.$$

Proof (cf. [Qia03] and [LZ17]). By Theorem 4.25 we only need to compute the error constants (4.67) and (4.80) for the Gaussian window function (4.60). Firstly, we study the regularization error constant (4.67). By (4.91) we recognize that the auxiliary function (4.72) is given by

$$\eta_{\mathrm{Gauss}}(v) = \chi_{[-\frac{M}{2},\,\frac{M}{2}]}(v) - \frac{1}{\sqrt{\pi}} \int_{\sqrt{2}\pi\alpha(v-L/2)}^{\sqrt{2}\pi\alpha(v+L/2)} \mathrm{e}^{-x^2}\,\mathrm{d}x, \quad v \in \mathbb{R}.$$

Note that by Lemma 4.31 we have

$$\eta_{\mathrm{Gauss}}(v) = 1 - L\,\hat{\psi}_{\mathrm{Gauss}}(v) \in [0,\,1], \quad v \in \left[-\tfrac{M}{2},\,\tfrac{M}{2}\right]. \tag{4.93}$$

Since $\int_{\mathbb{R}} \mathrm{e}^{-x^2}\,\mathrm{d}x = \sqrt{\pi}$ holds, this function η_{Gauss} can be evaluated for $v \in \left[-\frac{M}{2},\,\frac{M}{2}\right]$ as

$$\begin{aligned}
\eta_{\mathrm{Gauss}}(v) &= \frac{1}{\sqrt{\pi}}\left[\int_{\mathbb{R}} \mathrm{e}^{-x^2}\,\mathrm{d}x - \int_{\sqrt{2}\pi\alpha(v-L/2)}^{\sqrt{2}\pi\alpha(v+L/2)} \mathrm{e}^{-x^2}\,\mathrm{d}x\right] \\
&= \frac{1}{\sqrt{\pi}}\left[\int_{-\infty}^{\sqrt{2}\pi\alpha(v-L/2)} \mathrm{e}^{-x^2}\,\mathrm{d}x + \int_{\sqrt{2}\pi\alpha(v+L/2)}^{\infty} \mathrm{e}^{-x^2}\,\mathrm{d}x\right] \\
&= \frac{1}{\sqrt{\pi}}\left[\int_{\sqrt{2}\pi\alpha(L/2-v)}^{\infty} \mathrm{e}^{-x^2}\,\mathrm{d}x + \int_{\sqrt{2}\pi\alpha(v+L/2)}^{\infty} \mathrm{e}^{-x^2}\,\mathrm{d}x\right].
\end{aligned}$$

Using (4.92) we obtain the estimate

$$\eta_{\mathrm{Gauss}}(v) < \frac{1}{\sqrt{\pi}}\left(\frac{\mathrm{e}^{-2\pi^2\alpha^2(\frac{L}{2}-v)^2}}{2\sqrt{2}\pi\alpha(\frac{L}{2}-v)} + \frac{\mathrm{e}^{-2\pi^2\alpha^2(\frac{L}{2}+v)^2}}{2\sqrt{2}\pi\alpha(\frac{L}{2}+v)}\right), \quad v \in \left[-\tfrac{M}{2},\,\tfrac{M}{2}\right].$$

Since $\frac{L}{2}-v,\,\frac{L}{2}+v \in \left[\frac{L-M}{2},\,\frac{L+M}{2}\right]$ by $v \in \left[-\frac{M}{2},\,\frac{M}{2}\right]$, and the function $\frac{1}{x}\,\mathrm{e}^{-x^2/4}$ decreases for $x > 0$, we conclude that

$$\eta_{\mathrm{Gauss}}(v) < \frac{2\,\mathrm{e}^{-\pi^2\alpha^2(L-M)^2/2}}{\sqrt{2\pi}\,\pi\alpha(L-M)}, \quad v \in \left[-\tfrac{M}{2},\,\tfrac{M}{2}\right].$$

Hence, by (4.67) and (4.72) we receive

$$E_{\mathrm{r}}(\varphi_{\mathrm{Gauss}}, M, L) \le \frac{\sqrt{2M}}{\sqrt{\pi}\,\pi\alpha(L-M)}\,\mathrm{e}^{-\pi^2\alpha^2(L-M)^2/2}. \tag{4.94}$$

Now we examine the truncation error constant (4.80). For the Gaussian window function (4.60) we have

$$\begin{aligned}
&\frac{1}{m^2}\,\varphi_{\mathrm{Gauss}}^2\left(\tfrac{m}{L}\right) + \frac{1}{L}\int_{m/L}^{\infty} \frac{\varphi_{\mathrm{Gauss}}^2(t)}{t^2}\,\mathrm{d}t \\
&\qquad = \frac{1}{m^2}\,\mathrm{e}^{-m^2/(\alpha^2L^2)} + \frac{1}{\alpha L}\int_{m/(\alpha L)}^{\infty} \frac{\mathrm{e}^{-t^2}}{t^2}\,\mathrm{d}t.
\end{aligned}$$

By substituting $z = 1/t$, performing partial integration, and further substituting $y = 1/z$, we obtain

$$\begin{aligned}\int_{m/(\alpha L)}^{\infty} \frac{\mathrm{e}^{-t^2}}{t^2}\,\mathrm{d}t &= \int_0^{\alpha L/m} \mathrm{e}^{-1/z^2}\,\mathrm{d}z \\ &= \frac{\alpha L}{m}\,\mathrm{e}^{-m^2/(\alpha^2 L^2)} - 2\int_0^{\alpha L/m} \frac{\mathrm{e}^{-1/z^2}}{z^2}\,\mathrm{d}z \\ &= \frac{\alpha L}{m}\,\mathrm{e}^{-m^2/(\alpha^2 L^2)} - 2\int_{m/(\alpha L)}^{\infty} \mathrm{e}^{-y^2}\,\mathrm{d}y.\end{aligned}$$

Moreover, from (4.92) it follows

$$2\int_{m/(\alpha L)}^{\infty} \mathrm{e}^{-y^2}\,\mathrm{d}y \geq \frac{2\alpha^2 L^2}{\big(m + 2\alpha L\big)^2}\,\mathrm{e}^{-m^2/(\alpha^2 L^2)} > 0.$$

Thus, by (4.80) we obtain

$$E_{\mathrm{t}}(\varphi_{\mathrm{Gauss}}, m, L) \leq \frac{\sqrt{2L}}{\pi}\sqrt{\frac{1}{m^2} + \frac{1}{m}}\,\mathrm{e}^{-m^2/(2\alpha^2 L^2)}. \tag{4.95}$$

For the special parameter $\alpha = \sqrt{\frac{m}{\pi L\,(L-M)}} = \frac{1}{M}\sqrt{\frac{m}{\pi(1+\lambda)\lambda}}$, both error terms (4.94) and (4.95) have the same exponential decay such that

$$\begin{aligned}E_{\mathrm{r}}(\varphi_{\mathrm{Gauss}}, M, L) &\leq \frac{1}{\pi}\sqrt{\frac{2L}{m\lambda}}\,\mathrm{e}^{-m\pi\lambda/(2+2\lambda)}, \\ E_{\mathrm{t}}(\varphi_{\mathrm{Gauss}}, m, L) &\leq \frac{\sqrt{2L}}{\pi}\sqrt{\frac{1}{m^2} + \frac{1}{m}}\,\mathrm{e}^{-m\pi\lambda/(2+2\lambda)}.\end{aligned}$$

This completes the proof. ∎

Remark 4.34. Note that Theorem 4.33 enhances the corresponding results in [Qia03] and [LZ17] by improving the exponential decay rate from $(m-1)$ to m. In addition, the constant factor is slightly improved in comparison to [KPT22].

Furthermore, we remark that in [CZ19] a different parameter α is presented as the optimal one for the Gaussian window function (4.60), where, however, a slightly different truncation than in (4.74) was considered. Moreover, the rather artificial analysis in [CZ19] estimates the error only up to an

unknown constant and seems less intuitive than our result in Theorem 4.33. Nevertheless, both results, Theorem 4.33 and [CZ19, Theorem 1.1], possess the same asymptotic behavior. ◇

Remark 4.35. In [QO05, Theorem 2.3], the modified Gaussian window function

$$\varphi_{\text{modGauss}}(x) \coloneqq \mathrm{e}^{-x^2/(2\alpha^2)} \cos(\lambda x)\,, \quad x \in \mathbb{R}\,,$$

was used for the regularized Shannon sampling formulas (4.74), which could be seen as a combination of a regularization in the frequency domain, cf. (4.51), and a regularization in the spatial domain, cf. (4.60). However, by the same techniques as in Theorem 4.33 it can be shown that the approximation error of the regularized Shannon sampling formula with the modified Gaussian function $\varphi_{\text{modGauss}}$ has the best exponential decay in the case $\lambda = 0$, i. e., when using the original Gaussian window function (4.60). ◇

Now we show that for the regularization with the Gaussian window function (4.60) the uniform perturbation error (4.86) only grows as $\mathcal{O}(\sqrt{m})$, cf. [KPT22, Theorem 4.3]. We remark that a similar result can also be found in [QC06a].

Theorem 4.36. *Let $f \in \mathcal{B}_{M/2}(\mathbb{R})$ with $M \in \mathbb{N}$, $L = M(1+\lambda) \in \mathbb{N}$ with $\lambda > 0$ and $m \in \mathbb{N} \setminus \{1\}$ be given. Further let $R_{\text{Gauss},m}\tilde{f}$ be as in (4.85) with the noisy samples $\tilde{f}_\ell = f\big(\frac{\ell}{L}\big) + \varepsilon_\ell$, where $|\varepsilon_\ell| \leq \varepsilon$ for all $\ell \in \mathbb{Z}$ and $0 < \varepsilon \ll 1$. Then the regularized Shannon sampling formula with localized sampling (4.74) using the Gaussian window function (4.60) and $\alpha = \frac{1}{M}\sqrt{\frac{m}{\pi(1+\lambda)\lambda}}$ satisfies*

$$\|R_{\text{Gauss},m}\tilde{f} - R_{\text{Gauss},m} f\|_{C_0(\mathbb{R})} \leq \varepsilon \left(2 + \sqrt{\frac{2+2\lambda}{\lambda}}\,\sqrt{m}\right).$$

Proof. By Theorem 4.29 we only need to compute $\hat{\varphi}_{\text{Gauss}}(0)$ for the Gaussian window function (4.60). By (4.91) we recognize that

$$\hat{\varphi}_{\text{Gauss}}(0) = \sqrt{2\pi}\,\alpha = \frac{1}{L}\sqrt{\frac{2+2\lambda}{\lambda}}\,\sqrt{m},$$

such that (4.87) yields the assertion. ■

We remark that the triangle inequality combined with Theorems 4.33 and 4.36 also implies an estimate on the perturbation error $\|f - R_{\mathrm{Gauss},m}\tilde{f}\|_{C_0(\mathbb{R})}$, cf. (4.88).

B–spline window function

Secondly, we consider the modified B–spline window function (4.61). Note that (4.61) is supported on $\left[-\frac{m}{L}, \frac{m}{L}\right]$. According to (4.69) we form the B–*spline regularized sinc function*

$$\psi_{\mathrm{B}}(x) \coloneqq \operatorname{sinc}(L\pi x)\,\varphi_{\mathrm{B}}(x), \quad x \in \mathbb{R}. \tag{4.96}$$

Lemma 4.37. *Let $L \in \mathbb{N}$ and $s, m \in \mathbb{N} \setminus \{1\}$ be given. Then the Fourier transform of the* B*–spline regularized sinc function* (4.96) *reads as*

$$\hat{\psi}_{\mathrm{B}}(v) = \frac{m}{sL^2\,B_{2s}(0)} \int_{v-L/2}^{v+L/2} \left(\operatorname{sinc}\left(\frac{\pi u m}{sL}\right)\right)^{2s} \mathrm{d}u. \tag{4.97}$$

The function (4.97) *is even, positive, and belongs to $C^\infty(\mathbb{R})$, where*

$$\max_{v\in\mathbb{R}} \hat{\psi}_{\mathrm{B}}(v) = \hat{\psi}_{\mathrm{B}}(0) < \frac{1}{L}.$$

Proof. To compute the Fourier transform of (4.96) we apply the convolution property (4.66) using $f(x) = \operatorname{sinc}(L\pi x)$ and $g(x) = \varphi_{\mathrm{B}}(x)$. These functions possess the Fourier transforms

$$\begin{aligned} \hat{f}(v) &= \tfrac{1}{L}\,\chi_{\left[-\frac{L}{2},\frac{L}{2}\right]}(v), \\ \hat{g}(v) &= \frac{m}{sL\,B_{2s}(0)} \left(\operatorname{sinc}\left(\frac{\pi v m}{sL}\right)\right)^{2s}, \quad v \in \mathbb{R}, \end{aligned} \tag{4.98}$$

see [PT21b, PPST23]. Thus, we obtain

$$\begin{aligned} \hat{\psi}_{\mathrm{B}}(v) = \widehat{(f\,g)}(v) = (\hat{f} * \hat{g})(v) &= \int_{\mathbb{R}} \hat{f}(v-u)\,\hat{g}(u)\,\mathrm{d}u \\ &= \frac{1}{L}\int_{v-L/2}^{v+L/2} \hat{g}(u)\,\mathrm{d}u = \frac{m}{sL^2\,B_{2s}(0)} \int_{v-L/2}^{v+L/2} \left(\operatorname{sinc}\left(\frac{\pi u m}{sL}\right)\right)^{2s} \mathrm{d}u \end{aligned}$$

and thereby the assertion (4.97). It is easy to see by (4.97) that $\hat{\psi}_{\mathrm{B}}$ is even, positive, and belongs to $C^\infty(\mathbb{R})$. Moreover, since (4.97) is an integral of

fixed length over a positive function decaying as u^{-2s}, and $v \to \infty$ shifts the integral bounds towards infinity, its maximum is attained at $v = 0$. By inverse Fourier transform we have

$$1 = \varphi_{\mathrm{B}}(0) = \int_{\mathbb{R}} \hat{\varphi}_{\mathrm{B}}(v)\,\mathrm{d}v = \frac{m}{sL\,B_{2s}(0)} \int_{\mathbb{R}} \left(\operatorname{sinc}\left(\frac{\pi v m}{sL}\right)\right)^{2s} \mathrm{d}v,$$

such that

$$\int_{\mathbb{R}} \left(\operatorname{sinc}\left(\frac{\pi v m}{sL}\right)\right)^{2s} \mathrm{d}v = \frac{sL}{m}\, B_{2s}(0). \tag{4.99}$$

Then from (4.97) and (4.99) it follows that

$$\hat{\psi}_{\mathrm{B}}(0) = \frac{m}{sL^2\,B_{2s}(0)} \int_{-L/2}^{L/2} \left(\operatorname{sinc}\left(\frac{\pi u m}{sL}\right)\right)^{2s} \mathrm{d}u < \frac{1}{L}.$$

This completes the proof. ∎

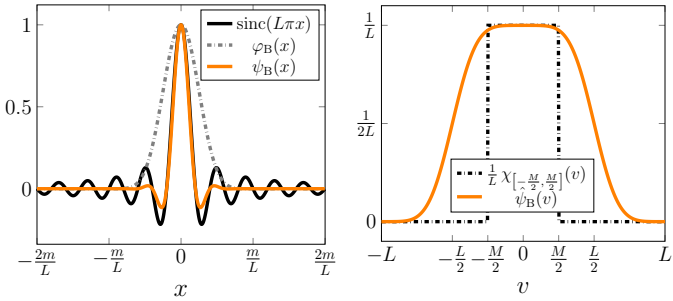

(a) ψ_{B} in (4.96) (b) $\hat{\psi}_{\mathrm{B}}$ in (4.97)

Figure 4.5: The B–spline regularized sinc function ψ_{B} as well as its Fourier transform $\hat{\psi}_{\mathrm{B}}$ with $m = 5$ and $s = 3$.

A visualization of the B–spline regularized sinc function (4.96) and its Fourier transform (4.97) can be found in Figure 4.5. Note that in comparison to Section 4.3.1 the function $\hat{\psi}_{\mathrm{B}}$ is not of the form (4.34). In addition, the B–spline regularized sinc function ψ_{B} is not bandlimited on any interval. However, the following lemma shows that this function (4.96) is essentially bandlimited on the interval $\left[-\frac{L}{2}(1+\varepsilon),\ \frac{L}{2}(1+\varepsilon)\right]$ with certain $\varepsilon > 0$, such that $\hat{\psi}_{\mathrm{B}}$ is negligible for $|v| > \frac{L}{2}(1+\varepsilon)$.

Lemma 4.38. *The* B*–spline regularized sinc function* ψ_{B} *in* (4.96) *is essentially bandlimited on the interval* $\left[-\frac{L}{2}(1+\varepsilon),\ \frac{L}{2}(1+\varepsilon)\right]$ *with* $\varepsilon > \frac{2s}{m\pi}$*, i. e., for all* $v \in \mathbb{R} \setminus \left[-\frac{L}{2}(1+\varepsilon),\ \frac{L}{2}(1+\varepsilon)\right]$ *we have*

$$0 < \hat{\psi}_{\mathrm{B}}(v) < \frac{1}{L\pi\,(2s-1)\,B_{2s}(0)} \left(\frac{2s}{\varepsilon\pi m}\right)^{2s-1}.$$

Proof. Since (4.97) is an integral over a positive function, we can estimate the Fourier transform of ψ_{B} for $v \in \mathbb{R} \setminus \left[-\frac{L}{2}(1+\varepsilon),\ \frac{L}{2}(1+\varepsilon)\right]$ as

$$\begin{aligned} 0 < \hat{\psi}_{\mathrm{B}}(v) &\leq \frac{m}{sL^2\,B_{2s}(0)} \int_{|v|-L/2}^{\infty} \left(\operatorname{sinc}\left(\frac{\pi u m}{sL}\right)\right)^{2s} \mathrm{d}u \\ &\leq \frac{s^{2s-1}\,L^{2s-2}}{\pi^{2s}\,m^{2s-1}\,B_{2s}(0)} \int_{|v|-L/2}^{\infty} u^{-2s}\,\mathrm{d}u \\ &= \frac{s^{2s-1}\,L^{2s-2}}{\pi^{2s}\,m^{2s-1}\,B_{2s}(0)} \cdot \frac{1}{(2s-1)\left(|v|-\frac{L}{2}\right)^{2s-1}}. \end{aligned}$$

Then by $|v| - \frac{L}{2} > \frac{L}{2}\,\varepsilon$ the assertion follows. In other words, for $\frac{2s}{\varepsilon\pi m} < 1$, namely $\varepsilon > \frac{2s}{\pi m}$, the Fourier transform $\hat{\psi}_{\mathrm{B}}$ is negligible for $|v| > \frac{L}{2}(1+\varepsilon)$. ∎

In order to estimate the uniform approximation error (4.78) when using the modified B–spline window function (4.61), we require the following lemma, cf. [KPT22, Lemma 5.1].

Lemma 4.39. *The sequence* $\left(\sqrt{2s}\,B_{2s}(0)\right)_{s=2}^{\infty}$ *is monotonously increasing with*

$$\lim_{s\to\infty} \sqrt{2s}\,B_{2s}(0) = \sqrt{\frac{6}{\pi}} \approx 1.3820, \tag{4.100}$$

such that we have

$$\frac{4}{3} \leq \sqrt{2s}\,B_{2s}(0) < \sqrt{\frac{6}{\pi}}, \quad s \in \mathbb{N} \setminus \{1\}. \tag{4.101}$$

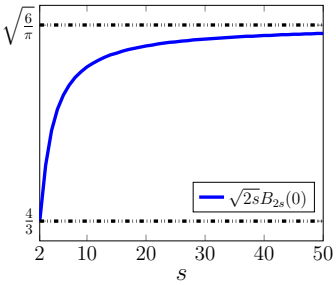

Figure 4.6: The sequence $\left(\sqrt{2s}\, B_{2s}(0)\right)_{s=2}^{50}$.

Proof. By (4.99) we have

$$\begin{aligned} B_{2s}(0) &= \frac{m}{sL} \int_{\mathbb{R}} \left(\operatorname{sinc}\left(\frac{\pi v m}{sL} \right) \right)^{2s} \mathrm{d}v \\ &= \frac{1}{\pi} \int_{\mathbb{R}} \left(\operatorname{sinc}(v) \right)^{2s} \mathrm{d}v = \frac{2}{\pi} \int_0^{\infty} \left(\operatorname{sinc}(v) \right)^{2s} \mathrm{d}v. \end{aligned}$$

The above integral can be determined in explicit form as

$$\int_0^{\infty} \left(\operatorname{sinc}(w) \right)^{2s} \mathrm{d}w = \frac{\pi}{2\,(2s-1)!} \sum_{j=0}^{s-1} (-1)^j \binom{2s}{j} (s-j)^{2s-1},$$

see [MR65], [Obe90, p. 20, 5.12] or [Chu92, (4.1.12)]. Especially, we have $B_2(0) = 1$, $B_4(0) = \frac{2}{3}$, $B_6(0) = \frac{11}{20}$, $B_8(0) = \frac{151}{315}$, $B_{10}(0) = \frac{15619}{36288}$, and $B_{12}(0) = \frac{655177}{1663200}$. A table including the decimal values of $B_{2s}(0)$ for $s = 15, \ldots, 50$, can be found in [MR65]. In Figure 4.6 we can see that the sequence $\left(\sqrt{2s}\, B_{2s}(0)\right)_{s=2}^{50}$ increases monotonously. For larger s we can use the asymptotic expansion

$$\sqrt{2s}\, B_{2s}(0) \approx \sqrt{\frac{6}{\pi}} \left[1 - \frac{3}{40\,s} - \frac{13}{4480\,s^2} + \frac{27}{25600\,s^3} + \frac{52791}{63078400\,s^4} + \frac{482427}{2129920000\,s^5} \right],$$

see [MR65], such that the whole sequence $\left(\sqrt{2s}\, B_{2s}(0)\right)_{s=2}^{\infty}$ increases monotonously. Moreover, by [UAE92, (3.6)] there exists the pointwise

limit

$$\lim_{s\to\infty} \sqrt{\frac{s}{6}}\, B_{2s}\left(\sqrt{\frac{s}{6}}\, x\right) = \frac{1}{\sqrt{2\pi}}\, \mathrm{e}^{-x^2/2},$$

such that for $x = 0$ we obtain (4.100) and hence we have (4.101). ■

Now we show that for the regularization with the modified B–spline window function (4.61) the uniform approximation error (4.78) decays exponentially with respect to m, cf. [KPT22, Theorem 5.3].

Theorem 4.40. *Let* $f \in \mathcal{B}_{M/2}(\mathbb{R})$ *with* $M \in \mathbb{N}$, $L = M\,(1+\lambda) \in \mathbb{N}$, *and* $m \in \mathbb{N} \setminus \{1\}$ *be given, where*

$$\lambda > \frac{m+2}{\pi m - (m+2)}. \tag{4.102}$$

Then the regularized Shannon sampling formula with localized sampling (4.74) *using the modified* B*–spline window function* (4.61) *and* $s = \left\lceil \frac{m+1}{2} \right\rceil$ *satisfies the error estimate*

$$\|f - R_{\mathrm{B},m} f\|_{C_0(\mathbb{R})} \le \frac{3\sqrt{sM}}{\sqrt{2}\,(2s-1)\,\pi}\, \mathrm{e}^{-m\,(\ln(\pi m\lambda) - \ln(2s(1+\lambda)))}\, \|f\|_{L_2(\mathbb{R})}.$$

Proof. By Corollary 4.26 we only need to estimate the regularization error constant (4.67), since we have $\operatorname{supp}(\varphi_{\mathrm{B}}) = \left[-\frac{m}{L}, \frac{m}{L}\right]$ and therefore the truncation error constant (4.80) vanishes for the modified B–spline window function (4.61).

By (4.98) we recognize that the auxiliary function (4.72) is given by

$$\eta_{\mathrm{B}}(v) = \chi_{\left[-\frac{M}{2}, \frac{M}{2}\right]}(v) - \frac{m}{sL\, B_{2s}(0)} \int_{v-L/2}^{v+L/2} \left(\operatorname{sinc}\left(\frac{\pi u m}{sL}\right)\right)^{2s} \mathrm{d}u, \quad v \in \mathbb{R}.$$

Note that by Lemma 4.37 we have

$$\eta_{\mathrm{B}}(v) = 1 - L\,\hat{\psi}_{\mathrm{B}}(v) \in [0,\, 1], \quad v \in \left[-\tfrac{M}{2}, \tfrac{M}{2}\right]. \tag{4.103}$$

Since (4.99) holds, this function η_{B} can be evaluated for $v \in \left[-\frac{M}{2}, \frac{M}{2}\right]$ as

$$\begin{aligned}\eta_{\mathrm{B}}(v) &= \frac{m}{sL\,B_{2s}(0)}\left(\int_{\mathbb{R}}\left(\operatorname{sinc}\left(\frac{\pi um}{sL}\right)\right)^{2s}\,\mathrm{d}u\right.\\ &\qquad\left.-\int_{v-L/2}^{v+L/2}\left(\operatorname{sinc}\left(\frac{\pi um}{sL}\right)\right)^{2s}\,\mathrm{d}u\right)\\ &= \frac{m}{sL\,B_{2s}(0)}\left(\int_{-\infty}^{v-L/2}\left(\operatorname{sinc}\left(\frac{\pi um}{sL}\right)\right)^{2s}\,\mathrm{d}u\right.\\ &\qquad\left.+\int_{v+L/2}^{\infty}\left(\operatorname{sinc}\left(\frac{\pi um}{sL}\right)\right)^{2s}\,\mathrm{d}u\right)\\ &= \frac{m}{sL\,B_{2s}(0)}\left(\int_{L/2-v}^{\infty}\left(\operatorname{sinc}\left(\frac{\pi um}{sL}\right)\right)^{2s}\,\mathrm{d}u\right.\\ &\qquad\left.+\int_{v+L/2}^{\infty}\left(\operatorname{sinc}\left(\frac{\pi um}{sL}\right)\right)^{2s}\,\mathrm{d}u\right).\end{aligned}$$

Applying the simple estimate

$$\begin{aligned}\int_{A}^{\infty}\left(\operatorname{sinc}\left(\frac{\pi um}{sL}\right)\right)^{2s}\,\mathrm{d}u &\le \frac{s^{2s}\,L^{2s}}{\pi^{2s}\,m^{2s}}\int_{A}^{\infty}u^{-2s}\,\mathrm{d}u\\ &= \frac{s^{2s}\,L^{2s}}{(2s-1)\,\pi^{2s}\,m^{2s}\,A^{2s-1}},\end{aligned}$$

for $A>0$, we obtain for $v\in\left[-\frac{M}{2},\,\frac{M}{2}\right]$ that

$$\eta_{\mathrm{B}}(v) \le \frac{s^{2s-1}\,L^{2s-1}}{(2s-1)\,\pi^{2s}\,m^{2s-1}\,B_{2s}(0)}\left(\frac{1}{\left(\frac{L}{2}-v\right)^{2s-1}}+\frac{1}{\left(\frac{L}{2}+v\right)^{2s-1}}\right).$$

Since $\frac{L}{2}-v,\ \frac{L}{2}+v\in\left[\frac{L-M}{2},\,\frac{L+M}{2}\right]$ by $v\in\left[-\frac{M}{2},\,\frac{M}{2}\right]$, and the function x^{1-2s} decreases for $x>0$, we conclude that

$$\eta_{\mathrm{B}}(v) \le \frac{2^{2s}\,s^{2s-1}\,L^{2s-1}}{(2s-1)\,\pi^{2s}\,m^{2s-1}\,B_{2s}(0)\,(L-M)^{2s-1}},\quad v\in\left[\tfrac{M}{2},\,\tfrac{M}{2}\right].$$

Hence, by (4.67), (4.72) and (4.101) we receive

$$E_{\mathrm{r}}(\varphi_{\mathrm{B}},M,L) \le \frac{2\sqrt{M}}{(2s-1)\,\pi\,B_{2s}(0)}\left(\frac{2sL}{\pi m(L-M)}\right)^{2s-1}$$

$$\leq \frac{3\sqrt{sM}}{\sqrt{2}\,(2s-1)\,\pi}\left(\frac{2sL}{\pi m(L-M)}\right)^{2s-1}. \tag{4.104}$$

For achieving convergence we need to satisfy

$$\frac{2sL}{\pi m(L-M)} = \frac{2s(1+\lambda)}{\pi m\lambda} =: c < 1.$$

By logarithmic laws we recognize that $c^{2s-1} = \mathrm{e}^{\ln(c^{2s-1})} = \mathrm{e}^{(2s-1)\,\ln c}$. Thus, the condition $c<1$ yields $\ln c < 0$ and therefore an exponential decay of (4.104) with respect to $(2s-1)$. To obtain an exponential decay rate of at least m, the condition $2s-1 \geq m$ can now be used to pick a suitable parameter $s \in \mathbb{N}$ in the form $s = \left\lceil \frac{m+1}{2} \right\rceil$. Then

$$\begin{aligned} c^{2s-1} &= \mathrm{e}^{(2s-1)\,\ln c} = \mathrm{e}^{(2s-1)\,(\ln(2s(1+\lambda))-\ln(\pi m\lambda))} \\ &= \mathrm{e}^{-(2s-1)\,(\ln(\pi m\lambda)-\ln(2s(1+\lambda)))} \leq \mathrm{e}^{-m\,(\ln(\pi m\lambda)-\ln(2s(1+\lambda)))} \end{aligned}$$

yields the assertion. In addition, the choice of $s = \left\lceil \frac{m+1}{2} \right\rceil$ implies $m+2 \geq 2s \geq m+1$, such that $c<1$ is ensured by $\pi m\lambda > (m+2)(1+\lambda)$, which can be rewritten as (4.102). ∎

Now we show that for the regularization with the modified B–spline window function (4.61) the uniform perturbation error (4.87) only grows as $\mathcal{O}(\sqrt{m})$, cf. [KPT22, Theorem 5.5].

Theorem 4.41. *Let $f \in \mathcal{B}_{M/2}(\mathbb{R})$ with $M \in \mathbb{N}$, $L = M(1+\lambda) \in \mathbb{N}$ with $\lambda \geq 0$ and $m \in \mathbb{N} \setminus \{1\}$ be given. Further let $R_{\mathrm{B},m}\tilde{f}$ be as in* (4.85) *with the noisy samples $\tilde{f}_\ell = f\left(\frac{\ell}{L}\right) + \varepsilon_\ell$, where $|\varepsilon_\ell| \leq \varepsilon$ for all $\ell \in \mathbb{Z}$ and $0 < \varepsilon \ll 1$. Then the regularized Shannon sampling formula with localized sampling* (4.74) *using the modified* B*–spline window function* (4.61) *and $s = \left\lceil \frac{m+1}{2} \right\rceil$ satisfies*

$$\|R_{\mathrm{B},m}\tilde{f} - R_{\mathrm{B},m}f\|_{C_0(\mathbb{R})} \leq \varepsilon\left(2 + \frac{3}{2}\sqrt{m}\right).$$

Proof. By Theorem 4.29 we only need to compute $\hat{\varphi}_{\mathrm{B}}(0)$ for the modified B–spline window function (4.61). By (4.98) and (4.101) we recognize that

$$\hat{\varphi}_{\mathrm{B}}(0) = \frac{m}{sL\,B_{2s}(0)} \leq \frac{3m\sqrt{2s}}{4sL} = \frac{3m}{2\sqrt{2s}L}.$$

Due to $s = \left\lceil \frac{m+1}{2} \right\rceil$ we have $\sqrt{2s} \geq \sqrt{m}$, such that (4.87) yields the assertion. ∎

We remark that the triangle inequality combined with Theorems 4.40 and 4.41 also implies an estimate on the perturbation error $\|f - R_{\mathrm{B},m}\tilde{f}\|_{C_0(\mathbb{R})}$, cf. (4.88).

sinh-type window function

Next, we proceed with the sinh-type window function (4.62) with the scaling parameter $\beta := \frac{b\pi\,(1+2\lambda)}{1+\lambda}$ for $b > 0$. Note that (4.62) is supported on $\left[-\frac{m}{L}, \frac{m}{L}\right]$. According to (4.69) we form the *sinh-type regularized sinc function*

$$\psi_{\sinh}(x) := \operatorname{sinc}(L\pi x)\,\varphi_{\sinh}(x), \quad x \in \mathbb{R}. \tag{4.105}$$

Lemma 4.42. *Let $L \in \mathbb{N}$ and $\beta := \frac{b\pi\,(1+2\lambda)}{1+\lambda}$ with $b > 0$ be given. Then the Fourier transform of the* sinh*-type regularized sinc function* (4.105) *reads as*

$$\hat{\psi}_{\sinh}(v) = \frac{m\beta}{2L^2\,\sinh\beta} \int_{v-L/2}^{v+L/2} \frac{J_1\left(2\pi\,\sqrt{\frac{m^2u^2}{L^2} - \frac{b^2(1+2\lambda)^2}{(2+2\lambda)^2}}\right)}{\sqrt{\frac{m^2u^2}{L^2} - \frac{b^2(1+2\lambda)^2}{(2+2\lambda)^2}}}\,\mathrm{d}u, \tag{4.106}$$

where J_α denotes the Bessel function of first kind. The function (4.106) *is even, real-valued, and belongs to $C^\infty(\mathbb{R})$.*

Proof. To compute the Fourier transform of (4.105) we apply the convolution property (4.66) using $f(x) = \operatorname{sinc}(L\pi x)$ and $g(x) = \varphi_{\sinh}(x)$. These functions possess the Fourier transforms

$$\begin{aligned}
\hat{f}(v) &= \tfrac{1}{L}\,\chi_{\left[-\frac{L}{2},\,\frac{L}{2}\right]}(v),\\
\hat{g}(v) &= \frac{\pi m\beta}{L\,\sinh\beta} \cdot \begin{cases} (w^2-\beta^2)^{-1/2}\,J_1\big(\sqrt{w^2-\beta^2}\big) & : w \in \mathbb{R}\setminus\{-\beta,\,\beta\},\\ \frac{1}{2} & : w = \pm\beta, \end{cases}
\end{aligned} \tag{4.107}$$

where $w := 2\pi m v/L$ denotes a scaled frequency, see [Obe90, p. 38, 7.58] or [PT21a]. Thus, we obtain

$$\begin{aligned}\hat{\psi}_{\sinh}(v) &= (f\,g)\hat{}(v) = (\hat{f} * \hat{g})(v) = \int_{\mathbb{R}} \hat{f}(v-u)\,\hat{g}(u)\,\mathrm{d}u \\ &= \frac{1}{L}\int_{v-L/2}^{v+L/2} \hat{g}(u)\,\mathrm{d}u \\ &= \frac{m\beta}{2L^2\sinh\beta}\int_{v-L/2}^{v+L/2} \frac{J_1\left(2\pi\sqrt{\frac{m^2u^2}{L^2}-\frac{b^2(1+2\lambda)^2}{(2+2\lambda)^2}}\right)}{\sqrt{\frac{m^2u^2}{L^2}-\frac{b^2(1+2\lambda)^2}{(2+2\lambda)^2}}}\,\mathrm{d}u\end{aligned}$$

and thereby the assertion (4.106). Note that the integrand of (4.106) is real-valued, since $J_1(\mathrm{i}\,z) = \mathrm{i}\,I_1(z)$ for $z \in \mathbb{C}$, where I_α denotes the modified Bessel function of first kind. Moreover, it is easy to see by (4.106) that $\hat{\psi}_{\sinh}$ is even and belongs to $C^\infty(\mathbb{R})$. ■

A visualization of the sinh-type regularized sinc function (4.105) and its Fourier transform (4.106) can be found in Figure 4.7. Note that in comparison to Section 4.3.1 the function $\hat{\psi}_{\sinh}$ is not of the form (4.34). In addition, the sinh-type regularized sinc function $\psi_{\sinh}$ is not bandlimited on any interval. However, the following lemma shows that this function (4.105) is essentially bandlimited on the interval $\left[-\frac{L}{2}(1+\varepsilon), \frac{L}{2}(1+\varepsilon)\right]$ with certain $\varepsilon > 0$, such that $\hat{\psi}_{\sinh}$ is negligible for $|v| > \frac{L}{2}(1+\varepsilon)$.

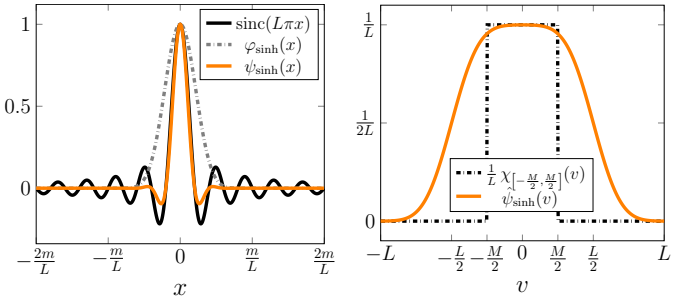

(a) $\psi_{\sinh}$ in (4.105) (b) $\hat{\psi}_{\sinh}$ in (4.106)

Figure 4.7: The sinh-type regularized sinc function $\psi_{\sinh}$ as well as its Fourier transform $\hat{\psi}_{\sinh}$ with $m = 5$ and $\beta = \frac{5}{2}\pi$.

Lemma 4.43. *The* sinh*-type regularized sinc function* $\psi_{\sinh}$ *in* (4.105) *is essentially bandlimited on the interval* $\left[-\frac{L}{2}(1+\varepsilon),\, \frac{L}{2}(1+\varepsilon)\right]$ *with* $\varepsilon \geq \frac{4b}{m}$, *i. e., for all* $v \in \mathbb{R} \setminus \left[-\frac{L}{2}(1+\varepsilon),\, \frac{L}{2}(1+\varepsilon)\right]$ *we have*

$$\left|\hat{\psi}_{\sinh}(v)\right| < \frac{5\sqrt{2b\beta}}{4L\sqrt{m\varepsilon}\,\sinh\beta}.$$

Proof. Due to the fact that (4.106) is an even function, it suffices to consider only $v > \frac{L}{2}(1+\varepsilon)$. Assume that for all $u \in \left[v-\frac{L}{2}, v+\frac{L}{2}\right]$ we have

$$\frac{m^2u^2}{L^2} - \frac{b^2(1+2\lambda)^2}{(2+2\lambda)^2} > 0, \tag{4.108}$$

such that from (4.106) it follows that

$$|\hat{\psi}_{\sinh}(v)| \leq \frac{m\beta}{2L^2\,\sinh\beta} \int_{v-L/2}^{v+L/2} \frac{\left|J_1\left(2\pi\sqrt{\frac{m^2u^2}{L^2} - \frac{b^2(1+2\lambda)^2}{(2+2\lambda)^2}}\right)\right|}{\sqrt{\frac{m^2u^2}{L^2} - \frac{b^2(1+2\lambda)^2}{(2+2\lambda)^2}}}\,\mathrm{d}u.$$

Since we have $|J_1(x)| < \frac{1}{\sqrt{x}}$ for all $x > 0$, cf. [PT21b, (3.4)], we obtain

$$\begin{aligned}|\hat{\psi}_{\sinh}(v)| &\leq \frac{m\beta}{2L^2\sqrt{2\pi}\,\sinh\beta} \int_{v-L/2}^{v+L/2} \left(\frac{m^2u^2}{L^2} - \frac{b^2(1+2\lambda)^2}{(2+2\lambda)^2}\right)^{-3/4} \mathrm{d}u \\ &< \frac{m\beta}{2L^2\sqrt{2\pi}\,\sinh\beta} \int_{\varepsilon L/2}^{\infty} \left(\frac{m^2u^2}{L^2} - \frac{b^2(1+2\lambda)^2}{(2+2\lambda)^2}\right)^{-3/4} \mathrm{d}u.\end{aligned}$$

Substituting $u = \frac{bL(1+2\lambda)}{m(2+2\lambda)}\,w$, we conclude

$$\begin{aligned}|\hat{\psi}_{\sinh}(v)| &< \frac{\sqrt{\beta}}{2L\,\sinh\beta} \int_{\varepsilon m\,(1+\lambda)/(b+2b\lambda)}^{\infty} (w^2-1)^{-3/4}\,\mathrm{d}w \\ &\leq \frac{\sqrt{\beta}}{2L\,\sinh\beta} \int_{\varepsilon m/(2b)}^{\infty} (w^2-1)^{-3/4}\,\mathrm{d}w,\end{aligned}$$

because of $\frac{\varepsilon m\,(1+\lambda)}{b+2b\lambda} \geq \frac{\varepsilon m}{2b}$ for $\lambda \geq 0$. Then by

$$\max_{w\geq 2} \frac{w^{3/2}}{(w^2-1)^{3/4}} < \frac{5}{4}$$

we receive

$$|\hat{\psi}_{\sinh}(v)| < \frac{5\sqrt{\beta}}{8L\sinh\beta}\int_{\varepsilon m/(2b)}^{\infty} w^{-3/2}\,\mathrm{d}w = \frac{5\sqrt{2b\beta}}{4L\sqrt{m\varepsilon}\sinh\beta}$$

for $\varepsilon m/(2b) \geq 2$, that means $\varepsilon \geq \frac{4b}{m}$. Note that in this setting also (4.108) is fulfilled, such that for $\varepsilon \geq \frac{4b}{m}$ the Fourier transform $\hat{\psi}_{\sinh}$ is negligible for $|v| > \frac{L}{2}(1+\varepsilon)$. ∎

Now we show that for the regularization with the sinh-type window function (4.62) the uniform approximation error (4.78) decays exponentially with respect to m, cf. [KPT22, Theorem 6.1].

Theorem 4.44. *Let $f \in \mathcal{B}_{M/2}(\mathbb{R})$ with $M \in \mathbb{N}$, $L = M(1+\lambda) \in \mathbb{N}$ with $\lambda > 0$, and $m \in \mathbb{N} \setminus \{1\}$ be given. Then the regularized Shannon sampling formula with localized sampling* (4.74) *using the* sinh*-type window function* (4.62) *and $\beta = \frac{\pi m\lambda}{1+\lambda}$ satisfies the error estimate*

$$\|f - R_{\sinh,m} f\|_{C_0(\mathbb{R})} \leq \sqrt{M}\,\mathrm{e}^{-m\pi\lambda/(1+\lambda)}\,\|f\|_{L_2(\mathbb{R})}.$$

Proof. By Corollary 4.26 we only need to estimate the regularization error constant (4.67), since we have $\operatorname{supp}(\varphi_{\sinh}) = \left[-\frac{m}{L}, \frac{m}{L}\right]$ and therefore the truncation error constant (4.80) vanishes for the sinh-type window function (4.62).

By (4.107) and the definition $\beta = \frac{b\pi(1+2\lambda)}{1+\lambda}$ we recognize that the auxiliary function (4.72) is given by

$$\eta_{\sinh}(v) = \chi_{\left[-\frac{M}{2}, \frac{M}{2}\right]}(v) - \frac{m\beta}{2L\sinh\beta}\int_{v-L/2}^{v+L/2} \frac{J_1\left(2\pi\sqrt{\frac{m^2u^2}{L^2} - \frac{b^2(1+2\lambda)^2}{(2+2\lambda)^2}}\right)}{\sqrt{\frac{m^2u^2}{L^2} - \frac{b^2(1+2\lambda)^2}{(2+2\lambda)^2}}}\,\mathrm{d}u, \quad v \in \mathbb{R}.$$

Substituting $u = \frac{bL(1+2\lambda)}{m(2+2\lambda)}\,w$, we obtain

$$\eta_{\sinh}(v) = 1 - \frac{\beta}{2\sinh\beta}\int_{-w_1(-v)}^{w_1(v)} \frac{J_1\left(\beta\sqrt{w^2-1}\right)}{\sqrt{w^2-1}}\,\mathrm{d}w, \quad v \in \left[-\tfrac{M}{2}, \tfrac{M}{2}\right], \tag{4.109}$$

with

$$w_1(v) \coloneqq \frac{(2v+L)\,m\,(1+\lambda)}{bL\,(1+2\lambda)} > 0, \quad v \in \left[-\tfrac{M}{2},\, \tfrac{M}{2}\right]. \tag{4.110}$$

By definition, $w_1(v)$ is linear and monotonously increasing, such that

$$\min_{v\in\left[-\frac{M}{2},\,\frac{M}{2}\right]} w_1(v) = w_1\big(-\tfrac{M}{2}\big) \quad \text{and} \quad \max_{v\in\left[-\frac{M}{2},\,\frac{M}{2}\right]} w_1(v) = w_1\big(\tfrac{M}{2}\big).$$

In the following we aim for an optimal parameter $b = b(M, m, \lambda) > 0$, such that $|\eta_{\sinh}(v)|$ is as small as possible for all $v \in \left[-\frac{M}{2},\, \frac{M}{2}\right]$. To this end, we have a closer look at the integral in (4.109). As known, the Bessel function J_1 oscillates on $[0, \infty)$ and has the non-negative simple zeros $j_{1,n}$, $n \in \mathbb{N}_0$, where $j_{1,0} = 0$ and $j_{1,n}$, $n = 1, \ldots, 40$, are tabulated in [Wat80, p. 748]. Therefore, the integrand of (4.109) has the zeros $\pm\xi_n$ with $\xi_n \coloneqq \sqrt{\left(\frac{j_{1,n}}{\beta}\right)^2 + 1} \geq 1$, $n \in \mathbb{N}$, and $\lim_{\beta\to\infty} \xi_1 = 1$. It is easy to see that

$$\int_{-a}^{b} \frac{J_1\big(\beta\sqrt{w^2-1}\big)}{\sqrt{w^2-1}}\,\mathrm{d}w \geq 0, \quad a, b \geq 0,$$

and that this integral is maximal for $a = b = \xi_1$, cf. Figure 4.8. Moreover, note that by [GR07, 6.681–3] and [AS72, 10.2.13] as well as $J_1(\mathrm{i}\,z) = \mathrm{i}\,I_1(z)$ for $z \in \mathbb{C}$ we have

$$\begin{aligned}\int_{-1}^{1} \frac{J_1\big(\beta\sqrt{w^2-1}\big)}{\sqrt{w^2-1}}\,\mathrm{d}w &= \int_{-1}^{1} \frac{I_1\big(\beta\sqrt{1-w^2}\big)}{\sqrt{1-w^2}}\,\mathrm{d}w = \int_{-\pi/2}^{\pi/2} I_1(\beta\,\cos t)\,\mathrm{d}t \\ &= \pi\left(I_{1/2}\Big(\frac{\beta}{2}\Big)\right)^2 = \frac{4}{\beta}\left(\sinh\frac{\beta}{2}\right)^2, \end{aligned} \tag{4.111}$$

and hence

$$\begin{aligned} h(\beta) &\coloneqq \frac{\beta}{2\,\sinh\beta}\int_{-1}^{1} \frac{J_1\big(\beta\sqrt{w^2-1}\big)}{\sqrt{w^2-1}}\,\mathrm{d}w \\ &= \frac{2\left(\sinh\frac{\beta}{2}\right)^2}{\sinh\beta} = \frac{\mathrm{e}^{\beta} - 2 + \mathrm{e}^{-\beta}}{\mathrm{e}^{\beta} - \mathrm{e}^{-\beta}} \in [0,\,1], \end{aligned}$$

where $h(\beta)$ is a monotonously increasing function with $\lim_{\beta\to 0} h(\beta) = 0$ and $\lim_{\beta\to\infty} h(\beta) = 1$. Thus, in order to achieve $|\eta_{\sinh}(v)|$ in (4.109) as

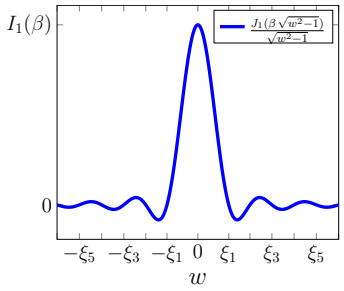

Figure 4.8: The function $\frac{J_1(\beta\sqrt{w^2-1})}{\sqrt{w^2-1}}$.

small as possible, we request $w_1(v) \geq 1$ for all $v \in \left[-\frac{M}{2}, \frac{M}{2}\right]$, which can be obtained by setting $w_1\left(-\frac{M}{2}\right) = 1$. Rearranging this by (4.110) in terms of b we obtain $b = \frac{m\lambda}{1+2\lambda}$ and therefore $\beta = \frac{\pi m\lambda}{1+\lambda}$.

Now given this scaling parameter β we are able to provide an estimate on the regularization error constant (4.67). From (4.109) it follows that

$$\eta_{\sinh}(v) = \eta_1(v) - \eta_2(v), \quad v \in \left[-\tfrac{M}{2}, \tfrac{M}{2}\right],$$

with

$$\eta_1(v) \coloneqq 1 - \frac{\beta}{2\sinh\beta} \int_{-1}^{1} \frac{I_1\left(\beta\sqrt{1-w^2}\right)}{\sqrt{1-w^2}}\,\mathrm{d}w,$$

$$\eta_2(v) \coloneqq \frac{\beta}{2\sinh\beta}\left(\int_{-w_1(-v)}^{-1} + \int_{1}^{w_1(v)}\right)\frac{J_1\left(\beta\sqrt{w^2-1}\right)}{\sqrt{w^2-1}}\,\mathrm{d}w.$$

By (4.111) we obtain

$$\eta_1(v) = 1 - \frac{2\left(\sinh\frac{\beta}{2}\right)^2}{\sinh\beta} = \frac{2\,\mathrm{e}^{-\beta}}{1+\mathrm{e}^{-\beta}} > 0.$$

Further we have

$$\eta_2(v) = \frac{\beta}{2\sinh\beta}\left(\int_{1}^{w_1(-v)} + \int_{1}^{w_1(v)}\right)\frac{J_1\left(\beta\sqrt{w^2-1}\right)}{\sqrt{w^2-1}}\,\mathrm{d}w.$$

Substituting $w = \cosh x$ in above integrals, we have

$$\eta_2(v) = \frac{\beta}{2\sinh\beta}\left(\int_{0}^{\operatorname{arcosh}(w_1(-v))} + \int_{0}^{\operatorname{arcosh}(w_1(v))}\right)J_1(\beta\sinh x)\,\mathrm{d}x.$$

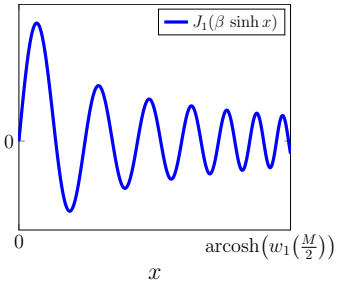

Figure 4.9: The function $J_1(\beta \sinh x)$ on the interval $\left[0, \operatorname{arcosh}\left(w_1\left(\frac{M}{2}\right)\right)\right]$.

In order to estimate these integrals properly we now have a closer look at the integrand. On each interval $\left[\operatorname{arsinh}\left(\frac{j_{1,2n}}{\beta}\right), \operatorname{arsinh}\left(\frac{j_{1,2n+2}}{\beta}\right)\right]$, $n \in \mathbb{N}_0$, the integrand $J_1(\beta \sinh x)$ is firstly non-negative and then non-positive, see Figure 4.9. Due to these properties and the fact that the amplitude is decreasing when $x \to \infty$, the integrals are positive on each interval $\left[\operatorname{arsinh}\left(\frac{j_{1,2n}}{\beta}\right), \operatorname{arsinh}\left(\frac{j_{1,2n+2}}{\beta}\right)\right]$, $n \in \mathbb{N}_0$. Note that by [GR07, 6.645–1] we have

$$\begin{aligned}\int_0^\infty J_1(\beta \sinh x)\,\mathrm{d}x &= I_{1/2}\Big(\frac{\beta}{2}\Big)\, K_{1/2}\Big(\frac{\beta}{2}\Big) \\ &= \frac{2}{\sqrt{\pi\beta}} \sinh\frac{\beta}{2} \cdot \sqrt{\frac{\pi}{\beta}}\, \mathrm{e}^{-\beta/2} = \frac{1-\mathrm{e}^{-\beta}}{\beta},\end{aligned}$$

where K_α denotes the *modified Bessel function of second kind* and $I_{1/2}$, $K_{1/2}$ denote modified Bessel functions of half order (see [AS72, 10.2.13, 10.2.14, and 10.2.17]). In addition, numerical experiments have shown that for all $T \geq 0$ we have

$$0 \leq \int_0^T J_1(\beta \sinh x)\,\mathrm{d}x \leq \frac{3\,(1-\mathrm{e}^{-\beta})}{2\,\beta}.$$

Therefore, we obtain

$$0 \leq \eta_2(v) \leq \frac{\beta}{2\,\sinh\beta} \cdot \frac{3\,(1-\mathrm{e}^{-\beta})}{\beta} = \frac{3\,\mathrm{e}^{-\beta}}{1+\mathrm{e}^{-\beta}}$$

and hence

$$\max_{v\in\left[-\frac{M}{2},\,\frac{M}{2}\right]} |\eta_{\sinh}(v)| = \max_{v\in\left[-\frac{M}{2},\,\frac{M}{2}\right]} |\eta_1(v) - \eta_2(v)| \le \frac{\mathrm{e}^{-\beta}}{1+\mathrm{e}^{-\beta}} \le \mathrm{e}^{-\beta} \le 1. \tag{4.112}$$

Thus, by (4.67) and (4.72) we conclude that

$$E_{\mathrm{r}}(\varphi_{\sinh}, M, L) \le \sqrt{M}\,\mathrm{e}^{-\beta}.$$

This completes the proof. ∎

Now we show that for the regularization with the sinh-type window function (4.62) the uniform perturbation error (4.87) only grows as $\mathcal{O}(\sqrt{m})$, cf. [KPT22, Theorem 6.3].

Theorem 4.45. *Let $f \in \mathcal{B}_{M/2}(\mathbb{R})$ with $M \in \mathbb{N}$, $L = M(1+\lambda) \in \mathbb{N}$ with $\lambda > 0$ and $m \in \mathbb{N} \setminus \{1\}$ be given. Further let $R_{\sinh,m}\tilde{f}$ be as in* (4.85) *with the noisy samples $\tilde{f}_\ell = f\big(\frac{\ell}{L}\big) + \varepsilon_\ell$, where $|\varepsilon_\ell| \le \varepsilon$ for all $\ell \in \mathbb{Z}$ and $0 < \varepsilon \ll 1$. Then the regularized Shannon sampling formula with localized sampling* (4.74) *using the* sinh*-type window function* (4.62) *and $\beta = \frac{\pi m \lambda}{1+\lambda}$ satisfies*

$$\|R_{\sinh,m}\tilde{f} - R_{\sinh,m} f\|_{C_0(\mathbb{R})} \le \varepsilon \left(2 + \sqrt{\frac{2+2\lambda}{\lambda}}\,\frac{1}{1-\mathrm{e}^{-2\beta}}\,\sqrt{m}\right).$$

Proof. By Theorem 4.29 we only need to compute $\hat{\varphi}_{\sinh}(0)$ for the sinh-type window function (4.62). By (4.107) we recognize that

$$\hat{\varphi}_{\sinh}(0) = \frac{\pi m \beta}{L \sinh\beta} \cdot \frac{I_1\big(\beta\big)}{\beta} = \frac{\pi m\, I_1\big(\beta\big)}{L \sinh\beta}.$$

Since $\sqrt{2\pi\beta}\,\mathrm{e}^{-\beta}\, I_1(\beta) < 1$, see [PT21b, Lemma 7], we have

$$\frac{\pi m\, I_1(\beta)}{\sinh\beta} \le \frac{\pi m\, \mathrm{e}^{\beta}}{\sqrt{2\pi\beta}\sinh\beta} = \frac{\sqrt{2\pi}\, m}{\sqrt{\beta}\,(1-\mathrm{e}^{-2\beta})},$$

such that (4.87) using $\beta = \frac{\pi m\lambda}{1+\lambda}$ yields the assertion. ∎

We remark that the triangle inequality combined with Theorems 4.44 and 4.45 also implies an estimate on the perturbation error $\|f - R_{\sinh,m}\tilde{f}\|_{C_0(\mathbb{R})}$, cf. (4.88).

Continuous Kaiser–Bessel window function

Finally, we consider the continuous Kaiser–Bessel window function (4.63) with the scaling parameter $\beta \coloneqq \frac{b\pi\,(1+2\lambda)}{1+\lambda}$ for $b > 0$. Note that (4.63) is supported on $\left[-\frac{m}{L}, \frac{m}{L}\right]$. According to (4.69) we form the *continuous Kaiser–Bessel regularized sinc function*

$$\psi_{\mathrm{cKB}}(x) \coloneqq \operatorname{sinc}(L\pi x)\,\varphi_{\mathrm{cKB}}(x), \quad x \in \mathbb{R}. \tag{4.113}$$

Lemma 4.46. *Let $L \in \mathbb{N}$ and $\beta \coloneqq \frac{b\pi\,(1+2\lambda)}{1+\lambda}$ with $b > 0$ be given. Then the Fourier transform of the continuous Kaiser–Bessel regularized sinc function* (4.113) *reads as*

$$\hat{\psi}_{\mathrm{cKB}}(v) = \frac{\beta}{L\pi\left(I_0(\beta)-1\right)} \int_{\frac{2\pi m}{\beta L}(v-L/2)}^{\frac{2\pi m}{\beta L}(v+L/2)} \frac{\sinh\left(\beta\sqrt{1-w^2}\right)}{\beta\sqrt{1-w^2}} - \operatorname{sinc}(\beta w)\,\mathrm{d}w. \tag{4.114}$$

The function (4.114) *is even, real-valued, and belongs to $C^\infty(\mathbb{R})$.*

Proof. To compute the Fourier transform of (4.113) we apply the convolution property (4.66) using $f(x) = \operatorname{sinc}(L\pi x)$ and $g(x) = \varphi_{\mathrm{cKB}}(x)$. These functions possess the Fourier transforms

$$\begin{aligned}
\hat{f}(v) &= \tfrac{1}{L}\,\chi_{\left[-\frac{L}{2},\,\frac{L}{2}\right]}(v),\\
\hat{g}(v) &= \frac{2m}{\left(I_0(\beta)-1\right)L} \cdot \begin{cases} \frac{\sinh\left(\beta\sqrt{1-w^2}\right)}{\beta\sqrt{1-w^2}} - \operatorname{sinc}(\beta w) & : w \in \mathbb{R}\setminus\{-1,\,1\},\\ 1-\operatorname{sinc}(\beta) & : w = \pm 1, \end{cases}
\end{aligned} \tag{4.115}$$

where $w = 2\pi m v/(\beta L)$ denotes a scaled frequency, see [Obe90, p. 3, 1.1, and p. 95, 18.31] or [PT21b]. Thus, by substituting $u = \beta L w/(2\pi m)$ we obtain

$$\begin{aligned}
\hat{\psi}_{\mathrm{cKB}}(v) = (f\,g)\hat{}(v) = (\hat{f} * \hat{g})(v) &= \int_{\mathbb{R}} \hat{f}(v-u)\,\hat{g}(u)\,\mathrm{d}u\\
&= \frac{1}{L}\int_{v-L/2}^{v+L/2} \hat{g}(u)\,\mathrm{d}u\\
&= \frac{\beta}{L\pi\left(I_0(\beta)-1\right)} \int_{\frac{2\pi m}{\beta L}(v-L/2)}^{\frac{2\pi m}{\beta L}(v+L/2)} \frac{\sinh\left(\beta\sqrt{1-w^2}\right)}{\beta\sqrt{1-w^2}} - \operatorname{sinc}(\beta w)\,\mathrm{d}w
\end{aligned}$$

and thereby the assertion (4.114). Note that the integrand of (4.114) is real-valued, since $\sinh(\mathrm{i}\, z) = \mathrm{i}\, \sin(z)$ for $z \in \mathbb{C}$. Moreover, it is easy to see by (4.114) that $\hat{\psi}_{\mathrm{cKB}}$ is even and belongs to $C^\infty(\mathbb{R})$. ■

A visualization of the continuous Kaiser–Bessel regularized sinc function (4.113) and its Fourier transform (4.114) can be found in Figure 4.10. Note that in comparison to Section 4.3.1 the function $\hat{\psi}_{\mathrm{cKB}}$ is not of the form (4.34). In addition, the continuous Kaiser–Bessel regularized sinc function ψ_{cKB} is not bandlimited on any interval. However, the following lemma shows that this function (4.96) is essentially bandlimited on the interval $\left[-\frac{L}{2}(1+\varepsilon), \frac{L}{2}(1+\varepsilon)\right]$ with certain $\varepsilon > 0$, such that $\hat{\psi}_{\mathrm{cKB}}$ is negligible for $|v| > \frac{L}{2}(1+\varepsilon)$.

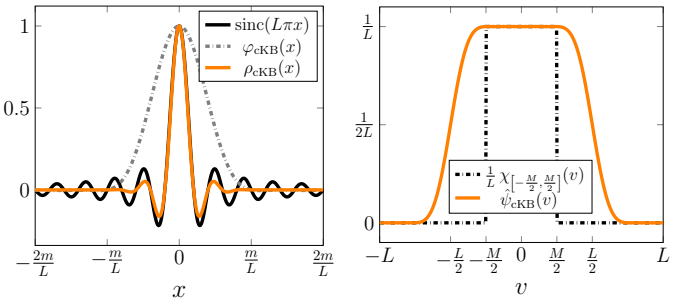

(a) ψ_{cKB} in (4.113) (b) $\hat{\psi}_{\mathrm{cKB}}$ in (4.114)

Figure 4.10: The continuous Kaiser–Bessel regularized sinc function ψ_{cKB} as well as its Fourier transform $\hat{\psi}_{\mathrm{cKB}}$ with $m = 5$ and $\beta = \frac{5}{2}\pi$.

Lemma 4.47. *The continuous Kaiser–Bessel regularized sinc function ψ_{cKB} in (4.113) is essentially bandlimited on the interval $\left[-\frac{L}{2}(1+\varepsilon), \frac{L}{2}(1+\varepsilon)\right]$ with certain $\varepsilon > \frac{\beta}{\pi m}$, i. e., for all $v \in \mathbb{R} \setminus \left[-\frac{L}{2}(1+\varepsilon), \frac{L}{2}(1+\varepsilon)\right]$ we have*

$$|\hat{\psi}_{\mathrm{cKB}}(v)| < \frac{2\beta^2}{L\pi^2 m\varepsilon\left(I_0(\beta) - 1\right)}.$$

Proof. Due to the fact that (4.114) is an even function, it suffices to consider only $v > \frac{L}{2}(1+\varepsilon)$. Assume that for all $w \in \frac{2\pi m}{\beta L}\left[v - \frac{L}{2}, v + \frac{L}{2}\right]$ we have

$$1 - w^2 < 0, \tag{4.116}$$

such that from (4.114) it follows that

$$\begin{aligned}&\left|\hat{\psi}_{\mathrm{cKB}}(v)\right| \\ &\quad\leq \frac{\beta}{L\pi\left(I_0(\beta)-1\right)} \int_{\frac{2\pi m}{\beta L} m(v-L/2)}^{\frac{2\pi m}{\beta L}(v+L/2)} \left|\operatorname{sinc}\bigl(\beta\sqrt{w^2-1}\,\bigr) - \operatorname{sinc}(\beta w)\right| \mathrm{d}w.\end{aligned}$$

Since we have

$$\left|\operatorname{sinc}\bigl(\beta\sqrt{w^2-1}\,\bigr) - \operatorname{sinc}(\beta w)\right| \leq \frac{2}{w^2} \tag{4.117}$$

for $|w| \geq 1$, see [PT21a, Lemma 4], we obtain

$$\begin{aligned}\left|\hat{\psi}_{\mathrm{cKB}}(v)\right| &\leq \frac{\beta}{L\pi\left(I_0(\beta)-1\right)} \int_{2\pi m(v-L/2)/(\beta L)}^{2\pi m(v+L/2)/(\beta L)} \frac{2}{w^2}\,\mathrm{d}w \\ &< \frac{\beta}{L\pi\left(I_0(\beta)-1\right)} \int_{\pi m\varepsilon/\beta}^{\infty} \frac{2}{w^2}\,\mathrm{d}w = \frac{2\beta^2}{L\pi^2 m\varepsilon\left(I_0(\beta)-1\right)}.\end{aligned}$$

Note that (4.116) is fulfilled in case $\frac{\pi m\varepsilon}{\beta} > 1$, such that for $\varepsilon \geq \frac{\beta}{\pi m}$ the Fourier transform $\hat{\psi}_{\mathrm{cKB}}$ is negligible for $|v| > \frac{L}{2}(1+\varepsilon)$. ■

Now we show that for the regularization with the continuous Kaiser–Bessel window function (4.63) the uniform approximation error (4.78) decays exponentially with respect to m, cf. [KPT24, Theorem 4.3].

Theorem 4.48. *Let $f \in \mathcal{B}_{M/2}(\mathbb{R})$ with $M \in \mathbb{N}$, $L = M(1+\lambda) \in \mathbb{N}$ with $\lambda \geq \frac{1}{m-1}$, and $m \in \mathbb{N} \setminus \{1\}$ be given. Then the regularized Shannon sampling formula with localized sampling* (4.74) *using the continuous Kaiser–Bessel window function* (4.63) *and $\beta = \frac{\pi m\lambda}{1+\lambda}$ satisfies the error estimate*

$$\|f - R_{\mathrm{cKB},m} f\|_{C_0(\mathbb{R})} \leq \frac{7\sqrt{M}\,\pi m\lambda\,(1+\lambda+4m\lambda)}{4\,(1+\lambda)^2}\,\mathrm{e}^{-m\pi\lambda/(1+\lambda)}\,\|f\|_{L_2(\mathbb{R})}.$$

Proof. By Corollary 4.26 we only need to estimate the regularization error constant (4.67), since we have $\operatorname{supp}(\varphi_{\mathrm{cKB}}) = \left[-\frac{m}{L}, \frac{m}{L}\right]$ and therefore the truncation error constant (4.80) vanishes for the continuous Kaiser–Bessel window function (4.63).

By (4.115) and substituting $w = \frac{2\pi m}{\beta L}\, u$ we recognize that the auxiliary function (4.72) is given by

$$\eta_{\mathrm{cKB}}(v) = 1 - \frac{\beta}{\pi\left(I_0(\beta) - 1\right)} \int_{-a(-v)}^{a(v)} \left(\frac{\sinh\left(\beta\sqrt{1-w^2}\right)}{\beta\sqrt{1-w^2}} - \operatorname{sinc}(\beta w) \right) \mathrm{d}w \tag{4.118}$$

with the increasing linear function $a(v) \coloneqq \frac{2m\pi}{\beta L}\left(v + \frac{L}{2}\right)$.

Similar to Theorem 4.44 we now aim to choose an optimal parameter $\beta > 0$, such that $|\eta_{\mathrm{cKB}}(v)|$ is as small as possible for all $v \in \left[-\frac{M}{2}, \frac{M}{2}\right]$. To this end, we have a closer look at the integral in (4.118). It is easy to see that

$$\int_{-a}^{b} \left(\frac{\sinh\left(\beta\sqrt{1-w^2}\right)}{\beta\sqrt{1-w^2}} - \operatorname{sinc}(\beta w) \right) \mathrm{d}w \geq 0, \quad a, b \geq 0,$$

and that this integral is maximal for $a = b = \xi_1$, when denoting the zeros of the integrand as $\pm\xi_n$, cf. Figure 4.11. Numerical experiments have shown that $\xi_n \geq 1$, $n \in \mathbb{N}$, and $\lim_{\beta\to\infty} \xi_1 = 1$. Moreover, by substituting $w = \sin(s)$ and [GR07, 3.997–1] we have

$$\begin{aligned} \int_{-1}^{1} \frac{\sinh\left(\beta\sqrt{1-w^2}\right)}{\beta\sqrt{1-w^2}}\, \mathrm{d}w &= \frac{2}{\beta} \int_{0}^{1} \frac{\sinh\left(\beta\sqrt{1-w^2}\right)}{\sqrt{1-w^2}}\, \mathrm{d}w \\ &= \frac{2}{\beta} \int_{0}^{\pi/2} \sinh(\beta\cos s)\, \mathrm{d}s = \frac{\pi}{\beta}\, \mathbf{L}_0(\beta), \end{aligned}$$

where $\mathbf{L}_0(x)$ denotes the *modified Struve function* given by (see [AS72, 12.2.1])

$$\mathbf{L}_0(x) \coloneqq \sum_{k=0}^{\infty} \frac{\left(\frac{x}{2}\right)^{2k+1}}{\left(\Gamma\left(k+\frac{3}{2}\right)\right)^2} = \frac{2x}{\pi} \sum_{k=0}^{\infty} \frac{x^{2k}}{\left((2k+1)!!\right)^2}.$$

Note that the function $I_0(x) - \mathbf{L}_0(x)$ is completely monotonic on $[0, \infty)$ (see [BP14, Theorem 1]) and tends to zero as $x \to \infty$. Applying the *sine integral function*

$$\mathrm{Si}(x) \coloneqq \int_0^x \frac{\sin(w)}{w}\, \mathrm{d}w = \int_0^x \operatorname{sinc}(w)\, \mathrm{d}w, \quad x \in \mathbb{R},$$

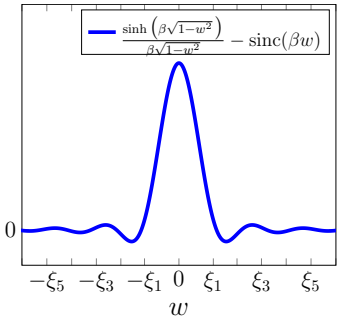

Figure 4.11: The function $\frac{\sinh\left(\beta\sqrt{1-w^2}\right)}{\beta\sqrt{1-w^2}} - \operatorname{sinc}(\beta w)$.

implies

$$\int_{-1}^{1} \operatorname{sinc}(\beta w)\,\mathrm{d}w = 2\int_{0}^{1} \operatorname{sinc}(\beta w)\,\mathrm{d}w = \frac{2}{\beta}\int_{0}^{\beta} \operatorname{sinc}(y)\,\mathrm{d}y = \frac{2}{\beta}\operatorname{Si}(\beta),$$

and hence

$$\begin{aligned} h(\beta) &:= \frac{\beta}{\pi\left(I_0(\beta)-1\right)}\int_{-1}^{1}\left(\frac{\sinh\left(\beta\sqrt{1-w^2}\right)}{\beta\sqrt{1-w^2}} - \operatorname{sinc}(\beta w)\right)\mathrm{d}w \\ &= \frac{1}{I_0(\beta)-1}\left(\mathbf{L}_0(\beta) - \frac{2}{\pi}\operatorname{Si}(\beta)\right), \quad \beta > 0. \end{aligned} \tag{4.119}$$

Numerical experiments have shown that $h(\beta) \in [0,\,1]$ is monotonously increasing with $\lim_{\beta\to 0} h(\beta) = 0$ and $\lim_{\beta\to\infty} h(\beta) = 1$, similar to Theorem 4.44. Thus, in order to achieve $|\eta_{\mathrm{cKB}}(v)|$ in (4.118) as small as possible, we request $a(v) \geq 1$ for all $v \in \left[-\frac{M}{2},\,\frac{M}{2}\right]$, which can be obtained by setting $a\left(-\frac{M}{2}\right) = 1$. Rearranging this by the definition of $a(v)$ we obtain $\beta = \frac{\pi m\lambda}{1+\lambda}$.

Now given this scaling parameter β we are able to provide an estimate on the regularization error constant (4.67). Using (4.118), we decompose $\eta_{\mathrm{cKB}}(v)$ in the form

$$\eta_{\mathrm{cKB}}(v) = \eta_3(v) - \eta_4(v), \quad v \in \left[-\tfrac{M}{2},\,\tfrac{M}{2}\right],$$

with

$$\eta_3(v) = 1 - \frac{\beta}{\pi\left(I_0(\beta)-1\right)} \int_{-1}^{1} \left(\frac{\sinh\left(\beta\sqrt{1-w^2}\,\right)}{\beta\sqrt{1-w^2}} - \operatorname{sinc}(\beta w) \right) \mathrm{d}w,$$

$$\eta_4(v) = \frac{\beta}{\pi\left(I_0(\beta)-1\right)} \left(\int_{-a(-v)}^{-1} \left(\operatorname{sinc}\left(\beta\sqrt{w^2-1}\,\right) - \operatorname{sinc}(\beta w) \right) \mathrm{d}w + \int_{1}^{a(v)} \left(\operatorname{sinc}\left(\beta\sqrt{w^2-1}\,\right) - \operatorname{sinc}(\beta w) \right) \mathrm{d}w \right).$$

By (4.119), we obtain

$$\begin{aligned} \eta_3(v) &= 1 - \frac{1}{I_0(\beta)-1} \left(\mathbf{L}_0(\beta) - \frac{2}{\pi}\operatorname{Si}(\beta) \right) \\ &= \frac{1}{I_0(\beta)-1} \left(I_0(\beta) - \mathbf{L}_0(\beta) - 1 + \frac{2}{\pi}\operatorname{Si}(\beta) \right). \end{aligned}$$

Note that for suitable $\beta > 0$ we find $\left[I_0(\beta) - \mathbf{L}_0(\beta) - 1 + \frac{2}{\pi}\operatorname{Si}(\beta)\right] \in \left[0,\, \frac{9}{20}\right)$, cf. Figure 4.12. In addition, it is known that $I_0(\beta) \geq 1$, $\beta > 0$, such that $\eta_3(v) > 0$.

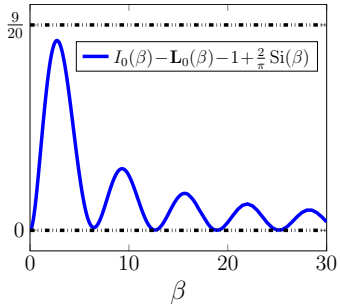

Figure 4.12: Visualization of $\left[I_0(\beta) - \mathbf{L}_0(\beta) - 1 + \frac{2}{\pi}\operatorname{Si}(\beta)\right] \in \left[0,\, \frac{9}{20}\right)$ for suitable $\beta > 0$.

Further, we estimate $\eta_4(v)$ for $v \in \left[-\frac{M}{2}, \frac{M}{2}\right]$ by the triangle inequality as

$$|\eta_4(v)| \leq \frac{\beta}{\pi\left(I_0(\beta)-1\right)}\Bigg(\int_{-a(-v)}^{-1}\Big|\operatorname{sinc}\big(\beta\sqrt{w^2-1}\,\big)-\operatorname{sinc}(\beta w)\Big|\,\mathrm{d}w + \int_{1}^{a(v)}\Big|\operatorname{sinc}\big(\beta\sqrt{w^2-1}\,\big)-\operatorname{sinc}(\beta w)\Big|\,\mathrm{d}w\Bigg).$$

Thus, by (4.117) we conclude

$$|\eta_4(v)| \leq \frac{4\beta}{\pi\left(I_0(\beta)-1\right)}\int_1^\infty \frac{1}{w^2}\,\mathrm{d}w = \frac{4\beta}{\pi\left(I_0(\beta)-1\right)}.$$

Combined with the estimate shown in Figure 4.12, this yields

$$\begin{aligned}|\eta_{\mathrm{cKB}}(v)| &\leq \eta_3(v)+|\eta_4(v)|\\ &\leq \frac{1}{I_0(\beta)-1}\left(I_0(\beta)-\mathbf{L}_0(\beta)-1+\frac{2}{\pi}\operatorname{Si}(\beta)+\frac{4\beta}{\pi}\right)\\ &\leq \frac{1}{I_0(\beta)-1}\left(\frac{9}{20}+\frac{4\beta}{\pi}\right).\end{aligned}$$

Note that this last term is strictly decreasing on $[0,\infty)$ and that by the assumption $\lambda \geq \frac{1}{m-1}$ we have $\beta = \frac{\pi m\lambda}{1+\lambda} \geq \pi$ for all $m \in \mathbb{N}\setminus\{1\}$, such that

$$|\eta_{\mathrm{cKB}}(v)| \leq \frac{1}{I_0(\pi)-1}\left(\frac{9}{20}+\frac{4\pi}{\pi}\right) = 0.993781\cdots \leq 1, \quad v \in \left[-\tfrac{M}{2}, \tfrac{M}{2}\right]. \tag{4.120}$$

By [Bar10, p. 577] the function $\frac{\mathrm{e}^x}{I_0(x)}$ is strictly decreasing on $[0,\infty)$ and tends to zero as $x \to \infty$. Numerical experiments have shown that $\frac{\mathrm{e}^x}{x\,(I_0(x)-1)}$ is strictly decreasing on $[\pi,\infty)$ as well. Hence, it follows that

$$\frac{\mathrm{e}^\beta}{\beta\,(I_0(\beta)-1)} \leq \frac{\mathrm{e}^\pi}{\pi\,(I_0(\pi)-1)} = 1.644967\ldots < \frac{7}{4}$$

and thus we conclude that

$$|\eta_{\mathrm{cKB}}(v)| \leq \frac{1}{I_0(\beta)-1}\left(\frac{9}{20}+\frac{4\beta}{\pi}\right) < \frac{7\beta}{4}\left(1+\frac{4\beta}{\pi}\right)\mathrm{e}^{-\beta}.$$

Using $\beta = \frac{\pi m\lambda}{1+\lambda}$ this completes the proof. ∎

Now we show that for the regularization with the continuous Kaiser–Bessel window function (4.63) the uniform perturbation error (4.87) only grows as $\mathcal{O}(\sqrt{m})$, cf. [KPT24, Theorem 4.6].

Theorem 4.49. *Let $f \in \mathcal{B}_{M/2}(\mathbb{R})$ with $M \in \mathbb{N}$, $L = M(1+\lambda) \in \mathbb{N}$ with $\lambda > 0$ and $m \in \mathbb{N} \setminus \{1\}$ be given. Further let $R_{\mathrm{cKB},m}\tilde{f}$ be as in (4.85) with the noisy samples $\tilde{f}_\ell = f\left(\frac{\ell}{L}\right) + \varepsilon_\ell$, where $|\varepsilon_\ell| \leq \varepsilon$ for all $\ell \in \mathbb{Z}$ and $0 < \varepsilon \ll 1$. Then the regularized Shannon sampling formula with localized sampling (4.74) using the continuous Kaiser–Bessel window function (4.63) and $\beta = \frac{\pi m \lambda}{1+\lambda}$ satisfies*

$$\|R_{\mathrm{cKB},m}\tilde{f} - R_{\mathrm{cKB},m} f\|_{C_0(\mathbb{R})} \leq \varepsilon \left(2 + \sqrt{\frac{2+2\lambda}{\lambda}}\,\sqrt{m}\right).$$

Proof. By Theorem 4.29 we only need to compute $\hat{\varphi}_{\mathrm{cKB}}(0)$ for the continuous Kaiser–Bessel window function (4.63). By (4.115) we recognize that

$$\hat{\varphi}_{\mathrm{cKB}}(0) = \frac{2m}{\big(I_0(\beta) - 1\big)\, L} \left(\frac{\sinh(\beta)}{\beta} - 1\right) = \frac{2m}{L\sqrt{\beta}} \cdot \frac{\sinh(\beta) - \beta}{\sqrt{\beta}\,\big(I_0(\beta) - 1\big)}.$$

Since it is known by [AS72, 9.7.1] that

$$\lim_{x \to \infty} \sqrt{2\pi x}\, \mathrm{e}^{-x} I_0(x) = 1,$$

we also have

$$\lim_{x \to \infty} \sqrt{2\pi x}\, \mathrm{e}^{-x} \big(I_0(x) - 1\big) = 1.$$

Moreover, for $\beta \in [0, \infty)$ the term $\frac{\sinh(\beta)-\beta}{\sqrt{\beta}\,\left(I_0(\beta)-1\right)}$ is monotonously increasing with

$$\lim_{\beta \to \infty} \frac{\sinh(\beta) - \beta}{\sqrt{\beta}\,\big(I_0(\beta) - 1\big)} = \lim_{\beta \to \infty} \frac{1 - \mathrm{e}^{-2\beta} - 2\beta\,\mathrm{e}^{-\beta}}{2\sqrt{\beta}\,\mathrm{e}^{-\beta}\,\big(I_0(\beta) - 1\big)} = \sqrt{\frac{\pi}{2}},$$

such that (4.87) using $\beta = \frac{\pi m \lambda}{1+\lambda}$ yields the assertion. ∎

We remark that the triangle inequality combined with Theorems 4.48 and 4.49 also implies an estimate on the perturbation error $\|f - R_{\mathrm{cKB},m}\tilde{f}\|_{C_0(\mathbb{R})}$, cf. (4.88).

Summary

Summarizing, we have seen that by the use of certain window functions $\varphi \in \Phi$ in spatial domain, or rather their truncated versions (4.73), the regularized Shannon sampling sums with localized sampling (4.74) possess exponential error decay rates. For a comparison of the theoretical error decay rates of the spatial window functions mentioned in Remark 4.22 we refer to Table 4.1, while a visualization of the error decay rates can be found in Examples 4.69 – 4.77.

4.3.3 Comparison of the two regularization methods

Finally, we compare the regularization methods studied in Sections 4.3.1 and 4.3.2. Similar to [KPT24], a summary of the theoretical error decay rates presented for the window functions in the frequency domain and in the spatial domain can be found in Table 4.1. It becomes apparent that regularization with a frequency window function is less effective, as an exponential decay can (up to now) only be realized using the regularization with a spatial window function. For a numerical comparison of these methods we refer to Example 4.78, which demonstrates that also in practice this second approach using window functions in spatial domain performs much better than window functions in frequency domain, since it produces much smaller errors using the same amount of samples.

In summary, we found that the regularized Shannon sampling formulas with localized sampling of Section 4.3.2 are much more powerful, since this approach is easy to compute, robust in the worst case error, and requires less data (for comparable accuracy) than the classical Shannon sampling sums or the regularization with a frequency window function, see also Section 4.5.

4.4 Multivariate regularized Shannon sampling formulas

In the following, we generalize the previous findings to $d > 1$ and present new d-dimensional regularized Shannon sampling formulas. As seen before, for regularizations with a window function in frequency domain from Section 4.3.1 only algebraic error decay rates are achievable, while regularizations with a window function in spatial domain from Section 4.3.2 possess

window function	error decay rate	see
$\operatorname{sinc}(L\pi\,\cdot)$	$(T-L)^{-1/2}$	Lemma 4.6
$\hat{\psi}_{\mathrm{lin}}$ in (4.44)	$(T-L)^{-3/2}$	Theorem 4.14
$\hat{\psi}_{\mathrm{cub}}$ in (4.47)	$(T-L)^{-5/2}$	Theorem 4.15
$\hat{\psi}_{\cos}$ in (4.50)	$(T-L)^{-5/2}$	Remark 4.16
$\hat{\psi}_{\mathrm{conv},2}$, cf. (4.57)	$(T-L)^{-5/2}$	cf. Lemma 4.12
φ_{const} in (4.84)	$\sqrt{\frac{1}{m}+\frac{1}{m^2}}$	Remark 4.28
φ_{Gauss} in (4.60)	$\mathrm{e}^{-m\pi\lambda/(2+2\lambda)}$	Theorem 4.33
φ_{B} in (4.61)	$\mathrm{e}^{-m\,(\ln(\pi m\lambda)-\ln(2s(1+\lambda)))}$	Theorem 4.40
$\varphi_{\sinh}$ in (4.62)	$\mathrm{e}^{-m\pi\lambda/(1+\lambda)}$	Theorem 4.44
φ_{cKB} in (4.63)	$\mathrm{e}^{-m\pi\lambda/(1+\lambda)}$	Theorem 4.48

Table 4.1: Summary of the theoretical results on decay rates for the window functions in frequency domain considered in Section 4.3.1 and the window functions in spatial domain considered in Section 4.3.2.

an exponential error decay and are numerically robust with respect to noisy samples, see also Section 4.5. Therefore, for $d > 1$ we consider only the second approach and focus on regularized Shannon sampling formulas with localized sampling, cf. (4.74), using window functions in spatial domain, cf. Remark 4.22.

For given $\varphi \in \Phi$ let φ_m be the truncated window function (4.73) and let (2.13) be the corresponding d-variate window function, where for simplicity we denote the d-variate versions by φ and φ_m as well. Then we approximate a function $f \in \mathcal{B}_{M/2}(\mathbb{R}^d)$ by the *d-dimensional regularized Shannon sampling formula*

$$(R_{\varphi,m} f)(\boldsymbol{x}) \coloneqq \sum_{\boldsymbol{\ell}\in\mathbb{Z}^d} f\big(\tfrac{\boldsymbol{\ell}}{L}\big)\operatorname{sinc}\big(L\pi\big(\boldsymbol{x}-\tfrac{\boldsymbol{\ell}}{L}\big)\big)\,\varphi_m\big(\boldsymbol{x}-\tfrac{\boldsymbol{\ell}}{L}\big), \quad \boldsymbol{x}\in\mathbb{R}^d. \tag{4.121}$$

As for the univariate version (4.74), this procedure is an interpolating approximation of f on the grid $\frac{1}{L}\,\mathbb{Z}^d$, i. e.,

$$(R_{\varphi,m} f)\big(\tfrac{\boldsymbol{k}}{L}\big) = f\big(\tfrac{\boldsymbol{k}}{L}\big), \quad \boldsymbol{k}\in\mathbb{Z}^d, \tag{4.122}$$

is fulfilled, since $\operatorname{sinc}(\pi \boldsymbol{k}) = 0$ for each $\boldsymbol{k} \in \mathbb{Z}^d \setminus \{\boldsymbol{0}\}$. Furthermore, the use of the compactly supported window function φ_m in (4.73) leads to localized sampling of the bandlimited function $f \in \mathcal{B}_{M/2}(\mathbb{R}^d)$, i. e., the computation of $(R_{\varphi,m} f)(\boldsymbol{x})$ for fixed $\boldsymbol{x} \in \mathbb{R}^d \setminus \frac{1}{L}\,\mathbb{Z}^d$ requires only $(2m+1)^d$ samples $f\big(\frac{\boldsymbol{\ell}}{L}\big)$, where $\boldsymbol{\ell} \in \mathbb{Z}^d$ fulfills the conditions $|\ell_t - L x_t| \le m$ for $t = 1, \ldots, d$.

Note that in comparison to the univariate regularized Shannon sampling formula (4.74) in the multivariate setting it is not sufficient to approximate f by $R_{\varphi,m} f$ in (4.121) only on the open sets $\frac{\boldsymbol{k}}{L} + \big(0,\, \frac{1}{L}\big)^d$, $\boldsymbol{k} \in \mathbb{Z}^d$, since by the interpolation property (4.122) we obtain equality only for the corners but not the whole edges of the respective hypercube. Hence, we have to approximate f by $R_{\varphi,m} f$ separately on each closed hypercube $\frac{\boldsymbol{k}}{L} + \big[0,\, \frac{1}{L}\big]^d$, $\boldsymbol{k} \in \mathbb{Z}^d$. For this reason, we also have to slightly enlarge the corresponding index set used for each hypercube, such that we now work with $\mathcal{J}_{m+1}^d \coloneqq \{-m, \ldots, m+1\}^d$, cf. (4.76). More precisely, by introducing the *d-variate regularized sinc function*

$$\psi(\boldsymbol{x}) \coloneqq \operatorname{sinc}(L\pi \boldsymbol{x})\, \varphi(\boldsymbol{x}), \quad \boldsymbol{x} \in \mathbb{R}^d, \tag{4.123}$$

analogous to (4.69), for $\boldsymbol{x} \in \big[0,\, \frac{1}{L}\big]^d$ the d-dimensional regularized Shannon sampling formula (4.121) reads as

$$(R_{\varphi,m} f)(\boldsymbol{x}) \coloneqq \sum_{\boldsymbol{\ell} \in \mathcal{J}_{m+1}^d} f\big(\tfrac{\boldsymbol{\ell}}{L}\big)\, \psi\big(\boldsymbol{x} - \tfrac{\boldsymbol{\ell}}{L}\big), \quad \boldsymbol{x} \in \big[0,\, \tfrac{1}{L}\big]^d.$$

Indeed, on any shifted hypercube $\frac{\boldsymbol{k}}{L} + \big[0,\, \frac{1}{L}\big]^d$ with $\boldsymbol{k} \in \mathbb{Z}^d$ the d-dimensional regularized Shannon sampling formula (4.121) has the form

$$(R_{\varphi,m} f)\big(\boldsymbol{x} + \tfrac{\boldsymbol{k}}{L}\big) = \sum_{\boldsymbol{\ell} \in \mathcal{J}_{m+1}^d} f\big(\tfrac{\boldsymbol{\ell}+\boldsymbol{k}}{L}\big)\, \psi\big(\boldsymbol{x} - \tfrac{\boldsymbol{\ell}}{L}\big), \quad \boldsymbol{x} \in \big[0,\, \tfrac{1}{L}\big]^d, \tag{4.124}$$

cf. (4.77).

Now for given $f \in \mathcal{B}_{M/2}(\mathbb{R}^d)$ and $\varphi \in \Phi$, we estimate the *uniform approximation error*

$$\|f - R_{\varphi,m} f\|_{C_0(\mathbb{R}^d)} = \max_{\boldsymbol{x} \in \mathbb{R}^d} \big|f(\boldsymbol{x}) - (R_{\varphi,m} f)(\boldsymbol{x})\big| \tag{4.125}$$

of the d-dimensional regularized Shannon sampling formula (4.121). Note that for $d = 1$ the following theorem coincides with Theorem 4.25.

Theorem 4.50. *Let* $f \in \mathcal{B}_{M/2}(\mathbb{R}^d)$ *with* $M \in \mathbb{N}$, $L = M(1+\lambda) \in \mathbb{N}$ *with* $\lambda \geq 0$ *and* $m \in \mathbb{N} \setminus \{1\}$. *Further let* $\varphi \in \Phi$ *with the truncated window function* (4.73) *as well as their* d*-variate versions* (2.13) *be given. Then the* d*-dimensional regularized Shannon sampling formula* (4.121) *satisfies*

$$\|f - R_{\varphi,m} f\|_{C_0(\mathbb{R}^d)} \leq \big(E_{\mathrm{r}}(\varphi, M, L, d) + E_{\mathrm{t}}(\varphi, m, L, d)\big)\, \|f\|_{L_2(\mathbb{R}^d)},$$

where the corresponding error constants are defined by

$$E_{\mathrm{r}}(\varphi, M, L, d) := M^{d/2} \max_{\boldsymbol{v} \in \left[-\frac{M}{2}, \frac{M}{2}\right]^d} \left| 1 - \prod_{t=1}^{d} \int_{v_t - L/2}^{v_t + L/2} \hat{\varphi}(u)\, \mathrm{d}u \right|, \tag{4.126}$$

$$E_{\mathrm{t}}(\varphi, m, L, d) := \frac{\sqrt{2d}\, L^{d/2}}{\pi} \left(\frac{1}{m^2}\, \varphi^2\big(\tfrac{m}{L}\big) + \frac{1}{L} \int_{m/L}^{\infty} \frac{\varphi^2(t)}{t^2}\, \mathrm{d}t \right)^{1/2}. \tag{4.127}$$

Proof. By (4.124) we approximate f by $R_{\varphi,m} f$ separately for each shifted hypercube $\frac{\boldsymbol{k}}{L} + [0, \frac{1}{L}]^d$, $\boldsymbol{k} \in \mathbb{Z}^d$, where we split the approximation error

$$f\big(\boldsymbol{x} + \tfrac{\boldsymbol{k}}{L}\big) - (R_{\varphi,m} f)\big(\boldsymbol{x} + \tfrac{\boldsymbol{k}}{L}\big) = e_{\mathrm{r}}\big(\boldsymbol{x} + \tfrac{\boldsymbol{k}}{L}\big) + e_{\mathrm{t},\boldsymbol{k}}(\boldsymbol{x}), \quad \boldsymbol{x} \in \big[0, \tfrac{1}{L}\big]^d,$$

into the *regularization error*

$$e_{\mathrm{r}}(\boldsymbol{x}) := f(\boldsymbol{x}) - \sum_{\boldsymbol{\ell} \in \mathbb{Z}^d} f\big(\tfrac{\boldsymbol{\ell}}{L}\big)\, \psi\big(\boldsymbol{x} - \tfrac{\boldsymbol{\ell}}{L}\big), \quad \boldsymbol{x} \in \mathbb{R}^d, \tag{4.128}$$

and the *truncation error*

$$e_{\mathrm{t},\boldsymbol{k}}(\boldsymbol{x}) := \sum_{\boldsymbol{\ell} \in \mathbb{Z}^d} f\big(\tfrac{\boldsymbol{\ell}+\boldsymbol{k}}{L}\big)\, \psi\big(\boldsymbol{x} - \tfrac{\boldsymbol{\ell}}{L}\big) - (R_{\varphi,m} f)(\boldsymbol{x}), \quad \boldsymbol{x} \in \big[0, \tfrac{1}{L}\big]^d. \tag{4.129}$$

Initially, we restrict ourselves to the hypercube $\big[0, \frac{1}{L}\big]^d$.

We start with the estimation of the regularization error (4.128). By the tensor product structure of ψ in (4.123) the d-dimensional Fourier transform $\hat{\psi}(\boldsymbol{v})$ equals the tensor product of one-dimensional Fourier transforms, see Remark 2.3, such that we obtain by (4.70) that

$$\hat{\psi}(\boldsymbol{v}) = \frac{1}{L^d} \prod_{t=1}^{d} \int_{v_t - L/2}^{v_t + L/2} \hat{\varphi}(u)\, \mathrm{d}u.$$

Using the shifting property of the Fourier transform, the Fourier transform of $\psi\big(\,\cdot - \frac{\boldsymbol{\ell}}{L}\big)$, $\boldsymbol{\ell} \in \mathbb{Z}^d$, reads as

$$\frac{1}{L^d}\,\mathrm{e}^{-2\pi\mathrm{i}\boldsymbol{v}\boldsymbol{\ell}/L} \prod_{t=1}^{d} \int_{v_t-L/2}^{v_t+L/2} \hat{\varphi}(u)\,\mathrm{d}u.$$

Therefore, the Fourier transform of the regularization error (4.128) has the form

$$\hat{e}_{\mathrm{r}}(\boldsymbol{v}) = \hat{f}(\boldsymbol{v}) - \sum_{\boldsymbol{\ell}\in\mathbb{Z}^d} \frac{1}{L^d}\, f\big(\tfrac{\boldsymbol{\ell}}{L}\big)\,\mathrm{e}^{-2\pi\mathrm{i}\boldsymbol{v}\boldsymbol{\ell}/L} \prod_{t=1}^{d} \int_{v_t-L/2}^{v_t+L/2} \hat{\varphi}(u)\,\mathrm{d}u. \tag{4.130}$$

Since $f \in \mathcal{B}_{M/2}(\mathbb{R}^d)$ and $L \geq M$ by assumption, we have

$$\operatorname{supp}(\hat{f}) \subseteq \big[-\tfrac{M}{2},\, \tfrac{M}{2}\big]^d \subset \big[-\tfrac{L}{2},\, \tfrac{L}{2}\big]^d.$$

Hence, the restriction of $\hat{f}$ to $\big[-\frac{L}{2},\, \frac{L}{2}\big]^d$ belongs to $L_2\big(\big[-\frac{L}{2},\, \frac{L}{2}\big]^d\big)$ and thus possesses the convergent L-periodic Fourier expansion

$$\hat{f}(\boldsymbol{v}) = \sum_{\boldsymbol{\ell}\in\mathbb{Z}^d} c_{\boldsymbol{\ell}}(\hat{f})\,\mathrm{e}^{2\pi\mathrm{i}\boldsymbol{v}\boldsymbol{\ell}/L}, \quad \boldsymbol{v} \in \big[-\tfrac{L}{2},\, \tfrac{L}{2}\big]^d,$$

with the Fourier coefficients

$$c_{\boldsymbol{\ell}}(\hat{f}) = \frac{1}{L^d} \int_{\left[-\frac{L}{2},\, \frac{L}{2}\right]^d} \hat{f}(\boldsymbol{v})\,\mathrm{e}^{-2\pi\mathrm{i}\boldsymbol{v}\boldsymbol{\ell}/L}\,\mathrm{d}\boldsymbol{v} = \frac{1}{L^d}\, f\left(-\tfrac{\boldsymbol{\ell}}{L}\right), \quad \boldsymbol{\ell} \in \mathbb{Z}^d.$$

In other words, since $f \in \mathcal{B}_{M/2}(\mathbb{R}^d)$ is bandlimited with bandwidth M, its Fourier transform $\hat{f}(\boldsymbol{v})$ with $\boldsymbol{v} \in \mathbb{Z}^d$ can be represented as

$$\hat{f}(\boldsymbol{v}) = \hat{f}(\boldsymbol{v})\,\chi_{\left[-\frac{M}{2},\, \frac{M}{2}\right]^d}(\boldsymbol{v}) = \left(\sum_{\boldsymbol{\ell}\in\mathbb{Z}^d} \frac{1}{L^d}\, f\big(\tfrac{\boldsymbol{\ell}}{L}\big)\,\mathrm{e}^{-2\pi\mathrm{i}\boldsymbol{v}\boldsymbol{\ell}/L} \right) \chi_{\left[-\frac{M}{2},\, \frac{M}{2}\right]^d}(\boldsymbol{v}). \tag{4.131}$$

Introducing the auxiliary function

$$\eta(\boldsymbol{v}) \coloneqq \chi_{\left[-\frac{M}{2},\, \frac{M}{2}\right]^d}(\boldsymbol{v}) - \prod_{t=1}^{d} \int_{v_t-L/2}^{v_t+L/2} \varphi(u)\,\mathrm{d}u,$$

cf. (4.72), we see by inserting (4.131) into (4.130) that $\hat{e}_{\mathrm{r}}(\boldsymbol{v}) = \hat{f}(\boldsymbol{v})\,\eta(\boldsymbol{v})$ and thereby $|\hat{e}_{\mathrm{r}}(\boldsymbol{v})| = |\hat{f}(\boldsymbol{v})|\,|\eta(\boldsymbol{v})|$. Thus, by inverse Fourier transform (4.4) we obtain

$$\begin{aligned} |e_{\mathrm{r}}(\boldsymbol{x})| &\le \int_{\mathbb{R}^d} |\hat{e}\mathrm{r}(\boldsymbol{v})|\,\mathrm{d}\boldsymbol{v} = \int_{\left[-\frac{M}{2},\,\frac{M}{2}\right]^d} |\hat{f}(\boldsymbol{v})|\,|\eta(\boldsymbol{v})|\,\mathrm{d}\boldsymbol{v} \\ &\le \max_{\boldsymbol{v}\in\left[-\frac{M}{2},\,\frac{M}{2}\right]^d} |\eta(\boldsymbol{v})| \int_{\left[-\frac{M}{2},\,\frac{M}{2}\right]^d} |\hat{f}(\boldsymbol{v})|\,\mathrm{d}\boldsymbol{v}. \end{aligned}$$

Using the Cauchy–Schwarz inequality and Parseval's identity, we see that

$$\begin{aligned} \int_{\left[-\frac{M}{2},\,\frac{M}{2}\right]^d} |\hat{f}(\boldsymbol{v})|\,\mathrm{d}\boldsymbol{v} &\le \left(\int_{\left[-\frac{M}{2},\,\frac{M}{2}\right]^d} 1^2\,\mathrm{d}\boldsymbol{v}\right)^{1/2} \left(\int_{\left[-\frac{M}{2},\,\frac{M}{2}\right]^d} |\hat{f}(\boldsymbol{v})|^2\,\mathrm{d}\boldsymbol{v}\right)^{1/2} \\ &= M^{d/2}\,\|\hat{f}\|_{L_2(\mathbb{R}^d)} = M^{d/2}\,\|f\|_{L_2(\mathbb{R}^d)}, \end{aligned}$$

which yields the estimate

$$\|e_{\mathrm{r}}\|_{C_0(\mathbb{R}^d)} \le E_{\mathrm{r}}(\varphi, M, L, d)\,\|f\|_{L_2(\mathbb{R}^d)}$$

with the error constant (4.126).

Now we estimate the truncation error (4.129). For $\boldsymbol{k} = \boldsymbol{0}$ the representation (4.124) implies

$$e_{\mathrm{t},\boldsymbol{0}}(\boldsymbol{x}) = \sum_{\boldsymbol{\ell}\in\mathbb{Z}^d\setminus\mathcal{J}_{m+1}^d} f\bigl(\tfrac{\boldsymbol{\ell}}{L}\bigr)\,\psi\bigl(\boldsymbol{x} - \tfrac{\boldsymbol{\ell}}{L}\bigr), \quad \boldsymbol{x} \in \bigl[0,\,\tfrac{1}{L}\bigr]^d.$$

Then by the Cauchy–Schwarz inequality and (4.9) it follows that

$$\begin{aligned} |e_{\mathrm{t},\boldsymbol{0}}(\boldsymbol{x})| &\le \left(\sum_{\boldsymbol{\ell}\in\mathbb{Z}^d\setminus\mathcal{J}_{m+1}^d} \bigl|f\bigl(\tfrac{\boldsymbol{\ell}}{L}\bigr)\bigr|^2\right)^{1/2} \left(\sum_{\boldsymbol{\ell}\in\mathbb{Z}^d\setminus\mathcal{J}_{m+1}^d} \bigl|\psi\bigl(\boldsymbol{x} - \tfrac{\boldsymbol{\ell}}{L}\bigr)\bigr|^2\right)^{1/2} \\ &\le L^{d/2}\,\|f\|_{L_2(\mathbb{R}^d)} \cdot \left(\sum_{\boldsymbol{\ell}\in\mathbb{Z}^d\setminus\mathcal{J}_{m+1}^d} \bigl|\psi\bigl(\boldsymbol{x} - \tfrac{\boldsymbol{\ell}}{L}\bigr)\bigr|^2\right)^{1/2}. \end{aligned}$$

Since

$$\mathbb{Z}^d \setminus \mathcal{J}_{m+1}^d \subseteq \bigcup_{t=1}^{d} \{\boldsymbol{\ell}\in\mathbb{Z}^d\colon\ \ell_t \in \mathbb{Z}\setminus\mathcal{J}_{m+1}\},$$

we conclude by (4.123), the product structure of $\bigl[\operatorname{sinc}(L\pi\boldsymbol{x}-\pi\boldsymbol{\ell})\bigr]^2$ and $\bigl[\varphi(\boldsymbol{x}-\frac{\boldsymbol{\ell}}{L})\bigr]^2$ as well as (4.10) that

$$\begin{aligned}\sum_{\boldsymbol{\ell}\in\mathbb{Z}^d\setminus\mathcal{J}_{m+1}^d}\bigl|\psi\bigl(\boldsymbol{x}-\tfrac{\boldsymbol{\ell}}{L}\bigr)\bigr|^2 &\le \sum_{t=1}^{d}\Biggl(\sum_{\ell\in\mathbb{Z}\setminus\mathcal{J}_{m+1}}\bigl|\psi\bigl(x_t-\tfrac{\ell}{L}\bigr)\bigr|^2\Biggr)\\ &\qquad\cdot\prod_{\substack{n=1\\ n\ne t}}\Biggl(\sum_{\ell\in\mathbb{Z}}\bigl[\operatorname{sinc}(L\pi x_n-\pi\ell)\bigr]^2\Biggr)\\ &\le \sum_{t=1}^{d} h_{m+1}(x_t)\cdot 1,\quad \boldsymbol{x}\in\bigl[0,\tfrac{1}{L}\bigr]^d,\end{aligned}$$

with the auxiliary function

$$h_{m+1}(x) \coloneqq \sum_{\ell\in\mathbb{Z}\setminus\mathcal{J}_{m+1}}\frac{1}{\pi^2\,|Lx-\ell|^2}\,\varphi^2\bigl(x-\tfrac{\ell}{L}\bigr)\ge 0,\quad x\in\bigl[0,\tfrac{1}{L}\bigr],$$

cf. (4.81). By analogy with (4.82) and (4.83) we can estimate

$$\begin{aligned}h_{m+1}(x) &\le \frac{2}{\pi^2}\sum_{\ell=m+1}^{\infty}\frac{\varphi^2(\frac{\ell}{L})}{\ell^2}\le\frac{2}{\pi^2}\sum_{\ell=m}^{\infty}\frac{\varphi^2(\frac{\ell}{L})}{\ell^2}\\ &\le\frac{2}{\pi^2}\left(\frac{\varphi^2(\frac{m}{L})}{m^2}+\frac{1}{L}\int_{m/L}^{\infty}\frac{\varphi^2(\frac{y}{L})}{y^2}\,\mathrm{d}y\right)\end{aligned}$$

for all $x\in[0,\frac{1}{L}]$, and hence we obtain

$$\max_{\boldsymbol{x}\in[0,\,1/L]^d}|e_{\mathrm{t},\mathbf{0}}(\boldsymbol{x})|\le E_{\mathrm{t}}(\varphi,m,L,d)\,\|f\|_{L_2(\mathbb{R}^d)}$$

with the error constant (4.127).

By the same technique, these error estimates can be obtained for each shifted hypercube $\frac{\boldsymbol{k}}{L}+\bigl[0,\frac{1}{L}\bigr]^d$ with arbitrary $\boldsymbol{k}\in\mathbb{Z}^d$, which completes the proof. ∎

Corollary 4.51. *Analogous to Corollary 4.26 the error estimate of Theorem 4.50 can be simplified, if the window function $\varphi \in \Phi$ vanishes on $\mathbb{R} \setminus \left[-\frac{m}{L}, \frac{m}{L}\right]$. Then the truncation errors $e_{\mathrm{t},\boldsymbol{k}}(x)$ are equal to zero for all $\boldsymbol{x} \in \left[0, \frac{1}{L}\right]^d$ and $\boldsymbol{k} \in \mathbb{Z}^d$, such that $E_{\mathrm{t}}(\varphi, m, L, d) = 0$ and we obtain the simple error estimate*

$$\|f - R_{\varphi,m} f\|_{C_0(\mathbb{R}^d)} \leq E_{\mathrm{r}}(\varphi, M, L, d)\, \|f\|_{L_2(\mathbb{R}^d)}.$$

Remark 4.52. As mentioned in Remark 4.27 for the univariate setting also the multivariate version in Corollary 4.51 applies to the modified B–spline window function (4.61), the sinh-type window function (4.62) and the continuous Kaiser–Bessel window function (4.63). Similarly, Corollary 4.51 does not hold for the Gaussian window function (4.60), since φ_{Gauss} does not vanish. ◇

Remark 4.53. Additionally, as in Remark 4.28, note that Theorem 4.50 could also be used to obtain a suitable error estimate for the constant window function (4.84). Since no regularization is done for the constant window function (4.84), we obviously have $E_{\mathrm{r}}(\varphi, M, L, d) = 0$ and therefore Theorem 4.50 provides the error estimate

$$\begin{aligned}\|f - R_{\mathrm{const},m} f\|_{C_0(\mathbb{R}^d)} &\leq E_{\mathrm{t}}(\varphi, m, L, d)\, \|f\|_{L_2(\mathbb{R}^d)} \\ &= \frac{\sqrt{2d}}{\pi}\, L^{d/2} \sqrt{\frac{1}{m} + \frac{1}{m^2}}\, \|f\|_{L_2(\mathbb{R}^d)},\end{aligned}$$

which can be seen as a consequence of a result in [MXZ09]. This again emphasizes that using localized sampling is not enough for obtaining fast convergence results for the Shannon sampling series (4.15), rather regularization is crucial as well. ◇

In order to apply Theorem 4.50 for a given window function $\varphi \in \Phi$, it merely remains to estimate the error constants (4.126) and (4.127). Since the estimation of the multivariate truncation error constant (4.127) reduces to the knowledge of the univariate truncation error constant (4.80), we now aim to simplify the multivariate regularization error constant (4.126) similarly. For this purpose, note that by definition (4.72) we have

$$\int_{v-L/2}^{v+L/2} \hat{\varphi}(u)\, \mathrm{d}u = 1 - \eta(v), \quad v \in \left[-\tfrac{M}{2}, \tfrac{M}{2}\right].$$

Consequently, with regard to (4.126), we consider the expression

$$1-\prod_{t=1}^{d}\int_{v_t-L/2}^{v_t+L/2}\hat{\varphi}(u)\,\mathrm{d}u = 1-\prod_{t=1}^{d}\big(1-\eta(v_t)\big), \quad \boldsymbol{v}=(v_1,\dots,v_d). \tag{4.132}$$

Lemma 4.54. *If the auxiliary function* $\eta\colon \left[-\frac{M}{2},\,\frac{M}{2}\right]\to\mathbb{R}$ *defined in* (4.72) *satisfies* $0\le\eta(v)\le 1$ *for* $v\in\left[-\frac{M}{2},\,\frac{M}{2}\right]$, *we have*

$$1-\prod_{t=1}^{d}\big(1-\eta(v_t)\big)\le\sum_{t=1}^{d}\eta(v_t), \quad \boldsymbol{v}=(v_1,\dots,v_d)\in\left[-\tfrac{M}{2},\,\tfrac{M}{2}\right]^d. \tag{4.133}$$

If η *in* (4.72) *at least fulfills* $|\eta(v)|\le 1$ *for* $v\in\left[-\frac{M}{2},\,\frac{M}{2}\right]$, *then we have*

$$\left|1-\prod_{t=1}^{d}\big(1-\eta(v_t)\big)\right|\le\frac{2^d-1}{d}\sum_{t=1}^{d}|\eta(v_t)|, \quad \boldsymbol{v}=(v_1,\dots,v_d)\in\left[-\tfrac{M}{2},\,\tfrac{M}{2}\right]^d, \tag{4.134}$$

where the factor $\frac{2^d-1}{d}$ *is best possible.*

Proof. The inequality (4.133) can easily be shown by induction. Obviously, the assertion (4.133) is valid for $d=1$ and $d=2$, since $\eta(v)\ge 0$, $v\in\left[-\frac{M}{2},\frac{M}{2}\right]$, by assumption. Assume that (4.133) holds for arbitrary $d\ge 2$. Then we conclude

$$\begin{aligned}1-\prod_{t=1}^{d+1}\big(1-\eta(v_t)\big) &= \left(1-\prod_{t=1}^{d}\big(1-\eta(v_t)\big)\right)+\eta(v_{d+1})\prod_{t=1}^{d}\big(1-\eta(v_t)\big)\\ &\le\sum_{t=1}^{d}\eta(v_t)+\eta(v_{d+1})\\ &=\sum_{t=1}^{d+1}\eta(v_t), (v_1,\dots,v_{d+1})\in\left[-\tfrac{M}{2},\,\tfrac{M}{2}\right]^{d+1},\end{aligned}$$

since $0\le 1-\eta(v)\le 1$ for $v\in\left[-\frac{M}{2},\frac{M}{2}\right]$ by assumption.

In case $|\eta(v)|\le 1$ for $v\in\left[-\frac{M}{2},\,\frac{M}{2}\right]$, the inequality (4.134) can be shown by the triangle inequality and the inequality of geometric and arithmetic

means $\sqrt[d]{x_1 \cdot \dots \cdot x_d} \le \frac{1}{d}(x_1 + \dots + x_d)$. Since (4.134) is obviously valid for $d = 1$, we demonstrate (4.134) only for $d = 2$ for simplicity. Here we have

$$\begin{aligned}\left|1 - \prod_{t=1}^{d} \big(1 - \eta(v_t)\big)\right| &= |\eta(v_1) + \eta(v_2) - \eta(v_1)\,\eta(v_2)| \\ &\le |\eta(v_1)| + |\eta(v_2)| + |\eta(v_1)\,\eta(v_2)| \\ &\le |\eta(v_1)| + |\eta(v_2)| + \sqrt{|\eta(v_1)\,\eta(v_2)|} \\ &\le |\eta(v_1)| + |\eta(v_2)| + \tfrac{1}{2}\big(|\eta(v_1)| + |\eta(v_2)|\big) \\ &= \tfrac{3}{2}\big(|\eta(v_1)| + |\eta(v_2)|\big).\end{aligned}$$

Analogously, the inequality (4.134) can be shown for $d > 2$. Moreover, the factor $\frac{2^d - 1}{d}$ is the best possible, since in case $\eta(v_t) = -1$, $t = 1, \dots, d$, we obtain equality in (4.134). ∎

Based on these properties, we can now simplify the estimate of the regularization error constant (4.126) from Theorem 4.50 as follows.

Corollary 4.55. *For a given window function $\varphi \in \Phi$ let $\eta\colon \big[-\frac{M}{2}, \frac{M}{2}\big] \to \mathbb{R}$ be its corresponding auxiliary function defined in* (4.72)*. Then the following holds.*

(i) If η in (4.72) *fulfills the condition $0 \le \eta(v) \le 1$ for $v \in \big[-\frac{M}{2}, \frac{M}{2}\big]$, then the error constant* (4.126) *can be bounded by*

$$E_{\mathrm{r}}(\varphi, M, L, d) \le d\, M^{d/2} \max_{v \in \left[-\frac{M}{2}, \frac{M}{2}\right]} \eta(v). \tag{4.135}$$

(ii) If η in (4.72) *fulfills the condition $|\eta(v)| \le 1$ for $v \in \big[-\frac{M}{2}, \frac{M}{2}\big]$, then the error constant* (4.126) *can be bounded by*

$$E_{\mathrm{r}}(\varphi, M, L, d) \le \big(2^d - 1\big)\, M^{d/2} \max_{v \in \left[-\frac{M}{2}, \frac{M}{2}\right]} |\eta(v)|. \tag{4.136}$$

Proof. (i) If for $\varphi \in \Phi$ the auxiliary function (4.72) fulfills the condition $0 \le \eta(v) \le 1$ for $v \in \big[-\frac{M}{2}, \frac{M}{2}\big]$, then we conclude by (4.126), (4.132) and (4.133) that

$$E_{\mathrm{r}}(\varphi, M, L, d) = M^{d/2} \max_{\boldsymbol{v} \in \left[-\frac{M}{2}, \frac{M}{2}\right]^d} \left|1 - \prod_{t=1}^{d} \int_{v_t - L/2}^{v_t + L/2} \hat{\varphi}(u)\,\mathrm{d}u\right|$$

$$= M^{d/2} \max_{\boldsymbol{v} \in \left[-\frac{M}{2}, \frac{M}{2}\right]^d} \left| 1 - \prod_{t=1}^{d} \big(1 - \eta(v_t)\big) \right|$$

$$\leq M^{d/2} \max_{\boldsymbol{v} \in \left[-\frac{M}{2}, \frac{M}{2}\right]^d} \left(\sum_{t=1}^{d} \eta(v_t) \right) = d\, M^{d/2} \max_{v \in \left[-\frac{M}{2}, \frac{M}{2}\right]} \eta(v).$$

(ii) If for $\varphi \in \Phi$ the auxiliary function (4.72) fulfills the condition $|\eta(v)| \leq 1$ for $v \in \left[-\frac{M}{2}, \frac{M}{2}\right]$, then we conclude by (4.126), (4.132) and (4.134) that

$$E_{\mathrm{r}}(\varphi, M, L, d) = M^{d/2} \max_{\boldsymbol{v} \in \left[-\frac{M}{2}, \frac{M}{2}\right]^d} \left| 1 - \prod_{t=1}^{d} \int_{v_t - L/2}^{v_t + L/2} \hat{\varphi}(u)\, \mathrm{d}u \right|$$

$$= M^{d/2} \max_{\boldsymbol{v} \in \left[-\frac{M}{2}, \frac{M}{2}\right]^d} \left| 1 - \prod_{t=1}^{d} \big(1 - \eta(v_t)\big) \right|$$

$$\leq \frac{2^d - 1}{d}\, M^{d/2} \max_{\boldsymbol{v} \in \left[-\frac{M}{2}, \frac{M}{2}\right]^d} \left(\sum_{t=1}^{d} |\eta(v_t)| \right)$$

$$= \big(2^d - 1\big)\, M^{d/2} \max_{v \in \left[-\frac{M}{2}, \frac{M}{2}\right]} |\eta(v)|.$$

This completes the proof. ■

Remark 4.56. As shown in (4.93) and (4.103), the Gaussian window function (4.60) and the B–spline window function (4.61) both satisfy the condition $0 \leq \eta(v) \leq 1$, i. e., for both window functions the estimate (4.135) can be applied.

Furthermore, it was demonstrated in (4.112) and (4.120), that the condition $|\eta(v)| \leq 1$ is satisfied for the sinh-type window function (4.62) and the continuous Kaiser–Bessel window function (4.63) with $\beta \geq \pi$, such that the estimate (4.136) can be applied for these window functions. ◇

Now, we will move on to the issue of numerical robustness. As seen in Theorem 4.7, if the samples $f\big(\frac{\boldsymbol{\ell}}{L}\big)$, $\boldsymbol{\ell} \in \mathbb{Z}^d$, of a bandlimited function $f \in \mathcal{B}_{M/2}(\mathbb{R}^d)$ are not known exactly, i. e., only erroneous samples $\tilde{f}_{\boldsymbol{\ell}} := f\big(\frac{\boldsymbol{\ell}}{L}\big) + \varepsilon_{\boldsymbol{\ell}}$ with $|\varepsilon_{\boldsymbol{\ell}}| \leq \varepsilon$, $\boldsymbol{\ell} \in \mathbb{Z}^d$, with sufficiently small $\varepsilon > 0$ are known, the corresponding Shannon sampling series (4.15) may differ

appreciably from f. Analogous to (4.85) we denote the d-dimensional regularized Shannon sampling formula with erroneous samples $\tilde{f}_\ell$ by

$$(R_{\varphi,m}\tilde{f})(\boldsymbol{x}) = \sum_{\boldsymbol{\ell}\in\mathbb{Z}^d} \tilde{f}_{\boldsymbol{\ell}}\, \operatorname{sinc}\big(L\pi\,\big(\boldsymbol{x}-\tfrac{\boldsymbol{\ell}}{L}\big)\big)\,\varphi_m\big(\boldsymbol{x}-\tfrac{\boldsymbol{\ell}}{L}\big), \quad \boldsymbol{x}\in\mathbb{R}^d. \quad (4.137)$$

Then, in contrast to the Shannon sampling series (4.15), the d-dimensional regularized Shannon sampling formula (4.121) is numerically robust, i. e., the *uniform perturbation error*

$$\|R_{\varphi,m}\tilde{f} - R_{\varphi,m}f\|_{C_0(\mathbb{R}^d)} \quad (4.138)$$

is small, as the following theorem shows. Note that for $d=1$ the following theorem coincides with Theorem 4.29.

Theorem 4.57. *Let $f\in\mathcal{B}_{M/2}(\mathbb{R}^d)$ with $M\in\mathbb{N}$, $L=M(1+\lambda)\in\mathbb{N}$ with $\lambda\geq 0$ and $m\in\mathbb{N}\setminus\{1\}$. Further let $\varphi\in\Phi$ be a univariate window function with its d-variate version (2.13). Moreover, let $\tilde{f}_{\boldsymbol{\ell}} = f\big(\frac{\boldsymbol{\ell}}{L}\big)+\varepsilon_{\boldsymbol{\ell}}$, $\boldsymbol{\ell}\in\mathbb{Z}^d$, be given, where we have $|\varepsilon_{\boldsymbol{\ell}}|\leq\varepsilon$ for all $\boldsymbol{\ell}\in\mathbb{Z}^d$ and $0<\varepsilon<1$. Then the d-dimensional regularized Shannon sampling formula (4.121) satisfies*

$$\begin{aligned}\|R_{\varphi,m}\tilde{f} - R_{\varphi,m}f\|_{C_0(\mathbb{R}^d)} &\leq \varepsilon\,\big(2+L\,\hat{\varphi}(0)\big)^d,\\ \|f-R_{\varphi,m}\tilde{f}\|_{C_0(\mathbb{R}^d)} &\leq \|f-R_{\varphi,m}f\|_{C_0(\mathbb{R}^d)} + \varepsilon\,\big(2+L\,\hat{\varphi}(0)\big)^d.\end{aligned} \quad (4.139)$$

Proof. By (4.124) we denote the error on each shifted hypercube $\frac{\boldsymbol{k}}{L}+\big[0,\,\frac{1}{L}\big]^d$ with $\boldsymbol{k}\in\mathbb{Z}^d$ and $\boldsymbol{x}\in\big[0,\,\frac{1}{L}\big]^d$ as

$$\tilde{e}_{\boldsymbol{k}}(\boldsymbol{x}) \coloneqq (R_{\varphi,m}\tilde{f})\big(\boldsymbol{x}+\tfrac{\boldsymbol{k}}{L}\big) - (R_{\varphi,m}f)\big(\boldsymbol{x}+\tfrac{\boldsymbol{k}}{L}\big) = \sum_{\boldsymbol{\ell}\in\mathcal{J}_{m+1}^d} \varepsilon_{\boldsymbol{\ell}+\boldsymbol{k}}\,\psi\big(\boldsymbol{x}-\tfrac{\boldsymbol{\ell}}{L}\big).$$

We start with the hypercube $\big[0,\,\frac{1}{L}\big]^d$. Using $|\varepsilon_{\boldsymbol{\ell}}|\leq\varepsilon$, the definition (4.123), and the non-negativity as well as the product structure of $\varphi\in\Phi$, we receive

$$\begin{aligned}\big|\tilde{e}_{\boldsymbol{0}}(\boldsymbol{x})\big| &\leq \sum_{\boldsymbol{\ell}\in\mathcal{J}_{m+1}^d} |\varepsilon_{\boldsymbol{\ell}}|\,\big|\psi\big(\boldsymbol{x}-\tfrac{\boldsymbol{\ell}}{L}\big)\big|\\ &\leq \varepsilon \sum_{\boldsymbol{\ell}\in\mathcal{J}_{m+1}^d} \varphi\big(\boldsymbol{x}-\tfrac{\boldsymbol{\ell}}{L}\big) = \varepsilon \prod_{t=1}^d \Big(\sum_{\ell\in\mathcal{J}_{m+1}} \varphi\big(x_t-\tfrac{\ell}{L}\big)\Big).\end{aligned}$$

Analogous to the proof of Theorem 4.29 it can be shown that for $\varphi \in \Phi$ and $x \in \left[0,\, \frac{1}{L}\right]$ we have

$$\sum_{\ell \in \mathcal{J}_{m+1}} \varphi\big(x - \tfrac{\ell}{L}\big) \le 2 \sum_{\ell=0}^{m} \varphi\big(\tfrac{\ell}{L}\big) < 2\,\varphi(0) + 2L \int_0^{m/L} \varphi(t)\,\mathrm{d}t \le 2\,\varphi(0) + L\,\hat{\varphi}(0).$$

Thus, we obtain

$$\max_{\boldsymbol{x} \in [0,\, 1/L]^d} \big|\tilde{e}_{\boldsymbol{0}}(\boldsymbol{x})\big| \le \varepsilon \left(2 + L\,\hat{\varphi}(0)\right)^d.$$

By the same technique, this error estimate can be shown for each shifted hypercube $\frac{\boldsymbol{k}}{L} + \left[0,\, \frac{1}{L}\right]^d$ with arbitrary $\boldsymbol{k} \in \mathbb{Z}^d$.

In addition, the triangle inequality yields (4.139), which completes the proof. ∎

In the remainder of this section we specify the results of Theorems 4.50 and 4.57 for the window functions in Remark 4.22. For this purpose, it merely remains to estimate the regularization error constant (4.126), the truncation error constant (4.127) as well as $\hat{\varphi}(0)$ for the different window functions, which shall be done in the following subsections.

Gaussian window function

Firstly, we consider the d-dimensional regularized Shannon sampling formula (4.121) with the Gaussian window function (4.60) and show that its uniform approximation error (4.125) decays exponentially with respect to m. Note that in case $d = 1$ the following theorem coincides with Theorem 4.33.

Theorem 4.58. *Let $f \in \mathcal{B}_{M/2}(\mathbb{R}^d)$ with $M \in \mathbb{N}$, $L = M\,(1+\lambda) \in \mathbb{N}$ with $\lambda > 0$ and $m \in \mathbb{N} \setminus \{1\}$ be given. Then the d-dimensional regularized Shannon sampling formula* (4.121) *using the Gaussian window function* (4.60) *and $\alpha = \frac{1}{M}\sqrt{\frac{m}{\pi(1+\lambda)\lambda}}$ satisfies the error estimate*

$$\|f - R_{\mathrm{Gauss},m} f\|_{C_0(\mathbb{R}^d)} \le \frac{d\,M^{d/2}\sqrt{2m(1+\lambda)} + \sqrt{2d}\,L^{d/2}\sqrt{\lambda(1+m)}}{m\pi\sqrt{\lambda}}\, \mathrm{e}^{-m\pi\lambda/(2+2\lambda)}\, \|f\|_{L_2(\mathbb{R}^d)}. \tag{4.140}$$

Proof. By Theorem 4.50 we only have to estimate the error constants (4.126) and (4.127) for the Gaussian window function (4.60). For the regularization error constant (4.126) we have seen in Corollary 4.55 and Remark 4.56 that this can easily be done by (4.135), i. e., we only have to consider the univariate function (4.72). Since the truncation error constant (4.127) also depends only on the univariate window function $\varphi \in \Phi$, and these univariate functions have already been estimated in Theorem 4.33, this completes the proof. ∎

Now we show that the d-dimensional regularized Shannon sampling formula with the Gaussian window function (4.60) is numerically robust with respect to noisy samples and that the uniform perturbation error (4.86) only grows as $\mathcal{O}(m^{d/2})$. Note that in case $d = 1$ the following theorem coincides with Theorem 4.36.

Theorem 4.59. *Let $f \in \mathcal{B}_{M/2}(\mathbb{R}^d)$ with $M \in \mathbb{N}$, $L = (1+\lambda)\,M \in \mathbb{N}$ with $\lambda > 0$ and $m \in \mathbb{N} \setminus \{1\}$ be given. Further let $R_{\mathrm{Gauss},m}\tilde{f}$ be defined as in (4.137) with the noisy samples $\tilde{f}_{\boldsymbol{\ell}} = f\big(\frac{\boldsymbol{\ell}}{L}\big) + \varepsilon_{\boldsymbol{\ell}}$, where $|\varepsilon_{\boldsymbol{\ell}}| \le \varepsilon$ for all $\boldsymbol{\ell} \in \mathbb{Z}^d$ and $0 < \varepsilon \ll 1$. Then the d-dimensional regularized Shannon sampling formula (4.121) using the Gaussian window function (4.60) and $\alpha = \frac{1}{M}\sqrt{\frac{m}{\pi(1+\lambda)\lambda}}$ satisfies*

$$\|R_{\mathrm{Gauss},m}\tilde{f} - R_{\mathrm{Gauss},m} f\|_{C_0(\mathbb{R}^d)} \le \varepsilon \left(2 + \sqrt{\frac{2+2\lambda}{\lambda}}\,\sqrt{m}\right)^d. \qquad (4.141)$$

Proof. By Theorem 4.57 we only need to compute $\hat{\varphi}_{\mathrm{Gauss}}(0)$ for the Gaussian window function (4.60), which has already been done in Theorem 4.36. ∎

We remark that the triangle inequality combined with Theorems 4.58 and 4.59 also implies an estimate on the perturbation error $\|f - R_{\mathrm{Gauss},m}\tilde{f}\|_{C_0(\mathbb{R}^d)}$, cf. (4.139).

B–spline window function

Secondly, we consider the d-dimensional regularized Shannon sampling formula (4.121) with the modified B–spline window function (4.61) and show that its uniform approximation error (4.125) decays exponentially

with respect to m, if the oversampling condition (4.102) is fulfilled. Note that in case $d = 1$ the following theorem coincides with Theorem 4.40.

Theorem 4.60. *Let $f \in \mathcal{B}_{M/2}(\mathbb{R}^d)$ with $M \in \mathbb{N}$, $L = M(1+\lambda) \in \mathbb{N}$ and $m \in \mathbb{N} \setminus \{1\}$ be given, where $\lambda > 0$ fulfills the oversampling condition (4.102). Then the d-dimensional regularized Shannon sampling formula (4.121) using the modified B–spline window function (4.61) and $s = \lceil \frac{m+1}{2} \rceil$ satisfies the error estimate*

$$\|f - R_{\mathrm{B},m} f\|_{C_0(\mathbb{R}^d)} \leq \frac{3d\sqrt{sM^d}}{\sqrt{2}\,(2s-1)\,\pi}\, \mathrm{e}^{-m\,(\ln(\pi m\lambda) - \ln(2s(1+\lambda)))}\, \|f\|_{L_2(\mathbb{R}^d)}. \tag{4.142}$$

Proof. By Corollary 4.51 we only have to estimate the regularization error constant (4.126) for the modified B–spline window function (4.61). As seen in Corollary 4.55 and Remark 4.56 this can easily be done by (4.135), i. e., we only have to consider the univariate function (4.72). Since this function has already been estimated in Theorem 4.40, this completes the proof. ∎

Now we show that the d-dimensional regularized Shannon sampling formula with the modified B–spline window function (4.61) is numerically robust with respect to noisy samples and that the uniform perturbation error (4.138) only grows as $\mathcal{O}(m^{d/2})$. Note that in case $d = 1$ the following theorem coincides with Theorem 4.41.

Theorem 4.61. *Let $f \in \mathcal{B}_{M/2}(\mathbb{R}^d)$ with $M \in \mathbb{N}$, $L = (1+\lambda)M \in \mathbb{N}$ with $\lambda > 0$ and $m \in \mathbb{N} \setminus \{1\}$ be given. Further let $R_{\mathrm{B},m}\tilde{f}$ be as in (4.137) with the noisy samples $\tilde{f}_{\boldsymbol{\ell}} = f\big(\frac{\boldsymbol{\ell}}{L}\big) + \varepsilon_{\boldsymbol{\ell}}$, where $|\varepsilon_{\boldsymbol{\ell}}| \leq \varepsilon$ for all $\boldsymbol{\ell} \in \mathbb{Z}^d$ and $0 < \varepsilon \ll 1$. Then the d-dimensional regularized Shannon sampling formula (4.121) using the B–spline window function (4.61) and $s = \lceil \frac{m+1}{2} \rceil$ satisfies*

$$\|R_{\mathrm{B},m}\tilde{f} - R_{\mathrm{B},m} f\|_{C_0(\mathbb{R}^d)} \leq \varepsilon \big(2 + \tfrac{3}{2}\sqrt{m}\big)^d. \tag{4.143}$$

Proof. By Theorem 4.57 we only need to compute $\hat{\varphi}_{\mathrm{B}}(0)$ for the B–spline window function (4.61), which has already been done in Theorem 4.41. ∎

We remark that the triangle inequality combined with Theorems 4.60 and 4.61 also implies an estimate on the perturbation error $\|f - R_{\mathrm{B},m}\tilde{f}\|_{C_0(\mathbb{R}^d)}$, cf. (4.139).

sinh-type window function

We proceed with the d-dimensional regularized Shannon sampling formula (4.121) with the sinh-type window function (4.62) and show that its uniform approximation error (4.125) decays exponentially with respect to m. Note that in case $d = 1$ the following theorem coincides with Theorem 4.44.

Theorem 4.62. *Let $f \in \mathcal{B}_{M/2}(\mathbb{R}^d)$ with $M \in \mathbb{N}$, $L = M(1+\lambda) \in \mathbb{N}$ with $\lambda > 0$ and $m \in \mathbb{N} \setminus \{1\}$ be given. Then the d-dimensional regularized Shannon sampling formula* (4.121) *using the* sinh*-type window function* (4.62) *and $\beta = \frac{\pi m \lambda}{1+\lambda}$ satisfies the error estimate*

$$\|f - R_{\sinh,m} f\|_{C_0(\mathbb{R}^d)} \leq \left(2^d - 1\right) M^{d/2} \, \mathrm{e}^{-m\pi\lambda/(1+\lambda)} \, \|f\|_{L_2(\mathbb{R}^d)}. \quad (4.144)$$

Proof. By Corollary 4.51 we only have to estimate the regularization error constant (4.126) for the sinh-type window function (4.62). As seen in Corollary 4.55 and Remark 4.56 this can easily be done by (4.136), i. e., we only have to consider the univariate function (4.72). Since this function has already been estimated in Theorem 4.44, this completes the proof. ∎

Now we show that the d-dimensional regularized Shannon sampling formula with the sinh-type window function (4.62) is numerically robust with respect to noisy samples and that the uniform perturbation error (4.86) only grows as $\mathcal{O}(m^{d/2})$. Note that in case $d = 1$ the following theorem coincides with Theorem 4.45.

Theorem 4.63. *Let $f \in \mathcal{B}_{M/2}(\mathbb{R}^d)$ with $M \in \mathbb{N}$, $L = (1+\lambda) M \in \mathbb{N}$ with $\lambda > 0$ and $m \in \mathbb{N} \setminus \{1\}$ be given. Further let $R_{\sinh,m}\tilde{f}$ be defined as in* (4.137) *with the noisy samples $\tilde{f}_{\boldsymbol{\ell}} = f\left(\frac{\boldsymbol{\ell}}{L}\right) + \varepsilon_{\boldsymbol{\ell}}$, where $|\varepsilon_{\boldsymbol{\ell}}| \leq \varepsilon$ for all $\boldsymbol{\ell} \in \mathbb{Z}^d$ and $0 < \varepsilon \ll 1$. Then the d-dimensional regularized Shannon sampling formula* (4.121) *using the* sinh*-type window function* (4.62) *and $\beta = \frac{\pi m \lambda}{1+\lambda}$ satisfies*

$$\|R_{\sinh,m}\tilde{f} - R_{\sinh,m} f\|_{C_0(\mathbb{R}^d)} \leq \varepsilon \left(2 + \sqrt{\frac{2+2\lambda}{\lambda}} \, \frac{1}{1 - \mathrm{e}^{-2\beta}} \, \sqrt{m}\right)^d. \quad (4.145)$$

Proof. By Theorem 4.57 we only need to compute $\hat{\varphi}_{\sinh}(0)$ for the sinh-type window function (4.62), which has already been done in Theorem 4.45. ∎

We remark that the triangle inequality combined with Theorems 4.62 and 4.63 also implies an estimate on the perturbation error $\|f - R_{\sinh,m}\tilde{f}\|_{C_0(\mathbb{R}^d)}$, cf. (4.139).

Continuous Kaiser–Bessel window function

Finally, we consider the d-dimensional regularized Shannon sampling formula (4.121) with the continuous Kaiser–Bessel window function (4.63) and show that its uniform approximation error (4.125) decays exponentially with respect to m. Note that in case $d = 1$ the following theorem coincides with Theorem 4.48.

Theorem 4.64. *Let $f \in \mathcal{B}_{M/2}(\mathbb{R}^d)$ with $M \in \mathbb{N}$, $L = M(1+\lambda) \in \mathbb{N}$ with $\lambda \geq \frac{1}{m-1}$ and $m \in \mathbb{N} \setminus \{1\}$ be given. Then the d-dimensional regularized Shannon sampling formula (4.121) using the continuous Kaiser–Bessel window function (4.63) and $\beta = \frac{\pi m \lambda}{1+\lambda}$ satisfies the error estimate*

$$\begin{aligned} &\|f - R_{\mathrm{cKB},m} f\|_{C_0(\mathbb{R}^d)} \\ &\quad \leq (2^d - 1)\, M^{d/2}\, \frac{7\pi m\lambda(1+\lambda+4m\lambda)}{4\,(1+\lambda)^2}\, \mathrm{e}^{-m\pi\lambda/(1+\lambda)}\, \|f\|_{L_2(\mathbb{R}^d)}. \end{aligned} \tag{4.146}$$

Proof. By Corollary 4.51 we only have to estimate the regularization error constant (4.126) for the continuous Kaiser–Bessel window function (4.63). As seen in Corollary 4.55 and Remark 4.56 this can easily be done by (4.136), i. e., we only have to consider the univariate function (4.72). Since this function has already been estimated in Theorem 4.48, this completes the proof. ∎

Now we show that the d-dimensional regularized Shannon sampling formula with the continuous Kaiser–Bessel window function (4.63) is numerically robust with respect to noisy samples and that the uniform perturbation error (4.86) only grows as $\mathcal{O}(m^{d/2})$. Note that in case $d = 1$ the following theorem coincides with Theorem 4.49.

Theorem 4.65. *Let $f \in \mathcal{B}_{M/2}(\mathbb{R}^d)$ with $M \in \mathbb{N}$, $L = (1+\lambda)M \in \mathbb{N}$ with $\lambda > 0$ and $m \in \mathbb{N} \setminus \{1\}$ be given. Further let $R_{\mathrm{cKB},m}\tilde{f}$ be defined as in (4.137) with the noisy samples $\tilde{f}_{\boldsymbol{\ell}} = f\big(\frac{\boldsymbol{\ell}}{L}\big) + \varepsilon_{\boldsymbol{\ell}}$, where $|\varepsilon_{\boldsymbol{\ell}}| \leq \varepsilon$ for all $\boldsymbol{\ell} \in \mathbb{Z}^d$ and $0 < \varepsilon \ll 1$. Then the d-dimensional regularized Shannon*

sampling formula (4.121) *using the continuous Kaiser–Bessel window function* (4.63) *and* $\beta = \frac{\pi m \lambda}{1+\lambda}$ *satisfies*

$$\|R_{\mathrm{cKB},m}\tilde{f} - R_{\mathrm{cKB},m} f\|_{C_0(\mathbb{R}^d)} \leq \varepsilon \left(2 + \sqrt{\frac{2+2\lambda}{\lambda}}\sqrt{m}\right)^d. \tag{4.147}$$

Proof. By Theorem 4.57 we only need to compute $\hat{\varphi}_{\mathrm{cKB}}(0)$ for the continuous Kaiser–Bessel window function (4.63), which has already been done in Theorem 4.49. ∎

We remark that the triangle inequality combined with Theorems 4.64 and 4.65 also implies an estimate on the perturbation error $\|f - R_{\mathrm{cKB},m}\tilde{f}\|_{C_0(\mathbb{R}^d)}$, cf. (4.139).

Summary

In summary, we have shown that for the window functions mentioned in Remark 4.22 the uniform approximation error (4.125) of the regularized Shannon sampling formula (4.121) can be bounded for all $d \in \mathbb{N}$, analogously to Section 4.3.2. For small $d \in \{1, 2, 3\}$ this is also useful in practice, see the numerical experiments in Section 4.5. Note, however, that for large values of d these error constants may not be appropriate due to the exponential term $M^{d/2}$. We remark that this behavior is similar to what is known for the FFT and the NFFT in Section 2 for dimensions $d > 1$.

4.5 Numerical examples & summary

Concluding this chapter, we have a look at some numerical examples, cf. [KPT22, KPT24]. Besides illustrating the nonrobustness of classical Shannon sampling series proven in Section 4.2 (see Example 4.66), we also visualize the error decay rates shown for the regularization using the frequency window functions considered in Section 4.3.1 (see Examples 4.67 and 4.68) as well as the spatial window functions studied in Sections 4.3.2 and 4.4 (see Examples 4.69 – 4.77). Finally, in a direct comparison of these methods (see Example 4.78), we demonstrate that this second approach using window functions in spatial domain is indeed more powerful as it produces much smaller errors using the same amount of samples.

Poor convergence of Shannon sampling sums

We start by visualizing that the convergence of the classical Shannon sampling series (4.15) may break down completely in the presence of noise in the samples.

Example 4.66. First of all, we exemplify the error bounds of the perturbation error in Theorem 4.7, similar to [KPT24, Figure 2.1]. Since the norm $\|\tilde{f} - f\|_{C_0(\mathbb{R}^d)}$ as well as the lower and upper bounds (4.29) and (4.27) do not depend on the actual choice of the function $f \in \mathcal{B}_{M/2}(\mathbb{R}^d)$, it is sufficient to consider only the sums (4.31) when using the special error terms (4.28). Note that by the tensor product structure of the sign and the sinc function (3.31) we may rewrite (4.31) for all $\boldsymbol{x} \in \mathbb{R}^d$ as

$$\tilde{f}(\boldsymbol{x}) - f(\boldsymbol{x}) = \varepsilon \prod_{t=1}^{d} \left(\sum_{k_t=-T}^{T} \operatorname{sign}\big(\operatorname{sinc}(\tfrac{\pi}{2} - \pi k_t)\big) \operatorname{sinc}(L\pi x_t - \pi k_t) \right).$$

Therefore, the computation of the multivariate approximation error

$$\begin{aligned} &\max_{\boldsymbol{x}\in[-1,\,1]^d} \left|\tilde{f}(\boldsymbol{x}) - f(\boldsymbol{x})\right| \\ &\quad = \varepsilon \max_{\boldsymbol{x}\in[-1,\,1]^d} \left| \prod_{t=1}^{d} \left(\sum_{k_t=-T}^{T} \operatorname{sign}\big(\operatorname{sinc}(\tfrac{\pi}{2} - \pi k_t)\big) \operatorname{sinc}(L\pi x_t - \pi k_t) \right) \right| \\ &\quad = \varepsilon \left(\max_{x\in[-1,\,1]} \left| \sum_{k=-T}^{T} \operatorname{sign}\big(\operatorname{sinc}(\tfrac{\pi}{2} - \pi k)\big) \operatorname{sinc}(L\pi x - \pi k) \right| \right)^d \end{aligned} \tag{4.148}$$

reduces to computing its univariate analogue, similar to the lower and upper bounds (4.29) and (4.27), respectively.

In this experiment the maximum approximation error (4.148) is estimated by evaluation at equidistant points $x_s = -1 + \frac{s}{S} \in [-1,\,1]$, $s = 0, \ldots, 2S$, with $S = 10^5$. For this purpose, we fix the bandwidth $M = 128$ and a maximum perturbation of $\varepsilon = 10^{-3}$, and consider the error behavior for increasing truncation parameters $T \in \mathbb{N}$, and several $L = M(1+\lambda)$ with oversampling parameters $\lambda \in \{0, 0.5, 1, 2\}$. The respective results for $T = 2^c$, $c \in \{0, \ldots, 15\}$, are depicted in Figure 4.14, while Figure 4.13 displays a detail for $T \in \{1, \ldots, 10\}$. As mentioned before, we recognize that the norm $\|\tilde{f} - f\|_{C_0(\mathbb{R}^d)}$ does not depend on the choice of the oversampling

parameter $\lambda = \frac{L-M}{M} \geq 0$. It can clearly be seen that the numerical outcomes perfectly fit the theoretical bounds, which are indeed very close to each other, see Figure 4.13. However, since for increasing dimension d the maximum approximation error (4.148) rises exponentially, Figure 4.14 also illustrates that for $T \to \infty$ the error behavior shown in Theorem 4.7 is not satisfactory and therefore the convergence of the Shannon sampling series (4.15) may even break down completely in the presence of noise in the samples $f\left(\frac{\boldsymbol{k}}{L}\right)$, $\boldsymbol{k} \in \mathbb{Z}^d$. ◇

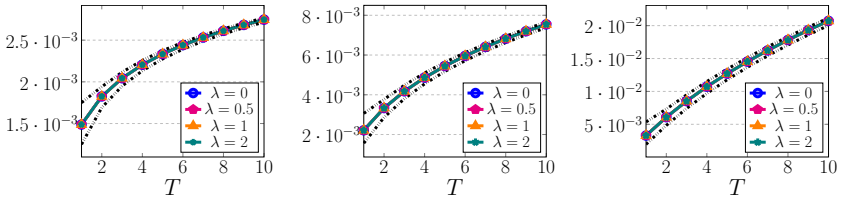

(a) $d = 1$ (b) $d = 2$ (c) $d = 3$

Figure 4.13: The maximum approximation error (4.148) as well as its lower and upper bounds (4.29) and (4.27), respectively, for $T \in \{1, \ldots, 10\}$, and $L = M(1 + \lambda)$ with $\lambda \in \{0, 0.5, 1, 2\}$, where $M = 128$ and $\varepsilon = 10^{-3}$ are chosen.

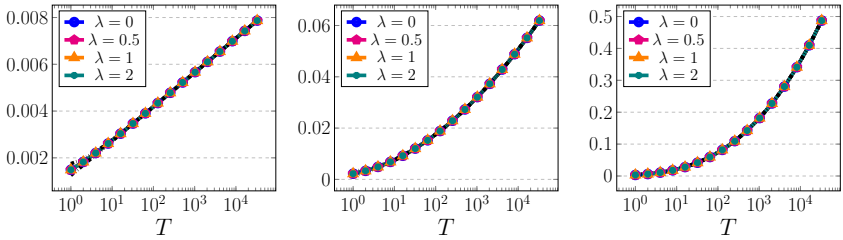

(a) $d = 1$ (b) $d = 2$ (c) $d = 3$

Figure 4.14: The maximum approximation error (4.148) as well as its lower and upper bounds (4.29) and (4.27), respectively, for $T = 2^c$, $c \in \{0, \ldots, 15\}$, and $L = M(1 + \lambda)$ with $\lambda \in \{0, 0.5, 1, 2\}$, where $M = 128$ and $\varepsilon = 10^{-3}$ are chosen.

Regularization with a window function in frequency domain

Next, we proceed with the illustration of the theoretical results regarding the regularization using the frequency window functions from Section 4.3.1. More precisely, in the following two examples we verify the error bounds of Theorems 4.14 and 4.15, and compare the frequency window functions considered throughout Section 4.3.1.

We start examining the linear frequency window ψ_{lin} in (4.45).

Example 4.67. As in [KPT24, Example 3.5], we now visualize the error bound of Theorem 4.14, i. e., for a given function $f \in \mathcal{B}_{M/2}(\mathbb{R})$ with $L = M(1+\lambda)$, $\lambda > 0$, we show that for the linear frequency window function ψ_{lin} in (4.45) the approximation error satisfies the estimate (4.46). For this purpose, the maximum approximation error

$$\max_{x \in [-1,\,1]} \left| f(x) - (P_{\mathrm{lin},T} f)(x) \right| \tag{4.149}$$

is estimated by evaluating the given function f as well as its approximation $P_{\mathrm{lin},T} f$, cf. (4.38), at equidistant points $x_s = -1 + \frac{s}{S} \in [-1,\,1]$, $s = 0, \ldots, 2S$, with $S = 10^5$. In this experiment we study the function $f(x) = \sqrt{M}\,\mathrm{sinc}(M\pi x)$, $x \in \mathbb{R}$, such that $\|f\|_{L_2(\mathbb{R})} = 1$. More specifically, we fix $M = 128$ and consider the error behavior for increasing truncation parameters $T \in \mathbb{N}$ and several oversampling parameters $\lambda \in \{0.5, 1, 2\}$. The corresponding results are depicted in Figure 4.15. Note that the error bound in (4.40) is only valid for $T > L$. Therefore, we have additionally marked the point $T = L$ for each λ as a vertical dash-dotted line. It can easily be seen that the numerical error results are also much better when $T > L$. Note, however, that increasing the oversampling parameter λ requires a much larger truncation parameter T to obtain errors of the same size. Hence, for the regularization with the linear frequency window function ψ_{lin} in (4.45) a small oversampling $\lambda > 0$ is desirable. ◇

As the error bound of Theorem 4.15 applies not only to the cubic frequency window function ψ_{cub} in (4.48) but also to the raised cosine frequency window function ψ_{cos} in (4.51) and the convolutional frequency window function $\psi_{\mathrm{conv},2}$ in (4.57), the next example combines the verification of this error bound with the comparison of all frequency window functions considered in Section 4.3.1.

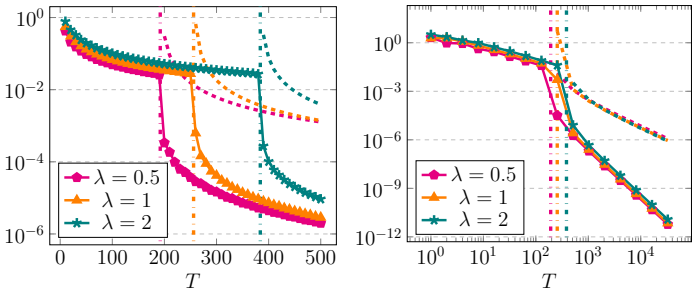

(a) $T \in \{10, 20, \dots, 500\}$ (b) $T = 2^c$, $c \in \{0, \dots, 15\}$

Figure 4.15: Maximum approximation error (4.149) (solid) and error constant (4.40) (dashed) using the linear frequency window ψ_{lin} from (4.45) in (4.38) for the function $f(x) = \sqrt{M}\,\operatorname{sinc}(M\pi x)$ with $M = 128$, $\lambda \in \{0.5, 1, 2\}$, and different $T \in \mathbb{N}$.

Example 4.68. Similar to [KPT24, Section 5], we compare the behavior of the regularization in frequency domain $P_{\psi,T} f$ in (4.38) of Section 4.3.1 to the classical Shannon sampling sums $S_T f$ in (4.12), i. e., for a given function $f \in \mathcal{B}_{M/2}(\mathbb{R})$ with $L = M(1+\lambda)$, $\lambda > 0$, we consider the approximation errors

$$\max_{x \in [-1,\,1]} \big| f(t) - (S_T f)(x) \big| \quad \text{and} \quad \max_{x \in [-1,\,1]} \big| f(x) - (P_{\psi,T} f)(x) \big| \tag{4.150}$$

for $\psi \in \{\psi_{\text{lin}}, \psi_{\text{cub}}, \psi_{\cos}, \psi_{\text{conv},2}, \psi_{\text{conv},3}, \psi_{\text{conv},4}, \psi_{\text{conv},\infty}, \psi_{\text{rat}}\}$, cf. (4.45), (4.48), (4.51), (4.57), (4.58), and Remark 4.21, as well as the corresponding error constants (4.46) and (4.49). As in Example 4.67 the errors (4.150) shall be estimated by evaluating a given function f and its approximation at equidistant points $x_s = -1 + \frac{s}{S} \in [-1, 1]$, $s = 0, \dots, 2S$, with $S = 10^5$. Analogous to [Obe90, Section IV, C] we choose the function

$$f(x) = \sqrt{\tfrac{4N}{5}} \left[\operatorname{sinc}(M\pi x) + \tfrac{1}{2} \operatorname{sinc}(M\pi(x-1)) \right], \quad x \in \mathbb{R}, \tag{4.151}$$

with $\|f\|_2 = 1$. Since the error bounds (4.46) and (4.49) are only valid for $T > L$, we fix $M = 256$ and consider several values of $T = L + m$ with $m \in \mathbb{N} \setminus \{1\}$ and $\lambda > 0$.

The associated results are displayed in Figure 4.16. We see that for all window functions the theoretical error behavior perfectly coincides with the

numerical outcomes. In this regard, see also Table 4.1 which summarizes the theoretical results. In particular, it can be seen that ψ_{cub} in (4.48), $\psi_{\cos}$ in (4.51), and $\psi_{\mathrm{conv},2}$ in (4.57) all meet the same error bound (4.49), while the error decay for $\psi_{\mathrm{conv},n}$ becomes faster as n increases. Moreover, note that $\psi_{\mathrm{conv},\infty}$ in (4.58) as well as ψ_{rat} from Remark 4.21 indeed behave similarly to the classical Shannon sampling sums (4.12), and thus the corresponding approaches for designing optimal window functions have not been successful. ◇

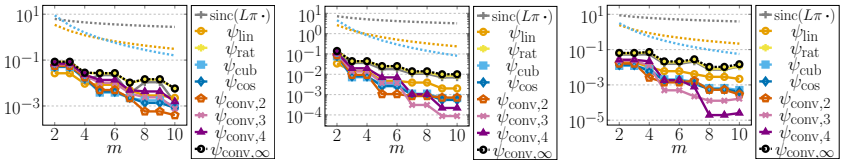

(a) $\lambda = 0.5$ (b) $\lambda = 1$ (c) $\lambda = 2$

Figure 4.16: Maximum approximation error (4.150) (solid) and error constants (dashed) using classical Shannon sampling sums compared to regularizations (4.36) with several frequency window functions for the function (4.151) where $M = 256$, $T = L + m$ with $m \in \{2, 3, \ldots, 10\}$, and $\lambda \in \{0.5, 1, 2\}$.

Regularization with a window function in spatial domain

Now let us move on to the regularization using the spatial window functions from Sections 4.3.2 and 4.4. Here we study the theoretical results regarding the uniform approximation error of Theorems 4.25 and 4.50 as well as the uniform perturbation error of Theorems 4.29 and 4.57. More specifically, we visualize the specified error bounds for each of the window functions mentioned in Remark 4.22 separately.

Gaussian window function We begin with the Gaussian window function (4.60).

Example 4.69. Analogous to [KPT22, Example 4.2] we now visualize the error bound of Theorems 4.33 and 4.58, respectively. For a given function $f \in \mathcal{B}_{M/2}(\mathbb{R}^d)$ with fixed $M \in \mathbb{N}$, $L = M(1+\lambda) \in \mathbb{N}$ with $\lambda \geq 0$,

and $m \in \mathbb{N} \setminus \{1\}$, we consider the approximation error

$$e_{m,\lambda}(f) \coloneqq \max_{\boldsymbol{x} \in [-1,\,1]^d} |f(\boldsymbol{x}) - (R_{\varphi,m} f)(\boldsymbol{x})|. \tag{4.152}$$

Using the Gaussian window function φ_{Gauss} in (4.60) with $\alpha = \frac{1}{M}\sqrt{\frac{m}{\pi(1+\lambda)\lambda}}$ we show that by (4.140) we have $e_{m,\lambda}(f) \le E_{m,\lambda} \|f\|_{L_2(\mathbb{R}^d)}$, where

$$\begin{aligned} E_{\mathrm{r}}(\varphi_{\mathrm{Gauss}}, M, L, d) + E_{\mathrm{t}}(\varphi_{\mathrm{Gauss}}, m, L, d) &\le E_{m,\lambda} \\ &\coloneqq \frac{d\, M^{d/2}\sqrt{2m(1+\lambda)} + \sqrt{2d}\, L^{d/2}\sqrt{\lambda(1+m)}}{m\pi\sqrt{\lambda}}\, \mathrm{e}^{-m\pi\lambda/(2+2\lambda)}. \end{aligned} \tag{4.153}$$

For this purpose, the error (4.152) shall be approximated by evaluating a given function f and its approximation $R_{\varphi,m} f$ on the equidistant grid $\otimes_{t=1}^{d} (x_0, \ldots, x_{2S^{1/d}})^{\top}$ with $x_s = -1 + \frac{s}{S} \in [-1,\,1]$, $s = 0, \ldots, 2S^{1/d}$, and $S = 2^{12}$. By the definition of the regularized Shannon sampling formula with localized sampling in (4.74) and (4.121), respectively, it can be seen that for $\boldsymbol{x} \in [-1,1]^d$ we have

$$(R_{\varphi,m} f)(\boldsymbol{x}) = \sum_{\boldsymbol{\ell} \in \mathcal{J}_{m,L}^{d}} f(\tfrac{\boldsymbol{\ell}}{L})\, \psi(\boldsymbol{x} - \tfrac{\boldsymbol{\ell}}{L})\, \chi_{[-\frac{m}{L},\,\frac{m}{L}]}(\boldsymbol{x} - \tfrac{\boldsymbol{\ell}}{L}) \tag{4.154}$$

with the regularized sinc function (4.123) and the index set

$$\begin{aligned} \mathcal{J}_{m,L}^{d} &\coloneqq \mathbb{Z}^d \cap [-m - L,\, m + L]^d \\ &= \{\boldsymbol{\ell} \in \mathbb{Z}^d \colon\, -m - L \le \ell_t \le m + L,\, t = 1, \ldots, d\}. \end{aligned}$$

Here we study the function $f(\boldsymbol{x}) = \left(\frac{3M}{4}\right)^{d/2} \operatorname{sinc}^2\left(\frac{M}{2}\pi\boldsymbol{x}\right)$, $\boldsymbol{x} \in \mathbb{R}^d$, such that we have $\|f\|_{L_2(\mathbb{R}^d)} = 1$. For $d \in \{1, 2, 3\}$ we fix $M = 2^{6/d}$ and choose different values for the truncation parameter $m \in \mathbb{N} \setminus \{1\}$ and the oversampling parameter $\lambda \ge 0$. Note that the error bound of Theorem 4.60 only holds for $\lambda > 0$, whereas the approximation error (4.152) can also be computed for $\lambda = 0$, since for the Gaussian window function (4.60) we have $\lim_{\lambda \to 0} \varphi_{\mathrm{Gauss}}(x) = 1$ for all $x \in \mathbb{R}$.

The associated results for $m \in \{2, 3, \ldots, 10\}$ and $\lambda \in \{0, 0.5, 1, 2\}$ are displayed in Figure 4.17. For all tested dimensions $d \in \{1, 2, 3\}$ it becomes evident that increasing the truncation parameter m and the oversampling

parameter λ results in strongly enhanced error results. Moreover, we remark that the experimental approximation error fully fits the theoretical bounds and the predicted decay rates. Note that for larger choices of M, the lines in Figure 4.17 would be shifted slightly upwards. ◇

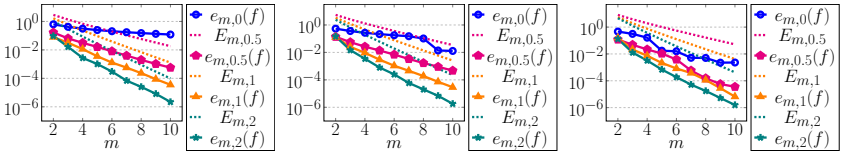

(a) $d = 1$ (b) $d = 2$ (c) $d = 3$

Figure 4.17: Maximum approximation error (4.152) (solid) and error constant (4.153) (dashed) using the Gaussian window function φ_{Gauss} in (4.60) with $\alpha = \frac{1}{M}\sqrt{\frac{m}{\pi(1+\lambda)\lambda}}$ for the function $f(\boldsymbol{x}) = \left(\frac{3M}{4}\right)^{d/2} \operatorname{sinc}^2\left(\frac{M}{2}\pi\boldsymbol{x}\right)$ with fixed $M = 2^{6/d}$ as well as $m \in \{2, 3, \dots, 10\}$, and $\lambda \in \{0, 0.5, 1, 2\}$.

Example 4.70. Next, analogous to [KPT22, Example 4.4], we visualize the error bound of Theorems 4.36 and 4.59, respectively. Similar to Example 4.69, we consider the perturbation error

$$\tilde{e}_{m,\lambda}(f) \coloneqq \max_{\boldsymbol{x}\in[-1,1]^d} |(R_{\varphi,m}\tilde{f})(\boldsymbol{x}) - (R_{\varphi,m}f)(\boldsymbol{x})|. \tag{4.155}$$

Using the Gaussian window function φ_{Gauss} in (4.60) with $\alpha = \frac{1}{M}\sqrt{\frac{m}{\pi(1+\lambda)\lambda}}$ we show that by (4.141) we have $\tilde{e}_{m,\lambda}(f) \le \tilde{E}_{m,\lambda}$, where

$$\tilde{E}_{m,\lambda} \coloneqq \varepsilon \left(2 + \sqrt{\frac{2+2\lambda}{\lambda}}\sqrt{m}\right)^d. \tag{4.156}$$

We conduct the same experiment as in Example 4.69 and introduce a maximum perturbation of $\varepsilon = 10^{-3}$ as well as uniformly distributed random numbers $\varepsilon_{\boldsymbol{\ell}} \in (-\varepsilon, \varepsilon)$, $\boldsymbol{\ell} \in \mathcal{J}_{m,L}^d$. Due to the randomness we perform the experiment ten times and then consider the maximum error. The corresponding outcomes are depicted in Figure 4.18. Clearly, the experimental error fully fits the theoretical bounds. ◇

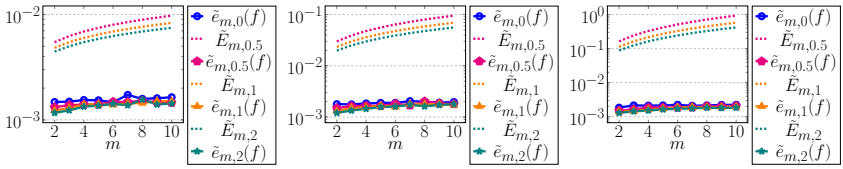

(a) $d = 1$ (b) $d = 2$ (c) $d = 3$

Figure 4.18: Maximum perturbation error (4.155) (solid) and error constant (4.156) (dashed) using the Gaussian window function φ_{Gauss} in (4.60) with $\alpha = \frac{1}{M}\sqrt{\frac{m}{\pi(1+\lambda)\lambda}}$ for the function $f(\boldsymbol{x}) = \left(\frac{3M}{4}\right)^{d/2} \operatorname{sinc}^2\left(\frac{M}{2}\pi\boldsymbol{x}\right)$ with fixed $M = 2^{6/d}$ as well as $\varepsilon = 10^{-3}$, $m \in \{2, 3, \dots, 10\}$, and $\lambda \in \{0, 0.5, 1, 2\}$.

B–spline window function Secondly, we consider the modified B–spline window function (4.61).

Example 4.71. Analogous to Example 4.69 and [KPT22, Example 5.4], we now visualize the error bound of Theorems 4.40 and 4.60, respectively, i. e., using the modified B–spline window function φ_{B} in (4.61) with $s = \left\lceil \frac{m+1}{2} \right\rceil$ we show that for the approximation error (4.152) we have by (4.142) that $e_{m,\lambda}(f) \leq E_{m,\lambda} \|f\|_{L_2(\mathbb{R}^d)}$, where

$$E_{\text{r}}(\varphi_{\text{B}}, M, L, d) \leq E_{m,\lambda} \coloneqq \frac{3d\sqrt{sM^d}}{\sqrt{2}\,(2s-1)\,\pi}\, \mathrm{e}^{-m\,(\ln(\pi m\lambda) - \ln(2s(1+\lambda)))}. \tag{4.157}$$

Additionally, we now have to observe the condition (4.102). Note that

$$\frac{m+2}{m\pi - (m+2)} \geq \frac{12}{10\pi - 12} \approx 0.6180, \quad m \in \{2, 3, \dots, 10\}.$$

Therefore, in Figure 4.19 the error bounds are plotted only for $\lambda \in \{1, 2\}$, since only then the requirements of Theorem 4.60 are fulfilled, while the approximation error (4.152) is computed for all constellations of the parameters as in Example 4.69. For all tested dimensions $d \in \{1, 2, 3\}$ it becomes evident that the experimental approximation error fully fits the theoretical results and that higher truncation parameters m and oversampling parameters λ reduce the error significantly. However, we recognize that compared

to Figure 4.17 there is hardly any improvement using the modified B–spline window function φ_{B} in (4.61) in comparison to the well-studied Gaussian window function φ_{Gauss} in (4.60). ◇

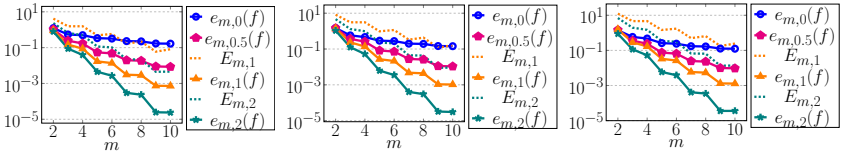

(a) $d = 1$ (b) $d = 2$ (c) $d = 3$

Figure 4.19: Maximum approximation error (4.152) (solid) and error constant (4.157) (dashed) using the modified B–spline window function φ_{B} in (4.61) with $s = \lceil \frac{m+1}{2} \rceil$ for the function $f(\boldsymbol{x}) = \left(\frac{3M}{4}\right)^{d/2} \operatorname{sinc}^2\left(\frac{M}{2}\pi\boldsymbol{x}\right)$ with fixed $M = 2^{6/d}$ as well as $m \in \{2, 3, \dots, 10\}$, and $\lambda \in \{0, 0.5, 1, 2\}$.

Example 4.72. Next, we visualize the error bound of Theorems 4.41 and 4.61, respectively. Using the modified B–spline window function φ_{B} in (4.61) with $s = \lceil \frac{m+1}{2} \rceil$, we show, similar to Example 4.70, that for the perturbation error (4.155) we have by (4.143) that $\tilde{e}_{m,\lambda}(f) \leq \tilde{E}_{m,\lambda}$, where

$$\tilde{E}_{m,\lambda} \coloneqq \varepsilon \left(2 + \tfrac{3}{2}\sqrt{m}\right)^{d}. \tag{4.158}$$

For the same experiment as in Example 4.70 the outcomes are depicted in Figure 4.20. Clearly, the experimental error fully fits the theoretical bounds. ◇

sinh-type window function We proceed with the sinh-type window function (4.62).

Example 4.73. Analogous to Example 4.69 and [KPT22, Example 6.2], we now visualize the error bound of Theorems 4.44 and 4.62, respectively, i. e., using the sinh-type window function $\varphi_{\sinh}$ in (4.62) with $\beta = \frac{\pi m \lambda}{1+\lambda}$ we show that for the approximation error (4.152) we have by (4.144) that $e_{m,\lambda}(f) \leq E_{m,\lambda} \|f\|_{L_2(\mathbb{R}^d)}$, where

$$E_{\mathrm{r}}(\varphi_{\sinh}, M, L, d) \leq E_{m,\lambda} \coloneqq \left(2^d - 1\right) M^{d/2}\, \mathrm{e}^{-m\pi\lambda/(1+\lambda)}. \tag{4.159}$$

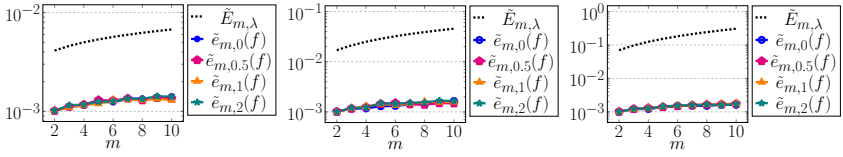

(a) $d = 1$ (b) $d = 2$ (c) $d = 3$

Figure 4.20: Maximum perturbation error (4.155) (solid) and error constant (4.158) (dashed) using the modified B–spline window function φ_{B} in (4.61) with $s = \lceil \frac{m+1}{2} \rceil$ for the function $f(\boldsymbol{x}) = \left(\frac{3M}{4}\right)^{d/2} \operatorname{sinc}^2\left(\frac{M}{2}\pi\boldsymbol{x}\right)$ with fixed $M = 2^{6/d}$ as well as $\varepsilon = 10^{-3}$, $m \in \{2, 3, \ldots, 10\}$, and $\lambda \in \{0, 0.5, 1, 2\}$.

Note that the error bound of Theorem 4.62 only holds for $\lambda > 0$, whereas the approximation error (4.152) can also be computed for $\lambda = 0$, since for the sinh-type window function (4.62) we have $\lim_{\lambda \to 0} \varphi_{\sinh}(x) = \sqrt{1 - \left(\frac{Lx}{m}\right)^2}$.

The associated results are displayed in Figure 4.21. For all tested dimensions $d \in \{1, 2, 3\}$ it becomes evident that the experimental approximation error fully fits the theoretical results and that higher truncation parameters m and oversampling parameters λ reduce the error significantly. Moreover, we see a substantial improvement in the results compared to both Figure 4.17 and 4.19. ◇

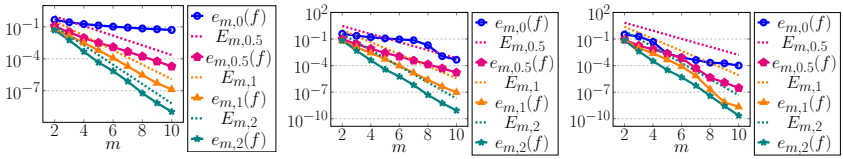

(a) $d = 1$ (b) $d = 2$ (c) $d = 3$

Figure 4.21: Maximum approximation error (4.152) (solid) and error constant (4.159) (dashed) using the sinh-type window function $\varphi_{\sinh}$ in (4.62) with $\beta = \frac{\pi m \lambda}{1+\lambda}$ for the function $f(\boldsymbol{x}) = \left(\frac{3M}{4}\right)^{d/2} \operatorname{sinc}^2\left(\frac{M}{2}\pi\boldsymbol{x}\right)$ with fixed $M = 2^{6/d}$ as well as $m \in \{2, 3, \ldots, 10\}$, and $\lambda \in \{0, 0.5, 1, 2\}$.

Example 4.74. Next, we visualize the error bound of Theorems 4.45 and 4.63, respectively. Using the sinh-type window function φ_{sinh} in (4.62) with $\beta = \frac{\pi m \lambda}{1+\lambda}$, we show, similar to Example 4.70, that for the perturbation error (4.155) we have by (4.145) that $\tilde{e}_{m,\lambda}(f) \leq \tilde{E}_{m,\lambda}$ where

$$\tilde{E}_{m,\lambda} := \varepsilon \left(2 + \sqrt{\frac{2+2\lambda}{\lambda}} \, \frac{1}{1 - \mathrm{e}^{-2\beta}} \, \sqrt{m} \right)^d . \tag{4.160}$$

For the same experiment as in Example 4.70 the outcomes are depicted in Figure 4.22. Clearly, the experimental error fully fits the theoretical bounds. ◇

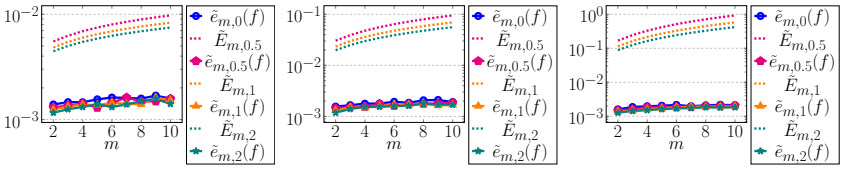

(a) $d = 1$ (b) $d = 2$ (c) $d = 3$

Figure 4.22: Maximum perturbation error (4.155) (solid) and error constant (4.160) (dashed) using the sinh-type window function φ_{sinh} in (4.62) with $\beta = \frac{\pi m \lambda}{1+\lambda}$ for the function $f(\boldsymbol{x}) = \left(\frac{3M}{4}\right)^{d/2} \operatorname{sinc}^2\left(\frac{M}{2}\pi \boldsymbol{x}\right)$ with fixed $M = 2^{6/d}$ as well as $\varepsilon = 10^{-3}$, $m \in \{2, 3, \ldots, 10\}$, and $\lambda \in \{0, 0.5, 1, 2\}$.

Continuous Kaiser–Bessel window function Finally, we study the continuous Kaiser–Bessel window function (4.63).

Example 4.75. Analogous to Example 4.69, we now visualize the error bound of Theorems 4.48 and 4.64, respectively, i. e., using the continuous Kaiser–Bessel window function φ_{cKB} in (4.63) with $\beta = \frac{\pi m \lambda}{1+\lambda}$ we show that for the approximation error (4.152) we have by (4.146) that $e_{m,\lambda}(f) \leq E_{m,\lambda} \, \|f\|_{L_2(\mathbb{R}^d)}$, where

$$\begin{aligned} E_{\mathrm{r}}(\varphi_{\text{cKB}}, M, L, d) &\leq E_{m,\lambda} \\ &:= (2^d - 1) \, M^{d/2} \, \frac{7\pi m \lambda (1 + \lambda + 4m\lambda)}{4\,(1+\lambda)^2} \, \mathrm{e}^{-m\pi\lambda/(1+\lambda)}. \end{aligned} \tag{4.161}$$

Note that the error bound of Theorem 4.64 only holds for $\lambda \geq \frac{1}{m-1} \geq 1$, $m \in \{2, 3, \dots, 10\}$. Therefore, Figure 4.23 displays the associated results only for $\lambda \in \{1, 2\}$ and $\lambda = 0.5$ with $m \geq 3$, whereas the approximation error (4.152) can also be computed for $\lambda = 0$, since for the continuous Kaiser–Bessel window function (4.63) we have $\lim_{\lambda \to 0} \varphi_{\mathrm{cKB}}(x) = 1 - \left(\frac{Lx}{m}\right)^2$.

For all tested dimensions $d \in \{1, 2, 3\}$ it becomes evident that the experimental approximation error fully fits the theoretical results and that higher truncation parameters m and oversampling parameters λ reduce the error significantly. Note that we see a substantial improvement in the results compared to both Figure 4.17 and 4.19, just as in Figure 4.21. ◇

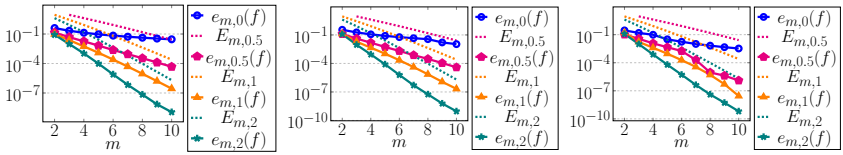

(a) $d = 1$ (b) $d = 2$ (c) $d = 3$

Figure 4.23: Maximum approximation error (4.152) (solid) and error constant (4.161) (dashed) using the continuous Kaiser–Bessel window function φ_{cKB} in (4.63) with $\beta = \frac{\pi m \lambda}{1+\lambda}$ for the function $f(\boldsymbol{x}) = \left(\frac{3M}{4}\right)^{d/2} \operatorname{sinc}^2\left(\frac{M}{2}\pi \boldsymbol{x}\right)$ with fixed $M = 2^{6/d}$ as well as $m \in \{2, 3, \dots, 10\}$, and $\lambda \in \{0, 0.5, 1, 2\}$.

Example 4.76. Next, we visualize the error bound of Theorems 4.49 and 4.65, respectively. Using the continuous Kaiser–Bessel window function φ_{cKB} in (4.63) with $\beta = \frac{\pi m \lambda}{1+\lambda}$, we show, similar to Example 4.70, that for the perturbation error (4.155) we have by (4.147) that $\tilde{e}_{m,\lambda}(f) \leq \tilde{E}_{m,\lambda}$ where

$$\tilde{E}_{m,\lambda} \coloneqq \varepsilon \left(2 + \sqrt{\frac{2+2\lambda}{\lambda}}\sqrt{m}\right)^d. \tag{4.162}$$

For the same experiment as in Example 4.70 the outcomes are depicted in Figure 4.24. Clearly, the experimental error fully fits the theoretical bounds. ◇

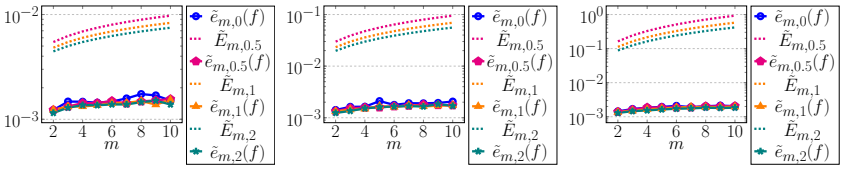

(a) $d = 1$ (b) $d = 2$ (c) $d = 3$

Figure 4.24: Maximum perturbation error (4.155) (solid) and error constant (4.162) (dashed) using the continuous Kaiser–Bessel window function φ_{cKB} in (4.63) with $\beta = \frac{\pi m \lambda}{1+\lambda}$ for the function $f(\boldsymbol{x}) = \left(\frac{3M}{4}\right)^{d/2} \operatorname{sinc}^2\left(\frac{M}{2}\pi \boldsymbol{x}\right)$ with fixed $M = 2^{6/d}$ as well as $\varepsilon = 10^{-3}$, $m \in \{2, 3, \ldots, 10\}$, and $\lambda \in \{0, 0.5, 1, 2\}$.

Comparison of the spatial window functions Summarizing, we compare the results for the spatial window functions considered above.

Example 4.77. Similar to [KPT22, Section 7], we consider a comparison using $\varphi \in \{\varphi_{\mathrm{const}}, \varphi_{\mathrm{Gauss}}, \varphi_{\mathrm{B}}, \varphi_{\mathrm{sinh}}, \varphi_{\mathrm{cKB}}\}$ in (4.84), (4.60), (4.61), (4.62), and (4.63). Here we restrict ourselves to $d = 1$, as we have previously observed that the regularized Shannon sampling sums with localized sampling exhibit analogous behavior for $d > 1$. For a given function $f \in \mathcal{B}_{M/2}(\mathbb{R})$ with $L = M(1 + \lambda)$, $\lambda > 0$, the maximum approximation error (4.152) shall be estimated by evaluating f and its approximation at equidistant points $x_s = -1 + \frac{s}{S} \in [-1, 1]$, $s = 0, \ldots, 2S$, with $S = 10^5$. As in Example 4.68 we choose the function (4.151) with $\|f\|_2 = 1$, fix $M = 256$ and consider several values of $m \in \mathbb{N} \setminus \{1\}$ and $\lambda > 0$. Comparing the corresponding results in Figure 4.25, the superiority of the sinh-type and continuous Kaiser–Bessel window function becomes apparent, since for all parameter choices these window functions yield by far the best results. ◇

Comparison of the two regularization methods

Finally, we draw a comparison between the regularization using a window function in frequency domain of Sections 4.3.1 and the regularization using a window function in spatial domain of Section 4.3.2.

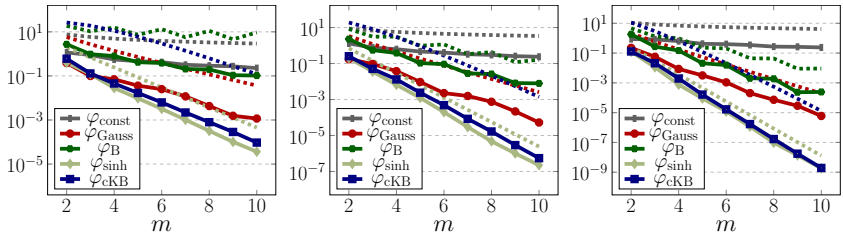

(a) $\lambda = 0.5$ (b) $\lambda = 1$ (c) $\lambda = 2$

Figure 4.25: Maximum approximation error (4.152) (solid) and error constant (4.79) (dashed) using $\varphi \in \{\varphi_{\text{const}}, \varphi_{\text{Gauss}}, \varphi_{\text{B}}, \varphi_{\text{sinh}}, \varphi_{\text{cKB}}\}$ for the function (4.151) with $M = 256$, $d = 1$, as well as $m \in \{2, 3, \dots, 10\}$, and $\lambda \in \{0.5, 1, 2\}$.

Example 4.78. Concluding, we compare the regularization methods presented in Sections 4.3.1 and 4.3.2, similar to [KPT24, Section 5]. Note that in the univariate setting $d = 1$ the regularized Shannon sampling formula with localized sampling (4.74) reads as

$$(R_{\varphi,m} f)(x) = \sum_{\ell=-L-m}^{L+m} f\big(\tfrac{\ell}{L}\big)\, \psi\big(x - \tfrac{\ell}{L}\big), \quad x \in [-1, 1], \tag{4.163}$$

with the regularized sinc function (4.69). Thus, in order to compare (4.163) to $P_{\psi,T} f$ in (4.38), we need to set $T = L + m$, such that both approximations use the same number of samples $f\big(\frac{\ell}{L}\big)$. This is to say, we conduct exactly the same experiment as already done in Examples 4.68 and 4.77, and therefore select only the best window functions for each of the approaches. In other words, for a given function $f \in \mathcal{B}_{M/2}(\mathbb{R})$ with $L = M(1 + \lambda)$, $\lambda > 0$, we consider the approximation error in (4.150) for $\psi_{\text{conv},n}$ with $n \in \{1, 2, 3, 4\}$, cf. (4.45) and (4.57), as well as the approximation error (4.152) with $\varphi \in \{\varphi_{\text{sinh}}, \varphi_{\text{cKB}}\}$, see (4.62) and (4.63), accompanied by the corresponding error constants (4.46), (4.49), (4.159) and (4.161).

The associated results are displayed in Figure 4.26. It can clearly be seen that for increasing oversampling parameter λ and truncation parameter m, the error results using the regularization (4.74) in spatial domain get much

better than the ones using the regularization (4.36) in frequency domain, due to the exponential error decay rate shown for (4.74). This is to say, our numerical results show that regularization with a spatial window function performs much better than regularization with a frequency window function, since an exponential decay can (up to now) only be realized using spatial window functions. ◇

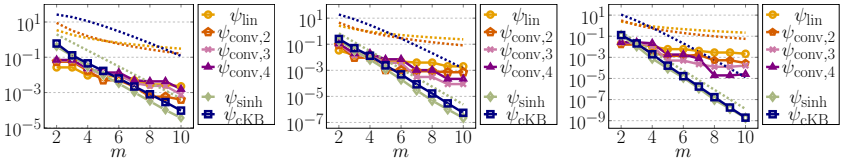

(a) $\lambda = 0.5$ (b) $\lambda = 1$ (c) $\lambda = 2$

Figure 4.26: Maximum approximation error (solid) and error constants (dashed) using regularizations (4.36) in frequency domain compared to regularizations (4.163) in spatial domain with selected window functions each, for the function (4.151), where $M = 256$, $m \in \{2, 3 \dots, 10\}$, and $\lambda \in \{0.5, 1, 2\}$.

Remark 4.79. Note that the code files for all the experiments in this chapter are available at [Kir] under `https://github.com/melaniekircheis/dissertation/tree/main/4-Regularized_Shannon_sampling_formulas`. ◇

In summary, comparing the proposed regularization methods as done in Figure 4.25, the superiority of the sinh-type and continuous Kaiser–Bessel window function can easily be seen, since rather small choices of the truncation parameter $m \leq 10$ are sufficient for achieving high precision. Due to the usage of localized sampling, the evaluation of (4.74) on an interval $[0, 1/L]$ requires only $2m$ samples and therefore has a computational cost of $\mathcal{O}(2m)$ flops. Thus, a reduction of the truncation parameter m is desirable to obtain an efficient method.

So, all in all, we found that the regularized Shannon sampling formula (4.74) with spatial window functions is the best of the considered methods, since this approach is the most accurate, easy to compute, robust in the worst case error, and requires less data (for comparable accuracy) than the classical Shannon sampling sums (4.12) or the regularization (4.36) with a frequency window function.

Summary

In this chapter, we gave the first comprehensive overview of the regularized Shannon sampling formulas along with a detailed comparison of the different regularization methods. For this purpose, the theoretical and numerical properties of several known as well as newly proposed window functions have been analyzed. In particular, we have adopted certain compactly supported window functions established in the context of the NFFT, which have been shown to be superior to previously known approaches. For the first time, the multivariate setting $d > 1$ is considered as well and we have presented error bounds that are valid for all $d \in \mathbb{N}$. However, since this error constant includes the term $M^{d/2}$, it has been noted that this estimate is only suitable for small $d \in \{1, 2, 3\}$.

5 Fast sinc methods

Previously, we have seen that the sinc function plays an important role in the context of the Whittaker–Kotelnikov–Shannon sampling theorem and the regularized Shannon sampling formulas. To emphasize the significance of the sinc function, in this chapter we focus especially on fast sinc methods, i. e., efficient and accurate algorithms, where the sinc function is a crucial ingredient.

Firstly, in Section 5.1 we consider the so-called discrete sinc transform and present an efficient evaluation scheme for these sinc sums. More precisely, we approximate the sinc function by means of an exponential sum, such that the NNFFT, see Algorithm 2.6, can be applied for a fast evaluation. Secondly, this fast sinc transform is generalized for the evaluation of the regularized Shannon sampling sums in Section 5.2. Afterwards, we slightly change the focus in Section 5.3 and introduce a new NFFT-like procedure for bandlimited functions, i. e., a fast method to approximate the function evaluations $f(\boldsymbol{x}_j)$ at given nonequispaced points $\boldsymbol{x}_j$, $j = 1, \dots N$, from given values $\hat{f}(\boldsymbol{k})$, $\boldsymbol{k} \in \mathcal{I}_{\boldsymbol{M}}$, of the Fourier transform (4.4) of the bandlimited function $f \in \mathcal{B}_{M/2}(\mathbb{R}^d)$. Subsequently, the concluding Section 5.4 contains several numerical examples that demonstrate the accuracy and efficiency of the new approaches, including a comparison with existing methods, as well as a brief summary.

5.1 Discrete sinc transform

In this section we consider an interesting signal processing application of the NNFFT, see Section 2.4. If a signal $h\colon \left[-\frac{1}{2}, \frac{1}{2}\right]^d \to \mathbb{C}$ is to be reconstructed from its samples at arbitrary points $\boldsymbol{a}_k \in \left[-\frac{1}{2}, \frac{1}{2}\right]^d$, $k \in \mathcal{I}_K$ with $K \in 2\mathbb{N}$, then h is often modeled as a linear combination of shifted sinc functions (3.31), i. e.,

$$h(\boldsymbol{x}) = \sum_{k \in \mathcal{I}_K} c_k \operatorname{sinc}\bigl(M\pi\,(\boldsymbol{x} - \boldsymbol{a}_k)\bigr), \quad \boldsymbol{x} \in \left[-\tfrac{1}{2}, \tfrac{1}{2}\right]^d, \tag{5.1}$$

with complex coefficients $c_k \in \mathbb{C}$, $k \in \mathcal{I}_K$. Since sums of the form (5.1) are often needed in practical applications, see for instance [LB92, Ste93], we

propose a fast algorithm for the approximate evaluation of the *discrete sinc transform*

$$h(\boldsymbol{b}_\ell) = \sum_{k \in \mathcal{I}_K} c_k \operatorname{sinc}\big(M\pi\,(\boldsymbol{b}_\ell - \boldsymbol{a}_k)\big), \quad \ell \in \mathcal{I}_L, \tag{5.2}$$

where $\boldsymbol{b}_\ell \in \big[-\frac{1}{2}, \frac{1}{2}\big]^d$, $\ell \in \mathcal{I}_L$ with $L \in 2\mathbb{N}$, are given arbitrary points and the coefficients $c_k \in \mathbb{C}$, $k \in \mathcal{I}_K$, are known.

Remark 5.1. Such a function (5.1) occurs for instance in numerical realizations of the famous sampling theorem of Whittaker–Kotelnikov–Shannon, see Theorem 4.2. By (4.7) a function $f \in \mathcal{B}_{M/2}(\mathbb{R}^d)$ can be represented in the form

$$f(\boldsymbol{x}) = \sum_{\boldsymbol{k} \in \mathbb{Z}^d} f\big(\tfrac{\boldsymbol{k}}{M}\big) \operatorname{sinc}\big(M\pi\big(\boldsymbol{x} - \tfrac{\boldsymbol{k}}{M}\big)\big), \quad \boldsymbol{x} \in \mathbb{R}^d.$$

Truncation of this series yields the Shannon sampling sum

$$\sum_{\|\boldsymbol{k}\|_\infty \le K} f\big(\tfrac{\boldsymbol{k}}{M}\big) \operatorname{sinc}\big(M\pi\big(\boldsymbol{x} - \tfrac{\boldsymbol{k}}{M}\big)\big), \quad \boldsymbol{x} \in \mathbb{R}^d,$$

cf. (4.12), which is a linear combination of shifted sinc functions and has the same form as (5.1) with $\boldsymbol{a}_k = \frac{\boldsymbol{k}}{M}$ equispaced. ◇

Since the naive computation of (5.2) requires $\mathcal{O}(KL)$ arithmetic operations, the aim is to find a more efficient method for the evaluation of (5.2). Up to now, several approaches for a fast computation of the discrete sinc transform (5.2) are known. In [GLI06] the discrete sinc transform (5.2) is realized by applying a Gauss–Legendre quadrature rule to a certain integral, such that the result can then be approximated by means of two NNFFTs with $\mathcal{O}(K + L)$ arithmetic operations. For the univariate setting with $d = 1$, a similar approach is taken in [LGBM18] using a corrected trapezoidal quadrature rule, cf. [KR97], and in [KPT23] using a Clenshaw–Curtis quadrature rule instead. Likewise, for $d = 1$ a multilevel algorithm with $\mathcal{O}(L \log(1/\delta))$ arithmetic operations, where δ is the desired evaluation accuracy, is presented in [LB11] which is most effective for equispaced points a_k and b_ℓ and, as the authors claim themselves, is only practical for rather large δ, i. e., low accuracy.

In the following, we present a multivariate approach for a fast approximate computation of the discrete sinc transform (5.2) in the fashion of [GLI06, KPT23], where we make use of exponential sums of the form (2.19).

5.1.1 Approximation of the sinc function by exponential sums

In order to approximate the discrete sinc transform (5.2), we firstly study the approximation of the sinc function $\operatorname{sinc}(M\pi\boldsymbol{x})$, which shall be realized by means of the exponential sums (2.19). For simplicity we start with the univariate setting $d = 1$, analogous to [KPT23].

Univariate setting

By [BM02] the exponential sums (2.19) can be used for a local approximation of functions F of the form

$$F(x) \coloneqq \int_{-1/2}^{1/2} w(\tau)\, \mathrm{e}^{-2\pi \mathrm{i} M\tau x}\, \mathrm{d}\tau, \quad x \in \mathbb{R}, \tag{5.3}$$

where $w\colon \left[-\frac{1}{2}, \frac{1}{2}\right] \to [0, \infty)$ is an integrable function with $\int_{-1/2}^{1/2} w(\tau)\, \mathrm{d}\tau > 0$. Substituting $v = -M\tau$ these functions (5.3) can be written as

$$F(x) = \frac{1}{M} \int_{-M/2}^{M/2} w\left(-\tfrac{v}{M}\right)\, \mathrm{e}^{2\pi \mathrm{i} v x}\, \mathrm{d}v,$$

such that by (4.4) the Fourier transform $\hat{F}(v) = \frac{1}{M}\, w\left(-\frac{v}{M}\right)$ of F is supported on $\left[-\frac{M}{2}, \frac{M}{2}\right]$, i. e., the function F in (5.3) is bandlimited with bandwidth M. Note that for $w(\tau) \coloneqq 1$, $\tau \in \left[-\frac{1}{2}, \frac{1}{2}\right]$, we obtain the sinc function $F(x) = \operatorname{sinc}(M\pi x)$, see (3.31).

Theorem 5.2. *Let $F \in \mathcal{B}_{M/2}(\mathbb{R})$ with $M \in \mathbb{N}$ be a bandlimited function of the form (5.3) and let $\varepsilon > 0$ be a given target accuracy. Then for sufficiently large $n \in \mathbb{N}$ with $n + 1 \geq 2M$, there exist quadrature weights $w_j > 0$ and quadrature points $z_j \in \left(-\frac{1}{2}, \frac{1}{2}\right)$, $j = 0, \ldots, n$, such that*

$$\left| F(x) - \sum_{j=0}^{n} w_j\, \mathrm{e}^{-2\pi \mathrm{i} M z_j x} \right| < \varepsilon, \quad x \in \left[-\tfrac{1}{2}, \tfrac{1}{2}\right]. \tag{5.4}$$

Proof. This result is a simple consequence of [BM02, Theorem 6.1]. Introducing $N \in \mathbb{N}$ with $N \geq 2M$ such that $\nu \coloneqq \frac{M}{N} \leq \frac{1}{2}$, we obtain by substituting $\tau \coloneqq -\frac{t}{2\nu}$ in (5.3) that

$$F(x) = \int_{-1/2}^{1/2} w(\tau)\, \mathrm{e}^{-2\pi \mathrm{i} M\tau x}\, \mathrm{d}\tau = \frac{1}{2\nu} \int_{-\nu}^{\nu} w\left(-\tfrac{t}{2\nu}\right)\, \mathrm{e}^{\pi \mathrm{i} N t x}\, \mathrm{d}t.$$

By setting $\sigma(t) \coloneqq \frac{1}{2\nu}\, w\big(-\frac{t}{2\nu}\big)$ and $y \coloneqq Nx \in \big[-\frac{N}{2},\, \frac{N}{2}\big]$, this yields

$$F\big(\tfrac{y}{n}\big) = \int_{-\nu}^{\nu} \sigma(t)\, \mathrm{e}^{\pi \mathrm{i} t y}\, \mathrm{d}t. \tag{5.5}$$

Then [BM02, Theorem 6.1 with $d = \frac{1}{2}$] implies the existence of $\kappa_j > 0$ and $|\theta_j| < \nu$, $j = 1, \dots, N$, such that

$$\left| \int_{-\nu}^{\nu} \sigma(t)\, \mathrm{e}^{\pi \mathrm{i} t y}\, \mathrm{d}t - \sum_{j=1}^{N} \kappa_j\, \mathrm{e}^{\pi \mathrm{i} \theta_j y} \right| < \varepsilon, \quad y \in \big[-\tfrac{N}{2} - 1,\, \tfrac{N}{2} + 1\big].$$

Hence, for all $x = \frac{y}{N} \in \big[-\frac{1}{2},\, \frac{1}{2}\big]$, we conclude by (5.5) as well as an index shift that

$$\left| F(x) - \sum_{j=0}^{N-1} \kappa_{j+1}\, \mathrm{e}^{\pi \mathrm{i} \theta_{j+1} N x} \right| = \left| F(x) - \sum_{j=0}^{n} w_j\, \mathrm{e}^{-2\pi \mathrm{i} M z_j x} \right| < \varepsilon,$$

where we set $w_j \coloneqq \kappa_{j+1}$ and $z_j \coloneqq -\frac{\theta_{j+1}}{2\nu} \in \big(-\frac{1}{2},\, \frac{1}{2}\big)$, $j = 0, \dots, n$, for $n \coloneqq N - 1$. This yields the assumption (5.4). ∎

We remark that the above Theorem 5.2 is a generalized version of [KPT23, Theorem 5.1], where only the sinc function $F(x) = \operatorname{sinc}(M\pi x)$ was considered.

Moreover, note that since we have $a_k, b_\ell \in \big[-\frac{1}{2},\, \frac{1}{2}\big]$ for $k \in \mathcal{I}_K$, $\ell \in \mathcal{I}_L$, in (5.2), we need to approximate the sinc function $\operatorname{sinc}(M\pi x)$ for all $x \in [-1,\, 1]$ to compute the discrete sinc transform (5.2). Therefore, we modify Theorem 5.2 by substituting $x = \frac{t}{2}$, $t \in [-1,\, 1]$, and replacing the bandwidth M by $2M$, such that we obtain the following uniform approximation of the sinc function on the interval $[-1,\, 1]$, see [KPT23, Corollary 5.2].

Corollary 5.3. *Let $\varepsilon > 0$ be a given target accuracy. Then for sufficiently large $n \in \mathbb{N}$ with $n + 1 \geq 4M$, there exist quadrature weights $w_j > 0$ and quadrature points $z_j \in \big(-\frac{1}{2},\, \frac{1}{2}\big)$, $j = 0, \dots, n$, such that*

$$\left| \operatorname{sinc}(M\pi x) - \sum_{j=0}^{n} w_j\, \mathrm{e}^{-2\pi \mathrm{i} M z_j x} \right| < \varepsilon, \quad x \in [-1,\, 1]. \tag{5.6}$$

In practice, the approximation of the sinc function $\operatorname{sinc}(M\pi x)$ by means of an exponential sum on the interval $[-1,1]$ shall be simplified by assuming that the points $z_j \in \left[-\frac{1}{2}, \frac{1}{2}\right]$, $j = 0, \ldots, n$, are given. Thus, we consider an approximation procedure using approximate values w_j. Apparently, the easiest way to obtain appropriate weights w_j, $j = 0, \ldots, n$, is a least squares approach, i. e., for suitable given evaluation points $y_p \in [-1,1]$, $p \in \mathcal{I}_P$, we consider the minimization problem

$$\underset{w_j \in \mathbb{C},\, j=0,\ldots,n}{\text{Minimize}} \sum_{p \in \mathcal{I}_P} \left| \operatorname{sinc}(M\pi y_p) - \sum_{j=0}^{n} w_j \, \mathrm{e}^{-2\pi \mathrm{i} M z_j y_p} \right|^2 . \tag{5.7}$$

As in [KPT23], we might also approximate the sinc function using Clenshaw–Curtis quadrature, see [Tre13, pp. 143–153] or [PPST23, pp. 393–400], where for given Chebyshev points

$$z_j = \tfrac{1}{2} \cos\!\left(\tfrac{j\pi}{n}\right) \in \left[-\tfrac{1}{2}, \tfrac{1}{2}\right], \quad j = 0, \ldots, n, \tag{5.8}$$

the weights $w_j > 0$ are explicitly known. In this case, we obtain the following explicit version of the error estimate (5.6), cf. [KPT23, Theorem 5.3].

Theorem 5.4. *Let the nonharmonic bandwidth $M \in 2\mathbb{N}$ with $M \gg 1$ be given. Then for sufficiently large $n \in \mathbb{N}$ with $n + 1 \geq 4M$, the estimate*

$$\left| \operatorname{sinc}(M\pi x) - \sum_{j=0}^{n} w_j \, \mathrm{e}^{-2\pi \mathrm{i} M z_j x} \right| \leq \frac{48}{35} \, 2^{-n} \, \cosh\left(\frac{3\pi M}{4}\right), \quad x \in [-1, 1], \tag{5.9}$$

holds for the explicitly known quadrature points (5.8) *and quadrature weights*

$$w_j = \varepsilon_n(j)^2 \, \frac{1}{n} \sum_{k=0}^{n/2} \varepsilon_n(2k)^2 \, \frac{2}{1 - 4k^2} \, \cos\!\left(\frac{2kj\pi}{n}\right) > 0, \quad j = 0, \ldots, n, \tag{5.10}$$

where $\varepsilon_n(0) = \varepsilon_n(n) = \frac{\sqrt{2}}{2}$ and $\varepsilon_n(k) = 1$ for $k = 1, \ldots, n-1$.

Proof. Initially, we rewrite the sinc function in the form

$$\operatorname{sinc}(M\pi x) = \frac{1}{2} \int_{-1}^{1} \mathrm{e}^{-\pi \mathrm{i} M t x} \, \mathrm{d}t = \frac{1}{2} \int_{-1}^{1} \cos(M\pi t x) \, \mathrm{d}t. \tag{5.11}$$

Then, for given Chebyshev points $z_j = \frac{1}{2}\cos(\frac{j\pi}{n}) \in \left[-\frac{1}{2}, \frac{1}{2}\right]$, $j = 0, \dots, n$, as well as $n \in 2\mathbb{N}$ with $n \geq 4M$, we apply the Clenshaw–Curtis quadrature rule, cf. [PPST23, Theorem 6.51], to the analytic function $f(t, x) = \frac{1}{2}\cos(M\pi t x)$ with $t \in [-1, 1]$ and fixed $x \in [-1, 1]$. In doing so, the integral (5.11) is approximated by

$$\operatorname{sinc}(M\pi x) \approx \sum_{j=0}^{n} w_j \cos(2M\pi z_j x) = \sum_{j=0}^{n} w_j \, \mathrm{e}^{-2\pi \mathrm{i} M z_j x}, \quad x \in [-1, 1], \tag{5.12}$$

with the explicit weights (5.10). If n is odd, then a similar formula holds, see [PPST23, Theorem 6.51]. Note that in (5.12) and (5.9) we may use the exponential form, since the imaginary part satisfies

$$\operatorname{Im}\left(\sum_{j=0}^{n} w_j \, \mathrm{e}^{-2\pi \mathrm{i} M z_j x}\right) = -\sum_{j=0}^{n} w_j \sin(2M\pi z_j x) = 0, \quad x \in [-1, 1],$$

due to the symmetry property of the weights $w_j = w_{n-j}$, $j = 0, \dots, n$, cf. [PPST23, p. 395], and the symmetry property of the Chebyshev points $z_j = -z_{n-j}$, $j = 0, \dots, \frac{n}{2} - 1$, and $z_{n/2} = 0$, which can be seen by trigonometric identities.

For the estimation of the approximation error, we make use of [Tre13], where an error estimate is given when $|f(z, x)|$ is bounded above for z on the Bernstein ellipse

$$E_\rho := \left\{ z \in \mathbb{C} \colon z = \tfrac{1}{2}(\rho + \rho^{-1})(\cos\theta + \mathrm{i}\sin\theta),\ \theta \in [0, 2\pi) \right\}.$$

Note that for all $z \in \mathbb{C}$ and fixed $x \in [-1, 1]$ we have

$$\begin{aligned} |\cos(M\pi z x)| &= \frac{1}{2}\left| \mathrm{e}^{\mathrm{i}M\pi x(\operatorname{Re}(z) + \mathrm{i}\operatorname{Im}(z))} + \mathrm{e}^{-\mathrm{i}M\pi x(\operatorname{Re}(z) + \mathrm{i}\operatorname{Im}(z))} \right| \\ &\leq \frac{1}{2}\left| \mathrm{e}^{\mathrm{i}M\pi x \operatorname{Re}(z)} \right| \mathrm{e}^{-M\pi x \operatorname{Im}(z)} + \frac{1}{2}\left| \mathrm{e}^{-\mathrm{i}M\pi x \operatorname{Re}(z)} \right| \mathrm{e}^{M\pi x \operatorname{Im}(z)} \\ &\leq \cosh(M\pi x \operatorname{Im}(z)). \end{aligned}$$

Therefore, the integrand $f(t, x) = \frac{1}{2}\cos(M\pi t x)$ is bounded on the interior of the Bernstein ellipse E_ρ with

$$|f(z, x)| \leq \frac{1}{2}\cosh(M\pi x \operatorname{Im}(z)) \leq \frac{1}{2}\cosh\left(\frac{M\pi\,(\rho - \rho^{-1})}{2}\right), \quad x \in [-1, 1],$$

since cosh is even and monotonously increasing on $[0, \infty)$. Accordingly, the estimate in [Tre13, Theorem 19.3] with $\rho = 2$ yields the assertion (5.9). ■

In practice, the weights w_j in (5.10) can be computed by means of a fast algorithm, the so-called *discrete cosine transform of type I (DCT-I)* of length $n+1$ (see [PPST23, Algorithm 6.28]), which uses the orthogonal cosine matrix of type I

$$\mathbf{C}^{\mathrm{I}}_{n+1} \coloneqq \sqrt{\frac{2}{n}} \left(\varepsilon_n(k)\, \varepsilon_n(j)\, \cos\left(\frac{kj\pi}{n} \right) \right)_{k,j=0}^{n}.$$

In doing so, the computation of the weights w_j in (5.10) can be summarized as follows, cf. [KPT23, Algorithm 5.4].

Algorithm 5.5 (Fast computation of the weights w_j)**.**

For $n \in \mathbb{N} \setminus \{1\}$ let $\varepsilon_n(0) = \varepsilon_n(n) = \frac{\sqrt{2}}{2}$ and $\varepsilon_n(k) = 1$ for $k = 1, \dots, n-1$, be given.

1. Form the vector $(\upsilon_k)_{k=0}^n$ with $\mathcal{O}(n)$

$$\upsilon_k \coloneqq \begin{cases} \varepsilon_n(2\ell)\, \frac{2}{1-4\ell^2} & : k = 2\ell,\ \ell = 0, \dots, \frac{n}{2}, \\ 0 & : k = 2\ell+1,\ \ell = 0, \dots, \frac{n}{2} - 1. \end{cases}$$

2. Compute $(\hat{\upsilon}_j)_{j=0}^n \coloneqq \mathbf{C}^{\mathrm{I}}_{n+1} (\upsilon_k)_{k=0}^n$ by means of a fast DCT-I. $\mathcal{O}(n \log(n))$

3. Set $\tilde{\omega}_j \coloneqq \frac{1}{\sqrt{2n}}\, \varepsilon_n(j)\, \hat{\upsilon}_j$, $j = 0, \dots, n$. $\mathcal{O}(n)$

Output: $\tilde{\omega}_j \approx w_j$, $j = 0, \dots, n$, cf. (5.10).

Complexity: $\mathcal{O}(n \log(n))$

Remark 5.6. In [GLI06] a Gauss–Legendre quadrature was applied to obtain explicit weights w_j for given Legendre points

$$z_j = \tfrac{1}{2}\, \zeta_j \in \left[-\tfrac{1}{2}, \tfrac{1}{2} \right], \quad j = 0 \dots, n, \tag{5.13}$$

where ζ_j denote the zeros of the $(n+1)$-th Legendre polynomial. Due to their error estimate the authors claimed that $n \in \mathbb{N}$ with $n \geq \frac{\pi}{2} M$ would be sufficient in this setting. However, the computation of the weights w_j using our approach in Algorithm 5.5 is more effective for large M even though here an oversampling of $n \geq 4M$ is needed, see Example 5.17. ⋄

Multivariate setting

Now we proceed with the approximation of the sinc function $\operatorname{sinc}(M\pi\boldsymbol{x})$ in the multivariate setting $d > 1$. By the tensor product structure of the d-variate sinc function (3.31), we recognize that by means of (5.12) we are immediately given the approximation

$$\begin{aligned}\operatorname{sinc}(M\pi\boldsymbol{x}) &= \prod_{t=1}^{d} \operatorname{sinc}(M\pi x_t) \\ &\approx \prod_{t=1}^{d} \left(\sum_{j=0}^{n} w_j \, \mathrm{e}^{-2\pi \mathrm{i} M z_j x_t} \right), \quad \boldsymbol{x} = (x_1, \ldots, x_d)^\top \in [-1,1]^d.\end{aligned} \tag{5.14}$$

Note that also the error estimate of Theorem 5.4 can be extended to $d > 1$ with the help of the following lemma.

Lemma 5.7. *For $d \in \mathbb{N}$ let the vectors $\boldsymbol{a} \coloneqq (a_t)_{t=1}^d$, $\boldsymbol{b} \coloneqq (b_t)_{t=1}^d \in \mathbb{C}^d$ with $|a_t|, |b_t| \leq 1$, $t = 1, \ldots, d$, be given. Then we have*

$$\left| \prod_{t=1}^{d} a_t - \prod_{t=1}^{d} b_t \right| \leq \sum_{t=1}^{d} |a_t - b_t| \,. \tag{5.15}$$

Proof. This statement can be shown by induction. Since the inequality is trivial for $d = 1$, we start with $d = 2$. By using a constructive zero, the triangle inequality as well as the assumption $|a_t|, |b_t| \leq 1$, $t = 1, \ldots, d$, we obtain

$$\begin{aligned}|a_1 a_2 - b_1 b_2| &= |a_1(a_2 - b_2) + b_2(a_1 - b_1)| \\ &\leq |a_1| \cdot |a_2 - b_2| + |b_2| \cdot |a_1 - b_1| \\ &\leq |a_2 - b_2| + |a_1 - b_1| \,.\end{aligned}$$

Now assume the assertion holds for $d = 1, \ldots, k$. Then we conclude for $d = k + 1$ by the same techniques as used above that

$$\begin{aligned}\left| \prod_{t=1}^{k+1} a_t - \prod_{t=1}^{k+1} b_t \right| &= \left| a_{k+1} \cdot \left(\prod_{t=1}^{k} a_t - \prod_{t=1}^{k} b_t \right) + (a_{k+1} - b_{k+1}) \cdot \prod_{t=1}^{k} b_t \right| \\ &\leq |a_{k+1}| \cdot \left| \prod_{t=1}^{k} a_t - \prod_{t=1}^{k} b_t \right| + |a_{k+1} - b_{k+1}| \cdot \prod_{t=1}^{k} |b_t|\end{aligned}$$

$$\leq \sum_{t=1}^{k} |a_t - b_t| + |a_{k+1} - b_{k+1}| = \sum_{t=1}^{k+1} |a_t - b_t| \,.$$

This completes the proof. ∎

Now we can give an error estimate for the approximation (5.14).

Corollary 5.8. *Let the nonharmonic bandwidth $M \in 2\mathbb{N}$ with $M \gg 1$, the quadrature points* (5.8)*, and the quadrature weights* (5.10) *be given. Then for sufficiently large $n \in \mathbb{N}$ with $n + 1 \geq 4M$, we obtain the error estimate*

$$\left| \operatorname{sinc}(M\pi \boldsymbol{x}) - \prod_{t=1}^{d} \left(\sum_{j=0}^{n} w_j \, \mathrm{e}^{-2\pi \mathrm{i} M z_j x_t} \right) \right| \leq d \cdot \frac{48}{35} \, 2^{-n} \, \cosh\left(\frac{3\pi M}{4} \right),$$

$$\boldsymbol{x} \in [-1,\, 1]^d.$$

Proof. The given error estimate is a simple consequence of Lemma 5.7 and Theorem 5.4. Note that we have $\operatorname{sinc}(M\pi \boldsymbol{x}) = \prod_{t=1}^{d} \operatorname{sinc}(M\pi x_t) = \prod_{t=1}^{d} a_t$ and $|\operatorname{sinc}(M\pi x)| \leq 1,\ x \in \mathbb{R}^d$. Additionally, by the triangle inequality and [PPST23, Theorem 6.51] we obtain

$$|b_t| = \left| \sum_{j=0}^{n} w_j \, \mathrm{e}^{-2\pi \mathrm{i} M z_j x_t} \right| \leq \sum_{j=0}^{n} |w_j| \cdot \left| \mathrm{e}^{-2\pi \mathrm{i} M z_j x_t} \right|$$

$$\leq \sum_{j=0}^{n} w_j = 1, \quad t = 1, \ldots, d,$$

such that combining (5.15) and (5.9) yields the assertion. ∎

Remark 5.9. We remark that for the approximation (5.14) we used a product of one-dimensional exponential sums instead of a d-dimensional exponential sum of the form (2.19). However, using suitable tensor decompositions, it can be shown that the corresponding d-dimensional exponential sum and the tensor product (5.14) are identical. To do so, we introduce the notations

$$\vec{\boldsymbol{w}} \coloneqq (\vec{w}_j)_{j=0}^{\vec{n}} \in \mathbb{C}^{\vec{n}+1} \quad \text{and} \quad \vec{\boldsymbol{z}} \coloneqq (\vec{\boldsymbol{z}}_j)_{j=0}^{\vec{n}} \in \mathbb{C}^{(\vec{n}+1)\times d}, \quad \vec{n} \in \mathbb{N}, \tag{5.16}$$

for the d-dimensional expressions, as distinct from the one-dimensional quadrature weights w_j in (5.10) and quadrature points z_j, $j = 0, \ldots, n$,

in (5.8) with $n \geq 4M$. Then the corresponding d-dimensional exponential sum of the form (2.19) can be written as

$$\sum_{j=0}^{\vec{n}} \vec{w}_j \, \mathrm{e}^{-2\pi \mathrm{i} M \vec{\boldsymbol{z}}_j \boldsymbol{x}}, \quad \boldsymbol{x} = (x_1, \ldots, x_d)^\top \in [-1,1]^d. \tag{5.17}$$

In order to establish the connection between (5.17) and (5.14), the notions (5.16) still need to be defined properly in accordance with (5.10) and (5.8). For instance, for $d = 2$ the right-hand side of (5.14) reads as

$$\begin{aligned}
&\prod_{t=1}^{2} \left(\sum_{j=0}^{n} w_j \, \mathrm{e}^{-2\pi \mathrm{i} M z_j x_t} \right) \\
&\quad = \left(\sum_{j_1=0}^{n} w_{j_1} \, \mathrm{e}^{-2\pi \mathrm{i} M z_{j_1} x_1} \right) \left(\sum_{j_2=0}^{n} w_{j_2} \, \mathrm{e}^{-2\pi \mathrm{i} M z_{j_2} x_2} \right) \\
&\quad = \sum_{j_1=0}^{n} \sum_{j_2=0}^{n} w_{j_1} w_{j_2} \, \mathrm{e}^{-2\pi \mathrm{i} M (z_{j_1} x_1 + z_{j_2} x_2)}.
\end{aligned}$$

Thus, by defining the notions (5.16) as

$$\vec{\boldsymbol{w}} \coloneqq \boldsymbol{w} \otimes \boldsymbol{w} = \begin{pmatrix} w_0 \cdot \boldsymbol{w} \\ \vdots \\ w_n \cdot \boldsymbol{w} \end{pmatrix} \in \mathbb{C}^{(n+1)^2} \tag{5.18}$$

and

$$\vec{\boldsymbol{z}} \coloneqq (\boldsymbol{z} \otimes \mathbf{1}_{n+1}, \mathbf{1}_{n+1} \otimes \boldsymbol{z}) = \begin{pmatrix} z_0 \cdot \mathbf{1}_{n+1} & \boldsymbol{z} \\ \vdots & \\ z_n \cdot \mathbf{1}_{n+1} & \boldsymbol{z} \end{pmatrix} \in \mathbb{C}^{(n+1)^2 \times 2}, \tag{5.19}$$

where $\boldsymbol{w} = (w_j)_{j=0}^{n} \in \mathbb{R}^{n+1}$ with the weights $w_j > 0$, $j = 0, \ldots, n$, in (5.10) and $\boldsymbol{z} = (z_j)_{j=0}^{n} \in \mathbb{R}^{n+1}$ with the points $z_j = \frac{1}{2} \cos(\frac{j\pi}{n}) \in \left[-\frac{1}{2}, \frac{1}{2}\right]$ in (5.8), as well as setting $\vec{n} \coloneqq (n+1)^2 - 1$, both representations (5.17) and (5.14) can be used interchangeably. For $d > 2$ this construction is repeated sequentially, such that we deal with

$$\vec{\boldsymbol{w}} \coloneqq \boldsymbol{w} \otimes \Big(\boldsymbol{w} \otimes \big(\cdots \otimes (\boldsymbol{w} \otimes \boldsymbol{w}) \big) \Big) \in \mathbb{C}^{(n+1)^d} \tag{5.20}$$

and

$$\vec{\boldsymbol{z}} \coloneqq \Big(\boldsymbol{z} \otimes \mathbf{1}_{(n+1)^{d-1}}, \mathbf{1}_{n+1} \otimes \big(\cdots \otimes (\boldsymbol{z} \otimes \mathbf{1}_{n+1}, \mathbf{1}_{n+1} \otimes \boldsymbol{z})\big)\Big) \in \mathbb{C}^{(n+1)^d \times d}. \tag{5.21}$$

However, despite the equality of these representations (5.17) and (5.14), comparing them in terms of the computational complexity, it turns out that the computation of (5.14) is much more efficient. This can be shown by assuming that both representations shall be evaluated at P arbitrary points $\boldsymbol{x}_p$, $p = 1, \ldots, P$. Then the computation of (5.14) can be realized by means of d one-dimensional NNFFTs, cf. Algorithm 2.6, and $(d-1)$ multiplications, such that we obtain a total arithmetic complexity of $\mathcal{O}(dM \log M + dn + dP)$. In contrast, for (5.17) it is sufficient to employ a single d-dimensional NNFFT (in addition to assembling the tensor products of the vectors), but this has a complexity of $\mathcal{O}(dM^d \log M + n^d + P)$. Accordingly, although both representations (5.17) and (5.14) are identical, for evaluation purposes it is recommended to use the much more efficient product of one-dimensional exponential sums (5.14) whenever possible. ⋄

5.1.2 The fast sinc transform

Given the approximation of the sinc function $\operatorname{sinc}(M\pi\boldsymbol{x})$ by means of the exponential sums (2.19), we can now state a fast approximate algorithm for the discrete sinc transform (5.2).

For simplicity, we start again with the univariate setting $d = 1$, analogous to [KPT23, Section 6]. Inserting the approximation (5.12) into the discrete sinc transform (5.2) with given a_k, $b_\ell \in \left[-\frac{1}{2}, \frac{1}{2}\right]$ yields

$$\begin{aligned} h(b_\ell) &= \sum_{k \in \mathcal{I}_K} c_k \operatorname{sinc}\big(M\pi(b_\ell - a_k)\big) \approx \sum_{k \in \mathcal{I}_K} c_k \sum_{j=0}^{n} w_j \, \mathrm{e}^{-2\pi \mathrm{i} M z_j (b_\ell - a_k)} \\ &= \sum_{j=0}^{n} w_j \Bigg(\sum_{k \in \mathcal{I}_K} c_k \, \mathrm{e}^{2\pi \mathrm{i} M z_j a_k} \Bigg) \mathrm{e}^{-2\pi \mathrm{i} M z_j b_\ell}, \quad \ell \in \mathcal{I}_L. \end{aligned} \tag{5.22}$$

Note that the term inside the brackets is an exponential sum of the form (2.19), which can be computed using an NNFFT, see Algorithm 2.6. The remaining outer sum is of the same form, and thus can also be computed using an NNFFT. Hence, similar to [GLI06], we may approximate the discrete sinc transform (5.2) for $d = 1$ by means of an NNFFT, a multiplication

by the given weights w_j, and another NNFFT in $\mathcal{O}(M \log M + K + L + n)$ arithmetic operations. We remark that for a fixed bandwidth M also the number n of quadrature points can be fixed for given target accuracy in Theorem 5.4, such that the actual computational complexity reduces to $\mathcal{O}(K + L)$.

In the multivariate setting with $d > 1$ we recognize that the decomposition (5.14) into a product of one-dimensional exponential sums is generally not useful, unless (5.2) possesses a certain tensor structure. In general, we rather have to make use of the tensor notation (5.17) introduced in Remark 5.9, such that the discrete sinc transform (5.2) is approximated by

$$\begin{aligned} h(\boldsymbol{b}_\ell) &= \sum_{k \in \mathcal{I}_K} c_k \operatorname{sinc}\bigl(M\pi(\boldsymbol{b}_\ell - \boldsymbol{a}_k)\bigr) \approx \sum_{k \in \mathcal{I}_K} c_k \left(\sum_{j=0}^{\vec{n}} \vec{w}_j \, \mathrm{e}^{-2\pi \mathrm{i} M \vec{\boldsymbol{z}}_j (\boldsymbol{b}_\ell - \boldsymbol{a}_k)} \right) \\ &= \sum_{j=0}^{\vec{n}} \vec{w}_j \left(\sum_{k \in \mathcal{I}_K} c_k \, \mathrm{e}^{2\pi \mathrm{i} M \vec{\boldsymbol{z}}_j \boldsymbol{a}_k} \right) \mathrm{e}^{-2\pi \mathrm{i} M \vec{\boldsymbol{z}}_j \boldsymbol{b}_\ell}, \quad \ell \in \mathcal{I}_L, \end{aligned} \tag{5.23}$$

with the tensorized quadrature weights (5.20) and the tensorized quadrature points (5.21). Thus, for $d > 1$ the discrete sinc transform (5.2) can be computed the same way as in the univariate setting (5.22) using d-dimensional NNFFTs, see Algorithm 2.6, which results in an arithmetic complexity of $\mathcal{O}(dM^d \log M + K + L + n^d)$. Similarly, for fixed parameters M and n this complexity reduces to $\mathcal{O}(K + L)$. In addition, note that this is basically the same procedure as in [GLI06], where the arithmetic complexity was overestimated as $\mathcal{O}((K + L) \log(K + L))$.

However, in the special case that the coefficients $\boldsymbol{c} \coloneqq (c_k)_{k \in \mathcal{I}_K}$ as well as the points $\boldsymbol{a} \coloneqq (\boldsymbol{a}_k)_{k \in \mathcal{I}_K}$ possess a tensor decomposition of the form

$$\boldsymbol{c} = \boldsymbol{\gamma}_1 \otimes \boldsymbol{\gamma}_2 = \begin{pmatrix} \gamma_{11} \cdot \boldsymbol{\gamma}_2 \\ \vdots \\ \gamma_{1\kappa} \cdot \boldsymbol{\gamma}_2 \end{pmatrix} \in \mathbb{C}^K, \quad \boldsymbol{\gamma}_1, \boldsymbol{\gamma}_2 \in \mathbb{C}^\kappa, \tag{5.24}$$

and

$$\boldsymbol{a} = (\boldsymbol{\alpha} \otimes \mathbf{1}_\kappa, \mathbf{1}_\kappa \otimes \boldsymbol{\alpha}) = \begin{pmatrix} \alpha_1 \cdot \mathbf{1}_\kappa & \boldsymbol{\alpha} \\ \vdots & \\ \alpha_\kappa \cdot \mathbf{1}_\kappa & \boldsymbol{\alpha} \end{pmatrix} \in \mathbb{C}^{K \times 2}, \quad \boldsymbol{\alpha} \in \mathbb{C}^\kappa, \tag{5.25}$$

with $\kappa \in \mathbb{N}$ and $\kappa^2 = K$, the fast sinc transform can be accelerated as follows. Note that, for the sake of simplicity, the procedure is described only for $d = 2$, while the generalization to $d > 2$ is straightforward with tensor decompositions analogous to (5.20) and (5.21). Using the structure of (5.24) and (5.25), as well as the quadrature points (5.19), the vector of the inner sums in (5.23) can be denoted as

$$\begin{aligned}
\vec{\boldsymbol{g}} = (\vec{g}_j)_{j=0}^{\vec{n}} &\coloneqq \left(\sum_{k \in \mathcal{I}_K} c_k \, \mathrm{e}^{2\pi \mathrm{i} M \vec{\boldsymbol{z}}_j \boldsymbol{a}_k} \right)_{j=0}^{\vec{n}} \\
&= \left(\sum_{k_1 \in I_\kappa} \sum_{k_2 \in I_\kappa} \gamma_{1k_1} \gamma_{2k_2} \, \mathrm{e}^{2\pi \mathrm{i} M \vec{z}_{j,1} \alpha_{k_1}} \, \mathrm{e}^{2\pi \mathrm{i} M \vec{z}_{j,2} \alpha_{k_2}} \right)_{j=0}^{\vec{n}} \\
&= \begin{pmatrix} \left(\sum_{k_1 \in I_\kappa} \sum_{k_2 \in I_\kappa} \gamma_{1k_1} \gamma_{2k_2} \, \mathrm{e}^{2\pi \mathrm{i} M z_0 \alpha_{k_1}} \, \mathrm{e}^{2\pi \mathrm{i} M z_{j_2} \alpha_{k_2}} \right)_{j_2=0}^{n} \\ \vdots \\ \left(\sum_{k_1 \in I_\kappa} \sum_{k_2 \in I_\kappa} \gamma_{1k_1} \gamma_{2k_2} \, \mathrm{e}^{2\pi \mathrm{i} M z_n \alpha_{k_1}} \, \mathrm{e}^{2\pi \mathrm{i} M z_{j_2} \alpha_{k_2}} \right)_{j_2=0}^{n} \end{pmatrix} \\
&= \left(\sum_{k_1 \in I_\kappa} \gamma_{1k_1} \, \mathrm{e}^{2\pi \mathrm{i} M z_{j_1} \alpha_{k_1}} \right)_{j_1=0}^{n} \otimes \left(\sum_{k_2 \in I_\kappa} \gamma_{2k_2} \, \mathrm{e}^{2\pi \mathrm{i} M z_{j_2} \alpha_{k_2}} \right)_{j_2=0}^{n} \\
&\eqqcolon \boldsymbol{g}_1 \otimes \boldsymbol{g}_2 .
\end{aligned}$$

Therefore, by additionally using the decomposition (5.18) of the quadrature weights, the outer sum in (5.23) can be computed by

$$\begin{aligned}
h_\ell &\coloneqq \sum_{j=0}^{\vec{n}} \vec{w}_j \, \vec{g}_j \, \mathrm{e}^{-2\pi \mathrm{i} M \vec{\boldsymbol{z}}_j \boldsymbol{b}_\ell} \\
&= \sum_{j_1=0}^{n} \sum_{j_2=0}^{n} w_{j_1} \, w_{j_2} \, g_{1j_1} \, g_{2j_2} \, \mathrm{e}^{-2\pi \mathrm{i} M z_{j_1} b_{\ell,1}} \, \mathrm{e}^{-2\pi \mathrm{i} M z_{j_2} b_{\ell,2}} \\
&= \left(\sum_{j_1=0}^{n} w_{j_1} \, g_{1j_1} \, \mathrm{e}^{-2\pi \mathrm{i} M z_{j_1} b_{\ell,1}} \right) \left(\sum_{j_2=0}^{n} w_{j_2} \, g_{2j_2} \, \mathrm{e}^{-2\pi \mathrm{i} M z_{j_2} b_{\ell,2}} \right), \quad \ell \in \mathcal{I}_L .
\end{aligned}$$

In other words, given a suitable tensor structure, we decomposed the discrete sinc transform (5.2) into a product of one-dimensional exponential

sums (5.14), as recommended in Remark 5.9. Thereby, instead of a single d-dimensional NNFFT we may use d one-dimensional NNFFTs, cf. Algorithm 2.6, which is much more efficient. Accordingly, in this setting the fast sinc transform, as an application of the NNFFT, can be summarized for all $d \geq 1$ as follows, cf. [KPT23, Algorithm 6.1].

Algorithm 5.10 (Fast sinc transform)**.**
For $d, M \in \mathbb{N}$ and $K, L \in 2\mathbb{N}$ let $\boldsymbol{a}_k \in \left[-\frac{1}{2}, \frac{1}{2}\right]^d$, $k \in \mathcal{I}_K$, and $\boldsymbol{b}_\ell \in \left[-\frac{1}{2}, \frac{1}{2}\right]^d$, $\ell \in \mathcal{I}_L$, be given nodes, as well as $c_k \in \mathbb{C}$ given coefficients. In addition, let $\kappa \in \mathbb{N}$ with $\kappa^d = K$, such that the coefficients satisfy the tensor decomposition $(c_k)_{k \in \mathcal{I}_K} = \bigotimes_{t=1}^{d} (\gamma_{tk})_{k \in \mathcal{I}_\kappa}$ and the nodes fulfill $(\boldsymbol{a}_k)_{k \in \mathcal{I}_K} = \Big(\boldsymbol{\alpha} \otimes \mathbf{1}_{\kappa^{d-1}}, \mathbf{1}_{d-1} \otimes \big(\cdots \otimes (\boldsymbol{\alpha} \otimes \mathbf{1}_\kappa, \mathbf{1}_\kappa \otimes \boldsymbol{\alpha})\big)\Big) \in \mathbb{C}^{K \times d}$ with $\boldsymbol{\alpha} = (\alpha_1, \ldots, \alpha_\kappa)^\top \in \mathbb{C}^\kappa$. Furthermore, we are given the quadrature points $z_j \in \left[-\frac{1}{2}, \frac{1}{2}\right]$, $j = 0, \ldots, n$, with $n \geq 4M$.

0. Precomputation: Compute the quadrature weights w_j, $j = 0, \ldots, n$, either by solving the least squares problem (5.7) or by means of Algorithm 5.5.

1. For $t = 1, \ldots, d$:

   a) Approximate the sums $\mathcal{O}(M \log M + \kappa + n)$

   $$g_j \approx \sum_{k \in \mathcal{I}_\kappa} \gamma_{tk} \, \mathrm{e}^{2\pi \mathrm{i} M z_j \alpha_k}, \quad j = 0, \ldots, n,$$

   by means of an NNFFT in Algorithm 2.6.

   b) Form the products $\mathcal{O}(n)$

   $$\tau_j \coloneqq w_j \cdot g_j, \quad j = 0, \ldots, n.$$

   c) Approximate the sums $\mathcal{O}(M \log M + L + n)$

   $$\tilde{h}_{\ell,t} \approx \sum_{j=0}^{n} \tau_j \, \mathrm{e}^{-2\pi \mathrm{i} M z_j b_{\ell,t}}, \quad \ell \in \mathcal{I}_L,$$

   by means of an NNFFT in Algorithm 2.6.

2. Compute $\mathcal{O}(dL)$

$$\tilde{h}_\ell \coloneqq \prod_{t=1}^{d} \tilde{h}_{\ell,t}, \quad \ell \in \mathcal{I}_L. \tag{5.26}$$

Output: $\tilde{h}_\ell \approx h(\boldsymbol{b}_\ell)$, $\ell \in \mathcal{I}_L$, cf. (5.2).

Complexity: $\mathcal{O}(dM \log M + d\kappa + dL + dn)$

Remark 5.11. Note that in the univariate case with $d = 1$ the error

$$\max_{\ell \in \mathcal{I}_L} |h(b_\ell) - \tilde{h}_\ell| \tag{5.27}$$

of the fast sinc transform in Algorithm 5.10 was estimated in [KPT23, Theorem 6.2]. There it was shown that (5.27) depends mainly on the quality of the precomputation of the weights w_j, $j = 0, \dots, n$. More precisely, when using the precomputation in Algorithm 5.5, this result ensures that we only need to choose n large enough such that $\frac{48}{35}\, 2^{-n} \cosh\bigl(\frac{3\pi M}{4}\bigr) \leq \varepsilon$ holds for a given target accuracy $\varepsilon > 0$, cf. Theorem 5.4. In other words, for a given target accuracy, the explicit error estimate (5.9) allows us to fix the parameters M and n, such that the complexity of Algorithm 5.10 is independent of these parameters. Consequently, the fast sinc transform can be realized with only $\mathcal{O}(d\kappa + dL)$ arithmetic operations.

For the least squares problem (5.7), however, the error of the precomputation depends strongly on the choice of the quadrature points z_j, $j = 0, \dots, n$, and the accuracy of the iteration procedure, which makes it impossible to bound the resulting error (5.27) or introduce such a simplification.

Finally, it should be noted that in case the coefficients vector $\boldsymbol{c}$ in (5.24) satisfies $\sum_{k \in \mathcal{I}_\kappa} |\gamma_{tk}| \leq 1$, $t = 1, \dots, d$, the estimate of the error (5.27) in [KPT23, Theorem 6.2] can be generalized to $d > 1$ by means of Lemma 5.7. ◇

Remark 5.12. Summarizing, we examine certain special cases, where the fast sinc transform in Algorithm 5.10 simplifies.

(i) If the coefficients of (5.2) satisfy $\boldsymbol{c} = \bigotimes_{t=1}^{d} \boldsymbol{\gamma}$, i. e., the factors in the decomposition (5.24) are all identical, then the steps a) and b) of Algorithm 5.10 are independent of d, and the overall complexity reduces to $\mathcal{O}(dM \log M + \kappa + dL + dn)$.

(ii) If the evaluation points $\boldsymbol{b} \coloneqq (\boldsymbol{b}_\ell)_{\ell \in \mathcal{I}_L}$ of (5.2) also possess a tensor decomposition of the form

$$\boldsymbol{b} = (\boldsymbol{\beta} \otimes \mathbf{1}_\lambda, \mathbf{1}_\lambda \otimes \boldsymbol{\beta}) = \begin{pmatrix} \beta_1 \cdot \mathbf{1}_\lambda & \boldsymbol{\beta} \\ \vdots & \\ \beta_\lambda \cdot \mathbf{1}_\lambda & \boldsymbol{\beta} \end{pmatrix} \in \mathbb{C}^{L \times 2}, \quad \boldsymbol{\beta} \in \mathbb{C}^\lambda, \quad (5.28)$$

with $\lambda \in \mathbb{N}$ and $\lambda^2 = L$ for $d = 2$, or analogous to (5.19) for $d > 2$, respectively, the outer sums in (5.23) can be computed by

$$\begin{aligned}
(h_\ell)_{\ell \in \mathcal{I}_L} &= \left(\sum_{j=0}^{\vec{n}} \vec{w}_j \, \vec{g}_j \, \mathrm{e}^{-2\pi \mathrm{i} M \boldsymbol{\vec{z}}_j \boldsymbol{b}_\ell} \right)_{\ell \in \mathcal{I}_L} \\
&= \left(\sum_{j_1=0}^{n} \sum_{j_2=0}^{n} w_{j_1} \, w_{j_2} \, g_{1 j_1} \, g_{2 j_2} \, \mathrm{e}^{-2\pi \mathrm{i} M z_{j_1} b_{\ell,1}} \, \mathrm{e}^{-2\pi \mathrm{i} M z_{j_2} b_{\ell,2}} \right)_{\ell \in \mathcal{I}_L} \\
&= \begin{pmatrix} \left(\sum_{j_1=0}^{n} \sum_{j_2=0}^{n} w_{j_1} \, w_{j_2} \, g_{1 j_1} \, g_{2 j_2} \, \mathrm{e}^{-2\pi \mathrm{i} M z_{j_1} \beta_1} \, \mathrm{e}^{-2\pi \mathrm{i} M z_{j_2} \beta_{\ell_2}} \right)_{\ell_2=1}^{\lambda} \\ \vdots \\ \left(\sum_{j_1=0}^{n} \sum_{j_2=0}^{n} w_{j_1} \, w_{j_2} \, g_{1 j_1} \, g_{2 j_2} \, \mathrm{e}^{-2\pi \mathrm{i} M z_{j_1} \beta_\lambda} \, \mathrm{e}^{-2\pi \mathrm{i} M z_{j_2} \beta_{\ell_2}} \right)_{\ell_2=1}^{\lambda} \end{pmatrix} \\
&= \left(\sum_{j_1=0}^{n} w_{j_1} \, g_{1 j_1} \, \mathrm{e}^{-2\pi \mathrm{i} M z_{j_1} \beta_{\ell_1}} \right)_{\ell_1=1}^{\lambda} \otimes \left(\sum_{j_2=0}^{n} w_{j_2} \, g_{2 j_2} \, \mathrm{e}^{-2\pi \mathrm{i} M z_{j_2} \beta_{\ell_2}} \right)_{\ell_2=1}^{\lambda} \\
&=: \boldsymbol{h}_1 \otimes \boldsymbol{h}_2.
\end{aligned}$$

Consequently, the complexity of step c) in Algorithm 5.10 reduces to $\mathcal{O}(M \log M + \lambda + n)$, and instead of computing the product (5.26) in step 2 of Algorithm 5.10, we have to compute the tensor product $(h_\ell)_{\ell \in \mathcal{I}_L} = \bigotimes_{t=1}^{d} \boldsymbol{h}_t$ in $\mathcal{O}(\lambda^d) = \mathcal{O}(L)$ arithmetic operations. Therefore, the overall complexity of Algorithm 5.10 reduces to $\mathcal{O}(dM \log M + d\kappa + L + dn)$.

(iii) In case that both of the aforementioned conditions are met, all the steps a), b) and c) are independent of d, thereby reducing the overall complexity of Algorithm 5.10 to $\mathcal{O}(M \log M + \kappa + L + n)$.

(iv) For equispaced points $\boldsymbol{a}_k$ with $\boldsymbol{\alpha} = \big(\frac{\tilde{k}}{M}\big)_{\tilde{k}\in\mathcal{I}_M}$ and $\kappa = M$ in (5.25), the NNFFT in step a) of Algorithm 5.10 turns into an NFFT, see Algorithm 2.2, such that the overall complexity of Algorithm 5.10 reduces to $\mathcal{O}(dM\log M + dL + dn)$.

(v) For equispaced evaluation points $\boldsymbol{b}_\ell$ in (5.2), i. e., points satisfying a decomposition of the form (5.28) with $\boldsymbol{\beta} = \big(\frac{\tilde{\ell}}{M}\big)_{\tilde{\ell}\in\mathcal{I}_M}$ and $\lambda = M$, the NNFFT in step c) of Algorithm 5.10 simplifies to an adjoint NFFT, see Algorithm 2.5. Note, however, that the overall complexity of Algorithm 5.10 remains $\mathcal{O}(dM\log M + d\kappa + M^d + dn)$.

(vi) In case that both sets of nodes $\boldsymbol{a}_k$ and $\boldsymbol{b}_\ell$ are equispaced, both steps a) and c) of Algorithm 5.10 turn into an (adjoint) NFFT and thus the computational cost reduces to $\mathcal{O}(dM\log M + dn + M^d)$. ◇

5.2 Application to regularized Shannon sampling formulas

In this section we consider a generalization of the fast sinc transform in Algorithm 5.10 to the regularized Shannon sampling sums from Section 4.3. More precisely, in case the direct evaluation of the partial sums (4.38) is too costly, we describe an efficient approximation procedure analogous to Algorithm 5.10 in Section 5.2.1. Similarly, an approximation procedure can also be derived for the regularized Shannon sampling formula with localized sampling (4.74) in Section 5.2.2.

5.2.1 Fast approximation using frequency window functions

Firstly, we introduce a method analogous to the fast sinc transform in Algorithm 5.10 for the regularization with a window function in frequency domain from Section 4.3.1. As observed previously, the partial sums (4.38) are dense, which is why a direct computation is rather costly, similar to (4.12). Likewise, by definition of the frequency window function (4.33) its corresponding function (4.34) in spatial domain is bandlimited with bandwidth L. Thereby, we immediately obtain the existence of suitable quadrature weights $w_j > 0$ and quadrature points $z_j \in \big(-\frac{1}{2}, \frac{1}{2}\big)$, $j = 0, \ldots, n$, by

means of Theorem 5.2. However, note that by Theorem 5.2 we only receive a good approximation of ψ on the interval $\big[-\frac{1}{2}, \frac{1}{2}\big]$. Since the partial sums $P_{\psi,T} f$ in (4.38) shall be evaluated at $x \in [-1, 1]$ with $\ell \in \{-T, \dots, T\}$, $T > L$, we have $|x - \frac{\ell}{L}| \le 1 + \frac{T}{L}$. Therefore, we adjust the result analogous to Corollary 5.3, such that the number of quadrature points needs to fulfill $n + 1 \ge 4\big(1 + \frac{T}{L}\big)M$.

Similar to Section 5.1.1, the practical approximation of the function ψ by means of an exponential sum shall be realized efficiently using Clenshaw–Curtis quadrature. To this end, explicit weights can be derived analogous to Theorem 5.4 by rewriting the function (4.34) as

$$\begin{aligned}\psi(x) &= \int_{\mathbb{R}} \hat{\psi}(v)\, \mathrm{e}^{2\pi \mathrm{i} v x}\, \mathrm{d}v = \int_{-L/2}^{L/2} \hat{\psi}(v)\, \mathrm{e}^{2\pi \mathrm{i} v x}\, \mathrm{d}v \\ &= \int_{-1}^{1} \tfrac{L}{2}\, \hat{\psi}\big(\tfrac{Lu}{2}\big)\, \mathrm{e}^{-\pi \mathrm{i} L u x}\, \mathrm{d}u.\end{aligned}$$

Thus, by utilizing the Clenshaw–Curtis quadrature rule for the integrand $h(u) \coloneqq \frac{L}{2}\, \hat{\psi}\big(\frac{Lu}{2}\big)\, \mathrm{e}^{-\pi \mathrm{i} L u x}$ with fixed parameter $x \in \big[-1 - \frac{T}{L}, 1 + \frac{T}{L}\big]$, we obtain

$$\frac{1}{L}\, \psi(x) = \frac{1}{L} \int_{-1}^{1} h(u)\, \mathrm{d}u \approx \frac{1}{L} \sum_{j=0}^{n} 2 w_j\, h(2 z_j) = \sum_{j=0}^{n} w_j\, \hat{\psi}(L z_j)\, \mathrm{e}^{-2\pi \mathrm{i} L z_j x},$$

with given Chebyshev points z_j in (5.8) and the quadrature weights w_j in (5.10). In other words, now we have the scaled weights

$$w_j^{\hat{\psi}} \coloneqq w_j\, \hat{\psi}(L z_j), \tag{5.29}$$

where in practice the weights w_j in (5.10) can be precomputed by means of the fast procedure in Algorithm 5.5 again.

In addition, we obtain the following error estimate analogous to Theorem 5.4.

Theorem 5.13. *Let the nonharmonic bandwidth $M \in 2\mathbb{N}$ with $M \gg 1$ be given. Then for sufficiently large $n \in \mathbb{N}$ with $n + 1 \ge 4\big(1 + \frac{T}{L}\big)M$, the estimate*

$$\left| \frac{1}{L} \psi(x) - \sum_{j=0}^{n} w_j^{\hat{\psi}}\, \mathrm{e}^{-2\pi \mathrm{i} L z_j x} \right| \le \frac{48}{35}\, 2^{-n}\, L \cosh\left(\frac{3\pi L}{4}\right),$$

holds for all $x \in \big[-1-\frac{T}{L},\, 1+\frac{T}{L}\big]$ *with the Chebyshev points* z_j *in* (5.8) *and the scaled quadrature weights* (5.29).

Proof. Analogous to the proof of Theorem 5.4. ∎

Finally, the T-th partial sums (4.38) can be approximated by

$$\begin{aligned}(P_{\psi,T} f)(x) \approx (\tilde{P}_{\psi,T} f)(x) &:= \sum_{\ell=-T}^{T} f\big(\tfrac{\ell}{L}\big) \sum_{j=0}^{n} w_j^{\hat{\psi}}\, \mathrm{e}^{-2\pi \mathrm{i} L z_j \left(x-\frac{\ell}{L}\right)} \\ &= \sum_{j=0}^{n} w_j^{\hat{\psi}} \left(\sum_{\ell=-T}^{T} f\big(\tfrac{\ell}{L}\big)\, \mathrm{e}^{2\pi \mathrm{i} z_j \ell} \right) \mathrm{e}^{-2\pi \mathrm{i} L z_j x}, \quad x \in [-1,\, 1], \end{aligned} \tag{5.30}$$

and thus a variant of the fast sinc transform in Algorithm 5.10 with the scaled weights (5.29) can be applied, where we only have $d = 1$. Note that by Remark 5.12 (iv) the fast sinc transform in Algorithm 5.10 simplifies since the inner sum of (5.30) can be computed by means of an NFFT. Hence, the obtained algorithm can be summarized as follows.

Algorithm 5.14 (Fast sinc transform for frequency regularization)**.**
For $M, P \in \mathbb{N}$ and $T > L := M\,(1+\lambda) \in \mathbb{N}$ with $\lambda > 0$, let $x_p \in [-1,\, 1]$, $p = 1, \ldots, P$, be given nodes, as well as $f\big(\frac{\ell}{L}\big)$, $\ell = -T, \ldots, T$, given samples of a bandlimited function $f \in \mathcal{B}_{M/2}(\mathbb{R})$. Furthermore, we are given the quadrature points $z_j \in \big[-\frac{1}{2},\, \frac{1}{2}\big]$, $j = 0, \ldots, n$, with $n+1 \geq 4\,\big(1+\frac{T}{L}\big) M$ and the corresponding evaluations $\hat{\psi}(L z_j)$ of the frequency window function (4.33).

0. Precomputation: Compute the quadrature weights w_j, $j = 0, \ldots, n$, either by solving the least squares problem (5.7) or by means of Algorithm 5.5.

1. Approximate the sums $\mathcal{O}(T \log T + n)$

$$g_j \approx \sum_{\ell=-T}^{T} f\big(\tfrac{\ell}{L}\big)\, \mathrm{e}^{2\pi \mathrm{i} z_j \ell}, \quad j = 0, \ldots, n,$$

by means of an NFFT in Algorithm 2.2.

2. Form the products $\mathcal{O}(n)$

$$\tau_j \coloneqq w_j \, \hat{\psi}(Lz_j) \cdot g_j, \quad j = 0, \dots, n.$$

3. Approximate the sums $\mathcal{O}(L \log L + P + n)$

$$(\tilde{P}_{\psi,T} f)(x_p) \approx \sum_{j=0}^{n} \tau_j \, \mathrm{e}^{-2\pi \mathrm{i} L z_j x_p}, \quad p = 1, \dots, P,$$

by means of an NNFFT in Algorithm 2.6.

Output: $(\tilde{P}_{\psi,T} f)(x_p) \approx (P_{\psi,T} f)(x_p)$, $p = 1, \dots, P$, cf. (4.38).

In order to compare the computational cost of the direct computation of $P_{\psi,T}$ in (4.38) and its approximation $\tilde{P}_{\psi,T}$ in (5.30), we assume that both representations shall be evaluated at P arbitrary points $x_p \in [-1/2, 1/2]$, $p = 1, \dots, P$. Then the direct computation of $P_{\psi,T}$ in (4.38) has a total arithmetic complexity of $\mathcal{O}(TP)$, while the approximation by means of the fast sinc transform in Algorithm 5.14 has a complexity of $\mathcal{O}(L \log L + T \log T + n + P)$. Thus, for the evaluation at a single point, i. e., for $P = 1$, the direct computation of (4.38) is obviously much faster, whereas for increasing numbers P the approximation by means of the fast sinc transform in Algorithm 5.14 becomes more efficient. For the numerical comparison of these two methods, we refer to Example 5.19.

5.2.2 Fast approximation using spatial window functions

A similar method can also be derived for the regularization with a window function in spatial domain from Sections 4.3.2 and 4.4. Namely, in case the regularized Shannon sampling formula with localized sampling (4.74) or (4.121) is too costly to be computed directly, an efficient approximation procedure analogous to Algorithm 5.10 can be used. Note, however, that in general these sums are sparse due to the characteristic function in their definition, i. e., this method might only be useful for rather large truncation parameters $m \in \mathbb{N}$ or higher dimensions $d > 1$. For the sake of simplicity, we firstly describe only the univariate version with $d = 1$.

As already observed in Lemmas 4.32, 4.38, 4.43, and 4.47, for the window functions mentioned in Remark 4.22 the regularized

sinc function $\psi(x) = \operatorname{sinc}(L\pi x)\,\varphi(x)$ is essentially bandlimited on the interval $\left[-\frac{L}{2}\,(1+\varepsilon),\ \frac{L}{2}\,(1+\varepsilon)\right]$ with certain $\varepsilon > 0$, where in practice $\varepsilon = 1$ always seems sufficient, cf. Figures 4.4, 4.5, 4.7, and 4.10. Thus, although Theorem 5.2 is not applicable since ψ is not bandlimited, we aim to use the fact that ψ is essentially bandlimited. To this end, similar to Section 5.1.1, the practical approximation of the function ψ by means of an exponential sum shall be realized efficiently using Clenshaw–Curtis quadrature. Note that since the regularized Shannon sampling formula with localized sampling (4.74) can be written as

$$(R_{\varphi,m} f)(x) \coloneqq \sum_{\ell \in \mathbb{Z}} f\left(\tfrac{\ell}{L}\right) \psi\left(x - \tfrac{\ell}{L}\right) \chi_{\left[-\frac{m}{L},\,\frac{m}{L}\right]}\left(x - \tfrac{\ell}{L}\right), \quad x \in \mathbb{R},$$

we only need to evaluate ψ for $\left|x - \frac{\ell}{L}\right| \leq \frac{m}{L}$ with $2m \leq L$. Hence, it suffices to consider the approximation of $\psi(x)$ for $x \in \left[-\frac{1}{2},\,\frac{1}{2}\right]$. In other words, although Theorem 5.2 is not applicable since ψ is only essentially bandlimited, we assume that the number of quadrature points should satisfy $n + 1 \geq 2M$ as well.

Since we have seen that $\hat{\psi}$ is negligible for $|v| > L$, we have by the inverse Fourier transform (4.4) that

$$\psi(x) = \int_{\mathbb{R}} \hat{\psi}(v)\,\mathrm{e}^{2\pi \mathrm{i} v x}\,\mathrm{d}v \approx \int_{-L}^{L} \hat{\psi}(v)\,\mathrm{e}^{2\pi \mathrm{i} v x}\,\mathrm{d}v = \int_{-1}^{1} L\,\hat{\psi}(Lu)\,\mathrm{e}^{-2\pi \mathrm{i} L u x}\,\mathrm{d}u.$$

We remark that we additionally used the fact that for the considered window functions from Remark 4.22 the regularized sinc function $\hat{\psi}$ is even by Lemmas 4.31, 4.37, 4.42, and 4.46. Then explicit weights can be derived analogous to Theorem 5.4 by means of Clenshaw–Curtis quadrature for the integrand $h(u) \coloneqq L\,\hat{\psi}(Lu)\,\mathrm{e}^{-2\pi \mathrm{i} L u x}$ with fixed parameter $x \in \left[-\frac{1}{2},\,\frac{1}{2}\right]$. This reads as

$$\begin{aligned}
\psi(x) &\approx \int_{-1}^{1} h(u)\,\mathrm{d}u \\
&\approx \sum_{j=0}^{n} 2 w_j\,L\,\hat{\psi}(2Lz_j)\,\mathrm{e}^{-2\pi \mathrm{i}(2L) z_j x} = \tilde{L} \sum_{j=0}^{n} w_j\,\hat{\psi}(\tilde{L} z_j)\,\mathrm{e}^{-2\pi \mathrm{i} \tilde{L} z_j x}
\end{aligned}$$

with given Chebyshev points $z_j = \frac{1}{2}\cos\left(\frac{j\pi}{n}\right) \in \left[-\frac{1}{2},\,\frac{1}{2}\right]$, $j = 0, \ldots, n$, in (5.8), the quadrature weights w_j in (5.10), and $\tilde{L} \coloneqq 2L$. In other words,

now we have the scaled weights

$$w_j^{\varphi} \coloneqq \tilde{L} w_j \, \hat{\psi}(\tilde{L} z_j). \tag{5.31}$$

In practice, the weights w_j in (5.10) can again be precomputed by means of the fast procedure in Algorithm 5.5, and the evaluations of $\hat{\psi}$ need to be precomputed according to Lemmas 4.31, 4.37, 4.42, and 4.46.

Finally, using the representation (4.77) the regularized Shannon sampling formula with localized sampling (4.74) can be approximated on any open interval $\left(\frac{k}{L}, \frac{k+1}{L}\right)$ with $k \in \mathbb{Z}$ by

$$\begin{aligned}(R_{\varphi,m} f)\big(x + \tfrac{k}{L}\big) &\approx (\tilde{R}_{\varphi,m} f)\big(x + \tfrac{k}{L}\big) \\ &\coloneqq \sum_{\ell \in \mathcal{J}_m} f\big(\tfrac{\ell+k}{L}\big) \sum_{j=0}^{n} w_j^{\varphi} \, \mathrm{e}^{-2\pi \mathrm{i} \tilde{L} z_j \left(x - \frac{\ell}{L}\right)} \\ &= \sum_{j=0}^{n} w_j^{\varphi} \left(\sum_{\ell \in \mathcal{J}_m} f\big(\tfrac{\ell+k}{L}\big) \, \mathrm{e}^{2\pi \mathrm{i} \tilde{L} z_j \ell / L} \right) \mathrm{e}^{-2\pi \mathrm{i} \tilde{L} z_j x}, \quad x \in \big(0, \tfrac{1}{L}\big),\end{aligned} \tag{5.32}$$

with the index set $\mathcal{J}_m$ defined in (4.76). Thus, a variant of the fast sinc transform in Algorithm 5.10 with the scaled weights (5.31) can be applied, where we only have $d = 1$. Note that by Remark 5.12 (iv) the fast sinc transform in Algorithm 5.10 simplifies since the inner sum of (5.32) is computed by means of an NFFT. Hence, the obtained algorithm can be summarized as follows.

Algorithm 5.15 (Fast sinc transform for spatial regularization)**.**

For $M, P \in \mathbb{N}$, $L \coloneqq M\,(1+\lambda) \in \mathbb{N}$ with $\lambda > 0$, and $\tilde{L} \coloneqq 2L$ let $x_p \in \big(0, \frac{1}{L}\big)$, $p = 1, \ldots, P$, be given nodes, as well as $f\big(\frac{\ell+k}{L}\big)$, $\ell \in \mathcal{J}_m$, cf. (4.76), given samples of a bandlimited function $f \in \mathcal{B}_{M/2}(\mathbb{R})$. Furthermore, we are given the quadrature points $z_j \in \big[-\frac{1}{2}, \frac{1}{2}\big]$, $j = 0, \ldots, n$, with $n + 1 \geq 2M$ and the corresponding evaluations $\hat{\psi}(\tilde{L} z_j)$ of the Fourier transform of the regularized sinc function (4.69).

0. Precomputation: Compute the quadrature weights w_j, $j = 0, \ldots, n$, either by solving the least squares problem (5.7) or by means of Algorithm 5.5.

1. Approximate the sums $\mathcal{O}(m \log m + n)$

$$g_j \approx \sum_{\ell \in \mathcal{J}_m} f\big(\tfrac{\ell+k}{L}\big)\, \mathrm{e}^{2\pi \mathrm{i} \tilde{L} z_j \ell / L}, \quad j = 0, \dots, n,$$

by means of an NFFT in Algorithm 2.2.

2. Form the products $\mathcal{O}(n)$

$$\tau_j \coloneqq \tilde{L} w_j\, \hat{\psi}(\tilde{L} z_j) \cdot g_j, \quad j = 0, \dots, n.$$

3. Approximate the sums $\mathcal{O}(L \log L + P + n)$

$$(\tilde{R}_{\varphi,m} f)(x_p) \approx \sum_{j=0}^{n} \tau_j\, \mathrm{e}^{-2\pi \mathrm{i} \tilde{L} z_j x_p}, \quad p = 1, \dots, P,$$

by means of an NNFFT in Algorithm 2.6.

Output: $(\tilde{R}_{\varphi,m} f)(x_p) \approx (R_{\varphi,m} f)(x_p)$, $p = 1, \dots, P$, cf. (4.74).

In order to compare the computational cost of the direct computation of $R_{\varphi,m} f$ in (4.74) and its approximation $\tilde{R}_{\varphi,m} f$ in (5.32), we assume that both representations shall be evaluated at P arbitrary points $x_p \in \big(0, \frac{1}{L}\big)$, $p = 1, \dots, P$. Then the direct computation of $R_{\varphi,m} f$ in (4.74) has a total arithmetic complexity of $\mathcal{O}(mP)$, while the approximation by means of the fast sinc transform in Algorithm 5.15 has a complexity of $\mathcal{O}(L \log L + m \log m + n + P)$. Thus, for the evaluation at a single point, i. e., for $P = 1$, the direct computation of (4.74) is obviously much faster, whereas for increasing numbers P the approximation by means of the fast sinc transform in Algorithm 5.15 becomes more efficient. For the numerical comparison of these two methods, we refer to Example 5.20.

Additionally, we remark that this procedure can be generalized to the multivariate setting (4.124) analogous to (5.23).

5.3 Approximation of bandlimited functions based on Fourier data

So far, this chapter was dedicated to the task of efficiently computing certain sinc sums including only terms in the spatial domain. In this section, we

consider a completely different problem, where the sinc function still plays an important role as it provides a fast and accurate approximation. More precisely, for given values $\hat{f}(\boldsymbol{k})$, $\boldsymbol{k} \in \mathcal{I}_{\boldsymbol{M}}$, of the Fourier transform (4.4) of a bandlimited function $f \in \mathcal{B}_{M/2}(\mathbb{R}^d)$, we are looking for function evaluations $f(\boldsymbol{x}_j)$ at given nonequispaced points $\boldsymbol{x}_j$, $j = 1, \dots N$. Note that if a trigonometric polynomial $f \in L_2(\mathbb{T}^d)$ is given, it is already known that this problem can be solved by means of the NFFT, see Algorithm 2.2. Hence, we aim to introduce a new NFFT-like procedure for bandlimited functions, which is based on the regularized Shannon sampling formulas, see Section 4.4.

5.3.1 Derivation of the fast algorithm

To this end, note that it is known by Section 4.3.2 that the regularized Shannon sampling formula $R_\varphi f$ in (4.64) with suitable window function $\varphi \in \Phi$ yields a good approximation of f. Further assume that the bandlimited function $f \in \mathcal{B}_{M/2}(\mathbb{R}^d)$ fulfills the condition (4.35) with $L > M$. Thus, inserting the approximation (4.64) into the Fourier transform (4.1) and using the definition (4.69) of the regularized sinc function $\psi(x) := \operatorname{sinc}(L\pi x)\,\varphi(x)$, we have

$$\begin{aligned}
\hat{f}(\boldsymbol{v}) &= \int_{\mathbb{R}^d} f(\boldsymbol{x})\, \mathrm{e}^{-2\pi \mathrm{i} \boldsymbol{v}\boldsymbol{x}}\, \mathrm{d}\boldsymbol{x} \approx \int_{\mathbb{R}^d} (R_\varphi f)(\boldsymbol{x})\, \mathrm{e}^{-2\pi \mathrm{i} \boldsymbol{v}\boldsymbol{x}}\, \mathrm{d}\boldsymbol{x} \\
&= \int_{\mathbb{R}^d} \sum_{\boldsymbol{\ell} \in \mathbb{Z}^d} f\big(\tfrac{\boldsymbol{\ell}}{L}\big)\, \psi\big(\boldsymbol{x} - \tfrac{\boldsymbol{\ell}}{L}\big)\, \mathrm{e}^{-2\pi \mathrm{i} \boldsymbol{v}\boldsymbol{x}}\, \mathrm{d}\boldsymbol{x} \\
&= \sum_{\boldsymbol{\ell} \in \mathbb{Z}^d} f\big(\tfrac{\boldsymbol{\ell}}{L}\big)\, \mathrm{e}^{-2\pi \mathrm{i} \boldsymbol{v}\boldsymbol{\ell}/L} \int_{\mathbb{R}^d} \psi(\boldsymbol{y})\, \mathrm{e}^{-2\pi \mathrm{i} \boldsymbol{v}\boldsymbol{y}}\, \mathrm{d}\boldsymbol{y} \\
&= \Bigg(\sum_{\boldsymbol{\ell} \in \mathbb{Z}^d} f\big(\tfrac{\boldsymbol{\ell}}{L}\big)\, \mathrm{e}^{-2\pi \mathrm{i} \boldsymbol{v}\boldsymbol{\ell}/L} \Bigg) \cdot \hat{\psi}(\boldsymbol{v}). \qquad (5.33)
\end{aligned}$$

We remark that summation and integration may be interchanged in (5.33) by the theorem of Fubini–Tonelli, since

$$\sum_{\boldsymbol{\ell} \in \mathbb{Z}^d} \big| f\big(\tfrac{\boldsymbol{\ell}}{L}\big) \big| \cdot \int_{\mathbb{R}^d} |\varphi\big(\boldsymbol{x} - \tfrac{\boldsymbol{\ell}}{L}\big)|\, \mathrm{d}\boldsymbol{x} < \infty$$

is fulfilled, by (4.35) and $\varphi \in L_1(\mathbb{R}^d)$ for all $\varphi \in \Phi$. By defining

$$\hat{\nu}(\boldsymbol{v}) \coloneqq \sum_{\boldsymbol{\ell} \in \mathbb{Z}^d} f\big(\tfrac{\boldsymbol{\ell}}{L}\big)\, \mathrm{e}^{-2\pi \mathrm{i} \boldsymbol{v}\boldsymbol{\ell}/L}, \quad \boldsymbol{v} \in \mathbb{R}^d, \tag{5.34}$$

we recognize that this function $\hat{\nu}$ is L-periodic, since

$$\begin{aligned} \hat{\nu}(\boldsymbol{v}+L) &= \sum_{\boldsymbol{\ell} \in \mathbb{Z}^d} f\big(\tfrac{\boldsymbol{\ell}}{L}\big)\, \mathrm{e}^{-2\pi \mathrm{i}(\boldsymbol{v}+L)\boldsymbol{\ell}/L} \\ &= \sum_{\boldsymbol{\ell} \in \mathbb{Z}^d} f\big(\tfrac{\boldsymbol{\ell}}{L}\big)\, \mathrm{e}^{-2\pi \mathrm{i} \boldsymbol{v}\boldsymbol{\ell}/L}\, \mathrm{e}^{-2\pi \mathrm{i} \boldsymbol{\ell}} = \hat{\nu}(\boldsymbol{v}), \quad \boldsymbol{v} \in \mathbb{R}^d, \end{aligned}$$

by $\mathrm{e}^{2\pi \mathrm{i} r} = 1$, $r \in \mathbb{Z}$. Thus, due to the fact that the Fourier transform of the bandlimited function $f \in \mathcal{B}_{M/2}(\mathbb{R}^d)$ is non-periodic, the approximation (5.33) can only be reasonable for $\boldsymbol{v} \in \big[-\frac{L}{2}, \frac{L}{2}\big]^d$.

As the goal is to recover the nonequispaced samples $f(\boldsymbol{x}_j)$, $j = 1, \ldots, N$, from given values $\hat{f}(\boldsymbol{k})$, $\boldsymbol{k} \in \mathcal{I}_{\boldsymbol{M}}$, we aim to use the approximation (5.34) in combination with a regularized Shannon sampling formula (4.121). For this purpose, we need access to as many equispaced samples $f\big(\frac{\boldsymbol{\ell}}{L}\big)$ as possible, i. e., we are looking for an inversion formula for (5.34). To this end, note that (5.34) can be written as

$$\begin{aligned} \hat{\nu}(\boldsymbol{v}) = &\sum_{\boldsymbol{\ell} \in \mathcal{I}_{\boldsymbol{\Theta}}} f\big(\tfrac{\boldsymbol{\ell}}{L}\big)\, \mathrm{e}^{-2\pi \mathrm{i} \boldsymbol{v}\boldsymbol{\ell}/L} \\ &+ \sum_{\boldsymbol{r} \in \mathbb{Z}^d \setminus \{\boldsymbol{0}\}} \sum_{\boldsymbol{\ell} \in \mathcal{I}_{\boldsymbol{\Theta}}} f\big(\tfrac{\boldsymbol{\ell} + \boldsymbol{r}\Theta}{L}\big)\, \mathrm{e}^{-2\pi \mathrm{i} \boldsymbol{v}(\boldsymbol{\ell} + \boldsymbol{r}\Theta)/L}, \quad \boldsymbol{v} \in \mathbb{R}^d, \end{aligned}$$

where the index set $\mathcal{I}_{\boldsymbol{\Theta}}$ is given in (2.1) with $\boldsymbol{\Theta} = \Theta \cdot \boldsymbol{1}_d$, $\Theta \in 2\mathbb{N}$. Since $f \in \mathcal{B}_{M/2}(\mathbb{R}^d) \subseteq C_0(\mathbb{R}^d)$, see Lemma 4.1, the equispaced samples $f\big(\frac{\boldsymbol{\ell}}{L}\big)$ are negligible for all $\|\boldsymbol{\ell}\|_\infty \geq \frac{\Theta}{2}$ with suitably chosen Θ. In order to avoid aliasing in the computation we assume that $\Theta = L$ is sufficient. Hence, we consider

$$\hat{\nu}(\boldsymbol{v}) \approx \hat{\vartheta}(\boldsymbol{v}) \coloneqq \sum_{\boldsymbol{\ell} \in \mathcal{I}_{\boldsymbol{L}}} f\big(\tfrac{\boldsymbol{\ell}}{L}\big)\, \mathrm{e}^{-2\pi \mathrm{i} \boldsymbol{v}\boldsymbol{\ell}/L}, \quad \boldsymbol{v} \in \mathbb{R}^d, \tag{5.35}$$

and thus by (5.33) the approximation

$$\hat{f}(\boldsymbol{v}) \approx \hat{\vartheta}(\boldsymbol{v}) \cdot \hat{\psi}(\boldsymbol{v}), \quad \boldsymbol{v} \in \big[-\tfrac{L}{2}, \tfrac{L}{2}\big]^d. \tag{5.36}$$

Since it is additionally known that $\hat{f}(\boldsymbol{v}) = 0$ for all $\boldsymbol{v} \notin \big[-\frac{M}{2}, \frac{M}{2}\big]^d$ and $\hat{\psi}(\boldsymbol{v}) \neq 0$ for all $\boldsymbol{v} \in \big[-\frac{L}{2}, \frac{L}{2}\big]^d$, we might use (5.36) and (5.35) for given $\hat{f}(\boldsymbol{k})$, $\boldsymbol{k} \in \mathcal{I}_{\boldsymbol{M}}$, to approximate the equispaced samples $f\big(\frac{\boldsymbol{\ell}}{L}\big)$, $\boldsymbol{\ell} \in \mathcal{I}_{\boldsymbol{L}}$, by setting

$$\hat{\vartheta}(\boldsymbol{k}) = \begin{cases} \frac{\hat{f}(\boldsymbol{k})}{\hat{\psi}(\boldsymbol{k})} & : \quad \boldsymbol{k} \in \mathcal{I}_{\boldsymbol{M}}, \\ 0 & : \quad \boldsymbol{k} \in \mathcal{I}_{\boldsymbol{L}} \setminus \mathcal{I}_{\boldsymbol{M}}, \end{cases}$$

and subsequently computing

$$f\big(\tfrac{\boldsymbol{\ell}}{L}\big) \approx \vartheta_{\boldsymbol{\ell}} := \frac{1}{|\mathcal{I}_{\boldsymbol{L}}|} \sum_{\boldsymbol{k} \in \mathcal{I}_{\boldsymbol{L}}} \hat{\vartheta}(\boldsymbol{k})\, \mathrm{e}^{2\pi \mathrm{i} \boldsymbol{k}\boldsymbol{\ell}/L}, \quad \boldsymbol{\ell} \in \mathcal{I}_{\boldsymbol{L}}, \tag{5.37}$$

by means of an iFFT.

To finally approximate the samples $f(\boldsymbol{x}_j)$, $j = 1, \ldots, N$, we make use of the regularized Shannon sampling formula $R_{\varphi,m} f$ with localized sampling in (4.121). This means, analogous to the NFFT we now assume that the window function $\varphi \in \Phi$ is well localized, such that it is small outside the square $\big[-\frac{m}{L}, \frac{m}{L}\big]^d$ and can be approximated by the compactly supported function φ_m in (4.73). In doing so, we benefit from the good approximation properties of the regularized Shannon sampling formula with localized sampling in (4.121) known by Section 4.4 as well as from its efficiency, since the computation of $(R_{\varphi,m} f)(\boldsymbol{x})$ for fixed $\boldsymbol{x} \in \mathbb{R}^d \setminus \frac{1}{L}\,\mathbb{Z}^d$ requires only $(2m+1)^d$ samples $f\big(\frac{\boldsymbol{\ell}}{L}\big)$, where $\boldsymbol{\ell} \in \mathbb{Z}^d$ fulfills the conditions $|\ell_t - L x_t| \leq m$ for $t = 1, \ldots, d$. However, we have already encountered that using (5.37) we might approximate only the equispaced samples $f\big(\frac{\boldsymbol{\ell}}{L}\big)$ with $\boldsymbol{\ell} \in \mathcal{I}_{\boldsymbol{L}}$. Thereby, the regularized Shannon sampling formula $(R_{\varphi,m} f)(\boldsymbol{x})$ can be evaluated only for $\boldsymbol{x} \in [-\frac{1}{2} + \frac{m}{L}, \frac{1}{2} - \frac{m}{L})^d$, since only in this case exclusively the evaluations $f\big(\frac{\boldsymbol{\ell}}{L}\big)$, $\boldsymbol{\ell} \in \mathcal{I}_{\boldsymbol{L}}$, are needed for the computation due to the fact that

$$\begin{aligned} \varphi_m\big(\boldsymbol{x} - \tfrac{\boldsymbol{\ell}}{L}\big) \neq 0 \iff \big(\boldsymbol{x} - \tfrac{\boldsymbol{\ell}}{L}\big) &\in \big[-\tfrac{m}{L}, \tfrac{m}{L}\big]^d \\ \iff -m + L\boldsymbol{x} \leq \boldsymbol{\ell} &\leq m + L\boldsymbol{x}. \end{aligned}$$

In other words, in order to avoid aliasing in the computation of the inverse Fourier transform in (5.37), we are confronted with a limitation of the feasible interval for the points $\boldsymbol{x}_j$, $j = 1, \ldots, N$. Nevertheless, for

given $\boldsymbol{x}_j \in [-\frac{1}{2} + \frac{m}{L}, \frac{1}{2} - \frac{m}{L})^d$, $j = 1, \ldots, N$, we may insert the approximated samples (5.37) into the definition of the regularized Shannon sampling formula with localized sampling (4.121). Thereby, the final approximation is computed by

$$\begin{aligned}(R_{\varphi,m} f)(\boldsymbol{x}_j) \approx f_j &:= \sum_{\boldsymbol{\ell} \in \mathcal{I}_{\boldsymbol{L}}} \vartheta_{\boldsymbol{\ell}} \operatorname{sinc}\big(L\pi\big(\boldsymbol{x}_j - \tfrac{\boldsymbol{\ell}}{L}\big)\big)\, \varphi_m\big(\boldsymbol{x}_j - \tfrac{\boldsymbol{\ell}}{L}\big) \qquad (5.38)\\ &= \sum_{\boldsymbol{\ell} \in \mathcal{J}_{\boldsymbol{L},m}(\boldsymbol{x}_j)} \vartheta_{\boldsymbol{\ell}} \operatorname{sinc}\big(L\pi\big(\boldsymbol{x}_j - \tfrac{\boldsymbol{\ell}}{L}\big)\big)\, \varphi_m\big(\boldsymbol{x}_j - \tfrac{\boldsymbol{\ell}}{L}\big),\end{aligned}$$

where the index set of the nonzero entries

$$\mathcal{J}_{\boldsymbol{L},m}(\boldsymbol{x}_j) := \big\{\boldsymbol{\ell} \in \mathbb{Z}^d \colon\ -m + L\boldsymbol{x}_j \le \boldsymbol{\ell} \le m + L\boldsymbol{x}_j\big\} \qquad (5.39)$$

contains at most $(2m+1)^d$ entries for each fixed $\boldsymbol{x}_j$, cf. (2.12). Thus, the obtained algorithm can be summarized as follows.

Algorithm 5.16 (NFFT-like procedure for bandlimited functions)**.**

For $d, m, N \in \mathbb{N}$ and $M \in 2\mathbb{N}$ let $\boldsymbol{x}_j \in [-\frac{1}{2} + \frac{m}{L}, \frac{1}{2} - \frac{m}{L})^d$, $j = 1, \ldots, N$, be given nodes as well as $\hat{f}(\boldsymbol{k}) \in \mathbb{C}$, $\boldsymbol{k} \in \mathcal{I}_{\boldsymbol{M}}$, given evaluations of the Fourier transform of the bandlimited function $f \in \mathcal{B}_{M/2}(\mathbb{R}^d)$. Furthermore, we are given the oversampling parameter $\lambda \ge 0$ with $L = M(1+\lambda) \in \mathbb{N}$, as well as the window function $\varphi \in \Phi$, the truncated window function φ_m, the corresponding regularized sinc function ψ and its Fourier transform $\hat{\psi}$.

0. Precomputation:
   a) Compute the nonzero values $\hat{\psi}(\boldsymbol{k})$ for $\boldsymbol{k} \in \mathcal{I}_{\boldsymbol{M}}$, cf. (2.1).
   b) Compute the evaluations $\operatorname{sinc}\big(L\pi\big(\boldsymbol{x}_j - \frac{\boldsymbol{\ell}}{L}\big)\big)\, \varphi_m\big(\boldsymbol{x}_j - \frac{\boldsymbol{\ell}}{L}\big)$ for $j = 1, \ldots, N$, and $\boldsymbol{\ell} \in \mathcal{J}_{\boldsymbol{L},m}(\boldsymbol{x}_j)$, cf. (5.39).
1. Set $\mathcal{O}(|\mathcal{I}_{\boldsymbol{M}}|)$
$$\hat{\vartheta}(\boldsymbol{k}) := \begin{cases} \frac{\hat{f}(\boldsymbol{k})}{\hat{\psi}(\boldsymbol{k})} & : \quad \boldsymbol{k} \in \mathcal{I}_{\boldsymbol{M}}, \\ 0 & : \quad \boldsymbol{k} \in \mathcal{I}_{\boldsymbol{L}} \setminus \mathcal{I}_{\boldsymbol{M}}. \end{cases}$$
2. Compute $\mathcal{O}(|\mathcal{I}_{\boldsymbol{M}}| \log(|\mathcal{I}_{\boldsymbol{M}}|))$
$$\vartheta_{\boldsymbol{\ell}} := \frac{1}{|\mathcal{I}_{\boldsymbol{L}}|} \sum_{\boldsymbol{k} \in \mathcal{I}_{\boldsymbol{L}}} \hat{\vartheta}(\boldsymbol{k})\, \mathrm{e}^{2\pi \mathrm{i} \boldsymbol{k}\boldsymbol{\ell}/L}, \quad \boldsymbol{\ell} \in \mathcal{I}_{\boldsymbol{L}},$$
by means of a d-variate iFFT.

3. Compute the short sums $\mathcal{O}(N)$

$$f_j \coloneqq \sum_{\boldsymbol{\ell} \in \mathcal{J}_{\boldsymbol{L},m}(\boldsymbol{x}_j)} \vartheta_{\boldsymbol{\ell}} \operatorname{sinc}\big(L\pi\big(\boldsymbol{x}_j - \tfrac{\boldsymbol{\ell}}{L}\big)\big)\, \varphi_m\big(\boldsymbol{x}_j - \tfrac{\boldsymbol{\ell}}{L}\big), \quad j = 1, \dots, N.$$

Output: $f_j \approx f(\boldsymbol{x}_j)$, cf. (4.4), $j = 1, \dots, N$.

Complexity: $\mathcal{O}(|\mathcal{I}_{\boldsymbol{M}}| \log(|\mathcal{I}_{\boldsymbol{M}}|) + N)$

Note that by defining the vectors $\boldsymbol{\vartheta} \coloneqq (\vartheta_{\boldsymbol{\ell}})_{\boldsymbol{\ell} \in \mathcal{I}_{\boldsymbol{L}}}$ and $\hat{\boldsymbol{f}} \coloneqq (\hat{f}(\boldsymbol{k}))_{\boldsymbol{k} \in \mathcal{I}_{\boldsymbol{M}}}$, as well as the matrix

$$\boldsymbol{D}_{\hat{\psi}} \coloneqq \operatorname{diag}\left(\frac{1}{|\mathcal{I}_{\boldsymbol{L}}| \cdot \hat{\psi}(\boldsymbol{k})}\right)_{\boldsymbol{k} \in \mathcal{I}_{\boldsymbol{M}}} \in \mathbb{C}^{|\mathcal{I}_{\boldsymbol{M}}| \times |\mathcal{I}_{\boldsymbol{M}}|}, \tag{5.40}$$

the definition (5.37) can be written as

$$\boldsymbol{\vartheta} = \boldsymbol{F} \boldsymbol{D}_{\hat{\psi}} \hat{\boldsymbol{f}},$$

where $\boldsymbol{F} \in \mathbb{C}^{|\mathcal{I}_{\boldsymbol{L}}| \times |\mathcal{I}_{\boldsymbol{M}}|}$ denotes the Fourier matrix (2.15) with $L = M_\sigma$. By additionally defining the vector $\boldsymbol{f} \coloneqq (f(\boldsymbol{x}_j))_{j=1}^N$ and the $(2m+1)^d$-sparse matrix

$$\boldsymbol{\Psi} \coloneqq \left(\operatorname{sinc}\big(L\pi\big(\boldsymbol{x}_j - \tfrac{\boldsymbol{\ell}}{L}\big)\big)\, \varphi_m\big(\boldsymbol{x}_j - \tfrac{\boldsymbol{\ell}}{L}\big)\right)_{j=1,\, \boldsymbol{\ell} \in \mathcal{I}_{\boldsymbol{L}}}^{N} \in \mathbb{R}^{N \times |\mathcal{I}_{\boldsymbol{L}}|}, \tag{5.41}$$

the approximation (5.38) can be written as $\boldsymbol{f} \approx \boldsymbol{\Psi}\boldsymbol{\vartheta}$. Thereby, the overall approximation of Algorithm 5.16 is given by

$$\boldsymbol{f} \approx \boldsymbol{\Psi}\boldsymbol{\vartheta} = \boldsymbol{\Psi}\boldsymbol{F}\boldsymbol{D}_{\hat{\psi}}\hat{\boldsymbol{f}}. \tag{5.42}$$

5.3.2 Comparison to the classical NFFT

Due to the fact that $f \in \mathcal{B}_{M/2}(\mathbb{R}^d)$ is a bandlimited function one could also directly apply an equispaced quadrature rule to the inverse Fourier transform (4.4), i. e., consider the approximation

$$f(\boldsymbol{x}) = \int_{\mathbb{R}^d} \hat{f}(\boldsymbol{v})\, \mathrm{e}^{2\pi \mathrm{i} \boldsymbol{v}\boldsymbol{x}}\, \mathrm{d}\boldsymbol{v} = \int_{[-\frac{M}{2}, \frac{M}{2}]^d} \hat{f}(\boldsymbol{v})\, \mathrm{e}^{2\pi \mathrm{i} \boldsymbol{v}\boldsymbol{x}}\, \mathrm{d}\boldsymbol{v} \approx \sum_{\boldsymbol{k} \in \mathcal{I}_{\boldsymbol{M}}} \hat{f}(\boldsymbol{k})\, \mathrm{e}^{2\pi \mathrm{i} \boldsymbol{k}\boldsymbol{x}}.$$

Thereby, the function evaluations $f(\boldsymbol{x}_j)$, $j = 1, \ldots, N$, might also be approximated efficiently by means of the NFFT, see Algorithm 2.2. Since this raises the question of which of the two methods, Algorithm 2.2 or Algorithm 5.16, is more advantageous, this section deals with the comparison of the two approaches.

Considering the matrix notations

$$\boldsymbol{B}\boldsymbol{F}\boldsymbol{D} \quad \text{and} \quad \boldsymbol{\Psi}\boldsymbol{F}\boldsymbol{D}_{\hat{\psi}},$$

cf. (2.17) and (5.42), the first thing to realize is that for $\boldsymbol{B} \in \mathbb{R}^{N \times |\mathcal{I}_{\boldsymbol{L}}|}$ in (2.16) the window function $\varphi_m(\boldsymbol{x})$ is used, while for $\boldsymbol{\Psi} \in \mathbb{R}^{N \times |\mathcal{I}_{\boldsymbol{L}}|}$ in (5.41) we consider the sinc regularized window function $\operatorname{sinc}(L\pi\boldsymbol{x})\,\varphi_m(\boldsymbol{x})$. A similar remark can also be made about the diagonal matrices $\boldsymbol{D} \in \mathbb{C}^{|\mathcal{I}_{\boldsymbol{M}}| \times |\mathcal{I}_{\boldsymbol{M}}|}$ in (2.14) and $\boldsymbol{D}_{\hat{\psi}} \in \mathbb{C}^{|\mathcal{I}_{\boldsymbol{M}}| \times |\mathcal{I}_{\boldsymbol{M}}|}$ in (5.40).

It is also important to note that the two methods can only be compared for $\boldsymbol{x} \in [-\frac{1}{2} + \frac{m}{L}, \frac{1}{2} - \frac{m}{L})^d$, as the approximation by Algorithm 5.16 is only reasonable in this case. This implies that the matrix $\boldsymbol{B}$ is, unlike usual, non-periodic in this setting, whereas the matrix $\boldsymbol{\Psi}$ is inherently non-periodic by definition.

To study the quality of both approaches, note that for $\boldsymbol{k} \in \mathcal{I}_{\boldsymbol{M}}$ fixed the NFFT gives the approximation

$$\mathrm{e}^{2\pi \mathrm{i} \boldsymbol{k}\boldsymbol{x}} \approx \frac{1}{|\mathcal{I}_{\boldsymbol{L}}| \cdot \hat{\varphi}(\boldsymbol{k})} \sum_{\boldsymbol{\ell} \in \mathcal{I}_{\boldsymbol{L}}} \mathrm{e}^{2\pi \mathrm{i} \boldsymbol{k}\boldsymbol{\ell}/L}\, \tilde{\varphi}_m\big(\boldsymbol{x} - \tfrac{\boldsymbol{\ell}}{L}\big), \quad \boldsymbol{x} \in \mathbb{T}^d, \tag{5.43}$$

cf. (2.17) with $L = M_\sigma$, where $\tilde{\varphi}_m(\boldsymbol{x}) = \sum_{\boldsymbol{r} \in \mathbb{Z}^d} \varphi_m(\boldsymbol{x} + \boldsymbol{r})$ denotes the 1-periodic version of the compactly supported window function φ_m. Thus, we look for a comparable approximation of the exponential function using our newly proposed method in Algorithm 5.16. For this purpose, we consider the regularized Shannon sampling formula with localized sampling (4.121), which is known to provide a good approximation $f(\boldsymbol{x}) \approx (R_{\varphi,m} f)(\boldsymbol{x})$, $\boldsymbol{x} \in \mathbb{R}^d$, for bandlimited functions $f \in \mathcal{B}_{M/2}(\mathbb{R}^d)$. It is easy to see that $f(\boldsymbol{x}) = \hat{\psi}(\boldsymbol{x})\,\mathrm{e}^{2\pi \mathrm{i} \boldsymbol{k}\boldsymbol{x}}$ with $\boldsymbol{k} \in \mathbb{R}^d$ fixed, possesses the Fourier transform $\hat{f}(\boldsymbol{v}) = \psi(\boldsymbol{k} - \boldsymbol{v})$. Therefore, we have $f \in \mathcal{B}_{M/2}(\mathbb{R}^d)$ for all $\boldsymbol{k} \in \big[-\frac{M}{2} + \frac{m}{L}, \frac{M}{2} - \frac{m}{L}\big]^d$ using the regularized sinc functions ψ_{B} in (4.96), $\psi_{\sinh}$ in (4.105) and ψ_{cKB} in (4.113), and f is essentially bandlimited with bandwidth M for all $\boldsymbol{k} \in \big[-\frac{M}{2} + \frac{m}{L}, \frac{M}{2} - \frac{m}{L}\big]^d$ using ψ_{Gauss} in (4.89). Hence, inserting this function $f(\boldsymbol{x}) = \hat{\psi}(\boldsymbol{x})\,\mathrm{e}^{2\pi \mathrm{i} \boldsymbol{k}\boldsymbol{x}}$ in (4.121) we

obtain

$$\hat{\psi}(\boldsymbol{x})\,\mathrm{e}^{2\pi\mathrm{i}\boldsymbol{k}\boldsymbol{x}} \approx \sum_{\boldsymbol{\ell}\in\mathbb{Z}^d} \hat{\psi}\big(\tfrac{\boldsymbol{\ell}}{L}\big)\,\mathrm{e}^{2\pi\mathrm{i}\boldsymbol{k}\boldsymbol{\ell}/L}\,\mathrm{sinc}\big(L\pi\big(\boldsymbol{x}-\tfrac{\boldsymbol{\ell}}{L}\big)\big)\,\varphi_m\big(\boldsymbol{x}-\tfrac{\boldsymbol{\ell}}{L}\big), \quad \boldsymbol{x}\in\mathbb{R}^d,$$

or rather

$$\mathrm{e}^{2\pi\mathrm{i}\boldsymbol{k}\boldsymbol{x}} \approx \sum_{\boldsymbol{\ell}\in\mathcal{I}_{\boldsymbol{L}}} \frac{\hat{\psi}\big(\frac{\boldsymbol{\ell}}{L}\big)}{\hat{\psi}(\boldsymbol{x})}\,\mathrm{e}^{2\pi\mathrm{i}\boldsymbol{k}\boldsymbol{\ell}/L}\,\mathrm{sinc}\big(L\pi\big(\boldsymbol{x}-\tfrac{\boldsymbol{\ell}}{L}\big)\big)\,\varphi_m\big(\boldsymbol{x}-\tfrac{\boldsymbol{\ell}}{L}\big), \quad \boldsymbol{x}\in\big[-\tfrac{1}{2}+\tfrac{m}{L},\tfrac{1}{2}-\tfrac{m}{L}\big)^d.$$

Numerical experiments, cf. Figures 4.4, 4.5, 4.7, and 4.10, have shown that $\hat{\psi}(\boldsymbol{y}) \approx \frac{1}{|\mathcal{I}_{\boldsymbol{L}}|}$, $\boldsymbol{y}\in\big[-\frac{M}{2},\frac{M}{2}\big)^d$, for all the window functions mentioned in Remark 4.22. Thereby, the above approximation simplifies to

$$\mathrm{e}^{2\pi\mathrm{i}\boldsymbol{k}\boldsymbol{x}} \approx \sum_{\boldsymbol{\ell}\in\mathcal{I}_{\boldsymbol{L}}} \mathrm{e}^{2\pi\mathrm{i}\boldsymbol{k}\boldsymbol{\ell}/L}\,\mathrm{sinc}\big(L\pi\big(\boldsymbol{x}-\tfrac{\boldsymbol{\ell}}{L}\big)\big)\,\varphi_m\big(\boldsymbol{x}-\tfrac{\boldsymbol{\ell}}{L}\big), \quad \boldsymbol{x}\in\big[-\tfrac{1}{2}+\tfrac{m}{L},\tfrac{1}{2}-\tfrac{m}{L}\big)^d, \tag{5.44}$$

which equals the approximation $\boldsymbol{\Psi F D}_{\hat{\psi}}$ of Algorithm 5.16 since $\hat{\psi}(\boldsymbol{k}) \approx \frac{1}{|\mathcal{I}_{\boldsymbol{L}}|}$, $\boldsymbol{k}\in\mathcal{I}_{\boldsymbol{M}}$. Therefore, we can compare the quality of the two methods by considering the approximations (5.43) and (5.44) of the exponential function.

For the sake of simplicity in the visualization, we restrict ourselves to the one-dimensional setting $d=1$. To estimate the quality of the approaches, we consider the approximation error

$$e(v) \coloneqq \max_{x_p,\,p=1,\dots,P} \big|\mathrm{e}^{2\pi\mathrm{i}vx_p} - h(x_p)\big|, \tag{5.45}$$

where the term $h(x_p)$ is a placeholder for the right hand sides of (5.43) and (5.44), respectively, evaluated at a fine grid of $P=10^5$ equispaced points x_p, $p=1,\dots,P$. This approximation error (5.45) shall now be computed for several values

$$v_s = -\tfrac{M}{2}-m+\tfrac{s}{S} \in \big[-\tfrac{M}{2}-m,\tfrac{M}{2}+m\big], \quad s=0,\dots,S(M+2m), \tag{5.46}$$

where $S=1$ corresponds to integer evaluation, whereas we use $S=32$ to examine the approximation at non-integer points as well. Note that (5.43)

is expected to provide a good approximation only for $v \in \big[-\frac{M}{2}, \frac{M}{2}\big]$, while (5.44) is expected to do so only for $v \in \big[-\frac{M}{2}+\frac{m}{L}, \frac{M}{2}-\frac{m}{L}\big]$. Nevertheless, we test for v from a larger interval to confirm this assumption.

The corresponding outcomes when computing the approximations (5.43) and (5.44) using the sinh-type window function (4.62) as well as the parameters $M = 20$, $\lambda = 1$, $L = (1+\lambda)M$, and $m = 5$, are displayed in Figure 5.1. For $x \in \big[-\frac{1}{2}, \frac{1}{2}\big)$ it is easy to see that our newly proposed method (5.44) indeed does not provide reasonable results, while the approximation (5.43) by means of the NFFT is only useful at integer points v. For the truncated interval $x \in \big[-\frac{1}{2}+\frac{m}{L}, \frac{1}{2}-\frac{m}{L}\big)$, however, both approximations (5.43) and (5.44) are clearly beneficial for non-integer points v as well, but as expected these methods only succeed when $|v| \leq \frac{M}{2}$. Nevertheless, although also the approximation (5.43) by means of the NFFT yields better results in this setting, the approximation (5.44) by means of our newly proposed method easily outperforms the classical NFFT in terms of the approximation error (5.45).

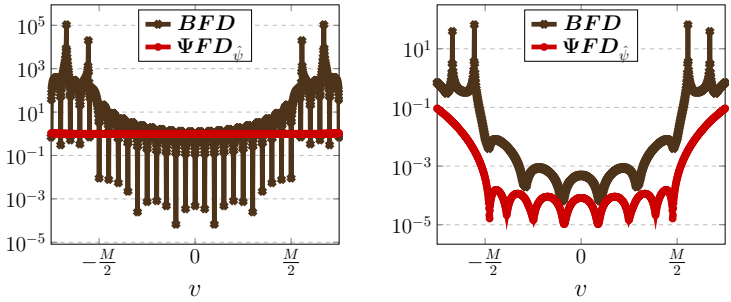

(a) $x \in \big[-\frac{1}{2}, \frac{1}{2}\big)$ (b) $x \in \big[-\frac{1}{2}+\frac{m}{L}, \frac{1}{2}-\frac{m}{L}\big)$

Figure 5.1: Maximum approximation error (5.45) for $P = 10^5$ computed for (5.46) with $S = 32$ using the sinh-type window function (4.62) as well as the parameters $M = 20$, $\lambda = 1$, $L = (1+\lambda)M$, and $m = 5$ in the one-dimensional setting $d = 1$.

That is to say, Figure 5.1 demonstrates that the novel NFFT-like approach in Algorithm 5.16 is better suited for bandlimited functions, as the errors are smaller. Note that this superiority is not limited to $k \in \mathcal{I}_M$ but extends to the entire domain $v \in \big[-\frac{M}{2}, \frac{M}{2}\big]$. Moreover, the error of Algorithm 5.16

is bounded by the error estimates of the regularized Shannon sampling formulas in Section 4.4, whereas the quadrature error of the NFFT is completely unclear.

5.4 Numerical examples & summary

Concluding this chapter, we have a look at some numerical examples. After investigating the accuracy of the fast sinc transform from Section 5.1 (see Examples 5.17 and 5.18), we also examine the quality and efficiency of its generalized versions for the evaluation of the regularized Shannon sampling sums introduced in Section 5.2 (see Examples 5.19 and 5.20). Moreover, also a test of the NFFT-like procedure for bandlimited functions from Section 5.3 is included (see Example 5.21).

Discrete sinc transform

We start by examining the quality of the approximation of the sinc function using the exponential sums (2.19).

Example 5.17. (a) Analogous to [KPT23, Example 5.5], we verify the result of Theorem 5.4, i. e., we visualize the error constant and the maximum approximation error, cf. (5.9). To this end, we compute the discrete maximum error

$$\max_{r\in\mathcal{I}_R}\left|\operatorname{sinc}(M\pi x_r)-\sum_{j=0}^{n} w_j\,\mathrm{e}^{-2\pi\mathrm{i}Mz_jx_r}\right| \tag{5.47}$$

on a fine evaluation grid $x_r=\frac{2r}{R}\in[-1,\,1]$, $r\in\mathcal{I}_R$, with $R=10^6$ fixed for certain bandwidths $M=2^s$, $s\in\{1,\dots,15\}$. More precisely, for several choices of $n=cM$ with $c\in\{1,\dots,10\}$ we compute the weights w_j, $j=0,\dots,n$, using Algorithm 5.5. Subsequently, the approximation (5.12) of the sinc function is computed by means of the NFFT, see Algorithm 2.2. The corresponding results are depicted in Figure 5.2. Note that Figure 5.2a shows only the error bound (5.9), thereby clearly illustrating the fact that $n+1\geq 4M$ is a necessary condition for the error constant to decay with respect to the bandwidth M. In Figure 5.2b it can be seen that the maximum approximation error (5.47) also gets as small as possible for $n+1\geq 4M$, where the optimal choice of the constant c appears to

depend on the size of the bandwidth M, with smaller c being sufficient for larger M. It should be noted that not all of the tested parameter constellations could be shown in Figure 5.2 since the error constant (5.9) might be huge for small $c < 4$ or smaller than machine precision for $c \geq 4$ depending on the size of M. Additionally, we remark that although Figure 5.2 displays only the results for $d = 1$, the results for $d > 1$ look the same due to tensorization, see (5.14) and Corollary 5.8, respectively.

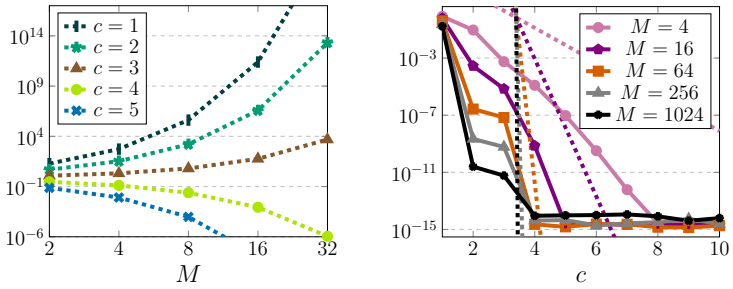

(a) Error constant (5.9)

(b) Maximum error (5.47) and error constant (5.9)

Figure 5.2: Error constant (5.9) (dashed) and maximum error (5.47) (solid) of the approximation of $\operatorname{sinc}(M\pi x)$, $x \in [-1, 1]$, with $R = 10^6$ for certain bandwidths $M = 2^s$, $s \in \{1, \dots, 15\}$, using the Chebyshev nodes (5.8) and the weigths computed by Algorithm 5.5, where $n = cM$ with $c \in \{1, \dots, 10\}$.

(b) Having verified the quality of the approximation (5.12) using the weights computed by means of Algorithm 5.5, we proceed with a comparison to other methods for choosing the weights w_j, $j = 0, \dots, n$. Especially, we consider the method from [GLI06] mentioned in Remark 5.6, where a Gauss–Legendre quadrature was used instead of the Clenshaw–Curtis quadrature in Theorem 5.4. For certain bandwidths $M = 2^s$, $s \in \{1, \dots, 15\}$, we compute the maximum error (5.47) of the approximation of the sinc function $\operatorname{sinc}(M\pi x)$, $x \in [-1, 1]$, with $R = 10^6$ using the Legendre points (5.13) and the weights proposed in [GLI06] with $n = 2M$. The corresponding results are depicted in Figure 5.3. Comparing Figures 5.3a and 5.2b it becomes apparent that indeed a smaller number n of quadrature weights is sufficient for the Gauss–Legendre weights men-

tioned in Remark 5.6. However, comparing the time needed to compute the approximation of the sinc function, we see that our method using the Clenshaw–Curtis weights computed by Algorithm 5.5 with $n = 4M$ is more efficient than the procedure of [GLI06] using the Gauss–Legendre weights mentioned in Remark 5.6 with $n = 2M$, see Figure 5.3b. Therefore, we consider our method to be at least a slight improvement on [GLI06].

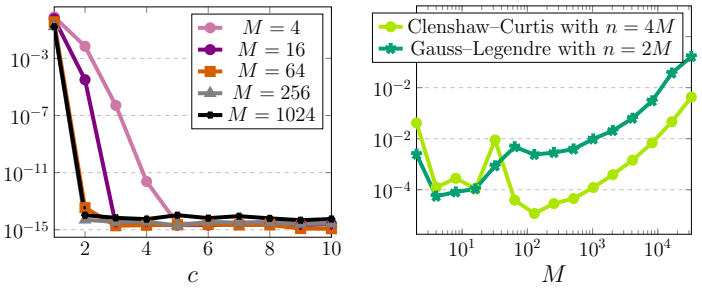

(a) Maximum error (5.47) using the weights mentioned in Remark 5.6

(b) Time needed to compute the approximation (in seconds)

Figure 5.3: Comparison of the approximation of $\operatorname{sinc}(M\pi x)$, $x \in [-1, 1]$, for certain bandwidths $M = 2^s$, $s \in \{1, \dots, 15\}$, using the Gauss–Legendre weights mentioned in Remark 5.6 and the Clenshaw–Curtis weights computed by Algorithm 5.5.

(c) Finally, we compare the analytic result of Theorem 5.4 to the empirical least squares approach (5.7), where for simplicity we describe only the one-dimensional case $d = 1$. Note that for (5.7) we are free to choose the quadrature points $z_j \in [-\frac{1}{2}, \frac{1}{2}]$, $j = 0, \dots, n$, as well as the evaluation points $y_p \in [-1, 1]$, $p \in \mathcal{I}_P$. Therefore, we consider different combinations of the equispaced points

$$z_j = -\tfrac{1}{2} + \tfrac{j}{n} \in [-\tfrac{1}{2}, \tfrac{1}{2}], \quad j = 0 \dots, n, \tag{5.48}$$

the Chebyshev points (5.8) and the Legendre points (5.13) with similarly chosen evaluation points $y_p \in [-1, 1]$, $p \in \mathcal{I}_P$, and investigate which choices of y_p and z_j lead to the best approximation results. More precisely, for the given sets of points we compute the corresponding weights $w_j \in \mathbb{C}$,

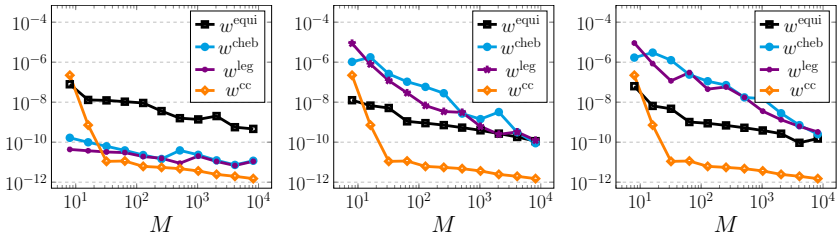

(a) Equispaced points y_p (b) Legendre points y_p (c) Chebyshev points y_p

Figure 5.4: Discrete maximum error (5.47) of the approximation of the sinc function $\operatorname{sinc}(M\pi x)$, $x \in [-1,1]$, with $R = 10^6$ for certain bandwidths $M = 2^s$, $s \in \{3,\dots,13\}$, shown for several choices of $y_p \in [-1,1]$, $p \in \mathcal{I}_P$, with $P = 2.5n$ and $n = 4M$, where the weights w^{equi}, w^{cheb} and w^{leg} are computed using the least squares approach (5.7) for $z_j \in [-\frac{1}{2}, \frac{1}{2}]$, $j = 0,\dots,n$, in (5.48), (5.8), and (5.13), compared to the analytic weights w^{cc} computed by Algorithm 5.5.

$j = 0,\dots,n$, iteratively as the least squares solution to the linear system (5.7), where for equispaced y_p we employ an NFFT and for nonequispaced y_p we make use of an NNFFT, respectively. Note that according to the choice of the quadrature points z_j we denote the weights as w^{equi}, w^{cheb} and w^{leg}. For comparison, we also compute the analytic weights w^{cc} in (5.10) by means of Algorithm 5.5. Consequently, we calculate the discrete maximum error (5.47), again choosing $R = 10^6$ with $R \gg P$, where $P = 2.5n$ and $n = 4M$.

The corresponding outcomes are depicted in Figure 5.4, where it becomes apparent that, except for very small bandwidths M, the analytic weights w^{cc} in (5.10) are superior to all tested least squares weights. Only in case of equispaced evaluation points y_p we see that choosing Chebyshev points (5.8) or Legendre points (5.13) leads to comparable results. Considering only the results of the least squares approach, we find that, regardless of the special choice, the approximation is best when equispaced points are combined with nonequispaced points. Furthermore, we observe that the best results can be obtained when (5.7) is an overdetermined problem with $P > 2n$, where $P = 2.5n$ has proven to be a good ratio. Additionally, we remark that for y_p other than equispaced we observe that the iteration procedure

did not yet converge to the desired accuracy 10^{-11} although 10000 iteration steps were permitted. Thus, for the least squares approach (5.7) the best choice is equispaced evaluation points y_p and nonequispaced quadrature points (5.8) or (5.13), since in this setting we obtain the best results with the least effort due to the NFFT. Nevertheless, these results are still being outperformed by the analytic approach using (5.10). ◇

Next we study the accuracy of the fast sinc transform in Algorithm 5.10.

Example 5.18. Similar to [KPT23, Example 6.3], we now compare the discrete sinc transform (5.2) with its approximation (5.26) by means of the fast sinc transform in Algorithm 5.10. To this end, we choose random nodes $\boldsymbol{a}_k, \boldsymbol{b}_\ell \in \left[-\frac{1}{2}, \frac{1}{2}\right]^d$, $k \in I_K$, $\ell \in I_L$, as well as random coefficients $c_k \in [0,1]^d$, and compute the maximum error (5.27). Due to the randomness of the given values, this test is repeated one hundred times and afterwards the maximum error over all repetitions is computed. In this experiment we consider certain bandwidths $M = 2^s$, $s \in \{5, \dots, 13\}$, and without loss of generality we choose $d = 1$ and $K = L = M$ for the visualization.

The only thing left to do to compute the fast sinc transform in Algorithm 5.10 is the specification of the precomputation scheme, which shall be either the least squares problem (5.7) or Algorithm 5.5. For the analytic weights w_j, $j = 0, \dots, n$, computed by means of Algorithm 5.5 the Chebyshev points (5.8) are used, such that only the number n of quadrature weights is free to choose. For the weights w_j computed by solving the least squares problem (5.7) we have seen in Example 5.17 that the best choice are equispaced evaluation points $y_p = \frac{2l}{P}$, $p \in I_P$, with $P = 2.5n$, and the nonequispaced quadrature points (5.8), such that also the parameter n is left to choose. To this end, we compare both approaches for several choices of $n = cM$ with $c \in \{2, 4, 6, 8\}$.

The corresponding outcomes are shown in Figure 5.5. For both precomputation schemes we recognize that for $n = 2M$ the approximation results are not as good as for larger n. This indicates that also for the least squares approach (5.7) the condition $n \geq 4M$ seems to be necessary to obtain the best approximation possible. Moreover, it can be seen that there is hardly any difference between the results for $c \in \{4, 6, 8\}$. However, we point out that a larger parameter $n = cM$ heavily increases the computational costs of the fast sinc transform in Algorithm 5.10. Therefore, it is recommended to use the smallest possible choice $n = 4M$.

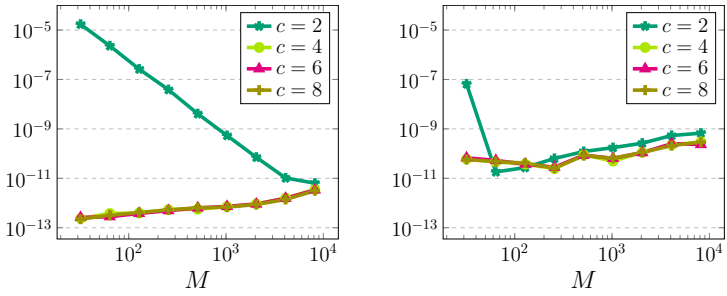

(a) Analytic weights obtained by Algorithm 5.5

(b) Least squares weights obtained by means of (5.7)

Figure 5.5: Maximum approximation error (5.27) of the fast sinc transform in Algorithm 5.10 for certain bandwidths $M = 2^s$, $s = 5, \dots, 13$, shown for several choices of $n = cM$ with $c \in \{2, 4, 6, 8\}$ when using random nodes $a_k, b_\ell \in \left[-\frac{1}{2}, \frac{1}{2}\right]$ and random coefficients $c_k \in [0, 1]$ with $d = 1$ and $K = L = M$, compared for different weights w_j, $j = 0, \dots, n$, obtained by Algorithm 5.5 or the least squares approach (5.7) with z_j in (5.8) each.

Comparing the two approaches in Figure 5.5a and 5.5b we recognize that, as expected by Figure 5.4, the errors obtained by using the analytic weights computed by Algorithm 5.5 are much smaller than by using the least squares weights computed by means of (5.7). Note that identical results are obtained for a_k or b_ℓ equispaced, for $d > 1$ and for $K \neq L \neq M$. This once more emphasizes the superiority of the analytic weights computed by Algorithm 5.5 and hence we strongly recommend to make use of Algorithm 5.5 in the precomputational step of Algorithm 5.10. ◇

Application to regularized Shannon sampling formulas

Next, we proceed with the examination of the generalization of the fast sinc transform introduced in Section 5.2. More precisely, we study the quality and efficiency for the evaluation of the regularized Shannon sampling sums, where Example 5.19 deals with the method for the regularization with a window function in frequency domain presented in Section 5.2.1 and Example 5.20 is concerned with the method for the regularization with a window function in spatial domain suggested in Section 5.2.2.

Example 5.19. Firstly, we have a look at the fast evaluation of the regularized Shannon sampling formulas with regularization in the frequency domain, see Section 5.2.1. More precisely, for the bandlimited function (4.151) we compare the regularization in frequency domain $P_{\psi,T}f$ in (4.38) of Section 4.3.1 with its approximation $\tilde{P}_{\psi,T}f$ in (5.30) by means of the fast sinc transform in Algorithm 5.14, where the weights w_j in (5.10) are precomputed by Algorithm 5.5. To this end, we consider the maximum approximation error

$$\max_{x\in[-1,\,1]} \left|(\tilde{P}_{\psi,T}f)(x) - (P_{\psi,T}f)(x)\right| \tag{5.49}$$

for several frequency window functions $\psi \in \{\psi_{\mathrm{lin}}, \psi_{\mathrm{cub}}, \psi_{\cos}, \psi_{\mathrm{conv},2}\}$, see (4.45), (4.48), (4.51), and (4.57). Similar to Example 4.67, the errors (5.49) shall be estimated by evaluating the approximations $P_{\psi,T}f$ and $\tilde{P}_{\psi,T}f$ at a fine grid of equidistant points $x_s = -1 + \frac{s}{S} \in [-1, 1]$, $s = 0, \ldots, 2S$, with $S = 10^5$. In addition, we also quantify the time needed for the naive computation of $P_{\psi,T}f$ in (4.38) as well as the computation of its approximation $\tilde{P}_{\psi,T}f$ in (5.30) by means of the fast sinc transform in Algorithm 5.14, where the precomputation of the corresponding coefficients $\hat{\psi}(Lz_j)$ and weights w_j, $j = 0, \ldots, n$, is excluded.

The results for fixed $M = 64$, $\lambda = 1$, and $L = (1 + \lambda)M$, as well as several values of the truncation parameter $T = cL$ with $c \in \{1, \ldots, 10\}$ are depicted in Figure 5.6. It can be seen in Figure 5.6a that the accuracy of the approximation $\tilde{P}_{\psi,T}f$ in (5.30) seems to depend strongly on the choice of the window function, as the maximum approximation error (5.49) differs appreciably for the considered $\psi \in \{\psi_{\mathrm{lin}}, \psi_{\mathrm{cub}}, \psi_{\cos}, \psi_{\mathrm{conv},2}\}$. Moreover, we recognize that the approximation $\tilde{P}_{\psi,T}f$ in (5.30) inexplicably improves for larger truncation parameter T, which was only expected for the approximation of f by means of $P_{\psi,T}f$ and $\tilde{P}_{\psi,T}f$, respectively. When considering Figure 5.6b, however, it becomes apparent that by using the fast sinc transform in Algorithm 5.14 the computation times are reduced by approximately two orders of magnitude for all considered window functions, thereby yielding a significant acceleration in the computation of the regularization in frequency domain $P_{\psi,T}f$. Thus, since we observed that the approximation of the bandlimited function f is almost equally good for $P_{\psi,T}f$ and $\tilde{P}_{\psi,T}f$, it is recommended to make use of the fast sinc transform in Algorithm 5.14, especially for large truncation parameters T. ◇

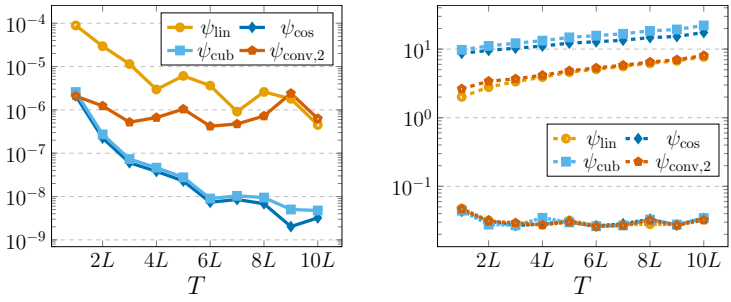

(a) Maximum approximation error (5.49)

(b) Time needed for the computation (in seconds)

Figure 5.6: Comparison of the regularization $P_{\psi,T}f$ in (4.38) in frequency domain (dashed) and its approximation $\tilde{P}_{\psi,T}f$ in (5.30) by means of the fast sinc transform in Algorithm 5.14 (dotted), for several $T = cL$ with $c \in \{1, \dots, 10\}$ and $\psi \in \{\psi_{\text{lin}}, \psi_{\text{cub}}, \psi_{\text{cos}}, \psi_{\text{conv},2}\}$, in (4.45), (4.48), (4.51), and (4.57), for the bandlimited function (4.151) with $M = 64$, $\lambda = 1$, and $L = (1+\lambda)M$.

Example 5.20. Secondly, we study the fast evaluation of the regularized Shannon sampling formulas with regularization in the spatial domain, see Section 5.2.2. Namely, for the bandlimited function (4.151) we compare the regularization in spatial domain $R_{\varphi,m}f$ in (4.74) of Section 4.3.2 with its approximation $\tilde{R}_{\varphi,m}f$ in (5.32) by means of the fast sinc transform in Algorithm 5.15, where the weights w_j in (5.10) are precomputed by Algorithm 5.5. Similar to Example 5.19 we consider the approximation error

$$\max_{x\in[-1,\,1]} \left|(\tilde{R}_{\varphi,m}f)(x) - (R_{\varphi,m}f)(x)\right| \tag{5.50}$$

for $\varphi \in \{\varphi_{\text{Gauss}}, \varphi_{\text{B}}, \varphi_{\text{sinh}}, \varphi_{\text{cKB}}\}$, see (4.60), (4.61), (4.62), and (4.63), which shall be estimated by evaluating the approximations $R_{\varphi,m}f$ and $\tilde{R}_{\varphi,m}f$ at a fine grid of equidistant points $x_s = -1 + \frac{s}{S} \in [-1, 1]$, $s = 0, \dots, 2S$, with $S = 10^5$. Moreover, we also quantify the time needed for the naive computation of $R_{\varphi,m}f$ in (4.74) as well as the computation of its approximation $\tilde{R}_{\varphi,m}f$ in (5.32) by means of the fast sinc transform

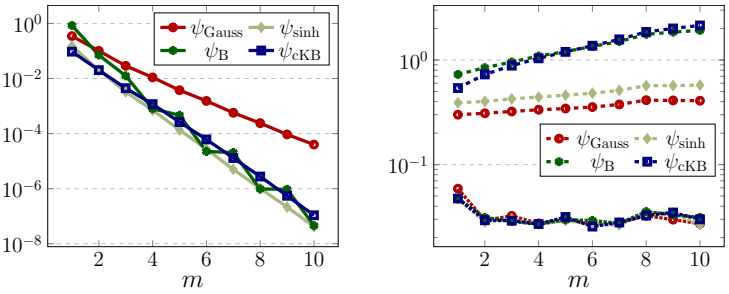

(a) Maximum approximation error (5.50)

(b) Time needed for the computation (in seconds)

Figure 5.7: Comparison of the regularization $R_{\varphi,m}f$ in (4.74) in spatial domain (dashed) and its approximation $\tilde{R}_{\varphi,m}f$ in (5.32) by means of the fast sinc transform in Algorithm 5.15 (dotted), for several $m \in \{1,\dots,10\}$ and $\varphi \in \{\varphi_{\text{Gauss}}, \varphi_{\text{B}}, \varphi_{\text{sinh}}, \varphi_{\text{cKB}}\}$, in (4.60), (4.61), (4.62), and (4.63), for the bandlimited function (4.151) with $M = 64$, $\lambda = 1$, and $L = (1+\lambda)M$.

in Algorithm 5.15, where the precomputation of the corresponding coefficients $\hat{\psi}(\tilde{L}z_j)$ and weights w_j, $j = 0,\dots,n$, is excluded.

The results for fixed $M = 64$, $\lambda = 1$, and $L = (1+\lambda)M$, as well as several values of the truncation parameter $m \in \{1,\dots,10\}$ are displayed in Figure 5.7. Considering Figure 5.7a we recognize that, in contrast to Example 5.19, the accuracy of the approximation $\tilde{R}_{\varphi,m}f$ in (5.32) does not depend much on the choice of the window function, as the maximum approximation error (5.50) is almost identical for all considered window functions φ, except for φ_{Gauss} in (4.60) being slightly worse. However, similarly as already observed in Example 5.19, it can be seen that the approximation $\tilde{R}_{\varphi,m}f$ in (5.32) inexplicably improves for larger truncation parameter m, which was only expected for the approximation of f by means of $R_{\varphi,m}f$ and $\tilde{R}_{\varphi,m}f$, respectively. In Figure 5.7b we see that the computation times are only slightly reduced by using the fast sinc transform in Algorithm 5.15. This means, when factoring in also the time needed for the precomputational step of Algorithm 5.15, there is hardly any difference between the two computation schemes. Hence, the approximate computation of $\tilde{R}_{\varphi,m}f$ by means of the fast sinc transform in Algorithm 5.15 might only

be useful for high dimension $d > 1$ or very large truncation parameters m, due to the sparse structure of $R_{\varphi,m} f$ in (4.74). $\diamond$

NFFT-like procedure for bandlimited functions

Finally, we test the NFFT-like procedure for bandlimited functions introduced in Section 5.3 in comparison to the classical NFFT.

Example 5.21. To examine the approximation quality of the NFFT-like procedure for bandlimited functions in Algorithm 5.16 we provide a function f with its corresponding Fourier transform $\hat{f}$ in (4.1), such that we have access to the exact values $\hat{f}(k)$, $k \in \mathcal{I}_M$, as input for Algorithm 5.16, as well as the exact function evaluations $f(x_j)$, $j = 1, \dots, N$. In doing so, we can compare the result f_j, $j = 1, \dots, N$, of Algorithm 5.16 to the exact function evaluations $f(x_j)$, $j = 1, \dots, N$, by computing the maximum approximation error

$$\max_{j=1,\dots,N} |f_j - f(x_j)|. \tag{5.51}$$

For the reason of comparison, we also compute the approximation error (5.51) when f_j, $j = 1, \dots, N$, is the result of the classical NFFT in Algorithm 2.2.

Here we consider the one-dimensional setting with $d = 1$ and for several bandwidth parameters $M \in \{20, 40, \dots, 1000\}$ we study the function $f(x) = \operatorname{sinc}^2\left(\frac{M}{2}\pi x\right)$ with the Fourier transform

$$\hat{f}(v) = \frac{2}{M} \cdot \begin{cases} 1 - \left|\frac{2v}{M}\right| & : |v| \le \frac{M}{2}, \\ 0 & : \text{otherwise.} \end{cases}$$

Note that the function f is scaled appropriately such that $\max_{x \in \mathbb{R}} f(x) = 1$ independent of the bandwidth M and thereby the approximation errors (5.51) are comparable for all considered M. As evaluation points $x_j \in \left[-\frac{1}{2} + \frac{m}{L}, \frac{1}{2} - \frac{m}{L}\right]$, $j = 1, \dots, N$, we choose the scaled Chebyshev nodes

$$x_j = \cos\left(\frac{(j-1)\pi}{N}\right) \cdot \left(\frac{1}{2} - \frac{m}{L}\right), \quad j = 1, \dots, N, \tag{5.52}$$

with $N = \frac{M}{2}$, $m = 5$, as well as $M_\sigma = L = M(1+\lambda)$ with $\lambda = 1$, and we use the sinh-type window function (4.62).

The corresponding results are depicted in Figure 5.8. As expected by the previous comparison of the two approaches in Figure 5.1, the new NFFT-like procedure for bandlimited functions presented in Algorithm 5.16 performs much better than the classical NFFT in Algorithm 2.2. While for $M \leq 80$ both approaches exhibit the same maximum approximation error (5.51), for larger bandwidth M the approximation error (5.51) gets smaller only for the NFFT-like procedure in Algorithm 5.16. That is to say, when approximating the evaluations $f(x_j)$, $j = 1, \ldots, N$, of the bandlimited function $f \in \mathcal{B}_{M/2}(\mathbb{R})$ by given samples $\hat{f}(k)$, $k \in \mathcal{I}_M$, of the corresponding Fourier transform (4.1), reasonable results can be obtained by the NFFT in Algorithm 2.2, yet evidence indicated that our newly proposed NFFT-like procedure for bandlimited functions in Algorithm 5.16 yields results that are at least as good, if not superior. Accordingly, the NFFT-like procedure in Algorithm 5.16 is the preferred approach in this context. ◇

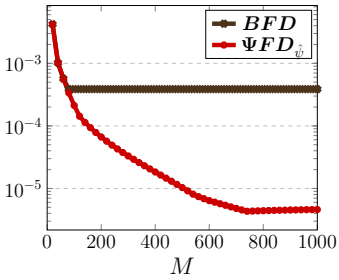

Figure 5.8: Maximum approximation error (5.51) of the NFFT-like procedure for bandlimited functions in Algorithm 5.16 and the classical NFFT in Algorithm 2.2 using the sinh-type window function (4.62) computed for the function $f(x) = \operatorname{sinc}^2\left(\frac{M}{2}\pi x\right)$ using several bandwidth parameters $M \in \{20, 40, \ldots, 1000\}$ and the scaled Chebyshev nodes (5.52) with $N = \frac{M}{2}$, $m = 5$, $M_\sigma = L = (1 + \lambda)M$, as well as $\lambda = 1$ and $d = 1$.

Remark 5.22. Note that the code files for all the experiments in this section are available at [Kir] under `https://github.com/melaniekircheis/dissertation/tree/main/5-Fast_sinc_methods`. ◇

Summary

In this chapter, we have studied several fast approximation schemes in which the sinc function plays an important role. On the one hand, we presented efficient and accurate algorithms for the evaluation of the Shannon sampling sums (4.12) and the regularized Shannon sampling formulas introduced in Sections 4.3.1 and 4.3.2, which were both theoretically and numerically verified. On the other hand, we proposed a new NFFT-like procedure for the approximation of function evaluations $f(\boldsymbol{x}_j)$, $j = 1, \ldots, N$, of a bandlimited function $f \in \mathcal{B}_{M/2}(\mathbb{R}^d)$ from given samples $\hat{f}(\boldsymbol{k})$, $\boldsymbol{k} \in \mathcal{I}_{\boldsymbol{M}}$, in the frequency domain. It has been shown that this new approach, which is based on regularized Shannon sampling formulas, can indeed outperform the classical NFFT in this context, thereby highlighting the importance of the sinc function.

6 Reconstruction of the Fourier transform of bandlimited functions from nonequispaced spatial data

So far, we have studied inversion approaches only for the NFFT, i. e., to efficiently find a solution to the discrete inversion problem (3.3) of computing the Fourier coefficients $\hat{f}_{\boldsymbol{k}} \in \mathbb{C}$, $\boldsymbol{k} \in \mathcal{I}_{\boldsymbol{M}}$, from given function evaluations $f(\boldsymbol{x}_j) \in \mathbb{C}$, $j = 1, \ldots, N$, of the trigonometric polynomial (2.8).

Various applications such as MRI, cf. [DAP22, EKP22], etc., however, deal with the analogous continuous problem, considering bandlimited functions $f \in \mathcal{B}_{M/2}(\mathbb{R}^d)$, cf. (4.3), instead of trigonometric polynomials (2.8). In this case the aim is the reconstruction of point evaluations $\hat{f}(\boldsymbol{k}) \in \mathbb{C}$, $\boldsymbol{k} \in \mathcal{I}_{\boldsymbol{M}}$, of an object $\hat{f}$ in (4.1) from given measurements $f(\boldsymbol{x}_j)$, $j = 1, \ldots, N$, of the form (4.4). Note that this can be seen as a generalization of the problem (3.3), as already mentioned in the frame theoretical approach in Section 3.3.4. Therefore, known approaches for the direct inversion of the NFFT from Section 3 shall now be extended to bandlimited functions $f \in \mathcal{B}_{M/2}(\mathbb{R}^d)$ with maximum bandwidth M, cf. [KP23b].

To this end, this chapter is organized as follows. Initially, in Section 6.1 we investigate the extension properties of the density compensation technique from Section 3.2.1, that leads to an exact reconstruction for all trigonometric polynomials (2.8) of degree $\boldsymbol{M}$. Subsequently, in Section 6.2 we comment on the analogous use of the matrix optimization approach from Section 3.3 for bandlimited functions. Finally, in Section 6.3 we show some numerical examples to investigate the accuracy of our approaches, including a short summary.

6.1 Density compensation factors

In this section the aim is to extend the density compensation method from Section 3.2.1 to bandlimited functions $f \in \mathcal{B}_{M/2}(\mathbb{R}^d)$ with maximum bandwidth M, as done in [KP23b]. For this purpose, we show in Section 6.1.1 that for any bandlimited function f there exists a certain corresponding

trigonometric polynomial $\tilde{f}$ that could be used for the reconstruction of the values $\hat{f}(\boldsymbol{k})$, $\boldsymbol{k} \in \mathcal{I}_{\boldsymbol{M}}$. Moreover, we show that it is reasonable to consider the inversion problem (3.3) for bandlimited functions $f \in \mathcal{B}_{M/2}(\mathbb{R}^d)$ as well. Besides, we describe a connection to some related approaches from the literature in Section 6.1.2. Finally, we provide some additional observations that can be made using the theory of tempered distributions in Section 6.1.3.

6.1.1 Reconsideration as trigonometric polynomials

To find a suitable reconstruction technique for a bandlimited function $f \in \mathcal{B}_{M/2}(\mathbb{R}^d)$, we assume that additionally $f \in L_1(\mathbb{R}^d)$ holds, such that we can consider its 1-periodized version

$$\tilde{f}(\boldsymbol{x}) \coloneqq \sum_{\boldsymbol{r} \in \mathbb{Z}^d} f(\boldsymbol{x} + \boldsymbol{r}), \quad x \in \mathbb{R}^d.$$

Further assume that $\sum_{\boldsymbol{k} \in \mathbb{Z}^d} |\hat{f}(\boldsymbol{k})| < \infty$. Then the Poisson summation formula, cf. [PPST23, Theorem 4.28], yields that $\tilde{f} \in L_1(\mathbb{T}^d)$ is uniquely representable in form of its absolute convergent Fourier series

$$\tilde{f}(\boldsymbol{x}) \coloneqq \sum_{\boldsymbol{k} \in \mathbb{Z}^d} c_{\boldsymbol{k}}(\tilde{f})\, \mathrm{e}^{2\pi \mathrm{i} \boldsymbol{k} \boldsymbol{x}}, \tag{6.1}$$

where the Fourier coefficients are given by

$$c_{\boldsymbol{k}}(\tilde{f}) = \int_{\mathbb{T}^d} \tilde{f}(\boldsymbol{x})\, \mathrm{e}^{-2\pi \mathrm{i} \boldsymbol{k} \boldsymbol{x}}\, \mathrm{d}\boldsymbol{x} = \int_{\mathbb{R}^d} f(\boldsymbol{x})\, \mathrm{e}^{-2\pi \mathrm{i} \boldsymbol{k} \boldsymbol{x}}\, \mathrm{d}\boldsymbol{x} = \hat{f}(\boldsymbol{k}), \quad \boldsymbol{k} \in \mathbb{Z}^d, \tag{6.2}$$

cf. (4.1). In addition, it is known that $f \in \mathcal{B}_{M/2}(\mathbb{R}^d)$ is a bandlimited function with bandwidth M, i. e., we have $\hat{f}(\boldsymbol{k}) = 0$, $\boldsymbol{k} \in \mathbb{Z}^d \setminus \mathcal{I}_{\boldsymbol{M}}$. Therefore, the periodic function (6.1) in fact is a trigonometric polynomial of degree $\boldsymbol{M}$ as in (2.8), which makes it reasonable to utilize the result from Section 3.2.1 to reconstruct the Fourier coefficients (6.2). In other words, for an exact solution of the linear system (3.12) we obtain an exact reconstruction of the form

$$\hat{f}(\boldsymbol{k}) = c_{\boldsymbol{k}}(\tilde{f}) = \sum_{j=1}^{N} w_j\, \tilde{f}(\boldsymbol{x}_j)\, \mathrm{e}^{-2\pi \mathrm{i} \boldsymbol{k} \boldsymbol{x}_j}, \quad \boldsymbol{k} \in \mathcal{I}_{\boldsymbol{M}}. \tag{6.3}$$

Note that using the nonequispaced Fourier matrix $\boldsymbol{A} \in \mathbb{C}^{N \times |\mathcal{I}_{\boldsymbol{M}}|}$ in (2.7), the weight matrix $\boldsymbol{W} = \operatorname{diag}(w_j)_{j=1}^N$ as well as the vectors $\tilde{\boldsymbol{f}} \coloneqq (\tilde{f}(\boldsymbol{x}_j))_{j=1}^N$ and $\hat{\boldsymbol{f}} \coloneqq (\hat{f}(\boldsymbol{k}))_{\boldsymbol{k} \in \mathcal{I}_{\boldsymbol{M}}}$, the reconstruction (6.3) can be denoted as $\hat{\boldsymbol{f}} = \boldsymbol{A}^* \boldsymbol{W} \tilde{\boldsymbol{f}}$. Moreover, by (6.1) we have $\tilde{\boldsymbol{f}} = \boldsymbol{A} \hat{\boldsymbol{f}}$, such that the property $\boldsymbol{A}^* \boldsymbol{W} \boldsymbol{A} = \boldsymbol{I}_{|\mathcal{I}_{\boldsymbol{M}}|}$ is fulfilled, cf. Remark 3.7.

However, in practical applications, such as MRI, this is only a hypothetical case, since the periodization $\tilde{f}$ in (6.1) cannot be sampled. Due to a limited coverage of space by the acquisition, the bandlimited function f is typically not known on whole $\mathbb{R}^d$, but only on a bounded domain, w.l.o.g. for $\boldsymbol{x} \in \left[-\frac{1}{2}, \frac{1}{2}\right)^d$, cf. [EKP22]. Thus, we need to assume that the given function f is small outside this interval $\left[-\frac{1}{2}, \frac{1}{2}\right)^d$, such that $\tilde{f}(\boldsymbol{x}_j) \approx f(\boldsymbol{x}_j)$, $j = 1, \ldots, N$, holds. Hence, we have to deal with the approximation

$$\hat{f}(\boldsymbol{k}) \approx \sum_{j=1}^{N} w_j \, f(\boldsymbol{x}_j) \, \mathrm{e}^{-2\pi \mathrm{i} \boldsymbol{k} \boldsymbol{x}_j}, \quad \boldsymbol{k} \in \mathcal{I}_{\boldsymbol{M}}, \tag{6.4}$$

which can also be written as $\hat{\boldsymbol{f}} \approx \boldsymbol{A}^* \boldsymbol{W} \boldsymbol{f}$ with $\boldsymbol{W} = \operatorname{diag}(w_j)_{j=1}^N$ from (3.12).

That is to say, by (6.3) the error in the approximation (6.4) solely occurs because the bandlimited function f is not known on whole $\mathbb{R}^d$. If we had access to the periodization $\tilde{f}$ or the function f would be supported on the interval $\left[-\frac{1}{2}, \frac{1}{2}\right)^d$, respectively, then (6.3) would guarantee an exact reconstruction. Therefore, the density compensation approach from Algorithm 3.2 using the weights computed by Algorithm 3.10, is also suitable for bandlimited functions $f \in \mathcal{B}_{M/2}(\mathbb{R}^d)$.

Remark 6.1. Typically, the approximation (6.4) is motivated the following way, cf. [KP23a, Section 3.2]. Considering the integral representation (4.1) we are provided with an exact formula for the evaluation of the Fourier transform $\hat{f}$. However, since in practical applications the function f is only known on a bounded domain, w.l.o.g. for $\boldsymbol{x} \in \left[-\frac{1}{2}, \frac{1}{2}\right)^d$, we have to deal with the approximation

$$\hat{f}(\boldsymbol{v}) \approx \int_{\left[-\frac{1}{2}, \frac{1}{2}\right)^d} f(\boldsymbol{x}) \, \mathrm{e}^{-2\pi \mathrm{i} \boldsymbol{v} \boldsymbol{x}} \, \mathrm{d}\boldsymbol{x}, \quad \boldsymbol{v} \in \left[-\tfrac{M}{2}, \tfrac{M}{2}\right)^d. \tag{6.5}$$

Then applying a nonequispaced quadrature rule, the evaluations of (6.5) at uniform grid points $\boldsymbol{k} \in \mathcal{I}_{\boldsymbol{M}}$ can be approximated via (6.4). However,

since this perspective does not immediately reveal the connection to the inversion problem (3.3) or directly suggests suitable quadrature weights, we prefer the explanation above. ◇

Summarizing, we present an error bound on density compensation factors computed by means of (3.12), analogous to Theorem 3.11, that applies to bandlimited functions $f \in \mathcal{B}_{M/2}(\mathbb{R}^d)$, cf. [KP23a, Theorem 3.14].

Theorem 6.2. *Let $p, q \in \{1, 2, \infty\}$ with $\frac{1}{p} + \frac{1}{q} = 1$. For given $d, N \in \mathbb{N}$, vector $\boldsymbol{M} = M \cdot \mathbf{1}_d \in (2\mathbb{N})^d$ and nonequispaced nodes $\boldsymbol{x}_j \in \left[-\frac{1}{2}, \frac{1}{2}\right)^d$, $j = 1, \dots, N$, let $\boldsymbol{A} \in \mathbb{C}^{N \times |\mathcal{I}_{\boldsymbol{M}}|}$ be the nonequispaced Fourier matrix in (2.7). Furthermore, we assume that we can compute density compensation factors $\boldsymbol{W} = \operatorname{diag}(w_j)_{j=1}^N \in \mathbb{C}^{N \times N}$ by means of Algorithm 3.10, such that*

$$\sum_{j=1}^{N} w_j \, \mathrm{e}^{2\pi \mathrm{i} \boldsymbol{k} \boldsymbol{x}_j} = \delta_{\mathbf{0}, \boldsymbol{k}} + \varepsilon_{\boldsymbol{k}}, \quad \boldsymbol{k} \in \mathcal{I}_{\boldsymbol{2M}},$$

with small $\varepsilon_{\boldsymbol{k}} \in \mathbb{R}$ for all $\boldsymbol{k} \in \mathcal{I}_{\boldsymbol{2M}}$. Then there exists an $\varepsilon \geq 0$ such that for any bandlimited function $f \in \mathcal{B}_{M/2}(\mathbb{R}^d)$ with bandwidth M the corresponding density compensation procedure satisfies

$$\left\| \hat{\boldsymbol{f}} - \boldsymbol{A}^* \boldsymbol{W} \boldsymbol{f} \right\|_p \leq |\mathcal{I}_{\boldsymbol{M}}| \, \varepsilon \cdot \left\| \hat{\boldsymbol{f}} \right\|_p + \left(N \, |\mathcal{I}_{\boldsymbol{M}}| \right)^{1/p} \|\boldsymbol{w}\|_q \cdot \|Q\|_{C(\mathbb{T}^d)}, \quad (6.6)$$

where $\hat{\boldsymbol{f}} \coloneqq (\hat{f}(\boldsymbol{k}))_{\boldsymbol{k} \in \mathcal{I}_{\boldsymbol{M}}}$ are the integer evaluations of (4.1) and Q is defined as the pointwise quadrature error

$$Q(\boldsymbol{x}) \coloneqq \int_{\left[-\frac{M}{2}, \frac{M}{2}\right)^d} \hat{f}(\boldsymbol{v}) \, \mathrm{e}^{2\pi \mathrm{i} \boldsymbol{v} \boldsymbol{x}} \, \mathrm{d}\boldsymbol{v} - \sum_{\boldsymbol{k} \in \mathcal{I}_{\boldsymbol{M}}} \hat{f}(\boldsymbol{k}) \, \mathrm{e}^{2\pi \mathrm{i} \boldsymbol{k} \boldsymbol{x}}, \quad \boldsymbol{x} \in \mathbb{T}^d. \quad (6.7)$$

Proof. Note that by (3.24) it only remains to estimate the error term $\left\| \boldsymbol{A} \hat{\boldsymbol{f}} - \boldsymbol{f} \right\|_p$. For any bandlimited function $f \in \mathcal{B}_{M/2}(\mathbb{R}^d)$ with bandwidth M we may use the notation $\hat{\boldsymbol{f}} \coloneqq (\hat{f}(\boldsymbol{k}))_{\boldsymbol{k} \in \mathcal{I}_{\boldsymbol{M}}}$ as well as the inverse Fourier transform (4.4) to estimate

$$\begin{aligned} \left| \left[\boldsymbol{A} \hat{\boldsymbol{f}} - \boldsymbol{f} \right]_j \right| &= \left| f(\boldsymbol{x}_j) - \sum_{\boldsymbol{k} \in \mathcal{I}_{\boldsymbol{M}}} \hat{f}(\boldsymbol{k}) \, \mathrm{e}^{2\pi \mathrm{i} \boldsymbol{k} \boldsymbol{x}_j} \right| \\ &= |Q(\boldsymbol{x}_j)| \leq \|Q\|_{C(\mathbb{T}^d)}, \quad j = 1, \dots, N, \end{aligned}$$

with the pointwise quadrature error (6.7). For detailed investigations of quadrature errors of bandlimited functions we refer to [GR23, KPT23]. Hence, we obtain $\left\|\boldsymbol{A}\hat{\boldsymbol{f}} - \boldsymbol{f}\right\|_p \leq N^{1/p} \, \|Q\|_{C(\mathbb{T}^d)}$, which by (3.24) implies the assertion (6.6). ∎

6.1.2 Linking to approaches in literature

In the literature, a density compensation approach is known which is closely related to our representation (6.3). Therefore, this approach is studied in the following.

Analogous to [GLI06] we now aim to compute weights w_j, $j = 1, \dots, N$, such that not only (6.3) holds, but its extension onto the whole interval, i. e.,

$$\hat{f}(\boldsymbol{v}) \approx \tilde{h}(\boldsymbol{v}) \coloneqq \sum_{j=1}^{N} w_j \, \tilde{f}(\boldsymbol{x}_j) \, \mathrm{e}^{-2\pi \mathrm{i} \boldsymbol{v} \boldsymbol{x}_j}, \quad \boldsymbol{v} \in \left[-\tfrac{M}{2}, \tfrac{M}{2}\right)^d, \tag{6.8}$$

is preferably a good approximation. Note that by inserting (6.8) into the inverse Fourier transform (4.4), we obtain the equivalent characterization

$$\begin{aligned} f(\boldsymbol{x}) &= \int_{\left[-\frac{M}{2}, \frac{M}{2}\right)^d} \hat{f}(\boldsymbol{v}) \, \mathrm{e}^{2\pi \mathrm{i} \boldsymbol{v} \boldsymbol{x}} \, \mathrm{d}\boldsymbol{v} \approx \int_{\left[-\frac{M}{2}, \frac{M}{2}\right)^d} \tilde{h}(\boldsymbol{v}) \, \mathrm{e}^{2\pi \mathrm{i} \boldsymbol{v} \boldsymbol{x}} \, \mathrm{d}\boldsymbol{v} \\ &= \sum_{j=1}^{N} w_j \, \tilde{f}(\boldsymbol{x}_j) \int_{\left[-\frac{M}{2}, \frac{M}{2}\right)^d} \mathrm{e}^{-2\pi \mathrm{i} \boldsymbol{v} (\boldsymbol{x}_j - \boldsymbol{x})} \, \mathrm{d}\boldsymbol{v} \\ &= \sum_{j=1}^{N} w_j \, \tilde{f}(\boldsymbol{x}_j) \cdot |\mathcal{I}_{\boldsymbol{M}}| \operatorname{sinc}\bigl(M\pi(\boldsymbol{x}_j - \boldsymbol{x})\bigr), \quad \boldsymbol{x} \in \mathbb{R}^d, \end{aligned}$$

with the d-variate sinc function (3.31). Since $\tilde{f}$ in (6.1) is still unknown in practical applications, we have to deal with the overall approximation

$$f(\boldsymbol{x}) \approx \sum_{j=1}^{N} w_j \, f(\boldsymbol{x}_j) \cdot |\mathcal{I}_{\boldsymbol{M}}| \operatorname{sinc}\bigl(M\pi(\boldsymbol{x}_j - \boldsymbol{x})\bigr), \quad \boldsymbol{x} \in \mathbb{R}^d. \tag{6.9}$$

That is to say, to obtain an approximation of the form (6.8) one might aim to choose suitable weights $w_j \in \mathbb{C}$, $j = 1, \dots, N$, based on (6.9). Especially,

by evaluation of (6.9) at the given nonequispaced nodes $\boldsymbol{x} = \boldsymbol{x}_h$ we obtain the condition

$$f(\boldsymbol{x}_h) \approx \sum_{j=1}^{N} w_j \, f(\boldsymbol{x}_j) \cdot |\mathcal{I}_{\boldsymbol{M}}| \operatorname{sinc}\big(M\pi(\boldsymbol{x}_j - \boldsymbol{x}_h)\big), \quad h = 1, \ldots, N.$$

By defining the nonequispaced sinc matrix

$$\boldsymbol{C}_{\mathrm{n}} \coloneqq \Big(\operatorname{sinc}\big(M\pi(\boldsymbol{x}_j - \boldsymbol{x}_h)\big)\Big)_{j,h=1}^{N} \in \mathbb{R}^{N\times N}, \tag{6.10}$$

and $\boldsymbol{f} = (f(\boldsymbol{x}_j))_{j=1}^{N}$ we see that this means that one may try to find a weight matrix $\boldsymbol{W} = \operatorname{diag}(w_j)_{j=1}^{N}$ such that the approximation $\boldsymbol{f} \approx |\mathcal{I}_{\boldsymbol{M}}| \cdot \boldsymbol{C}_{\mathrm{n}} \boldsymbol{W} \boldsymbol{f}$ is best as possible. Ideally, one would aim for equality $\boldsymbol{I}_N = |\mathcal{I}_{\boldsymbol{M}}| \cdot \boldsymbol{C}_{\mathrm{n}} \boldsymbol{W}$. Considering the main diagonal of $\frac{1}{|\mathcal{I}_{\boldsymbol{M}}|} \boldsymbol{I}_N = \boldsymbol{C}_{\mathrm{n}} \boldsymbol{W}$ the weights are given as

$$\tfrac{1}{|\mathcal{I}_{\boldsymbol{M}}|} = w_j \operatorname{sinc}\big(M\pi(\boldsymbol{x}_j - \boldsymbol{x}_j)\big) = w_j \operatorname{sinc}(0) = w_j, \quad j = 1, \ldots, N.$$

For all other entries with $j \neq h$, however, the condition

$$\operatorname{sinc}(M\pi(\boldsymbol{x}_j - \boldsymbol{x}_h)) = 0$$

can only be fulfilled for $\boldsymbol{x}_j$ equispaced. In other words, for arbitrarily spaced points $\boldsymbol{x}_j$ equality in $|\mathcal{I}_{\boldsymbol{M}}| \cdot \boldsymbol{C}_{\mathrm{n}} \boldsymbol{W} \approx \boldsymbol{I}_N$ is not possible for any weights.

Hence, one can only look for an approximate solution, e. g. by considering the least squares problem

$$\underset{\boldsymbol{W} = \operatorname{diag}(w_j)_{j=1}^{N}}{\text{Minimize}} \; \| |\mathcal{I}_{\boldsymbol{M}}| \cdot \boldsymbol{C}_{\mathrm{n}} \boldsymbol{W} - \boldsymbol{I}_N \|_{\mathrm{F}}^2. \tag{6.11}$$

By denoting the j-th column of $\boldsymbol{I}_N, \boldsymbol{C}_{\mathrm{n}} \in \mathbb{R}^{N\times N}$ and $\boldsymbol{W} \in \mathbb{C}^{N\times N}$ as $\boldsymbol{e}_j, [\boldsymbol{C}_{\mathrm{n}}]_j \in \mathbb{R}^N$ and $\boldsymbol{w}_j \in \mathbb{C}^N$, respectively, we may rewrite the Frobenius norm in (6.11) by means of the property (3.34), only considering the nonzero entries, as

$$\begin{aligned} \| |\mathcal{I}_{\boldsymbol{M}}| \cdot \boldsymbol{C}_{\mathrm{n}} \boldsymbol{W} - \boldsymbol{I}_N \|_{\mathrm{F}}^2 &= \sum_{j=1}^{N} \| |\mathcal{I}_{\boldsymbol{M}}| \cdot \boldsymbol{C}_{\mathrm{n}} \boldsymbol{w}_j - \boldsymbol{e}_j \|_2^2 \\ &= \sum_{j=1}^{N} \| |\mathcal{I}_{\boldsymbol{M}}| \cdot [\boldsymbol{C}_{\mathrm{n}}]_j \, w_j - \boldsymbol{e}_j \|_2^2 . \end{aligned}$$

Thus, as stated in [GLI06] (without proof) the least squares solution to the minimization problem (6.11) is given by

$$w_j = \frac{1}{|\mathcal{I}_{\boldsymbol{M}}|} [\boldsymbol{C}_{\mathrm{n}}]_j^{\dagger} \boldsymbol{e}_j = \frac{1}{|\mathcal{I}_{\boldsymbol{M}}|} \left([\boldsymbol{C}_{\mathrm{n}}]_j^{*} [\boldsymbol{C}_{\mathrm{n}}]_j \right)^{-1} [\boldsymbol{C}_{\mathrm{n}}]_j^{*} \boldsymbol{e}_j \tag{6.12}$$

$$= \frac{\operatorname{sinc}\big(M\pi(\boldsymbol{x}_j - \boldsymbol{x}_j)\big)}{|\mathcal{I}_{\boldsymbol{M}}| \sum_{h=1}^{N} \operatorname{sinc}^2(M\pi(\boldsymbol{x}_j - \boldsymbol{x}_h))}$$

$$= \frac{1}{|\mathcal{I}_{\boldsymbol{M}}|} \left(\sum_{h=1}^{N} \operatorname{sinc}^2(M\pi(\boldsymbol{x}_j - \boldsymbol{x}_h)) \right)^{-1}. \tag{6.13}$$

However, we see in the numerical examples in Section 6.3 that the reconstruction using the weights (6.12) seems to be much worse than the reconstruction (6.4) with weights computed such that the linear system (3.12) holds.

Remark 6.3. As already mentioned in Remark 3.16, it was claimed in [GLI06] that this approach coincides with the one in [PM99], considering finite sections of the sinc operator

$$\mathcal{C} \coloneqq \left(\operatorname{sinc}\big(M\pi\big(\boldsymbol{x}_j - \tfrac{\boldsymbol{\ell}}{M}\big)\big) \right)_{j=1,\, \boldsymbol{\ell} \in \mathbb{Z}^d}^{N} \tag{6.14}$$

with $\boldsymbol{\ell} \in \mathcal{I}_{\boldsymbol{M}}$. However, in the following we show that this claim only holds asymptotically for $|\mathcal{I}_{\boldsymbol{M}}| \to \infty$, i. e., when using $\mathcal{C}$ in (6.14), cf. [KP23b, Remark 3.2].

By the classical sampling theorem of Whittaker–Kotelnikov–Shannon, see Theorem 4.2, any bandlimited function $f \in \mathcal{B}_{M/2}(\mathbb{R}^d)$ can be recovered from its uniform samples $f\big(\frac{\boldsymbol{\ell}}{M}\big)$, $\boldsymbol{\ell} \in \mathbb{Z}^d$, as

$$f(\boldsymbol{x}) = \sum_{\boldsymbol{\ell} \in \mathbb{Z}^d} f\big(\tfrac{\boldsymbol{\ell}}{M}\big) \operatorname{sinc}\big(M\pi\big(\boldsymbol{x} - \tfrac{\boldsymbol{\ell}}{M}\big)\big), \quad \boldsymbol{x} \in \mathbb{R}^d. \tag{6.15}$$

Applying this sampling theorem to the shifted sinc function

$$f(\boldsymbol{x}) = \operatorname{sinc}(M\pi(\boldsymbol{x}_j - \boldsymbol{x})) \in \mathcal{B}_{M/2}(\mathbb{R}^d)$$

with j fixed, we find the equality

$$\operatorname{sinc}\big(M\pi(\boldsymbol{x}_j - \boldsymbol{x})\big) = \sum_{\boldsymbol{\ell} \in \mathbb{Z}^d} \operatorname{sinc}\big(M\pi\big(\boldsymbol{x}_j - \tfrac{\boldsymbol{\ell}}{M}\big)\big) \operatorname{sinc}\big(M\pi\big(\boldsymbol{x} - \tfrac{\boldsymbol{\ell}}{M}\big)\big). \tag{6.16}$$

Note that using the sinc operator $\mathcal{C}$ in (6.14) and the nonequispaced sinc matrix in (6.10), the evaluation of (6.16) at the given nonequispaced points $\boldsymbol{x} = \boldsymbol{x}_h$, $h = 1, \dots, N$, can be written as

$$\boldsymbol{C}_{\mathrm{n}} = \mathcal{C}\mathcal{C}^* \in \mathbb{R}^{N \times N}. \tag{6.17}$$

Hence, a restriction to finitely many $\boldsymbol{\ell}$ in (6.16) corresponds to a uniform truncation of the Shannon sampling series (6.15), which is known as a poor approximation due to the slow convergence of the sinc function, see Section 4.2. Thus, equality in (6.17) is only satisfied using the operator $\mathcal{C}$ in (6.14), while considering finite sections of (6.14) with $\boldsymbol{\ell} \in \mathcal{I}_{\boldsymbol{M}}$ implies a poor approximation of $\boldsymbol{C}_{\mathrm{n}}$. ◇

Remark 6.4. Additionally, note that the sinc operator (6.14) has an interesting property, cf. [KP23b, Remark 3.1]. First of all, by [LB92, Example 1.22] it is known that the M-periodization of the function $\mathrm{e}^{2\pi\mathrm{i}\boldsymbol{t}\boldsymbol{x}}$, $\boldsymbol{t} \in \big[-\frac{M}{2}, \frac{M}{2}\big)^d$, with $\boldsymbol{x} \in \mathbb{C}^d$ fixed, possesses the absolutely and uniformly convergent Fourier series

$$\mathrm{e}^{2\pi\mathrm{i}\boldsymbol{t}\boldsymbol{x}} = \sum_{\boldsymbol{\ell} \in \mathbb{Z}^d} \operatorname{sinc}\big(M\pi\big(\boldsymbol{x} - \tfrac{\boldsymbol{\ell}}{M}\big)\big)\, \mathrm{e}^{2\pi\mathrm{i}\boldsymbol{t}\boldsymbol{\ell}/M}. \tag{6.18}$$

Therefore, the terms $\operatorname{sinc}\big(M\pi\big(\boldsymbol{x} - \frac{\boldsymbol{\ell}}{M}\big)\big)$ as the Fourier coefficients of (6.18) are ℓ_2-summable, and thus the sinc operator (6.14) is well-defined, see also (4.10).

Based on this, by additionally defining the one-sided infinite Fourier matrix

$$\mathcal{F} \coloneqq \Big(\mathrm{e}^{2\pi\mathrm{i}\boldsymbol{k}\boldsymbol{\ell}/M}\Big)_{\boldsymbol{\ell} \in \mathbb{Z}^d,\, \boldsymbol{k} \in \mathcal{I}_{\boldsymbol{M}}},$$

cf. (2.15), the matrix product $\mathcal{C}\mathcal{F}$ can be written as

$$\mathcal{C}\mathcal{F} = \left(\sum_{\boldsymbol{\ell} \in \mathbb{Z}^d} \mathrm{e}^{2\pi\mathrm{i}\boldsymbol{k}\boldsymbol{\ell}/M} \operatorname{sinc}\big(M\pi\big(\boldsymbol{x}_j - \tfrac{\boldsymbol{\ell}}{M}\big)\big) \right)_{j=1,\, \boldsymbol{k} \in \mathcal{I}_{\boldsymbol{M}}}^{N} = \boldsymbol{A} \tag{6.19}$$

with the nonequispaced Fourier matrix $\boldsymbol{A} \in \mathbb{C}^{N \times |\mathcal{I}_{\boldsymbol{M}}|}$ in (2.7), since the components of (6.19) coincide with point evaluations of (6.18) at $\boldsymbol{x} = \boldsymbol{x}_j$, $j = 1, \dots, N$, and $\boldsymbol{t} = \boldsymbol{k} \in \mathcal{I}_{\boldsymbol{M}}$.

Note that in comparison to the series expansion (6.18) we already found the approximation (5.44) of the exponential function, where we obtained a finite sum by the use of the compactly supported window function φ_m and the restriction of $\boldsymbol{x} \in \mathbb{C}^d$ to $\boldsymbol{x} \in \big[-\frac{1}{2} + \frac{m}{L}, \frac{1}{2} - \frac{m}{L}\big)^d$. ◇

6.1.3 Exactness condition in the sense of tempered distributions

Similar to [KP23a], we now present some additional observations that can be made regarding the conditions for an exact reconstruction using the density compensation method. For this purpose, analogous to (6.8), we extend the approximation (6.4) onto the whole interval $\left[-\frac{M}{2}, \frac{M}{2}\right)^d$, i. e., we consider

$$\hat{f}(\boldsymbol{v}) \approx h(\boldsymbol{v}) \coloneqq \sum_{j=1}^{N} w_j \, f(\boldsymbol{x}_j) \, \mathrm{e}^{-2\pi \mathrm{i} \boldsymbol{v} \boldsymbol{x}_j}, \quad \boldsymbol{v} \in \left[-\tfrac{M}{2}, \tfrac{M}{2}\right)^d. \tag{6.20}$$

Note that in comparison to (6.8) here we directly consider the samples $f(\boldsymbol{x}_j)$ of the bandlimited function $f \in \mathcal{B}_{M/2}(\mathbb{R}^d)$ instead of the samples $\tilde{f}(\boldsymbol{x}_j)$ of its periodization.

Analogous to Section 3.2.1 we analyze (6.20) being exact and start our investigations with the continuous analogon of Theorem 3.4, cf. [KP23a, Theorem 3.8]

Theorem 6.5. *Let nonequispaced nodes $\boldsymbol{x}_j \in \left[-\frac{1}{2}, \frac{1}{2}\right)^d$ as well as quadrature weights $w_j \in \mathbb{C}$, $j = 1, \ldots, N$, be given. Then an exact reconstruction formula* (6.20) *for bandlimited functions $f \in \mathcal{B}_{M/2}(\mathbb{R}^d)$ with bandwidth $M \in \mathbb{N}$, i. e.,*

$$\hat{f}(\boldsymbol{v}) = h(\boldsymbol{v}) = \sum_{j=1}^{N} w_j f(\boldsymbol{x}_j) \, \mathrm{e}^{-2\pi \mathrm{i} \boldsymbol{v} \boldsymbol{x}_j}, \quad \boldsymbol{v} \in \left[-\tfrac{M}{2}, \tfrac{M}{2}\right)^d, \tag{6.21}$$

implies that the quadrature rule

$$\int_{\mathbb{R}^d} f(\boldsymbol{x}) \, \mathrm{d}\boldsymbol{x} = \sum_{j=1}^{N} w_j f(\boldsymbol{x}_j)$$

is exact for all bandlimited functions $f \in \mathcal{B}_{M/2}(\mathbb{R}^d)$ with bandwidth M.

Proof. Given the Fourier transform (4.1) we can express (6.21) as

$$\int_{\mathbb{R}^d} f(\boldsymbol{x}) \, \mathrm{e}^{-2\pi \mathrm{i} \boldsymbol{v} \boldsymbol{x}} \, \mathrm{d}\boldsymbol{x} = \hat{f}(\boldsymbol{v}) = \sum_{j=1}^{N} w_j f(\boldsymbol{x}_j) \, \mathrm{e}^{-2\pi \mathrm{i} \boldsymbol{v} \boldsymbol{x}_j}, \quad \boldsymbol{v} \in \left[-\tfrac{M}{2}, \tfrac{M}{2}\right)^d. \tag{6.22}$$

In particular, evaluating (6.22) at $\boldsymbol{v} = \boldsymbol{0}$ yields the assertion. ■

However, in contrast to Theorem 3.4, an explicit condition for the computation of suitable weights $w_j \in \mathbb{C}$, $j = 1, \dots, N$, such that the reconstruction formula (6.20) is preferably exact, could not be given in the above Theorem 6.5. Thus, in order to obtain a condition for exactness, we generalize the concept of an exact reconstruction h of f and employ the theory of tempered distributions. To this end, let

$$\mathscr{S}(\mathbb{R}^d) \coloneqq \left\{\varphi \in C^\infty(\mathbb{R}^d) \colon\ \boldsymbol{x}^{\boldsymbol{\beta}}(D^{\boldsymbol{\alpha}}\varphi)(\boldsymbol{x}) \in C_0(\mathbb{R}^d),\ \boldsymbol{\alpha}, \boldsymbol{\beta} \in \mathbb{N}_0^d\right\}$$

be the *Schwartz space* of rapidly decreasing functions, see [PPST23, Section 4.2.1]. Then a *tempered distribution* is a continuous linear functional on the Schwartz space $\mathscr{S}(\mathbb{R}^d)$ and the set of all tempered distributions is denoted by $\mathscr{S}'(\mathbb{R}^d)$, see [PPST23, Section 4.3.1]. For any slowly increasing function $f \colon \mathbb{R}^d \to \mathbb{C}$, satisfying $|f(\boldsymbol{x})| \leq c(1 + \|\boldsymbol{x}\|_2)^n$ almost everywhere with $c > 0$ and $n \in \mathbb{N}_0$, the *induced tempered distribution* T_f shall be defined by

$$\langle T_f, \varphi \rangle \coloneqq \int_{\mathbb{R}^d} \varphi(\boldsymbol{x})\, f(\boldsymbol{x})\, \mathrm{d}\boldsymbol{x}, \quad \varphi \in \mathscr{S}(\mathbb{R}^d).$$

The simplest tempered distribution, which cannot be described this way, is the tempered *Dirac distribution* δ defined by

$$\langle \delta, \varphi \rangle \coloneqq \int_{\mathbb{R}^d} \varphi(\boldsymbol{v})\, \delta(\boldsymbol{v})\, \mathrm{d}\boldsymbol{v} = \varphi(\boldsymbol{0}), \quad \varphi \in \mathscr{S}(\mathbb{R}^d),$$

cf. [PPST23, Example 4.37]. For a detailed introduction to the topic we refer to [PPST23, Sections 4.2.1 and 4.3.1].

Finally, utilizing these concepts of tempered distributions, the following generalized exactness property can be shown, cf. [KP23a, Theorem 3.9].

Theorem 6.6. *Let nonequispaced nodes $\boldsymbol{x}_j \in \left[-\frac{1}{2}, \frac{1}{2}\right)^d$, $j = 1, \dots, N$, and quadrature weights $w_j \in \mathbb{C}$ be given. Further let T_f be the distribution induced by some bandlimited function $f \in \mathcal{B}_{M/2}(\mathbb{R}^d)$ with bandwidth $M \in \mathbb{N}$. Then*

$$\langle \delta, \varphi \rangle = \langle T_\xi, \varphi \rangle, \quad \varphi \in \mathscr{S}(\mathbb{R}^d), \tag{6.23}$$

with

$$\xi(\boldsymbol{v}) \coloneqq \sum_{j=1}^{N} w_j \, \mathrm{e}^{2\pi \mathrm{i} \boldsymbol{v} \boldsymbol{x}_j}, \quad \boldsymbol{v} \in \mathbb{R}^d,$$

implies

$$\langle T_{\hat{f}}, \varphi \rangle = \langle T_h, \varphi \rangle, \quad \varphi \in \mathscr{S}(\mathbb{R}^d), \tag{6.24}$$

with the function h defined in (6.20).

Proof. Using the definition (6.20) of the function h as well as the fact that the inversion formula (4.4) holds for all $\boldsymbol{x} \in \mathbb{R}^d$, we have

$$\begin{aligned} \langle T_h, \varphi \rangle &= \int_{\mathbb{R}^d} h(\boldsymbol{v}) \, \varphi(\boldsymbol{v}) \, \mathrm{d}\boldsymbol{v} = \int_{\mathbb{R}^d} \varphi(\boldsymbol{v}) \sum_{j=1}^{N} w_j f(\boldsymbol{x}_j) \, \mathrm{e}^{-2\pi \mathrm{i} \boldsymbol{v} \boldsymbol{x}_j} \, \mathrm{d}\boldsymbol{v} \\ &= \int_{\mathbb{R}^d} \varphi(\boldsymbol{v}) \sum_{j=1}^{N} w_j \left(\int_{\mathbb{R}^d} \hat{f}(\boldsymbol{u}) \, \mathrm{e}^{2\pi \mathrm{i} \boldsymbol{u} \boldsymbol{x}_j} \, \mathrm{d}\boldsymbol{u} \right) \mathrm{e}^{-2\pi \mathrm{i} \boldsymbol{v} \boldsymbol{x}_j} \, \mathrm{d}\boldsymbol{v}. \end{aligned}$$

Since $f \in \mathcal{B}_{M/2}(\mathbb{R}^d)$ implies $\hat{f} \in L_1(\mathbb{R}^d)$, see the proof of Lemma 4.1, and $\varphi \in \mathscr{S}(\mathbb{R}^d)$, we obtain by Fubini's theorem that

$$\begin{aligned} \langle T_h, \varphi \rangle &= \int_{\mathbb{R}^d} \hat{f}(\boldsymbol{u}) \int_{\mathbb{R}^d} \varphi(\boldsymbol{v}) \sum_{j=1}^{N} w_j \, \mathrm{e}^{2\pi \mathrm{i} (\boldsymbol{u} - \boldsymbol{v}) \boldsymbol{x}_j} \, \mathrm{d}\boldsymbol{v} \, \mathrm{d}\boldsymbol{u} \\ &= \int_{\mathbb{R}^d} \hat{f}(\boldsymbol{u}) \int_{\mathbb{R}^d} \varphi(\boldsymbol{u} - \boldsymbol{v}) \sum_{j=1}^{N} w_j \, \mathrm{e}^{2\pi \mathrm{i} \boldsymbol{v} \boldsymbol{x}_j} \, \mathrm{d}\boldsymbol{v} \, \mathrm{d}\boldsymbol{u} \\ &= \int_{\mathbb{R}^d} \hat{f}(\boldsymbol{u}) \int_{\mathbb{R}^d} \varphi(\boldsymbol{u} - \boldsymbol{v}) \, \xi(\boldsymbol{v}) \, \mathrm{d}\boldsymbol{v} \, \mathrm{d}\boldsymbol{u}. \end{aligned}$$

Then we make of the equality (6.23), such that

$$\begin{aligned} \langle T_h, \varphi \rangle &= \int_{\mathbb{R}^d} \hat{f}(\boldsymbol{u}) \int_{\mathbb{R}^d} \varphi(\boldsymbol{u} - \boldsymbol{v}) \, \delta(\boldsymbol{v}) \, \mathrm{d}\boldsymbol{v} \, \mathrm{d}\boldsymbol{u} \\ &= \int_{\mathbb{R}^d} \hat{f}(\boldsymbol{u}) \int_{\mathbb{R}^d} \varphi(\boldsymbol{v}) \, \delta(\boldsymbol{u} - \boldsymbol{v}) \, \mathrm{d}\boldsymbol{v} \, \mathrm{d}\boldsymbol{u} = \int_{\mathbb{R}^d} \hat{f}(\boldsymbol{u}) \, \varphi(\boldsymbol{u}) \, \mathrm{d}\boldsymbol{u} = \langle T_{\hat{f}}, \varphi \rangle \end{aligned}$$

yields the assertion. ∎

Note that the property (6.24) states that h in (6.20) is an exact reconstruction of the function $\hat{f}$ in the sense of tempered distributions. However, this does not imply equality of point evaluations of the functions $\hat{f}$ and h. Moreover, in practice the condition (6.23) is hard to fulfill. Thus, although a generalization of the ideas of Section 3.2.1 to bandlimited functions is possible, the results are not directly helpful for the numerical computation of suitable weights $w_j \in \mathbb{C}$, $j = 1, \dots, N$. That is why, in numerical computations, we rather take the detour via trigonometric polynomials as described in Section 6.1.1, and look for an exact solution of the linear system (3.12).

6.2 Optimization of the sparse matrix B

As already seen in (6.4), we might use the density compensation approach from Algorithm 3.2 for bandlimited functions $f \in \mathcal{B}_{M/2}(\mathbb{R}^d)$ as well, i. e., we may try to find a solution to the continuous inversion problem by means of $\hat{\boldsymbol{f}} \approx \boldsymbol{D}^* \boldsymbol{F}^* \boldsymbol{B}^* \boldsymbol{W} \boldsymbol{f}$ with the matrices $\boldsymbol{D} \in \mathbb{C}^{|\mathcal{I}_{\boldsymbol{M}}| \times |\mathcal{I}_{\boldsymbol{M}}|}$, $\boldsymbol{F} \in \mathbb{C}^{|\mathcal{I}_{\boldsymbol{M}_\sigma}| \times |\mathcal{I}_{\boldsymbol{M}}|}$ and $\boldsymbol{B} \in \mathbb{R}^{N \times |\mathcal{I}_{\boldsymbol{M}_\sigma}|}$ defined in (2.14), (2.15) and (2.16).

However, similar to Section 3.2, this approach will be most useful in the highly overdetermined setting $|\mathcal{I}_{\boldsymbol{2M}}| \leq N$, since only in this case we are given a theoretical guarantee for (6.3) by Theorem 3.6. To relax this condition on overdetermination, we aim to generalize the method in Section 6.1 in the style of Remark 3.3. That is to say, as in Section 3.3 we consider the optimization of the sparse matrix $\boldsymbol{B} \in \mathbb{R}^{N \times |\mathcal{I}_{\boldsymbol{M}_\sigma}|}$ in (2.16) from the NFFT decomposition, see Section 2.2, such that an approximate solution to the continuous inversion problem can be computed by means of Algorithm 3.21 using the optimized matrix resulting from Algorithm 3.25. Note that this is reasonable due to the fact that the continuous inversion problem can be seen as a generalization of the discrete problem (3.3). Moreover, we remark that it was already mentioned in Section 3.3.4 that the frame theoretical approach, cf. [GS14], is originally designed for the continuous inversion problem anyway.

6.3 Numerical examples & summary

This chapter is concluded with a numerical example comparing the density compensation approach from Section 6.1 with the matrix optimization

approach from Section 6.2 for bandlimited functions, cf. [KP23a, KP23b].

Example 6.7. Similar to [KP23a, Example 5.5] and [KP23b, Example 4.2], we examine the reconstruction properties of the direct inversion methods for bandlimited functions $f \in \mathcal{B}_{M/2}(\mathbb{R}^d)$ with maximum bandwidth M. To determine the errors properly, we firstly specify a compactly supported function $\hat{f}$ in the Fourier domain and consequently compute its inverse Fourier transform (4.4), such that its samples $f(\boldsymbol{x}_j)$ for given $\boldsymbol{x}_j \in \left[-\frac{1}{2}, \frac{1}{2}\right)^2$, $j = 1, \dots, N$, can be used for the reconstruction of the samples $\hat{f}(\boldsymbol{k})$, $\boldsymbol{k} \in \mathcal{I}_{\boldsymbol{M}}$. Here we consider the tensorized function $\hat{f}(\boldsymbol{v}) = g(v_1) \cdot g(v_2)$, where $g(v)$ is the one-dimensional triangular pulse function (3.93). Then for all $b \in \mathbb{N}$ with $b \leq \frac{M}{2}$ the associated inverse Fourier transform

$$f(\boldsymbol{x}) = \int_{\mathbb{R}^2} \hat{f}(\boldsymbol{v})\, \mathrm{e}^{2\pi \mathrm{i} \boldsymbol{v}\boldsymbol{x}}\, \mathrm{d}\boldsymbol{v} = b^2 \operatorname{sinc}^2(b\pi\boldsymbol{x}), \quad \boldsymbol{x} \in \mathbb{R}^2, \tag{6.25}$$

is bandlimited with bandwidth M. For this function, we compare the density compensation methods from Section 6.1 and the matrix optimization approach from Section 6.2. On the one hand, we study Algorithm 3.2 with the weights computed via Algorithm 3.10 and the computation scheme (6.12). Since we have already seen in Example 3.33 that from the density compensation methods in Section 3.2.4 only the weights computed via (3.44) yield a reconstruction comparable to the one computed via Algorithm 3.10, the computation scheme (3.44) is considered as well. On the other hand, it is known by Example 3.35 that the best matrix optimization approach is given by Algorithm 3.21 with the optimized sparse matrix computed by Algorithm 3.25, such that we consider only this approach.

(a) As a first experiment we fix $M = 32$ and $b = 12$ and consider the case $|\mathcal{I}_{\boldsymbol{2M}}| \leq N$, which yields optimality for trigonometric polynomials, cf. Section 3.2.1. In addition to the real-world sampling of (6.25) we also examine the artificial sampling data

$$\tilde{f}(\boldsymbol{x}_j) = \sum_{\boldsymbol{k} \in \mathcal{I}_{\boldsymbol{M}}} \hat{f}(\boldsymbol{k})\, \mathrm{e}^{2\pi \mathrm{i} \boldsymbol{k}\boldsymbol{x}_j}, \quad j = 1, \dots, N, \tag{6.26}$$

of the periodization (6.1). A visualization of the chosen function f and the difference $f - \tilde{f}$ can be found in Figure 6.1.

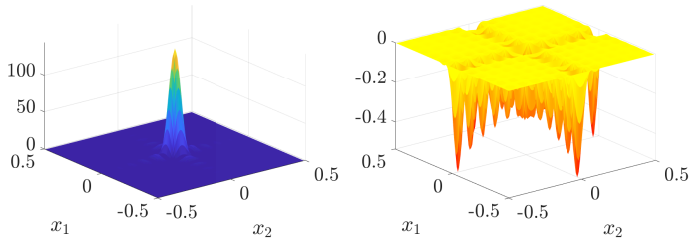

(a) The function f (b) The difference $f - \tilde{f}$

Figure 6.1: The function (6.25) with $b = 12$, and its periodization (6.26).

For the modified polar grid, cf. Figure 3.4b, of size $R = 2M$, $T = 2R$, we use these two kinds of sampling data to compute the reconstructions $\tilde{\boldsymbol{h}} \in \{\tilde{\boldsymbol{h}}^{\mathrm{w}}, \boldsymbol{h}_{\mathrm{opt}}\}$, cf. (3.6) and (3.60), and the respective pointwise errors $\left|\tilde{\boldsymbol{h}} - \hat{\boldsymbol{f}}\right|$. The corresponding results are displayed in Figure 6.2. It can easily be seen that for the artificial sampling data (6.26) our newly proposed weights computed by (3.15) indeed yield a nearly exact reconstruction, see Figure 6.2b (bottom), and thus are optimal. However, in the more realistic setting using the real-world sampling of (6.25) the results are not as good, see Figure 6.2b (top). Nevertheless, comparing to the equispaced setting in Figure 6.2a (top), it becomes apparent that Algorithm 3.2 using the weights computed by (3.15) and (3.44), as well as Algorithm 3.21 using the optimized sparse matrix $\boldsymbol{B}_{\mathrm{opt}} \in \mathbb{R}^{N \times |\mathcal{I}_{M\sigma}|}$ produce nearly the same error as a reconstruction on an equispaced grid. This nicely illustrates that for bandlimited functions the restricted knowledge of $f(\boldsymbol{x}_j)$, $j = 1, \ldots, N$, instead of $\tilde{f}(\boldsymbol{x}_j)$ is the dominating error term and therefore reconstruction errors smaller than the ones shown in Figure 6.2 cannot be expected. In addition, we remark that the reconstruction using the weights (6.12) is not competetive, for none of the sampling data, see Figure 6.2d. Finally, note that we chose comparatively small $M = 32$ in order that the computation schemes (3.44) and (6.12) are affordable.

(b) In a second experiment we sample the function (6.25) with parameters $M = 64$ and $b = 24$ at linogram grids, cf. Figure 3.4c, of different sizes $R \in \{40, 48, \ldots, 104\}$, $T = 2R$. The corresponding relative errors (3.99) can be found in Table 6.1. It should be noted that for $M = 64$ we have $|\mathcal{I}_{\boldsymbol{M}}| = 4096$ and $|\mathcal{I}_{\boldsymbol{2M}}| = 16384$, i. e., the underdetermined setting $|\mathcal{I}_{\boldsymbol{M}}| > N$ is considered once, while the setting $|\mathcal{I}_{\boldsymbol{2M}}| \leq N$ needed

for exactness of the weights in Section 3.2.1 is considered twice. In general, we observe that the use of the weights (3.15) and (3.44), as well as Algorithm 3.21, produces almost identical outcomes. Nevertheless, for $\frac{1}{2}|\mathcal{I}_{\mathbf{2}\boldsymbol{M}}| \geq N$ it can be seen that Algorithm 3.21 exhibits a marginal advantage, while for $|\mathcal{I}_{\mathbf{2}\boldsymbol{M}}| \approx N$ the scheme (3.15) is infinitesimally better. ◇

Remark 6.8. Note that the code files for all the experiments in this section are available at [Kir] under `https://github.com/melaniekircheis/dissertation/tree/main/6-Reconstruction_of_the_FT_of_bandlimited_functions`. ◇

Summary

In this chapter, we have examined direct inversion methods for the continuous analogon to problem (3.3), considering bandlimited functions $f \in \mathcal{B}_{M/2}(\mathbb{R}^d)$, cf. (4.3), instead of trigonometric polynomials (2.8). That is to say, in this setting the aim is the reconstruction of point evaluations $\hat{f}(\boldsymbol{k}) \in \mathbb{C}$, $\boldsymbol{k} \in \mathcal{I}_{\boldsymbol{M}}$, of an object $\hat{f}$ in (4.1) from given measurements $f(\boldsymbol{x}_j)$, $j = 1, \dots, N$, of the bandlimited function f. To solve this problem, we have extended the density compensation technique from Section 3.2.1 and the matrix optimization approach from Section 3.3 to bandlimited functions $f \in \mathcal{B}_{M/2}(\mathbb{R}^d)$. In doing so, we have demonstrated both theoretically, in Section 6.1.1, and numerically, in Example 6.7, that the reconstruction error is dominated by the fact that the bandlimited function f is not known on whole $\mathbb{R}^d$, but only on a bounded domain. Nevertheless, we have confirmed that our density compensation approach in Algorithm 3.2 with the weights computed by Algorithm 3.10 as well as our matrix optimization approach in Algorithm 3.21 with the optimized sparse matrix computed by Algorithm 3.25 yield the best results possible.

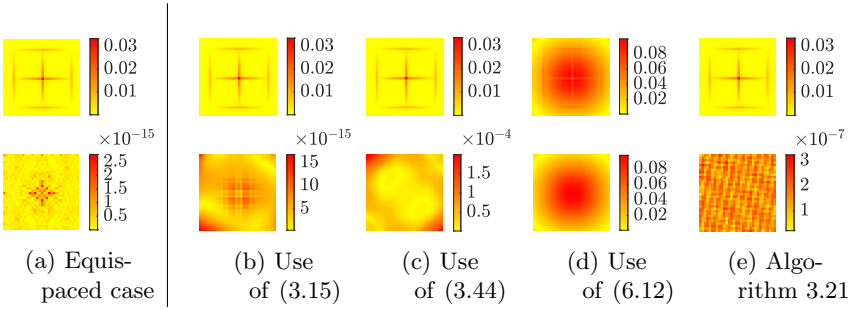

(a) Equispaced case (b) Use of (3.15) (c) Use of (3.44) (d) Use of (6.12) (e) Algorithm 3.21

Figure 6.2: Pointwise absolute error $|\tilde{\boldsymbol{h}} - \hat{\boldsymbol{f}}|$ of the reconstruction of the samples $\hat{f}(\boldsymbol{k})$, $\boldsymbol{k} \in \mathcal{I}_{\boldsymbol{M}}$, of the tensorized triangular pulse function (3.93) with $M = 32$ and $b = 12$, using the density compensation factors computed by (3.15), (3.44) and (6.12) as well as the optimization approach from Algorithm 3.21 for the modified polar grid, cf. Figure 3.4b, of size $R = 2M$, $T = 2R$, using samples $f(\boldsymbol{x}_j)$, $j = 1, \ldots, N$, (top) and artificial samples $\tilde{f}(\boldsymbol{x}_j)$ in (6.26) (bottom).

R	N	Use of (3.15)	Use of (3.44)	Use of (6.12)	Alg. 3.21
40	3120	8.4481–01	6.6334–01	7.8579–01	5.1464–01
48	4512	7.8774–01	4.7713–01	7.1759–01	2.1346–01
56	6160	7.4191–01	2.7790–01	5.5826–01	6.3496–02
64	8064	5.6105–01	3.8184–03	8.2305–02	3.7609–03
72	10224	3.7650–03	3.7651–03	3.3180–01	1.8321–02
80	12640	3.7724–03	3.8150–03	2.8526–01	4.8235–03
88	15312	3.7692–03	3.7689–03	2.1575–01	3.8691–03
96	18240	3.7599–03	3.7677–03	1.6278–01	3.7741–03
104	21424	3.7599–03	3.7517–03	1.3832–01	3.7620–03

Table 6.1: Relative errors (3.99) of the reconstruction of the samples $\hat{f}(\boldsymbol{k})$, $\boldsymbol{k} \in \mathcal{I}_{\boldsymbol{M}}$, of the tensorized triangular pulse function (3.93) with $M = 64$ and $b = 24$, using the density compensation factors computed by (3.15), (3.44) and (6.12) as well as the optimization approach from Algorithm 3.21 for linogram grids, cf. Figure 3.4c, of different sizes.

Bibliography

[ACD+06] A. Averbuch, R. Coifman, D. L. Donoho, M. Elad, and M. Israeli. Fast and accurate polar Fourier transform. *Appl. Comput. Harmon. Anal.*, 21:145–167, 2006. (Cited on page 41.)

[ACD+08] A. Averbuch, R. Coifman, D. Donoho, M. Israeli, and Y. Shkolnisky. A framework for discrete integral transformations I – the pseudopolar Fourier transform. *SIAM J. Sci. Comput.*, 30:764–784, 2008. (Cited on pages 41, 100, 101, and 102.)

[AGP16] R. Archibald, A. Gelb, and R. B. Platte. Image reconstruction from undersampled Fourier data using the polynomial annihilation transform. *J. Sci. Comput.*, 67(2):432–452, 2016. (Cited on page 40.)

[AGY05] R. Archibald, A. Gelb, and J. Yoon. Polynomial fitting for edge detection in irregularly sampled signals and images. *SIAM J. Numer. Anal.*, 43(1):259–279, 2005. (Cited on page 40.)

[AS72] M. Abramowitz and I. A. Stegun, editors. *Handbook of Mathematical Functions*. National Bureau of Standards, Washington, DC, USA, 1972. (Cited on pages 156, 171, 173, 178, and 182.)

[ASS16] A. Averbuch, G. Shabat, and Y. Shkolnisky. Direct inversion of the three-dimensional pseudo-polar Fourier transform. *SIAM J. Sci. Comput.*, 38(2):A1100–A1120, 2016. (Cited on page 41.)

[Bar10] Á. Baricz. Bounds for modified Bessel functions of the first and second kinds. *Proc. Edinb. Math. Soc. (2)*, 53:575–599, 2010. (Cited on page 181.)

[Bar21] A. H. Barnett. Aliasing error of the $\exp(\beta\sqrt{1-z^2})$ kernel in the nonuniform fast Fourier transform. *Appl. Comput. Harmon. Anal.*, 51:1–16, 2021. (Cited on page 29.)

[BES82] P. L. Butzer, W. Engels, and U. Scheben. Magnitude of the truncation error in sampling expansions of bandlimited signals. *IEEE Trans. Acoust. Speech Signal process*, ASSP-30(6):906–912, 1982. (Cited on page 119.)

[Bey95] G. Beylkin. On the fast Fourier transform of functions with singularities. *Appl. Comput. Harmon. Anal.*, 2:363–381, 1995. (Cited on pages 9, 25, and 28.)

[BG04] R. F. Bass and K. Gröchenig. Random sampling of multivariate trigonometric polynomials. *SIAM J. Math. Anal.*, 36:773–795, 2004. (Cited on page 39.)

[Bjö96] Å. Björck. *Numerical Methods for Least Squares Problems*. SIAM, Philadelphia, PA, USA, 1996. (Cited on pages 52, 58, 59, 60, 65, and 70.)

[BM02] G. Beylkin and L. Monzón. On generalized Gaussian quadratures for exponentials and their applications. *Appl. Comput. Harmon. Anal.*, 12:332–373, 2002. (Cited on pages 219 and 220.)

[BMK] A. H. Barnett, J. F. Magland, and L. A. Klinteberg. Flatiron Institute nonuniform fast Fourier transform libraries (FINUFFT). `http://github.com/flatironinstitute/finufft`. (Cited on pages 25 and 29.)

[BMK19] A. H. Barnett, J. F. Magland, and L. A. Klinteberg. A parallel non-uniform fast Fourier transform library based on an "exponential of semicircle" kernel. *SIAM J. Sci. Comput.*, 41:C479–C504, 2019. (Cited on pages 9 and 29.)

[BP07] A. Böttcher and D. Potts. Probability against condition number and sampling of multivariate trigonometric random polynomials. *Electron. Trans. Numer. Anal.*, 26:178–189, 2007. (Cited on page 39.)

[BP14] Á. Baricz and T. K. Pogány. Functional inequalities for modified Struve functions II. *Math. Inequal. Appl.*, 17:1387–1398, 2014. (Cited on page 178.)

[CAG19] V. Churchill, R. Archibald, and A. Gelb. Edge-adaptive ℓ_2 regularization image reconstruction from non-uniform Fourier data. *Inverse Probl. Imaging*, 13(5):931–958, 2019. (Cited on page 40.)

[Chr16] O. Christensen. *An introduction to frames and Riesz bases (Second Edition)*. Applied and Numerical Harmonic Analysis. Birkhäuser Basel, 2016. (Cited on page 83.)

[Chu92] C. K. Chui. *An Introduction to Wavelets*. Academic Press, Boston, 1992. (Cited on page 163.)

[CM82] S. Cambanis and E. Masry. Truncation error bounds for the cardinal sampling expansion of band-limited signals. *IEEE Trans. Inform. Theory*, IT-28(4):605–612, 1982. (Cited on page 119.)

[CM98] H. Choi and D. C. Munson. Analysis and design of minimax-optimal interpolators. *IEEE Trans. Signal Process.*, 46(6):1571–1579, 1998. (Cited on page 65.)

[CT65] J. W. Cooley and J. W. Tukey. An algorithm for machine calculation of complex Fourier series. *Math. Comput.*, 19:297–301, 1965. (Cited on pages 9 and 24.)

[CWB08] E. J. Candès, M. B. Wakin, and S. P. Boyd. Enhancing sparsity by reweighted ℓ_1 minimization. *J. Fourier Anal. Appl.*, 14(5):877–905, 2008. (Cited on page 40.)

[CY08] R. Chartrand and W. Yin. Iteratively reweighted algorithms for compressive sensing. In *IEEE International Conference on Acoustics, Speech and Signal Processing*, pages 3869–3872. IEEE, 2008. (Cited on page 40.)

[CZ19] L. Chen and H. Zhang. Sharp exponential bounds for the Gaussian regularized Whittaker–Kotelnikov–Shannon sampling series. *J. Approx. Theory*, 245:73–82, 2019. (Cited on pages 16, 123, 147, 158, and 159.)

[DAP22] M. Doneva, M. Akcakaya, and C. Prieto, editors. *Magnetic Resonance Image Reconstruction: Theory, Methods and Applications*, volume 6. Academic Press, 2022. (Cited on pages 9, 37, and 261.)

[Dau92] I. Daubechies. *Ten Lectures on Wavelets*. SIAM, Philadelphia, PA, USA, 1992. (Cited on pages 15, 123, 124, 131, and 141.)

[DD03] I. Daubechies and R. DeVore. Approximating a bandlimited function using very coarsely quantized data: A family of stable sigma-delta modulators of arbitrary order. *Ann. of Math.*, 158(2):679–710, 2003. (Cited on pages 14, 119, and 121.)

[DDFG10] I. Daubechies, R. DeVore, M. Fornasier, and C. S. Güntürk. Iteratively reweighted least squares minimization for sparse recovery. *Commun. Pure Appl. Math*, 63(1):1–38, 2010. (Cited on page 40.)

[DGS16] J. Davis, A. Gelb, and G. Song. A high-dimensional inverse frame operator approximation technique. *SIAM J. Numer. Anal.*, 54(4):2282–2301, 2016. (Cited on page 85.)

[DR93] A. Dutt and V. Rokhlin. Fast Fourier transforms for nonequispaced data. *SIAM J. Sci. Stat. Comput.*, 14:1368–1393, 1993. (Cited on pages 9, 25, and 28.)

[DR95] A. Dutt and V. Rokhlin. Fast Fourier transforms for nonequispaced data II. *Appl. Comput. Harmon. Anal.*, 2:85–100, 1995. (Cited on page 41.)

[DS99] A. J. W. Duijndam and M. A. Schonewille. Nonuniform fast Fourier transform. *Geophysics*, 64:539–551, 1999. (Cited on pages 9 and 28.)

[EKP22] H. Eggers, M. Kircheis, and D. Potts. Non-Cartesian MRI reconstruction. In M. Doneva, M. Akcakaya, and C. Prieto, editors, *Magnetic Resonance Image Reconstruction: Theory, Methods and Applications*, volume 6. Academic Press, 2022. (Cited on pages 9, 18, 19, 37, 58, 261, and 263.)

[Elb98] B. Elbel. Mehrdimensionale Fouriertransformation für nichtäquidistante Daten. Diplomarbeit, TH Darmstadt, 1998. (Cited on page 32.)

[ES98] B. Elbel and G. Steidl. Fast Fourier transform for nonequispaced data. In C. K. Chui and L. L. Schumaker, editors, *Approximation Theory IX*, pages 39–46, Nashville, 1998. Vanderbilt University Press. (Cited on pages 32 and 35.)

[Fas07] G. E. Fasshauer. *Meshfree approximation methods with MATLAB*. World Scientific Publishers, 2007. (Cited on pages 9 and 37.)

[Fei92a] H. G. Feichtinger. New results on regular and irregular sampling based on Wiener amalgams. In K. Jarosz, editor, *Function Spaces, Proc Conf, Edwardsville/IL (USA) 1990*, volume 136 of Lect. Notes Pure Appl. Math., pages 107—121. New York, 1992. (Cited on pages 14 and 119.)

[Fei92b] H. G. Feichtinger. Wiener amalgams over Euclidean spaces and some of their applications. In K. Jarosz, editor, *Function Spaces, Proc Conf, Edwardsville/IL (USA) 1990*, volume 136 of Lect. Notes Pure Appl. Math., pages 123—137. New York, 1992. (Cited on page 119.)

[FGS95] H. G. Feichtinger, K. Gröchenig, and T. Strohmer. Efficient numerical methods in non-uniform sampling theory. *Numer. Math.*, 69:423–440, 1995. (Cited on page 39.)

[FKP07] M. Fenn, S. Kunis, and D. Potts. On the computation of the polar FFT. *Appl. Comput. Harmon. Anal.*, 22:257–263, 2007. (Cited on page 88.)

[Fou03] K. Fourmont. Non equispaced fast Fourier transforms with applications to tomography. *J. Fourier Anal. Appl.*, 9:431–450, 2003. (Cited on page 29.)

[FS03] J. A. Fessler and B. P. Sutton. Nonuniform fast Fourier transforms using min-max interpolation. *IEEE Trans. Signal Process.*, 51:560–574, 2003. (Cited on page 40.)

[FTV23] F. Filbir, M. Tasche, and A. Veselovska. Regularized Shannon sampling formulas related to the special affine Fourier transform. *arXiv:2311.00610*, 2023. (Cited on page 153.)

[GJG23] D. Green, J. R. Jamora, and A. Gelb. Leveraging joint sparsity in 3d synthetic aperture radar imaging. *Appl. Math. Modern Chall.*, 1(1):61–86, 2023. (Cited on pages 9 and 37.)

[GKP09] M. Gräf, S. Kunis, and D. Potts. On the computation of nonnegative quadrature weights on the sphere. *Appl. Comput. Harmon. Anal.*, 27:124–132, 2009. (Cited on page 45.)

[GL04] L. Greengard and J.-Y. Lee. Accelerating the nonuniform fast Fourier transform. *SIAM Rev.*, 46:443–454, 2004. (Cited on pages 9, 25, and 29.)

[GLI06] L. Greengard, J.-Y. Lee, and S. Inati. The fast sinc transform and image reconstruction from nonuniform samples in k-space. *Commun. Appl. Math. Comput. Sci.*, 1:121–131, 2006. (Cited on pages 9, 16, 18, 37, 65, 218, 223, 227, 228, 249, 250, 265, and 267.)

[GR07] I. S. Gradshteyn and I. M. Ryzhik. *Table of Integrals, Series, and Products*. Academic Press New York, seventh edition, 2007. (Cited on pages 171, 173, and 178.)

[GR23] A. Gopal and V. Rokhlin. A fast procedure for the construction of quadrature formulas for bandlimited functions. *ACHA*, 66:193–210, 2023. (Cited on page 265.)

[Grö20] K. Gröchenig. Sampling, Marcinkiewicz–Zygmund inequalities, approximation, and quadrature rules. *J. Approx. Theory*, 257:105455, 2020. (Cited on pages 46 and 47.)

[GS13] A. Gelb and G. Song. Approximating the inverse frame operator from localized frames. *Appl. Comput. Harm. Anal.*, 35(1):94–110, 2013. (Cited on pages 84 and 85.)

[GS14] A. Gelb and G. Song. A frame theoretic approach to the nonuniform fast Fourier transform. *SIAM J. Numer. Anal.*, 52(3):1222–1242, 2014. (Cited on pages 41, 83, 84, 85, 86, 99, and 272.)

[H+19] E. S. Helou et al. The discrete Fourier transform for golden angle linogram sampling. *Inverse Problems*, 35(125004), 2019. (Cited on page 89.)

[HJ13] R. A. Horn and C. R. Johnson. *Matrix analysis*. Cambridge University Press, Cambridge, second edition, 2013. (Cited on page 63.)

[HJB85] M. T. Heideman, D. H. Johnson, and C. S. Burrus. Gauss and the history of the fast Fourier transform. *Arch. Hist. Exact Sci.*, 34:265–277, 1985. (Cited on page 9.)

[HR84] G. Heinig and K. Rost. *Algebraic methods for Toeplitz-like matrices and operators*, volume 19 of *Mathematical Research*. Akademie-Verlag, Berlin, 1984. (Cited on page 41.)

[Huy09] D. Huybrechs. Stable high-order quadrature rules with equidistant points. *J. Comput. Appl. Math.*, 231(2):933–947, 2009. (Cited on pages 46, 47, 48, 49, and 51.)

[Jag66] D. Jagerman. Bounds for truncation error of the sampling expansion. *SIAM J. Appl. Math.*, 14(4):714–723, 1966. (Cited on pages 14, 117, 118, and 119.)

[JG03] L. Jingfan and F. Gensun. On uniform truncation error bounds and aliasing error for multidimensional sampling expansion. *Sampl. Theory Signal Image Process.*, 2(2):103–115, 2003. (Cited on page 119.)

[Kir] M. Kircheis. `https://github.com/melaniekircheis/dissertation/`. (Cited on pages 20, 102, 215, 258, and 275.)

[KKP] J. Keiner, S. Kunis, and D. Potts. NFFT 3.5, C subroutine library. `http://www.tu-chemnitz.de/~potts/nfft`. Contributors: F. Bartel, M. Fenn, T. Görner, M. Kircheis, T. Knopp, M. Quellmalz, M. Schmischke, T. Volkmer, A. Vollrath. (Cited on page 25.)

[KKP07] T. Knopp, S. Kunis, and D. Potts. A note on the iterative MRI reconstruction from nonuniform k-space data. *Int. J. Biomed. Imag.*, 2007, 2007. ID 24727. (Cited on page 40.)

[KKP09] J. Keiner, S. Kunis, and D. Potts. Using NFFT3 - a software library for various nonequispaced fast Fourier transforms. *ACM Trans. Math. Software*, 36:Article 19, 1–30, 2009. (Cited on pages 9, 25, and 29.)

[KN21] S. Kunis and D. Nagel. On the condition number of Vandermonde matrices with pairs of nearly-colliding nodes. *Numer. Algor.*, 87:473–496, 2021. (Cited on page 39.)

[Kot01] V. A. Kotelnikov. On the transmission capacity of the "ether" and wire in electrocommunications. In *Modern Sampling Theory: Mathematics and Application*, pages 27–45. Birkhäuser,

Boston, 2001. Translated from Russian. (Cited on pages 11, 14, and 109.)

[KP07] S. Kunis and D. Potts. Stability results for scattered data interpolation by trigonometric polynomials. *SIAM J. Sci. Comput.*, 29:1403–1419, 2007. (Cited on pages 40 and 77.)

[KP08] S. Kunis and D. Potts. Time and memory requirements of the nonequispaced FFT. *Sampl. Theory Signal Image Process.*, 7:77–100, 2008. (Cited on page 39.)

[KP19] M. Kircheis and D. Potts. Direct inversion of the nonequispaced fast Fourier transform. *Linear Algebra Appl.*, 575:106–140, 2019. (Cited on pages 19, 41, 70, 83, 85, 86, 87, and 99.)

[KP21] M. Kircheis and D. Potts. Efficient multivariate inversion of the nonequispaced fast Fourier transform. *PAMM*, 20(1):e202000120, 2021. (Cited on pages 19, 69, and 71.)

[KP23a] M. Kircheis and D. Potts. Fast and direct inversion methods for the multivariate nonequispaced fast Fourier transform. *Front. Appl. Math. Stat.*, 9(1155484):27 pp., 2023. (Cited on pages 19, 20, 42, 45, 47, 52, 53, 56, 58, 69, 71, 78, 87, 91, 96, 99, 263, 264, 269, 270, and 273.)

[KP23b] M. Kircheis and D. Potts. Optimal density compensation factors for the reconstruction of the Fourier transform of bandlimited functions. *Fourteenth International Conference on Sampling Theory and Applications*, 2023. (Cited on pages 19, 47, 94, 261, 267, 268, and 273.)

[KPT22] M. Kircheis, D. Potts, and M. Tasche. On regularized Shannon sampling formulas with localized sampling. *Sampl. Theory Signal Process. Data Anal.*, 20(20):34 pp., 2022. (Cited on pages 19, 123, 141, 143, 147, 151, 156, 158, 159, 162, 164, 166, 170, 174, 200, 205, 207, 208, 209, and 213.)

[KPT23] M. Kircheis, D. Potts, and M. Tasche. Nonuniform fast Fourier transforms with nonequispaced spatial and frequency data and fast sinc transforms. *Numer. Algor.*, 92:2307–2339, 2023. (Cited on pages 19, 35, 218, 219, 220, 221, 223, 227, 230, 231, 248, 252, and 265.)

[KPT24] M. Kircheis, D. Potts, and M. Tasche. On numerical realizations of Shannon's sampling theorem. *Sampl. Theory Signal Process. Data Anal.*, 22(13):33 pp., 2024. (Cited on pages 19, 113, 114, 119, 121, 124, 132, 133, 134, 136, 141, 147, 177, 182, 183, 200, 201, 203, 204, and 214.)

[KR97] S. Kapur and V. Rokhlin. High-order corrected trapezoidal quadrature rules for singular functions. *SIAM J. Numer. Anal.*, 34(4):1331–1356, 1997. (Cited on page 218.)

[LB92] J. Lund and K. L. Bowers. *Sinc Methods for Quadrature and Differential Equations*. Society for Industrial and Applied Mathematics, 1992. (Cited on pages 16, 108, 217, and 268.)

[LB11] O. Livne and A. Brandt. MuST: The multilevel Sinc Transform. *SIAM J. Sci. Comput.*, 33(4):1726–1738, 2011. (Cited on pages 16 and 218.)

[LG05] J.-Y. Lee and L. Greengard. The type 3 nonuniform FFT and its applications. *J. Comput. Physics*, 206:1–5, 2005. (Cited on page 32.)

[LGBM18] H. Lawrence, L. Greengard, A. Barnett, and J. Magland. FINUFFT–associated sinc transform. `https://fast-sinc-transform.readthedocs.io/en/latest/index.html`, 2018. (Cited on page 218.)

[Li98] X. M. Li. Uniform bounds for sampling expansions. *J. Approx. Theory*, 93(1):100–113, 1998. (Cited on page 119.)

[LMFL12] Y. Liu, J. Ma, Y. Fan, and Z. Liang. Adaptive-weighted total variation minimization for sparse data toward low-dose x-ray computed tomography image reconstruction. *Phys. Med. Biol.*, 57(23):7923, 2012. (Cited on page 40.)

[LZ17] R. Lin and H. Zhang. Convergence analysis of the Gaussian regularized Shannon sampling formula. *Numer. Funct. Anal. Optim.*, 38(2):224–247, 2017. (Cited on pages 16, 123, 146, 147, 156, and 158.)

[Mar92] R. J. Marks II. *Advanced Topics on Shannon Sampling and Interpolation Theory*. Springer-Verlag, New York, 1992. (Cited on page 119.)

[MR65] R. Medhurst and J. Roberts. Evaluation of the integral $I_n(b) = \frac{2}{\pi}\int_0^\infty (\sin x/x)^n \cos(bx)\,\mathrm{d}x$. *Math. Comp.*, 19:113–117, 1965. (Cited on page 163.)

[MXZ09] C. Micchelli, Y. Xu, and H. Zhang. Optimal learning of bandlimited functions from localized sampling. *J. Complexity*, 25(2):85–114, 2009. (Cited on pages 16, 123, 150, and 190.)

[Nat86a] F. Natterer. *The Mathematics of Computerized Tomography*. John Wiley & Sons Ltd, Chichester, 1986. (Cited on pages 15 and 123.)

[Nat86b] F. Natterer. Efficient evaluation of oversampled functions. *J. Comput. Appl. Math.*, 14(3):303–309, 1986. (Cited on pages 136 and 140.)

[Nik75] S. M. Nikol'skii. *Approximation of Functions of Several Variables and Imbedding Theorems*. Grundlehren der mathematischen Wissenschaften. Springer Berlin, Heidelberg, 1975. (Cited on page 110.)

[NS03] A. Nieslony and G. Steidl. Approximate factorizations of Fourier matrices with nonequispaced knots. *Linear Algebra Appl.*, 266:337–351, 2003. (Cited on page 70.)

[NW01] F. Natterer and F. Wübbeling. *Mathematical Methods in Image Reconstruction*. SIAM, Philadelphia, PA, 2001. (Cited on pages 9 and 37.)

[Obe90] F. Oberhettinger. *Tables of Fourier Transforms and Fourier Transforms of Distributions*. Springer, Berlin, 1990. (Cited on pages 163, 167, 175, and 204.)

[Par97] J. R. Partington. *Interpolation, Identification, and Sampling*. Clarendon Press, London Mathematical Society Monographs New Series, 1997. (Cited on pages 15, 106, 107, 123, 124, 131, and 141.)

[Pip75] H. S. Piper Jr. Bounds for truncation error in sampling expansions of finite energy band-limited signals. *IEEE Trans. Inform. Theory*, IT-21:482–485, 1975. (Cited on page 119.)

[PM99] J. G. Pipe and P. Menon. Sampling density compensation in MRI: rationale and an iterative numerical solution. *Magn. Reson. Med.*, 41:179–186, 1999. (Cited on pages 65, 68, and 267.)

[PPST23] G. Plonka, D. Potts, G. Steidl, and M. Tasche. *Numerical Fourier Analysis*. Applied and Numerical Harmonic Analysis. Birkhäuser/Springer, Second edition, 2023. (Cited on pages 24, 25, 26, 29, 30, 31, 40, 41, 48, 52, 74, 106, 107, 109, 123, 126, 154, 160, 221, 222, 223, 225, 262, and 270.)

[Pre16] E. Prestini. *The Evolution of Applied Harmonic Analysis*. Applied and Numerical Harmonic Analysis. Birkhäuser/Springer, Second edition, 2016. (Cited on page 9.)

[PST01] D. Potts, G. Steidl, and M. Tasche. Fast Fourier transforms for nonequispaced data: A tutorial. In J. J. Benedetto and P. J. S. G. Ferreira, editors, *Modern Sampling Theory: Mathematics and Applications*, pages 247–270, Boston, MA, USA, 2001. Birkhäuser. (Cited on pages 9 and 32.)

[PT21a] D. Potts and M. Tasche. Continuous window functions for NFFT. *Adv. Comput. Math.*, 47(53):1–34, 2021. (Cited on pages 9, 28, 29, 167, and 177.)

[PT21b] D. Potts and M. Tasche. Uniform error estimates for nonequispaced fast Fourier transforms. *Sampl. Theory Signal Process. Data Anal.*, 19(17):1–42, 2021. (Cited on pages 29, 80, 142, 160, 169, 174, and 175.)

[PW01] K. P. Pruessmann and F. T. A. W. Wayer. Major speedup of reconstruction for sensitivity encoding with arbitrary trajectories. In *Proc. Intl. Soc. Mag. Reson. Med. 9*, page 767. Glasgow, Scotland, 2001. (Cited on page 40.)

[QC06a] L. Qian and D. Creamer. Localized sampling in the presence of noise. *Appl. Math. Letter*, 19:351–355, 2006. (Cited on pages 147 and 159.)

[QC06b] L. Qian and D. Creamer. A modification of the sampling series with a Gaussian multiplier. *Sampl. Theory Signal Image Process.*, 5(1):1–20, 2006. (Cited on page 147.)

[Qia03] L. Qian. On the regularized Whittaker–Kotelnikov–Shannon sampling formula. *Proc. Amer. Math. Soc.*, 131(4):1169–1176, 2003. (Cited on pages 16, 123, 146, 147, 156, and 158.)

[Qia04] L. Qian. *The regularized Whittaker-Kotelnikov-Shannon sampling theorem and its application to the numerical solutions of partial differential equations*. PhD thesis, National Univ. Singapore, 2004. (Cited on page 147.)

[QO05] L. Qian and H. Ogawa. Modified sinc kernels for the localized sampling series. *Sampl. Theory Signal Image Proc.*, 4(2):121–139, 2005. (Cited on pages 135 and 159.)

[Rap96] T. S. Rappaport. *Wireless Communications: Principles and Practice*. Prentice Hall, New Jersey, 1996. (Cited on pages 15, 123, and 134.)

[RAT18] D. Ruiz-Antolin and A. Townsend. A nonuniform fast Fourier transform based on low rank approximation. *SIAM J. Sci. Comput.*, 40(1):A529–A547, 2018. (Cited on page 39.)

[Ros98] D. Rosenfeld. An optimal and efficient new gridding algorithm using singular value decomposition. *Magn. Reson. Med.*, 40(1):14–23, 1998. (Cited on pages 61, 62, 82, 83, and 99.)

[RPS+99] V. Rasche, R. Proksa, R. Sinkus, P. Börnert, and H. Eggers. Resampling of data between arbitrary grids using convolution interpolation. *IEEE Trans. Med. Imag.*, 18:385–392, 1999. (Cited on page 44.)

[Sel18] J. Selva. Efficient type-4 and type-5 non-uniform FFT methods in the one-dimensional case. *IET Signal Processing*, 12(1):74–81, 2018. (Cited on page 41.)

[SFN01] B. P. Sutton, J. A. Fessler, and D. C. Noll. A min-max approach to the nonuniform N-dimensional FFT for rapid iterative reconstruction of MR images. In *Proc. ISMRM 9th Scientific Meeting*, page 763, 2001. (Cited on page 40.)

[SG19] T. Scarnati and A. Gelb. Accelerated variance based joint sparsity recovery of images from Fourier data. arXiv, 2019. (Cited on page 40.)

[Sha49] C. E. Shannon. Communication in the presence of noise. *Proc. I.R.E.*, 37:10–21, 1949. (Cited on pages 11, 14, and 109.)

[SN00] H. Sedarat and D. G. Nishimura. On the optimality of the gridding reconstruction algorithm. *IEEE Trans. Med. Imaging*, 19(4):306–317, 2000. (Cited on pages 59, 61, and 63.)

[SRG10] W. Stefan, R. A. Renaut, and A. Gelb. Improved total variation-type regularization using higher order edge detectors. *SIIMS*, 3(2):232–251, 2010. (Cited on page 40.)

[SS00] H. Schmeisser and W. Sickel. Sampling theory and function spaces. *Applied Mathematics Reviews*, pages 205–284, 2000. (Cited on pages 123, 128, 131, 135, and 138.)

[SS07] G. Schmeisser and F. Stenger. Sinc approximation with a Gaussian multiplier. *Sampl. Theory Signal Image Process.*, 6(2):199–221, 2007. (Cited on pages 16, 123, and 147.)

[ST05] T. Strohmer and J. Tanner. Implementations of shannon's sampling theorem, a time–frequency approach. *Sampl. Theory Signal Image Process.*, 4(1):1–17, 2005. (Cited on pages 15, 123, 124, 140, and 141.)

[ST06] T. Strohmer and J. Tanner. Fast reconstruction methods for bandlimited functions from periodic nonuniform sampling. *SIAM J. Numer. Anal.*, 44(3):1071–1094, 2006. (Cited on pages 117 and 141.)

[Ste93] F. Stenger. *Numerical Methods Based on Sinc and Analytic Functions*, volume 20 of *Springer Series in Computational Mathematics*. Springer-Verlag New York, 1993. (Cited on pages 16, 114, 116, and 217.)

[Ste98a] G. Steidl. A note on fast Fourier transforms for nonequispaced grids. *Adv. Comput. Math.*, 9:337–353, 1998. (Cited on pages 9, 25, and 28.)

[Ste98b] G. Stewart. *Matrix Algorithms: Basic decompositions*. SIAM, Philadelphia, 1998. (Cited on page 56.)

[Tch57] V. Tchakaloff. Formules de cubature mécaniques à coefficients non négatifs. *Bull. Sci. Math.*, 81:123–134, 1957. (Cited on page 46.)

[Tre13] L. N. Trefethen. *Approximation theory and approximation practice*. Society for Industrial and Applied Mathematics (SIAM), Philadelphia, PA, 2013. (Cited on pages 221, 222, and 223.)

[TSM08] K. Tanaka, M. Sugihara, and K. Murota. Complex analytic approach to the sinc-Gauss sampling formula. *Japan J. Ind. Appl. Math.*, 25:209–231, 2008. (Cited on page 147.)

[UAE92] M. Unser, A. Aldroubi, and M. Eden. On the asymptotic convergence of B-spline wavelets to Gabor functions. *IEEE Trans. Inform. Theory*, 38(2):864–872, 1992. (Cited on page 163.)

[WAG15] G. Wasserman, R. Archibald, and A. Gelb. Image reconstruction from Fourier data using sparsity of edges. *J. Sci. Comput.*, 65(2):533–552, 2015. (Cited on page 40.)

[War98] A. F. Ware. Fast approximate Fourier transforms for irregularly spaced data. *SIAM Rev.*, 40:838–856, 1998. (Cited on page 9.)

[Wat80] G. N. Watson. *A Treatise on the Theory of Bessel Functions*. Cambridge University Press, Cambridge, 1980. (Cited on page 171.)

[WEB24] H. Wilber, E. N. Epperly, and A. H. Barnett. A superfast direct inversion method for the nonuniform discrete Fourier transform. *arXiv:2404.13223*, 2024. (Cited on page 41.)

[Whi15] E. T. Whittaker. On the functions which are represented by the expansions of the interpolation theory. *Proc. R. Soc. Edinb.*, 35:181–194, 1915. (Cited on pages 11, 14, and 109.)

[WW20] E. T. Whittaker and G. N. Watson. *A Course of Modern Analysis*. Cambridge University Press, third edition, 1920. (Cited on page 117.)

[You91] R. M. Young. Euler's constant. *Math. Gaz.*, 75:187–190, 1991. (Cited on page 116.)

[YT66] K. Yao and J. B. Thomas. On truncation error bounds for sampling representations of band-limited signals. *IEEE Trans. Aerospace Electronic Syst.*, AES-2(6):640–647, 1966. (Cited on page 119.)

[Zay93] A. I. Zayed. *Advances in Shannon's Sampling Theory.* CRC Press, Boca Raton, 1993. (Cited on pages 117 and 119.)

Alphabetical Index

Approximation error, 186

Bandlimited functions, 105, 261
Bandwidth, 105
Bernstein space, 128
Bessel function
    modified, of first kind, 142, 168
    modified, of second kind, 173
    of first kind, 167
Best approximating trigonometric polynomial, 53
Block uniform resampling algorithm, 82

Cardinal B–spline, 142
Condition number, 56
Conjugate gradient algorithm (CG), 39, 63
Convolution, 135
    convolution property, 143
    convolution theorem, 26

Density compensation factors, 43
Direct methods, 41
Dirichlet kernel, 74
Dirichlet window function, 75
Discrete cosine transform of type I (DCT-I), 223

Error function, 154
Essentially bandlimited, 155
Euler's constant, 114, 116

Fourier coefficients, 24
Fourier matrix
    equispaced, 29
    nonequispaced, 25
Fourier series, 24
Fourier transform
    continuous, 105
    discrete (DFT), 26
    fast Fourier transform (FFT), 24
Frame, 83
Frame decomposition, 83
Frame operator, 83
Frequency window function, 124
    convolutional, 137
    cubic, 133
    de La Vallée-Poussin type, *see* linear
    linear, 131
    raised cosine, 134
    trapezoidal, *see* linear
Frobenius norm, 54, 70

Grids
    golden angle linogram, 89
    golden angle polar, 89
    jittered, 88
    linogram, 89
    modified polar, 89
    polar, 89
    pseudo-polar, *see* linogram
    random, 88

spiral, 90

Hadamard product, 63
Harmonic number, 115

Induced matrix norm, 70
Integral test for convergence of series, 117
Interpolating approximation, 143
Inverse Fourier transform
continuous, 107
inverse adjoint NFFT (iNFFT*), 38
inverse FFT (iFFT), 24
inverse NFFT (iNFFT), 38
Iterative inversion procedures, 39

Kronecker symbol, 45, 108

Least squares, 58, 60
Localized sampling, 146

Maclaurin–Cauchy test, *see* Integral test for convergence of series
Magnetic resonance imaging (MRI), 37, 261, 263
Mesh norm, 77
Modified Struve function, 178
Moore-Penrose pseudoinverse, 58

NFFT-like procedure, 243, 247, 257
Nonequispaced fast Fourier transform
adjoint NFFT, 30
NFFT, 25
NNFFT, 32
Nonharmonic bandwidth, 31

Normal equations
of first kind, 52, 60
of second kind, 51, 65

Oversampling, 122
Oversampling factor, 26
Oversampling parameter, 121

Paley–Wiener space, 106
Positive semidefinite, 63

Regularization
in frequency domain, 124
in spatial domain, 141
Regularization error, 144, 147, 148, 186
Regularization error constant, 145, 147, 153, 190, 192, 195
B–spline, 164, 197
sinh-type, 170, 198
continuous Kaiser–Bessel, 177, 199
Gaussian, 156, 196
Regularized sinc function, 185
B–spline, 160
sinh-type, 167
continuous Kaiser–Bessel, 175
Gaussian, 153
Regularized sinc function, 144
Regularized Shannon sampling formula, 143
Regularized Shannon sampling formula with localized sampling, 146, 184
sinh-type, 198
continuous Kaiser–Bessel, 199

modified B–spline, 196
truncated Gaussian, 195

Sampling density compensation, 42
Schatten 2-norm, 70
Schur product theorem, 63
Schwartz space, 270
Separation distance, 77
Shannon sampling series, 112
Shannon sampling sum, 111
Sinc function, 57
Sinc matrix, 57
Sinc transform
discrete, 218, 227
fast, 227, 230
Sine integral function, 178
Singular value decomposition (SVD), 59
Spatial window function, 141
sinh-type, 142
constant, 150, 190
continuous Kaiser–Bessel, 142
Gaussian, 142
modified B–spline, 142
Special affine Fourier transform (SAFT), 153
Spectral norm, 70

Tempered distributions, 270
Dirac distribution, 270
Induced distribution, 270
Tensor product, 28
Toeplitz matrix, 39, 41, 60
Torus, 23
Total variation (TV), 41
Triangular pulse function, 93, 99, 273
Trigonometric polynomial, 25
Truncated window function, 146
Truncation error, 147, 186, 188, 190
Truncation error constant, 147, 150, 153, 190, 195
B–spline, 164
sinh-type, 170
continuous Kaiser–Bessel, 177
Gaussian, 157, 196

Uncertainty principle, 126
Uniform approximation error, 119, 145, 147, 185
B–spline, 164, 196
sinh-type, 170, 198
continuous Kaiser–Bessel, 177, 199
Gaussian, 156, 195
Uniform perturbation error, 151, 194
B–spline, 166, 197, 208, 209
sinh-type, 174, 198, 209, 211
continuous Kaiser–Bessel, 182, 199, 211, 212
Gaussian, 159, 196, 206, 207
Uniform regularization error, 143

Voronoi weights, 39, 44

Well localized, 27
Whittaker–Kotelnikov–Shannon sampling theorem, 109
Window function for NFFT, 26
sinh-type, 29
B–spline, 28
continuous cosh-type, 29
continuous exp-type, 29
continuous Kaiser–Bessel, 29
Gaussian, 28

List of Symbols

$\lfloor x \rfloor$	Largest integer $\leq x$ for given $x \in \mathbb{R}$.
$\lceil x \rceil$	Smallest integer $\geq x$ for given $x \in \mathbb{R}$.
B_m	Centered cardinal B-spline of order m.
$\mathcal{B}_{M/2}(\mathbb{R}^d)$	Paley–Wiener space of bandlimited functions.
$\mathbb{C}$	Set of complex numbers.
$C(\mathbb{R}^d)$	Banach space of continuous functions $f\colon \mathbb{R}^d \to \mathbb{C}$.
$C_0(\mathbb{R}^d)$	Banach space of continuous functions $f\colon \mathbb{R}^d \to \mathbb{C}$ with $\lim_{\|\boldsymbol{x}\|_2 \to \infty} f(\boldsymbol{x}) = 0$.
$C^r(\mathbb{R}^d)$	Banach space of r-times continuously differentiable functions $f\colon \mathbb{R}^d \to \mathbb{C}$.
$\delta_{k,\ell}$	Kronecker symbol with $\delta_{k,\ell} = 1$, $k = \ell$, and $\delta_{k,\ell} = 0$, $k \neq \ell$.
δ	Dirac distribution.
$\operatorname{diag}(\boldsymbol{a})$	Diagonal matrix with the diagonal entries $\boldsymbol{a} = (a_j)_{j=1}^N$.
e	Euler's number.
$f\colon \mathbb{T}^d \to \mathbb{C}$	Complex-valued 1-periodic function.
$f\colon \mathbb{R}^d \to \mathbb{C}$	Complex-valued function.
$f * g$	Convolution of f, $g \in L_1(\mathbb{T}^d)$ or f, $g \in L_1(\mathbb{R}^d)$.
i	Imaginary unit.
$\boldsymbol{I}_N$	Identity matrix of size $N \times N$.
$\mathcal{I}_{\boldsymbol{M}}$	Multi-index set $\mathbb{Z}^d \cap \prod_{t=1}^d \left[-\frac{M_t}{2}, \frac{M_t}{2}\right)$.
I_ν	Modified Bessel function of first kind of order ν.
$\mathcal{J}_m$	Index set $\{-m+1, -m+2, \ldots, m\}$ for $m \in \mathbb{N}$.
J_ν	Bessel function of first kind of order ν.
K_ν	Modified Bessel function of second kind of order ν.

$L_p(X)$	Banach space of measurable functions $f\colon X \to \mathbb{C}$ with integrable $\lvert f\rvert^p$, $p \geq 1$.
$L_2(X)$	Hilbert space of square integrable functions $f\colon X \to \mathbb{C}$.
$\mathbb{N}$	Set of positive integers.
$\mathbb{N}_0$	Set of nonnegative integers.
$\mathcal{O}$	Landau symbol.
Φ	Set of window functions in spatial domain.
$\mathbb{R}$	Set of real numbers.
$\mathscr{S}(\mathbb{R}^d)$	Schwartz space of rapidly decreasing functions.
$\mathscr{S}'(\mathbb{R}^d)$	Space of tempered distributions on $\mathscr{S}(\mathbb{R}^d)$.
$\operatorname{sign}(x)$	Sign of $x \in \mathbb{R}$.
sinc	Cardinal sine function.
Si	Sine integral function.
$\operatorname{supp}(f)$	Support of $f\colon \mathbb{R}^d \to \mathbb{C}$.
$\mathbb{T}^d$	d-dimensional torus $\mathbb{R}^d \setminus \mathbb{Z}^d \cong \left[-\frac{1}{2}, \frac{1}{2}\right)^d$.
$\boldsymbol{v}$	Vector $\boldsymbol{v} = (v_j)_{j=1}^N \in \mathbb{C}^N$ with components $v_1, \ldots, v_N$.
$\mathbf{1}_d$	Vector of ones, $\mathbf{1}_d = (1, \ldots, 1)^T \in \mathbb{Z}^d$.
$\boldsymbol{xy}$	Inner product $\boldsymbol{xy} \coloneqq x_1 y_1 + \cdots + x_d y_d$ of two vectors $\boldsymbol{x}, \boldsymbol{y} \in \mathbb{R}^d$.
$\boldsymbol{x} \odot \boldsymbol{y}$	Componentwise product $\boldsymbol{x} \odot \boldsymbol{y} \coloneqq (x_1 y_1, \ldots, x_d y_d)^T$ of two vectors $\boldsymbol{x}, \boldsymbol{y} \in \mathbb{R}^d$.
$\boldsymbol{M}^{-1}$	Reciprocal $\boldsymbol{M}^{-1} \coloneqq \left(M_1^{-1}, \ldots, M_d^{-1}\right)^T$ of a vector $\boldsymbol{M} \in \mathbb{Z}^d$ with nonzero components.
$\chi_{[a,b]}$	Characteristic function of the interval $[a, b]$.
$\mathbb{Z}$	Set of integers.

The table above lists the most frequently used notations, but it is not comprehensive. Additional necessary notations may appear locally throughout the work.